

**POWER SYSTEM CONFIGURATION STUDY
AND RELIABILITY ANALYSIS**

**SPACECRAFT POWER SYSTEM
C O N F I G U R A T I O N R E F E R E N C E
M A N U A L**

by
W. G. Binckley

07171-6002-R000

18 September 1967

**This work was performed for the Jet Propulsion Laboratory,
California Institute of Technology, sponsored by the
National Aeronautics and Space Administration under
Contract No. 951574**

TRW
SYSTEMS GROUP OF TRW INC

ONE SPACE PARK • REDONDO BEACH, CALIFORNIA

This work was performed for the Jet Propulsion Laboratory, California Institute of Technology, sponsored by the National Aeronautics and Space Administration under Contract No. 951574

Prepared *W. G. Binckley*
W. G. Binckley
Project Manager

Approved *Arthur D. Schoenfeld*
A. D. Schoenfeld
Manager, Power Systems
and Conditioning Department

TRW Systems
One Space Park
Redondo Beach, California

DISCLAIMER CLAUSE

NOTICE

This report was prepared as an account of Government - sponsored work. Neither the United States, nor the National Aeronautics and Space Administration (NASA), nor any person acting on behalf of NASA:

- a. Makes warranty or representation, expressed or implied, with respect to the accuracy, completeness, or usefulness of the information contained in this report, or that the use of any information, apparatus, method, or process disclosed in this report may not infringe privately owned rights; or
- b. Assumes any liabilities with respect to the use of, or for damages resulting from, the use of any information, apparatus, method, or process disclosed in this report.

As used above, "person acting on behalf of NASA" includes any employee or contractor of NASA, or employee of such contractor, to the extent that such employees or contractor of NASA, or employee of such contractor prepares, disseminates, or provides access to, any information pursuant to his employment with such contractor.

Requests for copies of this report should be referred to:

National Aeronautics and Space Administration
Office of Scientific and Technical Information
Washington 25, D.C.

FOREWORD

This manual was prepared by TRW Systems for the Jet Propulsion Laboratory under Contract No. 951574. The author wishes to acknowledge the valuable contributions of the following personnel to this project: E. C. Jazwa, JPL technical representative, for his technical direction and guidance; W. S. Dixon, W. A. Klein and K. H. Meissner who formed the nucleus of the study team; P. Bauer, J. J. Biess, R. L. Brown, A. A. Conn, S. Green, W. R. Johnson, H. F. Meissinger, F. S. Osugi, B. M. Otzinger, A. D. Schoenfeld and J. W. Schrecengost for their significant technical contributions; and T. Byrne, G. A. Hetland and D. B. Ryder for their editorial assistance.

ABSTRACT

A method of performing preliminary power system tradeoffs to select optimum configurations on the basis of minimum weight and maximum reliability is presented. Model sets of power system requirements for interplanetary missions to Mercury, Venus, Mars and Jupiter and representative spacecraft configurations are provided. Candidate power system configurations and design approaches for each unit, and preferred methods of implementing unit redundancy and the effects of redundancy on unit weight and efficiency are described. A computer program to perform individual system reliability weight optimization and to select minimum weight system configurations as a function of reliability is described. Results of applying this optimization method to seven model spacecraft/mission applications are presented. Important system design considerations in the implementation of preferred system configurations are discussed and include electromagnetic compatibility, thermal interfaces, and command and telemetry provisions.

CONTENTS

	Page
1. INTRODUCTION	1-1
2. INTERPLANETARY MISSION CHARACTERISTICS	2-1
2.1 Typical Spacecraft and Mission Profiles	2-1
2.2 Typical Power Requirements	2-7
2.3 Solar Array Characteristics	2-25
3. BASELINE POWER SYSTEM CONFIGURATIONS	3-1
3.2 Methods of Implementing Functions	3-5
3.2.1 Battery Selection	3-5
3.2.2 Battery Control	3-5
3.2.3 Solar Array Controls	3-7
3.2.4 Line Regulators	3-8
3.2.5 Load Power Conditioning Equipment	3-8
3.2.6 Selection of Baseline System Configurations	3-9
3.3 Solar Array Power Utilization	3-33
4. METHODS OF IMPROVING SYSTEM RELIABILITY	4-1
4.1 Preferred Methods of Implementing Redundancy	4-1
4.2 Selected Redundant Configurations and Part Counts	4-7
4.2.1 Solar Array	4-7
4.2.2 Array Controls	4-7
4.2.3 Battery Controls	4-8
4.2.4 Battery	4-9
4.2.5 Line Regulators	4-9
4.2.6 Load Power Conditioner	4-10
4.3 Effect of Reliability Improvements on Unit Weight and Efficiency	4-47
4.3.1 Electronic Equipment	4-47
4.3.2 Batteries	4-48
5. RELIABILITY-WEIGHT OPTIMIZATION	5-1
5.1 Computer Program Description	5-1
5.2 Results of Reliability-Weight Optimization	5-40
5.2.1 Venus Orbiter No. 1	5-40
5.2.2 Venus Orbiter No. 2	5-41
5.2.3 Mercury Flyby	5-41
5.2.4 Mars Orbiter	5-42
5.2.5 Jupiter Flyby	5-43
5.2.6 Jupiter Orbiters	5-44

CONTENTS (Continued)

	Page
6. DESIGN CONSIDERATIONS AND CONCLUSIONS	6-1
6.1 Electromagnetic Compatibility	6-1
6.2 Thermal Control	6-5
6.3 Power System Flexibility	6-7
6.4 System Design Considerations	6-11
6.4.1 Command Provisions	6-11
6.4.2 Telemetry Provisions	6-15
6.4.3 Load Fault Protection	6-18
6.4.4 Electromagnetic Interference Control	6-21
6.5 Conclusions	6-28
6.5.1 Reliability-Weight Optimization Computer Program	6-28
6.5.2 Preferred Power System Configurations	6-30
6.5.3 Preferred Power Systems	6-32

ILLUSTRATIONS

	Page
1. Mission Profile: Mercury Flyby.	2-4
2. Mission Profile: Venus Orbiter	2-4
3. Mission Profile: Mars Orbiter (Launch May 1971).	2-5
4. Mission Profile: Jupiter Orbiter (Launch March 1972).	2-5
5. Eclipse Durations for Assumed Mars Orbit.	2-6
6. Eclipse Durations for Assumed Venus Orbit	2-6
7. Solar Array Maximum Power Capability and Conditioned Load Power Requirements versus Time - Mercury Flyby Mission	2-21
8. Solar Array Maximum Power Capability and Conditioned Load Power Requirements versus Time - Venus Orbiter No. 1 Mission.	2-21
9. Solar Array Maximum Power Capability and Conditioned Load Power Requirements versus Time - Venus Orbiter No. 2 Mission.	2-22
10. Solar Array Maximum Power Capability and Conditioned Load Power Requirements versus Time - Mars Orbiter Mission.	2-22
11. Solar Array Maximum Power Capability and Conditioned Load Power Requirements versus Time - Jupiter Flyby Mission.	2-23
12. Solar Array Maximum Power Capability and Conditioned Load Power Requirements versus Time - Jupiter Orbiter No. 1 Mission	2-23
13. Solar Array Maximum Power Capability and Conditioned Load Power Requirements versus Time - Jupiter Orbiter No. 2 Mission.	2-24
14. Comparison of Special Solar Cell with Standard Solar Cell at Light Intensity of 20 Suns.	2-26
15. Mercury Flyby Solar Array Characteristics	2-27
16. Venus Orbiter Solar Array Characteristics.	2-28
17. Mars Orbiter Solar Array Characteristics	2-28
18. Jupiter Mission Solar Array Characteristics.	2-29

ILLUSTRATIONS (Continued)

		Page
19.	Flow Diagram - Baseline System Configuration Analysis. . .	3-2
20.	Generalized Power System Concepts	3-3
21.	Basic Functional Power System Configurations	3-4
22.	Comparison of Required Solar Array Capabilities With and Without Momentary Line Booster for Unregulated Bus Systems.	3-10
23.	Dissipative Series Battery Charger.	3-11
24.	Pulsewidth Modulated Series Bucking Battery Charger	3-11
25.	Pulsewidth Modulated Buck-Boost Solar Array Regulator, Line Voltage Regulator or Battery Charger.	3-12
26.	Dissipative Battery Charge Regulator	3-12
27.	Pulsewidth Modulated Bucking Battery Charge Regulator. . .	3-13
28.	Pulsewidth Modulated Momentary Line Booster Used With Boosting Charger	3-13
29.	Pulsewidth Modulated Boosting Line Regulator, Battery Discharge Regulator and Momentary Line Booster Used with Bucking Charger	3-14
30.	Battery Control Block Diagram-Bucking Charger and Discharge Switch	3-14
31.	Battery Controls Block Diagram-Bucking Charger, Discharge Switch, and Line Booster	3-15
32.	Battery Controls Block Diagram-Boost Charger and Discharge Switch	3-16
33.	Battery Controls Block Diagram-Boost Charger, Discharge Switch, and Line Booster	3-17
34.	Battery Controls Block Diagram— Bucking Charge Regulator, Boost Discharge Regulator.	3-18
35.	Zener Diode Solar Array Voltage Limiter.	3-19
36.	Active Shunt Solar Array Voltage Limiter	3-19
37.	Pulsewidth Modulated Bucking Solar Array Voltage Limiter or Line Regulator.	3-20

ILLUSTRATIONS (Continued)

	Page
38. Maximum Power Tracking Solar Array Voltage Limiter . . .	3-20
39. Dissipative Series Line Regulator	3-20
40. Block Diagram. Load Power Conditioning Equipment Configuration. DC Distribution	3-21
41. Block Diagram Unregulated DC-DC Converter	3-21
42. Block Diagram. Load Power Conditioning Equipment Configuration - AC Distribution	3-21
43. Selected Alternative Methods of Implementing Basic Functional Configurations Having Unregulated Main Bus	3-22
44. Selected Methods of Implementing Basic Functional Configurations Having Regulated Main Bus	3-23
45. Solar Array Sizing Factors for Mercury Flyby Mission	3-36
46. Solar Array Utilization Factors for Venus Orbiter No. 1 Mission	3-37
47. Solar Array Sizing Factors for Venus Orbiter No. 2 Mission	3-38
48. Solar Array Sizing Factors for Mars Orbiter Mission	3-39
49. Solar Array Sizing Factors for Jupiter Missions	3-40
50. Basic System Reliability Model	4-4
51. Parallel Redundant System Reliability Model	4-4
52. Standby Redundant System Reliability Model	4-5
53. Quad Redundant System Reliability Model	4-5
54. Majority Voting System Reliability Model	4-6
55a. Nonredundant Voltage Sensing and Error Amplifier Block Diagram	4-11
55b. Majority Voting Redundant Configuration of Voltage Sensing and Error Amplifier	4-11
56. Methods of Implementing Part Redundancy	4-12

ILLUSTRATIONS (Continued)

		Page
57.	Array Controls, Baseline, Weight Versus Power Output. . .	4-49
58.	Array Controls, Redundant, Weight Versus Power Output. .	4-49
59.	Array Controls, Baseline, Efficiency Versus Power Output. ,	4-50
60.	Array Controls, Redundant, Efficiency Versus Power Output	4-50
61.	Battery Controls, Baseline, Weight Versus Power Output.	4-51
62.	Battery Controls, Redundant, Weight Versus Power Output.	4-51
63.	Battery Controls, Baseline, Efficiency versus Power Output,	4-52
64.	Battery Controls, Redundant, Efficiency versus Power Output.	4-52
65.	Low Voltage Battery Controls, Efficiency Versus Power Output.	4-53
66.	Low Voltage Battery Controls, Weight Versus Power Output.	4-53
67.	Line Regulators, Baseline, Weight Versus Power Output.	4-54
68.	Line Regulators, Redundant, Weight Versus Power Output.	4-54
69.	Line Regulator, Baseline, Efficiency Versus Power Output.	4-55
70.	Line Regulators, Redundant, Efficiency Versus Power Output.	4-55
71.	Load Power Conditioning Equipment, Baseline, Weight Versus Power Output ,	4-56
72.	Load Power Conditioning Equipment, Redundant, Weight Versus Power Output	4-56
73.	Load Power Conditioning Equipment, Baseline, Efficiency Versus Power Output	4-57
74.	Load Power Conditioning Equipment, Redundant, Efficiency Versus Power Output	4-57

ILLUSTRATIONS (Continued)

	Page
75. Bucking Line Regulator Power Loss Weight Product Versus Switching Frequency.	4-58
76. Twenty Cell Silver-Cadmium and Fifteen Cell Silver-Zinc Battery Weights as Functions of Capacity, Discharge Power and Mission.	4-59
77. Three Cell Battery Weights as Functions of Capacity, Discharge Power, and Mission	4-59
78. Reliability - Weight Optimization Matrix	5-8
79. Logic Diagram Computer Program	5-14
80. Locus of Optimum System Configurations, Venus Orbiter No. 1.	5-47
81. Comparison of Optimum System Configurations, Venus Orbiter No. 1.	5-47
82. Locus of Optimum System Configuration, Venus Orbiter No. 2	5-48
83. Comparison of Optimum System Configurations, Venus Orbiter No. 2.	5-49
84. Locus of Optimum System Configurations, Mercury Flyby.	5-50
85. Comparison of Optimum System Configurations, Mercury Flyby.	5-51
86. Locus of Optimum System Configuration, Mars Orbiter.	5-52
87. Comparison of Optimum System Configurations, Mars Orbiter.	5-53
88. Locus of Optimum System Configurations, Jupiter Flyby.	5-54
89. Comparison of Optimum System Configurations, Jupiter Flyby,	5-55
90. Locus of Optimum System Configurations, Jupiter Orbiter No. 1	5-56
91. Comparison of Optimum System Configurations, Jupiter No. 1.	5-57

ILLUSTRATIONS (Continued)

	Page
92. Locus of Optimum System Configurations, Jupiter Orbiter No. 2	5-58
93. Comparison of Optimum System Configurations, Jupiter Orbiter No. 2	5-59

TABLES

		Page
1.	Model Spacecraft Configurations	2-3
2.	Conditioned Power Requirements (in watts) is a Function of Mission Phase— Mercury Flyby Model.	2-9
3.	Conditioned Power Requirements (in watts) as a Function of Mission Phase— Venus Orbiter Model No. 1	2-10
4.	Conditioned Power Requirements (in watts) as a Function of Mission Phase— Venus Orbiter Model No. 2	2-11
5.	Conditioned Power Requirements (in watts) as a Function of Mission Phase— Mars Orbiter Model.	2-12
6.	Conditioned Power Requirements (in watts) as a Function of Mission Phase— Jupiter Flyby Model.	2-13
7.	Conditioned Power Requirements (in watts) as a Function of Mission Phase— Jupiter Orbiter Model No. 1	2-14
8.	Conditioned Power Requirements (in watts) as a Function of Mission Phase— Jupiter Orbiter Model No. 2	2-15
9.	Load Equipment Typical Input Power Characteristics.	2-16
10.	Mercury Flyby Mission, Load Power Conditioning Equipment.	3-24
11.	Venus Orbiter No. 1 Mission, Load Power Conditioning Equipment	3-25
12.	Venus Orbiter No. 2 Mission, Load Power Conditioning Equipment	3-26
13.	Mars Orbiter Mission, Load Power Conditioning Equipment	3-27
14.	Jupiter Flyby Mission Load Power Conditioning Equipment	3-28
15.	Jupiter Orbiter No, 1 Mission, Load Power Conditioning Equipment	3-29
16.	Jupiter Orbiter No. 2 Mission, Load Power Conditioning Equipment.	3-30
17.	Summary of Selected Baseline Power System Configurations	3-31

TABLES (Continued)

	Page
18. Justifications for Deletions of Power System Configurations	3-32
19. Baseline Parts Count, Array Control.	4- 13
20. Redundant Parts Count, Array Control.	4- 14
21. Baseline Parts Count, Battery Controls	4- 15
22. Redundant Parts Count, Battery Controls.	4- 16
23. Baseline Parts Count, Line Regulators	4-17
24. Redundant Parts Count, Line Regulators	4- 18
25. Load Power Conditioning Equipment, Baseline Parts Count, Mercury Flyby, AC Distribution System.	4-19
26. Load Power Conditioning Equipment, Redundant Parts Count, Mercury Flyby, AC Distribution System.	4-20
27. Load Power Conditioning Equipment, Baseline Parts Count, Mercury Flyby, DC Distribution System.	4-21
28. Load Power Conditioning Equipment, Redundant Parts Count, Mercury Flyby, DC Distribution System.	4-22
29. Load Power Conditioning Equipment, Baseline Parts Count, Venus Orbiter No. 1, AC Distribution System.	4-23
30. Load Power Conditioning Equipment, Redundant Parts Count, Venus Orbiter No. 1 AC Distribution System.	4-24
31. Load Power Conditioning Equipment, Baseline Parts Count, Venus Orbiter No. 1, DC Distribution System.	4-25
32. Load Power Conditioning Equipment, Redundant Parts Count, Venus Orbiter No. 1, DC Distribution System.	4-26
33. Load Power Conditioning Equipment, Baseline Parts Count, Venus Orbiter No. 2, AC Distribution System.	4-27
34. Load Power Conditioning Equipment, Redundant Parts Count, Venus Orbiter No. 2, AC Distribution System.	4-28
35. Load Power Conditioning Equipment, Baseline Parts Count, Venus Orbiter No. 2, DC Distribution System.	4-29
36. Load Power Conditioning Equipment, Redundant Parts Count, Venus Orbiter No. 2, DC Distribution System.	4-30

TABLES (Continued)

	Page
37. Load Power Conditioning Equipment, Baseline Parts Count, Mars Orbiter, AC Distribution System.	4-31
38. Load Power Conditioning Equipment, Redundant Parts Count, Mars Orbiter; AC Distribution System.	4-32
39. Load Power Conditioning Equipment, Baseline Parts Count, Mars Orbiter, DC Distribution System.	4-33
40. Load Power Conditioning Equipment, Redundant Parts Count, Mars Orbiter, DC Distribution System.	4-34
41. Load Power Conditioning Equipment, Baseline Parts Count, Jupiter Flyby, AC Distribution System.	4-35
42. Load Power Conditioning Equipment, Redundant Parts Count, Jupiter Flyby, AC Distribution System.	4-36
43. Load Power Conditioning Equipment, Baseline Parts Count, Jupiter Flyby, DC Distribution System.	4-37
44. Load Power Conditioning Equipment, Redundant Parts Count, Jupiter Flyby, DC Distribution System.	4-38
45. Load Power Conditioning Equipment, Baseline Parts Count, Jupiter Orbiter No. 1, AC Distribution System	4-39
46. Load Power Conditioning Equipment, Redundant Parts Count, Jupiter Orbiter No. 1, AC Distribution System.	4-40
47. Load Power Conditioning Equipment, Baseline Parts Count, Jupiter Orbiter No. 1, DC Distribution System.	4-41
48. Load Power Conditioning Equipment, Redundant Parts Count, Jupiter Orbiter No. 1, DC Distribution System	4-42
49. Load Power Conditioning Equipment, Baseline Parts Count, Jupiter Orbiter No. 2, AC Distribution System.	4-43
50. Load Power Conditioning Equipment, Redundant Parts Count, Jupiter Orbiter No. 2, AC Distribution System	4-44
51. Load Power Conditioning Equipment, Baseline Parts Count, Jupiter Orbiter No. 2, DC Distribution System	4-45
52. Load Power Conditioning Equipment, Redundant Parts Count, Jupiter Orbiter No. 2, DC Distribution System.	4-46
53. Recommended Failure Rates for Power System Configuration Study.	5-6

TABLES (Continued)

	Page
54. Part Type Demonstrated Orbital Operating Hours (Vela and OGO)	5-7
55. Part Group Total Number of Orbital Parts (Vela and OGO)	5-7
56. Weight Calculations for DC Distribution Systems.	5-9
57. Weight Calculations for AC Distribution Systems.	5-10
58. Glossary of Terms.	5-11
59. Program Listing	5-16
60. System Optimization Computer Printout, Mercury Flyby . . .	5-21
61. System Optimization Computer Printout, Venus Orbiter No. 1.	5-22
62. System Optimization Computer Printout, Venus Orbiter No. 2.	5-23
63. System Optimization Computer Printout, Mars Orbiter	5-24
64. System Optimization Computer Printout, Jupiter Flyby	5-25
65. System Optimization Computer Printout, Jupiter Orbiter No. 1	5-26
66. System Optimization Computer Printout, Jupiter Orbiter No. 2	5-27
67. Power System Configuration Code.	5-28
68. Computer Printout, Mercury Flyby.	5-29
69. Computer Printout, Venus Orbiter No. 1	5-31
70. Computer Printout, Venus Orbiter No. 2	5-32
71. Computer Printout, Mars Orbiter.	5-34
72. Computer Printout, Jupiter Flyby.	5-36
73. Computer Printout, Jupiter Orbiter No. 1	5-38
74. Computer Printout, Jupiter Orbiter No. 2	5-39
75. Configuration Code.	5-45
76. Analog Telemetry Measurements and Priorities	6-27

1. INTRODUCTION

The design of an electric power system for any spacecraft application necessarily begins with the comparative analysis of alternative power system configurations. These configurations are normally defined by a block diagram representing each of the functional units within the system. The functions essential to any photovoltaic power system which includes batteries are identified as the power source, power source control, energy storage (battery and battery controls), voltage regulation and load power conditioning ■

Since a large variety of power system configurations are conceptually feasible, it is normally necessary to limit the scope of these comparisons by selecting relatively few preferred approaches for comparison. The preferences leading to these selections are usually subjective in nature and tend to reflect, to a large extent, the experience of the organization or individual charged with the responsibility of performing this important phase of the system design task. The specific design requirements for the power system and the optimization criteria used to evaluate candidate configurations vary from one application to another. The two most common criteria, exclusive of cost however, are the conflicting requirements of maximizing reliability and minimizing weight. The validity of these preliminary system tradeoffs will clearly be reflected in the degree of optimization achieved in all subsequent phases of the power system design effort.

This manual is directed primarily toward the description of a method of conducting preliminary power system configuration tradeoffs to select optimized systems with respect to reliability and weight. The method was applied to seven specific spacecraft configuration models spanning the following five basic interplanetary missions:

Mission 1 - 0.3 AU Probe (Mercury Flyby)

Mission 2 - Venus Orbiters (two model spacecraft)

Mission 3 - Mars Orbiter

Mission 4 - 5.2 AU Probe (Jupiter Flyby)

Mission 5 - Jupiter Orbiters (two model spacecraft)

The assumptions made in performing these analyses, supporting parametric data and results of these optimization studies are included herein both to serve as examples of the application of the optimization method and to provide preliminary indications of the general power system configurations that are best suited to the five specified missions.

The optimization process makes use of a computer program to evaluate the relatively large number of possible power system configurations for each specific application. This program is arranged to first define minimum weight configurations of a given power system as a function of reliability by selecting optimum combinations of redundant and nonredundant units within this system. Secondly, the computer program compares these optimized configurations of all candidate power systems to determine their ranking by weight for a series of given reliability constraints. The program computes the reliability and weight of all possible combinations of redundant and nonredundant units within each system from the calculated reliability for each unit, the given output power requirements of the system, and a set of parametric data which defines the weight and efficiency of each unit as a function of its output power level. Minimum weight system configurations are then selected from the results of these computations for a series of reliability constraints ranging from .90 to the maximum achievable for any particular system. The results of these optimization computations are compared to define the minimum weight power systems as a function of reliability.

A specific optimum power system configuration cannot be validly determined independently from the spacecraft reliability-weight optimization analysis. As a result, the optimum power system configurations as a function of reliability serve as an input to such spacecraft analyses, which take into account all required spacecraft systems. These analyses determine the proper apportionment of total spacecraft weight to each system in order to achieve a maximum overall spacecraft reliability.

Following these spacecraft analyses and the definition of a preferred power system configuration the design implementation phase can be initiated. The salient design considerations which influence the implementation of the selected power system configuration are related primarily to the electrical, thermal and mechanical interfaces between the power

system and the spacecraft. Specific design considerations include electromagnetic compatibility, command and telemetry provisions, load fault protection, heat dissipation, temperature limits and unit dimensional constraints. Although command and telemetry provisions and load-fault protection are essentially common to all power system configurations, electromagnetic interference considerations, together with thermal and mechanical interface considerations, will influence the selection of a power system to a varying degree depending upon the particular application. As a result, discussions of each of these design considerations are included herein.

1.1 SUMMARY OF DATA

This reference manual presents the results of the "Power System Configuration Study and Reliability Analysis" Project performed for the Jet Propulsion Laboratory under Contract 951574. The power system analyses performed in the course of this study project are summarized herein. Complete discussion of these analyses are reported in Final Report No. 07171-6001-ROO0 which documents the entire study effort.

The data presented is divisible into four major groups. The first of these covers the definition of typical spacecraft configurations, mission profiles, power requirements and solar array characteristics for the five specified interplanetary missions. These data define representative design requirements for the electric power system for each of seven model spacecraft and the characteristics of the photovoltaic power source used with each. The results of these study investigations are contained in Section 2 of this manual, Interplanetary Mission Characteristics.

The second major group of data is presented in Section 3, Baseline Power System Configurations. In this case, the information defines a variety of candidate power system configurations and the method used to arrive at these specific configurations. Selected design approaches are provided in block diagram form for each functional element of these systems. These functional elements include load power conditioning units which consist of converters, inverters and transformer-rectifier units and which are considered an important part of the complete power system. This section of the manual also includes a description of a method of calculating the ratio of installed solar array power capability to required

power output at maximum load conditions for the various power system configurations and missions. The results of these calculations are presented for each of the seven model spacecraft and reflect variations in the ability of various types of power systems to utilize the maximum power capability of the solar array.

The third major group of data is presented in Section **4**, Methods of Improving System Reliability. In this section, the analyses leading to definition of preferred methods of implementing redundancy in each of the units of the different system configurations are summarized. The data consists of parts counts and parametric data covering unit weight and efficiency as functions of output power for each unit in its nonredundant and redundant configurations. The parts counts are used to determine unit and system reliability. The weight and efficiency data permit calculation of system weight. These data therefore constitute the principal inputs to the power system reliability and weight calculations and the subsequent selection of optimum system configurations.

The fourth major part of the manual, Section 5, Reliability-Weight Optimization, and Section **6**, Design Considerations, describes the computer program developed to perform the power system reliability-weight optimization, summarizes the results of these calculations for each of the seven model spacecraft, and discusses salient power system design considerations in addition to reliability and weight. These data show preferred types of power systems for the various missions and characteristic variations in system weight as a function of reliability for each. The discussion of additional design considerations highlights the impact of electromagnetic interference control and thermal interfaces on the power system design. Command and telemetry interfaces are also discussed relative to their incorporation in power system design.

This data organization reflects the necessary sequential steps in the design of any power system. Initially, the design requirements, mission and spacecraft constraints and power source characteristics must be defined. Candidate power system configurations which meet these criteria are determined. These basic configurations are then analyzed with respect to specific interface considerations, failure modes and effects, and performance characteristics to determine preferred design

implementations of each unit in the system with respect to both the basic design selection and the incorporation of provisions to protect each unit against failures in the system. These system designs are compared to determine those best suited to the particular application. The computer program described herein constitutes a method of performing these system tradeoffs with respect to reliability and weight optimization. System tradeoffs of this type may be required for other optimization criteria as well (e. g. cost, development time, mission flexibility, etc.). For the specified criteria of weight and reliability, preferred minimum weight system configurations are defined as a function of reliability. These data provide the necessary inputs to a spacecraft tradeoff which apportions the available weight among the various spacecraft systems to achieve overall maximum spacecraft reliability. These analyses at the spacecraft level will then determine the optimum power system configuration for the particular mission.

For purposes of this manual, "system" is used to denote the complete electric power system which consists of a solar array, battery, regulators and controls, and load power conditioning equipment. "Unit" is used to define one of the major functional elements in the system such as the solar array, battery, line regulator, etc. The term "part" is used for discrete components contained within a unit such as transistors, diodes, etc.

2. INTERPLANETARY MISSION CHARACTERISTICS

2.1 TYPICAL SPACECRAFT AND MISSION PROFILES

Seven typical model interplanetary spacecraft configurations are described in Table 1. In each case, salient features of the spacecraft systems having significant effects on the power system are listed.

In the case of both the Venus and Jupiter Orbiters, two classes of spacecraft are shown to reflect two weight categories and two power levels. In each, the power levels listed represent a rough estimate of the payload and spacecraft requirements. Detailed power requirements for the equipment and experiments carried on each of the missions are shown subsequently. Each of the model spacecraft is three-axis stabilized with exception of the 5.2 AU probe. In this case, spin stabilization is used with the spin axis of the vehicle directed towards the earth. The attitude control system for this model uses gas jets which precess the spin axis of the vehicle as required and which are controlled from the ground by scanning the rf beam from the vehicle.

The data rates listed for each of the model spacecraft are considered reasonable for the missions and objectives specified. Those models having larger payload capabilities and therefore greater quantities of experiment data to transmit require the higher bit rates. In all cases, high gain antennas are used to maintain the transmitter power requirements within reasonable levels and reduce power system weight.

The close proximity of Mercury to the Sun dictates special provisions to maintain solar array temperatures within an acceptable range for Model No. 1. The selected method employs temperature-controlled orientation of the solar panels away from normal to the sun vector to maintain a maximum 150°C limit. The increased solar intensity near Mercury of course, compensates for the resultant reduction in effective panel area.

Mission profiles as shown in Figure 1 through 4, were prepared to show variations in Earth-spacecraft and Sun-spacecraft distances with mission time. Significant mission events such as midcourse maneuvers, planetary encounter, and orbit insertion are identified. In addition, the

angle between the Sun and the Earth as viewed from the spacecraft is plotted as a function of mission time. This latter characteristic is particularly significant for the Jupiter missions where both the antenna and solar panels are earth oriented after reaching a Sun-spacecraft distance of approximately 1.3 AU. This permits a significant simplification of the spacecraft in that separate orientation of the solar array and antenna are not required. From Figure 4, it can be seen that the solar array orientation error resulting from this approach is only slightly greater than 10 deg at Jupiter, In the worst case this produces a solar array power loss of less than 2 percent. The trajectory data presented in the diagram are based on assumed launch dates for the Mars and Jupiter missions. Variations in these data with launch date will chiefly affect the early portion of the Sun-spacecraft Earth angle time history, and the late portion of the Earth-spacecraft distance time history.

Of major interest in the power system analysis for orbital missions are the eclipse time and sunlight time for any given orbit and the variations in these parameters during the assumed 6-month orbital phase of the missions. Orbits are assumed to be in the ecliptic plane for the Venus and Jupiter missions. The Mars orbit selection and resultant eclipse profile is based on analyses performed in the course of TRW's Voyager studies. The orbit parameters and variations in eclipse duration for the Mars and Venus missions are shown in Figures 5 and 6, Parameters for the assumed Jupiter orbit are as follows:

Orbit period	203 hr
Eclipse duration	1.6 hr maximum 1.1 hr minimum
Periapsis altitude	105,000 km
Apoapsis altitude	2,170,000 km

Mission Definition Spacecraft Type	1 0.3 AU Probe (or Mercury Flyby) Manner Class With Variable-Angle Array	2 Venus Orbiter No. 1 Mariner Class With Orbit Insertion Engine
Primary mission objectives	<ul style="list-style-type: none"> Interplanetary particles and fields Mercury scan 	<ol style="list-style-type: none"> Interplanetary and planetary particles and fields Venus scan
Mission C_3 (km^2/sec^2)	1 (50 to 60 for Mercury flyby)	14
Launch vehicle	Atlas/Centaur/HEKS or Titan IIIC/Centaur	Atlas/Centaur
Spacecraft injected weight (lb)	900	1500
Mission duration (yr)		
Transit	0.25 to perihelion	0.4
Orbit	0.25 - 0.32 to Mercury	0.5
Approx Power capability (w)		
At Earth	350	250
At target (planet)	350	300
Weight breakdown (lb)		
Injected weight	900	1490
Propellant exp en route	4 lb midcourse, if Mercury flyby)	60
Propellant exp orbit insertion		750
Lander or entry capsule		
Total weight expended		810
Total weight remaining	900	680
Science payload	60	50
Orbit characteristics		
Period (Earth days)	-	3.74, 1.52
Size (planetary radii from center of planet)	-	1.5 x 9.
Inclination		0 deg
Worst-case eclipse (h)		2.2
Configuration	Octagonal body, roll axis toward sun. Gimbale antenna and most experiment sensors away from sun.	Mariner II (Venus), with orbit insertion engine incorporated so as to point toward sun along roll axis. Thrust = 400 lb.
Stabilization and control	I-axis stabilized, using sun and Canopus optical sensors for errors, and gas jets. (Mariner).	3-axis stabilized, using sun and Canopus optical sensors and gas jets. Gimbale engines and gyros during firing.
Communications (downlink to 210-ft dish)	11-ft (Mariner) dish (23.3 db), double gimbale, and 20-w transmitter. After gimbale spacecraft distance)	3-ft (Mariner) dish (23.3 db) double gimbale, and 10-w solid-state transmitter: 3000 b/sec at 0.5 AU (Earth distance at encounter) 250 b/sec at 1.7 AU (1 yr after launch)
Thermal control	Reflecting shield on sun side of equipment compartment.	Standard Mariner
Estimated solar array size and configuration	Four panels totaling 75 ft^2 extend as elements of a cross from spacecraft perpendicular to roll axis. Each panel is oriented about its axis for temperature control.	Two panels totaling 40 ft^2 .

Table 1. Model Spacecraft Configurations

3 Venus Orbiter No. 2 Voyager Class With Entry Probe	4 Mars Orbiter Voyager Class Second-Generation With Lander	5 5.2 AU Probe (or Jupiter Flyby) APP Class Spin Stabilized	6 Jupiter Orbiter No. 1 APP Class Second-Generation	Jupiter Orbiter No. 2 Voyager Class With Multiple Entry Probes
Venus environment Venus atmosphere (scan and probe) Interplanetary environment	• Interplanetary/planetary science • Mars environment, atmos- phere, and surface data (including biological data, if any)	• Interplanetary particles and fields • Jupiter scan	• Interplanetary exploration • Jupiter environment and orbital scan	• Planetary/interplanetary data • Jupiter orbiter/entry probes
14	< 25	5 or 95 (Jupiter flyby)	10 to 100	10 to 100
Saturn IB/Centaur (or two larger vehicles on one Saturn V)	Saturn V (two spacecraft per launch)	Atlas/Centaur/TE-364 (C ₃ ≤ 86) or Atlas/Centaur/ HEKS (crowded)	Saturn IB/Centaur/HEKS	Saturn V
9000	20,500	650	2800	16,000
0.4 0.5	0.5 0.5	2.0	2.0 0.5	2.0 0.5
1000 1000	1010 600	> 5000 200	> 7000 300	> 14,000 600
9150 50	20,500 1,400	650	2800 80	16,000 170
4600 1000 5650 3500 250	3,650 plus 320 lb for orbit trim 3,000 14,370 6,130 400	- - - 650 50	1100 1180 1620 250	6,400 1,000 7,570 8,430 500
.74, 1.52	3.60		8.45	8.45
1.5 x 9,	1.6 x 7	-	1.5 x 32	1.5 x 32
deg .2	45 deg 2.3		10 deg 1.6	10 deg .6
similar to TRW Mars Voyager (Phase IA Task B, using LEM stage), but scaled down to 2500 lb thrust, 9000 lb injected weight.	Sun/Canopus oriented. 3-axis stabilized with fixed solar array and gimbaled h.g. antenna dish. Deployed planetary scan platform. Basi spaceframe is octagonal, with liquid propellant retro stage.	similar to APP spin-stabilized 500 lb spacecraft. Solar panels surrounding 7-ft D dish.	First sun/Canopus oriented; later Earth/Canopus oriented; large fixed antenna. Deploy solar panels.	Same as 6
3-axis, using sun and Canopus optical sensors and gas jets. Gimbaled engines and gyros during firing.	3-axis stabilized; requires sun and Canopus sensors, gyro package, possibly Mars sen- sors. TVC by retro engine gimbals. MC maneuvers by throttled retro.	Spin-stabilized. Axis near su until 1.3 AU, then directed toward Earth. Conical scan RF tracking and jet preces- sion.	3-axis stabilized; gas jets; su and Canopus sensors plus gyro package. Bias correc- tion for Earth pointing basec on signal strength. TVC by jet vanes.	Same as 6
12-ft dish (29.3 db), double- gimbaled, and 20-w TWT transmitter: 25,000 blsec at 0.5 AU (encounter) 2,000 b/sec at 1.7 AU (1 year after launch)	12-ft paraboloid dish, gimbal mounted. 50-w TWT transmitter 15,000 b/sec at 2.6 AU (end of mission)	12-ft dish (30.9 db), body- mounted, 20-w, Klystron transmitter. 270 b/sec at 6.0 AU.	32-ft dia paraboloid antenna 10-w TWT transmitter 2800 b/sec at 6 AU	Same as 6, except 40-w TWT 11,000 blsec
Louvers on equipment bays	Louvered equipment mounting panels, aluminized Mylar in- sulation. Thermostatically controlled heaters; thermal control of lander to be included.	Insulation from sun; thermal switches.	Insulation from sun; thermal switches or louvers	Same as 6
Solar panels totaling 140 ft ² .	20-ft dia circular array around retro engine nozzle. Eight fixed modular array plates; 280 ft ²	Solar panels (475 ft ² , deployed from perimeter of 7 ft dia rigid antenna and unfolded.	Deployed 8-panel array (each 10 x 10 ft) around sunflower antenna dish. Sequential deployment of solar array and antenna; (must with- stand orbit insertion loads.	Same (but each panel 12.5 x 16 ft)

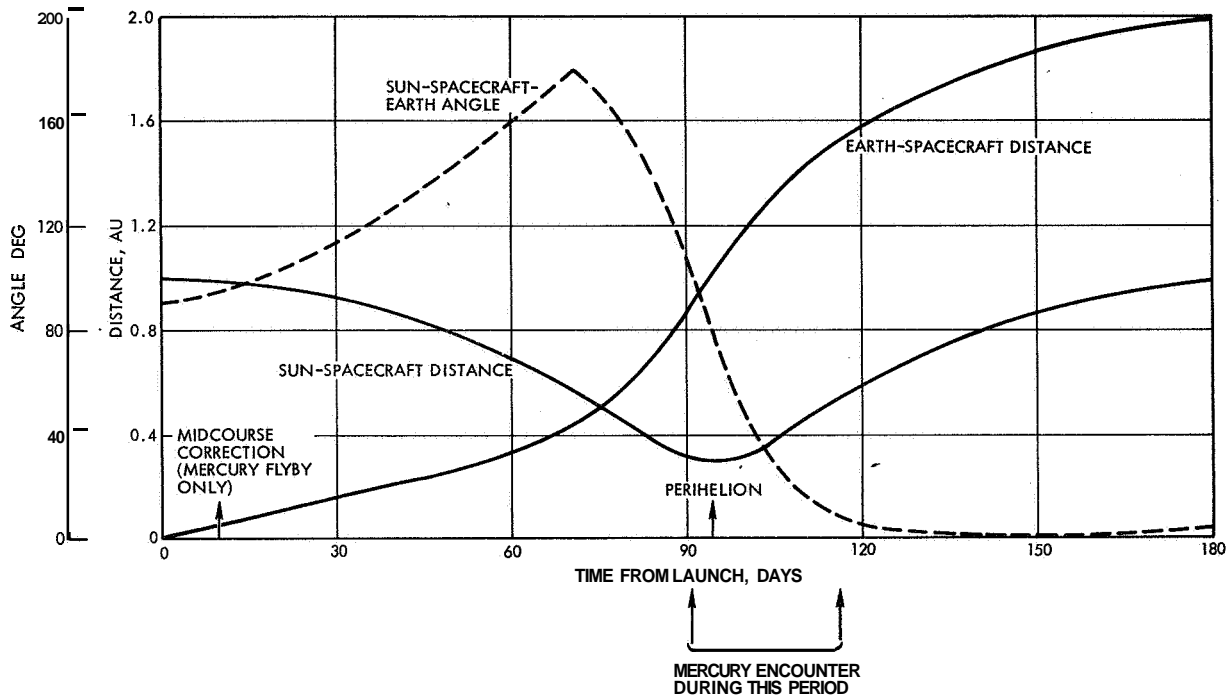


Figure 1. Mission Profile: Mercury Flyby

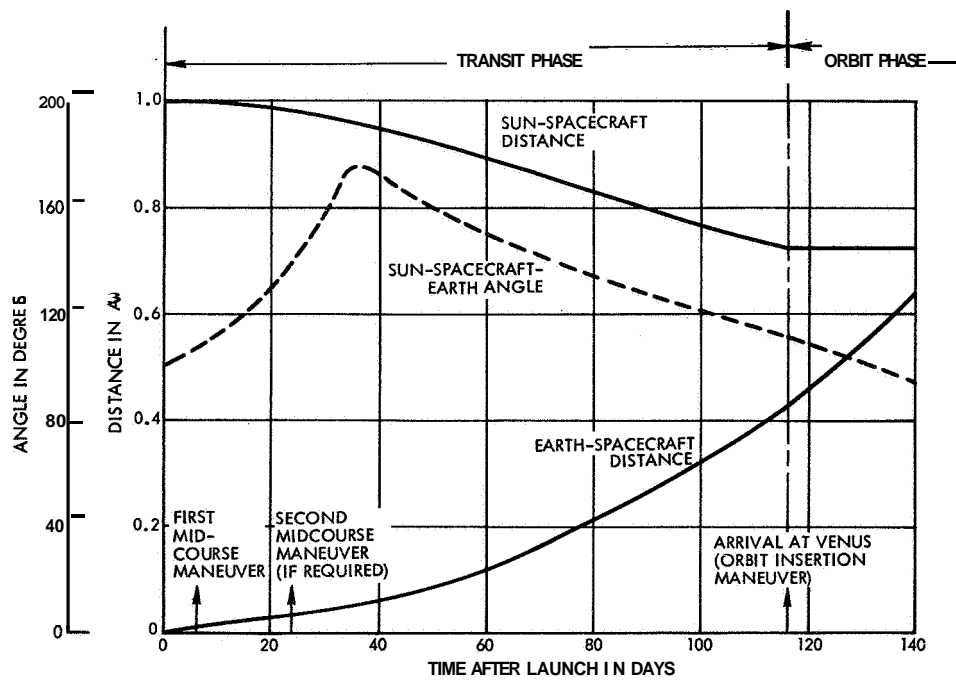


Figure 2. Mission Profile: Venus Orbiter

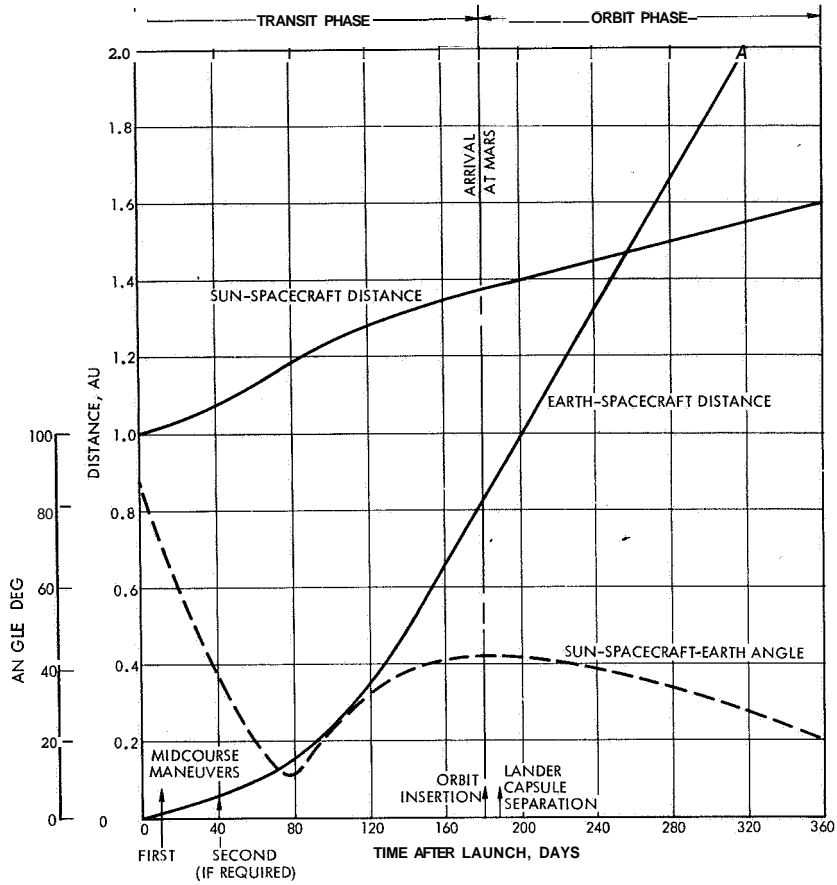


Figure 3. Mission Profile: Mars Orbiter (Launch May 1971)

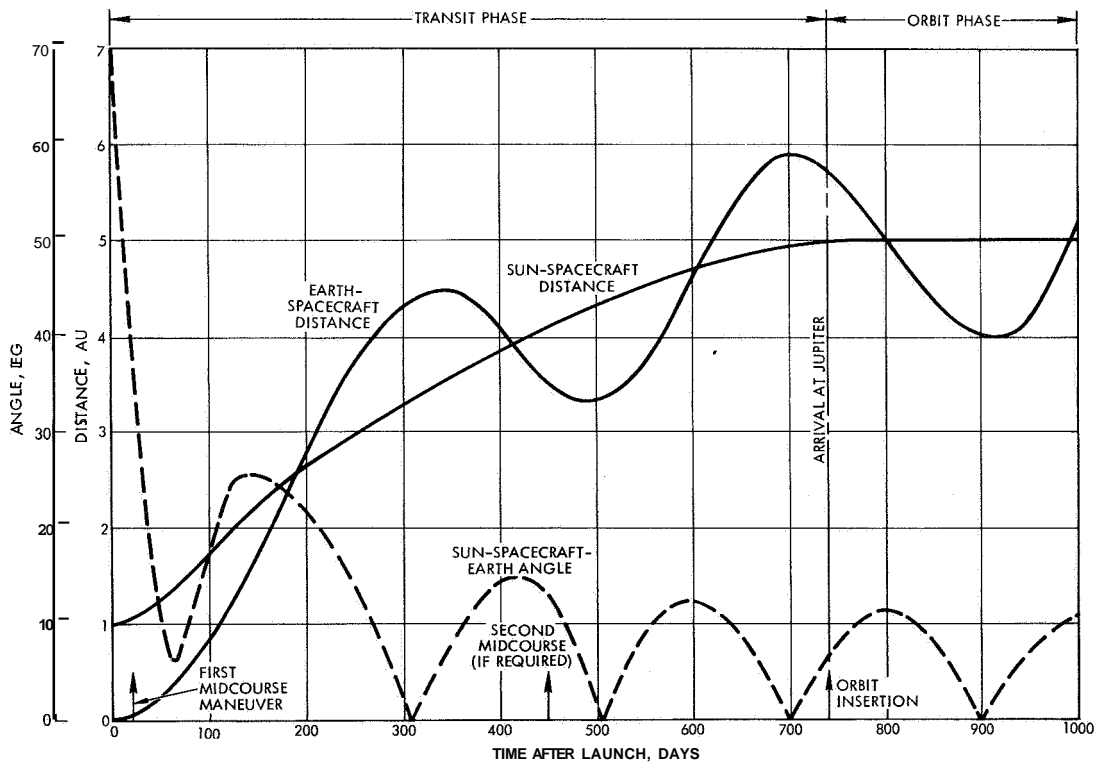


Figure 4. Mission Profile: Jupiter Orbiter (Launch March 1972)

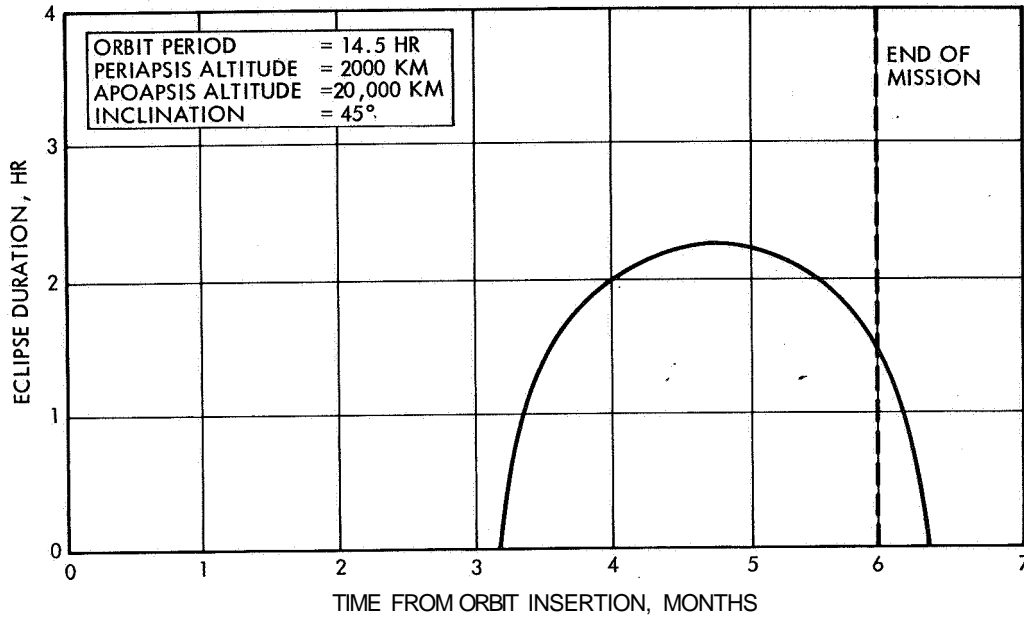


Figure 5. Eclipse Durations for Assumed Mars Orbit

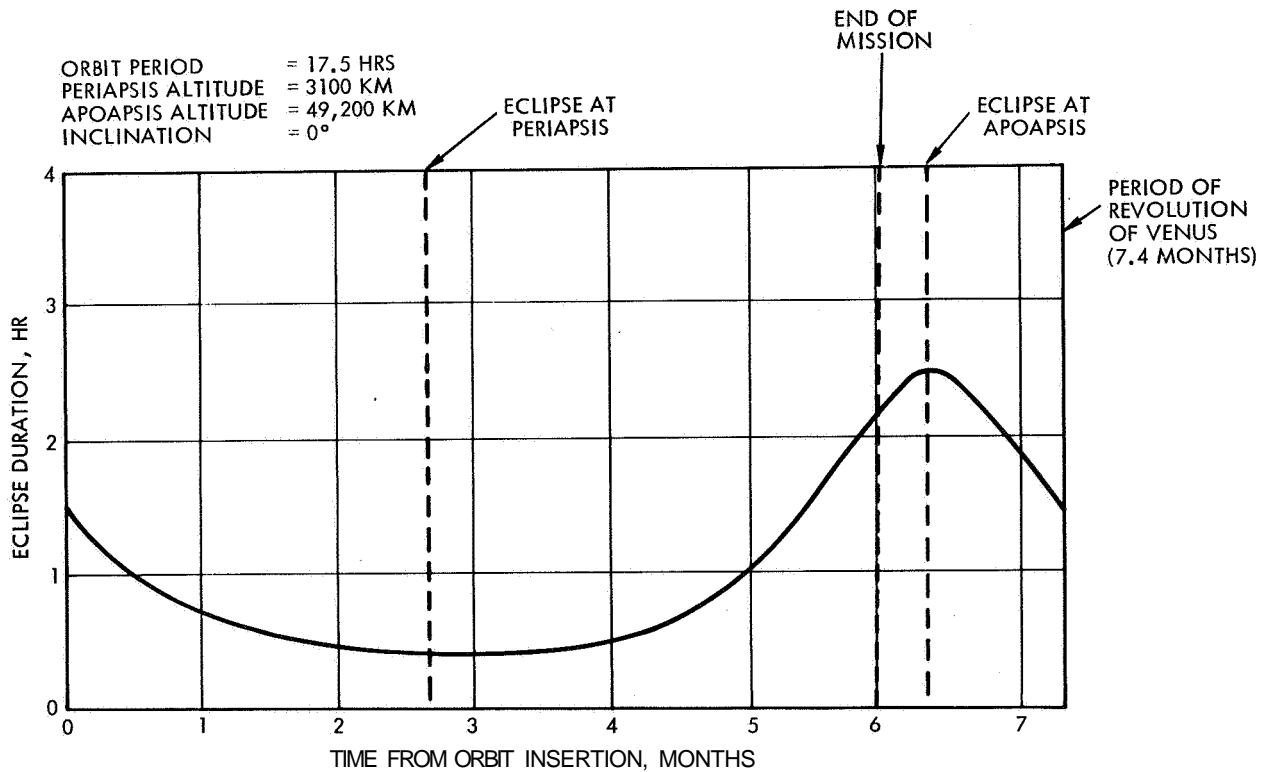


Figure 6. Eclipse Durations for Assumed Venus Orbit

2.2 TYPICAL POWER REQUIREMENTS

Selected load power requirements for each spacecraft model are shown in Tables 2 through 8. These estimates are based primarily on load data from existing spacecraft designs such as Mariner, Pioneer, and Voyager. Relatively high power requirements for thermal control of lander/probe payloads are assumed for the orbiting spacecraft missions based on the 200-w requirement used in the Voyager studies. In most cases, this requirement represents the largest single load in the spacecraft. A second major power-consuming load is the transmitter required to achieve suitable data rates at the extreme distances being considered in these studies. The largest transmitter selected is the 50-w TWT used on the Mars Orbiter model. In addition to the TWT, transmitters of the klystron and solid-state types are assumed for the Jupiter Flyby and Venus Orbiter No. 1 models respectively to reflect a broader spectrum of input power characteristics.

Table 9 lists each of the items of load equipment selected. Typical voltages, regulation levels, and apportionment of total power requirements among the several voltages for each item of equipment or each group of equipment are included.

Figures 7 through 12 show the time profiles of the conditioned load requirements in watts, for each of the model spacecraft. Also plotted are the time profiles of the solar array power capability, in percent, at the maximum power point. Additional solar array characteristics are presented in the succeeding subsection 2.3 of this manual. By comparing the relative solar array capability with the variations in load power requirements throughout the mission, it is possible to establish preliminary indications of the critical design points for each of the models. The critical design point is that condition during the mission at which the solar array power capability is a minimum relative to the power required from solar array. If the array power capability equals the demand at this point, then at all other times during a given mission the solar array power capability will exceed that required by the loads and battery charging. The critical design point, therefore, determines the required solar array capability in order to adequately support the loads over the complete mission.

For the Mercury Flyby model, Figure 7, the increased solar array capability at encounter relative to that at the beginning of the cruise phase indicates the critical design point to be at the beginning of the mission. This results from the fact that the load at encounter is only 3 percent greater than that during cruise. While the solar array capability is 23 percent greater at encounter than at cruise.

For the Venus Orbiter No. 1 model (Figure 8), the step decrease from 127 to 124 percent in solar array capability at encounter reflects an increased array temperature produced by the albedo of Venus. Comparison of the 189-w end-of-life load condition to the initial cruise load of 135-w indicates that the critical design point for this model occurs at end-of-life because the load is 40 percent higher than that at cruise.

For Venus Orbiter No. 2, the solar array characteristics are identical to that of Venus Orbiter No. 1. The large load subsequent to orbit insertion, due to the presence of the lander on the spacecraft, determines the critical design point for the mission. In this case it has been assumed that the lander will remain attached to the spacecraft for several orbits, the load is then reduced by approximately 50 percent upon capsule separation (Figure 9).

The solar array and load power profiles for the Mars Orbiter mission are shown in Figure 10. Comparison of the solar array capability with the load requirements indicates that the 46 percent array power output at the end of the mission, is the critical design point.

In the case of both the Jupiter probe (Figure 11) and Jupiter Orbiter No. 1 (Figure 12) missions, the maximum load is seen to occur at end-of-life. The minimum solar array capability at this same point clearly defines end-of-life as the critical design point for these missions. Figure 13 for the Jupiter Orbiter No. 2 mission shows again that the presence of planetary probes on the spacecraft, which are ejected during the orbit phase, produces a maximum load condition subsequent to insertion into orbit. As a result, the apparent critical design point for the Jupiter Orbiter No. 2 is at encounter.

Table 2. Conditioned Power Requirements (in watts) is a Function of Mission Phase - Mercury Flvby Model

LOAD GROUP	EQUIPMENT	PRE-LAUNCH	LAUNCH	ACQUIRE	CRUISE	MANUEVER	ENCOUNT.	PLAYBACK	
Stab and Control	Gyros and Electronics	25	25	25	0	25	0	0	
	Sensors	4	4	4	4	4	4	4	
	Control Elect.	12	12	12	5	25	5	5	
	Valves	0	0	0/0/30*	0/0/30	0/1/30	0/0/30	0/0/30	
Propulsion	Valves					Squibs			
	Actuators	(Not used for this model)							
Integration	Comp. Sequencer	5	5	5	5	5	5	5	
	Deploy. Actuators		Squibs						
Thermal Control	Heaters	(Not used for this model)							
	Transmitter **	1	1	1/70/70	70	70	70	70	
Communications	Tape Recorder	0	0	0	0	0	6	4	
	Data Handling	20	60	20	20	20	20	20	
	Cmd. Receiver	5	5	5	5	5	5	5	
	Cmd. Decoder	3	3	3	3	3	3	3	
	Relay Receiver	(Not used for this model)							
	Lander/Probe	(Not used for this model)							
Science/Payload	TV System	0	0	0	0	0	17	0	
	Exp. Pkg. Orient.	0	0	0	0	0	7	0	
	Dual Freq. Receiver	0	0	0	2	2	2	2	
	Trap. Radiation Det.	0	0	0	1	1	1	1	
	Plasma Probe	0	0	0	2	2	2	2	
	Spectrophotometer	0	0	0	0	0	25	0	
	Magnetometer	0	0	0	7	7	7	7	
	IR Radiometer	0	0	0	0	0	3	0	
	Cosmic Dust Det.	0	0	0	1	1	1	1	
	Cosmic Ray Telescope	0	0	0	1	1	1	1	
	Total Conditioned Power Ave		75	75	144	126	172	183	130

Indicates Min/Ave/Max Power level

** 20 w TWT and driver.

Table 3. Conditioned Power Requirements (in watts) as a Function of Mission Phase - Venus Orbiter Model No. 1

LOAD GROUP	EQUIPMENT	PRE-LAUNCH	LAUNCH	ACQUIRE	CRUISE	MANUEVER	INSERTION	ORBIT (SUN)	ORBIT (ECLIPSE)
Stab and Control	Gyros and Electronics	25	25	25	0	25	25	0	25
	Sensors	4	4	4	4	4	4	4	4
	Control Elect.	12	12	12	5	25	25	22	22
	Valves	0	0	0/0/30*	0/0/30	0/1/30	0/1/30	0/0/30	0/0/30
Propulsion	Valves	0	0	0	0	0/2/10	0/2/10	0	0
	Actuators	0	0	0	0	0/10/40	0/35/140	0	0
Integration	Comp. Sequencer	5	5	5	5	5	5	5	5
	Deploy. Actuators		Squibs						
Thermal Control	Heaters		(Not used for this model)						
	Transmitter**	50	50	50	50	50	50	50	50
Communications	Tape Recorder	0	0	0	0/4/10	0	0	0/4/10	0/4/10
	Data Handling	9	9	34	34	34	34	34	34
	Cmd. Receiver	8	8	8	8	8	8	8	8
	Cmd. Decoder	3	3	3	3	3	3	3	3
	Relay Receiver		(Not used for this model)						
	Antenna Orient.	0	0	0/2/8	0/2/8	0/2/25	0/2/25	0/2/25	0/2/25
Science/Payload	Lander/Probe		(Not used for this model)						
	TV System		(Not used for this model)						
	Exp. Pkg. Orient.	0	0	0	0	0	0	0/1/10	0/1/10
	Dual Freq. Receiver	0	0	0	2	2	2	2	2
	Trap Radiation Det.	0	0	0	1	1	1	1	1
	Plasma Probe	0	0	0	3	3	3	3	3
	UV Photometer	0	0	0	5	5	5	5	5
	Magnetometer	0	0	0	7	7	7	7	7
	IR Radiometer	0	0	0	0	0	0	0	0
	Cosmic Dust Det.	0	0	0	2	2	2	2	2
	Total Conditioned Power		116	116	143	135	189	214	156

*Indicates Min/Ave/Max power levels.

** -

Table 4. Conditioned Power Requirements (in watts) as a Function of Mission Phase - Venus Orbiter Model No. 2

LOAD GROUP	EQUIPMENT	PRE-LAUNCH	LAUNCH	ACQUIRE	CRUISE	MANUEVER	INSERTION	ORBIT (SUN)	ORBIT (ECLIPSE)	CAPSULE SEPARATE	ORBIT (SUN)	ORBIT (ECLIPSE)	
Stab and Control	Gyros and Electronics	25	25	25	0	25	25	0	25	0	0	25	
	Sensors	4	4	4	4	4	4	4	4	4	4	4	
Propulsion	Control Elect.	9/9/45*	9 9 45	9/9/45	9/9/45	9/9/45	9/9/45	9 9/45	9 9/45	9/9/45	9 9/45	9/9/45	
	Valves	0	0	0/0/50	0/0/50	0/1/50	0/1/50	0 0/50	0 0/50	0/0/50	0 0/50	0/0/50	
	Valves	0	0	0	0	0/2/15	0/2/15	0	0	0	0	0	
	Actuators	0	0	0	0	0/20/80	0/70/280	0	0	0	0	0	
Integration	Comp. Sequencer	18	18	18	18	18	18	18	18	18	18	18	
	Deploy. Actuators	Squibs	Squibs							Squibs			
Thermal Control	Heaters	(Not used for this model)											
	Communications	1	1	1/70/70	70	70	70	70	70	70	70	70	70
Science/Payload	Transmitter **	0	0	0	0/7/12	0/4/12	0/4/12	0/17/60	0/17/60	0/17/60	0/17/60	0/17/60	
	Tape Recorder	10	10	40	40	40	40	40	40	40	40	40	
	Data Handling	8	8	8	8	8	8	8	8	8	8	8	
	Cmd. Receiver	3	3	3	3	3	3	3	3	3	3	3	
	Cmd. Decoder	0	0	0	0	0	0	0	0	0	0	0	
	Relay Receiver	0	0	0	0	0	0	0	0	0	0	0	
	Antenna Orient.	0	0	0/2/15	0/2/15	0 3/40	0/3/40	0/3/40	0/3/40	0/3/40	0/3/40	0 3/40	0/3/40
	Lander/Probe	0	0	0/200/200	200	200	200	200	200	0/200/200	0/200/200	200	200
	TV System	0	0	0	0	0	0	0	0	0	0	0	0
	Exp. Pkg. Orient	0	0	0	0	0	0	0	0	0	0	0	0
Spectrometers (2)	Spectrometers (2)	0	0	0	0	0	0	0	0	0	0	0	
	Bistatic Radar	0	0	0	0	0	0	0	0	0	0	0	
IR Radiometer	IR Radiometer	0	0	0	0	0	0	0	0	0	0	0	
	Magnetometer (2)	0	0	0	6	6	6	6	6	6	6	6	
Ion Chamber	Ion Chamber	0	0	0	4	4	4	4	4	4	4	4	
	Cosmic Ray Telescope	0	0	0	5	5	5	5	5	5	5	5	
Trap. Radiation Det	Trap. Radiation Det	0	0	0	5	5	5	5	5	5	5	5	
	Gamma Ray	0	0	0	5	5	5	5	5	5	5	5	
Plasma Probe	Plasma Probe	0	0	0	5	5	5	5	5	5	5	5	
	Cosmic Dust Det.	0	0	0	2	2	2	2	2	2	2	2	
Total Conditioned Power		78	78	379	393	439	492	471	496	440	267	292	

* Indicates Min/Ave/Max power levels.

** 20 w TWT and driver.

Table 5. Conditioned Power Requirements (in watts) as a Function of Mission Phase — Mars Orbiter Model

LOAD GROUP	EQUIPMENT	PRE-LAUNCH	LAUNCH	ACQUIRE	CRUISE	MANUEVER	INSERTION	ORBIT (SUN)	SEPARATE LANDER	ORBIT (SUN)	ORBIT (ECLIPSE)	
Stab and Control	Cyros and Electronics	25	25	25	0	25	25	0	0	0	25	
	Sensors	4	4	4	4	4	4	4	4	4	4	
	Control Elect.	9	9	9/9/45	9/9/45	9/9/45	9/9/45	9/9/45	9/9/45	9/9/45	9/9/45	
	Valves	0	0	0/0/50	0/0/50	0/0/50	0/0/50	0/0/50	0/0/50	0/0/50	0/0/50	
	Valves	0	0	0	0	0/2/15	0/2/15	0	0	0	0	
Propulsion	Actuators	0	0	0	0	0/20/80	0/70/230	0	0	0	0	
	Comp. Sequencer	18	18	18	18	18	18	18	18	18	18	
Integration	Deploy. Actuators	0	Sq lbs	0	0	0	0	0	Squibs	0	0	
	Heaters	0	5	15	44	54	54	54	34	34	54	
Thermal Control Communications	Transmitter**	3	5	50/150	150	150	150	150	150	150	150	
	Tape Recorder	0	0	0	0/N/12	0/1/12	0/7/60	0/7/60	0/7/60	0/7/60	0/7/60	
	Data Handling	0	10	40	40	40	40	40	40	40	40	
	Cmd. Receiver	3	8	8	8	8	8	8	8	8	8	
	Cmd. Decoder	3	3	3	3	3	3	3	3	3	3	
	Relay Receiver	0	0	0	0	0	0	0	0	0	0	
	Lander/Probe	0	0	0/20/40	200	200	200	200	200	0/200/200	0/7/60	0/7/60
	TV System	0	0	0	0	0	0	0	0	0	0	
	Exp. Pkg. Orient.	0	0	0	0	0	0	0	0	0	0	
	Spectrometer (2)	0	0	0	0	0	0	0	0	0	0	
Science/Payload	Radiometer	0	0	0	0	0	0	0	0	0	0	
	Magnetometer	0	0	0	6	6	9	9	3	3	3	
	Micrometeoroid	0	0	0	2	2	2	2	2	2	2	
	Plasma Probe	0	0	0	5	5	5	5	5	5	5	
	Trap. Radiation Det.	0	0	0	5	5	5	5	5	5	5	
	Cosmic Ray (2)	0	0	0	10	10	10	10	10	10	10	
	Bistatic Radar	0	0	0	0	0	0	0	0	0	0	
	RF Noise Det.	0	0	0	3	3	3	3	3	3	3	
	Ion Chamber	0	0	0	5	5	5	5	5	5	5	
	Total Conditioned Power Ave	82	87	472	516	570	627	597	593	393	438	

*Indicates Min/Ave/Max power levels.

** 50 w TWT and driver.

Table 6. Conditioned Power Requirements (in watts) as a Function of Mission Phase — Jupiter Flyby Model

LOAD GROUP	EQUIPMENT	LAUNCH	LAUNCH	ACQUIRE	CRUISE	MANEUVER	ENCOUNT	PLAYBACK
Stab and control	Gyros and Electronics	(Not used for this model)	(Not used for this model)					
	Sensors (sun)	5	5	5	5	5	5	5
Propulsion	Control Elect.	0	0	0, 0, 6*	0, 0, 6	0, 0, 6	0, 0, 6	0, 0, 6
	Valves	0	0	0	0	Squibs	0	0
	Actuators	(Not used for this model)	(Not used for this model)					
Integration	Comp. Sequencers	5	5	5	5	5	5	5
	Deploy. Actuators		Squibs					
Thermal Control Communications	Heaters	0	0	0	0, 10/50	0	50	50
	Transmitter **	1	1	1, 80/30	30	80	80	80
	Tape Recorder	0	0	0	0	0	6	<
	Data Handling	10	10	10	10	10	10	10
	Cmd Receiver	2	2	2	2	2	2	2
	Cmd Decoder	2	2	2	2	2	2	2
	Relay Receiver							
	Antenna Orient.	(Not used for this model)	(Not used for this model)					
	Lander/Probe							
	TV System.	0	0	0	0	0	7	0
Science/Payload	Exp. Pkg. Orient.	0	0	0	0	0	7	0
	Magnetometer	0	0	0	4	4	4	4
	Trap. Radiation Det.	0	0	0	2	2	2	2
	Plasma Probe	0	0	0	2	2	2	2
	Cosmic Dust	0	0	0	1	1	1	1
	Dual Freq Rec	0	0	0	2	2	2	2
	Radiometer, IR	0	0	0	7	7	7	7
	Cosmic Ray (2)	0	0	0	4	4	4	4
	Total Conditioned Power	25	25	104	136	136	206	180

0.1W / save / max 0.001W levels
stron and driver

Table 7 Conditioned Power Requirements (in watts) as a Function of Mission Phase - Jupiter Orbiter Model No. 1

LOAD GROUP	EQUIPMENT	PRE-LAUNCH	LAUNCH	ACQUIRE	CRUISE	MANUEVER	INSERTION	ORBIT (SUN)	ORBIT (ECLIPSE)	
Stab and Control	Gyros and Electronics	25	25	25	0	25	25	0	25	
	Sensors	4	4	4	4	4	4	4	4	
Propulsion	Control Elect.	12	12	12	5	25	25	22	22	
	Valves	0	0	0/0/30*	0/0/30	0/1/30	0/1/30	0/1/30	0/0/30	
	Valves	0	0	0	0	0/2/20	0/4/20	0	0	
	Actuators	0	0	0	0	0/6/12	0/6/12	0	0	
Integration	Comp. Sequencer	5	5	5	5	5	5	5	5	
	Deploy. Actuators		Squibs							
Thermal Control	Heaters	0	5	20	100	100	100	100	150	
	Transmitter**	1	1	1/35/35	35	35	35	35	35	
Communications	Tape Recorder	0	0	0	0/4/10	0	0	0/4/10	0/4/10	
	Data Handling	9	9	34	34	34	34	34	34	
	Cmd. Receiver	8	8	8	8	8	8	8	8	
	Cmd. Decoder	3	3	3	3	3	3	3	3	
	Relay Receiver	(Not used for this model)								
	Lander/Probe	(Not used for this model)								
Science/Payload	RV System	0	0	0	0	0	0	15	15	
	Exp. Pkg. Orient.	0	0	0	0	0	0	1/2/20	1/2/20	
	Cosmic Ray (2)	0	0	0	4	4	4	4	4	
	Plasma Probe	0	0	0	2	2	2	2	2	
	Magnetometer	0	0	0	6	6	6	6	6	
	Micrometeoroid	0	0	0	1	1	1	1	1	
	Radio Propagation	0	0	0	3	3	3	3	3	
	Trap. Radiation Det	0	0	0	2	2	2	2	2	
	IR Radiometer	0	0	0	0	0	0	0	3	
	Auroral Detector	0	0	0	0	0	0	0	2	
Total Conditioned Power Ave		67	72	146	216	266	268	255	330	

* Indicates Min/Ave/Max power lev \$

** 10 w TWT and driver.

Table 8. Conditioned Power Requirements (in watts) as a Function of Mission Phase - Jupiter Orbiter Model No. 2

LOAD GROUP	EQUIPMENT	PRE-LAUNCH	LAUNCH	ACQUIRE	CRUISE	MIDCOURSE MANEUVER	ORBIT INSERTION	ORBIT (SUN)	ORBIT (ECLIPSE)	SEPARATE PROBE	TRACK PROBES	ORBIT (SUN)	ORBIT (ECLIPSE)
Stab and Control	Gyros and Electronics	25	4	2	0	25	25	0	25	0	0	0	0
	Sensors	4	4	4	4	4	4	4	4	4	4	4	4
	Control Elect.	10	10	10, 13/50*	10, 10/50	10, 10/50	10, 10/50	10, 10/50	10, 10/50	10, 10/50	10, 10/50	10, 10/50	10, 10/50
	Valves	0	0	0, 0/50	0, 0/50	0, 1/50	0, 1/50	0, 0/50	0, 0/50	0, 0/50	0, 0/50	0, 0/50	0, 0/50
	Valves	0	0	0	0	0, 4/25	0, 8/25	0	0	0	0	0	0
	Actuators	0	0	0	0	0, 8/15	0, 8/15	0	0	0	0	0	0
	Comp Sequencer	20	20	20	20	20	20	20	20	20	20	20	20
	Deploy. Actuators	5	5	5	5	5	5	5	5	5	5	5	5
	Heaters	0	0	0	0	0	0	0	0	0	0	0	0
	Transmitters**	15	15	15, 15	15	15	15	15	15	15	15	15	15
Thermal Control	Tape Recorder	0	0	0	0, 4/12	0, 4/12	0, 4/12	0, 17/60	0, 17/60	0, 17/60	0, 17/60	0, 17/60	0, 17/60
	Data Handling	10	10	0	40	40	40	40	40	40	40	40	40
	Cmd Receiver	8	8	8	8	8	8	8	8	8	8	8	8
	Cmd Decoder	5	5	5	5	5	5	5	5	5	5	5	5
	Relay Receiver	0	0	0	0	0	0	0	0	0	0	0	0
	Antenna Orient	(Not d to this model)											
	Lander/Probe	0	0	0, 150, 150	150	150	150	150	150	150	150	150	150
	TV System	0	0	0	0	0	0	0	0	0	0	0	0
	Exp Pkg Orient	0	0	0	0	0	0	0	0	0	0	0	0
	Cosmic Ray (2)	0	0	0	0	0	0	0	0	0	0	0	0
Science/Payload	Plasma Probe	0	0	0	5	5	5	5	5	5	5	5	5
	Magnetometers (2)	0	0	0	6	6	6	6	6	6	6	6	6
	Micrometeoroid	0	0	0	2	2	2	2	2	2	2	2	2
	Radio Propagation	0	0	0	3	3	3	3	3	3	3	3	3
	Trap Radiation	0	0	0	5	5	5	5	5	5	5	5	5
	Radiometers (2)	0	0	0	6	6	6	6	6	6	6	6	6
	Auroral Detector	0	0	0	0	0	0	0	0	0	0	0	0
	Spectrometer	0	0	0	0	0	0	0	0	0	0	0	0
	Topside Sounder	0	0	0	0	0	0	0	0	0	0	0	0
	Total Conditioned Power (Ave)	87	397	611	645	657	685	762	689	539/689	532	614	

*Indicates Min/Ave/Max power levels

** 40 w TWT and driver

*** Average power decreases to zero with separation of last probe

Table 9. Load Equipment Typical Input Power Characteristics

<u>Equipment</u>	<u>Typical Voltages (volts)</u>	<u>Typical Regulation \pm(%)</u>	<u>Percent of Total Power</u>	<u>Remarks</u>
<u>Stabilization and Control</u>				
Gyros and electronics	26 ac	2	90	400 cps *0. 01%, 3 ϕ
	+20	1	5	
	-20	1	5	
Star or sun sensor	20	1	100	
Control electronics	+20	2	5	
	-20	2	5	
	+15	1	20	
	-15	1	20	
	+6	1	25	
	-6	1	25	
Solenoid valves	bus	15	100	Peak only
Motor	bus	15	100	400 cps or dc
Heater	bus	15	100	
<u>Propulsion</u>				
Valve	bus	10 v min	100	Peak only
Solenoid	bus	15	100	Peak only
Heater	bus	15	100	
<u>Computer and Sequencer</u>				
	16	0.5	5	
	-16	0.5	5	
	+6	2	45	
	-3	2	45	
<u>Transmitters</u>				
10 w, solid state transmitter				
Driver	+6	1	5	
	-6	1	5	
Power amplifier	50	2	60	
	+15	1	5	
	-15	1	5	

Table 9. (continued)

<u>Equipment</u>	<u>Typical Voltages (volts)</u>	<u>Typical Regulation \pm(%)</u>	<u>Percent of Total Power</u>	<u>Remarks</u>
Thermoelectric cooler	+6	5	20	
20 w, Klystron transmitter				
Driver	+6 -6	1 1	5 5	
Klystron beam	1500	1	70	
Klystron heater	6	2	20	ac or dc
50 w, TWT transmitter				
Driver	+6 -6	1 1	5 5	
TWT helix	1500	0.2	70	
TWT collector	300	1	10	
TWT heater	6	1	10	dc
100 w, TWT transmitter				
Driver	16 6 -6	1 1 1	10	
TWT helix	3000	0.2	10	
TWT collector	800	1	60	
TWT heater	6	1	20	ac or dc
<u>Communications and Data Systems</u>				
Tape recorder	bus 16	2 1	50 50	
Data handling	bus -6 16 -16 +6 -6 16 -16	5 2 2 2 1 1 1 1	4 4 4 4 29 26 25 4	

Table 9. (continued)

<u>Equipment</u>	<u>Typical Voltages (volts)</u>	<u>Typical Regulation \pm(%)</u>	<u>Percent of Total Power</u>	<u>Remarks</u>
Antenna deployment (squibs)	bus	15	0	Peaks only
Antenna orientation	bus 16	15 1	95 5	ac or dc
Receiver	bus t i 6 t 6 -6	15 1 1 1	10 40 10 40	
Decoder	16 6 -6	2 2 2	20 40 40	
Switching and distribution	bus	5	0	Peaks only
<u>Science</u>				
Radio propagation	16 6 -6	1 0.1 0.1	40 30 30	
Whistlers	16	0.1	100	
Magnetometer	16 -16 6 -6 3	0.1 1 0.1 1 1	30 15 30 15 10	
Plasma probe	\pm 150 +6 165	1 1 1	30 65 5	
Coronagraph	3000 4-16 -16 t 6 -6	1 0.1 0.1 0.1 0.1	80 5 5 5 5	
Proton spectrometer	1000 +6 -6 t 3 -3 -16	0.1 1 0.1 1 1 1	15 40 15 10 10 10	

Table 9. (continued)

<u>Equipment</u>	<u>Typical Voltages (volts)</u>	<u>Typical Regulation \pm(%)</u>	<u>Percent of Total Power</u>	<u>Remarks</u>
Mass spectrometer	bus	5	25	
	300C	1	50	
	200	1	25	
	16	1		
	-16	1		
	t 6	1		
-6	1			
Cosmic ray	1000	0.1	50	
	16	1	30	
	6	1	20	
Ion chamber	6	1	100	
Scintollometer	1000	0.1	20	
	16	1	50	
	6	1	30	
Gamma ray	1000	0.1	10	
	16	0.1	90	
X-ray	1000	0.1	10	
	16	0.1	90	
Primary electrons	1500	0.1	20	
	16	0.5	50	
	3	2	30	
Micrometeorite	4-12	1	60	
	-6	1	20	
	t 3	1	20	
Television (ES vidicon)	500	0.2	5	Peaks only
	200	1	20	
	bus	5	0	
	t 16	1	10	
	- 16	1	5	
	t 6	5	50	
	- 6	0.2	10	
Probe Lander	bus	15	100	Thermal control

Table 9. (continued)

<u>Equipment</u>	<u>Typical Voltages (volts)</u>	<u>Typical Regulation \pm (%)</u>	<u>Percent of Total Power</u>	<u>Remarks</u>
Trapped radiation	1000	0.1	20	
	16	1	20	
	+6	1	30	
	-6	1	30	
IR radiometer (4 ch)	bus	2	20	Scanner
	6	1	40	
	-6	1	40	
UV spectrometer	bus	2	25	Scanner
	16	1	25	
	6	1	25	
	-6	1	25	
RF noise detector	+6	1	50	
	-6	1	50	
UV photometer	3000	1	70	
	35	1	10	
	± 20	1	10	
	± 10	1	10	
Bistatic radar	1500	1	70	
	+6	1	20	
	-6	1	10	

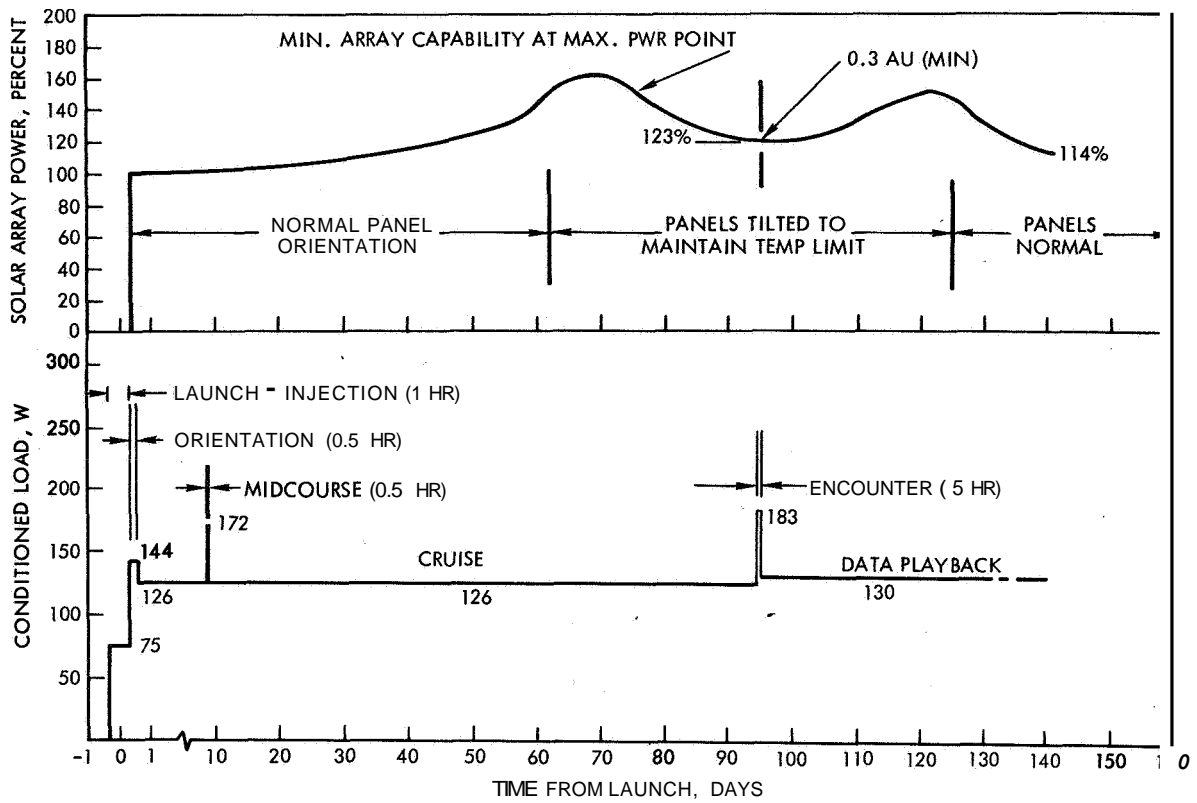
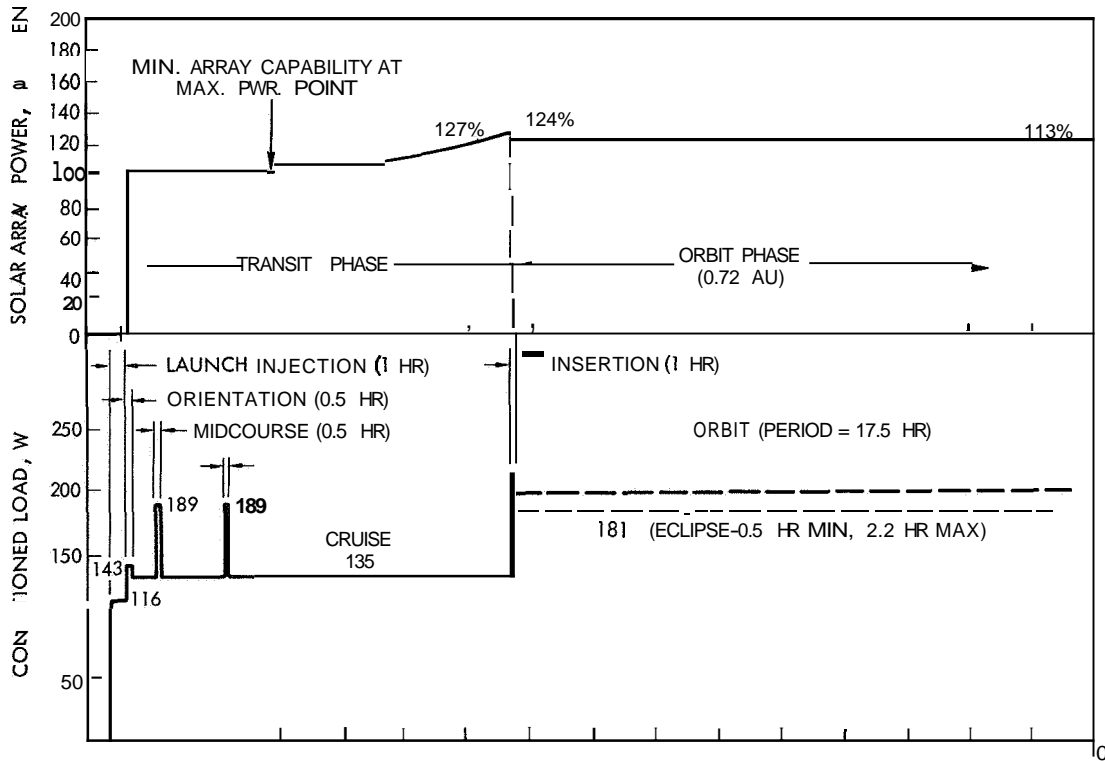


Figure 7. Solar Array Maximum Power Capability and Conditioned Load Power Requirements versus Time - Mercury Flyby Mission



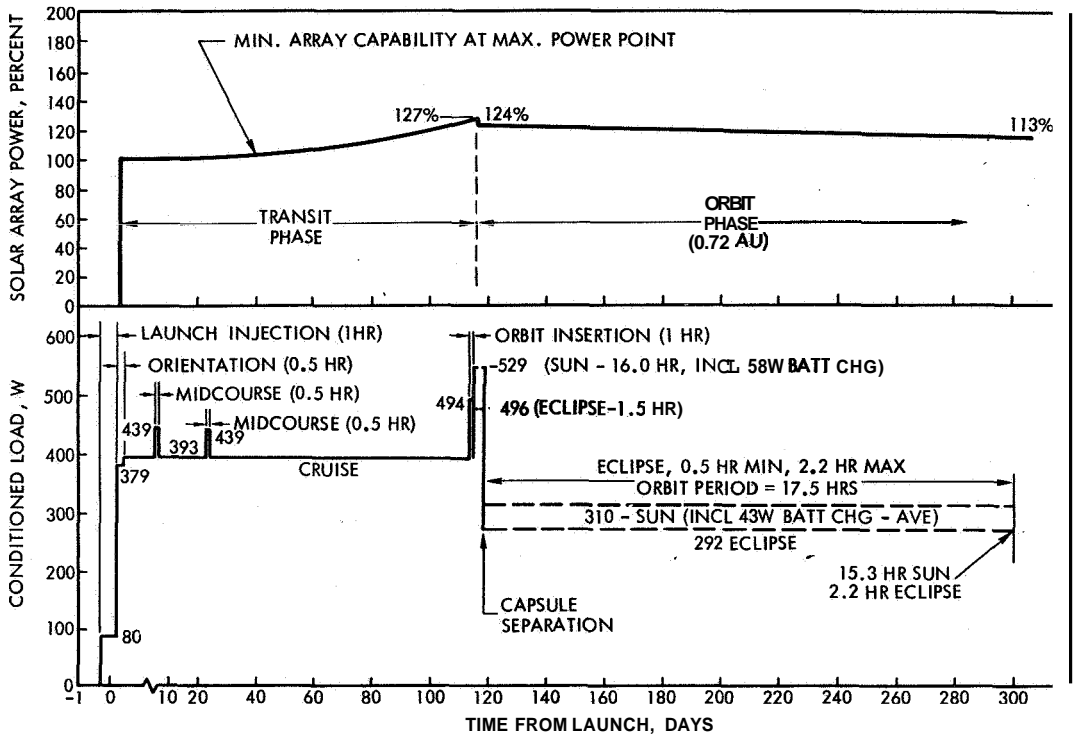


Figure 9. Solar Array Maximum Power Capability and Conditioned Load Power Requirements versus Time - Venus Orbiter No. 2 Mission

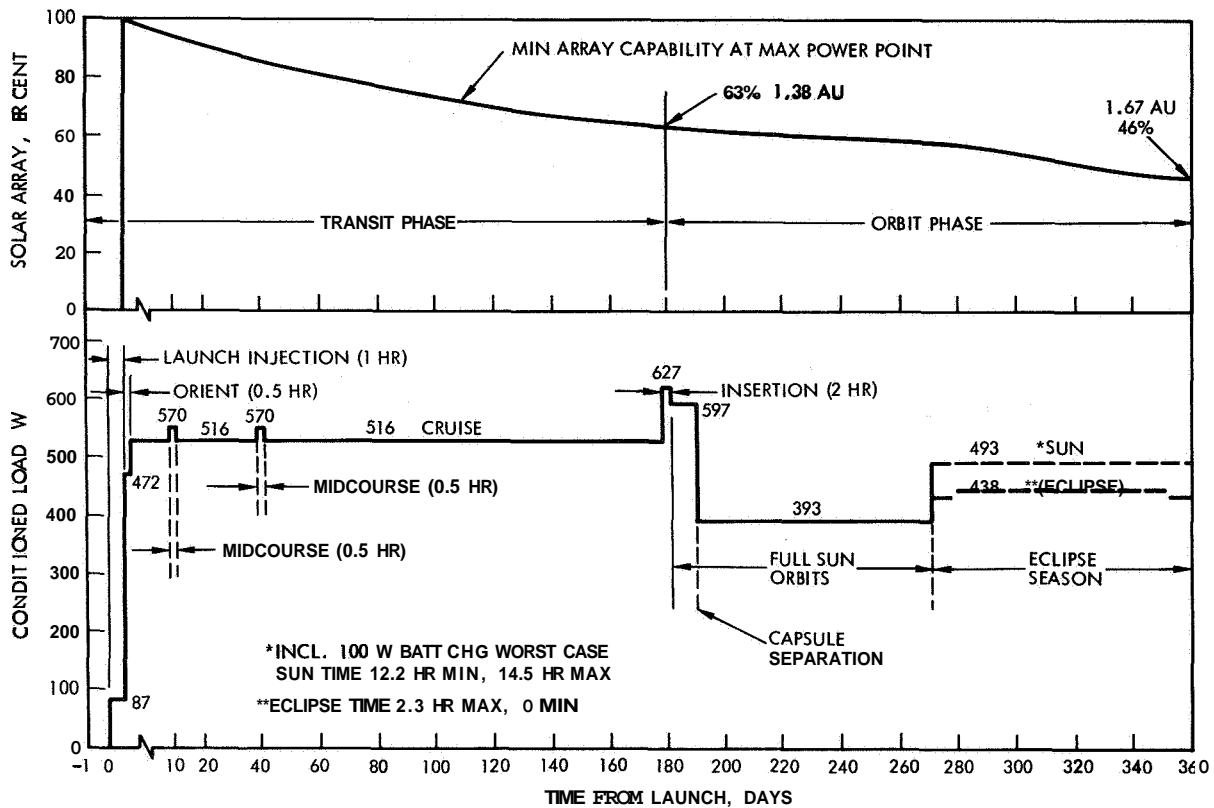


Figure 10. Solar Array Maximum Power Capability and Conditioned Load Power Requirements versus Time - Mars Orbiter Mission

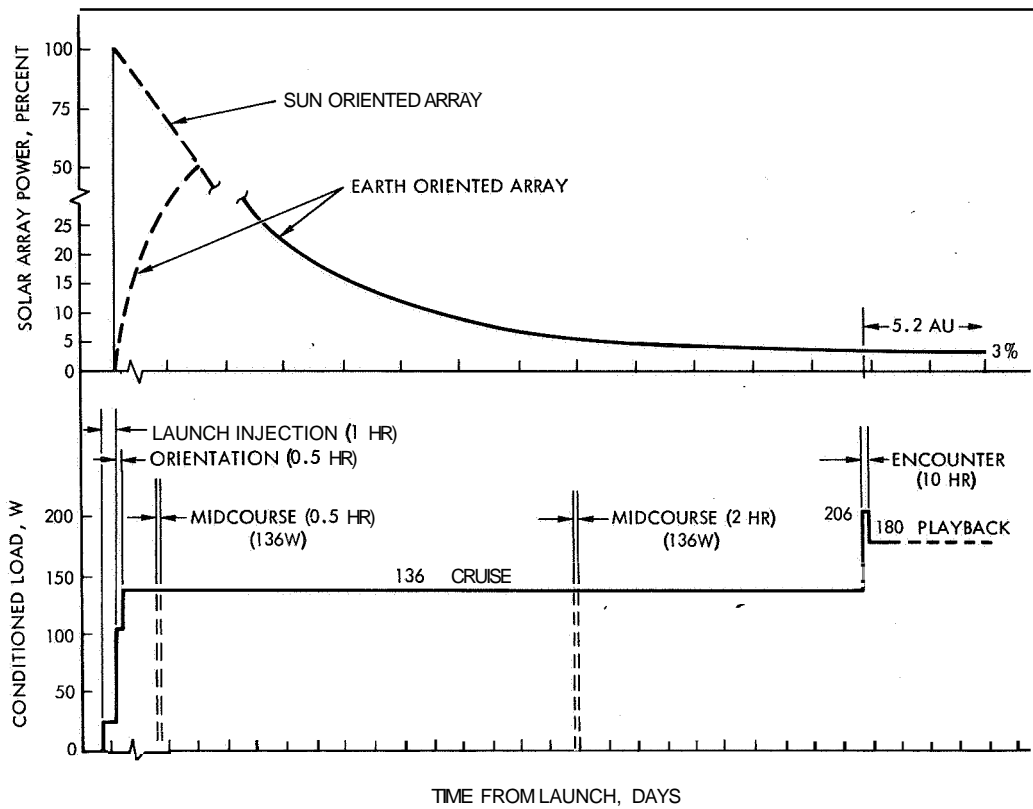


Figure 11. Solar Array Maximum Power Capability and Conditioned Load Power Requirements versus Time - Jupiter Flyby Mission

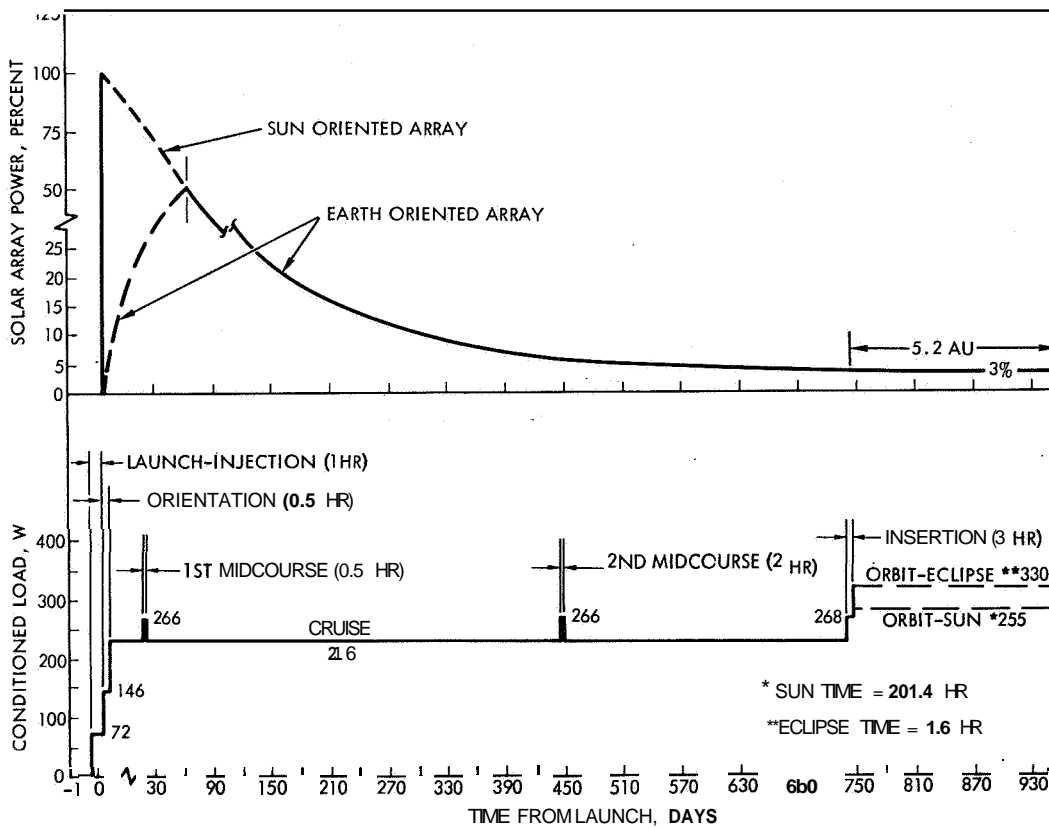


Figure 12. Solar Array Maximum Power Capability and Conditioned Load Power Requirements versus Time - Jupiter Orbiter No. 1 Mission

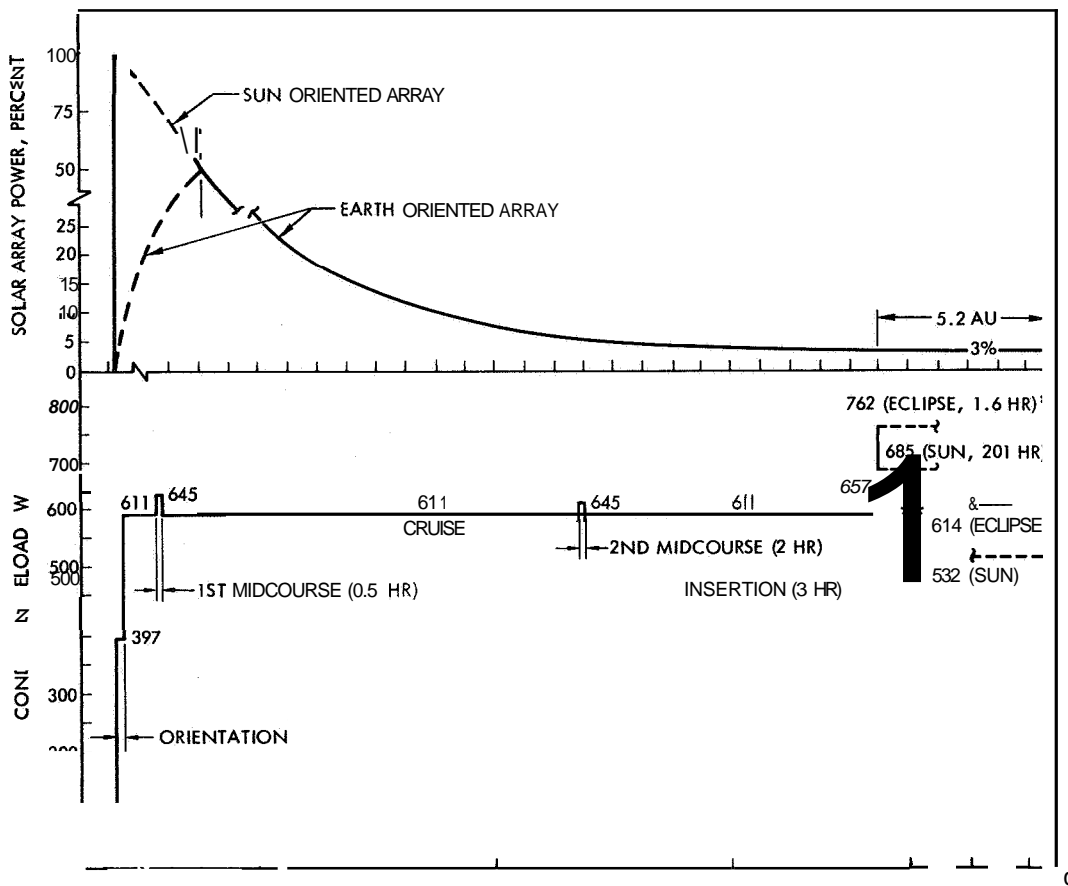


Figure 13. **Solar** Array Maximum Power Capability and Conditioned Load Power Requirements versus Time - Jupiter Orbiter No. 2 Mission

2.3 SOLAR ARRAY CHARACTERISTICS

The solar cells used in the analysis of inbound missions to Venus and Mercury are specially designed 1 x 2-cm size having a base resistivity of 10 ohm-cm, 10-percent AMO efficiency, and cover slides with a 420 μ cutoff filter. These cells were fabricated for high light-intensity operation with a low value of series resistance (approximately 0.2 ohm) through the use of twelve grids rather than the usual five. A comparison of the current-voltage characteristic of these cells with standard solar cells at high solar intensity is shown in Figure 14. The solar cell characteristics used in the analysis of the outbound missions to Mars and Jupiter are those of a 2 x 2-cm, 10.5-percent efficiency, 10 ohm-cm type covered by a 420 μ cutoff filter.

Output calculations in each case were based on a solar flare radiation environment equivalent to 10^{14} 1 mev electrons per cm² per year near the Earth (1 AU). It was assumed that the radiation levels at other than 1 AU varied inversely with the square of the Sun-spacecraft distance. For all of the Jupiter missions, an arbitrary 10 percent degradation in array performance has been assumed to reflect micrometeoroid damage during passage through the asteroid region at Sun-spacecraft distances of 2.0 to 4.0 AU.

Results of these calculations are shown in Figures 15, 16, 17, and 18 for the Mercury, Venus, Mars, and Jupiter missions, respectively. In addition to the array current-voltage characteristics at selected points in the mission, the variation in solar array current and voltage corresponding to the maximum power point throughout the mission is also indicated. For the Mercury mission, the maximum array power is shown to increase to a maximum and then decrease at lower values of Sun-spacecraft distance. This results from tilting the solar panels from their Sun-oriented position to prevent excessive cell temperatures at the lower values of Sun-spacecraft distance.

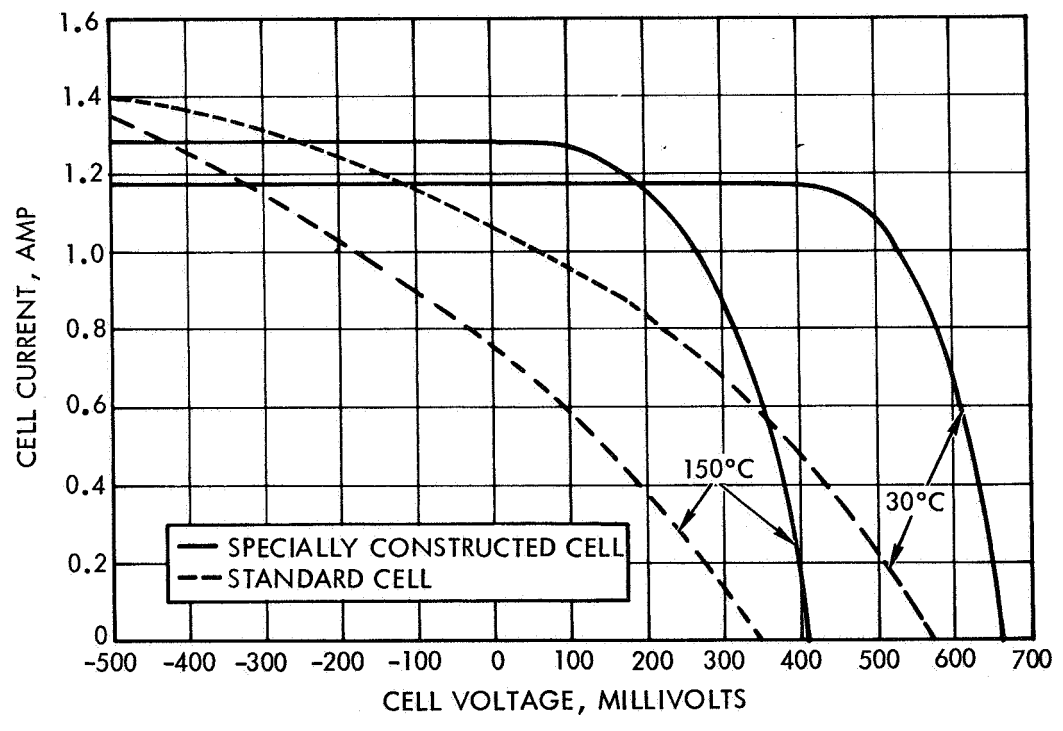


Figure 14. Comparison of Special Solar Cell with Standard Solar Cell at Light Intensity of 20 Suns

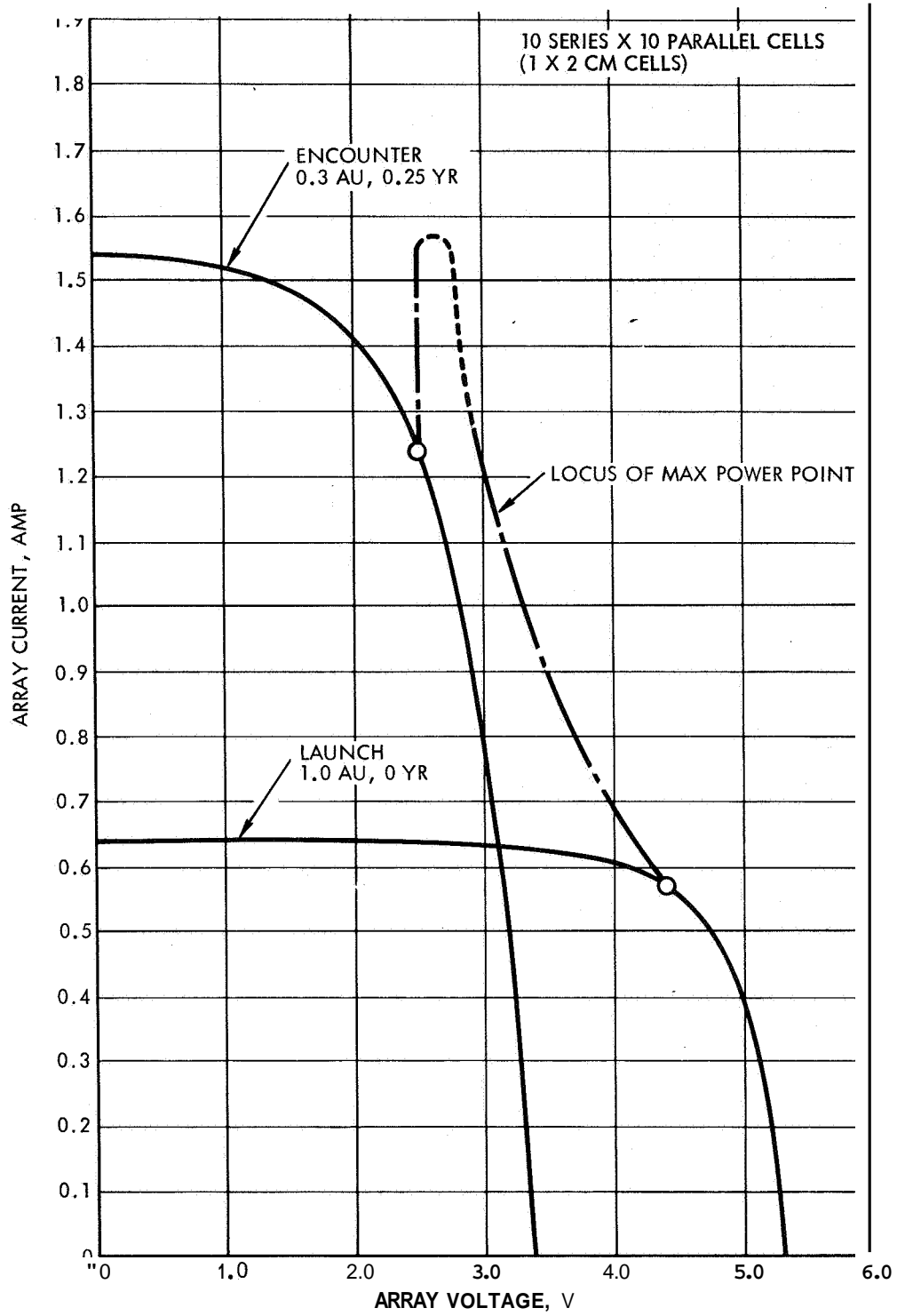


Figure 15. Mercury Flyby Solar Array Characteristics

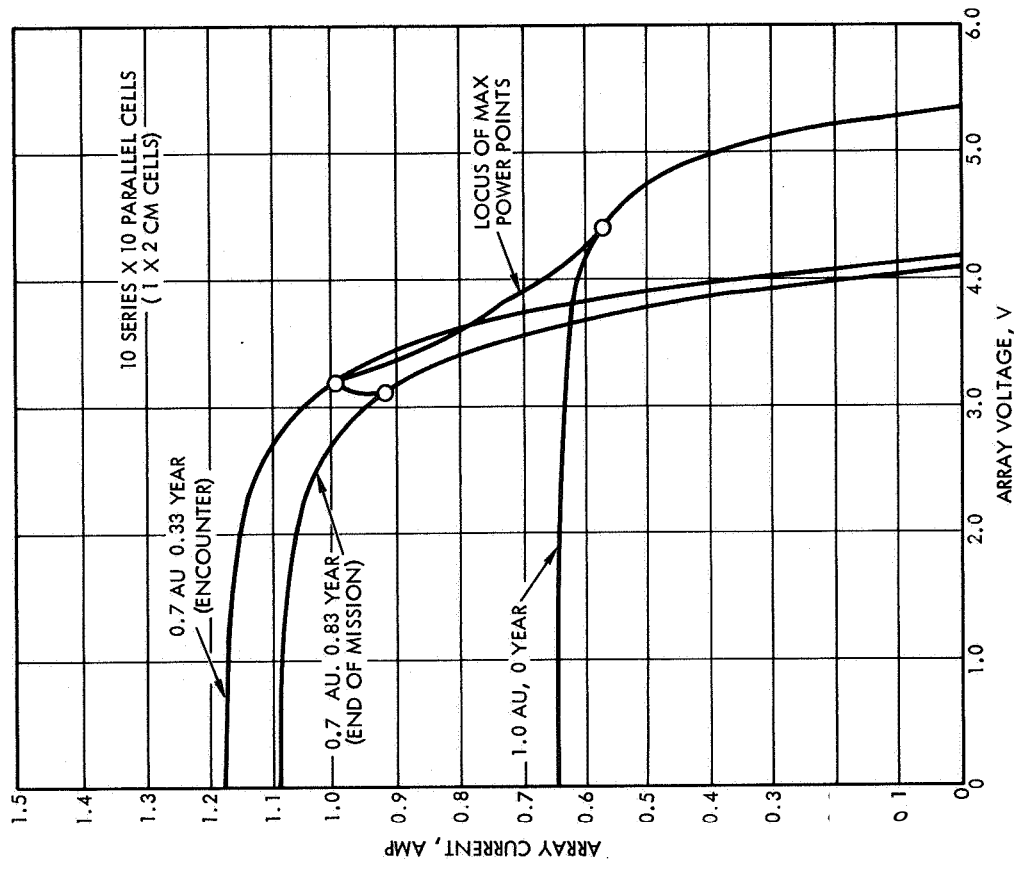


Figure 16. Venus Orbiter Solar Array Characteristics

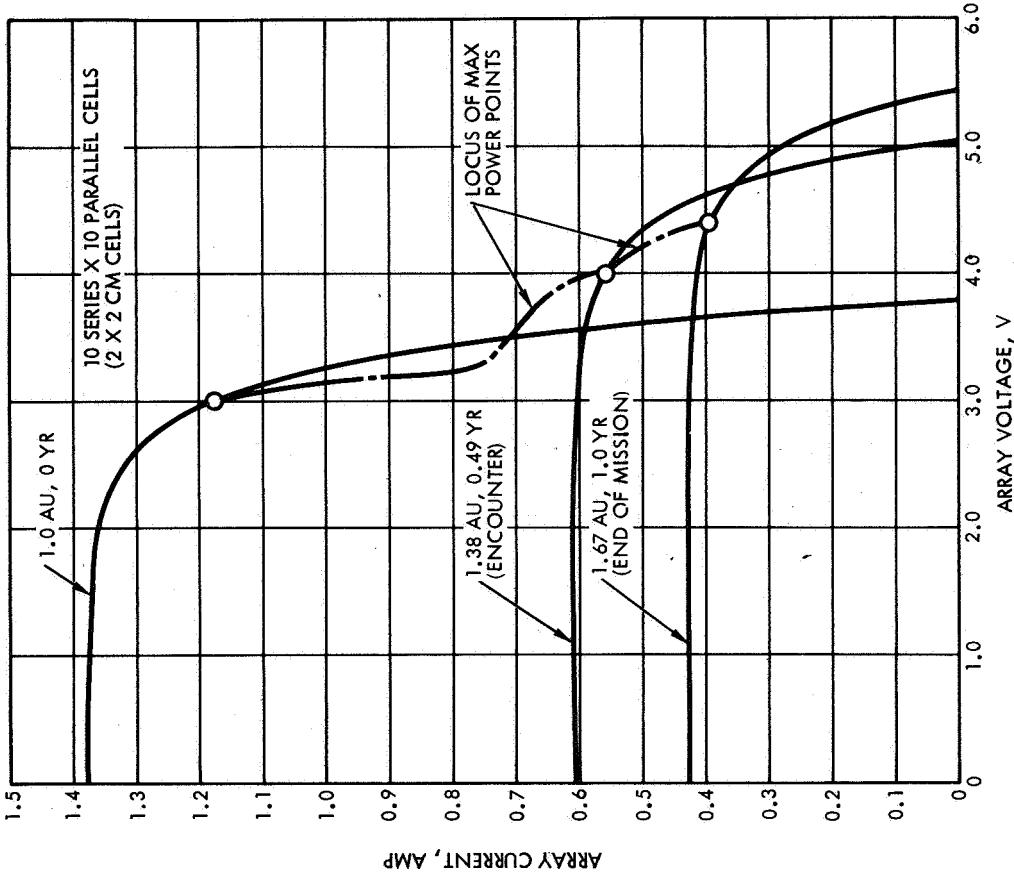


Figure 17. Mars Orbiter Solar Array Characteristics

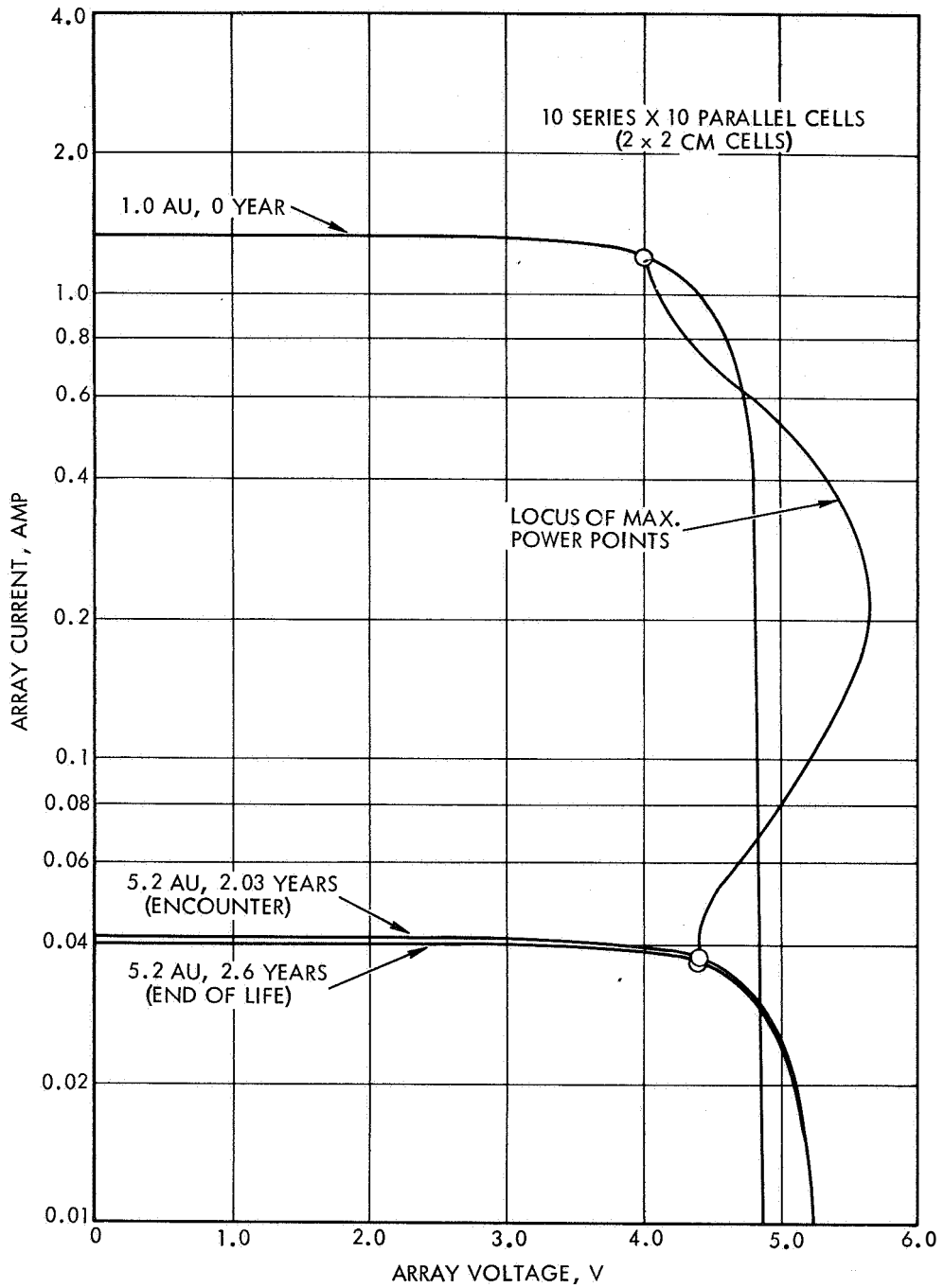


Figure 18. Jupiter Mission Solar Array Characteristics

3. BASELINE POWER SYSTEM CONFIGURATIONS

3.1 POWER SYSTEM SYNTHESIS

The selection of candidate power system configurations is based on progression from generalized system concepts to specific baseline implementations as shown in the flow diagram, Figure 19. Initially, all photovoltaic power systems are divided into two generalized concepts as shown in Figure 20. From these two concepts, the basic functional power system configurations shown in Figure 21 are developed. From these five functional system approaches, baseline system configurations are determined, based on selecting specific designs for each functional element of each basic configuration.

Referring to Figure 20, the first generalized concept combines the battery and solar array outputs at an unregulated bus with suitable controls. The unregulated bus supplies line regulation and power conditioning equipment which, in turn, supplies the regulated outputs of the system. In addition, the unregulated bus can directly supply certain of the spacecraft loads such as heaters and solenoids. The second approach employs regulators for both the solar array and battery to permit their electrical connection to a regulated dc bus which supplies the load power conditioning equipment and direct connected loads.

The five basic functional configurations are shown in Figure 21. In each system configuration specific functions are identified which satisfy the regulation requirements of the applicable generalized concept. For generalized Configuration 1, the three alternative approaches to accomplishing the line regulation function are shown.

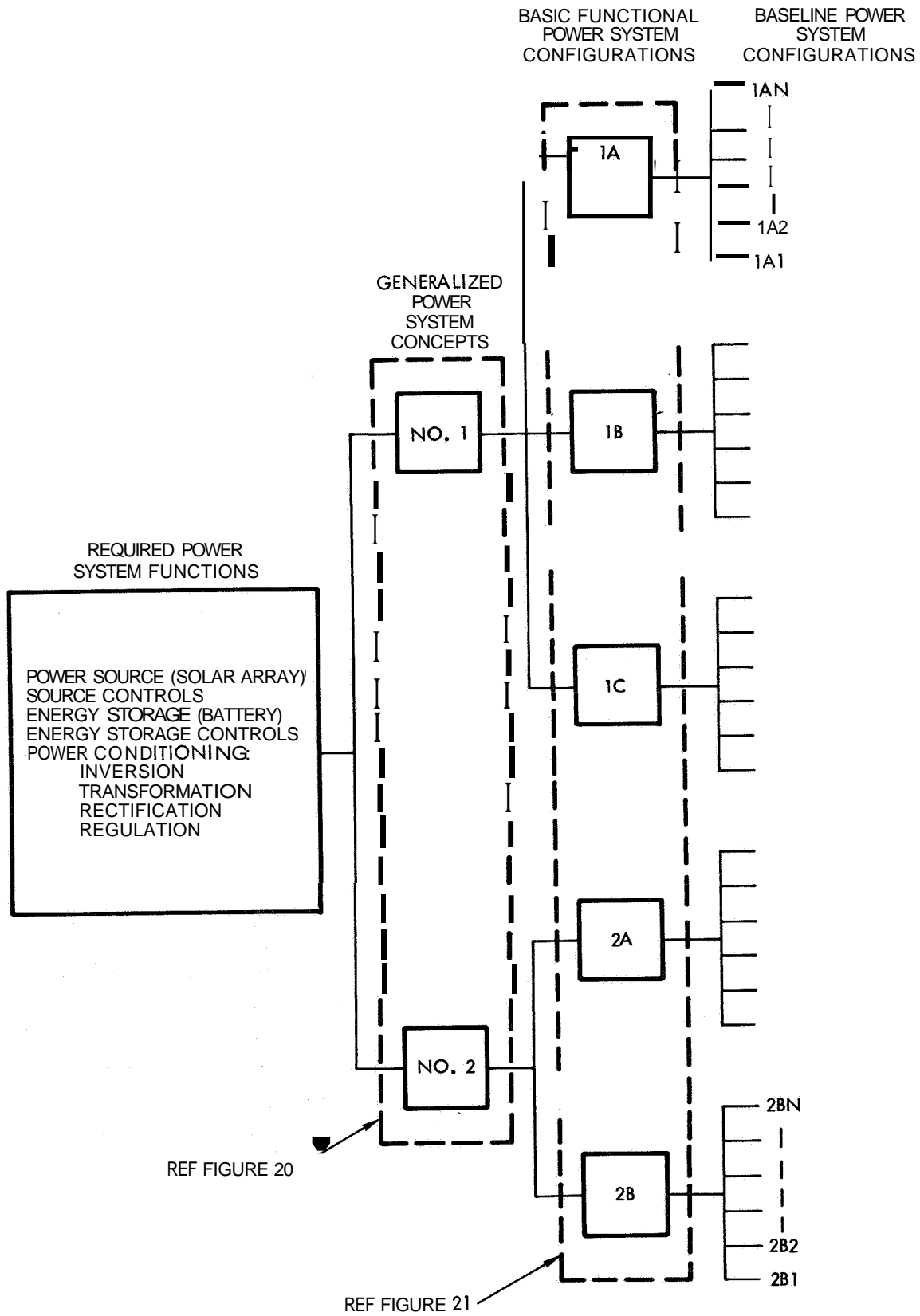


Figure 19. Flow Diagram - Baseline System Configuration Analysis

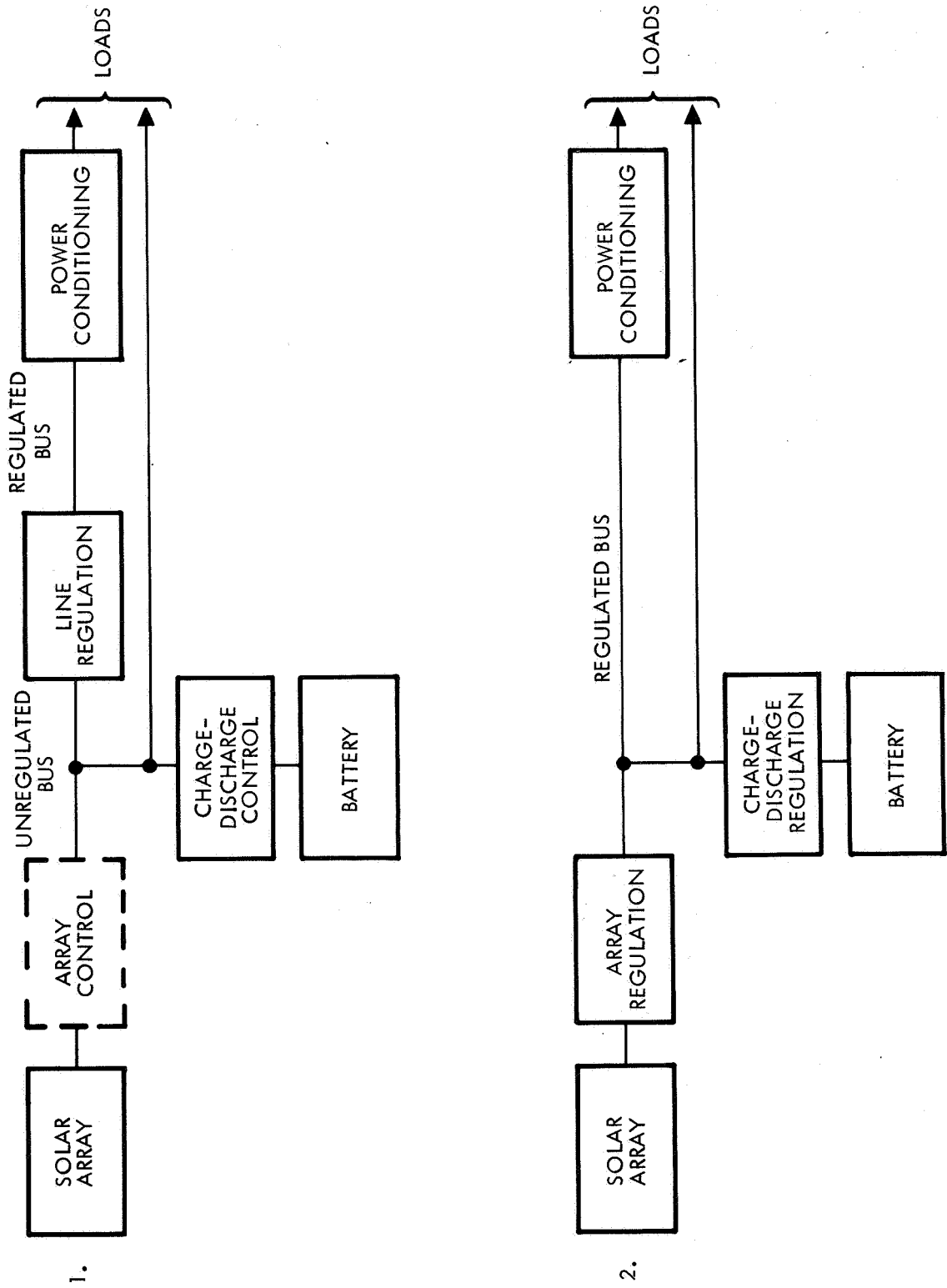


Figure 20. Generalized Power System Concepts

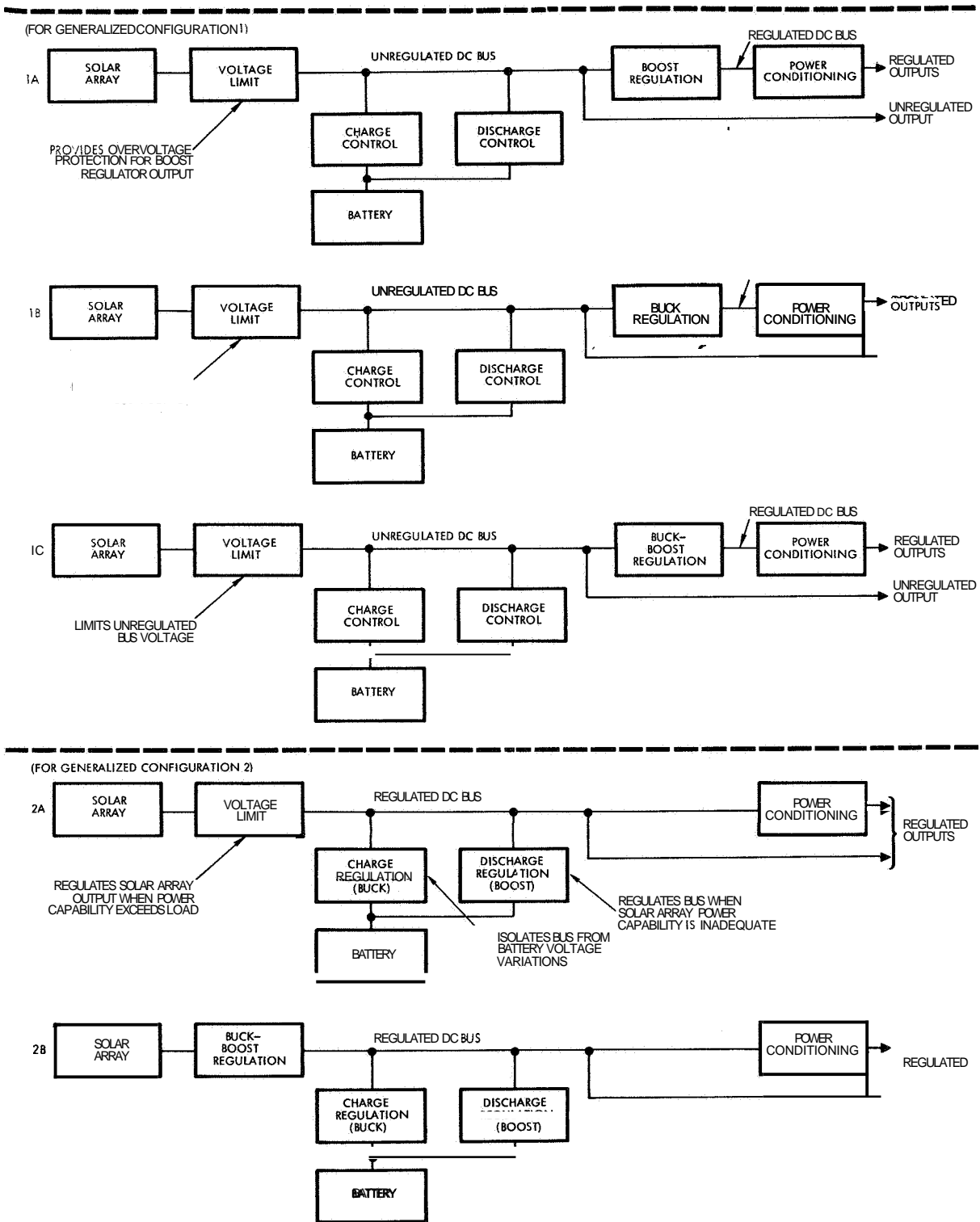


Figure 21.' Basic Functional Power System Configurations

3.2 METHODS OF IMPLEMENTING FUNCTIONS

3.2.1 Battery Selection

The selection of batteries for each of the model missions is based primarily on straightforward tradeoffs of weight and cycle life capability for the orbiting missions. The maximum number of cycles approach 300 for the Venus and Mars orbiters. This number of cycles is considerably lower than the capabilities of state-of-the-art silver-cadmium batteries operating at 50 percent depth of discharge which are selected for the orbiting missions. For the flyby missions, the silver-zinc battery is selected based on the low cycle life requirements and the improved energy density of the silver-zinc cell. Here again, a 50 percent maximum depth-of-discharge is assumed in sizing the battery.

3.2.2 Battery Control

The characteristics of both the silver-zinc and silver-cadmium batteries require a charge control method which limits battery charging current as a function of battery state-of-charge and prevents overcharge of the battery. The simplest scheme for implementing this method is to charge the battery from a constant potential bus through a series current limiting resistor. The current limiting function can be implemented by the use of a resistor or by any type of current limiting regulator.

Since it is preferable that silver-zinc and silver-cadmium batteries not be subjected to extended over-charge, charge termination by means of disconnecting the battery from its charging power source, is employed. Charge termination is controlled by determining that charging current has fallen below a low level indicative of full charge at a given voltage limit.

In those cases where the maximum main bus voltage is not equal to the maximum allowable battery voltage, a bucking or boosting regulator is used for control charge. These regulators and the associated controls must limit battery voltage, limit battery current as a function of battery voltage, detect a decrease in charging current below the desired charge termination value and terminate charge by de-energizing the regulator. This basic charge control approach is used for all of the missions.

For those power supply configurations employing a regulated main dc bus, the chargers include bus-voltage feedback to further limit battery charging current in those cases of marginal solar array capability where normal battery current could produce a main bus undervoltage condition.

For those power supplies in which the main bus voltage varies with the battery charge-discharge status, a switching function is incorporated to provide a direct loss-less-discharge path from battery to bus. The alternative approach of relying on a diode to provide an unidirectional discharge path is considered undesirable because of the voltage drop and power loss associated with this approach.

A potentially large penalty in solar array sizing results from those system configurations which combine the battery and solar array electrically at an unregulated bus. This results from the necessity of sizing the solar array to provide required power over a large range of operating voltages. Figure 22 illustrates the difference in required solar array capability between a system designed with appropriate controls to reduce the solar array operating voltage range and a system without such controls.

To improve the utilization of array power, a momentary battery discharge booster may be employed to force the bus voltage to a higher level where the increased array power capability can support the load and recharge the battery. With this approach, the solar array may be designed to provide required load current only at voltages corresponding to battery charging conditions (Point C).

Power sources which generate a regulated dc bus directly by regulating both battery and solar array outputs independently require a continuous boosting regulator for battery discharge. This approach, of course, permits designing the solar array for a particular main bus voltage and eliminates the problem of undesirable load sharing between battery and array.

The basic battery control designs selected are:

- Bucking charger and discharge switch
- Bucking charger, discharge switch and momentary line booster

- Boost charger and discharge switch
- Boost charger, discharge switch and momentary line booster
- Bucking charge regulator and boosting discharge regulator (continuous)

Three methods of implementing the bucking charger approach for the unregulated bus systems are: a series current limiting resistor and disconnect relay to terminate battery charging, a series dissipative regulator controlled to limit maximum battery voltage and battery charging current and to terminate charging, and a pulsewidth modulated series regulator controlled to limit battery voltage, current, and terminate charge.

For the regulated bus system, an active control is necessary to maintain the regulation of the main bus during battery charging. In this case, the appropriate methods of implementing this function are the dissipative and pulsewidth modulated series regulators.

The boost charger used with the unregulated bus systems and the boosting discharge regulator used with the regulated bus systems are dissimilar in that the former must have the capability of functioning in a bucking mode in those cases where the bus voltage exceeds the desired battery voltage limit. The momentary line booster used with a bucking charger is dissimilar from that used with a boosting charger in that the former is of the type wherein only an amount of power proportional to the difference in voltage between the battery and the bus is converted. This booster is similar to the continuous boost battery discharge regulator and is designed with a series diode which passes the major portion of the power. With a boost charger, the momentary line booster must be designed without such a diode path since this would short circuit the charger. Simplified block diagrams for all of these regulators are illustrated in Figures 23 through 29. Block diagrams of the associated battery controls are shown in Figures 30 through 34.

3.2.3 Solar Array Controls

Referring to the five basic functional system configurations, (Figure 21), solar array control functions are of two principal types. For all of the unregulated bus systems, the need for solar array control consists primarily of a need for voltage limiting of the solar array.

In the regulated bus systems, the solar array control function may be a voltage limiter or a buck-boost voltage regulator.

The selected alternative methods for implementing the array control functions are as follows:

- a) No array control
- b) Zener diode shunt
- c) Dissipative shunt voltage limiter
- d) Series pulsewidth modulated voltage limiter
- e) Maximum power point tracker (series bucking)
- f) Series PWM buck-boost regulator

Simplified block diagrams for each of the five array controls are shown in Figures 35 through 38.

3.2.4 Line Regulators

For those basic functional configurations employing an unregulated bus, the line regulator function is either of the buck, boost, or buck-boost type. The bucking type is further divided into dissipative and pulsewidth modulated approaches. Simplified block diagrams of the selected line regulators are illustrated in Figures 29, 37, 39 and 40.

3.2.5 Load Power Conditioning Equipment

The major simplifying assumption made in the selection of load power conditioning equipment is that voltage regulation requirements of the loads to closer than ± 5 percent are not included in this equipment. Since all of the power system configurations generate a regulated dc bus, the power conditioning equipment is simplified to consist of converters, inverters, and transformer rectifier units which are unregulated.

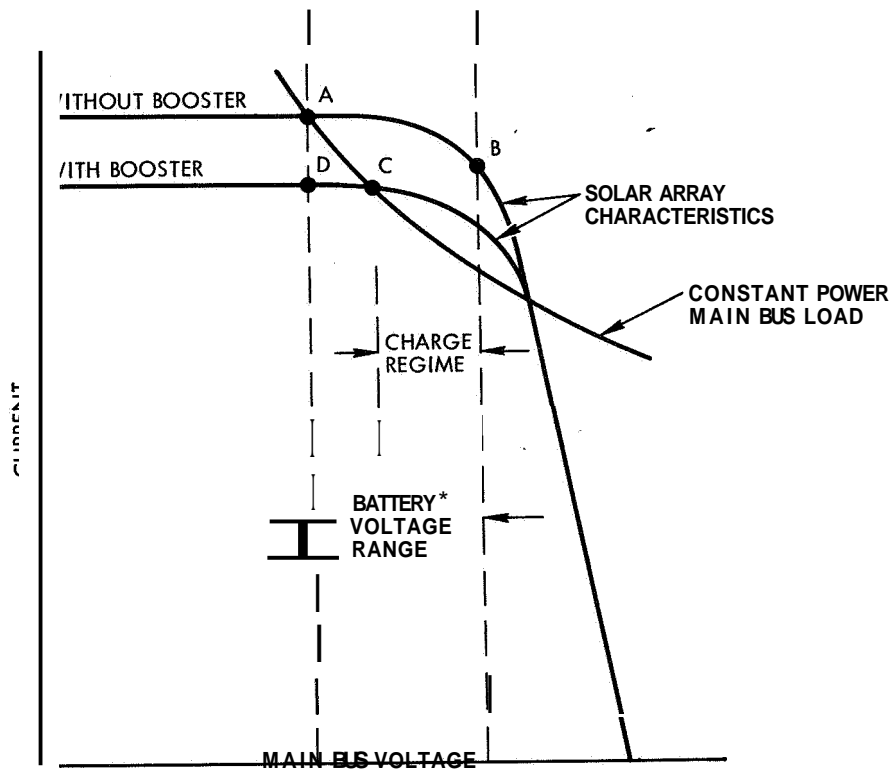
Identification of the specific load power conditioning equipment for both ac and dc distribution approaches for each of the model spacecraft is shown in Tables 10 to 16. For the dc case, these are divided normally into a main converter which supplies the standardized secondary voltage requirements of the majority of the load equipment, a transmitter converter, a gyro inverter, and auxiliary high voltage or low voltage converters to supply those loads not compatible with the standardized

secondary voltages. The block diagram of the selected load power conditioning equipment configuration, illustrated in Figure 44, is common to all baseline system configurations employing the dc distribution approach. A block diagram of the selected converter design is illustrated in Figure 41.

For the ac power distribution case, Figure 42, a central unregulated square-wave inverter is assumed to supply the major portion of the loads through transformer rectifier units. The transformer-rectifier units (TR's) are configured to combine as much power as possible in a main TR which furnishes the standard secondary dc voltages common to both ac and dc approaches. Auxiliary TR's are used to supply nonstandard voltages to the transmitter and experiments as required. A separate unregulated gyro inverter is included to furnish the required 3Ø 400 Hz output.

3.2.6 Selection of Baseline System Configurations

The appropriate methods of implementing various functions for each basic functional power system configuration are shown in Figures 43 and 44. The variations from system to system are primarily in the array control and battery control approaches. Logical combinations of these alternative control methods in each of the basic functional configurations define the baseline system configurations and are summarized in matrix form in Table 17. The uncircled numbers listed in each matrix cell reflect the appropriate array controls which are compatible with the line regulator and battery control defining the particular cell. The circled numbers within each cell refer to Table 18 which lists the reasons for deleting certain of the possible combinations of regulators and controls in defining these baseline systems. These deletions reflect cases where it is illogical to combine certain of the power control or regulation functions in the same system or where one control in a system depends on a specific performance characteristic in another.



*ASSUME EQUAL TO
BUS VOLTAGE RANGE

Figure 22. Comparison of Required Solar Array Capabilities With and Without Momentary Line Booster for Unregulated Bus Systems

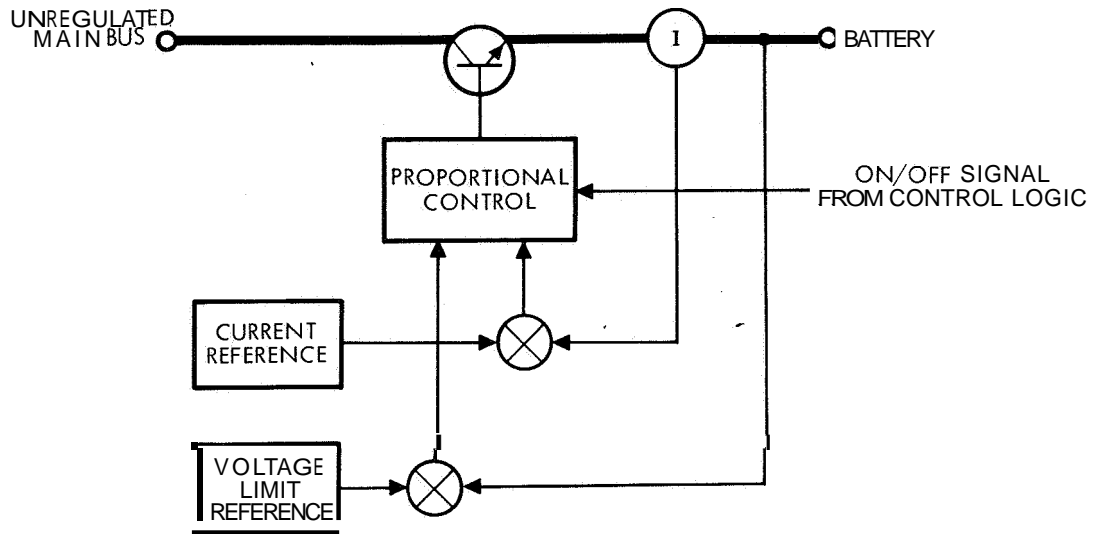


Figure 23. Dissipative Series Battery Charger

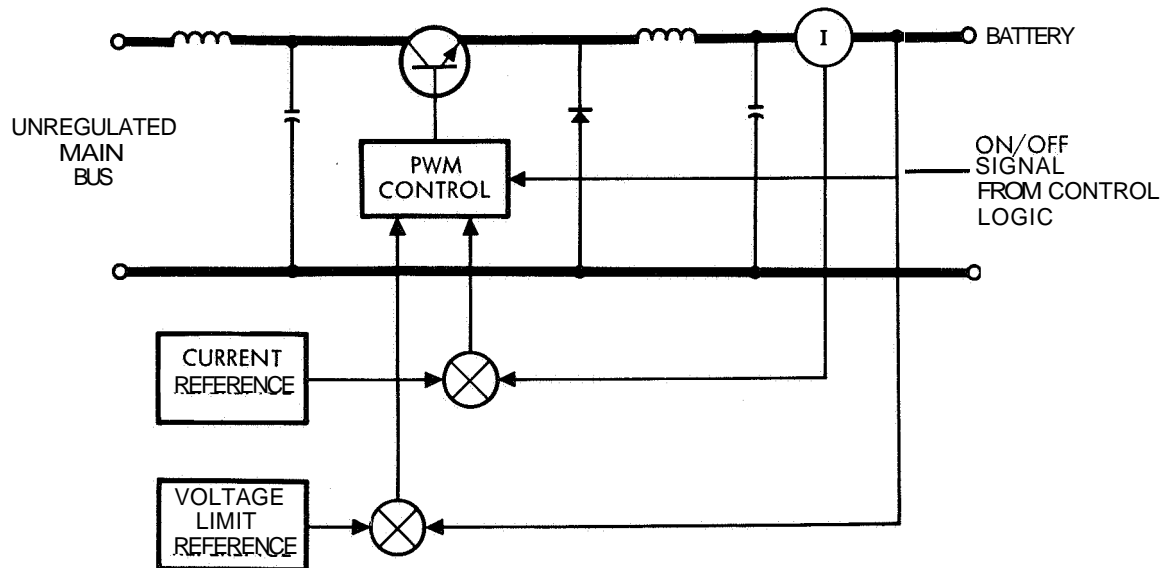


Figure 24. Pulsewidth Modulated Series Bucking Battery Charger

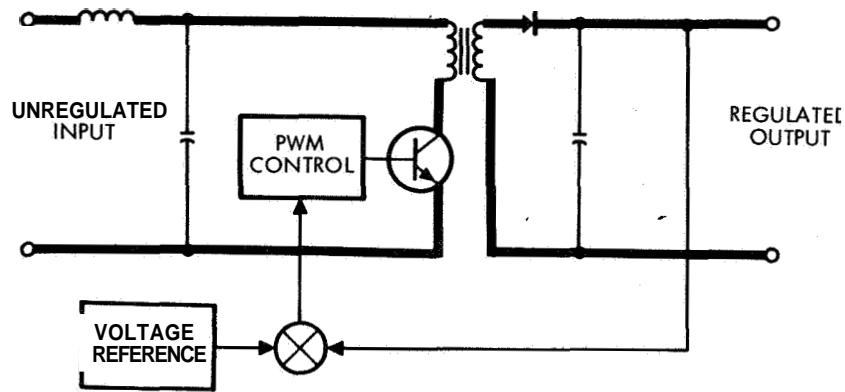


Figure 25. Pulsewidth Modulated Buck-Boost Solar Array Regulator, Line Voltage Regulator or Battery Charger

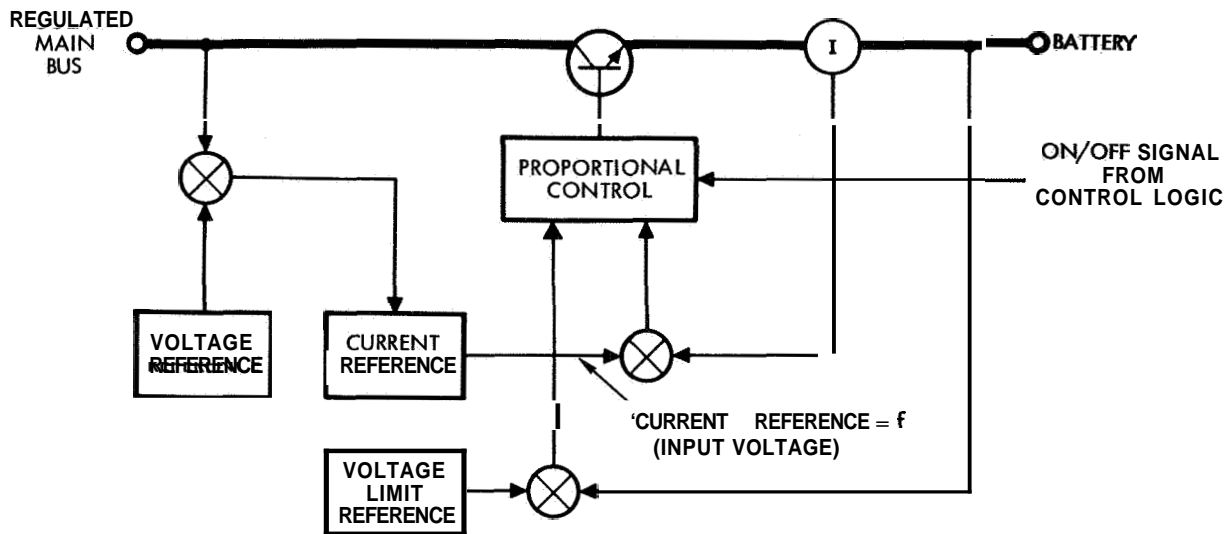


Figure 26. Dissipative Battery Charge Regulator

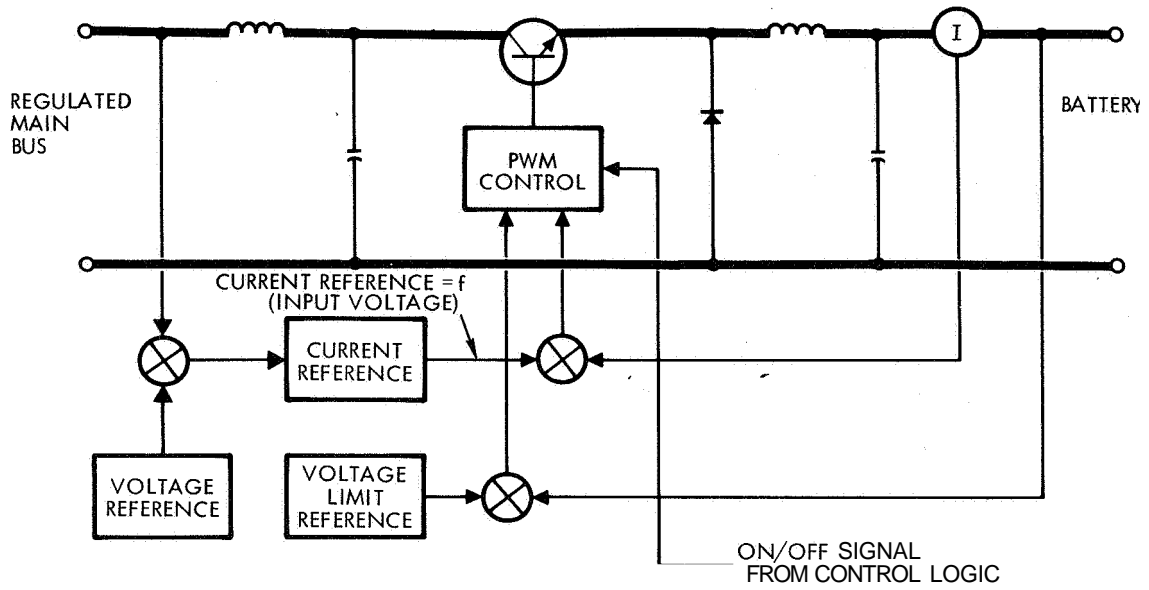


Figure 27. Pulsewidth Modulated Bucking Battery Charge Regulator

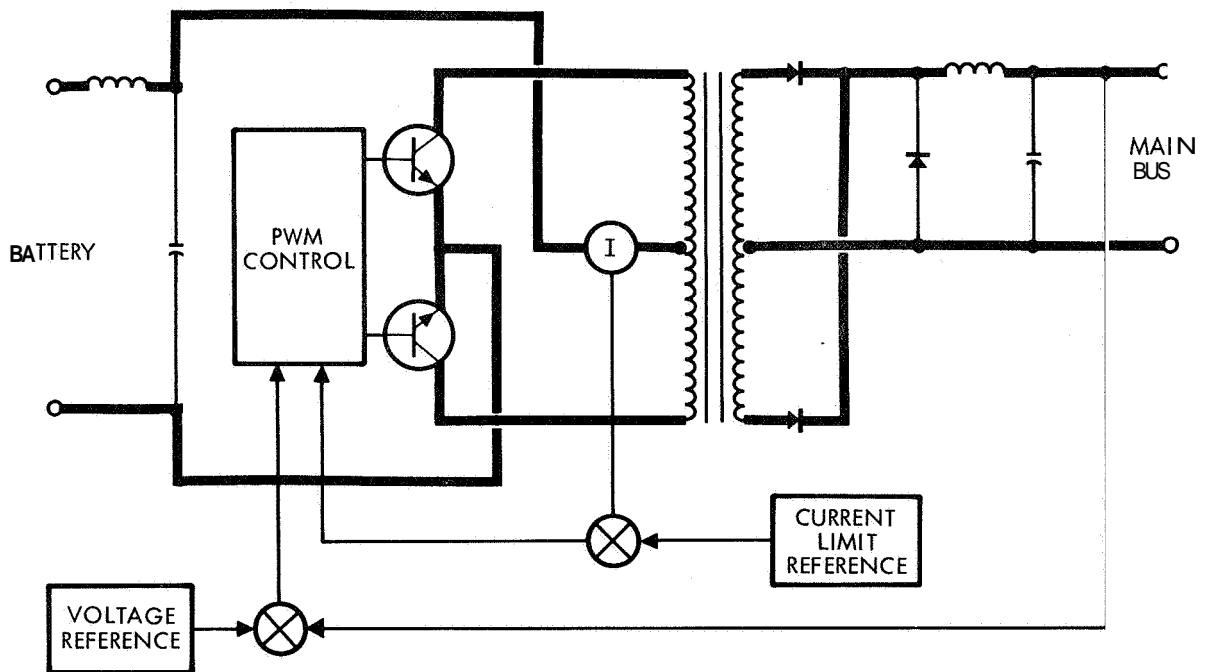


Figure 28. Pulsewidth Modulated Momentary Line Booster Used With Boosting Charger

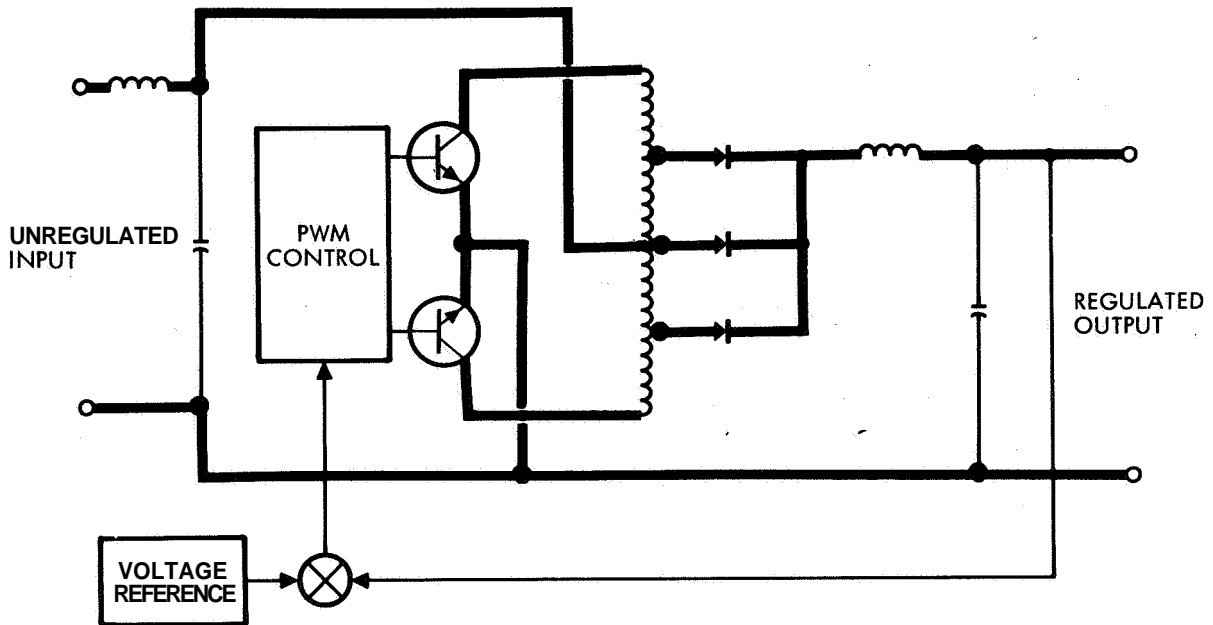


Figure 29. Pulsewidth Modulated Boosting Line Regulator, Battery Discharge Regulator and Momentary Line Booster Used with Bucking Charger

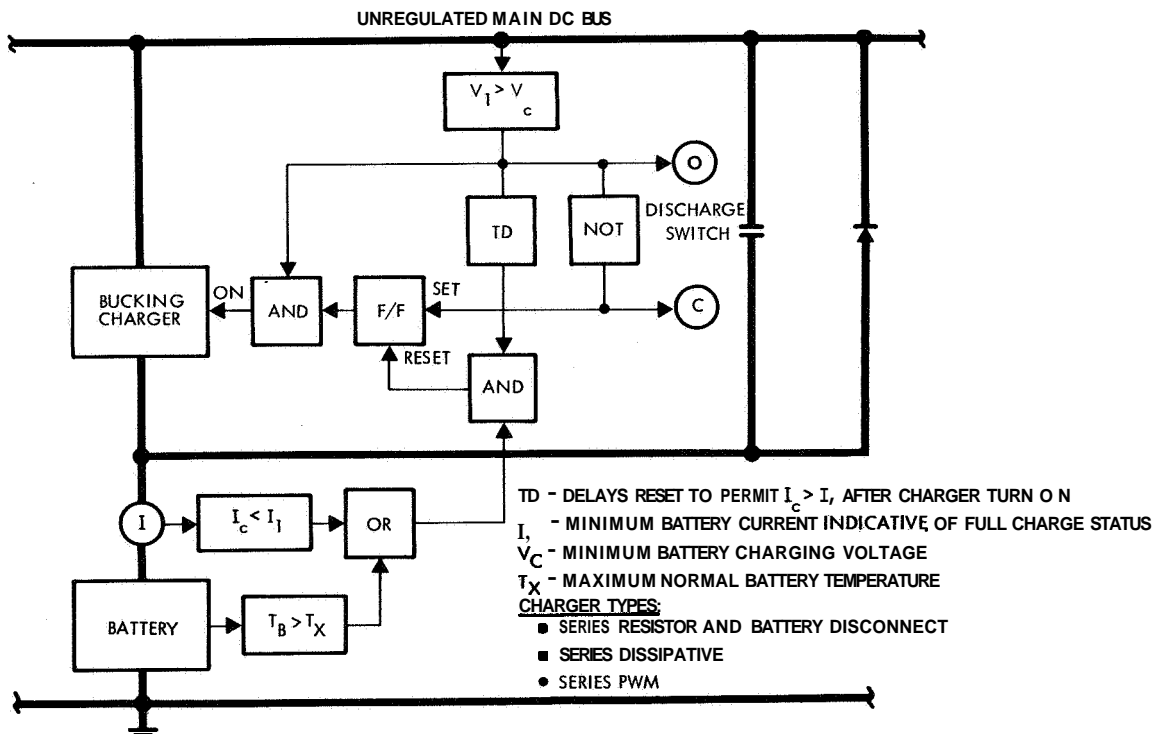


Figure 30. Battery Control Block Diagram - Bucking Charger and Discharge Switch

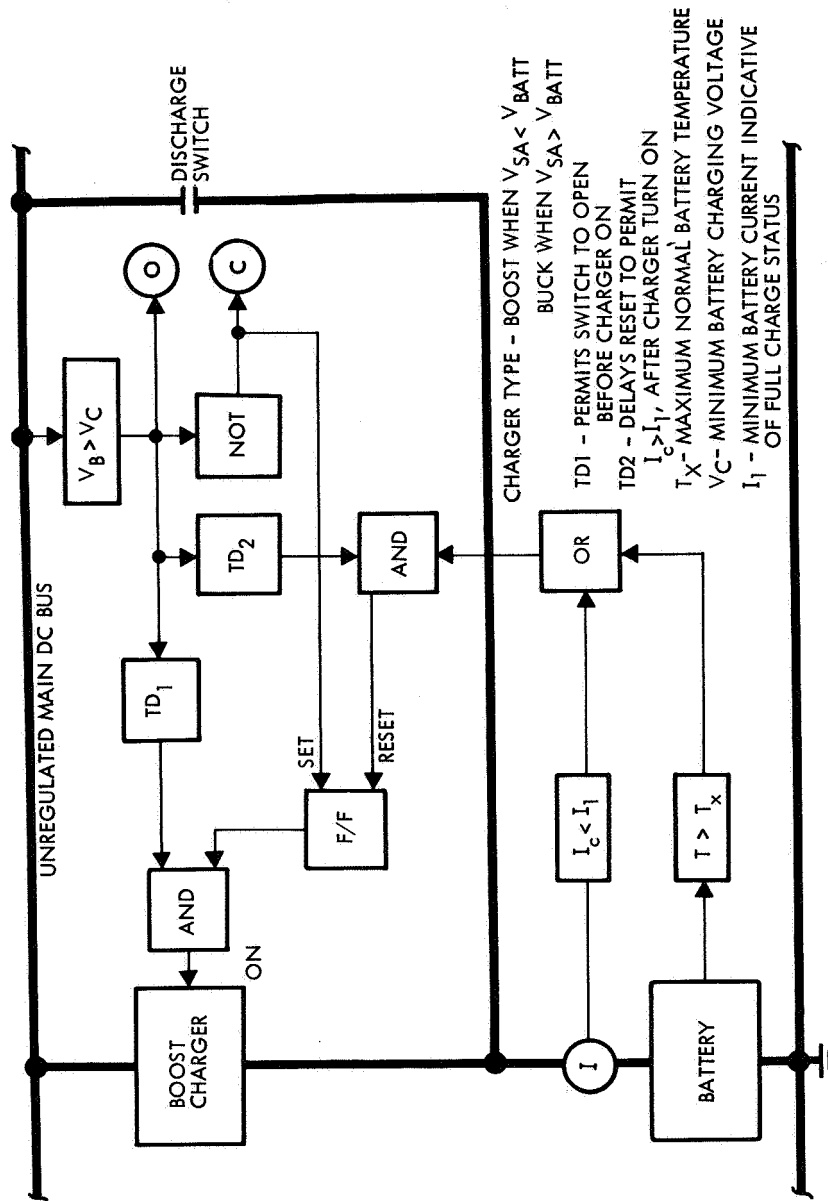


Figure 32 Battery Controls Block Diagram-Boost Charger and Discharge Switch

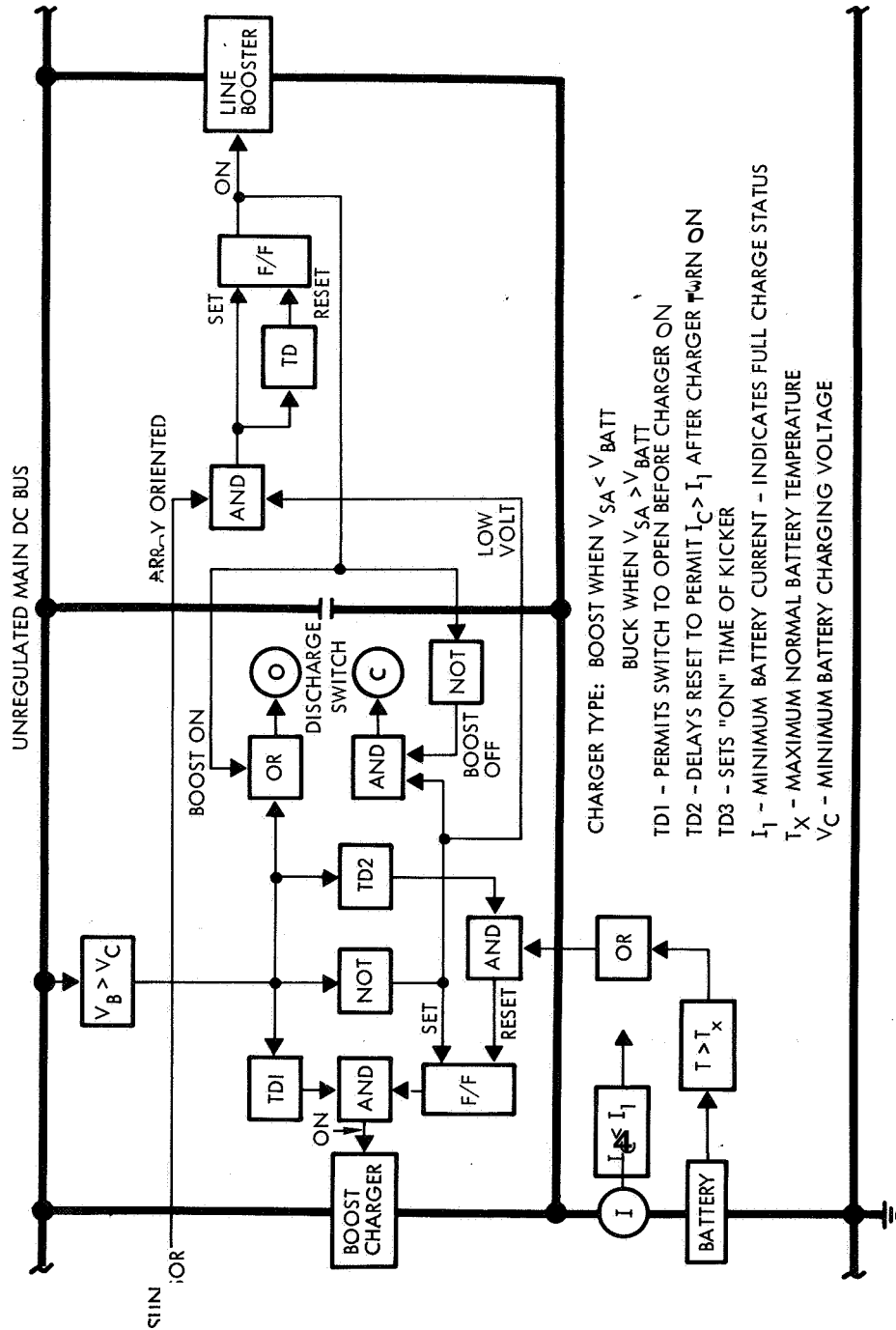


Figure 3k. Battery Controls Block Diagram-Boost Charger, Discharge Switch, and Line Booster

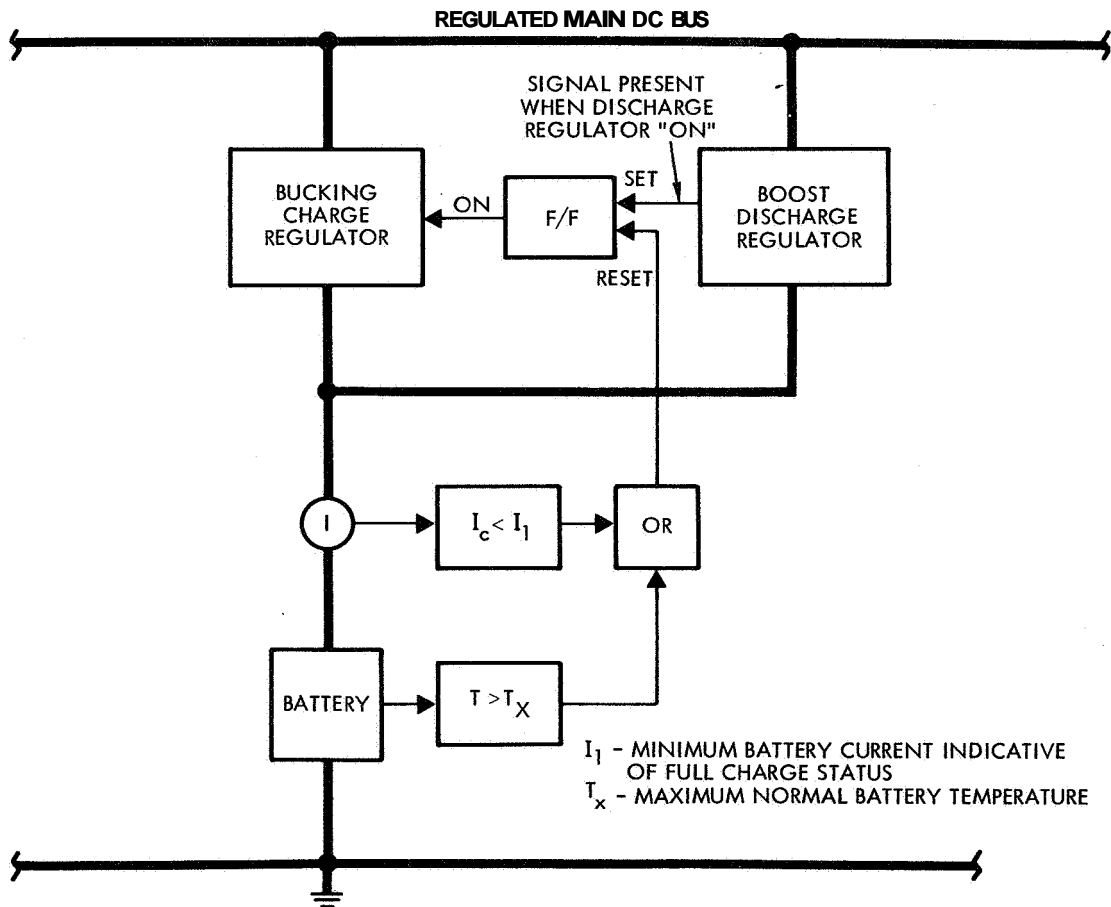


Figure 34. Battery Controls Block Diagram - Bucking Charge Regulator, Boost Discharge Regulator

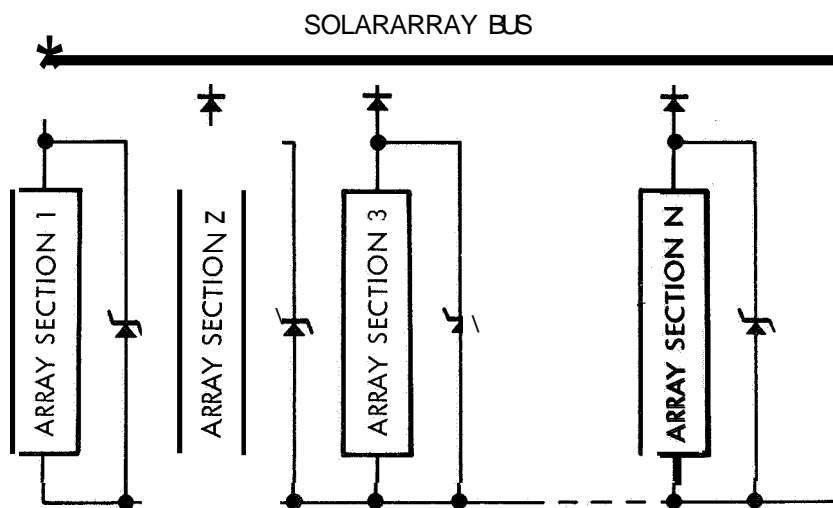


Figure 35. Zener Diode Solar Array Voltage Limiter

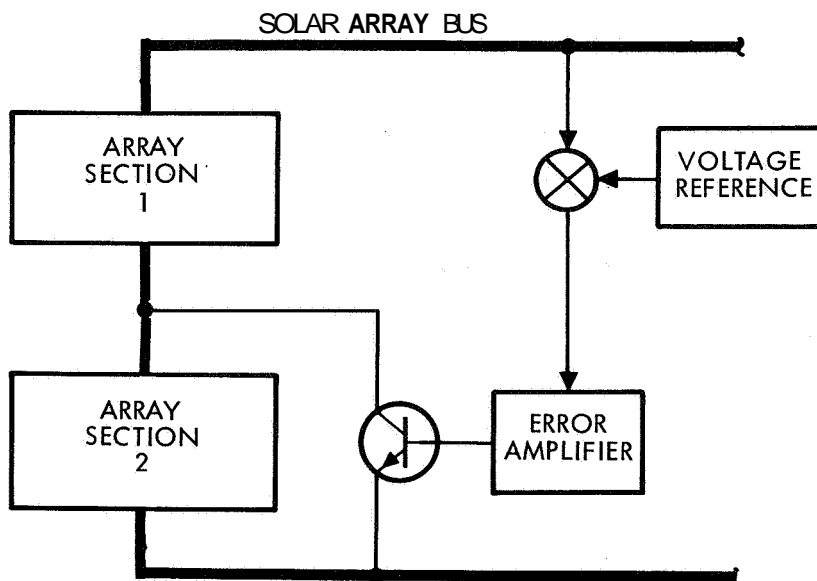


Figure 36. Active Shunt Solar Array Voltage Limiter

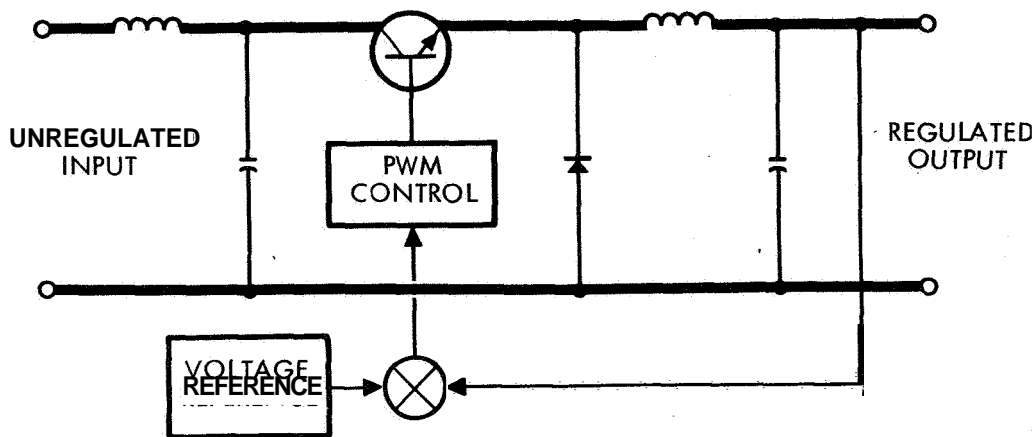


Figure 37. Pulsewidth Modulated Bucking Solar Array Voltage Limiter or Line Regulator

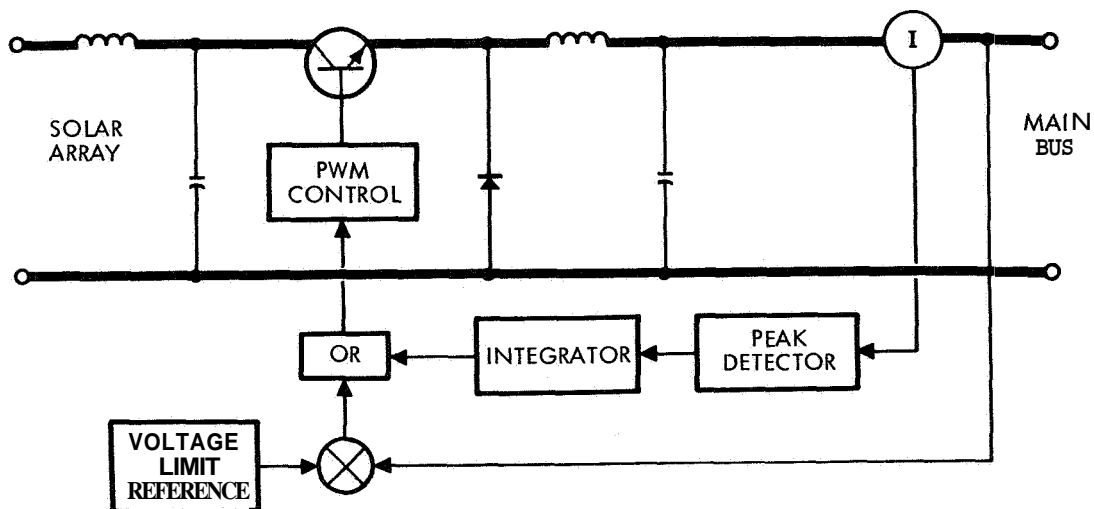


Figure 38. Maximum Power Tracking Solar Array Voltage Limiter

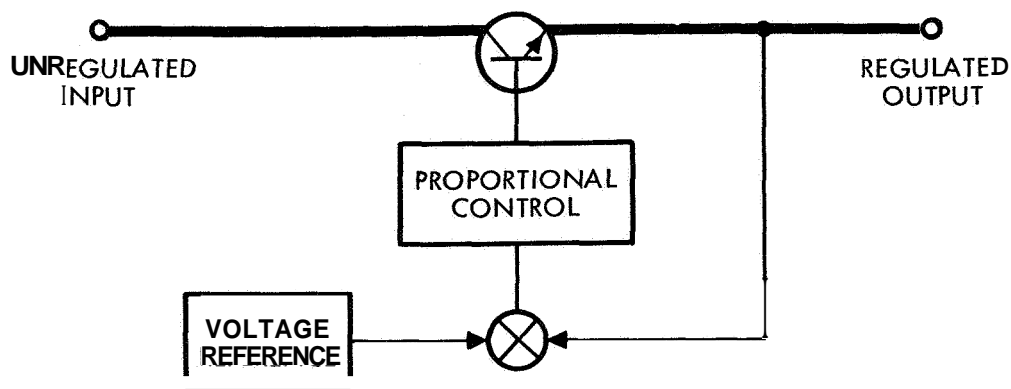


Figure 39. Dissipative Series Line Regulator

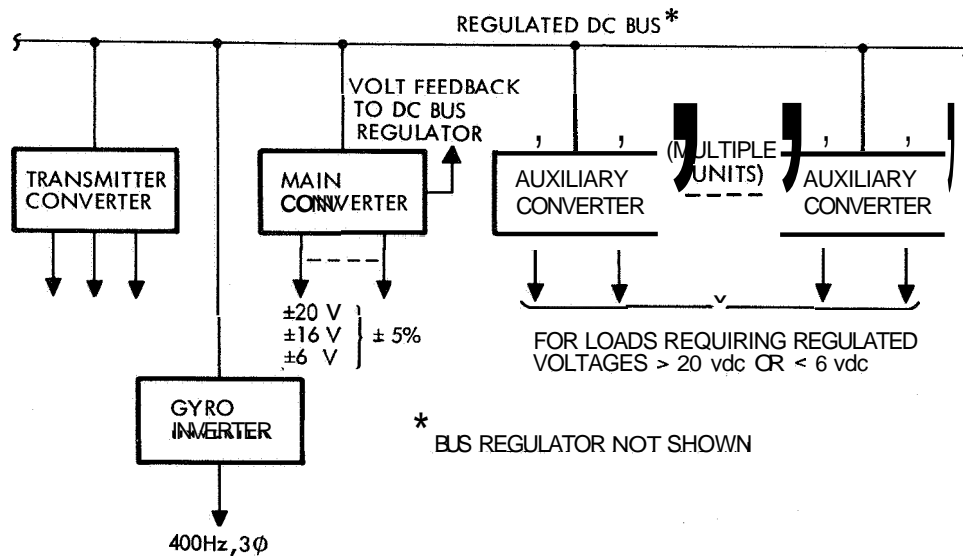


Figure 40. Block Diagram, Load Power Conditioning Equipment Configuration, DC Distribution

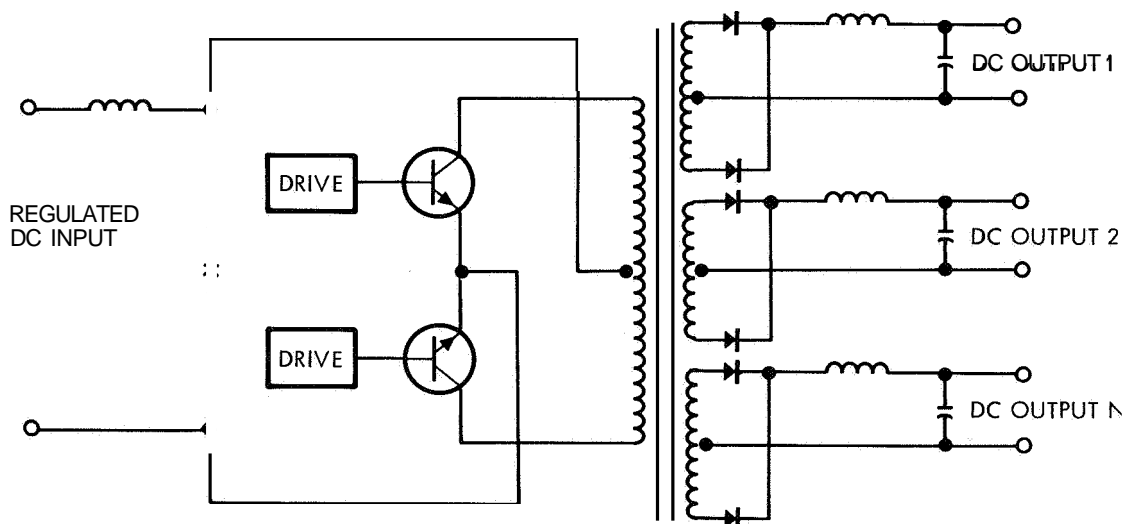


Figure 41. Block Diagram Unregulated DC-DC Converter

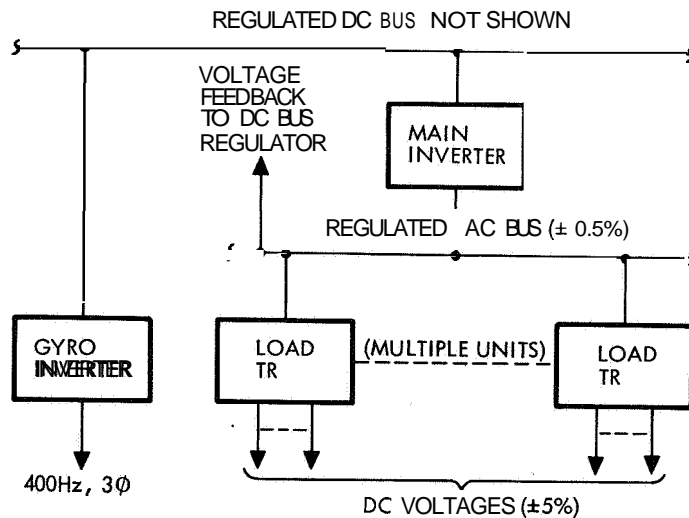
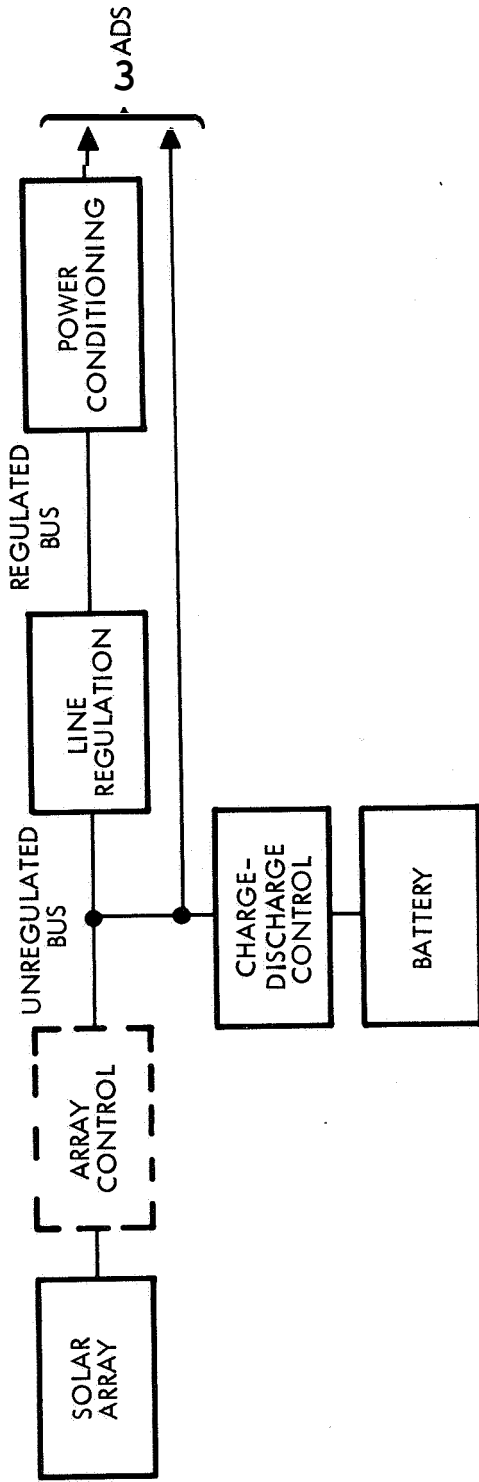
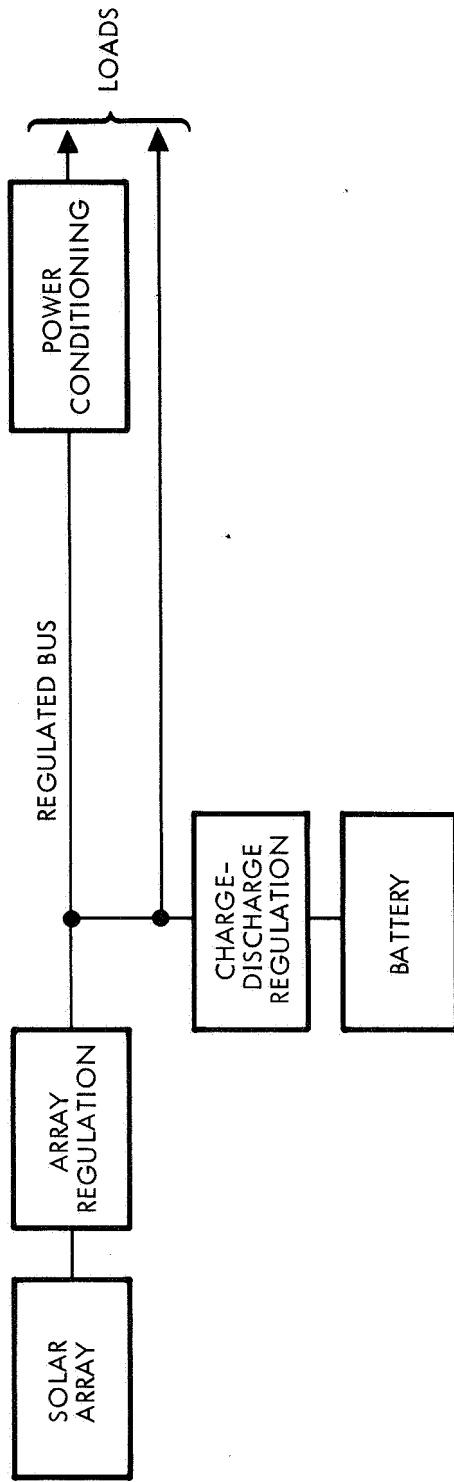


Figure 42. Block Diagram, Load Power Conditioning Equipment Configuration - AC Distribution



- | <u>ARRAY CONTROL</u> | <u>LINE REGULATION</u> | <u>BATTERY CONTROL</u> |
|-----------------------------------|--------------------------|--|
| CONFIGURATION 1A: | CONFIGURATION 1A: | (ALL CONFIGURATIONS) |
| • ZENER DIODE SHUNT | • PWM SERIES BUCK | • SWITCH & RESISTOR |
| • ACTIVE SHUNT | • DISS. SERIES BUCK | • SWITCH, RESISTOR & DISCHARGE BOOSTER |
| • PWM SERIES BUCK | CONFIGURATION 1B: | • DISS. CHARGER |
| • MAX. POWER TRACKING SERIES BUCK | • PWM SERIES BOOST | • DISS. CHARGER & DISCHARGE BOOSTER |
| CONFIGURATION 1B AND 1C: | CONFIGURATION 1C: | • PWM (BUCK) CHARGER |
| • NONE | • PWM SERIES | • PWM (BUCK) CHARGER & DISCHARGE BOOSTER |
| • ZENER DIODE SHUNT | • BUCK-BOOST | • BOOST CHARGER |
| • ACTIVE SHUNT | | • BOOST CHARGER & DISCHARGE BOOSTER |

Figure 43. Selected Alternative Methods of Implementing Basic Functional Configurations Having Unregulated Main Bus



ARRAY REGULATION

CONFIGURATION 2A:

- ACTIVE SHUNT VOLTAGE LIMITER
- PWM SERIES BUCKING, VOLTAGE LIMITER
- BUCKING MAX. POWER TRACKER-VOLTAGE LIMITER

CONFIGURATION 2B:

- BUCK-BOOST REGULATOR

CHARGE REGULATION

- DISSIPATIVE SERIES REGULATOR
- PWM SERIES BUCKING REGULATOR

DISCHARGE REGULATION

- PWM BOOST REGULATOR

Figure 44. Selected Methods of Implementing Basic Functional Configurations Having Regulated Main Bus

Table 10. Mercury Flyby Mission, Load Power Conditioning Equipment

<u>DC Distribution</u>			
<u>No.</u>	<u>Unit</u>	<u>Output</u>	<u>Power Rating</u>
1	Gyro Inverter	26 vac 30, 400 Hz	22 va
2	Main Converter	±20, ±16, ±6 vdc	73 watts
3	Transmitter (TWT) Converter	+1500, +300, ±6 vdc	70 watts
4	TV Converter	+500, +200, ±16, ±6 vdc	17 watts
5	Comp. -Sequencer Converter	±16, +6, -3 vdc	5 watts
6	Spectrophotometer Converter	+1000, -16, ±6, ±3 vdc	25 watts

<u>AC Distribution</u>			
1	Gyro Inverter	26 vac, 3 ϕ , 400 Hz	22 va
2	Main Inverter	1 ϕ , 6 KHz	*
3	Transmitter TR	+1500, +300, ±6 vdc	70 watts
4	TV TR	+500, +200, ±16, ±6 vdc	17 watts
5	Equipment TR	±20, ±16, ±6 vdc	78 watts
6	Spectrophotometer TR	+1000, -16, ±6, ±3 vdc	25 watts

*Power rating = total input power to TR units.

Table 11. Venus Orbiter No. 1 Mission, Load Power Conditioning Equipment

<u>No.</u>	<u>Unit</u>	<u>DC Distribution</u>	
		<u>output</u>	<u>Power Rating</u>
1	Gyro Inverter	26 vac, 3 ϕ , 400 Hz	22 va
2	Transmitter (Solid State) Converter	t50, ± 15 , ± 6 vdc	50 watts
3	Main Converter	± 20 , ± 16 , ± 6 vdc	94 watts
4	Comp. -Sequencer Converter	± 16 , t6, -3 vdc	5 watts
5	UV Photometer Exp. Converter	4-3000, 4-35, ± 20 , ± 10 vdc	5 watts
6	Cosmic Dust Exp. Converter	+12, -6, t 3 vdc	2 watts
<u>AC Distribution</u>			
1	Gyro Inverter	26 vac, 3 ϕ , 400 Hz	22 va
2	Main Inverter	1 ϕ , 6 KHz	*
3	Transmitter TR	4-50, ± 15 , ± 6 vdc	50 watts
4	Equipment TR	± 20 , ± 16 , ± 6 , -3 vdc	99 watts
5	UV Photometer Exp. TR	+3000, +35, ± 20 , ± 10 vdc	5 watts
6	Cosmic Dust Exp. TR	+12, -6, t 3 vdc	2 watts

*Power rating = total input power to TR units.

Table 12. Venus Orbiter No. 2 Mission, Load Power Conditioning Equipment

<u>No.</u>	<u>Unit</u>	<u>DC Distribution</u>	
		<u>output</u>	<u>Power Rating</u>
1	Gyro Inverter	26 vac, 3 ϕ , 400 Hz	22 va
2	Transmitter (TWT) Converter	+1500, +300, ± 6 vdc	70 watts
3	Main Converter	± 20 , ± 16 , ± 6 vdc	137 watts
4	Comp. -Sequencer Converter	± 16 , +6, -3 vdc	18 watts
5	TV Converter	+500, +200, ± 16 , 26 vdc	15 watts
6	Bistatic Radar Converter	+1500, ± 6 vdc	3 watts
7	Plasma Probe Exp. Converter	+165, ± 150 , t 6 vdc	5 watts
<u>AC Distribution</u>			
1	Gyro Inverter	26 vac, 3 ϕ , 400 Hz	22 va
2	Main Inverter	1 ϕ , 6 KHz	*
3	Transmitter TR	+1500, +300, ± 6 vdc	70 watts
4	Equipment TR	± 20 , ± 16 , ± 6 , -3 vdc	155 watts
5	TV TR	+500, +200, ± 16 , ± 6 vdc	15 watts
6	Bistatic Radar TR	t 1500 ± 6 vdc	3 watts
7	Plasma Probe Exp. TR	± 165 , ± 150 , +6 vdc	5 watts

* Power rating = total input power to TR units.

Table 13. Mars Orbiter Mission, Load Power Conditioning Equipment

<u>No.</u>	<u>Unit</u>	<u>DC Distribution</u>	
		<u>output</u>	<u>Power Rating</u>
1	Gyro Inverter	26 vac, 3 ϕ , 400 Hz	22 va
2	Transmitter (TWT) Converter	+1500, +300, ± 6 vdc	150 watts
3	Main Converter	± 20 , ± 16 , ± 6 vdc	181 watts
4	TV Converter	+500, +200, ± 16 , ± 6 vdc	26 watts
5	Comp. -Sequencer Converter	± 16 , t6, -3 vdc	18 watts
6	Bistatic Radar Converter	+1500, ± 6 vdc	3 watts
7	Cosmic Ray Exp. Converter	+1000, +16, t 6 vdc	10 watts
8	Plasma Probe Exp. Converter	+165, ± 150 , ± 16 , ± 6 vdc	5 watts
<u>AC Distribution</u>			
1	Gyro Inverter	26 vac, 3 ϕ , 400 Hz	22 va
2	Main Inverter	1 ϕ , 6 KHz	"
3	Transmitter TR	t 1500, +300, ± 6 vdc	150 watts
4	Equipment TR	± 20 , ± 16 , ± 6 , -3 vdc	199 watts
5	TV TR	+500, +200, ± 16 , ± 6 vdc	26 watts
6	Bistatic Radar TR	t 1500, ± 6 vdc	3 watts
7	Cosmic Ray Exp. TR	+1000, +16, t 6 vdc	10 watts
8	Plasma Probe Exp. TR	+165, ± 150 , 216, ± 6 vdc	5 watts

*Power rating = total input power to TR units.

Table 14. Jupiter Flyby Mission Load Power Conditioning Equipment

<u>DC Distribution</u>			
<u>No.</u>	<u>Unit</u>	<u>output</u>	<u>Power Rating</u>
1	Transmitter (klystron) Converter	+1500, ±6 vdc	80 watts
2	Main Converter	±20, ±16, ±6 vdc	39 watts
3	TV Converter	+500, +200, ±16, ±6 vdc	17 watts
4	Comp. -Sequencer Converter	±16, ±6, -3 vdc	5 watts
5	Plasma Probe Exp. Converter	+165, ±150, ±16, ±6 vdc	2 watts
6	Trap. Radiation Det. Exp. Conv.	+1000, ±16, ±6 vdc	2 watts
<u>AC Distribution</u>			
1	Main Inverter	10, 6 KHz	*
2	Transmitter TR	±1500, ±6 vdc	80 watts
3	Equipment TR	±20, ±16, ±6, -3 vdc	44 watts
4	TV TR	+500, +200, ±16, ±6 vdc	17 watts
5	Plasma Probe Exp. TR	+165, ±150, ±16, ±6 vdc	2 watts
6	Trap. Radiation Det. Exp. TR	+1000, ±16, ±6 vdc	2 watts

*Power rating = total input power to TR units.

Table 15. Jupiter Orbiter No. 1 Mission, Load Power Conditioning Equipment

<u>No.</u>	<u>Unit</u>	<u>DC Distribution</u>	
		<u>output</u>	<u>Power Rating</u>
1	Gyro Inverter	26 vac, 3 ϕ , 400 Hz	22 va
2	Main Converter	± 20 , ± 16 , ± 6 vdc	92 watts
3	Transmitter (TWT) Converter	+1500, +300, ± 6 vdc	35 watts
4	TV Converter	+500, +200, ± 16 , ± 6 vdc	15 watts
5	Comp. -Sequencer Converter	± 16 , +6, -3 vdc	5 watts
6	Auroral Detector Exp. Converter	+3000, ± 16 , ± 6 vdc	2 watts
7	Plasma Probe Exp. Converter	+165, ± 150 , ± 16 , ± 6 vdc	2 watts
<u>AC Distribution</u>			
1	Gyro Inverter	26 vac, 3 ϕ , 400 Hz	22 va
2	Main Inverter	1 ϕ , 6 KHz	*
3	Transmitter TR	+1500, +300, ± 6 vdc	35 watts
4	TV TR	+500, +200, ± 16 , ± 6 vdc	15 watts
5	Equipment TR	± 20 , ± 16 , ± 6 vdc	97 watts
6	Auroral Detector Exp. TR	+3000, ± 16 , ± 6 vdc	2 watts
7	Plasma Probe Exp. TR	+165, ± 150 , ± 16 , ± 6 vdc	2 watts

* Power rating = total input power to TR units.

Table 16. Jupiter Orbiter No. 2 Mission, Load Power Conditioning Equipment

<u>No.</u>	<u>Unit</u>	<u>DC Distribution</u>	
		<u>output</u>	<u>Power Rating</u>
1	Gyro Inverter	26 vac, 3 ϕ , 400 Hz	22 va
2	Transmitter (TWT) Converter	+1500, +300, \pm 6 vdc	135 watts
3	Main Converter	\pm 20, \pm 16, \pm 6 vdc	111 watts
4	Comp. -Sequencer Converter	\pm 16, +6, -3 vdc	20 watts
5	Cosmic Ray Exp. Converter	+1000, +16, \pm 6 vdc	10 watts
6	Spectrometer Exp. Converter	+3000, +200, \pm 16, \pm 6 vdc	15 watts

<u>AC Distribution</u>			
1	Gyro Inverter	26 vac, 3 ϕ , 400 Hz	22 va
2	Main Inverter	1 ϕ , 6 KHz	"
3	Transmitter TR	+1500, +300, \pm 6 vdc	135 watts
4	Equipment TR	\pm 20, \pm 16, \pm 6, -3 vdc	131 watts
5	Cosmic Ray Exp. TR	+1000, +16, \pm 6 vdc	10 watts
6	Spectrometer Exp. TR	+3000, +200, \pm 16, \pm 6 vdc	15 watts

*Power rating = total input power to TR units.

Table 17. Summary of Selected Baseline Power System Configurations

Note

- o Each configuration (combination of battery control, line regulator and array control) may be used with either AC or DC distribution.
- o Applicable array controls indicated by uncircled numbers in each cell.
- o Circled numbers in each cell designate reason for deleting certain configurations as listed in Table 18.

		LINE REGULATION					
		1	2	3	4	5	
		PWM Buck Line Reg	Diss Line Reg	Boost Line Reg	Bk-Boost Line Reg	No Reg	
BATTERY CONTROL	1	Switch t Resistor	3 (7)(9)	NA (3)	3, 4, 5 (7)(12)	3 (7)(9)	NA (2)
	2	Same + Dischg Booster	3 (7)(9)	NA (3)	3, 4 (7)(11)(12)	3 (7)(9)	NA (2)
	3	Dissipative Chg'r & Dischg. Sw.	1, 2, 3 (9)	NA (3)	2, 3, 4 (6)(10)(12)	1, 2, 3 (9)	NA (2)
		Same t Dischg. Booster	1, 2, 3 (9)	NA (3)	2, 3, 4 (6)(11)(12)	1, 2, 3 (9)	NA (2)
		PWM Buck Chg'r & Dischg. Sw.	1, 2, 3 (9)	NA (3)	2, 3, 4 (6)(10)(12)	1, 2, 3 (9)	NA (2)
	6	Same t Dischg. Booster	1, 2, 3 (9)	NA (3)	2, 3, 4 (6)(11)(12)	1, 2, 3 (9)	NA (2)
				2, 3 (5)(9)	2, 3, 4, 5 (6)(12)	1, 2, 3 (9)	NA (2)
	8	Same t Dischg. Booster	1, 2, 3 (9)	NA (4)	2, 3, 4 (6)(11)(12)	1, 2, 3 (9)	NA (2)
	9	Diss. Chg. & Boost Dischg. Regulators	NA (1)	NA (1)	NA (1)	NA (1)	3, 4, 5, 6 (8)
	10	PWM Buck Chg. & Boost Dischg. Regulators	NA (1)	NA (1)	NA (1)	NA (1)	3, 4, 5, 6 (8)

ARRAY CONTROL
1. None
2. Zener
3. Active Shunt
4. PWM Buck Series
5. PWM Buck Series t max Track Track
6. PWM Series Buck-Boost

Table 18. Justifications for Deletions of Power System Configurations

1. Not applicable. Array and battery controls provide regulated bus. Additional line regulation not required.
2. Not applicable. Required bus voltage regulation cannot be provided by these battery controls.
3. Not applicable. Power loss in line regulator with maximum voltage at unregulated bus considered excessive.
4. Not applicable. Series dissipative regulator tends to produce constant current load and eliminate possibility of undesirable load sharing.
5. Array Control 1 deleted. Unregulated bus voltage must be limited to minimize voltage drop across dissipative line regulator.
6. Array Control 1 deleted. Must limit unregulated bus voltage to prevent overvoltage at regulated bus.
7. Array Controls 1 and 2 deleted. Active regulator required by battery charge control to provide accurate voltage limit.
8. Array Controls 1 and 2 deleted. Will not provide required $\pm 1/2$ percent bus voltage regulation.
9. Array Controls 4, 5, and 6 deleted. Illogical to use two series bucking regulators in series.
10. Array Control 5 deleted. Illogical to use line regulator if solar array output well regulated. With bucking charge control, array voltage must always exceed battery voltage. Boosting required only during battery discharge and should be included in battery controls.
11. Array Control 5 deleted. Illogical to use discharge booster with maximum power tracking solar array control. Both prevent undesirable load sharing between array and battery.
12. Array Control 6 deleted. Illogical to use two boost regulators in series.

3.3 SOLAR ARRAY POWER UTILIZATION

To assess the impact of mismatch between the solar array maximum power point voltage and its operating voltages, a relatively simple computer program is used to determine the degree of matching of these voltages and also determines the critical design points for each of the candidate power systems for each of the missions. The results of these computations determine the oversizing required in the solar array for each case. Investigations of the solar array power capability as a function of mission time, and comparison of these capabilities with the load requirements as a function of mission time, clearly indicate that the critical design points occur at maximum load conditions at beginning of cruise, at encounter, or at end-of-life. The beginning of cruise and end-of-life conditions could be either at minimum or maximum Sun-spacecraft distance (AU) depending on the particular mission involved. Intermediate load conditions and solar array capabilities are always less critical than these three conditions,

The operation of the computer program is as follows. First the computer generates the current voltage characteristic of the solar array at the beginning of the mission, encounter, and end-of-life from input data which consist of an equation for the current-voltage characteristic, the appropriate short circuit current, open circuit voltage, and current and voltage at the maximum power point. Additional input data to the computer program consist of the appropriate ratio of maximum to minimum operating voltage for the solar array for the system configuration being analyzed and the power required for the given mission at these minimum and maximum voltage levels for the three discrete points in time within the mission.

The program then assumes that the power required at minimum voltage and minimum AU is just equal to the solar array capability at that condition. Starting at a given minimum voltage level the computer determines whether the solar array can support the power requirements at minimum and maximum voltages at all times in the mission. The program then gradually increases the minimum voltage in predetermined steps while maintaining the same maximum to minimum voltage ratio and maintaining the power requirement at minimum voltage and minimum AU equal

to the solar array capability at that voltage. For each step increase in minimum voltage at which all power requirements are satisfied by the solar array, the program calculates the corresponding required value of solar array power at its maximum power point.

These increases in voltage level are continued until such time as a minimum value of solar array power capability at the maximum power point is achieved. In those cases where further increases in operating voltage cause an increase in the maximum power capability of the solar array the program automatically stops. In some cases, the computer is not able to find the solution because the power required at both voltages and all AU conditions cannot be satisfied under the assumption that the minimum AU solar array capability is just adequate to support the load required at minimum voltage.

The program then repeats the operation with the constraint that the power required at maximum voltage at minimum AU is just equal to the solar array capability and again searches for the operating voltage levels that yield a minimum required capability of the solar array at its maximum power point. The program then performs a similar set of operations assuming the power requirement at minimum voltage to be equal to the solar array capability at conditions corresponding to either encounter or maximum AU as appropriate. Here again, the program shifts the operating voltage range from the given minimum value to increasingly higher values and searches for the solution wherein all power requirements are satisfied and the minimum capability of the solar array at its maximum power point is achieved.

Finally, the program performs a fourth set of computations at this second AU condition and in this case assumes the power required at maximum voltage to be just equal to the solar array capability. A fifth and sixth set of computations are performed to cover the third point in the mission in those cases where it is not obvious by inspection that the critical design point has been validly determined.

For these sets of calculations, the computer then compares the required maximum power point solar array capabilities at 1 AU for each case where solutions were found. That case which yields the lowest value of maximum power capability of the 1 AU solar array is then

identified as the critical design point for the mission. By comparing the relative solar array power capabilities at the critical design point and at the maximum power capability of the solar array at 1 AU, a factor is determined which reflects the solar array power capability that must be installed on the spacecraft in order to support a given load at the critical design point. This factor is used in subsequent calculations of the solar array size and weight required for each system configuration for the seven model spacecraft.

The results of the computer program are illustrated for the critical design point condition for each category of system in Figures 45 through 49. The resulting solar array sizing factor (**A**) is the ratio of solar array power required at 1 AU at the maximum power point, to the power required at maximum load conditions divided by the appropriate power per unit weight achievable for the particular solar array configuration at 1 AU. This factor includes a 5 percent contingency to accommodate solar cell or interconnection failures while still maintaining a high probability of successfully providing the required power output throughout the mission.

This factor, therefore, establishes the installed solar array weight per unit power at maximum load conditions. It is true that the maximum load conditions may not occur at the critical design point. The analysis, however, determines the relationships of solar array power capability to the load requirements at the several discrete points in the mission simultaneously. Thus the solar array size required to supply the maximum load condition is based on that solar array capability required to just satisfy the load at the critical design point. Obviously if the maximum load point is not at the critical design point, the solar array will have excess capability at this maximum load condition. The computer results in this case define the amount of this excess capability necessary to satisfy the power demand throughout the mission. Expressing the solar array sizing factor in terms of the maximum load condition permits application of this weight factor directly in subsequent system sizing analyses wherein maximum load conditions are used to determine the weight and size of each of the other system components.

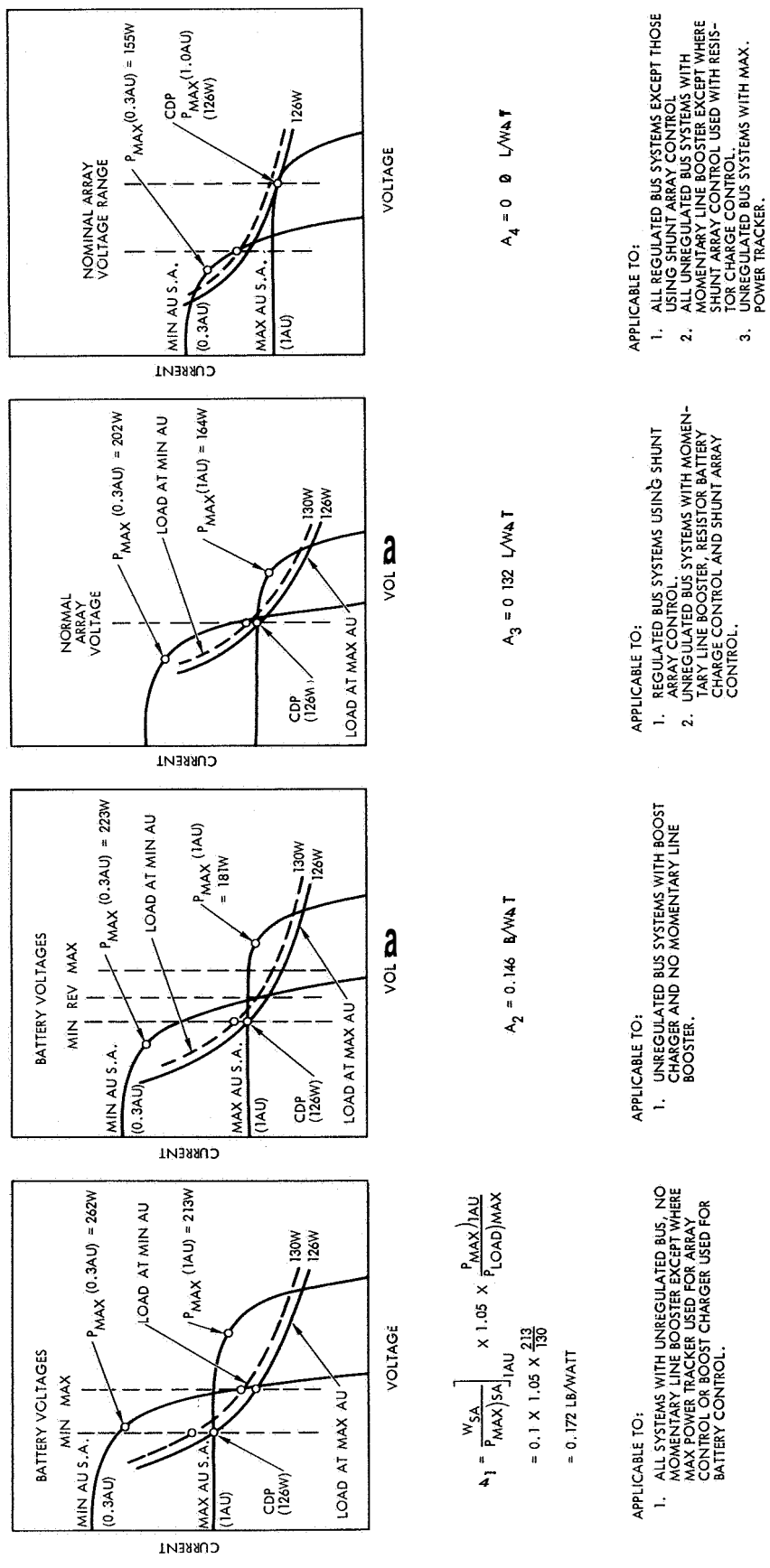
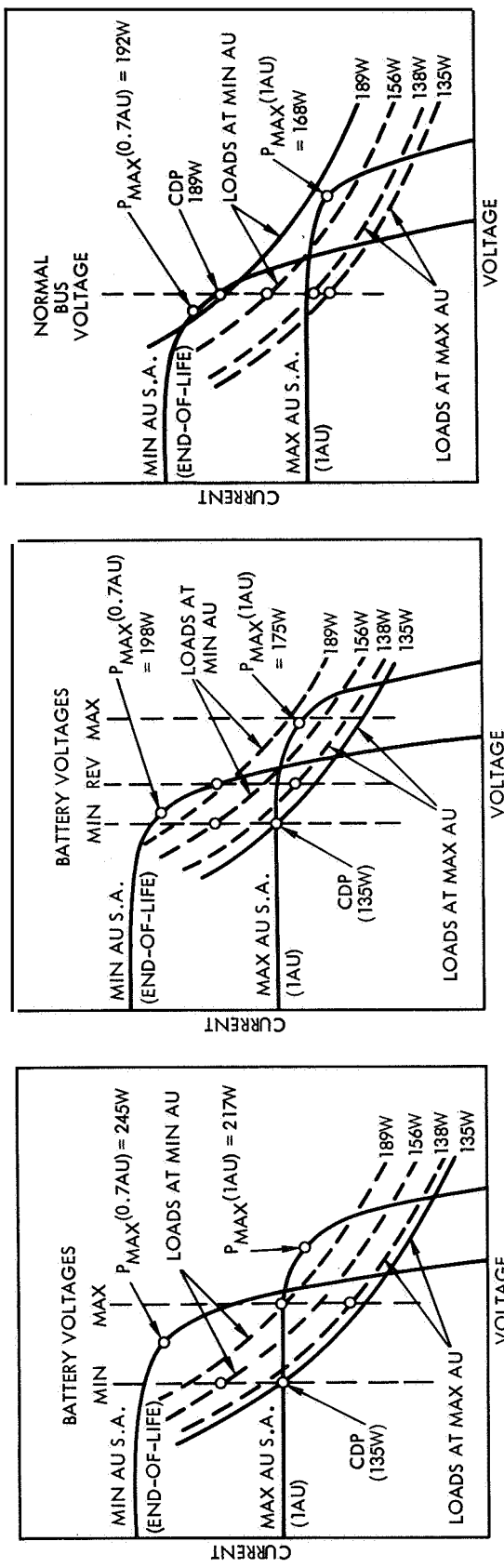


Figure 45. Solar Array Sizing Factors for Mercury Flyby Mission



$$\begin{aligned}
 \rho_1 &= \frac{W_{SA}}{P_{MAX}(SA)} \left[\frac{P_{MAX}(1AU)}{P_{LOAD}(MAX)} \right] \times 1.05 \times \frac{217}{189} \\
 &= 0.1 \times 1.05 \times \frac{217}{189} \\
 &= 0.121 \text{ LB/WATT}
 \end{aligned}$$

APPLICABLE TO:

1. ALL SYSTEM CONFIGURATIONS WITH UNREGULATED MAIN BUS AND NO MOMENTARY LINE BOOSTER EXCEPT WHERE MAX POWER TRACKER USED FOR ARRAY CONTROL OR BOOST CHARGER USED FOR BATTERY CONTROL.

$$A_2 = 0.0972 \text{ LB/WATT}$$

APPLICABLE TO:

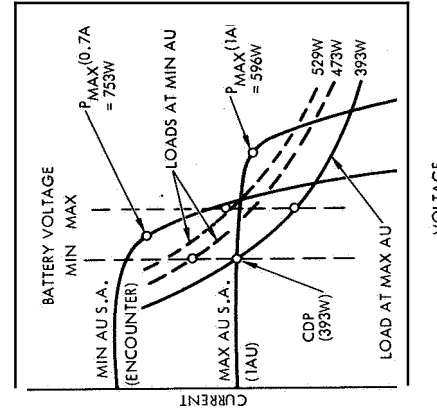
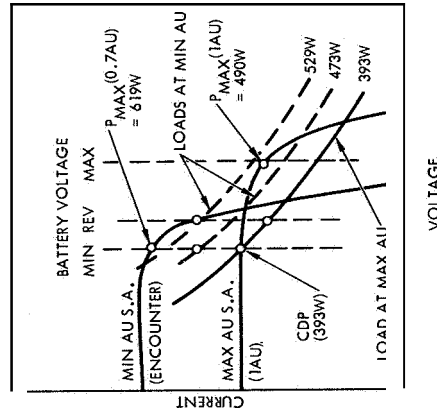
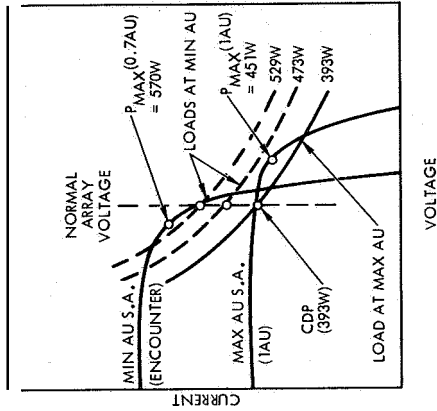
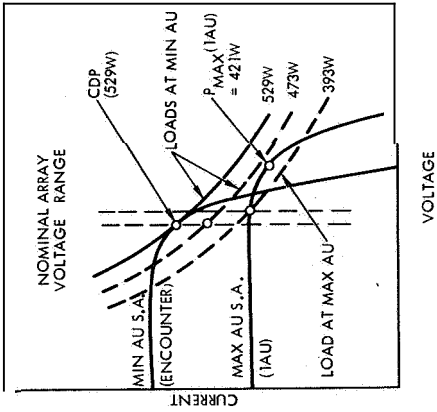
1. SYSTEM CONFIGURATIONS WITH UNREGULATED BUS, NO MOMENTARY LINE BOOSTER AND BOOST BATTERY CHARGER.

$$A_3 = 0.0935 \text{ LB/WATT}$$

APPLICABLE TO:

1. ALL SYSTEMS WITH REGULATED MAIN BUS.
2. ALL SYSTEMS WITH UNREGULATED MAIN BUS AND MOMENTARY LINE BOOSTER IN BATTERY CONTROL.
3. SYSTEMS WITH UNREGULATED MAIN BUS AND MAX POWER TRACKING ARRAY CONTROL.

Figure 46 Solar Array Utilization Factors for Venus Orbiter No 1 Mission



$$A_1 = \frac{W_{SA}}{P_{MAX SA}} \times 1.05 \times \frac{P_{MAX IAU}}{P_{LOAD MAX IAU}}$$

$$= 0.1 \times 1.05 \times \frac{596}{529}$$

$$= 0.1183 \text{ LB/WATT}$$

APPLICABLE TO:

- ALL SYSTEM CONFIGURATIONS WITH UNREGULATED MAIN BUS AND NO MOMENTARY LINE BOOSTER EXCEPT WHERE MAX POWER TRACKER USED FOR AREA CONTROL OR BOOST CHARGER (INSTR. FOR BATTERY CONTROL).

$$A_2 = 0.0973 \text{ LB/WATT}$$

APPLICABLE TO:

- SYSTEM CONFIGURATIONS WITH UNREGULATED BUS, NO MOMENTARY LINE BOOSTER AND BOOST BATTERY CHARGER.

$$A_3 = 0.0895 \text{ LB/WATT}$$

APPLICABLE TO:

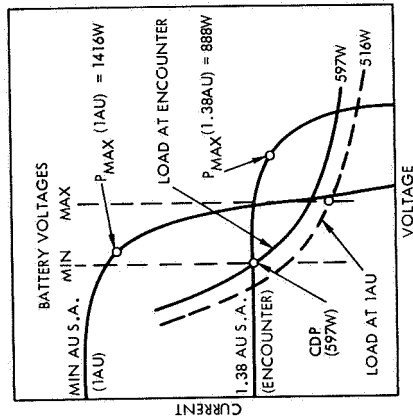
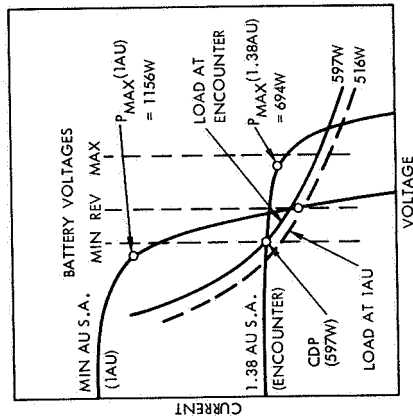
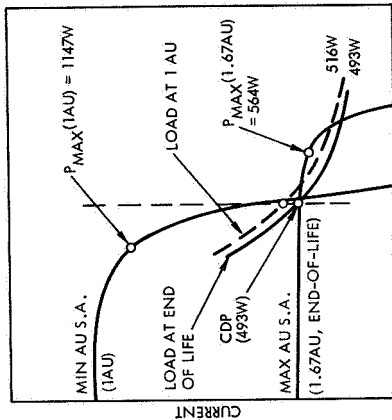
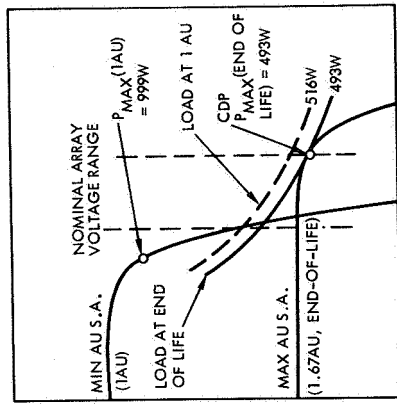
- REGULATED BUS SYSTEMS USING SHUNT ARRAY CONTROL.
- UNREGULATED BUS SYSTEMS WITH MOMENTARY LINE BOOSTER, RESISTOR BATTERY CHARGE CONTROL AND SHUNT ARRAY CONTROL.

$$A_4 = 0.0856 \text{ LB/WATT}$$

APPLICABLE TO:

- ALL SYSTEMS WITH REGULATED MAIN BUS EXCEPT THOSE USING SHUNT ARRAY CONTROL.
- ALL SYSTEMS WITH UNREGULATED MAIN BUS AND MOMENTARY LINE BOOSTER EXCEPT WHERE SHUNT ARRAY CONTROL USED WITH RESISTOR CHARGE CONTROL.
- SYSTEMS WITH UNREGULATED MAIN BUS AND MAX POWER TRACKING ARRAY CONTROL.

Figure 47. Solar Array Sizing Factors for Venus Orbiter No. 2 Mission



$A_4 = 0.337$ (BASED ON MAX LOAD AT ENCOUNTER)

$A_3 = 0.386$ (BASED ON MAX LOAD AT ENCOUNTER)

$$A_1 = \frac{W_{SA}}{P_{MAX}(SA)} \left[\frac{P_{MAX}(1AU)}{P_{LOAD}(MAX)} \right] \times 1.05 \times \frac{1416W}{597W}$$

$$= 0.189 \times 1.05 \times \frac{1416W}{597W}$$

$$= 0.470$$

$A_2 = 0.384$

APPLICABLE TO:

1. ALL SYSTEMS WITH REGULATED MAIN BUS EXCEPT THOSE USING SHUNT ARRAY CONTROL.
2. ALL SYSTEMS WITH UNREGULATED MAIN BUS AND MOMENTARY LINE BOOSTER EXCEPT WHERE SHUNT ARRAY CONTROL IS USED WITH RESISTOR CHARGE CONTROL.
3. SYSTEMS WITH UNREGULATED MAIN BUS AND MAX POWER TRACKING ARRAY CONTROL.

APPLICABLE TO:

1. REGULATED BUS SYSTEMS USING SHUNT ARRAY CONTROL.
2. UNREGULATED BUS SYSTEMS WITH MOMENTARY LINE BOOSTER, RESISTOR BATTERY CHARGE CONTROL AND SHUNT ARRAY CONTROL.

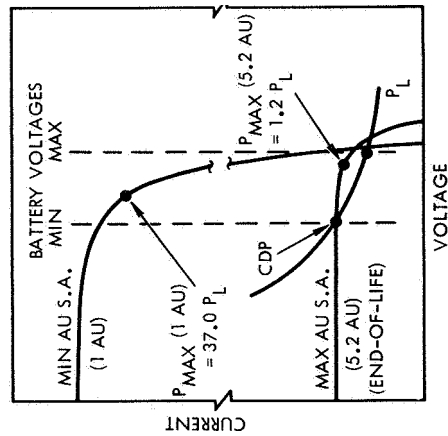
APPLICABLE TO:

1. SYSTEM CONFIGURATIONS WITH UNREGULATED BUS, NO MOMENTARY LINE BOOSTER AND BOOST BATTERY CHARGER.

APPLICABLE TO:

1. ALL SYSTEM CONFIGURATIONS WITH UNREGULATED MAIN BUS AND NO MOMENTARY LINE BOOSTER EXCEPT WHERE MAX POWER TRACKER IS USED FOR ARRAY CONTROL OR BOOST CHARGER USED FOR BATTERY CONTROL.

Figure 48. Solar Array Sizing Factors for Mars Orbiter Mission



JUPITER PROBE

$$A_1 = 3.46 \text{ (CDP = MIN BATTERY VOLTAGE AT ENCOUNTER)}$$

JUPITER ORBITER NO. 1

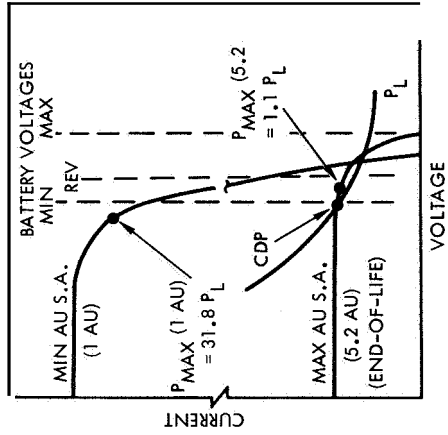
$$A_1 = 3.88 \text{ (CDP = MIN BATTERY VOLTAGE AT END-OF-LIFE)}$$

JUPITER ORBITER NO. 2

$$A_1 = 1.89 \text{ (CDP = MIN BATTERY VOLTAGE AT ENCOUNTER)}$$

APPLICABLE TO:

1. ALL SYSTEM CONFIGURATIONS WITH UNREGULATED MAIN BUS AND NO MOMENTARY LINE BOOSTER EXCEPT WHERE MAX POWER TRACKER USED FOR ARRAY CONTROL OR BOOST CHARGER USED FOR BATTERY CONTROL.



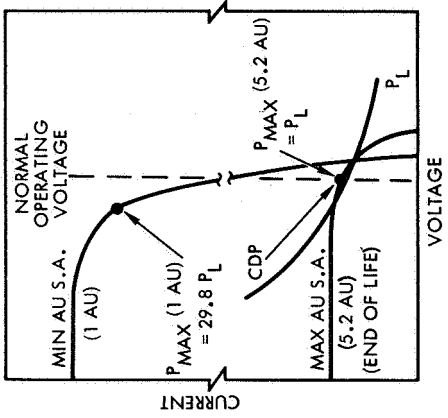
$$A_2 = 2.7 \text{ (CDP = MIN BATTERY VOLTAGE AT ENCOUNTER)}$$

$$A_2 = 2.34 \text{ (CDP = MIN BATTERY VOLTAGE AT END-OF-LIFE)}$$

$$A_2 = 1.63 \text{ (CDP = MIN BATTERY VOLTAGE AT ENCOUNTER)}$$

APPLICABLE TO:

1. SYSTEM CONFIGURATIONS WITH UNREGULATED MAIN BUS, NO MOMENTARY LINE BOOSTER AND BOOST BATTERY CHARGER.



$$A_3 = 3.12 \text{ (CDP = END-OF-LIFE)}$$

$$A_3 = 3.12 \text{ (CDP = END-OF-LIFE)}$$

$$A_3 = 1.53 \text{ (CDP = ENCOUNTER)}$$

APPLICABLE TO:

1. ALL SYSTEMS WITH REGULATED MAIN BUS
 2. ALL SYSTEMS WITH UNREGULATED MAIN BUS AND MOMENTARY LINE BOOSTER IN BATTERY CONTROL.
- ≡ SYSTEMS WITH UNREGULATED MAIN BUS AND MAX POWER TRACKING ARRAY CONTROL

Figure 9 Solar Array Sizing Factors for Jupiter Missions

4. METHODS OF IMPROVING SYSTEM RELIABILITY

4.1 PREFERRED METHODS OF IMPLEMENTING REDUNDANCY

There are four basic approaches to implementing redundancy for each power system unit: parallel, standby, quad, and majority voting. The reliability equations and basic configuration for each are described in the following paragraphs.

Since each part of a nonredundant unit has its own failure rate, the general equation for the probability of survival is:

$$P_S = e^{-At}$$

where

P_S = probability of survival or reliability

A = the summation of the failure rates for all parts

t = total operating time required.

Figure 50 shows a basic system configuration of "N" elements in series. The equation for the probability of survival of the system is

$$P_S = P_1 \times P_2 \times \dots \times P_n$$

where

$P_1 \rightarrow P_n$ are the reliabilities of each element.

Figure 51 shows a parallel redundant system comprised of two groups of 1 through "N" series elements. Each of the two parallel groups is completely independent and either one can perform the required function.

The probability of survival is:

$$P_S = 1 - [(1 - P_A)(1 - P_B)]$$

where

P_A and P_B are the survival probabilities of the independent strings.

Parallel operating channels have limited usage because there are some failure mode conditions which they cannot correct. For example, one of the two parallel channels could fail in a manner which causes its common output voltage to go above limits.

In the standby redundant configuration of Figure 52, there are two parallel channels, but only one is operating at any time. This configuration requires additional circuitry to sense a failure in the operating channel and a switching element to transfer to the standby elements in case of a primary element failure.

The equation for probability of survival is:

$$P_S = 1 - \left[(1 - P_1 P_{SW})(1 - P_2 P_{SW}) \right]$$

where

P_1 and P_2 are the reliabilities of the independent channels, and

P_{SW} = the reliability of the failure sensing and switching elements.

Standby redundancy is generally used for power circuits since it does not cause a significant loss in efficiency.

Quad redundancy is normally implemented at the part level and is illustrated in Figure 53. Either string can perform the required function. The reliability of this configuration is:

$$P_S = 1 - (1 - P_1^2)^2$$

where

P_1 = the reliability of a single part.

The quad configuration is normally not used for series power handling circuits because of its poor efficiency.

Figure 54 shows a block diagram of a majority voting configuration. Two out of the three elements must be operative in order to perform the required function. The probability of survival is:

$$P_S = 1 - \left[(1 - P_1 P_2)(1 - P_2 P_3)(1 - P_1 P_3) \right]$$

where

P_1 , P_2 , and P_3 are the reliabilities of each element.

In most cases $P_1 = P_2 = P_3$, therefore

$$P_S = 1 - (1 - P_1)^3$$

Majority voting redundancy is generally applied to low-power sensing circuits.

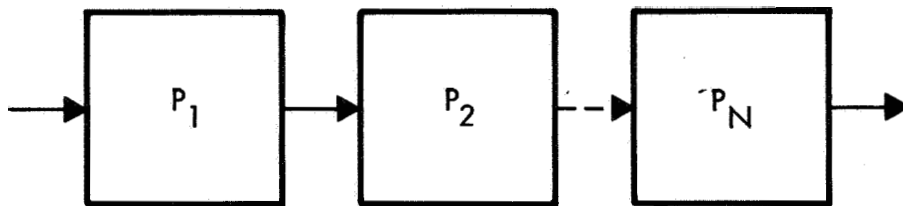


Figure 50. Basic System Reliability Model

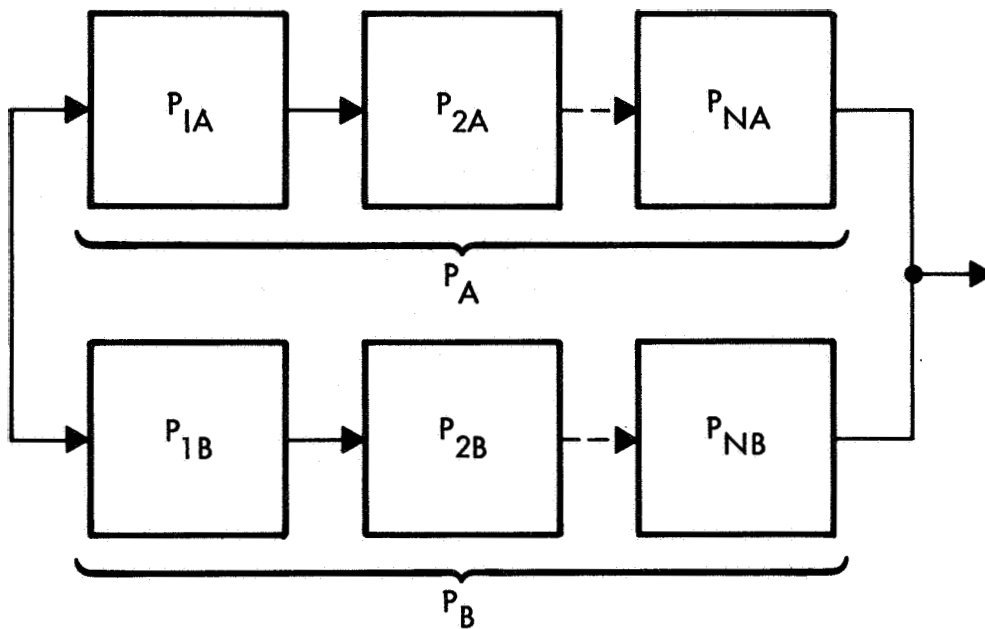


Figure 51. Parallel Redundant System Reliability Model

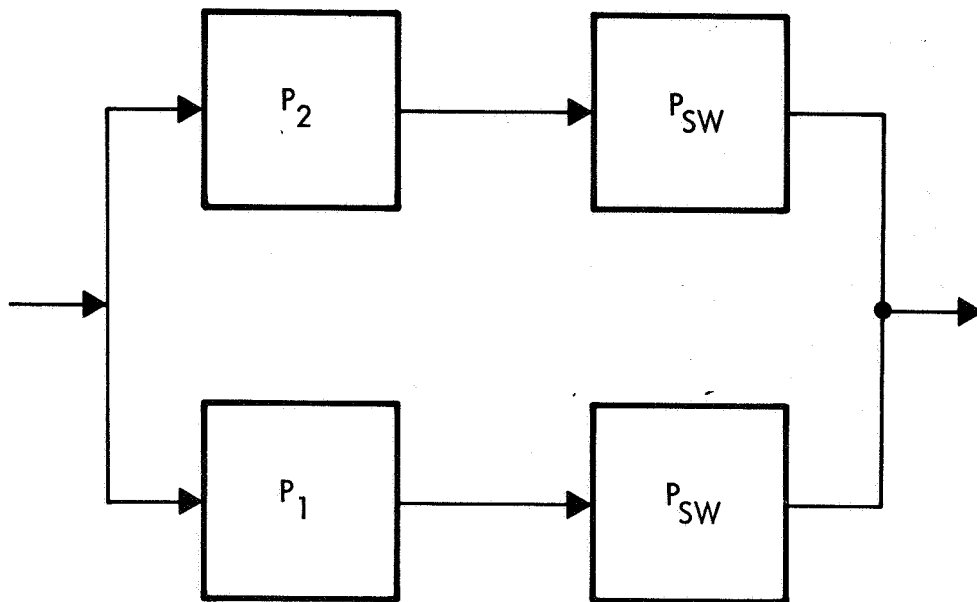


Figure 52. Standby Redundant System Reliability Model

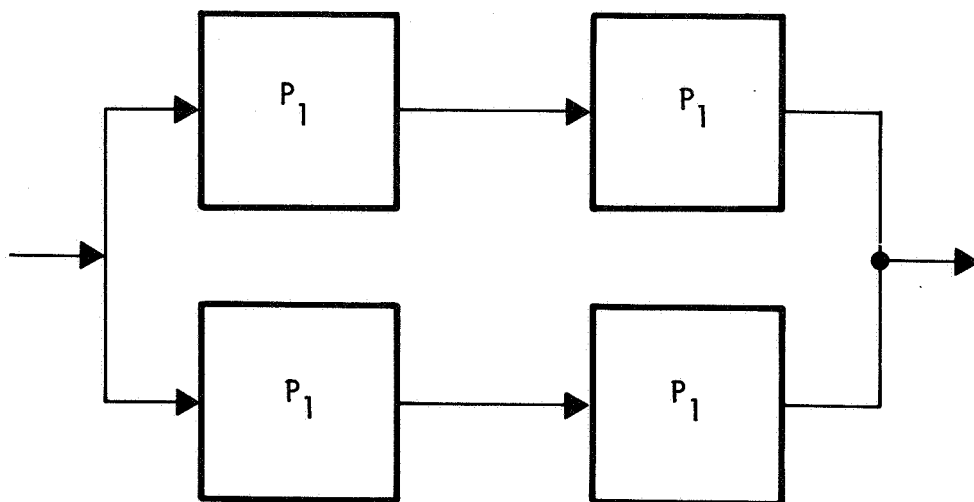


Figure 53. Quad Redundant System Reliability Model

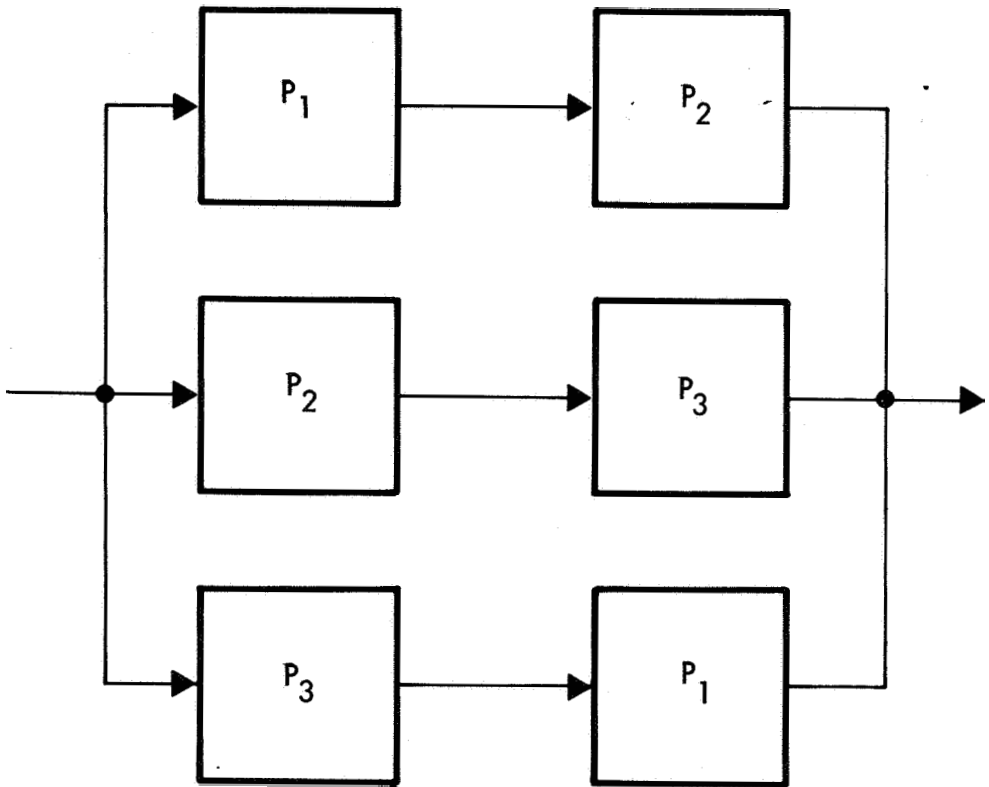


Figure 54. Majority Voting System Reliability Model

4.2 SELECTED REDUNDANT CONFIGURATIONS AND PART COUNTS

The power systems are divided into the following units, each of which may have many design configurations:

- o Solar array
- o Array contr'ol
- o Battery control
 - a Battery
 - a Line regulator
- o Load power conditioning units (ac or dc distribution)

4.2.1 Solar Array

The solar array configuration is the same for either a baseline system or a redundant system and includes a 5 percent design margin and multiple parallel interconnections of series strings of cells to minimize the effects of cell or connection open circuit failures on the output power of the array.

4.2.2 Array Controls

Five specific array control designs have been considered:

- o Zener diode shunt
- Active dissipative shunt
- o Pulsewidth modulated series bucking regulator
- o Pulsewidth modulated series bucking regulator with maximum power tracking
- o Pulsewidth modulated series buck-boost regulator.

The zener diode voltage limiter design is the same for the baseline and redundant configurations and uses multiple parallel shunt circuits, each controlling a parallel section of the array. If a diode shorts, the solar power will be degraded by $1/N$ where N is the number of parallel zener diodes. Series diodes between the zener diode connection and the common solar array bus prevent current flow through a shorted zener diode from the other parallel array sections. If a zener diode opens, the remaining diodes will limit total array voltage.

The active shunt redundant design uses the majority voting configuration for the voltage sensing and error amplifying stages as illustrated in Figure 55, and uses the quad part configuration for the power transistors and output filter. Figure 55a shows that the nonredundant configuration of the voltage sensing and error amplifier is composed of a voltage divider that reduces the magnitude of the sensed voltage to a level comparable to the reference, a precision voltage reference, a summing point, and an error amplifier stage. The redundant majority voting block diagram is illustrated in Figure 55b. It has three nonredundant parallel channels plus three AND gates and an OR gate. Each AND gate receives two amplified signals and if they are correct the signal is obtained.

The pulsewidth modulated series bucking regulator uses a switching series transistor that controls the power from the solar array to the spacecraft loads. The quad component configuration is not used for this series switch since it would cause a significant decrease in system efficiency. Parallel operating regulators cannot be used because if a switching transistor shorts, the full solar array voltage will appear on the output and the other parallel regulator could not control for this condition. Therefore the standby redundant configuration is used and if a failure occurs, the failed regulator is switched out and the standby regulator is energized to control the array output. Similarly, standby redundancy is used for the maximum power tracking and buck-boost array control. The parts count for baseline and redundant configurations of each array control are shown in Tables 19 and 20.

4.2.3 Battery Controls

Standby redundancy cannot be used for these controls because of the extreme difficulty in sensing a failure or out-of-tolerance condition over the wide range of charge and discharge operating conditions. Instead, majority voting redundancy is used for the low level signals and logic and part redundancy is used for the power circuits. The selected methods of implementing part redundancy are shown in Figure 56.

Tables 21 and 22 list the battery control parts counts for the non-redundant and redundant designs of each type of battery charger and its associated controls.

4.2.4 Battery

Two redundant configurations have been selected for analysis. The first of these consists of two parallel batteries, each containing 20 AgCd cells (or 15 AgZn cells) and each capable of satisfying the total energy storage requirement. Each battery is used with its own control circuitry which may be either baseline or redundant. The second redundant battery configuration consists of three batteries in a majority voting configuration with each containing only three series cells and each connected to the main power bus through a bucking charge regulator and a boosting discharge regulator! This approach is only applied to those systems which are configured with a regulated main bus. Each of the three batteries has an installed capacity equal to one-half that of the baseline battery capacity., The principal advantage of this second redundant battery configuration is the reduction in number of series connected cells per battery and the attendant improvement in the battery reliability. A second advantage is the reduced total battery weight (150 percent of baseline) in comparison to the first redundant approach (200 percent of baseline). The charge and discharge regulators may be either baseline or redundant.

4.2.5 Line Regulators

The following designs were selected for the line regulators:

- Pulsewidth modulated series bucking regulator
- Series dissipative
- Pulsewidth modulated boost regulator
- Pulsewidth modulated buck-boost regulator.

Because of the requirement to minimize weight and losses, standby redundancy configurations are used for the line regulators.

Tables 23 and 24 are the part counts for the baseline and redundant configurations of each line regulator.

† This configuration represents one method of applying the TRW Modular Energy Storage and Control concept (MESAC). This concept has been developed and tested under a company-sponsored research program.

4.2.6 Load Power Conditioner

The components used for load power conditioning have been analyzed with respect to the load requirements of each model spacecraft to define specific equipment groupings and performance requirements. The equipment for those systems using dc power distribution are as follows:

- 3 ϕ 400 Hz gyro inverter
- Central converter (dc to dc)
- Transmitter converter (high or low voltage)
- Computer – sequencer converter (low voltage)
- Television converter (high voltage)
- Experiment converter (low voltage)
- Experiment converter (high voltage)

The equipment selected for systems using ac power distribution are as follows:

- o 3 ϕ 400 Hz gyro inverter
- o Main central inverter (dc to ac)
- o Transmitter transformer-rectifier (TR) (high voltage or low voltage)
- o Equipment TR
- o Television TR – high voltage output
- e Experiment TR – low voltage output
- e Experiment TR – high voltage output

A distinction is being made between high voltage outputs and low voltage outputs. At high voltage, the transformer designs are heavier because of increased insulation requirements and the output filter capacitors are larger.

Each spacecraft will have its own set of equipment because of the variation in the equipment and the experiments to be performed. Standby redundancy has been selected for all the load power conditioning equipment.

Tables 25 through 52 list the parts counts for the power conditioning equipment for all missions.

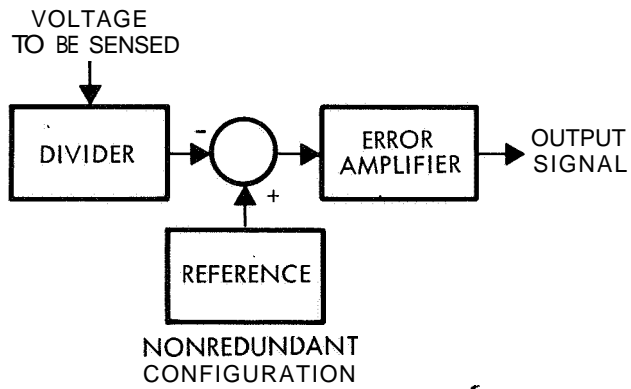


Figure 55a. Nonredundant Voltage Sensing and Error Amplifier Block Diagram

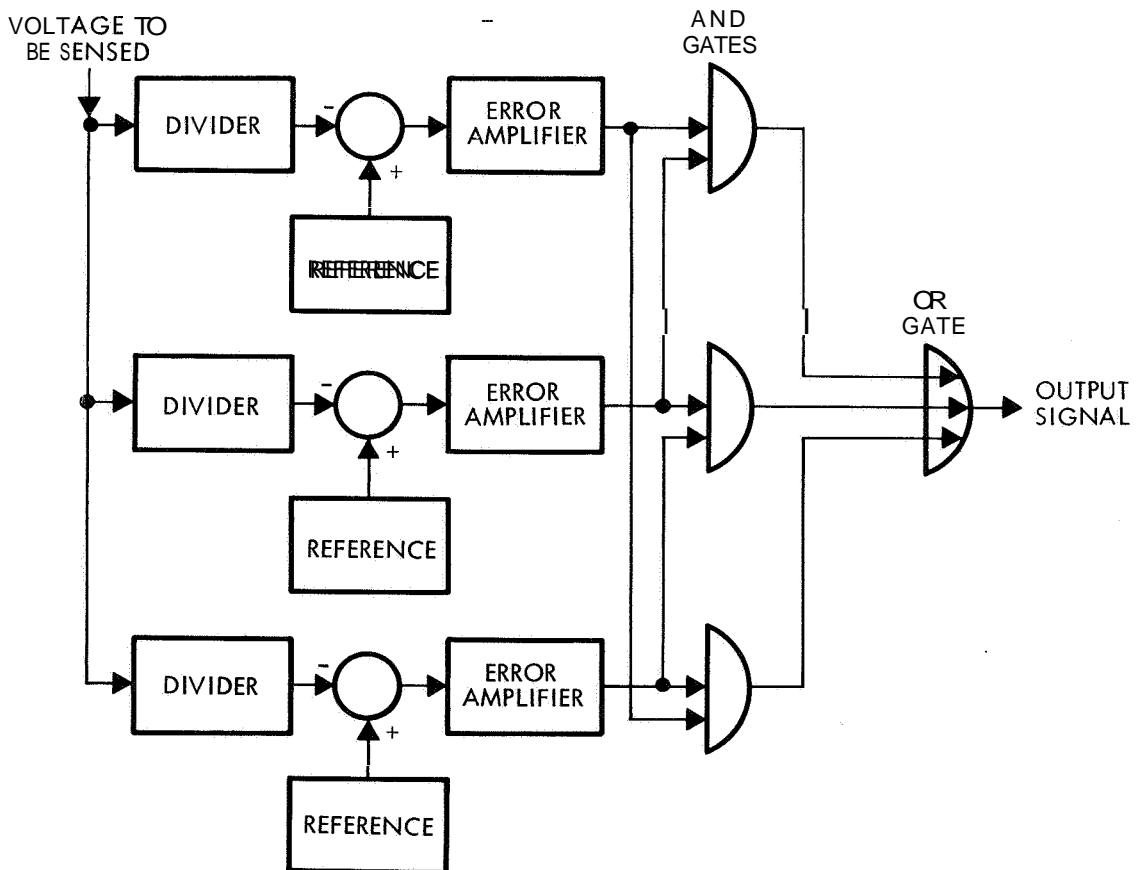


Figure 55b. Majority Voting Redundant Configuration of Voltage Sensing and Error Amplifier

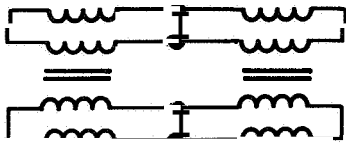
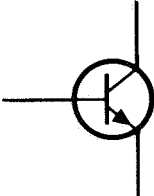
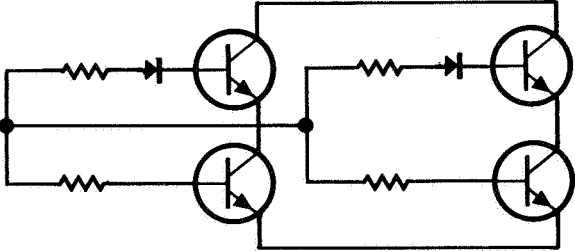
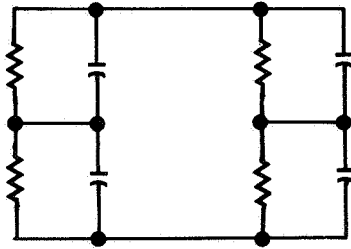
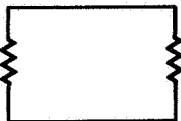
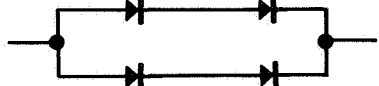
COMPONENT	REDUNDANT COMPONENT
a) MAGNETIC 	 <p data-bbox="756 655 1108 704">INSULATE BETWEEN PRIMARY AND SECONDARY</p>
b) TRANSISTOR 	
c) CAPACITOR 	
d) RESISTORS 	
e) DIODES 	

Figure 56. Methods of Implementing Part Redundancy

Table 19. Baseline Parts Count, Array Control

Unit	Resistors			Diodes			Capacitors			Transistor		Magnetics			Relays		Other/ Comments
	Carbon Composition	Metal Film	Wire Power	General- Purpose	Rectifiers	Zener	Ceramic	Tantalum Foil	Tantalum Solid	< 1 W	> 1 W	Transformers	Chokes	Mag-Amps	General 4 Sets	Latching 2 Coil	
Zener Diodes						15											
Active Shunt		13	4			1	1	3		4	3						
PWM Buck		21	4	13	1	2	2	3		6	2	3	2	1			
PWM Buck Maximum Power Tracker		40	4	1 ^a	1	4	3	4		16	2	6	2	1			
PWM Buck-Boost		21	3	13	1	2	1	3		6	2	4	1	1			

Table 20. Redundant Parts Count, Array Control

Unit	Resistors			Diodes		Capacitors			Transistor		Magnetics			Relays		Other/ Comments	
	Carbon Composition	Metal Film	Wire Power	General- Purpose	Rectifiers	Zener	Ceramic	Tantalum Foil	Tantalum Solid	< 1 W	> 1 W	Transformers	Chokes	Mag-Amps	General		Latching 2 Coil
Zener Diodes						15											
Active Shunt (Power Elements)			4		3			3									
Active Shunt (Controls)	15					1	2			6							Quad parts
PWM Buck	47		4	17	1	4	2	3	2	16	2	3	2	1		1	Majority voting
PWM Buck Maximum Power Tracker	66		4	20	1	6	3	3	6	26	2	6	2	1		1	Standby
PWM Buck-Boost	47		3	11	1	4	1	3	2	16	2	4	1	1		1	Standby

NOTE: Quantities shown are for each element of the applicable redundant configuration
 (i. e., total quantity per unit = number shown x 4 for quad, x 3 for majority voting
 and x 2 for standby redundancy).

Table 21. Baseline Parts Count, Battery Controls

Uni	Resistors			Diodes			Capacitors			Tran-sistor		Magnetics			Relays		Other/Comments		
	Carbon Comp.	Metal Film	Wire Power	General Purpose	Rectifiers	Zener	Ceramic	Tantalum Foil	Tantalum Solid	<1W	>1W	Transformers	Chokes	Mag-Amps	General 4 Sets	Latching 2 Coil			
Buck - Resistor		41	2	6	1	3			3	20						2		Used with systems having unregulated main bus	
Buck Resistor & Line Booster		69	2	8	4	4	1	1	6	31	2	3	2	1		2			
Buck Diss. Charger		49	1	4	1	4			2	23	2					1			
Buck Diss. Charger & Line Booster		77	1	6	4	5	2	1	5	34	4	3	2	1		1			
PWM Buck Charger		49	2	4	2	2	1	1	3	23	2					1			
PWM Buck Charger & Line Booster		77	2	6	5	3	2	2	6	34	4	3	4	1		1			
PWM Buck-Boost Charger		65	2	6	1	4	1	2	6	20	1	1	1	1		1			
PWM Buck-Boost Charger & Line Booster		92	4	8	5	5	1	4	8	32	3	2	3	2					
Diss. Regulator		13	5			1	1	2		4	3								Used with systems having regulated main bus
PWM Buck Regulator		21	4	13	1	2	2	2		6	2	2	2	1					

Table 22 Redundant Parts Count, Battery Controls

Unit	Resistors			Diodes		Capacitors			Transformer		Magnets		Relays		Other/Comments		
	Carbon Comp.	Metal Film	Wire Power	General Purpose	Rectifiers	Zener	Ceramic	Tantalum Foil	Tantalum Solid	<1W	>1W	Transformers	Chokes	Mag-Amps		General 4 Sets	Latching 2 Coil
Buck Resistor		44	2	6	1	3			3			3	2	1		2	Quad Comp. Majority Voting
Buck Resistor & Line Booster		4	2	4	1	4	1	1	6							2	Quad Comp. Majority Voting
Buck Diss. Charger		4	1	8	1	4	1	1	2							1	Quad Comp. Majority Voting
Buck Diss. Charger & Line Booster		45	1	4	4	4	1	1	5			3	2	1		1	Quad Comp. Majority Voting
PWM Buck Charger		6	2	2	2	5	1	1	3							1	Quad Comp. Majority Voting
PWM Buck Charger & Line Booster		45	2	2	2	2	2	1	3			3	2	1		1	Quad Comp. Majority Voting
PWM Buck-Boost Charger		71	2	6	9	3	3	1	6			1	1	1		1	Quad Comp. Majority Voting
PWM Buck-Boost Charger & Line Booster		65	2	4	6	4	1	2	6			2	3	2		1	Quad Comp. Majority Voting
PWM Buck-Boost Charger & Line Booster		90	4	8	5	5	1	4	8			2	3	2		1	Quad Comp. Majority Voting
Diss. Regulator		13	5	4	1	2	1	2									Quad Comp. Majority Voting
PWM Buck Regulator		2	4	4	1	2	1	2				2	2	1			Quad Comp. Majority Voting
		19		9	2		1										Quad Comp. Majority Voting

Note: Quantities listed are for each element of the applicable redundant configuration (i.e., total quantity per unit = number shown x 4 for quad and x 3 for majority voting redundancy).

Table 23. Baseline Parts Count, Line Regulators

Unit	Resistors				Diodes			Capacitors			Transistor		Magnetics			Relays		Other/Comments
	Carbon Comp.	Metal Film	Wire Power	General Purpose	Rectifiers	Zener	Ceramic	Tantalum Foil	Tantalum Solid	<1W	>1W	Transformers	Chokes	Mag-Amps	General 4 Sets	Latching 2 Coil		
PWM Buck		21	4	13	1	2	2	Z		6	2	2	2	1				
Diss. Series		13	5			1	1	Z		4	3							
Boost		16	2	6	3	2	2	Z		6	2	3	2	1				
Buck-Boost		21	3	13	1	2	2	Z		6	1	3	1	1				
																		Spec Note

Note: Boost line regulator also applicable to boost discharge regulator for battery in regulated lens systems

Table 24. Redundant Parts Count, Line Regulators

Unit	Resistors			Diodes			Capacitors			Transistor		Magnetics			Relays		Other/Comments
	Carbon Comp.	Metal Film	Wire Power	General Purpose	Rectifiers	Zener	Ceramic	Tantalum Foil	Tantalum Solid	<1W	>1W	Transformers	Chokes	Mag-Amps	General 4 Sets	Latching 2 Coil	
PWM Buck		47	4	17	1	4	2	Z	Z	16	2	2	2	1		1	Standby
Diss. Reg.		39	5	4		3	1	Z	Z	14	3					1	Standby
Boost		42	2	10	3	4	2	Z	Z	16	2	3	2	1		1	Standby
Buck-Boost		47	3	17	1	4	2	Z	Z	16	1	3	1	1		1	Standby

Note: Quantities listed must be doubled to determine total unit parts count.

Boost line regulator also applicable to boost discharge regulator for battery in regulated bus systems.

Table 25. Load Power Conditioning Equipment, Baseline Parts Count, Mercury Flyby, AC Distribution System

Unit	Resistors			Diodes			Capacitors				Transistors		Magnetics			Relays		Other / Comments
	Carbon Compound	Metal Film	Wire Power	General Purpose	Rectifiers	Zener	Ceramic	Tantalum Foil	Tantalum Solid	Plastic	< 1W	> 1W	Transformers	Chokes	Mag-Amps	General 4 Sets	Latching 2 Coil	
Gyro Inverter 3 ϕ (400~)		38	9	6	6		14	1	3		9	6	6	1				
Main Inverter		5		4			2	1			2	2	4	1				
Transmitter TR (HV)					8				2	2			1					
Equipment TR (LV)					14			2	5				1					
TV TR HV					12				4	2			1					
Experiment TR (LV)																		
Experiment TR (HV)				12					5	1			1					

Table 26. Load Power Conditioning Equipment, Redundant Parts Count, Mercury Flyby, AC Distribution System

Unit	Resistors			Diodes			Capacitors				Transistors		Magnetics			Relays		Other/Comments	
	Carbon Compound	Metal Film	Wire Power	General Purpose	Rectifiers	Zener	Ceramic	Tantalum Foil	Tantalum Solid	Plastic	<1W	>1W	Transformers	Chokes	Mag-Amps	General 4 Sets	Latching 2 Coil		
Gyro Inverter 3 ϕ (400~)		54	6	21	6	1	14	1	10		13	6	6	1			5		Standby ↔ Standby
Main Inverter		10		10		1	2	1	2		5	2	4	1			2		
Transmitter TR (HV)		15		6	8	1			4	2	3		1				1		
Equipment TR (LV)		19		6	14	1		2	7		3		1				1		
TV TR (HV)		18		6	12	1			6	2	3		1				1		
Experiment TR (LV)																			
Experiment TR (HV)		18		6	12	1			7	1	3		1						

Note: Parts count listed for one of two identical standby redundant channels in each unit.

Table 27. Load Power Conditioning Equipment, Baseline Parts Count, Mercury Flyby, DC Distribution System

Unit	Resistors			Diodes			Capacitors				Transistors		Magnetics			Relays		Other/Comments
	Carbon Compound	Metal Film	Wire Power	General Purpose	Rectifiers	Zener	Ceramic	Tantalum Foil	Tantalum Solid	Plastic	<1W	>1W	Transformers	Chokes	Mag-Amps	General 4 Sets	Latching 2 Coil	
Transmitter Converter (HV)	6			4	8		2	1	3	2	2	2	4	1				
Gyro Inverter 3 ϕ (400~)	38	6	6	6	6	14	2	1	3		9	6	6	1				
Main Converter (LV)	6	6		4	12	2	2	1	6		2	2	4	1				
TV Converter (HV)	6	6		4	12	2	2	1	4	2	2	2	4	1				
Computer and Sequencer Converter (LV)	6	6		4	8	2	2	1	4		2	2	4	1				
Experiment Converter (HV)	6			4	12	2	2	1	5	1	2	2	4	1				
Experiment Converter (LV)				Not Required														

Table 28. Load Power Conditioning Equipment, Redundant Parts Count, Mercury Flyby, DC Distribution System

Unit	Resistors			Diodes				Capacitors				Transistors		Magnetics			Relays		Other / Comments
	Carbon Compound	Metal Film	Wire Power	General Purpose	Rectifiers	Zener	Ceramic	Tantalum Foil	Tantalum Solid	Plastic	< 1W	> 1W	Transformers	Chokes	Mag-Amps	General 4 Sets	Latching 2 Coil		
Transmitter Converter (HV)	21			10	8	1	2	1	5	2	5	2	4	1			1	Standby	
Gyro Inverter 3 ϕ (400~)	54	0		21	6	1	14	1	10		13	6	6	1			5	Standby	
Main Converter (LV)	21			10	12	1	2	1	8		5	2	4	1			1	Standby	
TV Converter (HV)	21			10	12	1	2	1	6	2	5	2	4	1			1	Standby	
Computer and Sequencer Converter (LV)	21			10	8	1	2	1	6		5	2	4	1			1	Standby	
Experiment Converter (HV)	21			10	12	1	2	1	7	1	5	2	4	1			1	Standby	
Experiment Converter (LV)							NOT REQUIRED												

Note: Parts count listed for one of two identical redundant channels in each unit.

Table 29. Load Power Conditioning Equipment, Baseline Parts Count,
Venus Orbiter No. 1, AC Distribution System

Unit	Resistors			Diodes		Capacitors			Transistor			Magnetics			Relays		Other/ Comments	
	Carbon Comp.	Metal Film	Wire Power	General Purpose	Rectifiers	Zener	Ceramic	Tantalum Foil	Tantalum Solid	Plastic	<1W	>1W	Transformers	Chokes	Mag-Amps	General 4 Sets		Latching 2 Coil
Gyro Inverter		38	6	6	6		14	1	3		9	6	6	1				
Main Inverter		5		4			2	1			2	2	4	1				
Transmitter TR (LV)					12				6				1					
Equipment TR (LV)					14				7				1					
T.V. TR (HV)																		
Experiment TR (LV)					6				3				1					
Experiment TR (HV)					12				3	3			1					

Table 30. Load Power Conditioning Equipment, Redundant Parts Count, Venus Orbiter No. 1, AC Distribution System

Unit	Resistors			Diodes			Capacitors			Transistor			Magnetics			Relays		Other/ Comments
	Carbon Comp.	Metal Film	Wire Power	General Purpose	Rectifiers	Zener	Ceramic	Tantalum Foil	Tantalum Solid	Plastic	<1W	>1W	Transformers	Chokes	Mag-Amps	General 4 Sets	Latching 2 Coil	
Gyro Inverter		54	6	21	6	1	14	1	10		13	6	9	1			5	Standby ←————→
Main Inverter		10		10		1	2	1	2		5	2	4	1			2	
Transmitter TR (LV)		15		6	12	1			8		3		1				1	
Equipment TR (LV)		16		6	14	1			9		3		1				1	
T. V. TR (HV)		NOT REQUIRED																
Experiment TR (LV)		12		6	6	1			5		3		1				1	
Experiment TR (HV)		20		6	12	1			5	3	3		1				1	Standby

Note: Parts count listed for one of two identical standby redundant channels in each unit.

Table 31. Load Power Conditioning Equipment, Baseline Parts Count, Venus Orbiter No. 1, DC Distribution System

Unit	Resistors				Diodes				Capacitors				Transistor			Magnetics			Relays		Other/Comments
	Carbon Comp.	Metal Film	Wire Power	General Purpose	Rectifiers	Zener	Ceramic	Tantalum Foil	Tantalum Solid	Plastic	<1W	>1W	Transformers	Chokes	Mag-Amps	General 4 Sets	atching 2 Coil				
Transmitter Converter (LV)	6		4	12		2	1	6			2	2	4	1							
Gyro Inverter	38	6	6	6	14	1	1	3		9	6	6	6	1							
Main Converter (LV)	6		4	12	2	1	1	6		2	2	4	4	1							
TV Converter (HV)	NOT REQUIRED																				
Computer-Sequencer Converter (LV)	6		4	8	2	1	1	4		2	2	4	4	1							
Experiment Converter (HV)	6		4	12	2	1	1	3	3	2	2	4	4	1							
Experiment Converter (LV)	6		4	6	2	1	1	3		2	2	4	4	1							

Table 32. Load Power Conditioning Equipment, Redundant Parts Count, Venus Orbiter No. 1, DC Distribution System

Unit	Resistors				Diodes			Capacitors			Transistor			Magnetics			Relays		Other/Comments
	Carbon Comp.	Metal Film	Wire Power	General Purpose	Rectifiers	Zener	Ceramic	Tantalum Foil	Tantalum Solid	Plastic	<1W	>1W	Transformers	Chokes	Mag-Amps	General 4 Sets	Latching 2 Coil		
Transmitter Converter (LV)		21		10	12	1	2	1	3		5	2	4	0			1	1	Standby
Gyro Inverter		54	6	21	6	1	14	0	5		13	6	6	1			5		
Main Converter (LV)		21		10	12	1	2	0	3		5	2	4	1			1		
TV Converter (HV)	NOT REQUIRED																		
Computer-Sequencer Converter (LV)		19		10	8	0	2	1	6		5	2	4	1			0		
Experiment Converter (HV)		24		10	02	1	2	0	5	3	5	2	4	1			0		
Experiment Converter (LV)		18		10	6	1	2	0	5		5	2	4	1			1		Standby

Note: Parts count listed for one of two identical standby redundant channels in each unit.

Table 33. Load Power Conditioning Equipment, Baseline Parts Count, Venus Orbiter No. 2, AC Distribution System

Unit	Resistors			Diodes			Capacitors				Transistors		Magnetics			Relays		Other / Comments
	Carbon Compound	Metal Film	Wire Power	General Purpose	Rectifiers	Zener	Ceramic	Tantalum Foil	Tantalum Solid	Plastic	< 1W	> 1W	Transformers	Chokes	Mag-Amps	General 4 Sets	Latching 2 Coil	
Gyro Inverter 3 ϕ (400~)		38	6	6	6		14	1	3		9	6	6	1				
Main Inverter		5		4		2		1			2	2	4	1				
Transmitter TR (HV)					8				2	2			1					
Equipment TR (LV)				14				2	5				1					
TV TR (HV)				12					4	2			1					
Experiment TR (LV)				8				3	1				1					
Experiment TR (XV)				6					2	1			1					

Table 34. Load Power Conditioning Equipment, Redundant Parts Count, Venus Orbiter No. 2, AC Distribution System

Unit	Resistors			Diodes			Capacitors			Transistors		Magnetics			Relays		Other/Comments	
	Carbon Compound	Metal Film	Wire Power	General Purpose	Rectifiers	Zener	Ceramic	Tantalum Foil	Tantalum Solid	Plastic	V IM	V IM	Transformers	Chokes	Mag-Amps	General 4 Sets		Latching 2 Coil
Gyro Inverter 3 ϕ (400~)		54	6	21	6	1	14	1	10		13	6	6	1			5	Standby
Main Inverter		10		10		1	2	1	2		5	2	4	1			2	
Transmitter TR (HV)		15		6	8	1		4	2		3		1				1	
Equipment TR (LV)		19		6	14	1		7			3		1				1	
TV TR (HV)		18		6	12	1		6	2		3		1				1	
Experiment TR (LV)		16		6	8	1		3	3		3		1				1	
Experiment TR (HV)		15		6	6	1		4	1		3		1				1	Standby

Note: Parts count listed for one of two identical standby redundant channels in each unit.

Table 35. Load Power Conditioning Equipment, Baseline Parts Count, Venus Orbiter No. 2, DC Distribution System

Unit	Resistors			Diodes			Capacitors				Transistors		Magnetics			Relays		Other / Comments
	Carbon Compound	Metal Film	Wire Power	General Purpose	Rectifiers	Zener	Ceramic	Tantalum Foil	Tantalum Solid	Plastic	< 1W	> 1W	Transformers	Chokes	Mag-Amps	General 4 Sets	Latching 2 Coil	
Emitter Converter (XV)		6		4	8		2	1	3	2	2	2	4	1				
Gyro Inverter 3 ϕ (400V)		38	6	6	6	14	2	1	3		9	6	6	1				
Main Converter (LV)		6		4	12		2	1	6		2	2	4	1				
TV Converter (HV)		6		4	12		2	1	4	2	2	2	4	1				
Computer and Sequencer Converter (LV)		6		4	8		2	1	4		2	2	4	1				
Experiment Converter (HV)		6		4	6		2	1	2	1	2	2	4	1				
Experiment Converter (LV)		6		4	8		2	2	4		2	2	4	1				

Table 36. Load Power Conditioning Equipment, Redundant Parts Count, Venus Orbiter No. 2, DC Distribution System

Unit	Resistors			Diodes			Capacitors				Transistors		Magnetics			Relays		Other / Comments	
	Carbon Compound	Metal Film	Wire Power	General Purpose	Rectifiers	Zener	Ceramic	Tantalum Foil	Tantalum Solid	Plastic	< 1W	> 1W	Transformers	Chokes	Mag-Amps	General 4 Sets	Latching 2 Coil		
Transmitter Converter (HV)		21	10	10	8	1	2	1	5	2	5	2	4	1			1	1	Standby
Gyro Inverter 3 ϕ (400~)		54	6	21	9	1	14	1	10		13	6	6	1			5	5	
Main Converter (LV)		21	10	10	12	1	2	1	8		5	2	4	1			1	1	
TV Converter (HV)		21	10	10	12	1	2	1	6	2	5	2	4	1			1	1	
Computer and Sequencer Converter (LV)		21	10	10	8	1	2	1	6		5	2	4	1			1	1	
Experiment Converter (HV)		21	10	10	0	1	2	1	4	1	5	2	4	1			1	1	
Experiment Converter (LV)		21	10	10	0	1	2	2	6		5	2	4	1			1	1	Standby

Note: Parts count listed for one of two identical standby redundant channels in each unit.

Table 37. Load Power Conditioning Equipment, Baseline Parts Count, Mars Orbiter, AC Distribution System

Unit	Resistors			Diodes			Capacitors				Transistors		Magnetics			Relays		Other / Comments
	Carbon Compound	Metal Film	Wire Power	General Purpose	Rectifiers	Zener	Ceramic	Tantalum Foil	Tantalum Solid	Plastic	< 1W	> 1W	Transformers	Chokes	Mag-Amps	General 4 Sets	Latching 2 Coil	
Gyro Inverter x 3 (400~)		38	6	6			14	1	3		9	6	6					
Main Inverter		5		4			2	1			2	2	4	1				
Transmitter TR (HV)					8				2	2		1	1					
Equipment TR (LV)				14				2	5				1					
TV TR (HV)				12					4	2		1	1					
Experiment TR (LV)				14				3	4			1	1					
Experiment TR (HV)				6					2	1		1	1					
Experiment TR (HV)				6					2	1		1	1					

Table 38. Load Power Conditioning Equipment, Redundant Parts Count, Mars Orbiter, AC Distribution System

Unit	Resistors			Diodes			Capacitors				Transistors		Magnetics			Relays		Other/Comments
	Carbon Compound	Metal Film	Wire Power	General Purpose	Rectifiers	Zener	Ceramic	Tantalum Foil	Tantalum Solid	Plastic	< 1W	> 1W	Transformers	Chokes	Mag-Amps	General 4 Sets	Latching 2 Coil	
Gyro Inverter 3φ (400~)		54	9	21	6	1	14	1	10		13	6	6	1			5	Standby
Main Inverter		10		1.0	8	1	2	1	2		5	2	4	1			2	Standby
Transmitter TR (HV)		15		6	14	1			4	2	3		1				1	
Equipment TR (LV)		19		6	12	1		2	7		3		1				1	
TV TR (HV)		18		6	14	1			6	2	3		1				1	
Experiment TR (LV)		19		6	14	1		3	6		3		1				1	
Experiment TR (HV)		15		6	6	1			4	1	3		1				1	
Experiment TR (HV)		15		6	6	1			4	1	3		1				1	Standby

Note: Parts count listed are for one of two identical standby redundant channels in each unit.

Table 39. Load Power Conditioning Equipment, Baseline Parts Count, Mars Orbiter, DC Distribution System

Unit	Resistors			Diodes			Capacitors				Transistors		Magnetics			Relays		Other / Comments
	Carbon Compound	Metal Film	Wire Power	General Purpose	Rectifiers	Zener	Ceramic	Tantalum Foil	Tantalum Solid	Plastic	<1W	>1W	Transformers	Chokes	Mag-Amps	General 4 Sets	Latching 2 Coil	
Transmitter Converter (HV)		6		4	8		2	1	3	2	2	2	4	1				
Gyro Inverter 3 ϕ (400~)	38		0	9	6	14		1	3		9	6	6	1				
Main Converter (LV)	6			4	12		2	1	6		2	2	4	1				
TV Converter (HV)	6			4	12		2	1	4	2	2	2	4	1				
Computer and Sequencer Converter (LV)	6			4	8		2	1	4		2	2	4	1				
Experiment Converter (HV)	6			4	12		2	1	2	1	2	2	4	1				
Experiment Converter (LV)	6			4	14		2	2	7		2	2	4	1				
Experiment Converter (HV)	6			4	12		2	1	2	1	2	2	4	1				

Table 40. Load Power Conditioning Equipment, Redundant Parts Count, Mars Orbiter, DC Distribution System

Unit	Resistors			Diodes			Capacitors				Transistors		Magnetics			Relays		Other / Comments	
	Carbon Compound	Metal Film	Wire Power	General Purpose	Rectifiers	Zener	Ceramic	Tantalum Foil	Tantalum Solid	Plastic	< 1W	> 1W	Transformers	Chokes	Mag-Amps	General 4 Sets	Latching 2 Coil		
Transmitter Converter (HV)		21		10	8	1	2	1	5	2	5	2	4	1			1	1	Standby
Gyko Inverter 3 ϕ (400~)		54	6	21	6	1	14	1	10		13	6	6	1			5		
Main Converter (LV)		21		10	12	1	2	1	8		5	2	4	1			1		
TV Converter (HV)		21		10	12	1	2	1	6	2	5	2	4	1			1		
Computer and Sequencer Converter (LV)		21		10	8	1	2	1	6		5	2	4	1			1		
Experiment Converter (HV)		21		10	12	1	2	1	4	1	5	2	4	1			1		
Experiment Converter (LV)		21		10	14	1	2	2	9		5	2	4	1			1		
Experiment Converter (HV)		21		10	12	1	2	1	4	1	5	2	4	1			1		Standby

Note: Parts count listed are for one of two identical standby redundant channels in each unit.

Table 41. Load Power Conditioning Equipment, Baseline Parts Count, Jupiter Flyby, AC Distribution System

Unit	Resistors			Diodes			Capacitors				Transistors		Magnetics			Relays		Other / Comments
	Carbon (powder)	Metal Film	Wire Power	General Purpose	Rectifiers	Zener	Ceramic	Tantalum Foil	Tantalum Solid	Plastic	< 1M	> 1M	Transformers	Chokes	Mag-Amps	General 4 Sets	Latching 2 Coil	
Gyro Inverter 3φ (400~)		14		4			2	1			2	2	4	1				
Main Inverter					6			2	1				1					
Transmitter TR (HV)					14			2	5				1					
Equipment TR (LV)					12				4	2			1					
TV TR (HV)					14			3					1					
Experiment TR (LV)					10				4	1			1					
Experiment TR (HV)													1					

Table 42. Load Power Conditioning Equipment, Redundant Parts Count, Jupiter Flyby, AC Distribution System

Unit	Resistors			Diodes			Capacitors				Transistors		Magnetics			Relays		Other/Comments
	Carbon Compound	Metal Film	Wire Power	General Purpose	Rectifiers	Zener	Ceramic	Tantalum Foil	Tantalum Solid	Plastic	< 1W	> 1W	Transformers	Chokes	Mag-Amps	General 4 Sets	Latching 2 Coil	
Gyro Inverter 30 (400~)		10		10		1	2	1	2	NOT REQUIRED	5	2	4	1			2	Standby
Main Inverter		15		6	6	1					3		1				1	
Transmitter TR (HV)		19		6	14	1		2	7		3		1				1	
Equipment TR (LV)		18		6	12	1			6	2	3		1				1	
TV TR (XV)		19		6	14	1		3	6		3		1				1	
Experiment TR (LV)		17		6	10	1		6	6	1	3		1				1	Standby

Note: Parts count listed are for one of two identical standby redundant channels in each unit.

Table 43. Load Power Conditioning Equipment, Baseline Parts Count, Jupiter Flyby, DC Distribution System

Unit	Resistors			Diodes			Capacitors				Transistors		Magnetics			Relays		Other / Comments
	Carbon Compound	Metal Film	Wire Power	General Purpose	Rectifiers	Zener	Ceramic	Tantalum Foil	Tantalum Solid	Plastic	<1W	>1W	Transformers	Chokes	Mag-Amps	General 4 Sets	Latching 2 Coil	
Transmitter Converter (HV)	6			4	6		2	1	3	1	2	2	4	1				
Gyro Inverter 3 ϕ (400~)	NOT REQUIRED						2	1										
Main Converter (LV)	6			4	12		2	1	6		2	2	4	1				
TV Converter (HV)	6			4	12		2	1	4	2	2	2	4	1				
Computer and Sequencer Converter (LV)	6			4	8		2	1	4		2	2	4	1				
Experiment Converter (HV)	6			4	12		2	1	2	1	2	2	4	1				
Experiment Converter (LV)	6			4	14		2	2	7		2	2	4	1				

Table 44. Load Power Conditioning Equipment, Redundant Parts Count, Jupiter Flyby, DC Distribution System

Unit	Resistors			Diodes			Capacitors				Transistors		Magnetics			Relays		Other / Comments
	Carbon Compound	Metal Film	Wire Power	General Purpose	Rectifiers	Zener	Ceramic	Tantalum Foil	Tantalum Solid	Plastic	<1W	>1W	Transformers	Chokes	Mag-Amps	General 4 Sets	Latching 2 Coil	
Transmitter Converter (HV)	21			10	6	1	2	1	5	1	5	2	4	1			1	Standby
Gyro Inverter 3 ϕ (400~)	NOT REQUIRED																	
Main Converter (LV)	21			10	12	1	2	1	0		5	2	4	1			1	
TV Converter HV	21			10	12	1	2	1	0	2	5	2	4	1			1	
Computer and Sequencer Converter (LV)	21			10	8	1	2	1	0		5	2	4	1			1	
Experiment Converter (HV)	21			10	12	1	2	1	4	1	5	2	4	1			1	
Experiment Converter (LV)	21			10	14	1	2	2	9		5	2	4	1			1	Standby

Note: Parts count listed are for one of two identical standby redundant channels in each unit.

Table 45. Load Power Conditioning Equipment, Baseline Parts Count
 Jupiter Orbiter No. 1, AC Distribution System

Unit	Resistors			Diodes			Capacitors				Transistors		Magnetics			Relays		Other/ Comments
	Carbon Compound	Metal Film	Wire Power	General Purpose	Rectifiers	Zener	Ceramic	Tantalum Foil	Tantalum Solid	Plastic	< 1W	> 1W	Transformers	Chokes	Mag-Amps	General 4 Sets	Latching 2 Coil	
Gyro Inverter 3 ϕ (400~)		3	6	6			14	1	3		9	6	6	1				
Main Inverter		3		4			2	1			2	2	4	1				
Transmitter TR (HV)					8				2	2			1					
Equipment TR (LV)					14			2	5				1					
TV TR (2)					12				4	2			1					
Experiment TR (LV)					14			3	4				1					
Experiment TR (HV)					10			4	4	1			1					

Table 46. Load Power Conditioning Equipment, Redundant Parts Count, Jupiter Orbiter No. 1, AC Distribution System

Unit	Resistors			Diodes			Capacitors				Transistors		Magnetics			Relays		Other / Comments	
	Carbon Compound	Metal Film	Wire Power	General Purpose	Rectifiers	Zener	Ceramic	Tantalum Foil	Tantalum Solid	Plastic	< 1W	> 1W	Transformers	Chokes	Mag-Amps	General 4 Sets	Latching 2 Coil		
Gyro Inverter 3φ (400~)		54	6	21	6	1	14	1	10		13	6	6	1			5	5	Standby ↔
Maio Inverter		10		10		1	2	1	2		5	2	4	1			2	2	
Transmitter TR (HV)		15		6	8	1			4	2	3		1						
Equip ment TR (LV)		19		6	14	1		2	7		3		1				1	1	
TV TR (XV)		18		6	12	1			6	2	3		1				1	1	
Experiment TR (LV)		19		6		1		3	6		3		1				1	1	
Experiment TR (HV)		17		6		1			6	1	3		1				1	1	Standby

Note: Parts count listed are for one of two identical standby redundant channels in each unit.

Table 47. Load Power Conditioning Equipment, Baseline Parts Count, Jupiter Orbiter No. 1, DC Distribution System

Unit	Resistors			Diodes			Capacitors				Transistors		Magnetics			Relays		Other / Comments
	Carbon Compound	Metal Film	Wire Power	General Purpose	Rectifiers	Zener	Ceramic	Tantalum Foil	Tantalum Solid	Plastic	< 1W	> 1W	Transformers	Chokes	Mag-Amps	General 4 Sets	Latching 2 Coil	
Transmitter Converter (HV)		6		4	8		2	1	3	2	2	2	4	1				
Gyro Inverter 3 ϕ (400~)		38	6	6	6		14	1	3		9	6	6	1				
Main Converter (LV)		6		4	12		2	1	6		2	2	4	1				
TV Converter (HV)		6		4	12		2	1	4	2	2	2	4	1				
Computer and Sequencer Converter (LV)		6		4	8		2	1	4		2	2	4	1				
Experiment Converter (HV)		6		4	6		2	1	2	1	2	2	4	1				
Experiment Converter (HV)		6		4	12		2	1	4	2	2	2	4	1				

Table 48. Load Power Conditioning Equipment, Redundant Parts Count, Jupiter Orbiter No. 1, DC Distribution System

Unit	Resistors			Diodes			Capacitors				Transistors		Magnetics			Relays		Other / Comments
	Carbon Compound	Metal Film	Wire Power	General Purpose	Rectifiers	Zener	Ceramic	Tantalum Foil	Tantalum Solid	Plastic	< 1W	> 1W	Transformers	Chokes	Mag-Amps	General 4 Sets	Latching 2 Coil	
Transmitter Converter (HV)	21			10	8	1	2	1	5	2	4	1	4	1			1	Standby
Gyro Inverter 3 ϕ (400~)	54	6		21	6	1	14	1	10	13	6	1	6	1			5	Standby
Main Converter (LV)	21			10	12	1	2	1	8	5	2	1	4	1			1	
TV Converter (HV)	21			10	12	1	2	1	6	5	2	2	4	1			1	
Computer and Sequencer Converter (LV)	21			10	8	1	2	1	6	5	2	4	1	1			1	
Experiment Converter (HV)	21			10	6	1	2	1	4	5	2	4	1	1			1	
Experiment Converter (HV)	21			10	12	1	2	1	6	5	2	4	1	1			1	Standby

Note: Parts count listed are for one of two identical standby redundant channels in each unit.

Table 49. Load Power Conditioning Equipment, Baseline Parts Count
 Jupiter Orbiter No. 2, AC Distribution System

Unit	Resistors			Diodes			Capacitors				Transistors		Magnetics			Relays		Other / Comments
	Carbon Compound	Metal Film	Wire Power	General Purpose	Rectifiers	Zener	Ceramic	Tantalum Foil	Tantalum Solid	Plastic	< 1W	> 1W	Transformers	Chokes	Mag-Amps	General 4 Sets	Latching 2 Coil	
Gyro Inverter 3 ϕ (400~)		38	6	6	6		14	1	3		9	6	6	1				
Main Inverter		5		4			2	1			2	2	4	1				
Transmitter TR (HV)					8			2	2				1					
Equipment TR (LV)				14				2	5				1					
TV TR (HV)				12				4	2				1					
Experiment TR (HV)				6				2	1				1					
Experiment TR (HV)				12				4	2				1					

Table 50. Load Power Conditioning Equipment, Redundant Parts Count, Jupiter Orbiter No. 2, AC Distribution System

Unit	Resistors			Diodes			Capacitors				Transistors		Magnetics			Relays		Other / Comments	
	Carbon Compound	Metal Film	Wire Power	General Purpose	Rectifiers	Zener	Ceramic	Tantalum Foil	Tantalum Solid	Plastic	< 1W	> 1W	Transformers	Chokes	Mag-Amps	General 4 Sets	Latching 2 Coil		
Gyro Inverter 3 ϕ (400~)		54	6	21	6	1	14	1	10		13	6	6	1			5		Standby ↕ Standby
Main Inverter		10		10		1	2	1	2		5	2	4	1			2		
Transmitter TR (HV)		15		6	8	1			4	2	3		1				1		
Equipment TR (LV)		19		6	14	1		2	7		3		1				1		
TV TR (HV)		18		6	12	1			6	2	3		1				1		
Experiment TR (HV)		15		6	6	1			4	1	3		1				1		
Experiment TR (HV)		18		6	12	1		6	6	2	3		1				1		

Note: Parts count listed are for one of two identical standby redundant channels in each unit.

Table 51. Load Power Conditioning Equipment, Baseline Parts Count, Jupiter Orbiter No. 2, DC Distribution System

Item	Resistors			Diodes			Capacitors				Transistors		Magnetics			Relays		Other / Comments
	Carbon Compound	Metal Film	Wire Power	General Purpose	Rectifiers	Zener	Ceramic	Tantalum Foil	Tantalum Solid	Plastic	< 1W	> 1W	Transformers	Chokes	Mag-Amps	General 4 Sets	Latching 2 Coil	
Transmitter Converter (XV)		6		4	8		2	1	3	2	2	2	4	1				
Gyro Inverter 3 ϕ (400~)		≥ 8	6	6	6	14	1	1	3		9	6	6	1				
Main Converter (LV)		6		4	12	2	1	1	6		2	2	4	1				
AC Converter (XV)		6		4	12	2	1	1	4	2	2	2	4	1				
Computer and Sequencer Converter (LV)		6		4	8	2	1	1	4		2	2	4	1				
Experiment Converter (HV)		6		4	10	2	1	1	4	1	2	2	4	1				
Experiment Converter (LV)		6		4	8	2	2	2	4		2	2	4	1				

Table 52. Load Power Conditioning Equipment, Redundant Parts Count, Jupiter Orbiter No. 2, DC Distribution System

	Resistors			Diodes			Capacitors				Transistors		Magnetics			Relays		Other / Comments
	Carbon Compound	Metal Film	Wire Power	General Purpose	Rectifiers	Zener	Ceramic	Tantalum Foil	Tantalum Solid	Plastic	< 1W	> 1W	Transformers	Chokes	Mag-Amps	General 4 Sets	Latching 2 Coil	
Transmitter Converter (HV)		21		10	8	1	2	1	5	2	5	2	4	1			1	Standby
Gyro Inverter 3 ϕ (400~)		54	6	21	6	1	14	1	10		13	6	6	1			5	Standby
Main Converter (LV)		21		10	12	1	2	1	8		5	2	4	1			1	Standby
TV Converter (HV)		21		10	12	1	2	1	6	2	5	2	4	1			1	Standby
Computer and Sequencer Converter (LV)		21		10	8	1	2	1	6		5	2	4	1			1	Standby
Experiment Converter (HV)		21		10	10	1	2	1	6	1	5	2	4	1			4	Standby
Experiment Converter (LV)		21		10	8	1	2	2	6		5	2	4	1			4	Standby

Note: Parts count listed are for one of two identical standby redundant channels in each unit.

4.3 EFFECT OF RELIABILITY IMPROVEMENTS ON UNIT WEIGHT AND EFFICIENCY

4.3.1 Electronic Equipment

The effects of implementing the preferred redundant configurations in each unit on their weights and efficiencies are shown in Figures 57 through 72.

In calculating efficiency, the losses in all the following elements were accounted for:

- e Input filter (capacitor and inductor)
- o Transformers
- a Rectifiers - both forward losses and recovery losses
- e Output filter (capacitor and inductor)
- o Transistor - both saturated and switching losses
- o Error amplifier losses
- Logic losses
- o Failure sensing losses.

The same items were accounted for in calculating the weight. An allowance was also made for the packaging of the components, the mechanical assembly, and the electrical connectors.

One of the most significant design parameters affecting unit efficiency and weight is the switching frequency of the inverter and pulse-width modulated regulator circuits. Preliminary designs were made at switching frequencies ranging from 400 Hz to 20 kHz. A figure-of-merit relating both unit efficiency and weight was selected as the product of the unit losses in percent times the unit weight in pounds. Comparisons of the figure-of-merit as a function of frequency for different types of switching units showed a minimum at 6 kHz. Figure 73 is a plot of the loss-weight product versus switching frequency for a 100-w bucking series regulator. At frequencies lower than 6 kHz, the losses decrease but are more than offset by the increased weights of the magnetics and filters. At frequencies greater than 6 kHz, the weight decreases but the increased

losses become the predominant characteristic. A **6-kHz** switching frequency was selected, therefore, for all ac circuits with the exception of the gyro inverters, which require a **400-Hz** output.

4.3.2 Batteries

Parametric weight data for both the silver-cadmium and silver-zinc batteries are shown in Figures 74 and 75 as a function of rated capacity and the maximum discharge power level for each mission. Calculations for each mission are based on an allowable depth of discharge of 50 percent.

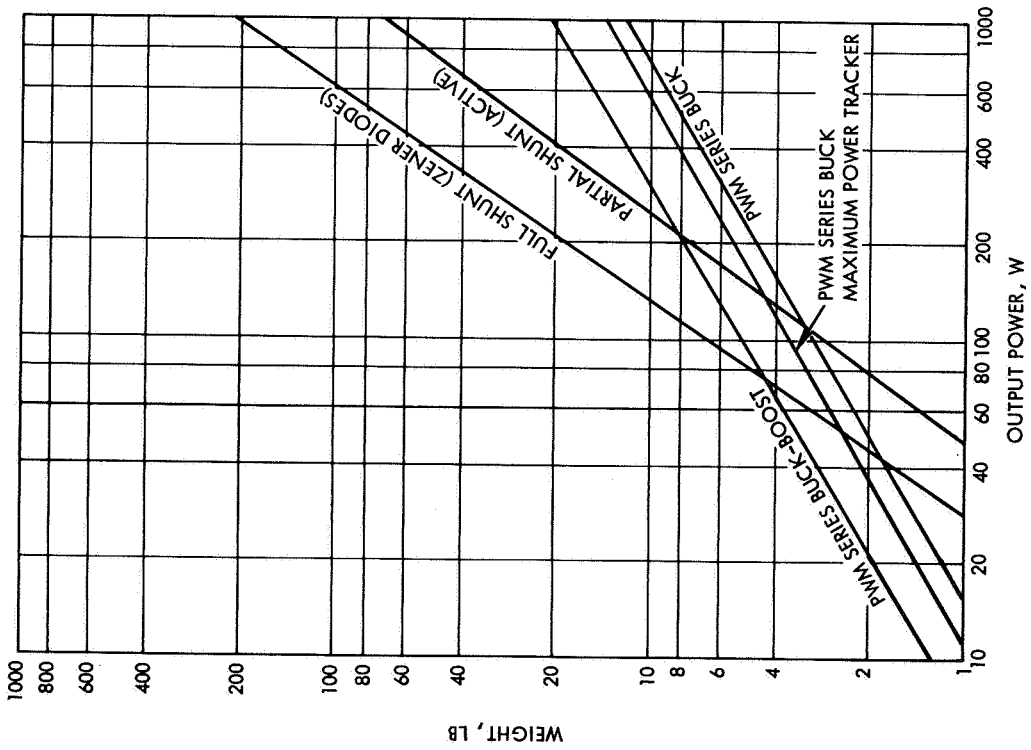


Figure 57. Array Controls, Baseline Weight Versus Power Output

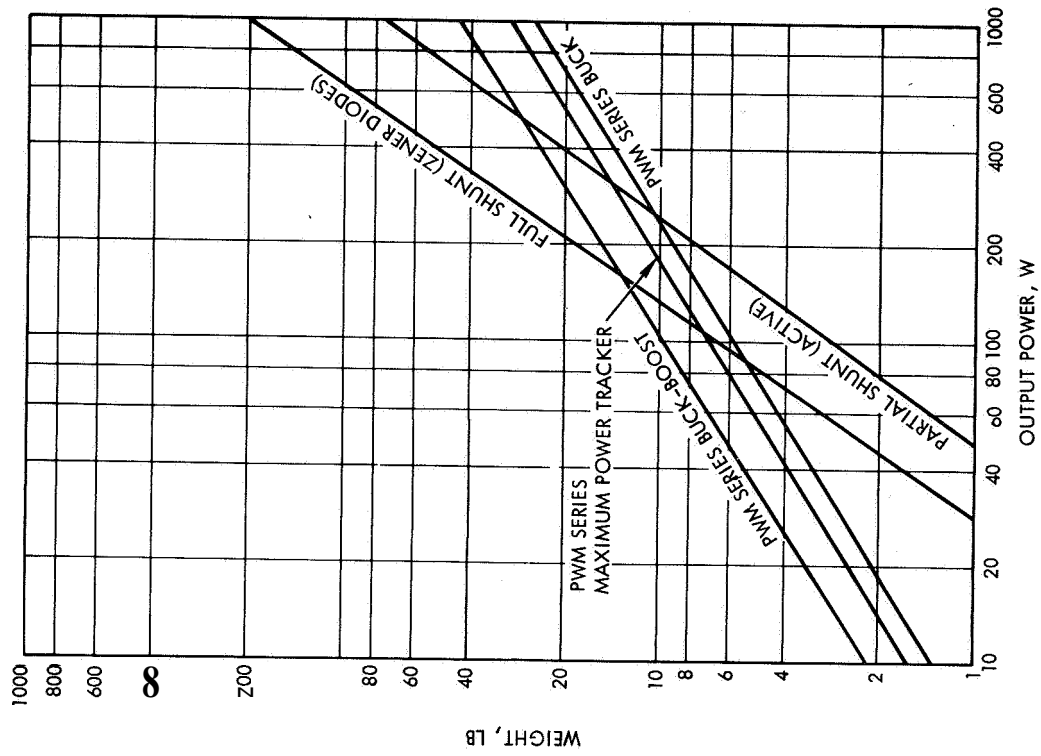


Figure 58. Array Controls, Redundant, Weight Versus Power Output

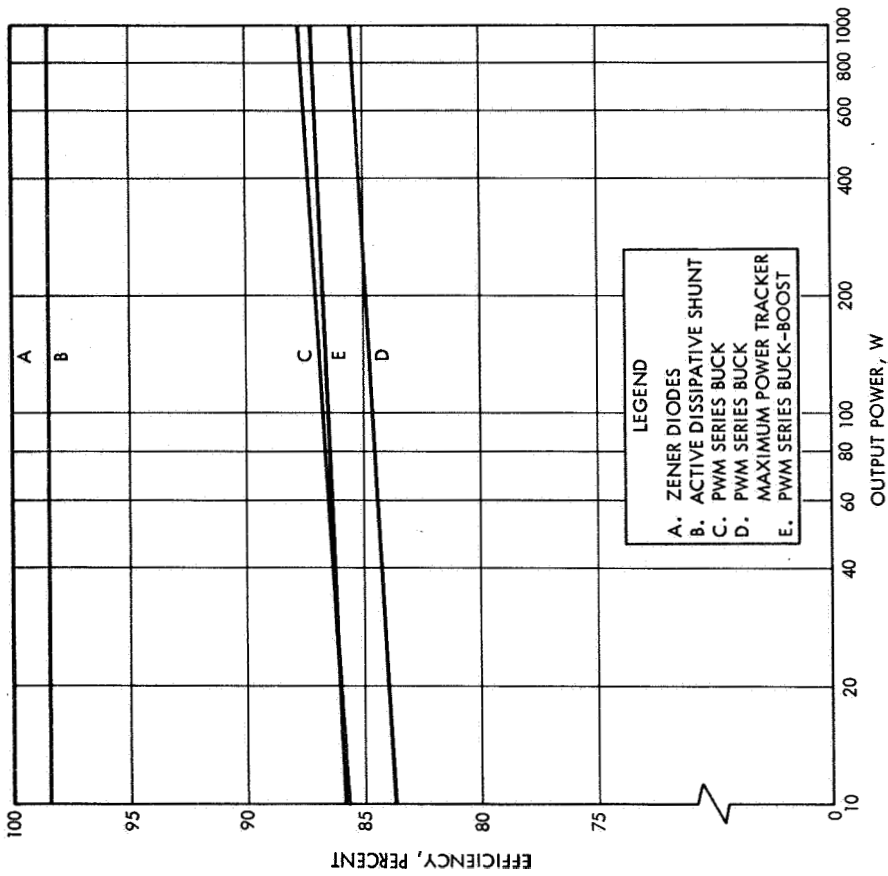


Figure 59. Array Controls, Baseline, Efficiency Versus Power Output

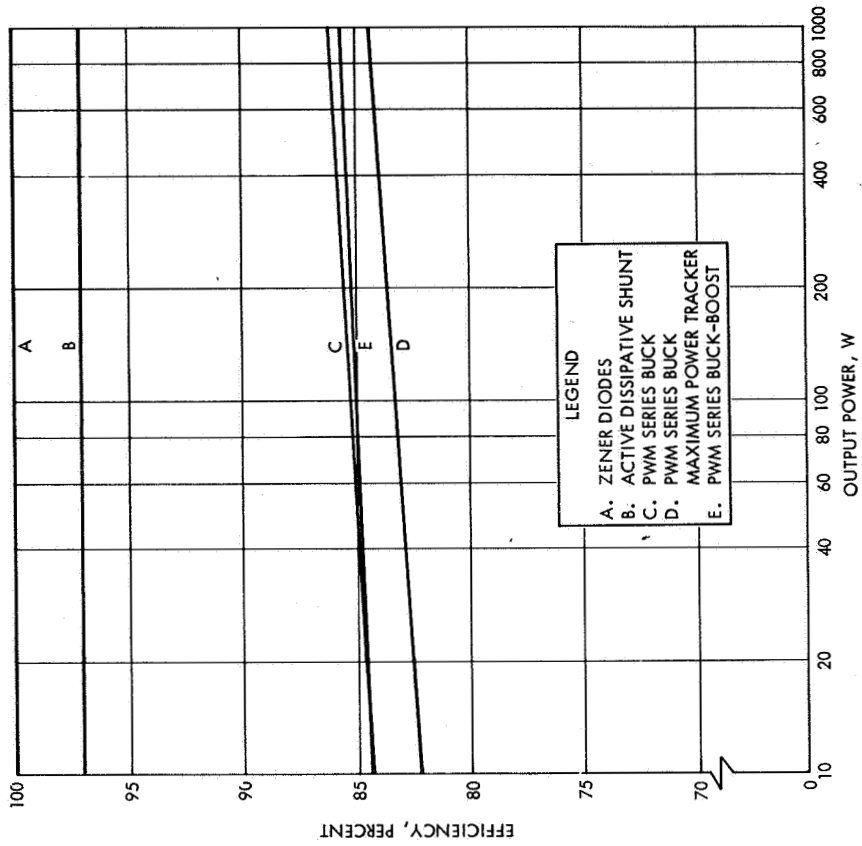


Figure 60. Array Controls, Redundant, Efficiency Versus Power Output

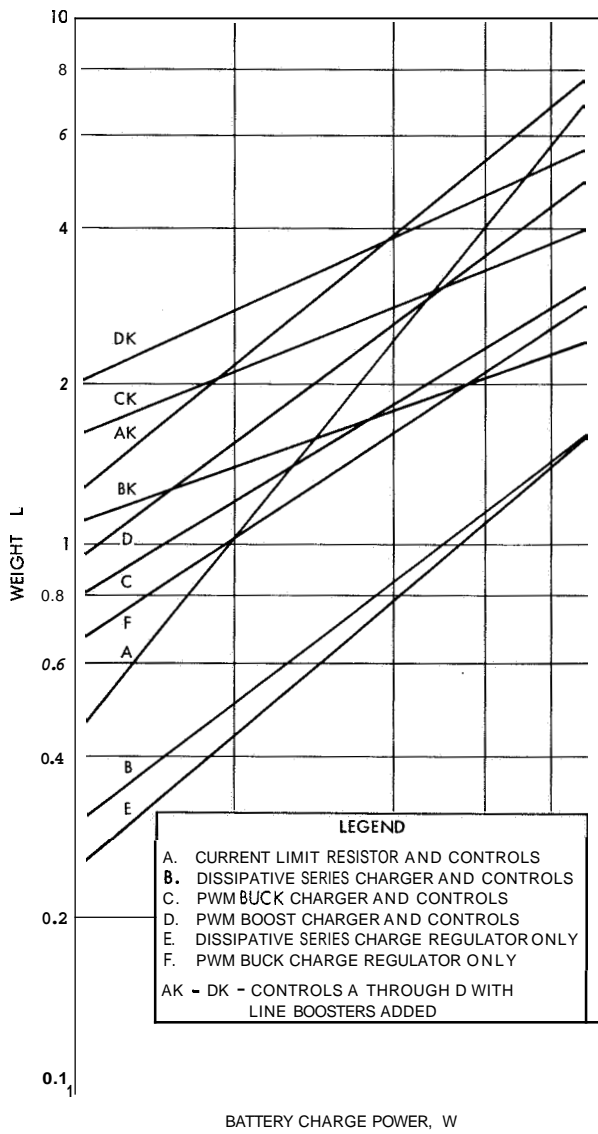


Figure 61. Battery Controls, Baseline, Weight Versus Power output

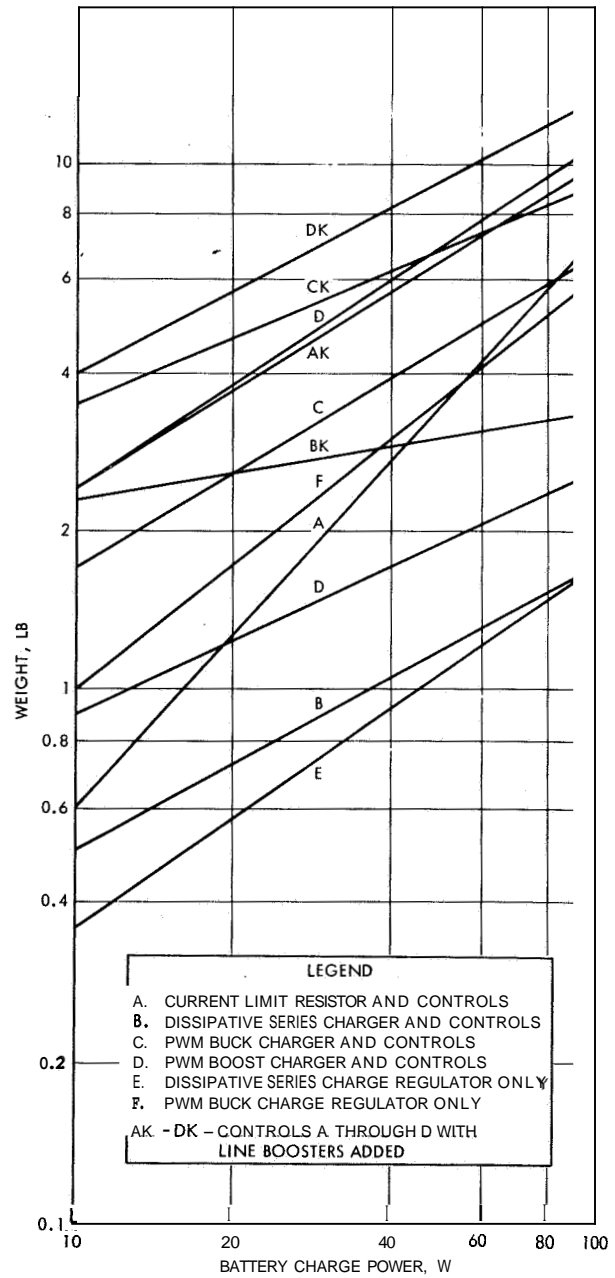


Figure 62. Battery Controls, Redundant, Weight Versus Power output

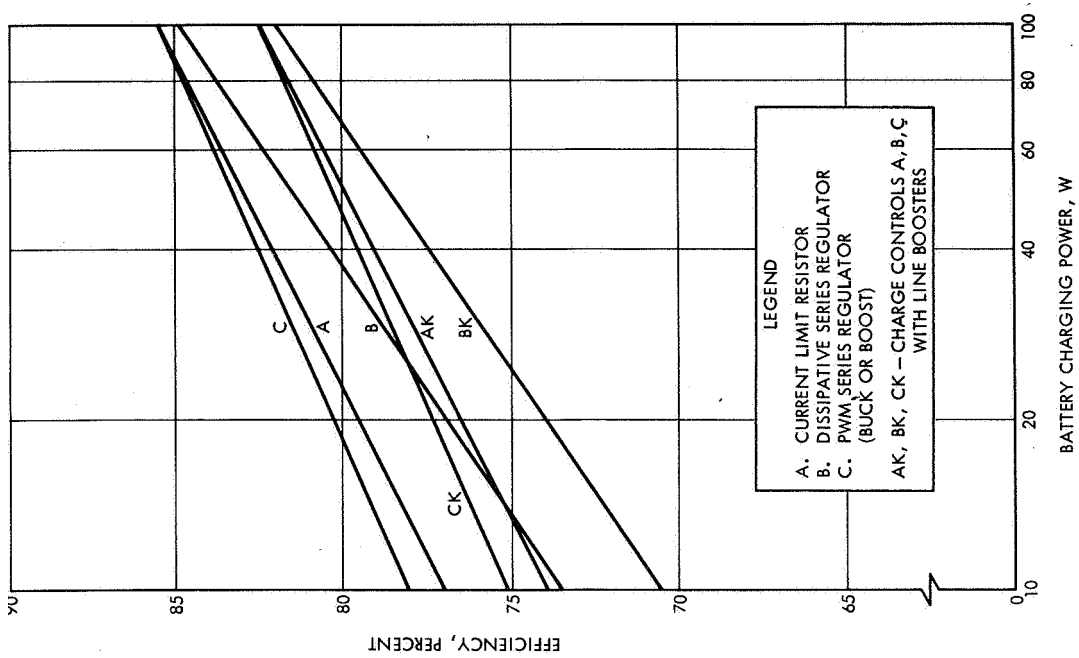


Figure 63. Battery Controls, Baseline, Efficiency versus Power Output

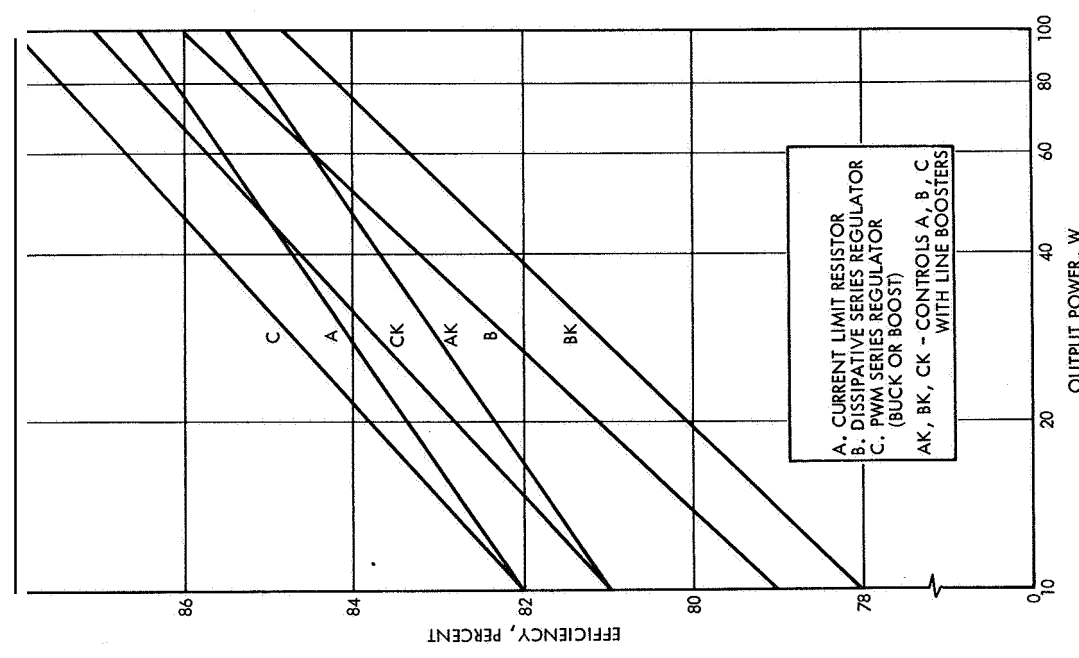


Figure 64. Battery Controls, Redundant, Efficiency versus Power Output

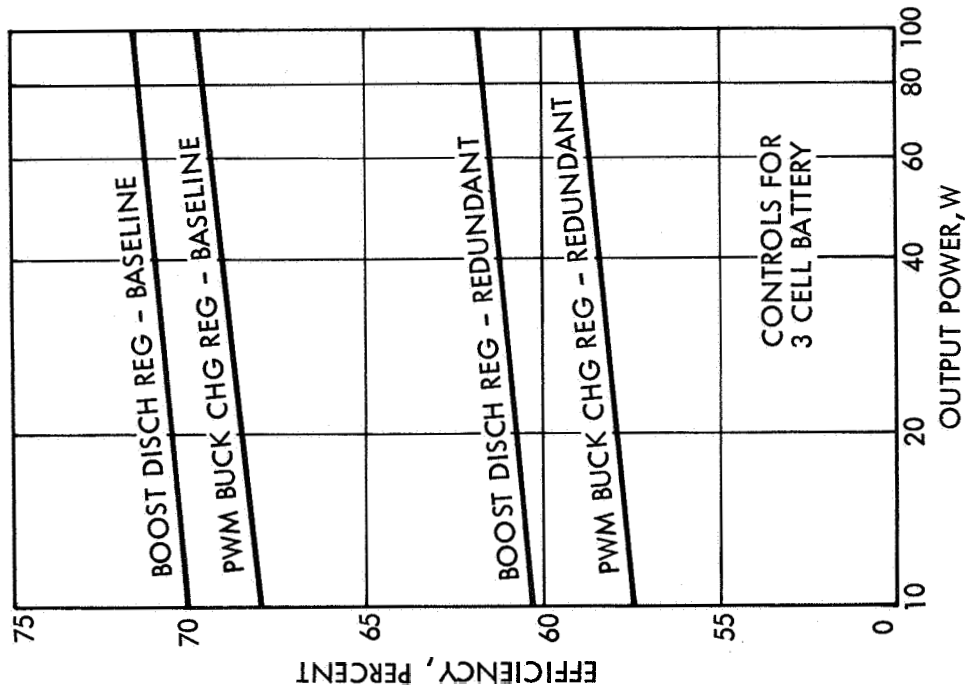


Figure 65. Low Voltage Battery Controls, Efficiency Versus Power Output

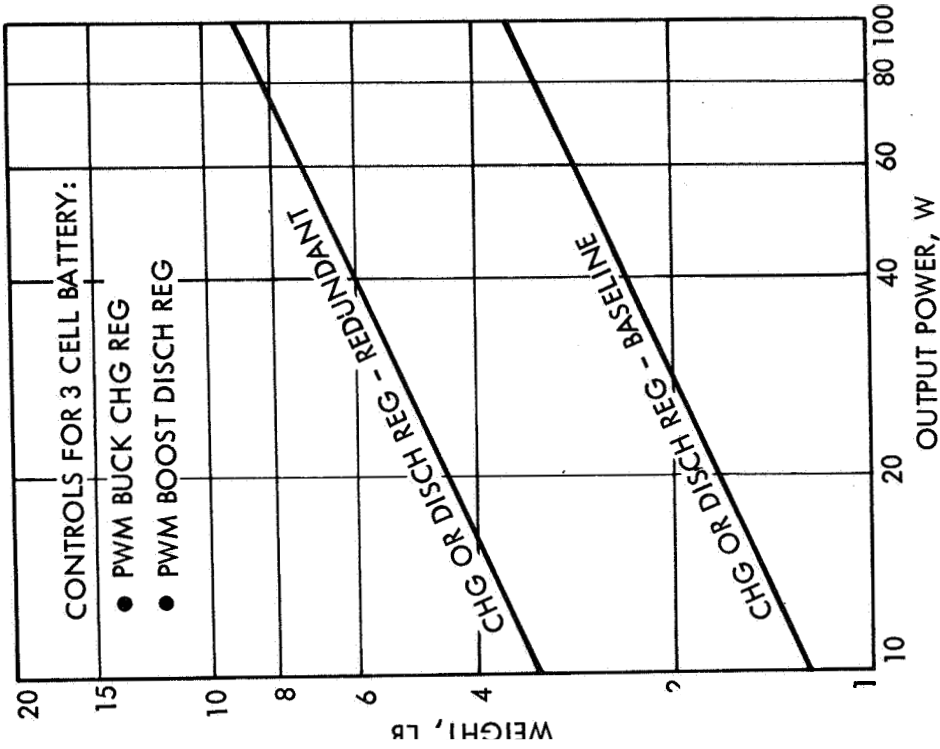


Figure 66. Low Voltage Battery Controls, Weight Versus Power Output

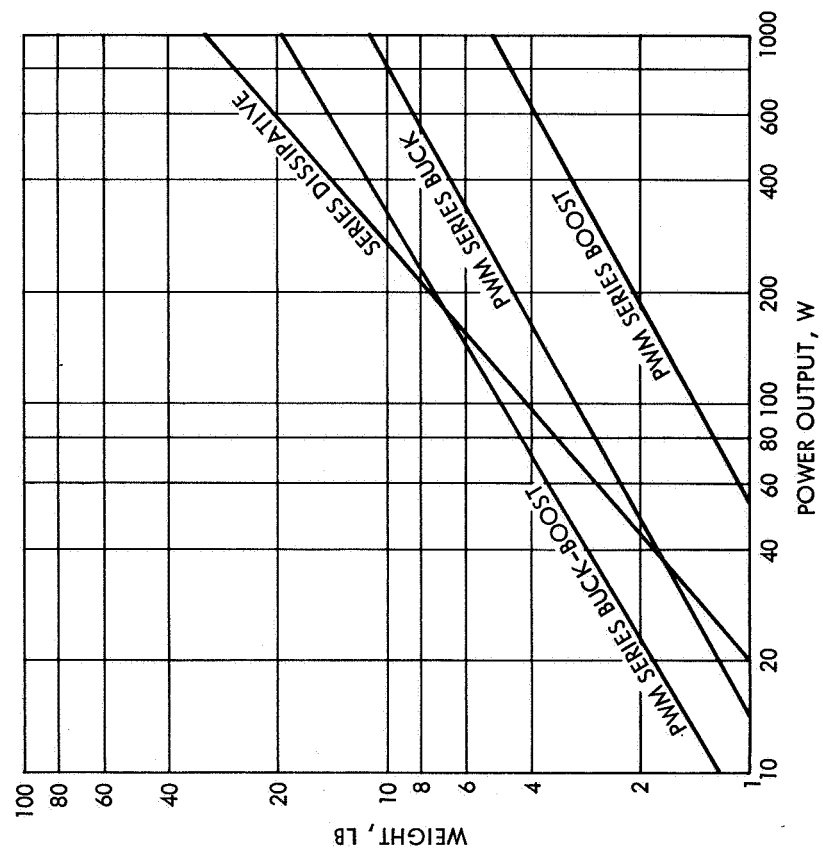


Figure 67. Line Regulators, Baseline, Weight Versus Power Output

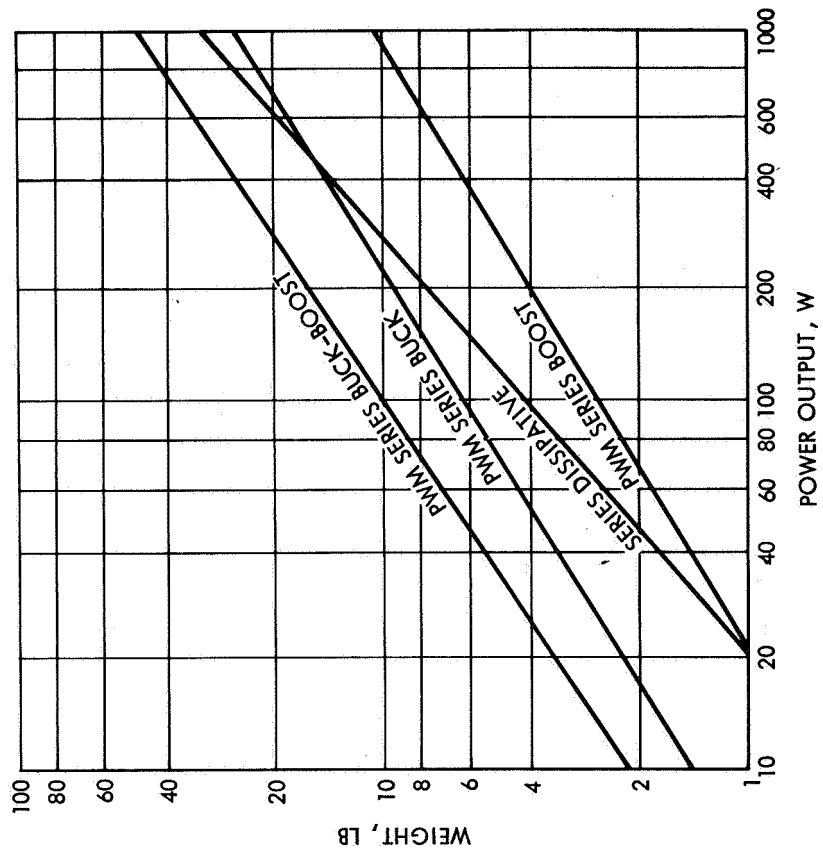


Figure 68. Line Regulators, Redundant, Weight Versus Power Output

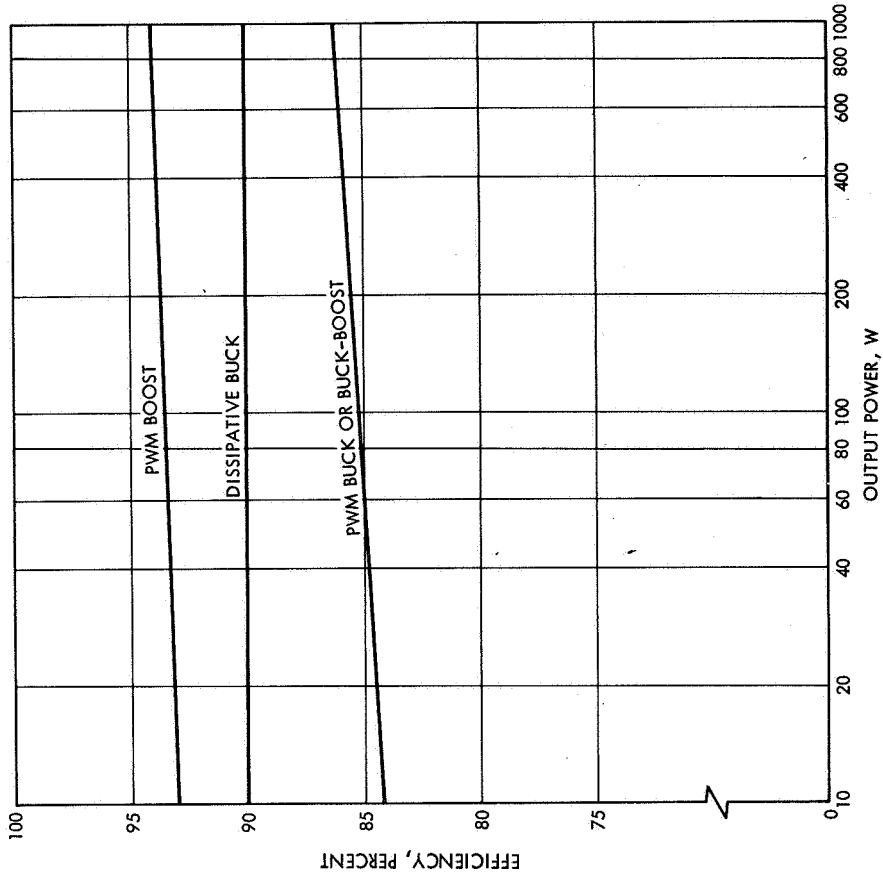


Figure 70. Line Regulators, Redundant, Efficiency Versus Power Output

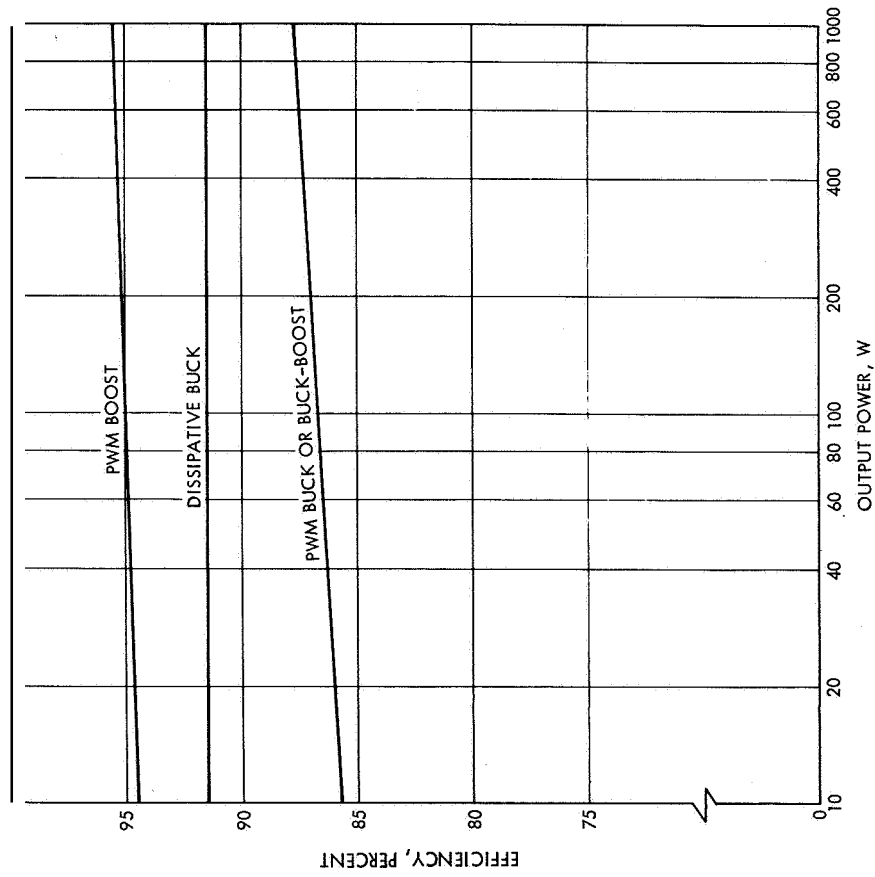


Figure 69. Line Regulator, Baseline, Efficiency Versus Power Output

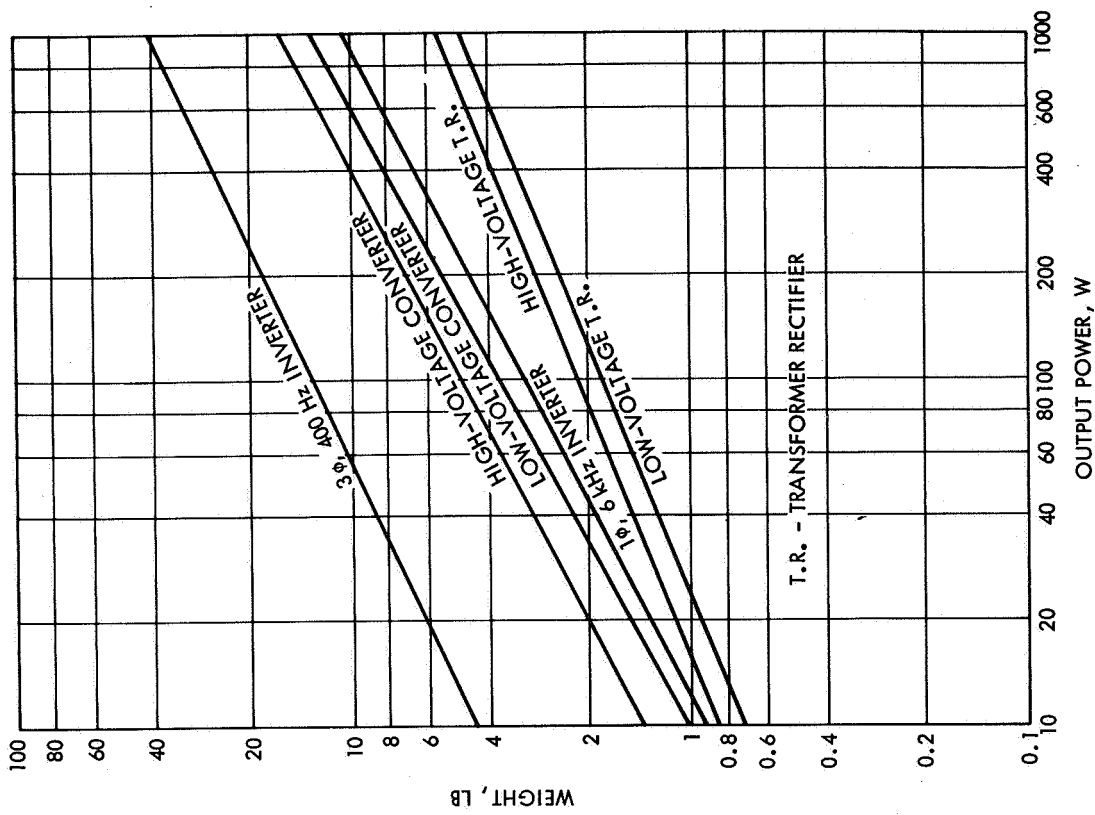


Figure 71. Load Power Conditioning Equipment, Baseline, Weight Versus Power Output

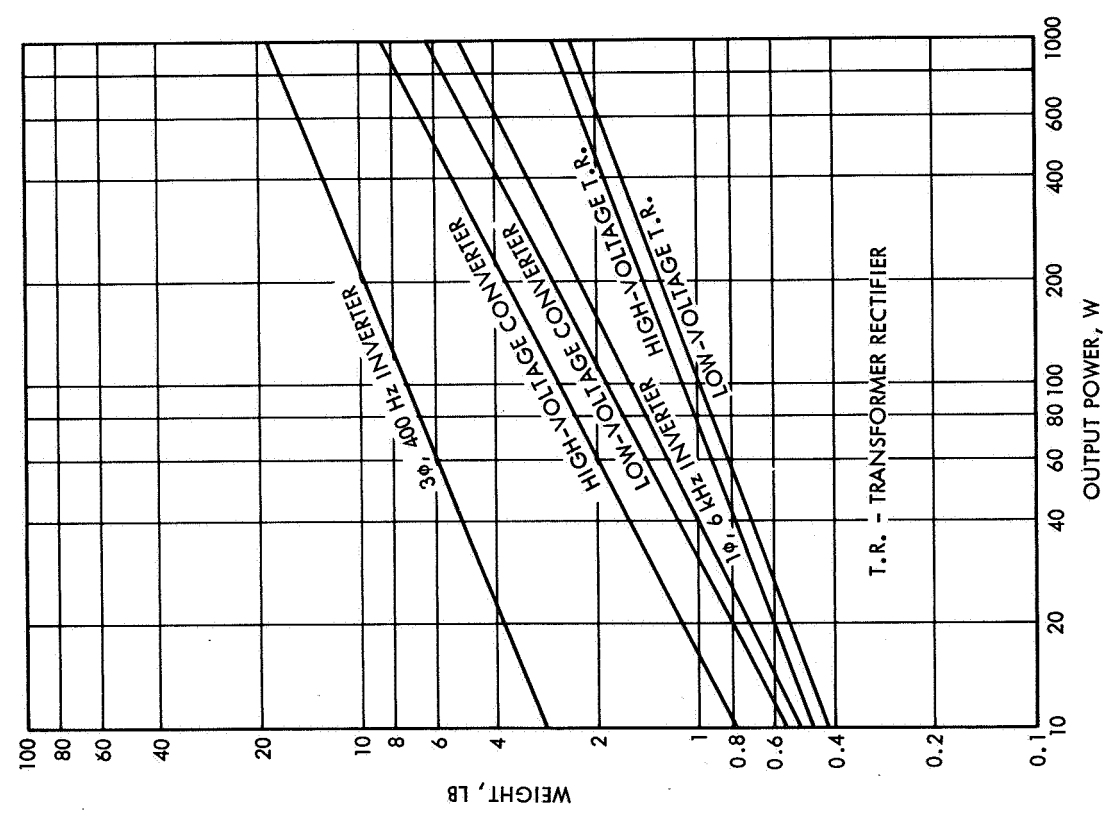


Figure 72. Load Power Conditioning Equipment, Redundant, Weight Versus Power Output

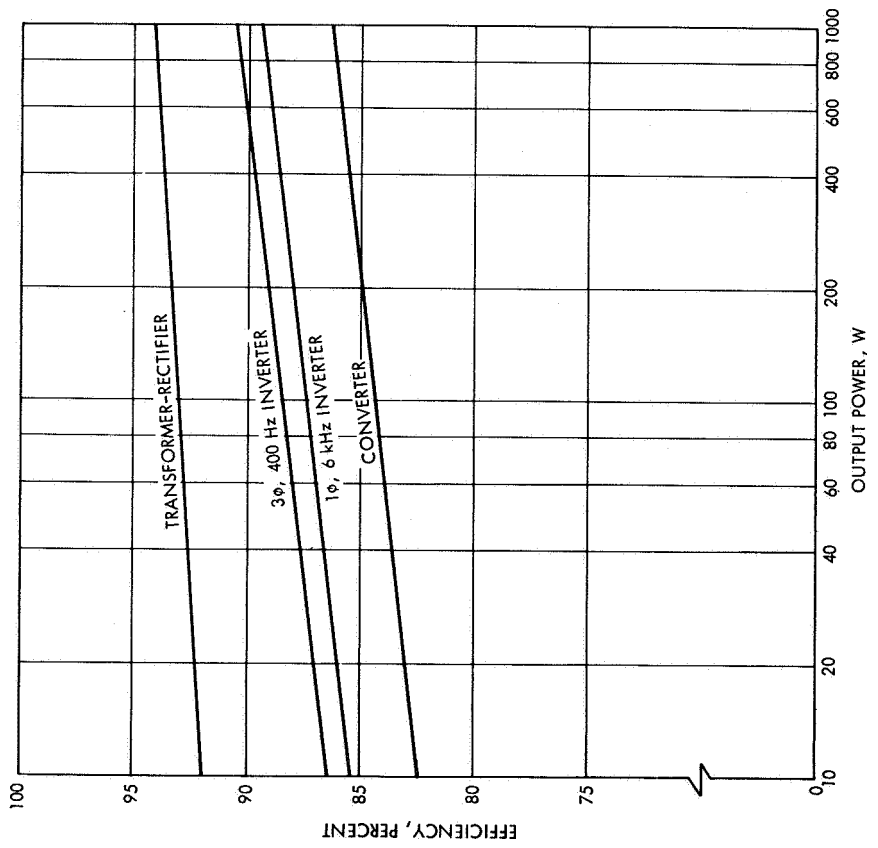


Figure 73. Load Power Conditioning Equipment, Baseline, Efficiency Versus Power Output

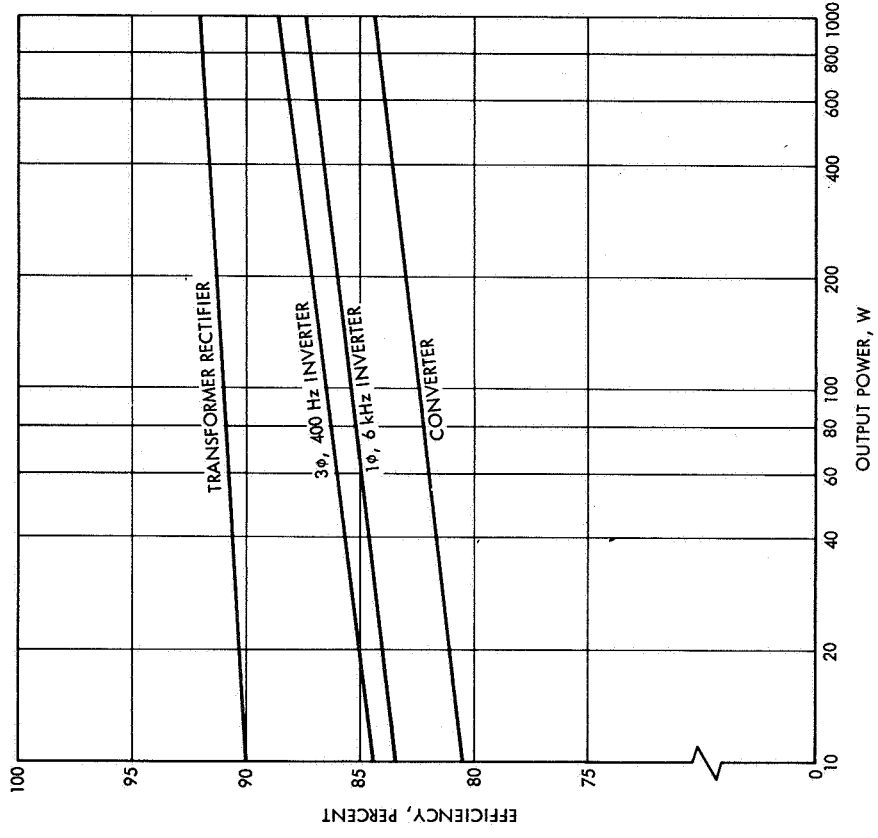


Figure 74. Load Power Conditioning Equipment, Redundant, Efficiency Versus Power Output

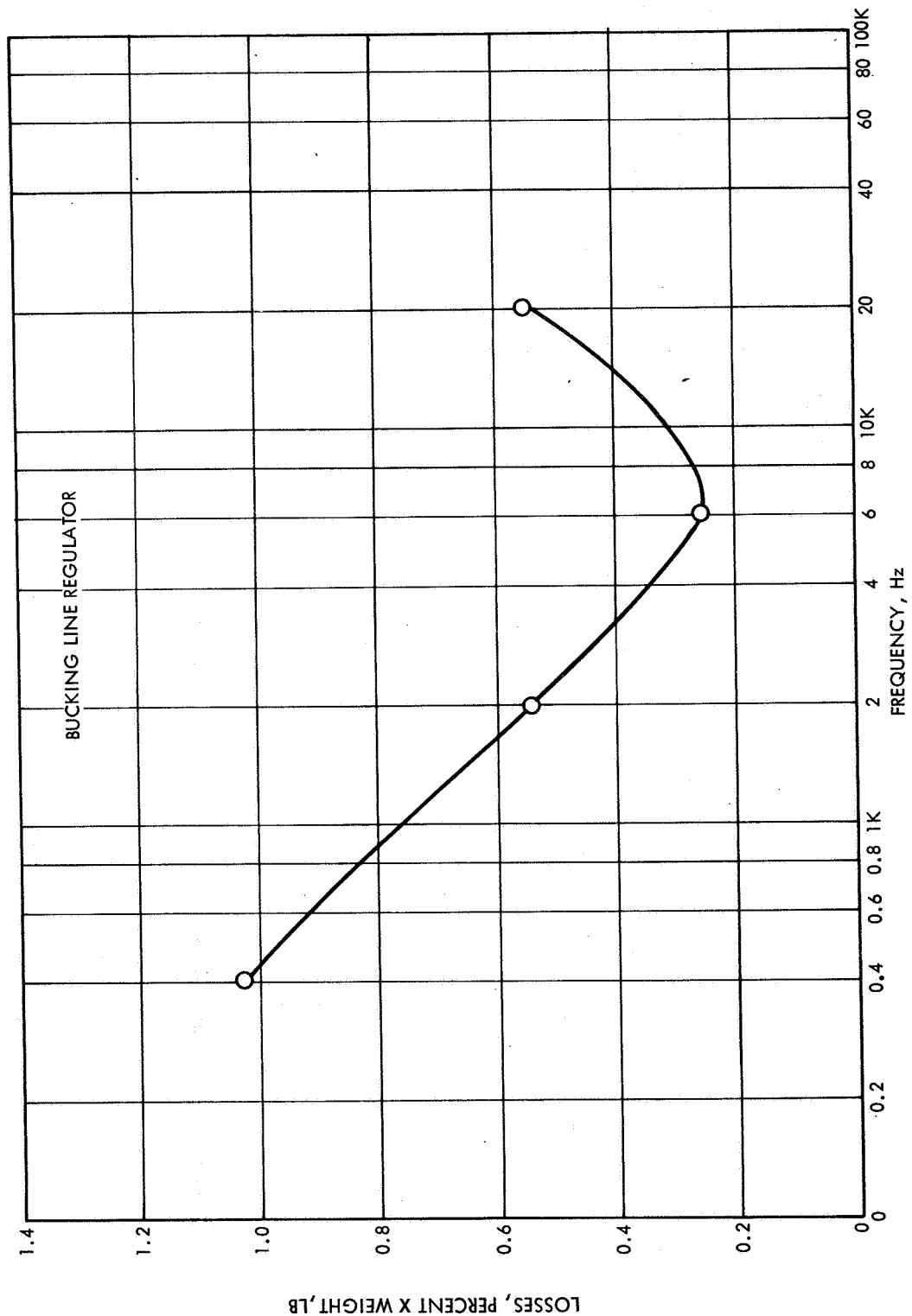


Figure 75. Bucking Line Regulator Power Loss Weight Product Versus Switching Frequency

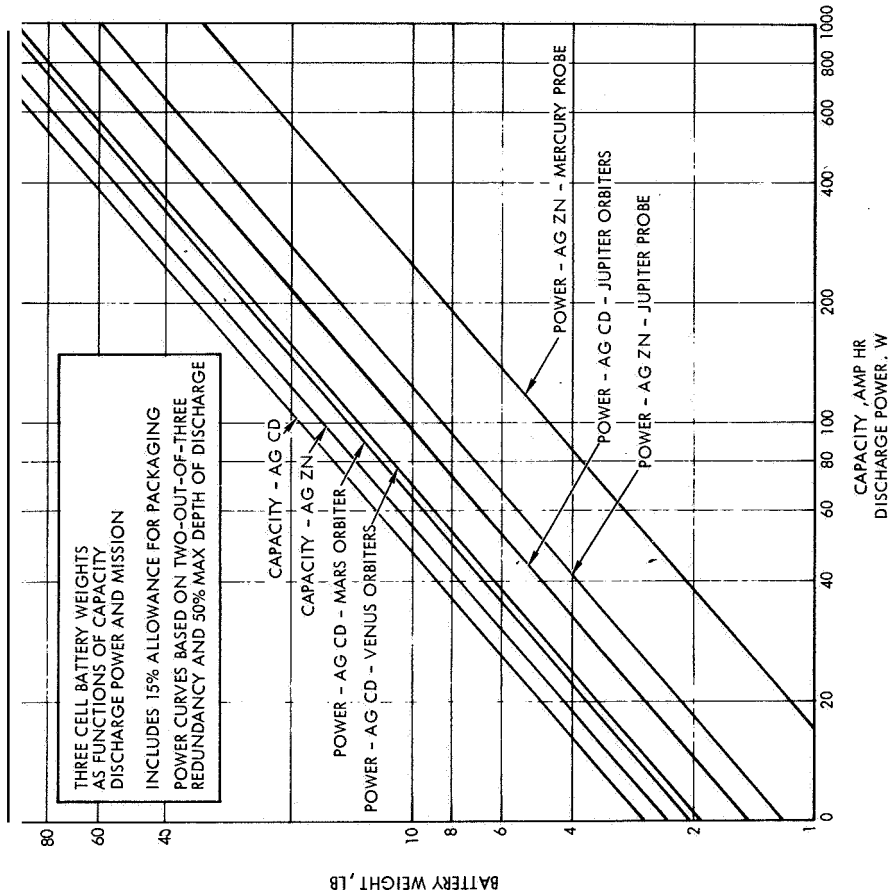


Figure 77 Three Cell Battery Weights as Functions of Capacity, Discharge Power, and Mission

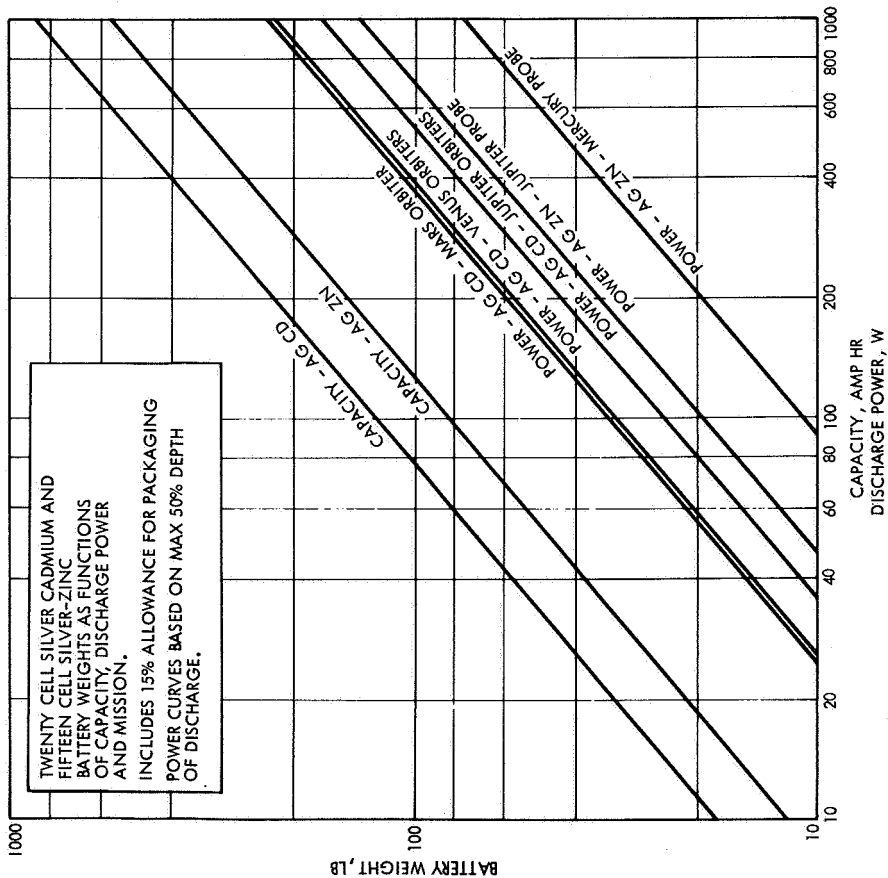


Figure 76. Twenty Cell Silver-Cadmium and Fifteen Cell Silver-Zinc Battery Weights as Functions of Capacity, Discharge Power and Mission

5. RELIABILITY-WEIGHT OPTIMIZATION

5.1 COMPUTER PROGRAM DESCRIPTION

The power system reliability-weight optimization program determines the best combinations of redundant and nonredundant units within one system configuration as a function of either a reliability or weight allocation. The computer program enumerates all possible combinations of unit redundancy, and selects those that provide minimum weight for system reliabilities ranging from a minimum of 0.90 to the maximum achievable. These selected combinations then represent the optimum reliability versus weight characteristic for a given system configuration. By comparing these characteristics for all candidate system configurations, the best designs for each mission are determined.

The reliability calculations are based on the assumption that any single part failure in a nonredundant unit constitutes a power system failure. This simplification permits the analysis of a relatively large number of power system configurations leading to the determination of one or more "best" candidates for each mission. The reliability of each unit in the various systems is established on the basis of its parts count and the part failure rates listed in Table 53. These failure rates are based primarily on TRW OGO, Vela, and Pioneer spacecraft flight experience. Demonstrated orbital operating times and numbers of parts by type are shown in Tables 54 and 55, respectively. Battery cell failure rates represent estimated values based on the very limited data available for the silver-zinc and silver-cadmium types in space applications.

The matrix shown in Figure 78 represents the basic arrangement of the computer program. Each column represents one essential unit of the system, and each cell represents one of the alternative choices of redundancy in the unit of the appropriate column. Several numbers may be associated with each cell in the matrix, plus additional numbers which are common to all the cells of a column. For the cells, the numbers used are as follows:

R = unit reliability for appropriate level of redundancy

M = intercept of log weight versus log power plot for particular unit

N = intercept of efficiency versus log power plot for particular unit

K = number of batteries

W = unit weight (when independent of other units)

η_E = unit efficiency in eclipse (when independent of other units)

η_D = unit efficiency in daylight (when independent of other units)

For the columns, the numbers used are as follows:

θ = slope of log weight versus log power plot for each unit

S = slope of efficiency versus log power plot for each unit

π_E = load for particular unit in eclipse? (when independent of other units)

π_D = load for particular unit in daylight? (when independent of other units)

F = ratio of battery charge power to discharge power for particular mission.

The computer calculates efficiency and weight for the unit configuration represented by each cell in the matrix according to the following general equations:

$$\text{Efficiency } (\eta) = S \log P + N$$

$$\text{Weight } (W) = MP\theta$$

From the required output power, P , and the calculated efficiency, the computer determines the input power to each unit. The program proceeds from specified output requirements back through the various series elements of the system to determine required unit power levels and weights, taking into account the required operation of each in sunlight and eclipse.

The matrix is then scanned, and necessary calculations performed to determine total system weight and reliability for each possible combination of system units.

†Represents only part of total load for array control, energy storage, and line regulator.

Specific calculation methods for the weight of the power system are shown in Tables 56 and 57. Terms for these calculations are listed in Table 58. The computer program logic block diagram and program listing are shown in Figure 79 and Table 59, respectively, Table 59 also includes brief descriptions of the function of each routine in the program.

Referring to Figure 78, four alternate configurations for the energy storage which combines the battery and its controls are defined as follows: 1) a single nonredundant battery with nonredundant controls, 2) a nonredundant battery with redundant controls, 3) redundant batteries each having nonredundant controls, and 4) redundant batteries each having redundant controls. For those cases where the battery controls perform a line regulation function to generate a regulated main bus directly, the appropriate factors are used for the line regulator to permit the computer to calculate its efficiency at 100 percent and its weight at 0. The reliability number for each energy storage configuration contains the reliability of both battery and control. A single solar array configuration is used. For all other units within any system, two configurations, that is, the baseline nonredundant configuration or the preferred redundant configuration, are used. These units are identified as the array control, line regulator, and several units which combine to perform the load power conditioning function.

Typical examples of the computer printouts for the optimization of one system for each mission are illustrated in Tables 60 to 66. System configurations are coded in accordance with Table 57. The computer optimization results for a series of 20 reliability constraints are shown in each case. For each reliability constraint, the number of feasible combinations of redundant and nonredundant units within the system which meet or surpass the reliability constraint are listed. The weight of each of the feasible combinations is computed and the configuration which yields minimum weight for each of the reliability constraints is selected.

The digits in the configuration column represent the individual units within the system; "1" indicates nonredundant and "2" indicates redundant. The first column represents the selected configuration for the array control, the second column is for the energy storage, the third column represents the configuration of the line regulator, and the remaining six columns represent the power conditioning equipment. For

the energy storage column, numbers up to **4** may appear reflecting the existence of four alternative choices of battery and battery controls redundancy.

Progressing from the first reliability constraint where the largest number of units within the system are nonredundant, redundant configurations of selected units within a system are added as the reliability constraint is increased. In each case the added redundancy is selected by the computer such as to achieve a minimum system weight for the appropriate reliability constraint.

Having evaluated each system configuration for a particular mission to ascertain its lightest weight combinations of redundant and nonredundant units for a series of given reliability constraints, the computer program then performs a second operation which consists of scanning all of the available optimized system configurations, at each reliability constraint, to rank all of them in order of weight. Examples of the computer printouts for this operation are shown in Tables 68 to **74**. System identifications in the column headed "CASE" are in accordance with the coding shown in Table 67.

The approach to reduce this data in order to define the optimum system configurations as a function of weight and reliability is as follows. Starting with the ranking by type for Constraint No. 1, which is similar to that shown in Table 68 for Constraint No. 17, the minimum weight system is identified and the listing then scanned to determine the next system of higher reliability that yields a minimum increase in weight. This eliminates from consideration those systems of lower reliability and higher weight than the first system. The optimum systems are recorded and the procedure is repeated until a system is found having a reliability equal to or greater than a higher reliability constraint or a weight greater than the minimum weight system of a higher reliability constraint. The ranking by type for this higher constraint is then scanned in the same way. This procedure is continued through the highest reliability systems listed in the ranking by type for Constraint No. 20. With this approach, the optimum systems are identified over the entire reliability range. These systems dominate all other system configurations because they represent the minimum achievable weight for a given reliability level. Conversely,

all of the systems rejected are either less reliable for an equivalent weight or heavier for an equivalent reliability. The systems identified as optimum constitute an envelope of minimum weight maximum reliability configurations.

The specific configurations of these selected systems relative to the degree of redundancy used are then determined by referring to the matrix of optima for that particular system. As an example, referring to Table 68, the sixth ranked system (3495) for this 17th reliability constraint for the Mercury mission is assumed to be one of the optimum systems selected by the above process. Referring to Table 67, system 3495 is of the regulated bus type and consists of a PWM bucking solar array regulator, a dissipative battery charge regulator, a nominal 28-v battery (15 AgZn cells for this mission), a PWM boosting discharge regulator, no line regulator and a dc distribution system. The matrix of optima for this system, 3495, is shown in Table 60. For constraint 17, the system configuration is shown to be 2-3-1-2-2-2-2-2-2, which identifies the redundancy in the system as follows:

<u>Digit</u>	<u>Value</u>	<u>Unit</u>	<u>Redundancy</u>
1st	2	Array control	Standby redundant
2nd	3	Energy storage	Redundant batteries, each having nonredundant charge & discharge regulators
3rd	1	Line regulator	None
4th-9th	2	Load power conditioning equipment	Standby redundant

Table 53. Recommended Failure Rates for Power System Configuration Study

Part Type	Principal Electrical and Other Stress	Spacecraft Equipment Failures/10 ⁹ Hr at Case Temperature 30°C
	<u>Rated Power, Percent</u>	
<u>Diode:</u>		
Silicon (< 1 w)	25	5
Silicon power (> 1 w)	25	14
Zener	25	55
<u>Transistor:</u>		
Silicon (< 1 w)	25	28
Silicon power (> 1 w)	25	56
<u>Resistor:</u>		
Carbon composition	25	12
Metal film	25	3
Wirewound, power	25	65
	<u>Rated Voltage, Percent</u>	
<u>Capacitor:</u>		
Ceramic	25	25
Mica, dipped	25	3
Paper, Mylar	25	40
<u>Tantalum:</u>		
Foil	25	21
Solid (series resistance ≥ 3 ohms/v)	25	21
<u>Transformer:</u>		
Low voltage, class H or T insulation	Hot spot ≤ 125°C	30 t 30/winding
<u>Inductor:</u>		
Low voltage, class H or T insulation	Hot spot ≤ 125°C	30
<u>Relay:</u>		
Base rate, class H or T coil insulation, magnetic latching (2 coils)	Hot spot ≤ 125°C	15 (failures/10 ⁹ cycles)
<u>Connector:</u>		
Per active pin (soldered)		10
<u>Connector:</u>		
Per active pin (crimped)		5
<u>Connection:</u>		
Soldered		0.5
<u>Connection:</u>		
Welded		0.5
<u>Solar Cell:</u>	Orbital conditions	1
<u>Battery Cell:</u>		
Silver cadmium in 20 cell pack		150
Silver cadmium in 3 cell pack		300
<u>Battery Cell:</u>		
Silver zinc in 15 cell pack		300
Silver zinc in 3 cell pack		600

Table 54. Part Type Demonstrated Orbital Operating Hours
(Vela and OGO)

Part Type	Number of Failures	Operating Hours Vela and OGO
<u>Transistors:</u>		
Silicon	2	106,073,965
<u>Diodes:</u>		
Silicon	1	385,629,667
Zener		7,508,145
<u>Resistors:</u>		
Carbon composition		74,482,179
Metal film		292,450,010
Wirewound		4,374,113
<u>Capacitors:</u>		
Ceramic	1	63,428,620
Dipped mica		2,926,213
Tantalum foil		1,030,847
Tantalum solid		42,916,870
Plastic		233,919
Mylar paper		387,862
<u>Magnetics:</u>		
Transformer		25,782,120
Inductor		1,397,461
Filter		3,281,707
<u>Relays:</u>		
Latching		5,630,944

Table 55. Part Group Total Number of Orbital Parts
(Vela and OGO)

Part Group	Number of Parts
Transistors	13,989
Diodes	45,855
Capacitors	15,505
Resistors	44,541
Magnetics	3,531
Relays	408

Table 56. Weight Calculations for DC Distribution

1	$P_{LWE} = \frac{\pi_{E1}}{\eta_{1PE}} + \frac{\pi_{E2}}{\eta_{2PE}} + \frac{\pi_{EN}}{\eta_{NPE}} + \frac{\pi_{RPE}}{\eta_{RPE}}$	10.	$\pi_{<R} = FP_B$
2	$\pi_{LRD} = \frac{\pi_{D1}}{\eta_{1DN}} + \frac{\pi_{D2}}{\eta_{2DN}} + \dots + \frac{\pi_{DN}}{\eta_{NDN}} + \pi_{R\theta D}$	11	$W_{ES} = KM_{DR} \pi_{ES}^{\theta_{DR}} + KM_B \pi_{\omega}^{\theta_B} + KM_{BR} P_{C\omega} <R$
3	$\pi_{L\omega\omega} = \text{greater of } \pi_{LRE} \text{ or } \pi_{L\omega D}$	12	$\eta_{<R} = S_{<R} \log \frac{P_{CR}}{K} + N_{C\omega}$
4.	$W_{TRP} = M_{TRP} P_{TRP}^{\theta_{LR}}$	13	$\pi_{A<} = \frac{P_{LRD}}{\eta_{LRD}} + \frac{P_{CR}}{\eta_{CR}} + \pi_{UBD}$
5	$\pi_{LWE} = S_{LR} \log \pi_{LRE} + N_{LR}$	14.	$W_{AC} = M_{A\theta} \pi_{AC}^{\theta_{AC}}$
6	$\pi_{LRD} = S_{LR} \log \pi_{LRD} + N_{LR}$	15.	$\pi_{A<} = S_{A<} \log P_{A<} + N_{A<}$
7.	$P_{ES} = \frac{P_{LRE}}{\eta_{LRE}} + \pi_{UBE}$	16	$\pi_{SA} = \frac{P_{AC}}{\eta_{AC}}$
8	$\pi_{DR} = S_{D\omega} \log \frac{P_{ES}}{K} + N_{D\omega}$	17	$\omega_{SA} = A P_{SA}$
9.	$P_B = \frac{P_{ES}}{\eta_{DR}}$	18	$W_{SYS} = \omega_{SA} + W_{AC} + W_{ES} + W_{L\omega} + W_{1\pi} + W_{2\pi} + \dots + P$

Table 57. Weight Calculations for AC Distribution Systems

1.	$P_{MIE} = \frac{\pi_{E1}}{\eta_{1TE}} + \frac{\pi_{E2}}{\eta_{2TE}} + \dots + \frac{\pi_{EN}}{\eta_{NTE}}$	13.	$P_{ES} = \frac{P_{LRE}}{\eta_{LRE}} + \pi_{UBE}$
2.	$P_{MID} = \frac{\pi_{D1}}{\eta_{1TD}} + \frac{\pi_{D2}}{\eta_{2TD}} + \dots + \frac{\pi_{DN}}{\eta_{NTD}}$	14.	$\eta_{DR} = S_{DR} \log \frac{P_{ES}}{K} + N_{DR}$
3.	$P_{MIR} = \text{greater of } P_{MIE} \text{ or } P_{MID}$	15.	$P_B = \frac{P_{ES}}{\eta_{DR}}$
4.	$W_{MI} = M_{MI} P_{MIR}^{\theta_{MI}}$	16.	$P_{CB} = F_{PB}$
5.	$\eta_{MIE} = S_{MI} \log P_{MIE} + N_{MI}$	17.	$W_{EB} = KM_{DR} P_{CB}^{\theta_{DB}} + KM_B P_B^{\theta_B} + KM_{CR} P_{CB}^{\theta_{CB}}$
6.	$M_{MID} = S_{MI} \log P_{MID} + N_{MI}$	18.	$\eta_{CR} = S_{CR} \log \frac{P_{CR}}{K} + N_{CR}$
7.	$P_{L\omega E} = \frac{P_{MIE}}{\eta_{MIE}} + \frac{P_{MID}}{\eta_{MID}} + P_{CB}$	19.	$P_{AC} = \frac{P_{LRD}}{\eta_{LRD}} + \frac{P_{CR}}{\eta_{CR}} + \pi_{UBD}$
8.	$P_{LRD} = \frac{P_{MID}}{\eta_{MID}} + \frac{\pi_{GD}}{\eta_{GD}} + \pi_{RBD}$	20.	$W_{AC} = M_{AC} P_{AC}^{\theta_{AC}}$
9.	$P_{L\omega\omega} = \text{greater of } P_{LRE} \text{ or } P_{LRD}$	21.	$\eta_A = S_{AC} \log P_{AC} + N_{AC}$
10.	$W_{LR} = M_{LR} P_{LRR}^{\theta_{LR}}$	22.	$P_{SA} = \frac{P_{AC}}{\eta_{AC}}$
11.	$\eta_{L\omega E} = S_{L\omega} \log P_{L\omega E} + N_{L\omega}$	23.	$W_{SA} = A P_{SA}$
12.	$\eta_{LRD} = S_{L\omega} \log P_{LRD} + N_{L\omega}$	24.	$W_{SYS} = W_{SA} + C_C + \omega_{ES} + W_{L\omega} + W_{1P} + W_{2P} + W_{NP}$

Table 58. Glossary of Terms

Power Terms

$P_{MIE, MID}$	=	Main inverter output power in eclipse, sunlight
P_{MIR}	=	Main inverter rated output power
$P_{LRE, LRD}$	=	Line regulator output power in eclipse, sunlight
P_{LRR}	=	Line regulator rated output power
	=	Energy storage output power
P_B	=	Battery output power
P_{CR}	=	Battery charger output power
P_{AC}	=	Array control output power
P_{SA}	=	Solar array output power
$\pi_{E1, E2, EN}$	=	Output power in eclipse for power conditioning equipments 1, 2, ---N
$\pi_{D1, D2, DN}$	=	Output power in sunlight for power conditioning equipments 1, 2, ---N
$\pi_{GE, GD}$	=	Output power for gyro inverter in eclipse, sunlight
$\pi_{RBE, RBD}$	=	Direct connected regulated bus load in eclipse, sunlight
$\pi_{UBE, UBD}$	=	Direct connected unregulated bus load in eclipse, sunlight

Efficiency Terms

$\eta_{ITE, 2TE, NTE}$	=	Efficiency in eclipse of transformer rectifiers 1, 2, ---N
$\eta_{ITD, 2TD, NTD}$	=	Efficiency in sunlight of transformer rectifiers 1, 2, ---N
$\eta_{MIE, MID}$	=	Efficiency of main inverter in eclipse, sunlight
$\eta_{GE, GD}$	=	Efficiency of gyro inverter in eclipse, sunlight
$\eta_{IPE, 2PE, NPE}$	=	Efficiency in eclipse of power conditioning equipments 1, 2, ---N

Table 58. (Continued)

Efficiency Terms (Continued)

- $\eta_{IPD,2PD,NPD}$ - Efficiency in sunlight of power conditioning equipments 1, 2, ---N
- $\eta_{LRE,LRD}$ = Efficiency of line regulator in eclipse, sunlight
- η_{DR} = Efficiency of discharge regulator
- η_{CR} = Efficiency of charge regulator
- η_{AC} = Efficiency of array control
- K = Number of batteries
- F = Ratio of battery charge power to battery discharge power
- S_{MI}, N_{MI} = Slope and intercept of main inverter efficiency vs power curve
- S_{LR}, N_{LR} - Slope and intercept of line regulator efficiency vs power curve
- S_{DR}, N_{DR} - Slope and intercept of discharge regulator efficiency vs power curve
- S_{CR}, N_{CR} = Slope and intercept of charge control efficiency vs power curve
- S_{AC}, N_{AC} = Slope and intercept of array control efficiency vs power curve

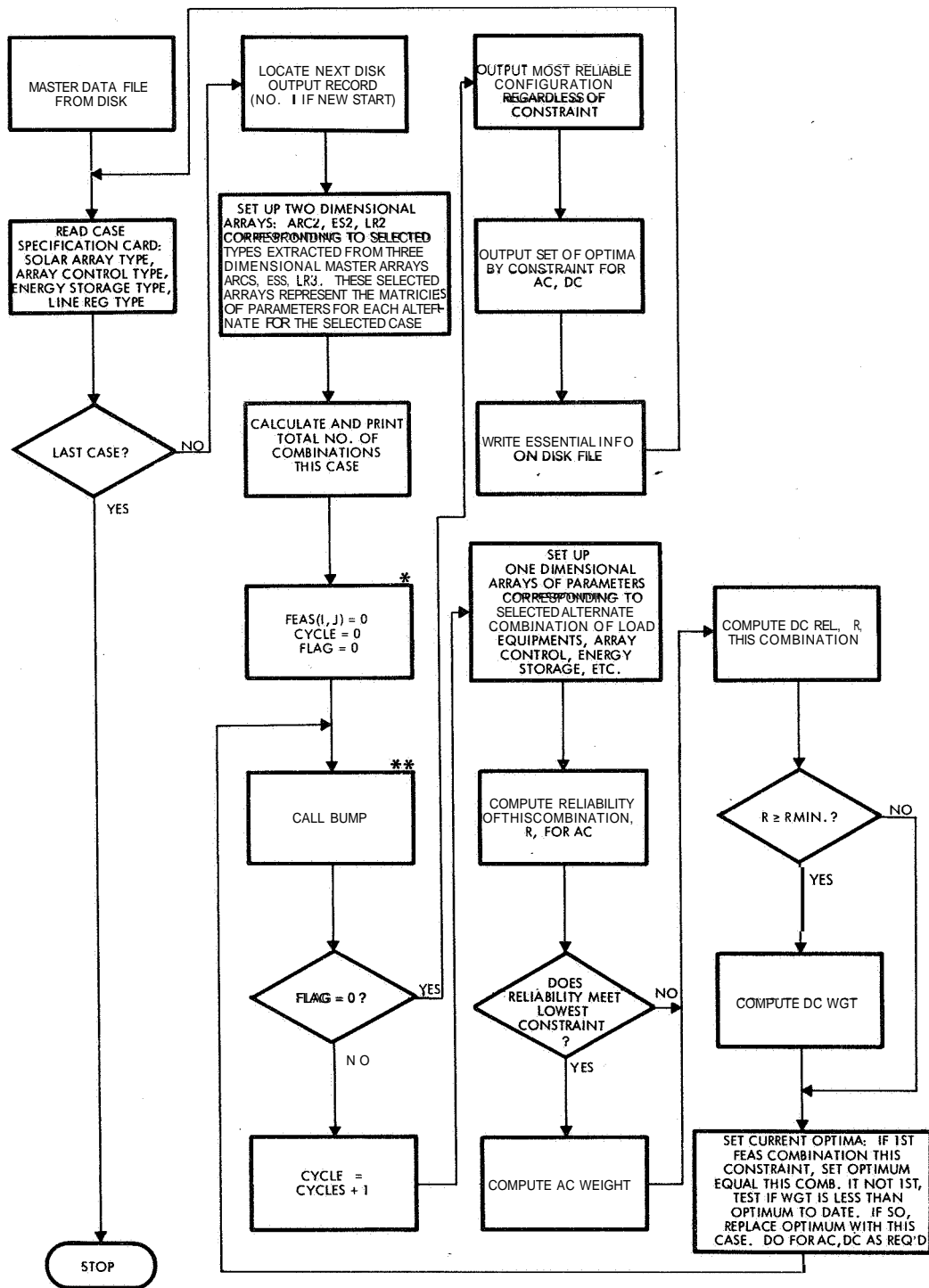
Weight Terms

- $W_{IP, 2P, NP}$ = Weight of power conditioning equipments 1, 2, ---N including main inverter when used
- W_{MI} = Weight of main inverter
- W_{LR} = Weight of line regulator
- W_{ES} = Weight of energy storage
- W_{AC} = Weight of array control
- W_{SA} = Weight of solar array
- A = Weight per unit power output of solar array at critical design point

Table 58. (Continued)

Weight Terms (Continued)

K	=	Number of batteries
M_{MI}, θ_{MI}	=	Intercept and slope of main inverter weight vs power curve
M_{LR}, θ_{LR}	=	Intercept and slope of line regulator weight vs power curve
M_{DR}, θ_{DR}	=	Intercept and slope of discharge regulator weight vs power curve
M_B, θ_B	=	Intercept and slope of battery weight vs power curve
M_{CR}, θ_{CR}	=	Intercept and slope of charge control weight vs power curve
M_{AC}, θ_{AC}	=	Intercept and slope of array control weight vs power curve

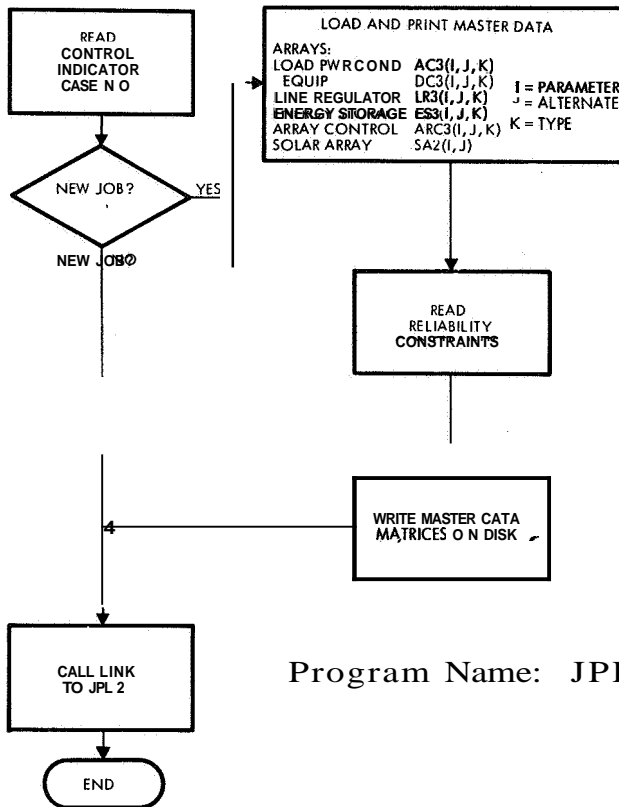


* FEAS (I, J) CONTAINS COUNTS OF COMBINATIONS THAT MEET THE JTH RELIABILITY CONSTRAINT I=1 AC, I=2 DC. FLAG = 0 CAUSES "BUMP" ROUTINE TO INITIALIZE

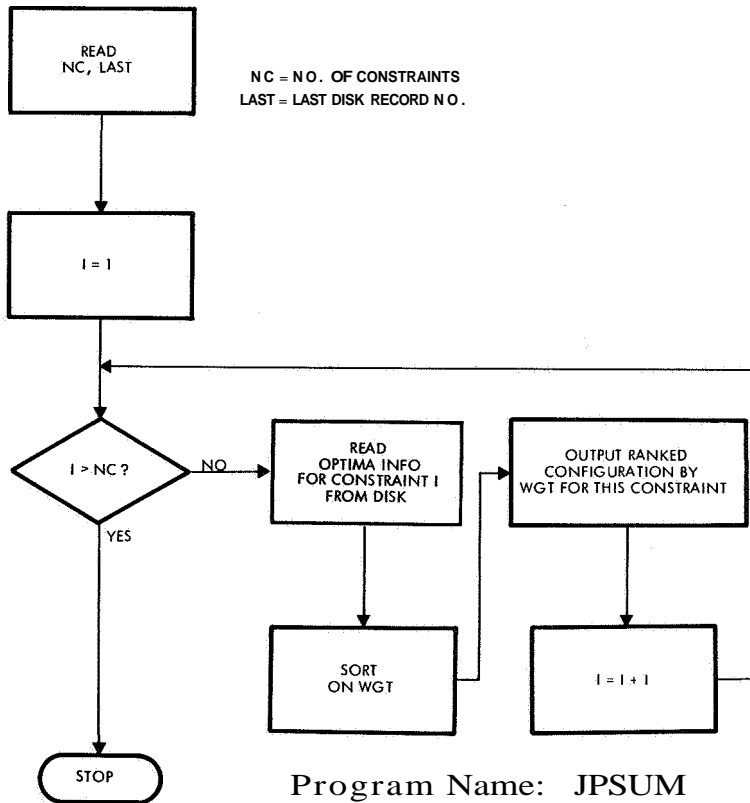
** "BUMP" SYSTEMATICALLY GENERATES EVERY COMBINATION OF ALTERNATES. ON FIRST SETS FLAG ≠ 0, ON LAST SETS FLAG = 0.

Program Name: JPL2

Figure 79. Logic Diagram Computer Program



Program Name: JPL



Program Name: JPSUM

Figure 79. (Continued)

Table 59. Program Listing

JPL		
	REAL AC3(4,3,8),DC3(4,3,8),LR3(4,3,5),ES3(7,3,11),ARC3(3,3,6),	
	S SA2(2,4),C(50),HEAD(20)	
	INTEGER ALR(5),AES(11),AARC(6),LMAX(11),L(11),FLAG	
	COMMON N, FLAG, LMAX, L	
	COMMON KK	
	DEFINE PILE 2(5,320,U,IX2)	
	READ(2,1)JOB, KK	
	GOTO(50,150),JOB	
50	READ(2,10)HEAD	
	WRITE(3,11)HEAD	FUNCTION
	WRITE(3,12)HEAD	Reads the input data (which is constant
	WRITE(3,13)	from case to case) and stores it on the
	WRITE(3,20)	disc. Calls execution of JPLZ. Provides
	READ(2,1)NLE	for a switch direct to JPL2 if Job is
	DO 60 NU=1,NLE	being restarted.
	READ(2,2) (AC3(I,1,NU),I=1,4)	
	WRITE(3,21)NU,(AC3(I,1,NU),I=1,4)	
	DO 60 J=1,2	
	READ(2,2) (AC3(I,J&1,NU),I=1,4)	
60	WRITE(3,22)J,(AC3(I,J&1,NU),I=1,4)	
	WRITE(3,12)HEAD	
	WRITE(3,14)	
	WRITE(3,20)	
	DO 70 NU=1,NLE	
	READ(2,2) (DC3(I,1,NU),I=1,4)	
	WRITE(3,21)NU,(DC3(I,1,NU),I=1,4)	
	DO 70 J=1,2	
	READ(2,2) (DC3(I,J&1,NU),I=1,4)	
70	WRITE(3,22)J,(DC3(I,J&1,NU),I=1,4)	Note: & is equivalent to +
	WRITE(3,12)HEAD	
	WRITE(3,15)	
	WRITE(3,20)	
	READ(2,1)KLR,(ALR(I),I=1,KLR)	
	DO 80 NU=1,KLR	
	READ(2,2) (LR3(I,1,NU),I=1,4)	
	WRITE(3,21)NU,(LR3(I,1,NU),I=1,4)	
	M=ALR(NU)	
	DO 80 J=1,M	
	READ(2,2) (LR3(I,J&1,NU),I=1,4)	
80	WRITE(3,22)J,(LR3(I,J&1,NU),I=1,4)	
	WRITE(3,12)HEAD	
	WRITE(3,16)	
	WRITE(3,20)	
	READ(2,1)KES,(AES(I),I=1,KES)	
	DO 90 NU=1,KES	
	READ(2,2) (ES3(I,1,NU),I=1,7)	
	WRITE(3,21)NU,(ES3(I,1,NU),I=1,7)	
	M=AES(NU)	
	DO 90 J=1,M	
	READ(2,2) (ES3(I,J&1,NU),I=1,7)	
90	WRITE(3,22)J,(ES3(I,J&1,NU),I=1,7)	
	WRITE(3,12)HEAD	
	WRITE(3,17)	
	WRITE(3,20)	
	READ(2,1)KAC,(AARC(I),I=1,KAC)	
	DO 100 NU=1,KAC	
	READ(2,2) (ARC3(I,1,NU),I=1,3)	
	WRITE(3,21)NU,(ARC3(I,1,NU),I=1,3)	
	M=AARC(NU)	
	DO 100 J=1,M	
	READ(2,2) (ARC3(I,J&1,NU),I=1,3)	
100	WRITE(3,22)J,(ARC3(I,J&1,NU),I=1,3)	
	WRITE(3,12)HEAD	
	WRITE(3,18)	
	WRITE(3,20)	
	READ(2,1)KSA	
	DO 110 NU=1,KSA	
	READ(2,2) (SA2(I,NU),I=1,2)	
110	WRITE(3,21)NU,(SA2(I,NU),I=1,2)	
	WRITE(3,12)HEAD	
	WRITE(3,19)	
	READ(2,1)NC	
	READ(2,2) (C(I),I=1,NC)	
	WRITE(3,23) (I,C(I),I=1,NC)	
	WRITE(1,24)	
	PAUSE 1111	
C	SAVE MASTER DATA ON DISK	
	WRITE(2,1)HEAD,NLE,AC3,DC3,KLR,ALR,LR3,KES,AES,ES3,KAC,AARC,ARC3,	
	SKSA,SA2,NC,C	
150	CALL LINK(JPL2)	
1	FORMAT (16I5)	
12	FORMAT (1H1,10X,20A4)	
10	FORMAT (20A4)	
11	FORMAT(1H1,'NEW RUN START'//1X, 20A4//1X,'MASTER DATA LOAD=='//)	

Table 59 (Continued)

```

23 FORMAT(1H0,'TYPE',1X,'ALT',9X,'P1',11X,'P2',11X,'P3',11X,'P4',11X,
S'P5',11X,'P6',11X,'P7'//)
13 FORMAT(1H0,'AC LOAD EQUIPMENT'//)
21 FORMAT(1H0,13,3X,'C',3X,7E13,6)
22 FORMAT(1H ,17,3X,7E13,6)
2 FORMAT(8F10,0)
14 FORMAT(1H0,'DC LOAD EQUIPMENT'//)
15 FORMAT(1H0,'LINE REGULATOR'//)
16 FORMAT(1H0,'ENERGY STORAGE'//)
17 FORMAT(1H0,'ARRAY CONTROL'//)
18 FORMAT(1H0,'SOLAR ARRAY'//)
19 FORMAT(1H0,'RELIABILITY CONSTRAINTS....'//)
23 FORMAT(1H ,15,F12,6)
24 FORMAT(1H ,1,'CHECK FOREGOING INPUT--IF O.K. PRESS START!')

```

JPL2

FUNCTION

	<p>Reads input data card describing a case. selects a combination of baseline and redundant units (begins with all baseline and cycles through to all most highly redundant) and assembles the data appropriately. computes reliability (keeps track of AC and DC systems separately), computes weights of AC and DC systems (skips calculations if reliability does not meet the minimum constraint), stores data (reliability, weight and alternates selected) if this cycle gives a lower weight while meeting a given reliability constraint. After all possible combinations have been explored, outputs data on best combinations as a function of the reliability constraints. Also writes this information in a file on the disc.</p>
(Main)	
	<p>Selects next combination of alternates to be considered in the coming cycle. Sets a flag if all possible combinations have been explored.</p>
(BUMP)	

```

REAL AC3(4,3,8),DC3(4,3,8),LR3(4,3,5),ES3(7,5,11),ARC3(3,3,6),
SSA2(2,4),LR2(4,3),ES2(7,5),ARC2(3,3),SA(2),C(50),
SAC2(4,8),DC2(4,8),LR(4),ES(7),ARC(3),HEAD(20)
SMOP(50,2),MMI,NMI,MLR,NLR,MB,MCR,MDR,NCR,NDR,MAC,NAC

```

```

INTEGER ALR(5),AES(11),AARC(6),LMAX(11),L(11),LOP(50,11,2),
SFEAS(50,2),CYCLE,FLAG

```

```

COMMON N,FLAG,LMAX,L
COMMON IX1

```

```

EQUIVALENCE (TMI,AC3(1,1,2)),(SMI,AC3(2,1,2)),(MMI,AC2(2,2)),
S(NMI,AC2(3,2)),(TLR,LR2(1,1)),(SLR,LR2(2,1)),(PRBD,LR2(3,1)),
S(PRBE,LR2(4,1)),(MLR,LR(2)),(NLR,LR(3)),(TB,ES2(1,1)),(TCR,ES2(2,1
S)),(TDR,ES2(3,1)),(PUBE,ES2(4,1)),(SCR,ES2(5,1)),(SDR,ES2(6,1)),
S(F,ES2(7,1)),(MB,ES(2)),(MCR,ES(3)),(MDR,ES(4)),(NCR,ES(5)),
S(NDR,ES(6)),(FK,ES(7)),(TAC,ARC2(1,1)),(SAC,ARC2(2,1))

```

```

EQUIVALENCE (PUBD,ARC2(3,1)),(MAC,ARC(2)),(NAC,ARC(3)),(RLR,LR(1))
S,(RES,ES(1)),(RAC,ARC(1)),(RSA,SA(1)),(A,SA(2))

```

```

OEFINE FILE 1(320,202,U,IX1)
DEFINE FILE 2( 5,320,U,IX2)

```

```

150 READ(2,1)HEAD,NLE,AC3,DC3,KLR,ALR,LR3,KES,AES,ES3,KAC,AARC,ARC3,
SKSA,SA2,NC,C
WRITE(3,25)HEAD

```

C READ CASE SPECIFICATION AND SETUP CASE MATRICIES

```

160 READ(2,1)JSA,JARC,JES,JLR
IF(JSA)700,700,165
165 CONTINUE
WRITE(3,12)HEAD
WRITE(3,26)JSA,JARC,JES,JLR
SA(1)=SA2(1,JSA)
SA(2)=SA2(2,JSA)
166 FIND(1,IX1)

```

Table 59. (Continued)

```

WGT=WGT&A*PSA
GOTO(350,390),KOB
350 WA=WGT
360 IF(R2-C(1)) 400,370,370

C COMPUTE CC-WEIGHT
370 KOB=2
DIRF=PRRF
PLRD=PRBD
WGT=0.0
DO 380 NU=1,NLE
PLRE=PLRE&DC3(1,1,NU)/DC2(3,NU)
PLRD=PLRD&DC3(2,1,NU)/DC2(4,NU)
380 WGT=WGT&DC2(2,NU)
GOTO 325
390 WD=WGT

RT1,CYCLE)=10000*R1&.5
R(2,CYCLE)=10000*R2&.5
W(1,CYCLE)=10*WA&.5
W(2,CYCLE)=10*WD&.5
GOTO 225

C SETUP CURRENT OPTIMA
400 DO 450 I=1,NC
IF(R1-C(I))460,410,410
410 IF(FEAS(I,1))430,430,420
420 IF(MOP(I,1)-WA)450,450,430
430 MOP(I,1)=WA
ROP(I,1)=R1
DO 440 J=1,N
440 LOP(I,J,1)=L(J)
450 FEAS(I,1)=FEAS(I,1)&1
460 OO 510 I=1,NC
IF(R2-C(I))520,470,470
470 IF(FEAS(I,2))490,490,480
480 IF(MOP(I,2)-WD)510,510,490
490 MOP(I,2)=WD
ROP(I,2)=R2
DO 500 J=1,N
500 LOP(I,J,2)=L(J)
510 FEAS(I,2)=FEAS(I,2)&1
520 IF(CYCLE=M)225,530,530
530 WRITE(3,50)R1,WA,R2,WD

RZ=RSA*AC*RES*RLR
R1=1.0
R2=1.0
DO 280 J=1,NLE
R1=R1*AC2(1,J)
280 R2=R2*DC2(1,J)
R1=R1*R
R2=R2*R
IF(R1-C(1)) 360,290,290

C COMPUTE AC WEIGHT
290 KOB=1
PME=0.0
PMD=0.0
WGT=AC2(2,1)
DO 300 NU=3,NLE
PME=PME&AC3(1,1,NU)/AC2(3,NU)
PMD=PMD&AC3(2,1,NU)/AC2(4,NU)
300 WGR=WGT&AC2
IF(PMD=PMR)320,320,310
310 PMR=PMD
320 WGT=WGT&MMI*PMR**TMI
EMIE=SMI*0.4342945*ALOG(PME)+NMI
EMID=SMI*0.4342945*ALOG(PMD)+NMI
PLRE=PME/EMIE&AC3(1,1,1)/AC2(3,1)&PRBE
PLRD=PMD/EMID&AC3(2,1,1)/AC2(4,1)&PRBD
325 PLRR=PLRE
IF(PLRD-PLRR)340,340,330
330 PLRR=PLRD
340 WGT=WGT&MLR*PLRR**TLR
ELRE=SLR*0.4342945*ALOG(PLRE)+NLR
ELRD=SLR*0.4342945*ALOG(PLRD)+NLR
PES=PLRE/ELR&PUBE
EDR=SDR*0.4342945*ALOG(PES/FK)+NDR
PB=PES/EDR
PCR=F*PB
WGT=WGT&FK*(MDR*PES**TDR+MB*PB**TB+MCR*PCR**TCR)
ECR=SCR*0.4342945*ALOG(PCR/FK)+NCR
PAC=PLRD/ELRD&PCR/ECR&PUBD
WGT=WGT&MAC*PAC**TAC
EAC=SAC*0.4342945*ALOG(PAC)+NAC
PSA=PAC/EAC

```

Table 59. (Continued)

```

SUBROUTINE BUMP
INTEGER FLAG,LMAX(11),L(11)
COMMON N,FLAG,LMAX,L
IF(FLAG) 40,40,10
10 DO 20 I=1,N
L(I)=L(I)&1
IF(L(I)-LMAX(I)) 30,30,20
20 L(I)=1
FLAG=0
30 RETURN
40 FLAG=1
DO 50 I=1,N
50 L(I)=1
GOTO 30
END

```

	FUNCTION
<pre> JPSUM KEAL MOP(50,2),ROP(50,2),WGT(320),REL(320) INTEGER JN(4), JC(4,320),IX(320) DEFINE FILE 1(320,202,U,JJ) 10 WRITE(1,5) READ(6,1)NC,NCASE JCB=0 50 JOB=JOB+1 IF(JOB-NC)60,60,55 CALL EXTT JJ=1 DO 80 J=1,NCASE READ(1,JJ) (JN(I),I=1,4),MOP,ROP FIND(I,JJ) K=2*J-1 WGT(K)=MOP(JOB,1) WGT(K+1)=MOP(JOB,2) REL(K)=ROP(JOB,1) REL(K+1)=ROP(JOB,2) DO 70 I=1,4 JC(I,K)=JN(I) 70 JC(I,K+1)=JN(I) 80 JC(I,K)=-JC(I,K) N=2*NCASE CALL SORT(WGT,N,IX) WRITE(3,2)JOB DO 90 J=1,N K=IX(J) 90 WRITE(3,3)J,WGT(J),REL(K),(JC(I,K),I=1,4) GOTO 50 1 FORMAT(1615) 2 FORMAT(1H1,'RANKING BY TYPE FOR CONSTRAINT NO.',15//1X, \$TX,'NO.',4X,'WEIGHT',7X,'REL',9X,'CASE'//) 3 FORMAT(1H,10, F10.2, F10.6, 5X, 4I3) 5 FORMAT('ENTER(215), NO. CONSTRAINTS, NO. CASES'//) </pre>	<p>For each reliability constraint, reads the disc file of system optima saved by JPL2, sorts on the weight values, and outputs weight, reliability, and case designation (preceded by a - for AC systems) from least to heaviest weight for all 156 systems.</p> <p>Sorts a list of floating point values and retains an index of their original order in the list.</p>

Table 59. (Continued)

```

LMAX(1)=AARC(JARC)
OO 170 I=1,3
DO 170 J=1,3
170 ARC2(I,J)=ARC3(I,J,JARC)
LMAX(2)=AES(JES)
DO 180 I=1,7
OO 180 J=1,5
180 ES2(I,J)=ES3(I,J,JES)
LMAX(3)=ALRIJLR)
OO 190 I=1,4
OO 190 J=1,3
190 LR2(I,J)=LR3(I,J,JLR)
OO 200 J=1,NLE
200 LMAX(J&3)=2
M=LMAX(1)*LMAX(2)*LMAX(3)
DO 210 J=1,NLE
210 M=M*LMAX(J+3)
WRITE(3,27)M
N=NLE&3
FLAG=0
CYCLE=0

C BEGIN COMBINATORIAL SEARCH
DO 220 I=1,NC
DO 220 J=1,2
220 FEAS(I,J)=0
225 CALL BUMP
IF(FLAG)550,550,230
230 CYCLE=CYCLE&1
J=L(I)&1
DO 240 I=1,3
240 ARC(I)=ARC2(I,J)
J=L(2)&1
OO 250 I=1,7
250 ES(I)=ES2(I,J)
J=L(3)&1
OO 260 I=1,4
260 LR(I)=LR2(I,J)
OO 270 NU=1,NLE
J=L(NU&3)&1
OO 270 I=1,4
AC2(I,NU)=AC3(I,J,NU)
270 DC2(I,NU)=DC3(I,J,NU)
C COMPUTE RELIABILITY
I
GOTO 225

OUTPUT CASE
550 WRITE(3,30)
WRITE(3,28)
OO 563 I=1,NC
IF(FEAS(I,1))562,562,560
560 WRITE(3,29)I,FEAS(I,1),MOP(I,1),ROP(I,1),(LOP(I,J,1),J=1,N)
561 GOTO 563
562 WRITE(3,29)I,FEAS(I,1)
563 CONTINUE
WRITE(3,31)
WRITE(3,28)
DO 573 I=1,NC
IF(FEAS(I,2))572,572,570
570 WRITE(3,29)I,FEAS(I,2),MOP(I,2),ROP(I,2),(LOP(I,J,2),J=1,N)
571 GOTO 573
572 WRITE(3,29)I,FEAS(I,2)
573 CONTINUE
WRITE(1,35)IX1,JSA,JARC,JES,JLR,MOP,ROP
WRITE(1,35)IX1,JSA,JARC,JES,JLR
GOTO 160
600 CALL EXIT

1 FORMAT(16I5)
12 FORMAT(1H1,10X,20A4)
25 FORMAT(1H1,10X,20A4//1X,'CONTINUED')
26 FORMAT(1H0,'SOLAR ARRAY TYPE=',I3/1X,'ARRAY CONTROL TYPE=',I3/1X,
$'ENERGY STORAGE TYPE=',I3/1X,'LINE REGULATOR TYPE=',I3//)
27 FORMAT(1H,'NO. COMBINATIONS=',I-//)
29 FORMAT(1H,'110.19,F12.2,F13.6,5X,11I3)
30 FORMAT(1H0,'AC SYSTEM')
31 FORMAT(1H0,'DC SYSTEM')
35 FORMAT(1H0,'CASE',I5,5X,4I3)
28 FORMAT(1H0,'MATRIX OF OPTIMA//1X,'CONSTRAINT FEASBLE MIN WEIGHT
$,'2X,'RELIABILITY',5X,'CONFIGURATION...')
50 FORMAT(1H0,'MAX AC SYSTEM'/1X,'R=',F10.6,10X,'WGT=',F10.2//1X,
$ 'MAX DC SYSTEM'/1X,'R=',F10.6,10X,'WGT=',F10.2//)
END

```

Table 60. System Optimization Computer Printout,
Mercury Flyby

MERCURY FLYBY

SOLAR ARRAY TYPE= 3
 ARRAY CONTROL TYPE= 4
 ENERGY STORAGE TYPE= 9
 LINE REGULATOR TYPE= 5

NO. COMBINATIONS= 512

MAX AC SYSTEM
 R= 0.999549 WGT= 99.64

YAX OC SYSTEY
 R= 0.999487 WGT= 98.44

AC SYSTEM

MATRIX OF OPTIMA

CONSTRAINT	FEASBLE	MIN WEIGHT	RELIABILITY	CONFIGURATION....
1	512	55.94	0.950386	1 1 1 1 1 1 1 1 1
2	512	55.94	0.950386	1 1 1 1 1 1 1 1 1
3	512	55.94	0.950386	1 1 1 1 1 1 1 1 1
4	512	55.94	0.950386	1 1 1 1 1 1 1 1 1
5	512	55.94	0.950386	1 1 1 1 1 1 1 1 1
6	500	58.01	0.955617	1 1 1 1 1 1 2 2 2
7	463	58.74	0.9961539	1 1 1 2 1 1 1 2 1
8	408	60.36	0.965055	1 1 1 2 1 1 2 2 2
9	348	61.85	0.971021	1 2 1 2 1 1 1 2 2
10	285	66.12	0.976430	1 2 1 2 2 1 2 2 2
11	225	69.83	0.980084	2 2 1 2 1 2 2 2 2
12	142	82.48	0.986361	1 3 1 2 1 1 1 2 2
13	114	83.72	0.989216	1 3 1 2 1 1 2 2 2
14	80	86.71	0.990101	1 3 1 2 2 1 2 2 1
15	54	88.17	0.99222 1	2 3 1 2 1 1 1 2 2
16	24	90.79	0.995567	2 3 1 2 1 2 2 2 2
17	10	93.08	0.997748	2 3 1 2 2 1 2 2 2
18	2	94.46	0.999233	2 3 1 2 2 2 2 2 2
19	2	94.46	0.999233	2 3 1 2 2 2 2 2 2
20	1	99.64	0.999549	2 4 1 2 2 2 2 2 2

DC SYSTEM

MATRIX OF OPTIYA

CONSTRAINT	FEASBLE	PIN WEIGHT	RELIABILITY	CONFIGURATION....
1	512	56.09	0.938768	1 1 1 1 1 1 1 1 1
2	512	56.09	0.938768	1 1 1 1 1 1 1 1 1
3	511	56.42	0.942895	1 1 1 1 1 1 2 1 1
4	505	57.27	0.947493	1 1 1 1 1 1 2 2 1
5	488	58.34	0.951578	1 1 1 1 1 1 2 2 2
6	452	59.63	0.956851	1 1 1 2 1 1 2 2 1
7	398	60.70	0.960976	1 1 1 2 1 1 2 2 2
8	338	62.54	0.965540	1 1 1 2 2 1 2 2 2
9	275	65.06	0.973336	1 2 1 2 2 1 2 2 2
10	203	67.15	0.977823	1 2 1 2 2 2 2 2 2
11	136	72.82	0.983632	2 2 1 2 2 2 2 2 2
12	73	85.45	0.988712	1 3 1 2 2 1 2 2 2
13	46	85.45	0.988712	1 3 1 2 2 1 2 2 2
14	29	87.72	0.993270	1 3 1 2 2 2 2 2 2
15	14	87.72	0.993270	1 3 3 2 2 2 2 2 2
16	4	93.39	0.99917 1	2 3 1 2 2 2 2 2 2
17	2	93.39	0.99917 1	2 3 1 2 2 2 2 2 2
18	2	93.39	0.99917 1	2 3 1 2 2 2 2 2 2
19	1	98.44	0.999487	2 4 1 2 2 2 2 2 2
20	0			

**Table 61. System Optimization Computer Printout,
Venus Orbiter No. 1**

VENUS ORBITER NO. 1

SOLAR ARRAY TYPE= 2
 ARRAY CONTROL TYPE= 4
 ENERGY STORAGE TYPE= 9
 LINE REGULATOR TYPE= 5

NO. COMBINATIONS* 256

MAX AC SYSTEM
 R= 0.998970 WGT= 205.28

MAX DC SYSTEM
 R= 0.998733 WGT= 198.32

AC SYSTEM

MATRIX OF OPTIMA CONSTRAINT	FEASBLE	MIN WEIGHT	RELIABILITY	CONFIGURATION....
1	256	109.80	0.913026	1 1 1 1 1 1 1 1
2	256	109.80	0.913026	1 1 1 1 1 1 1 1
3	256	109.80	0.913026	1 1 1 1 1 1 1 1
4	255	110.28	0.918705	1 1 1 1 1 1 1 2
5	250	111.34	0.921856	1 1 1 1 1 2 1 2
6	245	112.28	0.931155	1 1 1 2 1 1 1 1
7	236	112.28	0.931155	1 1 1 2 1 1 1 1
8	221	112.76	0.936947	1 1 1 2 1 1 1 2
9	209	113.82	0.940161	1 1 1 2 1 2 1 2
10	131	115.68	0.946287	1 2 1 2 1 1 1 1
11	172	116.16	0.952173	1 2 1 2 1 1 1 2
12	151	117.24	0.955439	1 2 1 2 1 2 1 2
13	125	121.29	0.962524	1 2 1 2 2 2 1 2
14	102	123.22	0.966169	1 2 1 2 2 2 2 2
15	79	125.31	0.970517	2 2 1 2 1 2 2 2
16	58	129.49	0.977713	2 2 1 2 2 2 2 2
17	39	189.11	0.983588	2 3 1 2 1 1 1 2
18	24	190.56	0.986963	2 3 1 2 1 2 1 2
19	12	193.14	0.990700	2 3 1 2 1 2 2 2
20	4	198.46	0.998046	2 3 1 2 2 2 2 2

DC SYSTEM

MATRIX OF OPTIMA CONSTRAINT	FEASBLE	MIN WEIGHT	RELIABILITY	CONFIGURATION....
1	252	108.17	0.906388	1 1 1 1 1 1 1 2
2	250	108.17	0.906388	1 1 1 1 1 1 1 2
3	242	108.53	0.914413	1 1 1 1 1 1 2 2
4	238	109.97	0.915056	1 1 1 1 1 2 1 2
5	226	110.33	0.923158	1 1 1 1 1 2 2 2
6	209	111.01	0.932570	1 1 1 2 1 1 2 2
7	199	111.01	0.932570	1 1 1 2 1 1 2 2
8	175	112.81	0.941489	1 1 1 2 1 2 2 2
9	164	112.81	0.941489	1 1 1 2 1 2 2 2
10	132	114.36	0.947725	1 2 1 2 1 1 2 2
11	119	115.59	0.950493	1 1 1 2 2 2 2 2
12	92	116.18	0.956789	1 2 1 2 1 2 2 2
13	70	118.99	0.965939	1 2 1 2 2 2 2 2
14	55	118.99	0.965939	1 2 1 2 2 2 2 2
15	38	125.08	0.977480	2 2 1 2 2 2 2 2
16	27	125.08	0.977480	2 2 1 2 2 2 2 2
17	13	185.61	0.986026	1 3 1 2 2 2 2 2
18	10	185.61	0.986026	1 3 1 2 2 2 2 2
19	2	191.68	0.997808	2 3 1 2 2 2 2 2
20	2	191.68	0.997808	2 3 1 2 2 2 2 2

Table 62. System Optimization Computer Printout,
Venus Orbiter No. 2

VENUS ORBITER NO. 2

SOLAR ARRAY TYPE= 3
 ARRAY CONTROL TYPE= 4
 ENERGY STORAGE TYPE= 9
 LINE REGULATOR TYPE= 5

NO. COMBINATIONS= 1024

MAX AC SYSTEM
 R= 0.998983 WGT= 426.21

MAX DC SYSTEM
 R= 00399031 WGT= 419.52

AC SYSTEM

MATRIX OF OPTIMA					CONFIGURATION....														
CONSTRAINT	FEASBLE	MIN WEIGHT	RELIABILITY																
1	1024	233.30	0.910938		1	1	1	1	1	1	1	1	1	1	1	1	1	1	1
2	1024	233.30	0.910938		1	1	1	1	1	1	1	1	1	1	1	1	1	1	1
3	1024	233.30	0.910938		1	1	1	1	1	1	1	1	1	1	1	1	1	1	1
4	1018	233.78	0.915706		1	1	1	1	1	1	1	1	1	1	2	2	2	2	2
5	999	235.51	0.921854		1	1	1	1	1	2	1	2	1	2	2	2	2	2	2
6	973	235.76	0.929038		1	1	1	2	1	1	1	1	1	1	1	1	1	1	1
7	936	235.99	0.931366		1	1	1	2	1	1	1	1	1	1	1	1	1	1	2
8	878	236.45	0.935020		1	1	1	2	1	1	1	1	2	2	2	1	2	2	1
9	817	237.96	0.940171		1	1	1	2	1	2	1	2	1	2	2	2	2	2	2
10	752	242.29	0.946501		1	2	1	2	1	1	1	1	1	1	1	2	2	2	2
11	674	242.74	0.950010		1	2	1	2	1	1	1	1	2	1	2	1	2	1	2
12	576	244.28	0.955450		1	2	1	2	1	2	1	2	1	2	2	2	2	2	2
13	479	249.40	0.960131		1	2	1	2	2	2	2	1	2	2	2	1	2	2	1
14	390	252.19	0.966181		1	2	1	2	2	2	2	2	2	2	2	2	2	2	2
15	295	257.94	0.970527		2	2	1	2	1	2	2	2	2	2	2	2	2	2	2
16	207	263.19	0.8975072		2	2	1	2	2	2	2	2	2	2	2	1	2	2	2
17	142	398.78	0.980098		1	3	1	2	2	2	2	2	2	2	2	2	2	2	1
18	86	402.53	0.986274		1	3	1	2	2	2	2	2	2	2	2	2	2	2	2
19	37	406.63	0.990710		2	3	1	2	1	2	2	2	2	2	2	2	2	2	2
20	10	411.97	0.995076		2	3	1	2	2	2	1	2	2	2	2	2	2	2	2

DC SYSTEM

MATRIX OF OPTIMA					CONFIGURATION....														
CONSTRAINT	FEASBLE	MIN WEIGHT	RELIABILITY																
1	999	233.43	0.905808		1	1	1	1	1	1	2	1	2	2	2	2	2	2	2
2	989	233.43	0.905808		1	1	1	1	1	1	2	1	2	2	2	2	2	2	2
3	946	234.29	0.914761		1	1	1	1	1	1	2	2	2	2	2	2	2	2	2
4	923	235.09	0.915760		1	1	1	2	1	1	1	1	2	2	2	2	2	2	2
5	864	235.89	0.923903		1	1	1	2	1	1	2	1	2	2	2	2	2	2	2
6	796	236.31	0.925013		1	1	1	2	1	1	2	2	2	2	2	1	2	2	1
7	745	236.74	0.933035		1	1	1	2	1	1	2	2	2	2	2	2	2	2	2
8	636	239.17	0.941733		1	1	1	2	1	2	2	2	2	2	2	2	2	2	2
9	592	239.17	0.941733		1	1	1	2	1	2	2	2	2	2	2	2	2	2	2
10	454	242.70	0.950783		1	1	1	2	2	2	2	2	2	2	2	2	2	2	2
11	409	242.70	0.950783		1	1	1	2	2	2	2	2	2	2	2	2	2	2	2
12	287	245.44	0.957037		1	2	1	2	1	2	2	2	2	2	2	2	2	2	2
13	238	249.00	0.8966233		1	2	1	2	2	2	2	2	2	2	2	2	2	2	2
14	152	249.00	0.966233		1	2	1	2	2	2	2	2	2	2	2	2	2	2	2
15	107	260.07	0.977779		2	2	1	2	2	2	2	2	2	2	2	2	2	2	2
16	61	260.07	0.977779		2	2	1	2	2	2	2	2	2	2	2	2	2	2	2
17	37	396.22	0.986327		1	3	1	2	2	2	2	2	2	2	2	2	2	2	2
18	16	396.22	0.986327		1	3	1	2	2	2	2	2	2	2	2	2	2	2	2
19	5	407.25	0.998113		2	3	1	2	2	2	2	2	2	2	2	2	2	2	2
20	2	407.25	0.998113		2	3	1	2	2	2	2	2	2	2	2	2	2	2	2

Table 63. System Optimization Computer Printout, Mars Orbiter

MARS ORBITER

SOLAR-ARRAY TYPE= 3
 ARRAY CONTROL TYPE= 4
 ENERGY STORAGE TYPE= 9
 LINE REGULATOR TYPE= 5

NO. COMBINATIONS= 512

MAX AC SYSTEM
 R= Om998540 WGT= 707.93

MAX DC SYSTEM
 R= 0.998035 WGT= 690.19

AC SYSTEM

CONSTRAINT	FEASBLE	MIN WEIGHT	RELIABILITY	CONFIGURATION...
1	504	497.14	0.90048 1	1 1 1 1 1 1 1 1 2
	495	498.58	0.912181	1 1 1 2 1 1 1 1 1
	484	498.58	0.912181	1 1 1 2 1 1 1 1 1
4	470	499.61	0.916202	1 1 1 2 1 1 1 1 2 1
5	444	499.65	0.921756	1 1 1 2 1 1 1 1 1 2
6	420	500.68	0.925819	1 1 1 2 1 1 1 1 2 2
7	387	507.24	0.933905	1 2 1 2 1 1 1 1 2 1
8	357	507.28	Om939566	1 2 1 2 1 1 1 1 1 2
9	323	508.31	0.943708	1 2 1 2 1 1 1 1 2 2
10	284	512.53	0.947073	1 2 1 2 1 2 1 2 2 2
11	244	517.42	0.951338	1 2 1 2 1 2 2 2 2 2
12	205	524.27	0.955428	1 2 1 2 2 2 1 2 2 2
13	165	529.90	0.960526	2 2 1 2 1 2 1 2 2 2
14	131	537.47	0.965557	2 2 1 2 2 1 1 2 2 2
15	96	546.93	0.973364	2 2 1 2 2 2 2 2 2 2
16	67	665.05	0.975390	1 3 1 2 2 1 1 2 2 2
17	44	668.08	0.980596	2 3 1 2 1 1 1 2 2 2
18	23	674.26	0.985012	2 3 1 2 1 1 2 2 2 2
19	10	687.78	0.992774	2 3 1 2 2 2 1 2 2 2
20	2	694.08	0.997245	2 3 1 2 2 2 2 2 2 2

DC SYSTEM

CONSTRAINT	FEASBLE	MIN WEIGHT	RELIABILITY	CONFIGURATION...
1	407	494.73	0.900 188	1 1 1 2 1 1 1 1 1 2
2	392	495813	0.909669	1 1 1 2 1 1 2 1 2 2
3	353	496.31	0.910723	1 1 1 2 1 1 1 1 2 2
4	330	497.31	0.920315	1 1 1 2 1 1 2 2 2 2
5	293	497.31	0.920315	1 1 1 2 1 1 2 2 2 2
6	260	503.23	0.930476	1 1 1 2 1 2 2 2 2 2
7	229	503.23	0.930476	1 1 1 2 1 2 2 2 2 2
8	189	504885	0.938097	1 2 1 2 1 1 2 2 2 2
9	169	509.29	0.941 062	1 1 1 2 2 2 2 2 2 2
10	124	510.81	Om948454	1 2 1 2 1 2 2 2 2 2
11	116	516.93	0.959245	1 2 1 2 2 2 2 2 2 2
12	72	516.93	Om959245	1 2 1 2 2 2 2 2 2 2
13	71	528.01	0.961928	2 2 1 2 1 2 2 2 2 2
14	38	534.22	0.972872	2 2 1 2 2 2 2 2 2 2
15	35	534.22	0.972872	2 2 1 2 2 2 2 2 2 2
16	21	659.48	0.982780	1 3 1 2 2 2 2 2 2 2
17	12	659.48	0.982780	1 3 1 2 2 2 2 2 2 2
18	10	669.31	0.985528	2 3 1 2 1 2 2 2 2 2
19	2	676.71	0.996741	2 3 1 2 2 2 2 2 2 2
20	2	676.71	0.996741	2 3 1 2 2 2 2 2 2 2

Table 64. System Optimization Computer Printout, Jupiter Flyby

JUPITER FLYBY

SOLAQ ARRAY TYPE= 2
 ARRAY CONTROL TYPE= 4
 ENERGY STORAGE TYPE= 9
 LINE REGULATOR TYPE= 5

NO. COMBINATIONS= 512

YAX AC SYSTEM
 R= 0.000000 WGT= 1003.67

MAX DC SYSTEM
 R= 0.000000 WGT= 969.79

AC SYSTEK

YATRIX OF OPTIMA

CONSTRAINT	FEASBLE	MIN WEIGHT	RELIABILITY	CONFIGURATION.....
1	133	941.90	0.912860	1 3 1 1 1 1 1 1 2
2	131	941.90	0.912860	1 3 1 1 1 1 1 1 2
3	124	941.90	0.912860	1 3 1 1 1 1 1 1 2
4	118	943.95	0.921961	1 3 1 1 1 1 1 1 2
5	112	943.95	0.921961	1 3 1 1 1 1 1 1 2
6	104	948.94	0.929168	1 4 1 1 1 1 1 1 2
7	95	954.10	0.936466	1 4 1 1 1 1 1 1 2
8	84	954.10	0.936466	1 4 1 1 1 1 1 1 2
9	73	962.69	0.941447	2 3 1 1 1 1 1 1 2
10	62	964.77	0.950533	2 3 1 1 1 1 1 1 2
11	52	964.77	0.950533	2 3 1 1 1 1 1 1 2
12	41	969.77	0.958266	2 4 1 1 1 1 1 1 2
13	30	975.02	0.965792	2 4 1 1 1 1 1 1 2
14	22	075.02	0.965792	2 4 1 1 1 1 1 1 2
15	14	984.60	0.972158	2 4 1 1 1 1 1 1 2
16	9	988.52	0.976988	2 4 1 1 2 1 1 1 2
17	5	993.88	0.984661	2 4 1 1 2 1 1 1 2
18	1	1003.67	0.991152	2 4 1 1 2 2 2 2 2
19	1	1003.67	0.991152	2 4 1 1 2 2 2 2 2
20	0			

DC SYSTEM

MATRIX OF OPTIMA

CONSTRAINT	FEASBLE	MIN WEIGHT	RELIABILITY	CONFIGURATION.. ..
1	65	027.53	0.907298	1 3 1 1 1 1 2 2 2
2	64	927.53	0.907298	1 3 1 1 1 1 2 2 2
3	57	932.44	0.914391	1 4 1 1 1 1 2 2 2
4	43	933.01	0.930145	1 3 1 1 2 1 2 2 2
5	36	933.01	0.930145	1 3 1 1 1 1 2 2 2
6	34	933.01	0.930145	1 3 1 1 2 1 2 2 2
7	31	933.01	0.930145	1 3 1 1 2 1 2 2 2
8	26	937.91	0.937416	1 4 1 1 2 1 2 2 2
9	19	944.07	0.951670	1 3 1 1 2 2 2 2 2
10	12	944.07	0.951670	1 3 1 1 2 2 2 2 2
11	12	944.07	0.951670	1 3 1 1 2 2 2 2 2
12	11	949.05	0.959110	1 4 1 1 2 2 2 2 2
13	6	958.50	0.966771	2 4 1 1 2 1 2 2 2
14	4	958.50	0.966771	2 4 1 1 2 1 1 2 2
15	2	964.81	0.981472	2 3 1 1 2 2 2 2 2
16	2	964.81	0.981472	2 3 1 1 2 2 2 2 2
17	2	964.81	0.981472	2 3 1 1 2 2 2 2 2
18	1	969.79	0.989145	2 4 1 1 2 2 2 2 2
19	0			
20	0			

Table 65. System Optimization Computer Printout,
Jupiter Orbiter No. 1

JUPITER ORBITER NO. 1

SOLAR ARRAY TYPE= 2
 ARRAY CONTROL TYPE= 4
 ENERGY STORAGE TYPE= 9
 LINE REGULATOR TYPE= 5

NO. COMBINATIONS= 512

MAX AC SYSTEM
 R= 0.990829 WGT= 1249.52

MAX DC SYSTEM
 R= 0.988150 WGT= 1216.57

AC SYSTEM

MATRIX OF OPTIMA

CONSTRAINT	FEASBLE	MIN WEIGHT	RELIABILITY	CONFIGURATION....
1	157	1143.03	0.901069	2 2 1 2 1 1 2 2 2
2	146	1147.29	0.909235	2 2 1 2 1 2 2 2 2
3	125	1151.07	0.910869	2 2 1 2 2 1 1 2 2
4	116	1155.43	0.919123	2 2 1 2 2 2 1 2 2
5	95	1160.87	0.921295	2 2 1 2 2 1 2 2 2
6	87	1165.23	0.929644	2 2 1 2 2 2 2 2 2
7	71	1205.35	0.931782	2 3 1 2 1 1 1 1 2
8	64	1206.20	0.938386	1 3 1 2 2 2 1 2 2
9	53	1207.51	0.942225	2 3 1 2 1 1 1 1 2
10	44	1211.94	0.950764	2 3 1 2 1 2 1 2 2
11	35	1211.94	0.950764	2 3 1 2 1 2 1 2 2
12	26	1220.69	0.958110	2 4 1 2 1 2 1 2 2
13	21	1221.96	0.961646	2 3 1 2 1 2 2 2 2
14	13	1230.40	0.972105	2 3 1 2 2 2 1 2 2
15	11	1230.40	0.972105	2 3 1 2 2 2 1 2 2
16	5	1239.22	0.979616	2 4 1 2 2 2 1 2 2
17	3	1240.65	0.983232	2 3 1 2 2 2 2 2 2
18	1	1249.52	0.990829	2 4 1 2 2 2 2 2 2
19	1	1249.52	0.990829	2 4 1 2 2 2 2 2 2
20	0			

DC SYSTEM

MATRIX OF OPTIMA

CONSTRAINT	FEASBLE	MIN WEIGHT	RELIABILITY	CONFIGURATION....
1	70	1123.28	0.901065	2 2 1 2 1 2 2 2 2
2	49	1133.95	0.927130	2 2 1 2 2 2 2 2 2
3	38	1133.95	0.927130	2 2 1 2 2 2 2 2 2
4	37	1133.95	0.927130	2 2 1 2 2 2 2 2 2
5	35	1133.95	0.927130	2 2 1 2 2 2 2 2 2
6	33	1133.95	0.927130	2 2 1 2 2 2 2 2 2
7	20	1184.08	0.946560	1 3 1 2 2 2 2 2 2
8	15	1184.08	0.946560	1 3 1 2 2 2 2 2 2
9	12	1184.08	0.946560	1 3 1 2 2 2 2 2 2
10	12	1184.08	0.946560	1 3 1 2 2 2 2 2 2
11	11	1192.80	0.953873	1 4 1 2 2 2 2 2 2
12	6	1235.39	0.960369	2 4 1 2 1 2 2 2 2
13	5	1205.39	0.960369	2 4 1 2 1 2 2 2 2
14	2	1207.84	0.900573	2 3 1 2 2 2 2 2 2
15	2	1207.84	0.980573	2 3 1 2 2 2 2 2 2
16	2	1207.84	0.980573	2 3 1 2 2 2 2 2 2
17	2	1207.84	0.980573	2 3 1 2 2 2 2 2 2
18	1	1216.57	0.988150	2 4 1 2 2 2 2 2 2
19	0			
20	0			

Table 66. System Optimization Computer Printout,
Jupiter Orbiter No. 2

JUPITER ORBITER NO 2

SOLAR ARRAY TYPE= 2
 ARRAY CONTROL TYPE= 4
 ENERGY STORAGE TYPE= 9
 LINE REGULATOR TYPE= 5

NO. COMBINATIONS= 512

MAX AC SYSTEM
 R= 0.990753 WGT= 1765.30

MAX DC SYSTEM
 R= 0.988133 WGT= 1733.10

AC SYSTEM

MATRIX OF OPTIMA

CONSTRAINT	FEASBLE	MIN WEIGHT	RELIABILITY	CONFIGURATION....
1	162	1570.01	0.900999	2 2 1 2 1 1 2 2 2
2	147	1578.23	0.909165	2 2 1 2 1 2 2 2 2
3	128	1583.03	0.910799	2 2 1 2 2 1 1 2 2
4	116	1590.77	0.921224	2 2 1 2 2 1 2 2 2
5	98	1590.77	0.921224	2 2 1 2 2 1 2 2 2
6	87	1599.16	0.929572	2 2 1 2 2 2 2 2 2
7	75	1704.76	0.930107	1 3 1 2 2 1 2 1 2
8	65	1706.74	0.940530	1 3 1 2 2 1 2 2 2
9	56	1706.74	0.940530	1 3 1 2 2 1
10	46	1715.55	0.949054	1 3 1 2 2 2 2 2 2
11	37	1719.59	0.952937	2 3 1 2 1 1 2 2 2
12	27	1728.35	0.961572	2 3 1 2 1 2 2 2 2
13	22	1728.35	0.961572	2 3 1 2 1 2 2 2 2
14	13	1741.71	0.974327	2 3 1 2 2 1 2 2 2
15	11	1741.71	0.974327	2 3 1 2 2 1 2 2 2
16	5	1750.65	0.983157	2 3 1 2 2 2 2 2 2
17	3	1750.65	0.983157	2 3 1 2 2 2 2 2 2
18	1	1765.30	0.990753	2 4 1 2 2 2 2 2 2
19	1	1765.30	0.990753	2 4 1 2 2 2 2 2 2
20	0			

DC SVSTEC

MATRIX OF OPTIMA

CONSTRAINT	FEASRLR	MIN WEIGHT	RELIABILITY	CONFIGURATION....
1	69	1559.51	0.901797	2 2 1 2 2 1 2 2 2
2	49	1569.63	0.927115	2 2 1 2 2 2 2 2 2
3	38	1569.63	0.927115	2 2 1 2 2 2 2 2 2
4	37	1569.63	0.927115	2 2 1 2 2 2 2 2 2
5	35	1569.63	0.927115	2 2 1 2 2 2 2 2 2
6	33	1569.63	0.927115	2 2 1 2 2 2 2 2 2
7	20	1684.17	0.946545	1 3 1 2 2 2 2 2 2
8	15	1684.17	0.946545	1 3 1 2 2 2 2 2 2
9	12	1684.17	0.946545	1 3 1 2 2 2 2 2 2
10	12	1684.17	0.946545	1 3 1 2 2 2 2 2 2
11	11	1698.62	0.953858	1 4 1 2 2 2 2 2 2
12	6	1718.64	0.980557	2 3 1 2 2 2 2 2 2
13	5	1718.64	0.980557	2 3 1 2 2 2 2 2 2
14	2	1718.64	0.980557	2 3 1 2 2 2 2 2 2
15	2	1718.64	0.980557	2 3 1 2 2 2 2 2 2
16	2	1718.64	0.980557	2 3 1 2 2 2 2 2 2
17	2	1718.64	0.980557	2 3 1 2 2 2 2 2 2
18	1	1733.10	0.988133	2 4 1 2 2 2 2 2 2
19	0			
20	0			

Table 67. Power System Configuration Code

Code Identification:	Distribution Method	Energy Storage
1	AC Distribution	Disconnect switch plus current limiting resistor
2	DC Distribution	Disconnect switch plus current limiting resistor plus discharge booster
<u>Array Sizing Factor</u>		
1	Sizing Factor A ₁	Dissipative bucking charger and discharge switch
2	Sizing Factor A ₂	Dissipative charger, discharge switch and discharge booster
3	Sizing Factor A ₃	PWM bucking charger and discharge switch
4	Sizing Factor A ₄	PWM bucking charger, discharge switch and discharge booster
<u>Array Control</u>		
1	None	PWM boost charger and discharge switch and discharge booster
2	Zener Shunt	Dissipative charger and boost discharge regulator (normal voltage battery)
3	Active Shunt	PWM bucking charger and boost discharge regulator (normal voltage battery)
4	PWM Series Buck	PWM bucking charger and boost discharge regulator (low voltage battery)
5	Max. Pwr. Tracker-Buck	
6	PWM Series Buck-Boost	
<u>Line Regulator</u>		
1	PWM bucking line regulator	
2	Dissipative bucking line regulator	
3	Boost line regulator	
4	Buck-boost line regulator	
5	No line regulator	

Example Configuration Code:

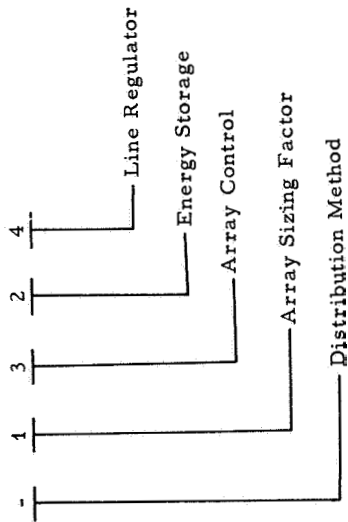


Table 68. Computer Printout, Mercury Flyby

RANKING BY TYPE FOR CONSTRAINT NO. 17 (R = 0.997)

NO.	WEIGHT	REL	CASE				
1	89.40	0.997771	- 3 3 9 5	74	102.65	0.999039	3 2 8 4
2	89.56	0.999194	3 3 9 5	75	104.47	0.999395	1 3 1 3
3	89.77	0.997649	-3 3 10 5	76	104.75	0.999741	1 1 5
4	89.93	0.999072	3 3 10 5	77	104.84	0.997972	- 1 3 1 3
5	93.08	0.997748	- 3 4 9 5	78	104.93	0.999296	1 3 7 3
6	93.39	0.999171	3 4 9 5	79	104.96	0.999897	1 1 5
7	93.43	0.997650	- 3 3 4 3	80	104.97	0.999353	1 3 5 3
8	93.45	0.9997626	-3 4 10 5	81	105.31	0.997873	- 1 3 7 3
9	93.48	0.999073	3 3 4 3	82	105.34	0.997930	- 1 3 5 3
10	93.72	0.997628	- 3 3 6 3	83	106.11	0.999074	3 3 4 1
11	93.75	0.999049	3 4 10 5	84	106.26	0.999368	
12	93.76	0.999051	3 3 6 3	85	106.39	0.599352	3 3 6 1
13	93.96	0.997606	-3 3 8 3	96	106.41	3.997651	- 3 3 4 1
14	93.96	0.997500	1 1 5	87	106.65	0.999030	3 3 8 1
15	94.00	0.999029	3 3 8 3	88	106.65	0.999030	1 2 7 2
16	94.10	0.998922	3 3 8 3	106.67	0.997945		
17	94.43	0.997663	-3 1 4 1	90	106.70	0.997629	- 3 3 6 1
18	94.43	0.997663	-3 2 4 1	91	106.88	0.999308	1 2 7 1
19	94.69	0.999085	3 2 4 1	92	106.88	0.999308	1 1 7 1
20	94.69	0.999085	3 1 4 1	93	106.91	0.999365	1 2 5 1
21	94.73	0.997640	- 3 2 6 1	94	106.91	0.999365	1 1 5 1
22	94.73	0.997640	- 3 1 6 1	95	106.96	0.997607	- 1 2 7 2
23	94.98	0.999063	3 1 6 1	96	106.96	0.997607	-3 3 8 1
24	94.98	0.999063	3 2 6 1	97	107.08	0.997885	-1 2 7 1
25	94.99	0.997619	- 3 2 2 1	98	107.08	0.997885	- 1 1 7 1
26	94.99	0.997619	- 3 1 8 1	99	107.11	0.997942	-1 2 5 1
27	95.24	0.999041	3 1 8 1	100	107.11	0.997942	- 1 1 5 1
28	95.24	0.999041	3 2 8 1	101	107.31	0.999388	
29	95.70	0.997705	- 3 5 9 5	102	108.31	0.999388	1 1 5 1
30	95.96	0.999128	3 5 9 5	103	108.55	0.997942	1 1 5 1
31	96.08	0.997584	-3 5 10 5	104	108.55	0.997942	1 1 5 1
32	96.08	0.997606	1 1 5	135	109.69	0.999372	1 4 1 3
33	96.08	0.997656	- 3 4 2 3	106	109.95	0.997949	-1 4 1 3
34	96.30	0.999077	1 2 2 2	107	110.15	0.9999273	1 4 7 3
35	96.30	0.999079	3 4 2 3	108	110.19	0.999330	3 2 6 3
36	96.32	0.999006	3 5 10 5	109	110.19	0.999330	1 4 5 3
37	96.80	0.997627	- 1 2 5 3	110	110.42	0.997850	- 1 4 7 3
38	96.80	0.997627	- 3 4 4 3	111	110.45	0.597907	- 3 2 6 3
39	97.02	0.999050	3 4 4 3	112	110.45	0.597907	-1 4 5 3
40	97.02	0.999050	1 2 5 3	113	111.30	0.999065	2 3 2 1
41	97.09	0.597605	- 1 2 7 3	114	111.48	0.999345	3 2 4 3
42	97.09	0.997605	- 3 4 6 3	115	111.73	0.999345	
43	97.31	0.999028	3 4 6 3	116	111.73	0.999313	1 3 7 2
44	97.31	0.999028	1 2 7 3	117	111.78	0.997922	- 3 2 4 3
45	97.33	0.997583	- 3 4 8 3	118	111.78	0.997922	
46	97.54	0.9999306	3 4 8 3	119	111.81	0.997642	- 2 3 2 1
47	97.61	0.997477	1 1 5	120	112.40	0.997890	- 1 3 7 2
48				121	113.53	0.999072	3 3 4 4
49	98.17	0.999064	2 3 2 3	122	113.81	0.999050	3 3 6 4
50	98.21	0.997852	- 3 5 1 3	123	114.01	0.997649	- 3 3 4 4
51	98.31	0.997641	- 2 3 2 3	124	114.06	0.999028	3 3 8 4
52	98.38	0.999275	3 5 1 3	125	114.29	0.9997627	-3 3 6 4
53	98.68	0.997753	- 3 2 8 3	126	114.30	0.999306	1 2 7 4
54	98.68	0.997753	- 3 5 7 3	127	114.30	0.999306	1 1 7 4
55	98.84	0.999176	3 5 7 3	128	114.33	0.999363	1 2 5 4
56	98.84	0.999176	3 2 8 3	129	114.33	0.999363	1 1 5 4
57	100.18	0.997746	- 3 6 9 5	130	114.56	0.997605	-3 3 8 4
58	100.25	0.997434	3 5 11 5	131	114.68	0.997883	- 1 2 7 4
59	100.33	0.999169	3 6 9 5	132	114.68	0.997883	-1 1 7 4
60	100.55	0.997624	-3 6 10 5	133	114.71	0.997940	-1 2 5 4
61	100.56	0.998850	1 1 5	134	114.71	0.997940	- 1 1 5 4
62	100.70	0.999047	3 6 10 5	135	115.22	0.999378	1 2 3 4
63	102.03	0.997660	- 3 2 4 4	136	115.22	0.999378	1 1 3 4
64	102.03	0.997660	- 3 1 4 4	137	116.14	0.997955	1 2 3 4
65	102.10	0.999083	3 1 4 4	138	116.14	0.997955	1 1 5 4
66	102.10	0.999083	3 2 4 4	139	118.21	0.999396	1 3 1 1
67	102.32	0.997638	- 3 2 6 4	140	118.69	0.999297	1 3 7 1
68	102.32	0.997638	- 3 1 6 4	141	118.71	0.999063	2 3 2 4
69	102.40	0.999061	3 1 6 4	142	118.73	0.909354	1 3 5 1
70	102.40	0.9999061	3 2 6 4	143	118.97	0.997973	- 1 3 1 1
71	102.59	0.997617	- 3 2 8 4	144	119.41	0.997640	-2 3 2 4
72	102.59	0.997617	- 3 1 8 4	145	119.47	0.997874	- 1 3 7 1
73	102.65	0.999039	3 1 8 4	146	119.50	0.997931	-1 3 5 1

Table 68. (Continued)

147	120.12	0.999369					1
148	120.93	0.997946					
149	125.62	0.999394	1	3	1	4	
150	126.11	0.999295	1	3	7	4	
151	126.14	0.999352	1	3	5	4	
152	126.57	0.997971	-	1	3	1	4
153	127.06	0.997872	-	1	3	7	4
154	127.09	0.997929	-1	3	5	4	
155	127.54	0.999367					
156	128.53	0.997944					

RANKING BY TYPE FOR CONSTRAINT NO. 17 (R=0.997)

(Partial Rerun)

NO.	WEIGHT	REL	CASE
1	89.10	0.997500	-3 3 11 5
2	89.40	0.998922	3 3 11 5
3	92.74	0.997477	-3 4 11 5
4	93.19	0.998099	3 4 11 5
5	95.39	0.997434	-3 5 11 5
6	95.77	0.998856	3 5 11 5
7	99.88	0.997475	-3 6 11 5
8	100.17	0.998897	3 6 11 5
9	106.29	0.999368	1 3 3 3
10	106.71	0.997945	- 1 3 3 3
11	108.34	0.999380	1 2 3 1
12	108.34	0.999380	1 1 3 1
13	108.57	0.997957	- 1 2 3 1
14	108.57	0.997957	- 1 1 3 1
15	111.51	0.999345	1 4 3 3
16	111.81	0.997922	- 1 4 3 3
17	115.75	0.999378	1 2 3 4
18	115.75	0.999378	1 1 3 4
19	116.17	0.997955	- 1 2 3 4
20	116.17	0.997955	- 1 1 3 4
21	120.16	0.999369	1 2 3 3
22	120.16	0.999369	1 3 3 1
23	120.97	0.997946	- 1 2 3 3
24	120.97	0.997946	- 1 3 3 1
25	127.58	0.999367	1 3 3 4
26	128.57	0.997944	- 1 3 3 4

Table 69. Computer Printout, Venus Orbiter No. 1

RANKING BY NO.	TYPE WEIGHT	FOR CONSTRAINT REL	NO.	17 CASE	(R.0 980)				
1	183.56	0.983324		2 3 9 5	75	209.28	0.981884	2 3 8 1	
2	184.94	0.983678		-2 3 9 5	76	209.44	0.980035	- 2 3 6 1	
3	185.61	0.986026		2 4 9 5	77	209.70	0.981807	- 1 3 7 2	
4	185.69	0.982949		2 3 10 5	78	209.76	0.982111	2 3 2 1	
5	187.10	0.983302		-2 3 10 5	79	209.97	0.980104	- 2 3 4 1	
6	187.67	0.985650		2 4 10 5	80	210.03	0.982544	1 3 3 3	
7	189.11	0.983588		- 2 4 9 5	81	210.12	0.981346	2 3 6 4	
8	189.29	0.985596		2 6 9 5	82	210.62	0.981415	2 3 4 4	
9	190.94	0.981752		2 3 6 3	83	211.24	0.980738	- 2 2 6 3	
10	190.99	0.988185		2 5 9 5	94	211.87	0.980807	- 2 2 4 3	
11	191.21	0.983213		-2 4 10 5	85	211.90	0.98 1767	1 2 5 3	
12	191.38	0.985220		2 6 10 5	86	212.20	0.980194	- 2 3 2 1	
13	191.38	0.981921		2 3 4 3	87	212.30	0.981279	2 3 8 4	
14	191.98	0.983418		- 2 5 9 5	88	212.55	0.980626	- 1 3 3 3	
15	193.01	0.991635		2 3 9 3	99	212.78	0.981506	2 3 2 4	
16	193.10	0.987808		2 5 10 5	90	212.90	0.980147	- 2 3 8 1	
17	193.23	0.981912		2 3 2 3	91	212.93	0.982701	1 3 5 1	
18	193.39	0.982112		- 2 6 9 5	92	213.35	0.980671	- 2 2 8 3	
19	193.52	0.983212		-2 3 6 3	93	213.42	0.981598	1 2 7 3	
20	193.53	0.985559		2 4 5 3	94	213.84	0.986354	1 4 3 3	
21	193.92	0.985629		2 4 4 3	95	214.49	0.982821	1 3 1 1	
22	193.97	0.983281		- 2 3 4 3	95	214.60	0.982532	1 3 7 1	
23	194.10	0.983043		-2 5 10 5	97	215.24	0.987909	1 1 3 1	
24	194.175	0.987113		2 1 6 1	98	215.37	0.982972	- 2 3 6 4	
25	195.15	0.987182		2 1 4 1	99	215.58	0.980793	- 1 3 5 1	
26	195.51	0.981738		-2 6 10 5	100	215.91	0.983041	- 2 3 4 4	
27	195.61	0.983144		- 2 3 8 3	101	215.95	0.982096	1 3 5 4	
28	195.61	0.965491		2 4 8 3	102	216.47	0.981487	- 1 2 5 3	
29	195.87	0.985719		2 4 2 3	103	217.18	0.980871	- 1 1 3 1	
30	195.88	0.983372		- 2 3 2 3	104	217.24	0.980903	- 1 3 1 1	
31	196.15	0.982502		1 3 5 3	105	217.29	0.980614	- 1 3 7 1	
32	196.25	0.980080		- 2 1 6 1	106	217.35	0.980537	- 1 4 3 3	
33	196.66	0.980149		- 2 1 4 1	107	217.41	0.980676	- 2 3 2 4	
34	196.93	0.987044		2 1 9 1	108	217.51	0.982216	1 3 1 4	
35	197.33	0.983122		- 2 4 6 3	109	217.60	0.982904	- 2 3 8 4	
36	197.37	0.982622		1 3 1 3	110	217062	0.981927	1 3 7 4	
37	197.45	0.987485		2 5 1 3	111	218.04	0.981318	- 1 2 7 3	
38	197.67	0.982333		1 3 7 3	112	218.26	0.987300	1 1 3 4	
39	197.76	0.983191		- 2 4 4 3	113	218.64	0.980179	- 1 3 5 4	
40	197.77	0.987194		2 5 7 3	114	220.24	0.980266	- 1 1 3 4	
41	197.77	0.986504		2 1 6 4	115	220.30	0.980298	- 1 3 1 4	
42	198.17	0.986573		2 1 4 4	116	220.35	0.980010	- 1 3 7 4	
43	199.43	0.980584		- 1 3 5 3	117	225.28	0.981217	2 2 6 1	
44	198.46	0.980013		- 2 1 8 1	118	225.70	0.982771	1 2 7 2	
45	199.37	0.980450		- 2 5 1 3	119	225.94	0.981809	1 2 3 3	
46	199.34	0.980161		- 2 5 7 3	120	225.96	0.981286	2 2 4 1	
47	199.43	0.983055		- 2 4 8 3	121	227.46	0.981150	2 2 8 1	
48	199.70	0.983282		- 2 4 2 3	122	227.78	0.982744	1 3 3 1	
49	199.73	0.980704		- 1 3 1 3	123	228.29	0.980613	2 2 6 4	
50	199.83	0.986312		1 4 5 3	124	228.98	0.980682	2 2 4 4	
51	199.95	0.986436		2 1 8 4	125	229.47	0.981385	-2 2 28 7 4 2	
52	199.99	0.980415		- 1 3 7 3	126	230.47	0.980545		
53	200.50	0.987866		1 1 5 1	127	230.68	0.980825	- 1 3 3 1	
54	201.10	0.986432		1 4 1 3	128	230.79	0.982138	1 3 3 4	
55	201.38	0.986142		1 4 7 3	129	230.80	0.981529	- 1 2 3 3	
56	202.02	0.983017		- 2 1 6 4	130	230.92	0.981967	1 2 5 1	
57	202.17	0.987696		1 1 7 1	131	232.59	0.981797	1 2 7 1	
58	202.19	0.900828		- 1 1 5 1	132	233.74	0.980221	- 1 3 3 4	
59	202.44	0.983086		- 2 1 4 4	133	233.94	0.981361	1 2 5 4	
60	203.25	0.980495		- 1 4 5 3	134	234.27	0.981451	- 2 2 6 1	
61	203.52	0.987257		1 1 5 4	135	235.01	0.981520	- 2 2 4 1	
62	203.90	0.980660		- 1 1 7 1	136	235.61	0.981192	1 2 7 4	
63	204.25	0.982949		- 2 1 0 4	137	236.51	0.981383	- 2 2 8 1	
64	204.55	0.980615		- 1 4 1 3	138	237.38	0.980846	- 2 2 6 4	
65	204.81	0.980326		- 1 4 7 3	139	138.11	0.980915	- 2 2 4 4	
66	205.19	0.987087		1 1 7 4	140	239.61	0.980778	- 2 2 8 4	
67	205.25	0.980224		- 1 1 5 4	141	240.27	0.982200	- 1 2 5 1	
68	206.65	0.983194		1 3 7 2	142	242.02	0.982031	- 1 2 7 1	
69	206.86	0.981018		2 2 6 3	143	243.37	0.981595	- 1 2 5 4	
70	206.96	0.980055		- 1 1 7 4	144	245.12	0.981426	- 1 2 7 4	
71	207.10	0.981952		2 3 6 1	145	245.94	0.982009	1 2 3 1	
72	207.46	0.981087		2 2 4 3	146	248.96	0.981403	1 2 3 4	
73	207.61	0.982021		2 3 4 1	147	255.79	0.982243	- 1 2 3 1	
74	208.93	0.980950		2 2 8 3	148	258.89	0.981637	- 1 2 3 4	

Table 70. Computer Printout, Venus Orbiter No. 2

RANKING BY TYPE FOR CONSTRAINT NO.			17		(R= 0.980)						
NO.	WEIGHT	REL	CASE								
1	354.83	0.985513	3	4 11 5	74	441.93	0.980098	-	3 3 6 1		
2	356.88	0.981743	-3	4 11 5	75	442.27	0.982323	3	3 4 1		
3	362.43	0.985083	3	6 11 5	76	442.65	0.982636	1	3 7 3		
4	364.57	0.981315	-3	6 11 5	77	443.50	0.980157	-	3 3 4 1		
5	366.52	0.900374	-3	5 11 5	78	444.11	0.980472	-	1 3 7 3		
6	368.49	0.987626	3	5 11 5	79	444.51	0.982184	3	3 8 1		
7	376.97	0.980675	-3	3 11 5	80	444.89	0.981646	-	3 3 6 4		
8	377.70	0.902768	3	3 11 5	81	445.74	0.980020	-	3 3 8 1		
9	396.22	0.986327	3	4 9 5	82	446.44	0.981715	3	3 4 4		
10	396.69	0.980091	-3	1 6 1	83	447.135	0.980020	1	3 1 3		
11	397.20	0.987414	3	1 6 1	84	448.09	0.980009	-3	3 6 4		
12	397.95	0.980160	-3	1 4 1	85	448.66	0.980002				
13	398.45	0.987483	3	1 4 1	86	448.67	0.981578	3	3 8 4		
14	398.78	0.980098	-3	4 9 5	87	448.75	0.980005				
15	399.53	0.985951	3	4 10 5	88	446.99	0.980761	-1	3 1 3		
16	400.36	0.985860	3	4 6 3	89	449.66	0.980158	-	3 3 4 4		
17	400.50	0.980023	-3	1 8 1	90	451.96	0.980021	-3	3 8 4		
18	400.99	0.987345	3	1 8 1	91	452.02	0.987605				
19	401.37	0.986805	3	1 6 4	92	452.06	0.980280				
20	401.61	0.985929	3	4 4 3	93	452.07	0.986659				
21	402.37	0.982179	-3	4 10 5	94	454.26	0.982411	2	3 2 1		
22	402.61	0.986874	3	1 4 4	95	455.72	0.980247	-2	3 2 1		
23	402.72	0.980092	-3	1 6 4	96	455.97	0.980004				
24	403.21	0.985897	3	6 9 5	97	458.42	0.981805	2	3 2 4		
25	403.34	0.982088	-3	4 6 3	98	455.54	0.983495	1	3 7 2		
26	403.98	0.980161	-3	1 4 4	99	460.05	0.981864	-	1 3 7 2		
27	404.04	0.985792	3	4 8 3	100	461.91	0.980248	-2	3 2 4		
28	404.62	0.982157	-3	4 4 3	101	463.64	0.983005	1	3 5 1		
29	405.15	0.986737	3	1 8 4	102	465.55	0.980840	-	1 3 5 1		
30	406.10	0.982125	-3	6 9 5	103	466.06	0.982040				
31	406.26	0.980221	-3	5 9 5	104	467.72	0.980003				
32	406.53	0.980024	-3	1 8 4	105	467.78	0.982836	1	2 7 1		
33	406.56	0.985521	3	6 10 5	106	467.80	0.982399	1	3 5 4		
34	407.06	0.982020	-3	4 8 3	107	469.74	0.980671	-	1 3 7 1		
35	408.17	0.988442	3	5 9 5	108	469.77	0.980255	-	1 3 5 4		
36	409.10	0.986020	3	4 2 3	109	471.94	0.982230	1	3 7 4		
37	409.49	0.981750	-3	6 10 5	110	473.14	0.983125	1	3 1 1		
38	409.94	0.9808 10	-3	5 10 5	111	473.96	0.980067	-1	3 7 4		
39	411.58	0.988065	3	5 10 5	112	475.26	0.980960	-	1 3 1 1		
40	412.27	0.982248	-3	4 2 3	113	477.30	0.082519	1	3 1 4		
41	412.29	0.980522	-3	3 9 5	114	479.47	0.980355	-	1 3 1 4		
42	412.59	0.980172	-3	5 7 3	115	486.83	0.981317	3	2 6 3		
43	413.01	0.980030	3	3 9 5	116	488.83	0.981336	3	2 4 3		
44	413.08	0.987495	3	5 7 3	117	490.49	0.981250	3	2 6 3		
45	416.01	0.980147	-3	3 10 5	118	491.25	0.980749	-	3 2 6 3		
46	416.84	0.983204	3	3 10 5	119	492.15	0.983047				
47	417.13	0.982052	3	3 6 3	120	493.28	0.980818	-	3 2 4 3		
48	417.34	0.980460	-3	5 1 3	121	494.33	0.980002				
49	417.41	0.980108	3	5 1 3	122	494.94	0.980621	-3	2 8 3		
50	413.31	0.980057	-3	3 6 3	123	496.31	0.982441				
51	418.59	0.982121	3	3 4 3	124	498.55	0.980277				
52	419.68	0.980843	-1	1 5 1	125	507.85	0.082071	1	2 5 3		
53	419.79	0.980126	-3	3 4 3	126	511.77	0.981902	1	2 7 3		
54	419.87	0.988171	1	1 5 1	127	512.61	0.981502	-	1 2 5 3		
55	420.79	0.981984	3	3 8 3	128	516.47	0.981517	3	2 4 1		
56	422.28	0.980953	-3	3 8 3	129	516.59	0.981333	-	1 2 7 3		
57	423.87	0.980674	-1	1 7 1	130	518.61	0.981580	3	2 4 1		
58	423.90	0.980238	-1	1 5 4	131	520.26	0.981449	3	2 8 1		
59	424.01	0.0988001	1	1 7 1	132	520.64	0.980912	3	2 6 4		
60	424.03	0.987562	1	1 5 4	133	522.77	0.980981	3	2 4 4		
61	425.32	0.986617	1	4 5 3	134	524.42	0.980844	3	2 8 4		
62	428.09	0.980070	-1	1 7 4	135	528.02	0.981464	-	3 2 6 1		
63	428.17	0.987392	1	1 7 4	136	530.21	0.981533	-	3 2 4 1		
64	428.50	0.980174	-1	4 5 3	137	531.86	0.981396	-	3 2 8 1		
65	429.28	0.986447	1	4 7 3	138	532.29	0.980859	-	3 2 6 4		
66	429.83	0.982211	2	3 2 3	139	533.77	0.983030	1	2 7 2		
67	430.82	0.980048	-2	3 2 3	140	534.48	0.980928	-	3 2 4 4		
68	432.53	0.980006	-1	4 7 3	141	534.60	0.982113				
69	434.04	0.986737	1	4 1 3	142	536.13	0.980791	-3	2 8 4		
70	435.85	0.980025	-1	4 1 3	143	536.74	3.981400	-	1 2 7 2		
71	438.73	0.982806	1	3 5 3	144	538.77	0.982270	1	2 5 1		
72	440.15	0.980641	-1	3 5 3	145	539.75	0.981000				
73	440.73	0.982251	3	3 6 1	146	542.90	0.982101	1	2 7 1		
					147	542.93	0.981665	1	2 5 4		

Table 70. (Continued)

148	547.07	0.981495	1	2	7	4	
149	550096	0.982217	-	1	2	5	1
150	555.21	0.982048	-1	2	7	1	
151	555.24	0.981612	-	1	2	5	4
152	559.48	0.981443	-	1	2	7	4
153	566.74	0.982312	1	2	3	1	
154	570.90	0.981707	1	2	3	4	
155	579.49	0.982259	2	2	1	1	
156	583.76	0.981654	7	1	4		

RANKING BY TYPE FOR CONSTRAINT NO. 17 (R = 0.980)

(Partial Rerun)

NO.	WEIGHT	REL	CASE
1	449.43	0.987876	1 1 3 1
2	449.53	0.980885	- 1 1 3 1
3	453.60	0.987267	1 1 3 4
4	453.75	0.980280	- 1 1 3 4
5	453.94	0.986322	1 4 3 3
6	456.30	0.980410	- 1 4 3 3
7	467.33	0.982511	1 3 3 3
8	469.02	0.980641	- 1 3 3 3
9	493.50	0.982711	1 3 3 1
10	495.71	0.980840	- 1 3 3 1
11	497.66	0.982105	1 3 3 4
12	499.93	0.980235	- 1 3 3 4
13	536.98	0.981777	1 2 3 3
14	542.09	0.981544	- 1 2 3 3
15	569.19	0.981976	1 2 3 1
16	573.36	0.981371	1 2 3 4
17	582.02	0.982259	- 1 2 3 1
18	586030	0.981654	- 1 2 3 4

Table 71. Computer Printout, Mars Orbiter

RANKING BY TYPE FOR CONSTRAINT NO.		17		(R = 0.980)	
NO.	WEIGHT	REL	CASE		
1	563.93	0.989875	3 4 2 3	74	783.48 0.980426 1 1 5 1
2	565.03	0.981715	- 3 4 2 3	75	794.98 0.980955 - 1 1 7 1
3	588.79	0.983908	2 3 2 3	76	795.13 0.989196 3 2 6 3
4	596.08	0.981901	- 2 3 2 3	77	795.22 0.980080 1 3 7 3
5	642.37	0.983912	2 3 2 1	78	798.73 0.981192 - 1 1 5 1
6	650.88	0.981905	- 2 . 2 1	79	798.85 0.989293 3 2 4 3
7	655.76	0.983898	2 3 2 4	80	799.39 0.989101 3 2 8 3
8	659.48	0.982790	3 4 9 5	E1	800.32 0.980216 1 3 5 3
9	661.53	0.980781	- 3 3 9 5	82	800.74 0.981041 - 3 2 6 3
10	662.57	0.985715	3 3 9 5	93	801.05 0.980948 - 1 3 7 3
11	664.42	0.981891	- 2 3 2 4	84	801.98 0.980416 1 1 5 4
12	665.48	0.982254	3 4 10 5	85	802.68 0.980411 1 1 7 4
13	667.88	0.980257	-3 3 10 5	86	803.40 0.980157 1 3 1 3
14	668.08	0.980596	- 3 4 9 5	87	804.52 0.981138 - 3 2 4 3
15	668.80	0.982271	3 6 9 5	88	805.04 0.980947 -3 2 8 3
16	668.88	0.985187	3 3 10 5	89	806.31 0.981184 - 1 3 5 3
17	674.19	0.980071	-3 4 10 5	90	808.32 0.980486
18	674.85	0.981745	3 6 10 5	91	808.37 0.980942 - 1 1 7 4
19	677.34	0.981101	3 1 4 1	92	809.02 0.982946 1 4 7 3
20	678.05	0.980136	- 3 1 6 1	93	809.88 0.981351 - 1 3 1 3
21	678.25	0.981109	3 1 6 1	94	810.28 0.980203 - 1 1 5 4
22	680.75	0.980357	- 3 5 9 5	95	813.69 0.983194 1 4 5 3
23	680.84	0.980232	- 3 1 4 1	96	817.78 0.983351 1 4 1 3
24	681.90	0.985288	3 5 9 5	97	818.33 0.980416
25	682.55	0.980042	- 3 1 8 1	98	820.34 0.980762 - 1 4 7 3
26	682.79	0.980381	3 1 4 4	99	821.31 0.980050
27	683.57	0.984971	3 1 8 1	100	823.96 0.981252 - 3 2
28	683.70	0.980389	3 1 6 4	101	825.29 0.960999 - 1 4 5 3
29	685.11	0.982125	3 4 6 3	02	827.76 -
30	685.45	0.980585	-3 6 9 5	103	829.13 0.981166 -1 4 1 3
31	686.97	0.980407	3 4 4 3	104	832.32 0.980174 1 3 7 2
32	687.91	0.982222	3 4 4 3	105	835.76 0.980252 - 3 2
33	688.08	0.984761	3 5 10 5	106	835.88 0.98324 -
34	689.16	0.980128	- 3 3 6 3	107	838.68 0.981042 -1 3 7 2
35	689.37	0.982031	3 4 8 3	108	841.15 0.981050
36	690.01	0.985058	3 3 6 3	109	854.51 0.980186 1 3 7 1
37	690.15	0.980311	3 4 4 3	110	860.15 0.980422 1 3 5 1
38	691.44	0.980122	- 3 1 6 4	111	864.54 0.980589 1 3 1 1
39	691.68	0.980060	-3 6 10 5	112	868.69 0.989200 3 2 6 1
40	692.15	0.980224	- 3 3 4 3	113	871.45 0.980952 -1 3 7 1
41	692.26	0.983326	-3 5 10 5	114	872.75 0.989297 1 2 4 1
42	692.97	0.985155	3 3 4 3	115	873.19 0.989105 3 2 6 1
43	693.42	0.980034	-3 3 8 3	116	875.55 0.991345 - 3 2 6 1
44	694.23	0.980219	- 3 1 4 4	117	875.89 0.980414 1 3 1 4
45	694.24	0.984963	3 3 8 3	118	877.23 0.98118E - 1 3 5 1
46	695.82	0.980384	3 1 8 4	119	877.56 0.980070 1 3 7 4
47	695.93	0.980028	-3 1 8 4	120	879.59 0.980412 1 3 5 4
48	697.21	0.980039	- 3 4 4 3	121	879.67 0.981142 -3 2 4 1
49	698.00	0.980347	3 4 4 3	122	880.09 0.980951 -3 2 8 1
50	699.48	0.980035	- 3 4 6 3	123	881.92 0.981355 -1 3 1 1
51	700.53	0.980271	3 4 8 3	124	882.08 0.989186 3 2 6 4
52	703.98	0.983343	- 3 4 8 3	125	882.54 0.980492
53	704.16	0.980072	3 5 11 5	126	884.84 0.980938 -1 3 7 4
54	709.00	0.980301	3 5 11 5	127	886.13 0.989243 3 2 4 4
55	710.47	0.980523	- 3 5 7 3	128	886.58 0.989091 3 2 8 4
56	711.39	0.985455	3 5 7 3	129	883.39 0.981032 -3 2 6 4
57	714.00	0.980352	3 5 7 3	130	890.11 0.080198 -1 3 5 4
58	718.98	0.980927	- 3 5 1 3	131	893.21 0.981128 -3 2 4 4
59	719.19	0.0980471	3 5 1 3	132	893.41 0.980412
60	719.65	0.983281	3 6 11 3	133	893.63 0.980937 -3 2 8 4
61	750.86	0.981097	3 3 4 1	134	895.00 0.980365 - 1 3 1 4
62	751.00	0.981105	3 3 6 1	135	899.95 0.981246
63	751.22	0.980132	- 3 3 6 1	136	903.44 0.0990025 1 2 7 3
64	754.46	0.980228	- 3 3 4 1	137	910.56 0.081862 - 1 2 7 3
65	755.71	0.980038	- 3 3 8 1	138	911.70 0.990262 1 2 5 3
66	756.01	0.984967	3 3 8 1	139	913.05 0.98002
67	756.31	0.980377	3 3 4 4	140	918.99 0.982099 - 1 2 5 3
68	756.45	0.980385	3 3 6 4	141	926.70 0.98000
69	764.60	0.980118	- 3 3 6 4	142	926.89 0.98200
70	767.85	0.980215	- 3 3 4 4	143	946.05 0.990118 1 2 7 2
71	768.56	0.980380	3 3 8 4	144	954.00 0.981956 - 1 2 7 7
72	769.10	0.980024	3 3 8 4	145	985.07 0.990027 - 1 2 7 1
73	779.82	0.0980190	1 1 7 1	145	993.58 0.981855 -1 2 7 1
				147	994.26 0.990266 1 2 5 1

Table 71. (Continued)

148	998.45	0.990013	1	2	7	4	
149	1002.95	0.982102	-1	2	5	1	
150	1007.12	0.981852	-1	2	7	4	
151	1007.64	0.990252	1	2	5	4	
152	1010.00	0.980166					
153	1016.49	0.982089	-	1	2	5	4
154	1021.60	0.982163					
155	1023.31	0.980147					
156	1025.14	0.982149					

RANKING BY TYPE FOR CONSTRAINT NO.			17 (R = 0 980)				(Partial Rerun)
NO.	WEIGHT	REL	CASE				
1	668462	0.981643	3	4	1	1	5
2	676.85	0.984515	3	3	1	1	5
3	678.84	0.981135	3	6	1	1	5
4	681.35	0.983080	-3	3	1	1	5
5	684.06	0.982955	-3	4	1	1	5
6	694.04	0.984148	3	5	1	1	5
7	696.17	0.981631	-3	6	1	1	5
8	698.24	0.982715	-3	5	1	1	5
9	812.25	0.980486	1	1	3	1	
10	819.59	0.900416	1	1	3	4	
11	825.74	0.980050	1	3	3	3	
12	827.98	0.981252	-	1	1	3	1
13	832.30	0.981185	-	1	3	3	3
14	839.85	0.980262	-	1	1	3	4
15	840.14	0.983244	1	4	3	3	
16	851.52	0.901059	-	1	4	3	3
17	887.39	0.980423	1	3	3	1	
18	895.17	0.980352	1	3	3	4	
19	904.91	0.981188	-	1	3	3	1
20	918.08	0.980199	-	1	3	3	4
21	928.83	0.980156	1	2	3	3	
22	942.93	0.982159	-	1	2	3	3
23	1012.34	0.980160	1	2	3	1	
24	1025.66	0.980147	1	2	3	4	
25	1028.26	0.982163	-	1	2	3	1
26	1041.80	0.982149	-	1	2	3	4

Table 72. Computer Printout, Jupiter Flyby

RANKING BY TYPE FOR CONSTRAINT NO. 14 (R = 0.965)			
NO.	WEIGHT	REL	CASE
1	846.73	0.968871	2 3 9 5
2	847.50	0.968872	2 3 10 5
3	864.64	0.9755	2 3 11 5
4	867.80	0.966393	- 2 3 9 5
5	869.06	0.966284	-2. 3 10 5
6	886.11	0.971097	- 3 11
7	888.95	0.966607	2 3 2 3
8	890.08	0.965391	2 3 6 3
9	890.22	0.965903	2 3 4 3
10	893.03	0.975206	2 3 8 3
11	895.41	0.973577	2 2 4 3
12	896.03	0.973343	2 2 6 3
13	396.83	0.973280	2 2 8 3
14	906.81	3.965311	- 2 3 2 3
15	908.86	0.965903	-2 3 4 3
16	909.48	0.965230	- 2 3 6 3
17	910.29	0.965167	- 2 3 8 3
18	918.41	0.969164	- 2 2 4 3
19	919.02	0.968932	- 2 2 6 3
20	919.85	0.968868	- 2 2 8 3
21	928.18	0.966770	2 1 4 1
22	928.83	0.966538	2 1 6 1
23	929.67	0.966475	2 1 8 1
24	934.76	0.966705	2 1 4 4
25	935.41	3.966473	2 1 6 4
26	936.25	0.966410	2 1 8 4
27	944.82	0.965790	- 2 1 4 1
28	945.46	0.965559	- 2 1 6 1
29	946.32	0.965496	- 7 1 8 1
30	951.51	0.965725	- 2 1 4 4
31	752.15	0.965494	- 2 1 6 4
32	953.01	0.965431	-2 1 8 4
33	958.50	0.966771	2 4 9 5
34	959.30	0.966662	2 4 1 c 5
35	961.18	0.966528	2 3 2 1
35	962.33	0.965413	2 3 6 1
37	962.49	0.965925	2 3 4 1
38	965.44	0.975227	2 3 8 1
39	967.82	0.966564	2 3 2 4
43	967.85	0.966721	2 6 9 2
41	058.78	0.973598	2 2 4 1
42	968.96	0.965348	2 3 6 4
43	969.13	0.965862	2 3 4 4
44	969.16	0.965612	2 6 10 5
45	969.39	0.973365	2 2 6 1
46	970.24	0.973301	2 2 6 1
47	971.55	0.974912	2 2 7 2
48	972.08	0.975162	2 3 8 4
(14)	975.02	0.965792	-2 4 9 2
50	975.42	0.973533	2 2 4 4
51	975.71	0.972340	1 3 1 3
52	976.02	0.973300	2 2 6 4
53	975.25	3.969951	1 3 7 3
54	976.31	0.971336	1 3 5 3
55	075.35	3.965683	-2 4 10 2
56	976.88	0.973236	2 2 8 4
57	977.92	0.971694	2 2 8 4
58	978.74	0.968035	1 2 7 3
59	978.79	0.969418	1 2 5 3
60	979.80	0.969375	2 3 3
61	980.89	3.965332	-2 3 2 1
62	981.04	0.974861	2 3 11 5
63	981.31	3.965641	2 5 9 5
54	992.62	3.905532	2 5 10 5
65	983.03	0.965483	- 2 3 4 1
66	983.64	0.965252	- 2 3 6 1
67	984.50	0.965188	- 2 3 8 1
68	984.53	0.965742	- 2 6 9 5
69	985.86	0.965633	-2 5 10 5
70	987.58	0.965268	- 7 3 2 6
71	989.72	0.965418	-2 3 4 4
72	990.33	0.965187	-2 3 6 4
73	991.19	0.965124	-2 3 8 4
74	994.26	0.969185	-2 2 4 1
75	994.73	0.973772	2 5 11 5
76	994.86	0.968953	-2 2 6 1
77	995.58	0.970493	2 4 11 5
78	995.70	0.965656	-1 3 1 3
79	995.73	0.968089	-2 2 8 1
80	996.67	0.965556	-1 3 7 3
81	996.78	0.965627	-1 3 5 3
82	997.35	0.965670	-1 3 3 3
83	1001.05	0.969120	-2 2 4 4
84	1001.44	0.965659	2 4 2 3
85	1001.65	0.968888	-2 2 6 4
86	1002.53	0.968824	-2 2 8 4
87	1003.56	0.965439	2 4 4 3
88	1004.09	0.965024	-1 2 5 3
89	1004.11	0.965009	2 4 6 3
90	1004.91	0.965545	2 4 8 3
91	1005.04	0.969259	-1 2 7 3
92	1005.13	0.969370	-1 2 3 3
93	1005.29	0.970443	-2 6 11 5
94	1006.98	0.968276	-2 5 9 5
95	1007.84	0.968277	-2 5 10 5
96	1009.20	0.970401	1 3 7 2
97	1012.04	0.968484	1 2 7 2
98	1013.04	0.966064	1 1 7 1
99	1018.14	0.966935	1 1 5 1
100	1018.75	0.966920	1 1 3 1
101	1019.38	0.968359	-2 5 11 5
102	1024.62	0.966799	1 1 7 4
103	1024.72	0.966870	1 1 5 4
104	1025.33	0.966864	1 1 3 4
105	1029.13	0.971069	-2 4 2 3
106	1033.52	0.966204	-1 3 7 2
107	1031.30	0.971221	-2 4 4 3
108	1031.84	0.970988	-2 4 6 3
109	1032.66	0.970924	-2 4 8 3
110	1036.49	0.965985	-1 1 7 1
111	1036.59	0.965956	-1 1 5 1
112	1037.21	0.965549	-1 1 3 1
113	1039.67	0.969709	-1 2 7 2
114	1043.18	0.965820	-1 1 7 4
115	1043.28	0.965891	-1 1 5 4
116	1043.90	0.965884	-1 1 3 4
117	1054.50	0.972362	1 3 1 1
118	1055.06	0.969972	1 3 7 1
119	1055.13	0.971358	1 3 5 1
120	1056.21	0.971715	1 3 3 1
121	1058.46	0.968056	1 2 7 1
122	1058.50	0.969439	1 2 5 1
123	1059.59	0.968796	1 2 3 1
124	1061.13	0.972297	1 3 1 4
125	1061.72	0.969907	1 3 7 4
126	1061.76	0.971293	1 3 5 4
127	1062.85	0.971650	1 3 3 4
128	1065.09	0.967991	1 2 7 4
129	1065.14	0.969374	1 2 5 4
130	1066.22	0.969731	1 2 3 4
131	1076.52	0.965677	-1 3 1 1
132	1077.54	0.965577	-1 3 7 1
133	1077.64	0.965648	-1 3 5 1
134	1078.27	0.965641	-1 3 3 1
135	1083.21	0.965613	-1 3 1 4
136	1084.23	0.965513	-1 3 7 4
137	1084.34	0.965584	-1 3 5 4
138	1084.96	0.965577	-1 3 3 4
139	1086.51	0.965045	-1 2 5 1
140	1087.53	0.969280	-1 2 7 1
141	1087.62	0.965400	-1 2 3 1
142	1094.33	0.969215	-1 2 7 4
143	1094.41	0.965336	-1 2 3 4
144	1094.43	0.969286	-1 2 5 4
145	1100.52	0.966034	1 4 1 3
146	1101.48	0.965934	1 4 7 3

Table 72. (Continued)

147	1101.59	0.966005	1	4	5	3
148	1102.16	0.965994	1	4	5	3
149	1120.08	0.965055	-1	4	1	3
153	1121.17	0.965026	-1	4	5	3
151	1121.75	0.965019	1	4	5	3
152	1131.01	0.965692	-1	4	7	3
153	1139.32	0.983835	1	5	1	3
154	1129.90	0.981417	1	5	7	3
155	1157.53	0.966940	-1	5	1	3
156	1159.15	0.970180	-1	5	7	3

RANKING BY TYPE FOR CONSTRAINT NO.

14 (R = 0.965)

(Partial Rerun)

NO.	WEIGHT	REL	CASE
1	860.34	0.975519	2 3 1 1 5
2	881.75	0.971097	-2 3 1 1 5
3	967.26	0.974912	2 4 1 1 5
4	976.74	0.974861	2 6 1 1 5
5	977.84	0.971694	1 3 3 3
6	980.32	0.969775	1 2 3 3
7	990.43	0.973772	2 5 1 1 5
8	991.22	0.970493	-2 4 1 1 5
9	997.54	0.965620	-1 3 3 3
10	1000.93	0.970443	-2 6 1 1 5
11	1005.67	0.965379	-1 2 3 3
12	1015.02	0.969359	-2 5 1 1 5
13	1018.94	0.966928	1 1 3 1
14	1025.52	0.966864	1 1 3 4
15	1037.41	0.965949	-1 1 3 1
16	1044.10	0.965884	-1 1 3 4
17	1056.77	0.965715	1 3 3 1
18	1060.15	0.969796	1 2 3 1
19	1063.40	0.971650	1 3 3 4
20	1066.79	0.969731	1 2 3 4
21	1078.48	0.965641	-1 3 3 1
22	1085.17	0.965577	-1 3 3 4
23	1088.20	0.965400	-1 2 3 1
24	1094.99	0.965336	-1 2 3 4
25	1102.37	0.965998	1 4 3 3
26	1121.97	0.965019	-1 4 3 3

Table 73. Computer Printout, Jupiter Orbiter No. 1

RANKING BY NO.	TYPE FOR WEIGHT	CONSTRAINT REL	NO.	14 CASE	(R ≥ 0 965)	76	1251.55	0.977953	2 4 2 3
1	1072.42	0.966262		2 3 9 5		77	1252.83	0.976643	2 4 6 3
2	1080.39	0.974674		2 3 1 1 5		78	1253.20	0.976089	2 4 8 3
3	1083.40	0.973702		2 3 1 0 5		79	1253.45	0.977206	2 4 4 3
4	1100.56	0.966251		-2 3 11 5		80	1257.77	0.970615	-2 5 9 5
5	1101.21	0.965319		-2 3 9 5		81	1259.35	0.966264	-2 5 11 5
6	1103.21	0.965825		-2 3 10 5		82	1259.42	0.967552	-2 5 10 5
7	1112.06	0.972375		2 3 2 3		83	1268.18	0.967730	-2 4 2 3
8	1115.06	0.972176		2 3 4 3		84	1271.43	0.967532	-2 4 4 3
9	1115.43	0.972288		2 3 6 3		a5	1271.63	0.967644	-2 4 6 3
10	1116.81	0.972220		2 3 8 3		86	1273.01	0.967577	-2 4 8 3
11	1121.06	0.969967		2 2 4 3		87	1335.56	3.969570	1 3 1 3
12	1121.40	0.1970079		2 2 6 3		88	1336.43	0.968566	1 3 5 3
13	1122.78	0.970012		2 2 8 3		89	1336.44	3.967162	1 3 7 3
14	1138.93	0.966255		-2 3 2 3		90	1338.99	0.966365	1 2 5 3
15	1141.96	0.966057		-2 3 4 3		91	1339.44	0.968924	1 3 3 3
16	1142.32	0.966169		-2 3 6 3		92	1340.98	0.970425	1 2 7 3
17	1143.71	0.966102		-2 3 8 3		93	1342.00	0.966723	1 2 3 3
18	1152.81	0.972597		-2 2 4 3		94	1369.66	0.966618	-1 3 1 3
19	1153.14	0.972710		-2 2 6 3		95	1371.21	0.966588	-1 3 5 3
20	1154.54	0.972642		-2 2 8 3		95	1371.22	0.966513	-1 3 7 3
21	1156.61	0.977882		2 1 6 1		97	1372.84	0.966580	-1 3 3 3
22	1157.01	0.977328		2 1 8 1		98	1373.40	0.967753	1 3 7 2
23	1157.14	0.978446		2 1 4 1		99	1376.31	3.965554	1 2 7 2
24	1164.05	0.977795		2 1 6 4		100	1377.29	0.968986	-1 2 5 3
25	1164.45	0.977241		2 1 8 4		101	1377.30	0.967581	-1 2 7 3
26	1164.58	0.978358		2 1 4 4		102	1380.37	0.969345	-1 2 3 3
27	1174.10	0.968759		-2 1 4 1		103	1391.64	3.984158	1 1 5 1
28	1174.47	0.968871		-2 1 6 1		104	1391.66	0.982732	1 1 7 1
29	1175.91	0.968804		-2 1 8 1		105	1394.76	0.984523	1 1 3 1
30	1181.64	0.968673		-2 1 4 4		106	1399.08	0.984071	1 1 5 4
31	1182.02	0.968785		-2 1 6 4		107	1399.10	0.982644	1 1 7 4
32	1183.45	0.968718		-2 1 8 4		108	1402.20	0.984435	1 1 3 4
33	1185.34	0.972403		2 3 2 1		109	1409.62	0.965162	-1 1 5 1
34	1188.43	0.972204		2 3 4 1		110	1409.83	0.967104	-1 3 7 2
35	1188.17	0.972316		2 3 6 1		111	1411.70	0.969217	-1 1 7 1
36	1190.20	0.972249		2 3 8 1		112	1412.77	0.965520	-1 1 3 1
37	1192.78	0.972316		2 3 2 4		113	1416.47	0.968172	-1 2 7 2
38	1195.55	0.969995		2 2 4 1		114	1417.16	0.965076	-1 1 4 4
39	1195.86	0.970107		2 2 6 1		115	1419.24	0.969131	-1 1 7 4
40	1195.87	0.972117		2 3 4 4		116	1420.31	0.965434	-1 1 3 4
41	1196.21	0.972229		2 3 6 4		117	1422.96	0.969598	1 3 1 1
42	1197.28	0.970040		2 2 8 1		118	1423.85	0.968594	1 3 5 1
43	1197.64	0.972162		2 3 8 4		119	1423.87	0.967190	1 3 7 1
44	1202.99	0.969908		2 2 4 4		120	1427.00	0.968952	1 3 3 1
45	1203.30	0.970021		2 2 6 4		121	1427.31	0.966393	1 2 5 1
46	1203.40	0.973876		2 4 1 5		122	1429.41	0.970453	1 2 7 1
47	1204.72	0.969953		2 2 8 4		123	1430.40	0.969512	1 3 1 4
48	1207.84	0.980573		2 4 9 5		124	1430.47	0.96675 1	1 2 3 1
49	1209.45	0.977479		2 4 1 0 5		125	1431.29	0.968508	1 3 5 4
50	1214.31	0.973810		2 6 1 1 5		126	1431.31	0.967104	1 3 7 4
51	1214.96	0.966283		-2 3 2 1		127	1434.44	0.968866	1 3 3 4
52	1218.09	0.966085		-2 3 4 1		128	1434.75	0.966307	1 2 5 4
53	1218.41	0.966197		-2 3 6 1		129	1436.85	0.970367	1 2 7 4
54	1218.63	0.980506		2 6 9 5		130	1437.91	0.966665	1 2 3 4
55	1219.86	0.966130		-2 3 8 1		131	1460.45	0.966646	-1 3 1 1
56	1220.24	0.977412		2 6 1 0 5		132	1462.04	0.966616	-1 3 5 1
57	1222.59	0.966197		-2 3 2 4		133	1462.07	0.966541	-1 3 7 1
58	1225.71	0.965999		-2 3 4 4		134	1463.76	0.966609	-1 3 3 1
59	1225.82	0.0965466		-2 4 11 5		135	1468.08	0.966560	-1 3 1 4
60	1226.04	0.966111		-2 3 6 4		136	1469.44	0.969014	-1 2 5 1
61	1227.48	0.966044		-2 3 8 4		137	1469.46	0.967610	-1 2 7 1
62	1230.40	0.972105		-2 4 9 5		138	1469.66	0.966530	-1 3 5 4
63	1230.51	0.972625		-2 2 4 1		139	1469.69	0.966455	-1 3 7 4
64	1230.54	0.972383		2 5 1 1 5		140	1471.38	0.966522	-1 3 3 4
65	1230.80	0.972738		-2 2 6 1		141	1472.67	0.969373	-1 2 3 1
66	1232.03	0.969037		-2 4 10 5		142	1477.09	0.968920	-1 2 5 4
67	1232.25	0.972690		-2 2 8 1		143	1477.11	0.967523	-1 2 7 4
68	1234.65	0.979070		2 5 9 5		144	1490032	0.969286	-1 2 3 4
69	1236.29	0.975980		2 5 1 0 5		145	1510.76	0.98393 1	1 4 1 3
70	1236.93	0.965400		-2 6 11 5		146	1511.67	0.982911	1 4 5 3
71	1238.15	0.972539		-2 2 4 4		147	1511.68	0.981487	1 4 7 3
72	1238.44	0.972651		-2 2 6 4		148	1514.81	0.983275	1 4 3 3
73	1239.90	0.972584		-2 2 8 4		149	1531.30	0.968094	-1 4 1 3
74	1241.39	0.1972039		-2 6 9 5		150	1532.85	0.968014	-1 4 5 3
75	1243.02	0.968972		-2 6 10 5		151	1532.86	0.967989	-1 4 7 3
						152	1534.54	0.968056	-1 4 3 3
						153	1544.96	0.982422	1 5 1 3
						154	1545.89	0.979982	1 5 7 3
						155	1566.06	0.966610	-1 5 1 3
						156	1567.62	0.966505	-1 5 7 3

Table 74. Computer Printout, Jupiter Orbiter No. 2

RANKING BY TYPE FOR CONSTRAINT NO.			14 (R ≥ 0.965)	77	1792.19	0.970024	2 2 8 1
NO.	WEIGHT	REL	CASE				
1	1560.71	0.974658	2 3 1 1 5	78	1800.94	0.969893	2 2 4 4
2	1571.39	0.966246	2 3 9 5	79	1801.56	0.970005	2 2 6 4
3	1581.74	0.968465	-2 3 11 5	80	1803.96	0.969938	2 2 8 4
4	1589.02	0.973686	2 3 1 0 5	81	1827.30	0.972550	- 2 2 4 1
5	1600.99	0.968807	- 2 3 9 5	82	1827.90	0.972663	- 2 2 6 1
6	1602.86	0.965750	-2 3 10 5	83	1830.32	0.972595	- 2 2 8 1
7	1613.81	0.972359	2 3 2 3	84	1839.36	0.972464	-2 2 4 4
8	1616.70	0.972160	2 3 4 3	85	1839.97	0.972576	- 2 2 6 4
9	1617.48	0.972272	2 3 6 3	86	1842.39	0.972509	- 2 2 8 4
10	1619.80	0.972205	2 3 8 3	87	1900.09	0.969554	1 3 1 3
11	1629.06	0.977866	2 1 6 1	88	1900.95	0.968550	1 3 5 3
12	1629.59	0.978430	2 1 4 1	89	1901.13	0.967146	1 3 7 3
13	1629.80	0.977312	2 1 8 1	90	1905.80	0.968909	1 3 3 3
14	1636.53	0.966181	- 2 3 2 3	91	1927.62	0.984142	1 1 5 1
15	1639.44	0.965983	- 2 3 4 3	92	1927.62	0.982716	1 1 7 1
16	1640.21	0.966094	- 2 3 6 3	93	1929.19	0.966544	- 1 3 1 3
17	1640.83	0.977779	2 1 6 4	94	1931.28	0.966514	- 1 3 5 3
18	1641.36	0.978343	2 1 4 4	95	1931.65	0.966439	- 1 3 7 3
19	1641.57	0.977225	2 1 8 4	96	1932.41	0.984507	1 1 3 1
20	1642.55	0.966027	- 2 3 8 3	97	1934.13	0.966506	- 1 3 3 3
21	1642.61	0.968685	- 2 1 4 1	98	1939.19	0.984055	1 1 5 4
22	1643.45	0.968797	- 2 1 6 1	99	1939.39	0.982618	1 1 7 4
23	1645.85	0.968730	- 2 1 8 1	100	1940.49	0.965088	- 1 1 5 1
24	1654.51	0.968598	- 2 1 4 4	101	1943.59	0.969142	- 1 1 7 1
25	1655.35	0.968711	- 2 1 6 4	102	1944.18	0.984419	1 1 3 4
26	1657.76	0.968643	- 2 1 8 4	103	1945.52	0.965445	- 1 1 3 1
27	1690.52	0.973860	2 4 1 1 5	104	1952.02	0.967737	1 3 7 2
28	1692.10	0.969951	2 2 4 3	105	1952.39	0.965002	- 1 1 5 4
29	1692.75	0.970063	2 2 6 3	106	1955.50	0.969056	- 1 1 7 4
30	1695.07	0.969996	2 2 8 3	107	1957.43	0.965359	- 1 1 3 4
31	1704.09	0.972387	2 3 2 1	108	1971.70	0.966350	1 2 5 3
32	1707.03	0.972188	2 3 4 1	109	1974.81	0.970409	1 2 7 3
33	1707.78	0.972300	2 3 6 1	110	1976.63	0.966707	1 2 3 3
34	1710.17	0.972233	2 3 8 1	111	1984.28	0.967029	- 1 3 7 2
35	1711.74	0.973794	2 6 1 1 5	112	2005.36	0.969583	1 3 1 1
36	1713.12	0.967672	-2 4 11 5	113	2006.21	0.968578	1 3 5 1
37	1715.86	0.972301	2 3 2 4	114	2006.42	0.9671 74	1 3 7 1
38	1718.64	0.980557	2 4 9 5	115	201.1027	0.968937	1 3 3 1
39	1718.80	0.972101	2 3 4 4	116	2012.34	0.968911	- 1 2 5 3
40	1719.55	0.972214	2 3 6 4	117	2012.54	0.967507	- 1 2 7 3
41	1720.57	0.977463	2 4 1 0 5	118	2017.13	0.969496	1 3 1 4
42	1721.94	0.972146	2 3 8 6	119	2017.36	0.969270	- 1 2 3 3
43	1726.51	0.972522	- 2 2 4 3	120	2017.98	0.968492	1 3 5 4
44	1727.15	0.972635	- 2 2 6 3	121	2016.19	0.967088	1 3 7 4
45	1728.92	0.972368	2 5 1 1 5	122	2023.04	0.968850	1 3 3 6
46	1729.40	0.966209	- 2 3 2 1	123	2025.62	0.965538	1 2 7 2
47	1729.50	0.972567	- 2 2 8 3	124	2037.60	0.966572	- 1 3 1 1
48	1732.36	0.966011	- 2 3 4 1	125	2039.71	0.966542	- 1 3 5 1
49	1733.10	0.966122	- 2 3 6 1	126	2040.12	0.966467	-1 3 7 1
50	1734.65	0.967607	-2 6 11 5	127	2042.69	0.966534	- 1 3 3 1
51	1735.52	0.966055	- 2 3 8 1	128	2049.60	0.966486	- 1 3 1 4
52	1739.69	0.980491	2 6 9 5	129	2051.71	0.966456	- 1 3 5 4
53	1741.40	0.966123	- 2 3 2 4	130	2052.12	0.966381	- 1 3 7 4
54	1741.64	0.977396	2 6 1 0 5	131	2054.69	0.966448	-1 3 3 4
55	1741.71	0.974327	-2 4 9 5	132	2068.60	0.968098	- 1 2 7 2
56	1743.67	0.971252	-2 4 10 5	133	2083.47	0.966378	1 2 5 1
57	1744.36	0.965925	- 2 3 4 4	134	2086.72	0.970437	1 2 7 1
58	1745.11	0.966036	- 2 3 6 4	135	2088.61	0.966735	1 2 3 1
59	1747.52	0.965969	- 2 3 8 4	136	2093.84	0.983915	1 4 1 3
60	1752.16	0.966189	-2 5 11 5	137	2094.72	0.982895	1 4 5 3
61	1756.67	0.979054	2 5 9 5	138	2094.90	0.981471	1 4 7 3
62	1758.64	0.975965	2 5 1 0 5	139	2095.25	0.966292	1 2 5 4
63	1763.05	0.974261	- 2 6 9 5	140	2098.49	0.970351	1 2 7 4
64	1763.50	0.977938	2 4 2 3	141	2099.67	0.983259	1 4 3 3
65	1764.44	0.976621	2 4 6 3	142	2100.38	0.966649	1 2 3 4
66	1765.03	0.971186	-2 6 10 5	143	2109.32	0.968019	- 1 4 1 3
67	1765.06	0.977190	2 4 4 3	144	2111.39	0.967989	- 1 4 5 3
68	1765.15	0.976074	2 4 0 3	145	2111.75	0.967914	- 1 4 7 3
69	1775.85	0.967656	- 2 4 2 3	146	2114.26	0.967982	- 1 4 3 3
70	1778.90	0.967457	- 2 4 4 3	147	2128.40	0.968939	- 1 2 5 1
71	1779.57	0.967569	- 2 4 6 3	148	2128.62	0.967535	- 1 2 7 1
72	1780.37	0.972833	-2 5 9 5	149	2133.63	0.969298	- 1 2 3 1
73	1781.90	0.967502	- 2 4 8 3	150	2140.47	0.968853	-1 2 5 4
74	1782.36	0.969763	-2 5 10 5	151	2140.68	0.967449	1 2 7 4
75	118901.7	0.969979	2 2 4 1	152	2141.46	0.982406	1 5 1 3
76	1789.79	0.970091	2 2 6 1	153	2142.53	0.979966	1 5 7 3
				154	2145.69	0.969212	- 1 2 3 4
				155	2157.45	0.966535	- 1 5 1 3
				156	2159.88	0.966431	- 1 5 7 3

5.4 RESULTS OF RELIABILITY –WEIGHT OPTIMIZATION

5.4.1 Venus Orbiter No. 1

The results of the optimization analysis for the Venus Orbiter No. 1 model are illustrated in Figure 84. The points plotted here represent the optimum system configurations as a function of reliability and weight over the complete range of reliabilities. Five different system configurations were identified as optimum and all of these employ a regulated bus system approach. All other system configurations analyzed fall above the locus of optima plotted on the curve. This locus of points has no meaning between the particular points identified. Although systems exist at these intermediate reliability levels, their weights are always higher than the weight of the next higher reliability system plotted on the curve.

A comparison of these five optimum system configurations for the Venus Orbiter No. 1 mission is shown in Figure 85. This is a plot of the matrix of optima (Reference Table 25) for each of the systems, as determined by the computer analysis of each of the candidate systems. Systems 2395 and 2495 employ 20-cell silver-cadmium batteries with charge and discharge regulators to control the regulated bus (Reference, Configuration Code, Table 62). A large increase in weight is required for these systems to achieve reliabilities greater than 0.98 because of the need to change from nonredundant to fully redundant batteries at this point. Since the battery weight is a relatively large portion of the total system weight for this mission, a characteristic large increase in weight at intermediate reliability levels was found to exist in all systems using 100 percent battery redundancy.

The reliability-weight relationship for these types of systems results from starting with a minimum weight, nonredundant system and selectively adding redundancy to the control, regulation and conditioning equipment. This yields a relatively large increase in reliability for small increase in weight. When reliabilities of approximately 0.977 are achieved, all the electronic equipment is in its redundant configuration. Any further increase in reliability requires that the battery be made redundant. When this is done, it is possible to then minimize the system weight at these increased reliabilities by returning to the baseline configurations of selected units within the system. Further increases in reliability are then

achieved by again making the electronic equipment redundant until the maximum redundant configuration of the system is reached at a reliability of approximately 0.999.

Systems 23115 and -23115 employ low-voltage batteries in a two-out-of-three majority voting Configuration. This alternative approach to implementing battery redundancy in a regulated bus system produces a significant weight advantage at reliability levels between 0.98 and 0.997. Since this approach was used only in a redundant battery configuration, the system weight remains high at lower reliabilities. In order to achieve reliabilities higher than 0.997 with this approach it is necessary to make the battery controls redundant. This produces a significant decrease in system efficiency, a corresponding by large increase in system weight and the highest reliability of all systems considered.

5.4.2 Venus Orbiter No. 2

The locus of optimum systems for Venus Orbiter No. 2 is shown in Figure 86. As indicated in Figure 87, the low voltage battery system, **34115**, offers a significant weight advantage at the intermediate reliability levels. The remaining eight optimum systems are closely grouped with respect to weight over the whole reliability range. For this mission the unregulated bus systems 1171, 3161 and **3141** are competitive with the regulated bus systems. As is true with Venus Orbiter No. 1, the maximum reliability is achievable with the low voltage system configuration. The weight penalty associated with this maximum reliability, however, represents a smaller weight penalty on a percentage basis in comparison to the competitive systems than for the lower power Venus Orbiter No. 1 mission. System 1151, although optimum at one reliability level, is not competitive over the remainder of the reliability range.

5.4.3 Mercury Flyby

The Mercury Flyby mission represents the shortest time duration of the seven missions considered in the study. As a result, the minimum reliability for a given system based on a nonredundant configuration of that system was determined to exceed 0.90 by considerable margin. The 20 reliability constraints were therefore revised to reflect a range from 0.93 to 0.9995. The locus of optimum system configurations for this

mission is illustrated in Figure 88. Eight system configurations were determined to be optimum at different reliability values over the entire reliability range. Four of these systems are of the unregulated bus type and four of them utilize the regulated bus technique.

The locus of optima for each of these systems is plotted in Figure 89. The achievable reliability and weights of all the systems are fairly closely grouped. Systems 1171 and -1171, however, were generally higher in weight than the other systems over the range of reliabilities, and, since each of these systems appears as the optimum at only a single reliability value, these systems are considered to be less desirable approaches. The low-voltage battery configurations 34115 and -34115 for this study are shown to be approximately 20 percent higher in weight than the majority of the systems at their maximum reliability values. These lower voltage battery systems are also seen to be characteristically higher in weight at the lower reliability levels because they were analyzed only in redundant battery configuration. At intermediate reliability values ranging from approximately 0.99 to 0.9992 the regulated bus systems (3495 and 34115) offer the lightest weight approach. Unregulated bus systems 3141 and -3141 are optimum at higher and lower reliability values.

5.4.4 Mars Orbiter

The locus of optimum systems for the Mars Orbiter mission is illustrated in Figure 90. Nine different system configurations were determined to be optimum at various values of reliability over the entire range. The optimized reliability versus weight relationship for each of these nine systems is illustrated in Figure 91. Here again, the lines connecting points serve only to facilitate examination of the data and as such have no meaning relative to achievable reliability and weight of the various systems.

At reliabilities between 0.9 and approximately 0.97, the majority of these optimum systems are relatively closely grouped in weight. Two higher weight systems exist within the lower reliability range and these systems, 2323 and 2321, may be observed to be only optimum at a reliability level of slightly greater than 0.99. The weight penalty associated with these two systems at all other reliability levels is considered sufficient justification for eliminating them from further consideration.

The characteristic step increase in weight produced by changing from the nonredundant to redundant battery configurations is seen to occur at reliabilities of approximately 0.98 for five of the systems. It is significant that four of the unregulated bus systems can achieve a reliability of approximately 0.99 prior to the need for adding redundant batteries. At this reliability level, systems 3423 and -3423 offer a significant weight advantage. At the higher reliability levels between 0.997 and 0.999, the regulated bus systems 3495 and unregulated bus systems 3161 and 3141 all are competitive from a weight standpoint.

5.4.5 Jupiter Flyby

The locus of optimum power system configurations for the Jupiter Flyby mission is illustrated in Figure 92. Four different systems were determined to be optimum at various specific reliability levels over the total range. Comparison of the optimized weight and reliability for each of these four systems is shown in Figure 93. The maximum achievable reliability is seen to be relatively low in comparison to the previously discussed mission. This results from the much longer mission time required to reach Jupiter.

The advantage of regulated bus systems employing a shunt solar array regulator is apparent because the solar array is operated at its maximum power point at the critical design point and this power is delivered directly to the load power conditioning equipment without incurring efficiency penalties in series regulators. The inefficiency of charge and discharge regulators produces a minimal effect on the system because of the very low-battery utilization requirement on a nonorbiting mission of this type. The ac distribution system is shown to produce a significant advantage in reliability for this particular mission. The weight penalty associated with this advantage in comparison to the less reliable lighter-weight dc systems shown is approximately 6 percent.

The optimum power system weights vary from approximately 800 to 900 lb which clearly exceeds the allowable weight for this mission. Referring to Table 1, the estimated spacecraft weight is 650 lbs including payload. The assumption that state-of-art solar arrays at 0.1 lb/watt would be used for this mission is therefore not valid. Since the solar array constitutes the major portion of the system weight, a 0.5 lb/watt design,

or better, is essential to the feasibility of this model mission. However, such a change would not appear to affect the selection of optimum systems.

5.4.6 Jupiter Orbiters

The locus of optima for the Jupiter Orbiter No. 1 mission is plotted in Figure 94. Only four system configurations comprise this locus. The plot of the individual optimized weight versus reliability for each of these four systems is shown in Figure 95. The same four systems were determined to be optimum for the Jupiter Orbiter No. 2 mission as shown in Figure 96. The individual plots for this mission are shown in Figure 97. For both of these missions, the regulated bus systems employing the shunt regulator for solar array control were determined to be optimum. Characteristically, the AC versions produced the higher achievable reliabilities and the low voltage battery systems yielded the maximum achievable reliability.

The resultant optimum power system weights for the Jupiter Orbiter No. 1 mission represent 60 to 70 percent of the estimated spacecraft weight of 1620 lbs. Thus, a lighter weight array design is essential to perform this mission with the assumed loads. For the Jupiter Orbiter No. 2 mission, the lighter 0.5 lb/w array design was assumed and the resultant optimum system weights represent less than 20 percent of the 8430-lb spacecraft weight.

Table 75. Configuration Code

<u>Example Configuration Code:</u>		<u>Code Identification:</u>
1		<u>Energy Storage</u>
2		1 Disconnect switch plus current limiting resistor
3		2 Disconnect switch plus current limiting resistor plus discharge booster
4		3 Dissipative bucking charger and discharge switch
1	<u>Distribution Method</u>	<u>Energy Storage</u>
2		1 AC Distribution
3		2 (no symbol) DC Distribution
4		3 Dissipative charger, discharge switch and discharge booster
1	<u>Array Sizing Factor</u>	<u>Energy Storage</u>
2		1 Sizing Factor A ₁
3		2 Sizing Factor A ₂
4		3 Sizing Factor A ₃
1	<u>Array Control</u>	<u>Energy Storage</u>
2		1 None
3		2 Zener Shunt
4		3 Active Shunt
1	<u>Line Regulator</u>	<u>Energy Storage</u>
2		1 PWM bucking charger and boost discharge regulator (normal voltage battery)
3		2 Max. Pwr. Tracker - Buck
4		3 PWM Series Buck-Boost
1	<u>Line Regulator</u>	<u>Energy Storage</u>
2		1 PWM bucking charger and boost discharge regulator (normal voltage battery)
3		2 Max. Pwr. Tracker - Buck
4		3 PWM Series Buck-Boost

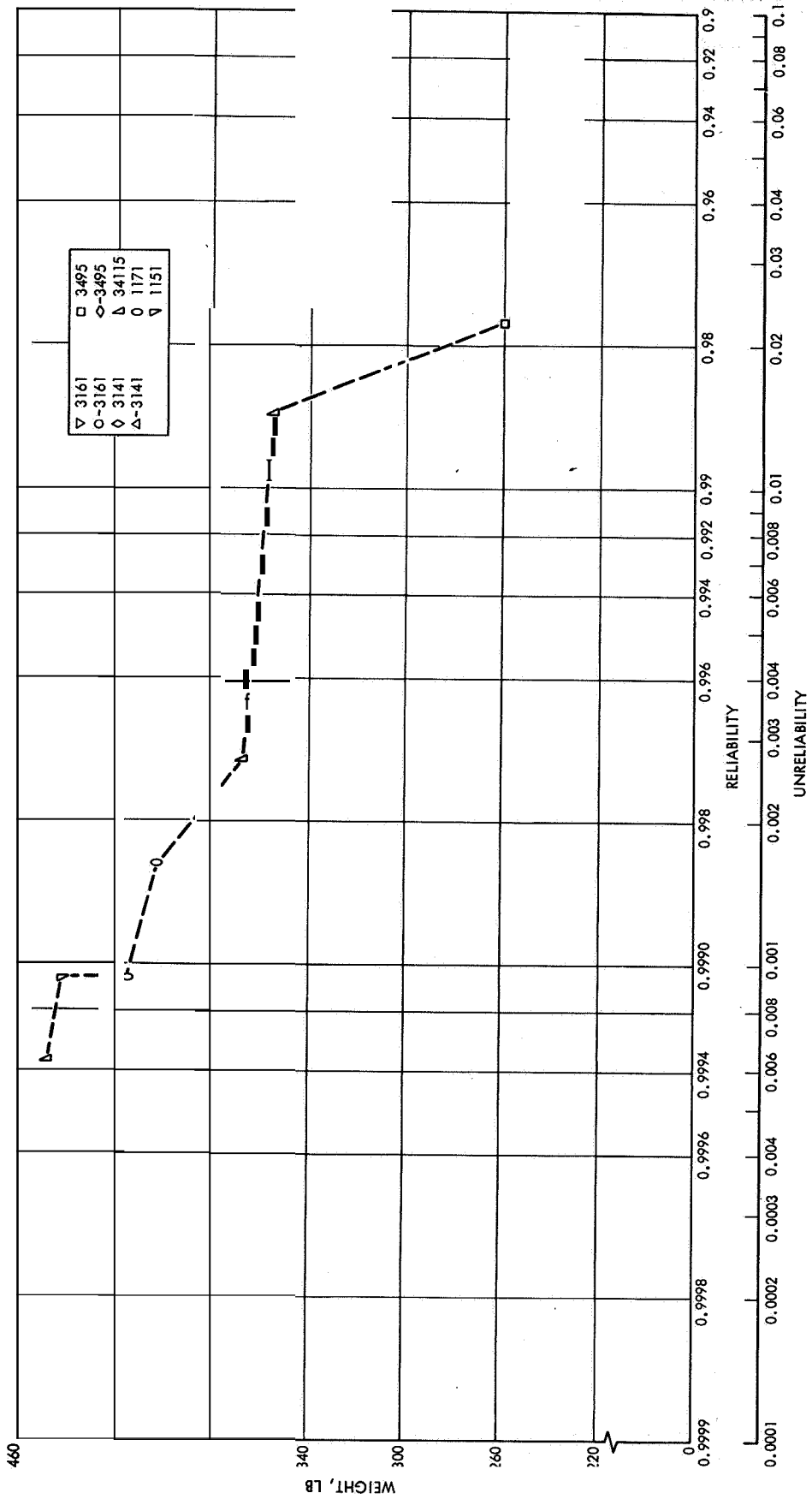


Figure 82. Locus of Optimum System Configuration, Venus Orbiter No. 2

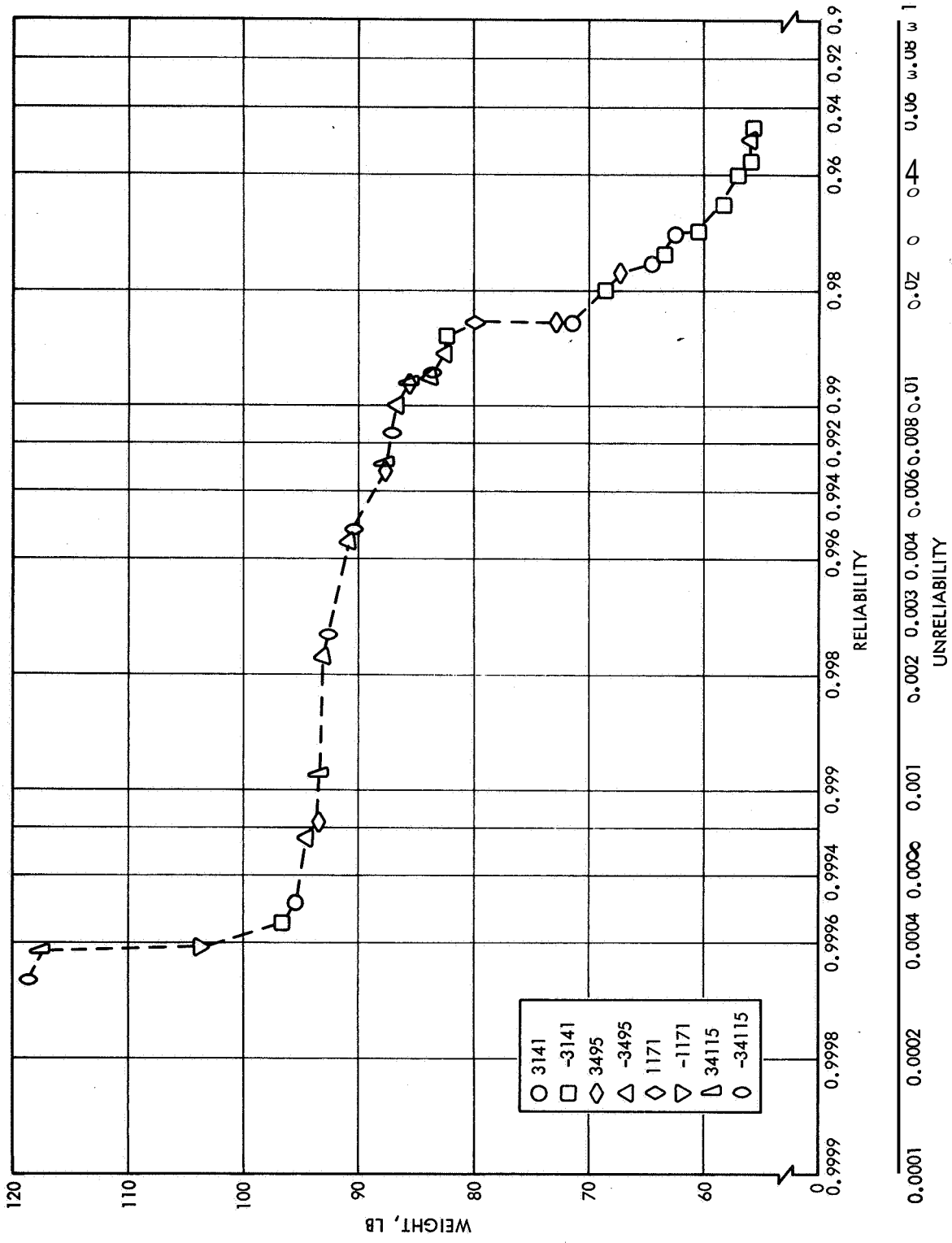


Figure 84. Locus of Optimum System Configurations, Mercury Flyby

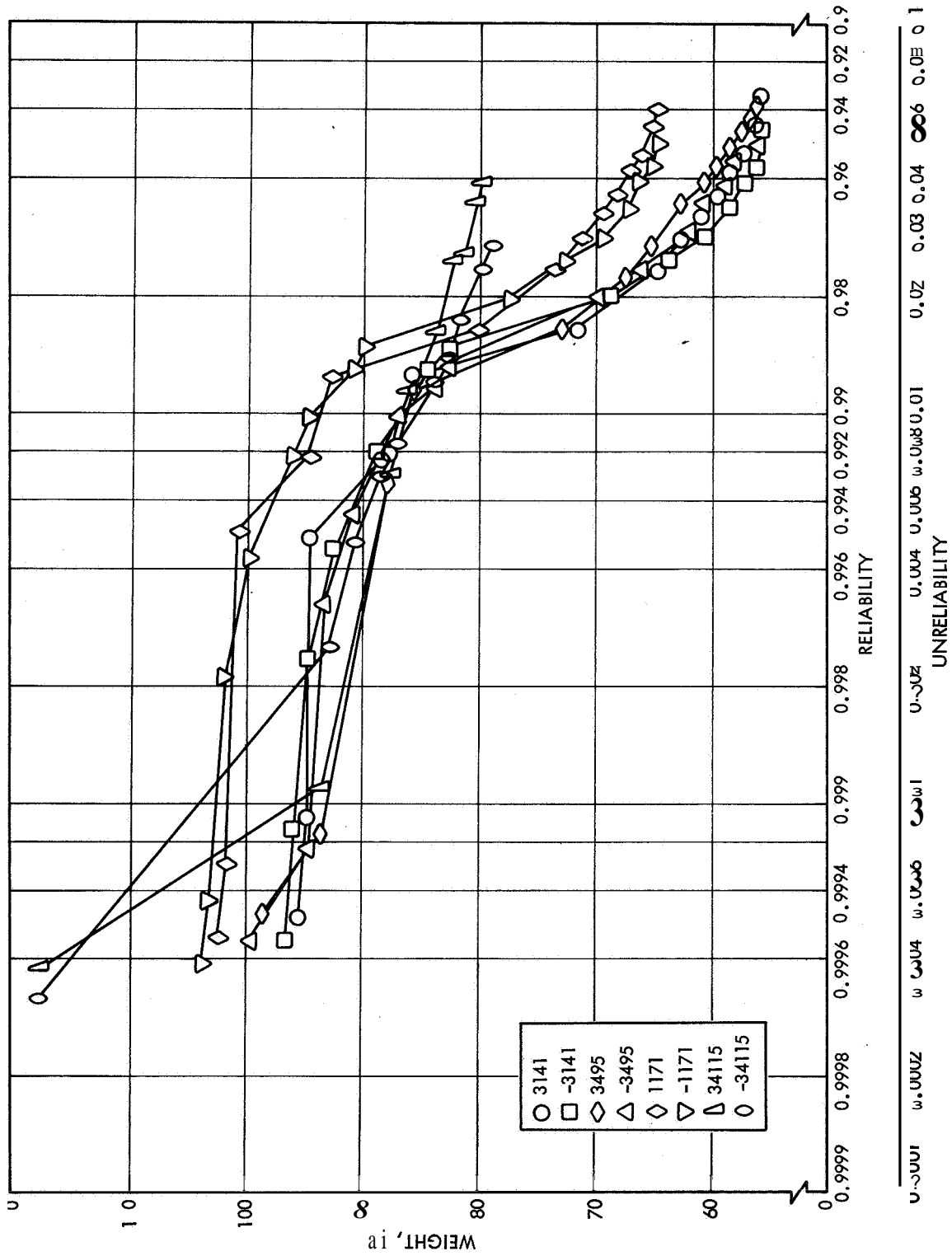


Figure 85. Comparison of Optimum System Configurations, Mercury Flyby

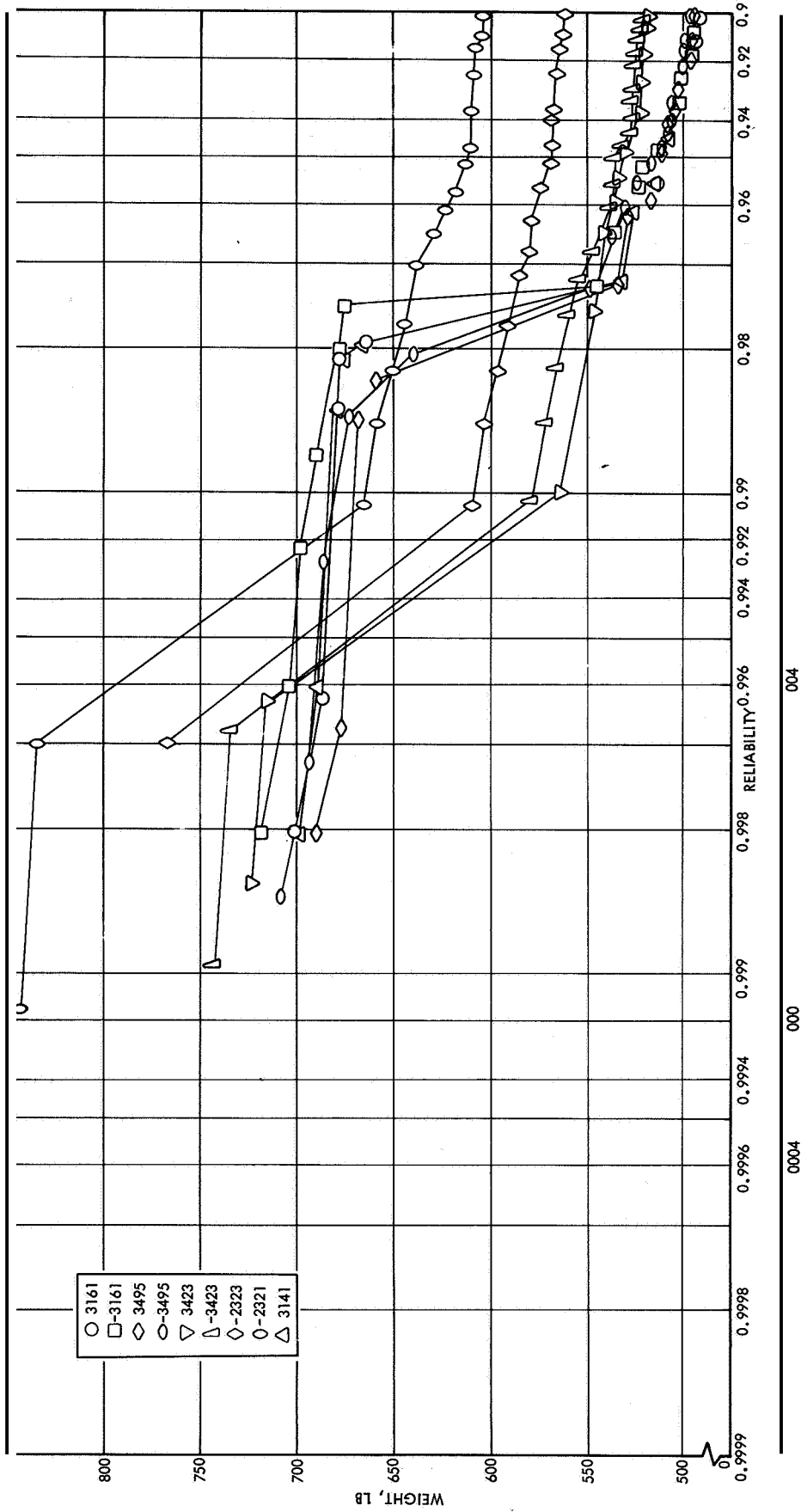


Figure 87. Comparison of Optimum System Configurations, Mars Orbiter

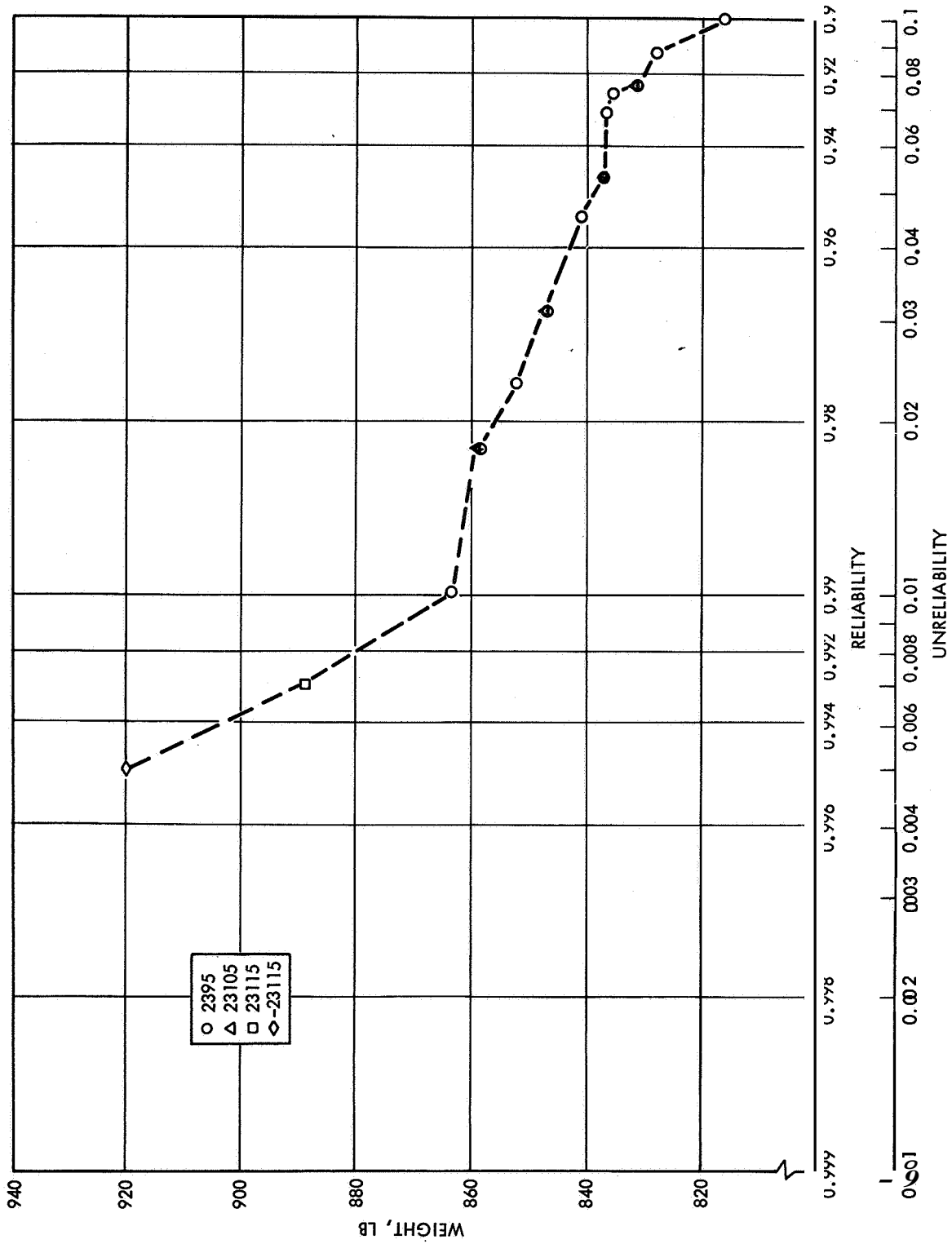


Figure 44 Locus of Optimum System Configurations, Jupiter Flyby

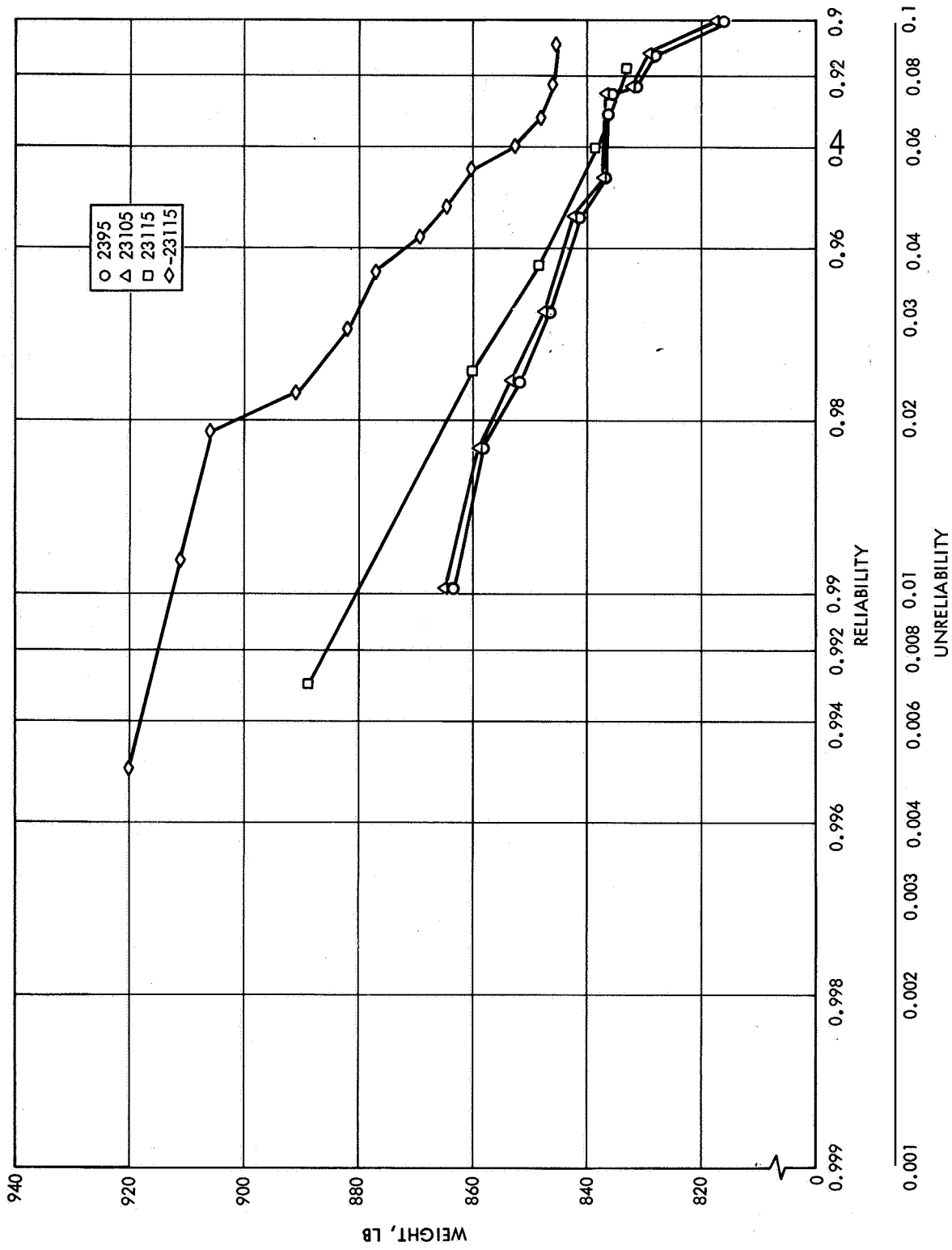


Figure 89. Comparison of Optimum System Configurations, Jupiter Flyby

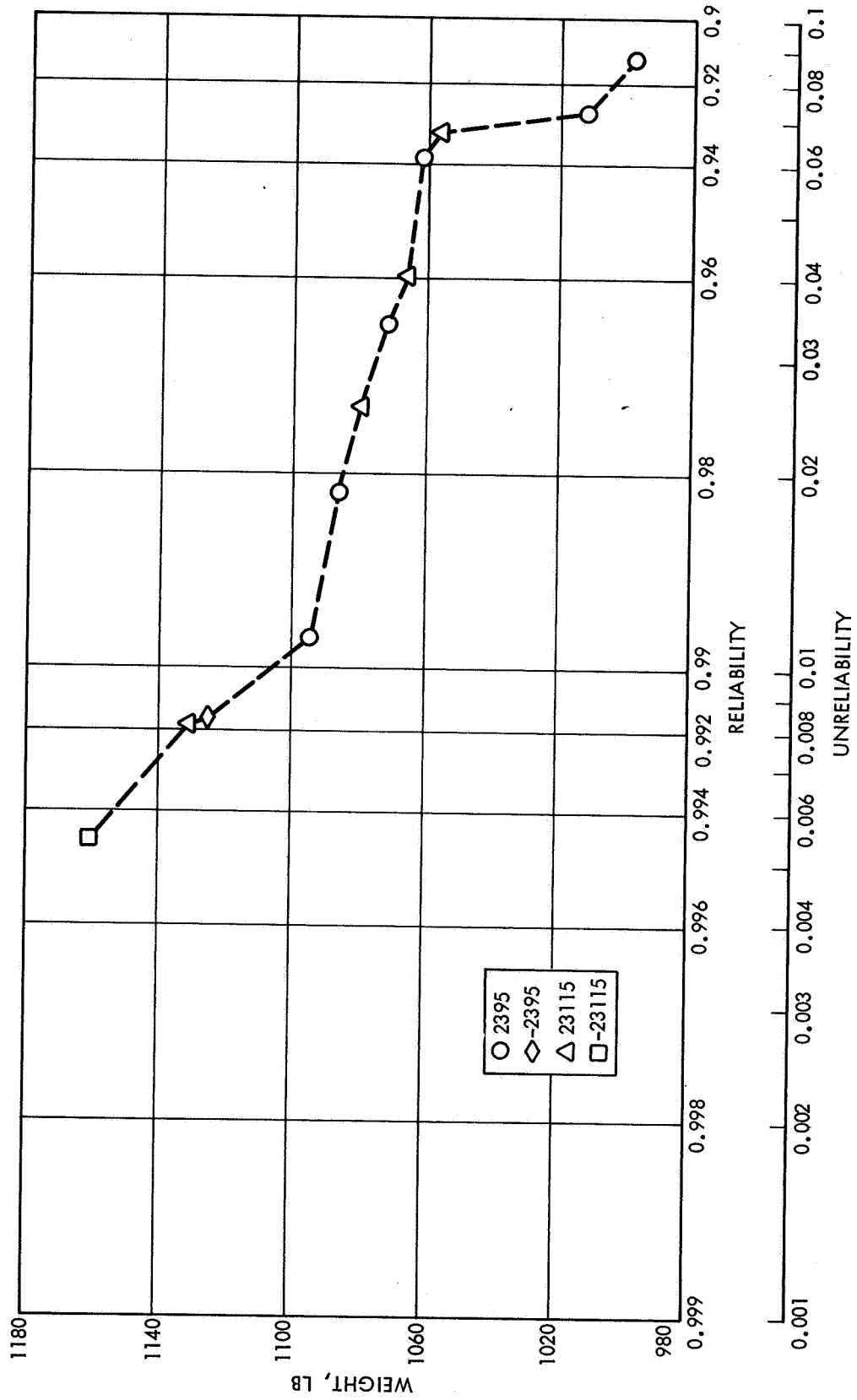


Figure 90. Locus of Optimum System Configurations, Jupiter Orbiter No. 1

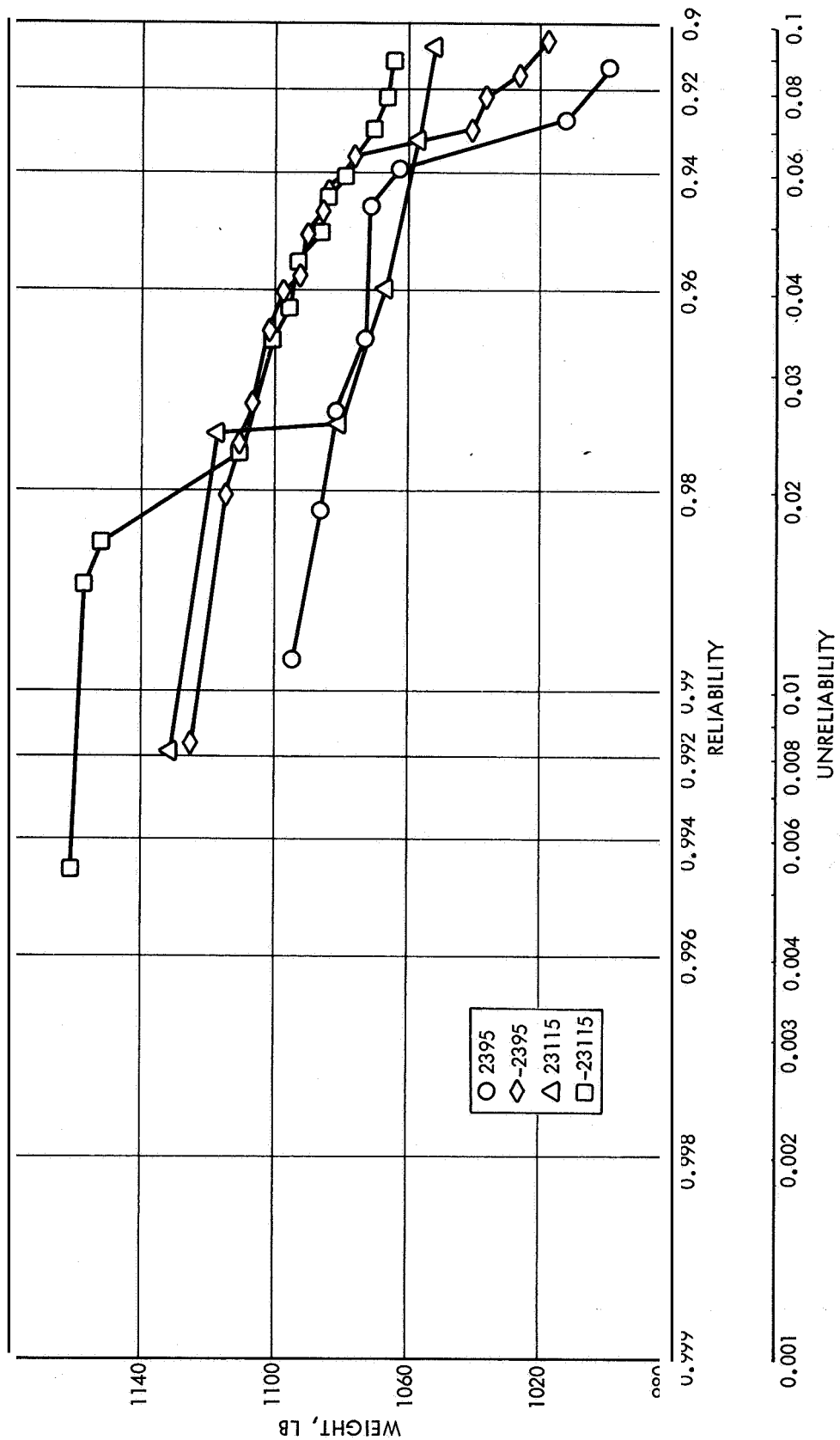


Figure 91. Comparison of Optimum System Configurations, Jupiter No. 1

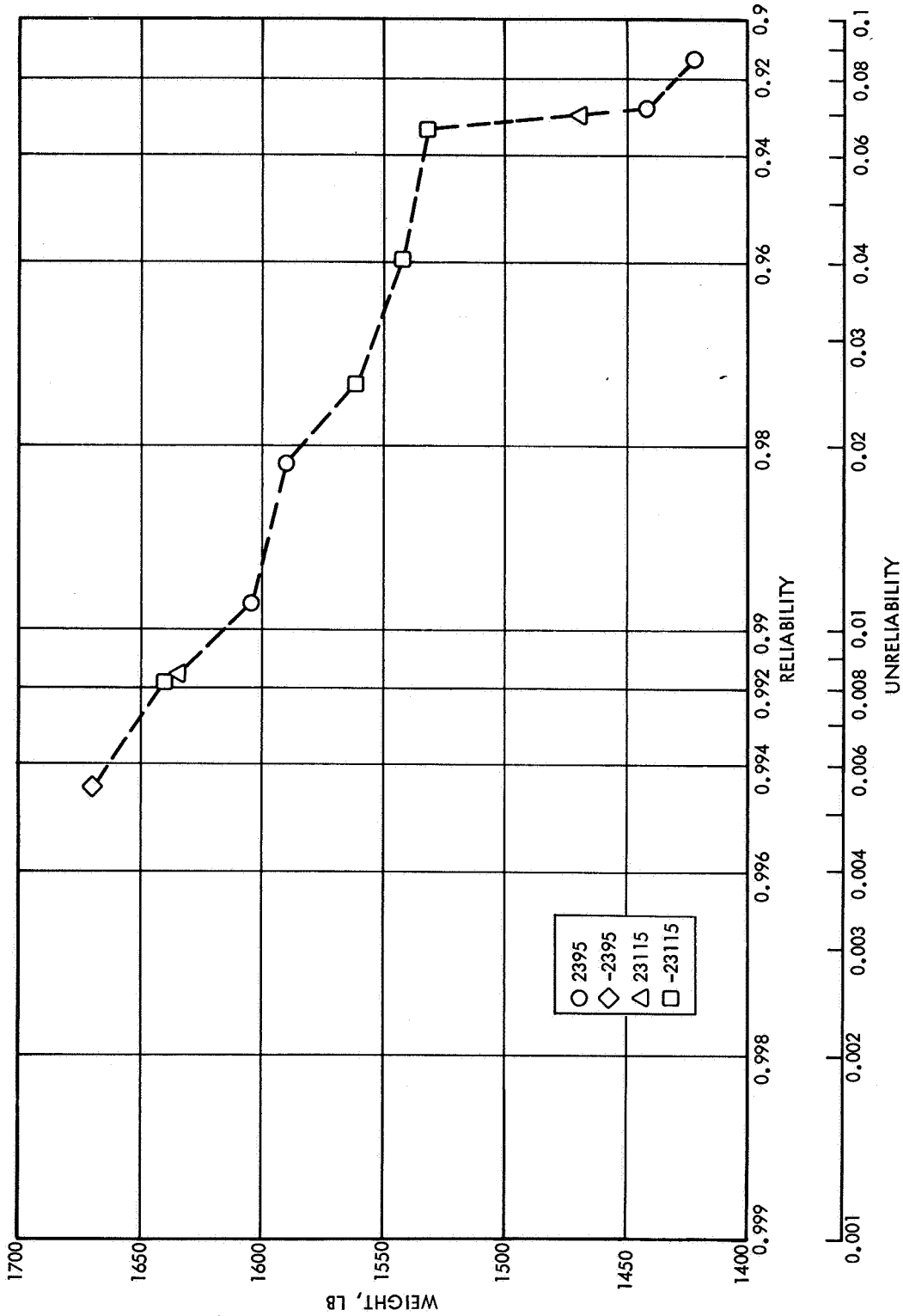


Figure 92 Locus of Optimum System Configurations, Jupiter Orbiter No. 2

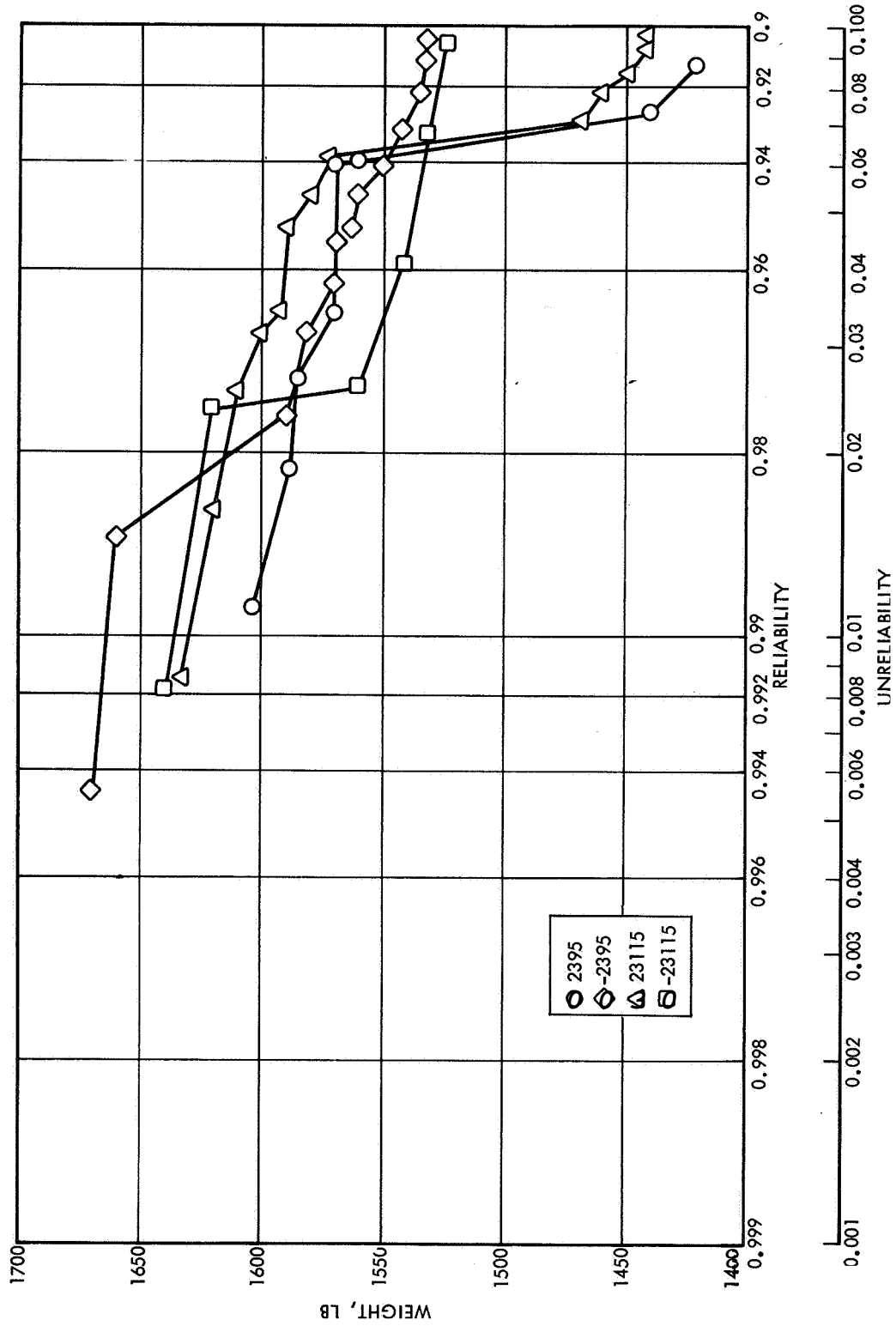


Figure 93. Comparison of Optimum System Configurations, Jupiter Orbiter No. 2

6. DESIGN CONSIDERATIONS AND CONCLUSIONS

6.1 ELECTROMAGNETIC COMPATIBILITY

One of the most important interface considerations which influence the design of spacecraft power systems is that of electromagnetic compatibility (EMC). Since the power system has some type of conductive interface with each equipment on the spacecraft, interference generated by the power subsystem will exist at these interfaces. In addition, interference, generated by any of the equipments using this power, can use the power subsystem as a medium to couple interference to any other equipment.

As a result of these considerations and the fact that EMC problems are often not fully appreciated by power system designers, emphasis was placed on this aspect of the power system interface studies for this program.

Typical problem areas of incompatibility occur in two distinctive areas:

- a) Effects of electromagnetic interference on phenomena being measured by spacecraft experiments.
- b) Effects of electromagnetic interference on spacecraft electronic systems by various coupling methods.

In the first area, the effect is generally due to the electric and magnetic fields created by the power system equipment and the distribution system. These fields may modulate or change the electromagnetic fields existing in and around the spacecraft or may dominate the space fields so as to make them unmeasurable,

In the second area, interference may couple voltages and/or currents into sensitive electronic circuits and cause irregular behavior of the affected system,

The spectral distribution of the power system interference may be classified into two general categories. The first is discrete line spectra at the regulator switching frequency, converter switching frequency and/or the frequency of ac distribution. Harmonics generally exist above

general random spacecraft noise out to the region of 5 to 10 mc. The second type noise is transient in nature existing at turn on—turn off occurrences. The continuous-spectrum nature of transients may be quite large in amplitude when integrated over the bandwidth of the affected system, and consequently the systems will respond to this energy.

While any system will respond to energy within its passband, some categorization of typical problems is possible for general systems. The magnitude of overall interference problems is generally an inverse function of spacecraft maximum distance for a given power available since data rates are of necessity low for long-distance missions. Consequently, the information bandwidths of experiments and telemetry functions are narrow and the probability of intercepting an intolerable amount of noise is decreased. If the discrete frequencies associated with the power system are above approximately half the maximum data rate, small interference problems should result provided the sensitivities are not excessively high. The nature of the problems, which occur under these conditions, is generally one of sampling. The interference frequencies, which are high compared to the data rate, may be sampled each time a particular data word is transmitted. If the noise frequency and data rates are synchronous, a constant off-set will occur. If they are asynchronous, a modulation of data will occur at some low frequency, dependent upon the difference between the noise frequency and the particular harmonic of the data rate, which results in an inband signal.

Onboard systems, whose outputs are utilized onboard and not transmitted to earth, are not necessarily limited by the data bandwidth. These systems may well have bandwidths which allow them to see the power system interference over a broad range.

Specifically, the primary compatibility problems relating to the spacecraft power system are due to:

- **Type** of power distribution used (ac or dc)
- Waveform of ac distribution
- Frequency of ac distribution
- **Type** of voltage regulator circuit used (dissipative or switching type)

- o Power circuit grounding
- Power circuit wiring practices
- o Power converter "Bandpass Characteristic" to interference at its input.

These compatibility problems can be minimized by the use of judicious circuit design and interference control measures, such as circuit grounding, bonding, shielding, circuit isolation, and filtering.

The impact of EMC considerations on selection of a power system design is divisible into two areas of consideration. The first area concerns the desirability of minimizing the number of power handling units which employ pulsewidth modulation types of switching circuits for regulation and control of the solar array, battery and main power bus. Both series and shunt-type voltage regulators used in spacecraft power systems may employ either switching (pulsewidth-modulated) or dissipative techniques. From the interference generation standpoint, the dissipative type is preferable since it generates negligible interference. In contrast, the pulsewidth-modulated type of regulator is a prolific generator of impulse-type interference.

The second area in which **EMC** considerations strongly influence power system design is that of selection of the power distribution system. Because of the fewer parts in the ac distribution system it was determined to be the most reliable system. However, in comparing redundant dc systems versus redundant ac systems the differences were only in the third or fourth decimal place of the calculated reliability values. The ac systems were selected with one transformer in the main inverter and a second transformer in each of the transformer-rectifier units. This series transformer configuration produced a penalty in system efficiency which was then reflected in a greater system weight in comparison to the dc systems. Here again, the magnitude of the impact of this poorer efficiency on system weight was not significant. As a result, selection of either ac or dc distribution cannot be based strictly on comparisons of power system reliability and weight.

A squarewave ac versus dc tradeoff performed for a typical state-of-the-art spacecraft indicated, in general, a definite advantage for the dc power distribution system with respect to **EMC**. The analysis indicated that the dc distribution system could be designed to be acceptably low in interference with proper filtering at its interference producing loads (solenoids, relays, etc.), 'dc to dc converters and PWM regulators. In contrast, the squarewave ac distribution system inherently produces interference fields due to the transmission of squarewave power throughout the spacecraft. The interference control techniques of slowing pulse rise and fall times, wire twisting and shielding, and proper cable routing reduce the generation and crosscoupling of the switching interference, but not sufficiently in every case.

The necessity of shielding on the ac distribution cabling increases the weight of cabling by approximately **45** percent. For the larger spacecraft, this penalty becomes increasingly significant. The possibility of using higher voltage (>100 V) ac distribution can offset this penalty by reducing load currents and wire sizes. The use of higher voltage dc distribution systems has been limited to about 50 V in the past, based on available transistor voltage ratings. For larger spacecraft, distribution voltages of 100 V or greater (whether ac or dc) would provide significant improvements in the efficiency and weight of the distribution system. Development of parts to provide reliable operation at these higher voltages is considered mandatory to optimize the weight of systems using dc distribution for power levels in the kilowatt range.

6.2 THERMAL CONTROL

The most common interface problem between the power subsystem and spacecraft thermal control system is that of maintaining a relatively close range of operating temperatures for the battery to assure its reliable operation. The typical 50 to 90°F range desired for the battery has, in several spacecraft designs, constituted the single most difficult control problem for the thermal control system. The magnitude of this problem is a function not only of the variations in heat dissipation of the battery which are in turn directly related to its charge rates and charge control methods, but also the influence of other spacecraft equipment, the heat dissipation of which may influence the operating temperature of the battery. Maintaining desirable battery-operating temperatures throughout a mission is a problem common for the most part to all power system configurations, and it does not, therefore, materially effect the selection of power system designs.

A second important thermal interface which could influence the design of the power system is that relating to the thermal control of dissipative regulators. This is particularly true with the shunt dissipative regulator. Techniques have been developed to reduce the magnitude of the heat dissipation in shunt regulators. For the larger spacecraft and for the interplanetary missions studied, however, these techniques may prove inadequate. As a result, the use of series PWM regulators to control the output voltage of the solar array appear clearly advantageous from the thermal control standpoint. The principal advantage of the series regulator is to proportionately reduce the power drawn from the solar array if the load power demand is significantly less than the solar array power capability. This is accomplished by causing the solar array to operate at a voltage and current at which the efficiency with which it converts solar energy into electric power is relatively low.

Concerning the missions investigated in this study, the large variation in solar array capability during the Jupiter Mission would produce the largest thermal control problem relative to the use of the shunt regulator. The shunt regulator, however, is most advantageous for the Jupiter missions because of its ability to optimize the operating point of

the solar array at the critical design point of the mission. This advantage is particularly significant because of the very large solar array required for the Jupiter missions; thus it is desirable to add additional complexity to switch-out sections of the solar array during the early phases of the mission when a large excess capability exists. **This** will reduce the amount of heat dissipation in the shunt regulator such that the thermal control system can accommodate this approach.

6.3 POWER SYSTEM FLEXIBILITY

The term flexibility, as used in this study, pertains to the ability of the power system to tolerate variations in load power requirements during the various mission phases or changes in the specific power characteristics required by the loads without necessitating extensive redesign of the power system or producing detrimental effects on the power system reliability and weight. The first area of concern is the effect of changes in power levels or power characteristics required by the loads when supplied from the dc distribution system. When dc to dc converters are used to generate the voltages required by the loads, any variation in load requirements could necessitate the redesign of one or more of these converters. The advantage gained by using an ac distribution system as configured in this study is small in this respect, in that centralized TR units were used wherever possible to minimize the number of parts in the system and to maximize system efficiency. These would also require redesign in the event of load requirement changes.

It is clear that, from the standpoint of flexibility, power system configurations which supply a common ac or dc bus to the loads and permit the load equipment to condition that power as necessary offer large advantages in terms of flexibility. The disadvantage is the duplication of power conditioning functions in the various load equipment with its attendant reduction in system reliability and increase in system weight. This reliability penalty results from the increased number of parts required to provide power conditioning for the essential loads but must also take into account the advantage of having separate power conditioners for the nonessential loads. Obviously, redundancy can be employed in these power conditioning functions to minimize the **loss** in reliability. **As** a result, the poorer efficiency of many small power conditioning elements in comparison to centralized power conditioning is the major reason for considering this to be an undesirable approach.

It is extremely difficult to quantitatively trade off the gains in system flexibility against losses in system efficiency. The design of an optimum power system, however, must assume adequate definition of load power requirements and must permit the power system designer to optimize the necessary power conditioning equipment. The approach of supplying an ac bus to all of the load equipment from a central inverter is a compromise,

in this respect, which permits consolidating all power inversion functions into one power system unit and requires transformer rectifier units in the load equipment. If the power requirements of each of these items of load equipment are small, relative to the total power demand, it is reasonable to assume that an advantage will be gained with this approach over that of supplying a dc bus to all of the load equipment and including dc-to-dc converters within each of the loads. The reason for this is that at low power levels the decrease in efficiency of a dc-to-dc converter is larger than that associated with transformer-rectifiers. If a relatively small number of dc-to-dc converters may be used, as occurred for the assumed load power conditioning equipment configurations in this study, then the efficiency of the dc distribution system is improved and the efficiency penalty of having transformers in the main inverter and additional transformers in the TR units tends to offset the apparent efficiency advantage of the ac distribution system.

A second area of consideration relative to load growth is in the power sources and their control and regulation functions. Any increased continuous load power demand will normally require redesign of these power system elements. With respect to transient or peak load demands, however, if the additional load can be supplied from an unregulated bus, then those system configurations which permit the battery to discharge directly to the main bus would appear to have an advantage over the regulated bus system unless these transient load demands can be supplied directly from the battery.

The use of a low-voltage battery with a regulated bus system has a significant disadvantage in this respect. For this type of system, all continuous or transient load demands which exceed the solar array capability must be supplied from the battery through its boost discharge regulator. An increase in steady state or peak loads would necessitate adequate power-handling capability in this regulator. In addition to the probable redesign required, the regulator efficiency at normal load conditions would, as a result, be decreased with an attendant increase in battery and system weight.

A method under investigation by TRW to overcome this disadvantage with a low-voltage battery system is incorporated in the modular energy storage and control (MESAC) system which is based on a modular approach to performing the energy storage function. Each module within such a system contains the low voltage battery and its charge and discharge regulators. This system has an inherent large degree of flexibility in that load growth can be accommodated by adding modules without necessitating new design or the redesign of any of the other existing modules.

With respect to transient or peak loads, the use of a transient load bus isolated from the main bus and supplied through separate boosters from the batteries, or the use of separate energy sources, such as capacitors or a primary battery, appear to be feasible alternatives to the addition of energy storage modules.

In this study, the low-voltage battery concept was configured with three batteries, two of which are required to support the requirements. In the actual application of the modular energy storage concept, the number of batteries is a variable which can be optimized for the specific use. The analyses leading to the selection of the optimum system must take into account the availability of battery cells of given capacities as well as the reliability-weight tradeoff of using a larger number of batteries in parallel. Thus, it is possible to consider a system as an example having twelve batteries in parallel, ten of which are required to support the mission. The potential advantage is that due to the relatively small number of cells required, an adequate reliability may be achieved with only 20 percent redundancy.

From these general considerations, it appears that the ac distribution approach and the modular energy storage concept offer advantages relative to flexibility in terms of load growth. The reliability weight analyses that have been performed indicate that changes in the battery duty cycle may have a more significant impact on the selection of a power system. Here again the distinction between the regulated bus concept and the unregulated bus concept is made. The former is clearly advantageous for those missions in which battery discharge requirements are relatively small. The Mars Orbiter mission represented the greatest ratio of

eclipse time to sunlight time during its orbiting phase. The study results for this mission showed that certain of the unregulated bus systems offered weight advantages in comparison to the regulated bus systems.

Analyses have shown that if this ratio is further increased, the unregulated bus approach, because of its more efficient energy-storage capability, becomes even more favorable than the regulated bus approach. **As** a result, consideration of flexibility in terms of variations in the orbit parameters may lead either type of system to become less optimum and possible variations in these parameters must **be** taken into account in the initial power system design.

6.4 SYSTEM DESIGN CONSIDERATIONS

There are several specific power system design considerations that are common to all power system configurations. These are:

- o Command provisions
- o Telemetry provisions
- Protection against load faults
- Electromagnetic interference control

6.4. 1 Command Provisions

In those spacecraft applications where continuous surveillance from the ground is possible, many operations of the power system can be controlled by ground command. In some cases, this results in a significant simplification of the onboard automatic control circuitry. The approach favored for the interplanetary missions considered in this study is that of providing onboard automatic controls and relying on ground command only as a backup to the onboard control. The reliability of these automatic controls is maximized by the addition of redundancy within the control circuits. Care must be exercised in implementing the backup command circuits to assure that their failure modes are such that they will not cause improper operation of the power system.

The need for automatic controls is particularly important in considering missions with large earth-spacecraft distances such as that of the Jupiter missions. In these missions, the time lapse between the transmittal of telemetry data from the spacecraft and the receipt of that data at the earth can be as great as 50 minutes. This corresponds to a distance of 6 AU. Maximum distances and approximate corresponding one-way transmission times for each of the missions are as follows:

Jupiter :	6 AU	(at encounter)	50 minutes
Mars :	2.6 AU	(end-of-life)	22 minutes
Venus :	1.2 AU	(end-of-life)	15 minutes
Mercury :	1.4 AU	(end-of-life)	12 minutes

For the Jupiter mission, if the reaction time at the ground station is as rapid as five minutes to determine necessary action on receipt of abnormal telemetry data, the corrective action for a possible dangerous situation on the spacecraft would take about two hours. In reviewing typical power system failure modes and effects, it is considered impractical to allow any of these failure modes to exist for that period of time without corrective action.

The second reason for recommending the use of reliable automatic controls is that the penalty in weight resulting from incorporating automatic power system control functions in the spacecraft and in implementing these circuits in a redundant fashion to assure their-reliable operation is relatively small. Nevertheless, unforeseen eventualities do exist and, whether they occur within the power system or external to the power system, the desirability of having the flexibility of changing operating modes by command in response to abnormal conditions is clearly advantageous.

Command capability is considered most desirable in those areas relating to battery-charge control and load switching. The safe operation of the battery is dependent upon the ability of the spacecraft thermal control system to maintain desirable operating temperatures. If these operating temperatures are exceeded for reasons of abnormal orientation conditions, abnormal heat dissipation in any spacecraft equipment or abnormal operating conditions of the battery itself, the probability of completing the mission is reduced. Ground command capabilities are considered necessary to terminate battery charging, regardless of the status of the on-board control circuitry, and to restore normal automatic operation when desired. Secondary command requirements relative to battery control are the ability to initiate battery charging at any time as a backup to the automatic on-board charge control function and the provision to adjust battery charge rates or voltage limits to accommodate abnormal operating conditions.

The second command requirement of providing the capability for switching loads may serve as a backup to on-board load sequencing provisions, permit gross adjustments of heat dissipation within the vehicle, control the amount of available battery charging power, or limit battery discharge energy requirements. An automatic control feature in most power systems consist's of a battery under voltage sensor which effects an automatic load reduction in the event that battery capacity is inadequate.

The preferred implementation of this feature is to provide a non-essential load bus which can be deenergized in the event of an undervoltage of the battery. All loads not required for survival of the spacecraft should be energized from such a bus since, in the event'of a battery undervoltage, the remaining battery capacity is usually relatively small. If battery undervoltage occurs early during an eclipse period, the remaining battery capacity must support all essential or critical loads throughout the remainder of the eclipse period. The voltage setting for this undervoltage disconnect of nonessential loads is critical in that it must be sufficiently high to assure adequate remaining battery capacity for spacecraft survival and, on the other hand, sufficiently low to prevent premature load disconnect.

Here again, the operation of such a load disconnect function could be implemented by relying on a ground command for cases where the surveillance of the spacecraft is continuous and the transmission times are relatively small. Neither of these conditions is applicable to the interplanetary missions considered in this study. As a result, the need for a nonessential load bus and automatic deenergiation of that bus in the event of low-battery voltage during discharge is considered imperative. The simplest example of this is the Jupiter Orbiter mission. If such an event were to occur at the beginning of the 1.6-hr. eclipse period, a probable complete loss of power would occur before corrective action could be taken by ground command. Ground command load-switching capabilities are necessary in this case to restore the nonessential loads when desired, and to effect a load reduction prior to entry into each subsequent eclipse if the battery capacity is not recovered.

Another ground command capability often provided in earth-orbiting spacecraft is that for reconditioning batteries. This operation consists of removing a battery from the main system, discharging it completely through an auxiliary load and then returning it to the system for complete recharge. This reconditioning cycle is employed routinely in the storage of battery cells and has been determined to be an effective way of overcoming a major portion of the loss of battery capacity attributable to repeated charge-discharge cycling or long term storage.

Although the numbers of cycles required in the interplanetary missions considered in this study do not appear sufficiently large to necessitate the addition of battery-reconditioning capability, it is considered desirable to include this provision as it is not a significant penalty in weight or reliability and it affords the possibility of extending the mission considerably beyond its design life in the orbiting phase. It also permits diagnosis of suspected battery malfunctions by removing a battery from the system and discharging it through a separate auxiliary load. The battery-reconditioning provision may also serve to restore battery capacity lost through self discharge during an extended cruise phase prior to a spacecraft maneuver or other battery discharge requirement.

Another type of command often employed in power system design is that used to reset automatic switching of a standby redundant unit. This provision is necessitated primarily by practical consideration of pre-launch checkout requirements to ensure that both channels of redundant units are operative. The recommended implementation of standby redundancy and that used in the reliability weight tradeoffs in this study provide for switching from either channel to the second channel in the event of a failure. **As** such, the possibility of a subsequent failure or apparent failure in the second channel could cause switching back to the failed channel.

The probability of having failures in both channels of redundant units is extremely low; however, the possibility of a failure in an item of load equipment or other power system unit which appears as a failure in the operating channel is much higher. The result of such an apparent failure would be

to switch back to the failed channel and this would, in turn, cause a cycling condition between the two channels until such time as the malfunction which produced this apparent failure was corrected or isolated. It appears clear that with properly designed redundancy in the other power system units and with proper load fault isolation provisions, this cycling condition will be terminated automatically.

Command provisions are recommended, therefore, to provide the following capabilities:

- a) Terminate/initiate battery charging
- b) Change battery charge current/voltage limits
- c) Energize/deenergize nonessential load bus
- d) Energize/deenergize individual nonessential loads
- e) Initiate/terminate battery reconditioning discharge
- f) Select operative channel of standby redundant units

6.4.2 Telemetry Provisions

The judicious implementation of telemetry provisions constitutes an important task in the design of an electrical power system. It may be said that in the event of proper operation of all elements of the power system during a given mission the telemetry data for the power system will be excessive. On the other hand, in the event of a malfunction within the power system or a malfunction attributed to the power system, the telemetry provisions will be typically inadequate. Whereas in the case of operational satellite systems such as those used for global communications, navigational, or weather observation networks, power system telemetry provisions may be minimized, the exploratory nature of the interplanetary missions considered in this study amplify the desirability of maximizing these provisions.

Power system telemetry, however, normally competes with scientific communications and other prime spacecraft functions for the available telemetry channels so that it is a rare case when all desirable engineering measurements can be transmitted. Priorities for selection of telemetry points must therefore be developed for the spacecraft as a whole. To this end, five general categories of telemetry provisions were developed and they are listed in order of descending priority as follows:

- 1) Measurements required for the performance of normal flight operations by ground command.
- 2) Measurements required for the performance of alternate or abnormal modes of operation by ground command.
- 3) Measurements required to verify the performance of specific systems either in flight or during prelaunch checkout activities.
- 4) Measurements required to evaluate detailed performance of critical or newly developed units.
- 5) Measurements required to diagnose malfunctions which may result in a mission failure.

Recommended analog telemetry measurements and the assigned priority for each as applied to electric power systems are illustrated in Table 76. For each parameter listed, the typical range of nominal values, the required variation's of each about that nominal value and the desired measurement accuracy are shown. These values reflect the range of typical operating characteristics of the interplanetary mission considered in this study.

The assignment of priorities reflects the possibility of changing battery operating modes or adjusting spacecraft loads by command. As a result, all of the battery parameters and key current measurements are listed as priority 2. Since load adjustments can be made to change shunt regulator heat dissipation, the shunt element temperature measurement is **also** assigned this higher priority. The remaining parameters are required to verify power system performance (priority 3) or diagnose serious malfunctions (priority 5).

To conserve telemetry channels it is desirable to combine several output voltage measurements of load power conditioners in one word. In this case, only a qualitative indication is provided in the event that one or more voltages deviate from their normal value. When all voltages are correct, a single value telemetry indication will be received.

In addition to the analog measurements listed in the table, discrete status indications are required for all on-off switching functions in the power system. The priorities assigned to these are either 2 or 5 depending on whether command operation of these switching functions is provided. As the transmission time between the spacecraft and the ground station is increased, the importance of these status indications **also** increases. The reason for this is that the effect of sending a given command cannot be rapidly ascertained and thus the exact status of the on-board controls must be **known** to minimize the possibility of transmitting a wrong command for the particular situation.

Several of the diagnostic measurements become meaningless if they are not made with high accuracy. Some errors can be eliminated by repeated automatic calibration, but analog systems are usually limited to ± 3 percent accuracy. Several power system measurements need, therefore, pulse modulation telemetry of considerable word length. Sampling rates, however, can be slow in all cases, about one sample every 1 to 10 minutes. During certain mission phases, a speed-up of this rate may be desirable, but telemetry of transient conditions is rarely attempted.

Any telemetry is costly, either in complexity, power consumption, reliability, etc. The simplest parameter to telemeter is voltage, since it needs no further conversion. Biased measurements (suppressed zero) require well stabilized Zener diode networks. Current measurements require conversion into analog voltages with an attendant increased complexity. Temperature measurements suffer from the low accuracy achievable with wide-range thermistors or similar temperature/voltage converters.

Since none of the power system telemetry has a priority 1, the guiding criterion in the implementation of these monitors is to achieve fail-safe designs. Where separate power sources are required to supply de-bias voltages or ac excitation to the telemetry monitors, it is essential that these power supplies be fused or otherwise protected to assure that their failure will not jeopardize the mission. The most common case where this consideration applies is the inverter necessary to supply ac excitation to magnetic-amplifier-type current monitors. Although more

costly in terms of power consumption, it is recommended that separate inverters be provided for each current monitor and that each inverter be fused to isolate it from the system in event of a short-circuit failure.

6.4.3 Load Fault Protection

In all of the study investigations, the failures considered in calculating the probability of success of the power system were based solely on the reliabilities of the units within the power system. It is recognized that failures in other subsystems of a spacecraft may precipitate failures in the power system itself. The possibility that a given and perhaps non-essential load could fail the power system and the mission cannot be overlooked in actual applications.

In analyzing failure modes of typical load equipment, the predominant failure which can damage the power system is a gross overload produced by shorting of a part connected in a shunt configuration. The distinction made here is between series parts in a load circuit which may short and produce an increase in current and shunt parts which short circuit the power supply output in event of a failure. A detailed failure mode analysis of the load equipment is essential to the optimization of overload protection provisions within any power system.

The providing of overload protection against short circuits in the distribution system wiring itself is not recommended. The probability of short circuit failures in the interconnecting wiring of the spacecraft is normally made extremely low through proper design, manufacturing and installation of the harness assemblies to maintain adequate insulation between circuits and between each circuit and the spacecraft structure.

Several approaches exist for protecting the power system against gross overloads caused by load equipment failures. These are:

- a) Fuse protection for each item of load equipment.
- b) Circuit breaker protection for each (not remotely resettable).
- c) Latching relay with excess current trip.
- d) Individual unit current limiting.

- 1) Solid state series element
- 2) Series regulator control

e) Bus undervoltage detection and associated bus disconnect.

6.4.3. 1 Fuse Protection for Each Major Component

The use of fusing in the power input to each major load unit constitutes a simple and effective approach to overload protection. Weight penalties and power losses associated with this approach are quite small. One problem with this approach, however, is the relatively high probability of undesired loss of power to the load because of the variability of "blow" values for fuses. This may be further complicated by a wide range of component power requirements or component turn-on current surges. This latter problem may be partly or completely alleviated by use of delayed-blow type fuses.

The use of fuses does introduce another series element in the system reliability model, and the possibility of failure due to environmental factors such as vibration, humidity or shock must be taken into account. Fuses alone can provide adequate isolation of failed nonessential loads. The use of fuses also lends itself to use with redundant essential loads of either parallel or standby types. Operation of the fuse in a standby redundant unit configuration offers an easily detectable signal to effect transfer to the standby unit and helps to protect other series power system units against damage or unnecessary switching in the event of a short circuit prior to its detection and isolation by standby redundant switching provisions in the failed unit.

6.4.3.2 Circuit Breaker Protection for Each Major Component

Circuit breakers offer a second simple approach to load fault isolation. The variability of their trip point is narrower than that of fuses. A prime drawback is the size and weight penalty that will be incurred with their use. If used with a load subject to a wide range of input requirements, circuit breakers are not effective. **As** in the case of fuses, circuit breakers are a one-shot protection means when used in unmanned applications. The power loss in the protective device is very minimal and a voltage drop of 20 to 100 mv is typical.

6.4.3.3 Latching Relay with Excess Current Trip

This approach is very similar to the use of circuit breakers, including their advantages and disadvantages. The principal difference is the advantage offered by incorporating automatic or ground command controlled reset provisions with the relay approach.

The protective device power loss can be kept to a level comparable to that for circuit breakers.

6.4.3.4 Unit Current Limiting

The use of a separate self-sufficient current limiting device would appear to hold considerable promise if implemented in a solid-state approach. The principal advantages of this approach appear to be a narrow range of operating values and high resistance to environmental effects. Significant disadvantages however are that the series voltage drop and power loss will be appreciable.

Current limiting can also be provided by appropriate current feedback circuits to provide override control of series voltage regulating functions in line regulation or load power conditioning equipment.

If integrated with the load equipment, it is quite possible that an automatically variable current limit point could be achieved to make the limiting value a function of the mode of operation of the unit, and weight and size penalties would be minimized. A large advantage of this approach is that it can be automatically reset. The major disadvantage is that complete isolation of a faulted unit from the power source is not normally achievable.

6.4.3 .5 Bus Undervoltage Detection

The use of bus undervoltage detection and consequent automatic removal of all nonessential loads is a relatively effective approach in most circumstances. Provisions to reconnect these loads by command of each individual load is considered desirable. This approach is most effective in detecting large magnitude faults, particularly if the power source has relatively high impedance such as a solar array.

The weight penalty attributable to this form of protection will be quite negligible if provision for on/off control of the loads is provided for other reasons. The reliability of this approach can be maximized through the use of redundancy and the power loss and series voltage drop will be negligible. Insensitivity to small magnitude faults, particularly with a low impedance power source is the principal area of weakness of this approach,

6.4.4 Electromagnetic Interference Control

The overriding aim in designing for electromagnetic compatibility (EMC) is to prevent any system from having adverse effects on the operation of any other system of the spacecraft. From the packaging and equipment interfacing considerations, there are two fundamental approaches to spacecraft EMC success. The first approach is to utilize individual source suppression on a building block or unit basis. The second approach involves not employing source suppression, but rather shielding the unit containing the interference source and filtering its inputs and outputs.

The first approach, where possible to implement, simplifies the interconnection and interfacing problem, whereas the second approach requires filtering all inputs and outputs and places additional burdens on the designers concerned with spacecraft EMC. Where an internal compatibility problem is essentially nonexistent or the susceptible circuits are easily separated from the high internal interference levels, the second approach is satisfactory. The first proposed approach includes three identifiable EMC actions:

- a) Prevention of the generation of interference at the source. In many cases, it will be found easier to prevent the generation of interference than to prevent its transmittal to susceptible circuits, or to reduce the effect of interference which reaches other circuits.
- b) Prevention of any residual interference, remaining after the above step, from either being conducted or radiated from the generating circuit to any of the susceptible circuits.
- c) Prevention of any remaining interference which reaches the susceptible circuit from adversely affecting performance.

The three above activities are suppression, shielding, and desensitizing. They should be carried out in the entire equipment design, starting with the design of the smallest circuit board all the way through the complete power system with nearby spacecraft equipment taken into consideration.

Shielding and other suppression measures may prove quite ineffective unless supplemented by adequate and consistent grounding. Grounding deficiencies may be the source of problems of internal system interaction, as well as excessive interference propagation and susceptibility to external fields.

Because of the wide range of frequencies involved, careful consideration must be given to the grounding practices employed throughout a spacecraft. The grounding techniques employed must be effective over the entire range of frequencies generated and in the electromagnetic environment in which the spacecraft must operate. The extensive use of solid-state devices greatly increases the susceptibility of circuits to RF energy well beyond their design passband. This must be taken into account in the grounding and shielding practices employed.

A prerequisite to the effective reduction of interference interaction is the establishment of an effective ground plane. When the first functional electronic circuit or module is assembled into a metallic housing or chassis, that housing or chassis becomes its ground plane and, ultimately, the spacecraft structure becomes the ground plane for each unit and all systems. The effectiveness of the ground plane in dissipating undesired electromagnetic energy is dependent upon its proper utilization with respect to the circuitry with which it is associated.

The equipment mountings and structural members of the spacecraft should be electrically bonded together to form a low-impedance reference plane. The mating surface areas between structural members should have an electrically-conductive finish equivalent to bare metal. All units or assemblies of the power system should be electrically bonded to the spacecraft structure **via** the mounting panels or pads. Bonding should be accomplished by metal-to-metal contact over the entire surface areas, which are held in mechanical contact. Where metal-to-metal contact

cannot be employed, at least two metallic bonding straps of minimum practical length and maximum width compatible with the mechanical considerations should be used.

6.4.4.1 Unit Packaging and Installation

Preventing the generation of unwanted signals begins with the earliest power system concept analyses. First, the types of circuits, waveforms, devices, etc., are chosen and then the specific units, circuits, and parts with favorable EMC characteristics are selected. At this point, the packaging engineer can assist by applying the following measures or by examining the design to ensure that the following have been done:

- a) Proper bonding to the ground plane of all metal, not a direct part of the circuit, will prevent those materials from possibly becoming antennas, resonant circuits, etc. Bonding will also prevent changes in resistance between portions of the structure which would generate rather large interference signals,
- b) Proper suppression of switching transients from electromechanical relays or fast squarewave rise and fall times.
- c) Reduction of generated and coupled interference by proper orientation of components and proper wire routing, twisting, and shielding.
- d) Proper design of the equipment enclosure to prevent the escape of radiated interference energy.

The discrete line spectrum produced by the fast rise and fall times of switching circuits, such as those used in pulsewidth modulated regulators, converters, and inverters, can be greatly reduced by slowing the switching times. The amount of slowing required is a function of the current being switched and the level of interference generation which can be tolerated.

Separation of generating circuits from susceptible circuits is best accomplished by placing them at opposite ends of the equipment or circuit board or by enclosing one or the other inside a shielded compartment. As an example, a dc-dc converter located at a spacecraft

experiment package, should be enclosed in a shielded compartment within the experiment package with its input/output leads properly bypassed with feedthrough filters.

Of prime importance is the handling of the wiring within the densely packaged equipments which make up the typical spacecraft power system. For purposes of example, it is assumed that one unit is the Power Distribution Unit (PDU), whose function is the distribution of electrical power throughout the spacecraft. A typical PDU measures 6 x 6 x 8 in. and contains circuitry for primary and secondary dc power, squarewave ac power, input and output discrete command circuitry, and relay power switching. Since this unit interfaces with every other equipment on the spacecraft, it can become a coupling medium for interference generated within the PDU, or to any one of the interfaced loads, if improperly designed with respect to **EMC**. To minimize this coupling and suppress the power switching transients, the following interference control measures must be implemented:

- a) Locate power switching relays in a shielded compartment and decouple the contact circuits with bulkhead mounted, feedthrough filters.
- b) Twist and shield all circuits which generate interference or are susceptible to interference.
- c) Ground the wire shields at each end to maximize their shielding efficiency. Bundle interference-sensitive wiring separately from noisy wiring, including wiring going to interference-sensitive spacecraft equipments.
- d) Locate the squarewave ac power bus in a shielded compartment with its input and output leads shielded to minimize its radiation.
- e) Route ac power, primary dc power, secondary dc power, and commands on separate output connectors to avoid coupling. In passing through these connectors, carry each two-wire circuit on adjacent pins to minimize the circuit area and, in turn, the interference pickup or generation.

These measures are similarly applicable to other units of the power system: particularly dc/dc converters and pulsewidth modulated regulators.

The packaging activity must, in general, conform to the shielding design and be assisted by the EMC engineer. The enclosure requires attention in the "RF-tight" sealing seams and cover plates and the removal of nonconductive materials from electrical bonding surfaces. It is important that the shielding be electrically continuous with high conductivity across each seam, joint, or other discontinuity. In general, shield thickness is governed by the required mechanical properties for strength rather than by shielding effectiveness requirements.

6.4.4.2 Grounding

For all units energized from the primary dc bus, the power returns should be grounded at a single electrical reference point only. All load returns should be carried to this point on individual conductors. Steady-state loads of less than 1 amp may be returned to structure within or adjacent to the load unit.

If separate power sources are used for individual systems, separate electrical reference points should be established for each system. These points will normally be located at, or adjacent to, the power sources. Exceptions to this criterion may be warranted by the physical separation of the load units.

Secondary power (dc outputs of transformer-rectifiers or converters) returns should be dc isolated from the primary power and connected directly to chassis in each load power conditioner, and at each unit supplied. Power return wires should not carry signal returns except in short runs within a circuit where power and signal returns are necessarily common. In all cases, circuit returns should be individually connected to chassis at the closest accessible point.

In transformer-rectifiers or converters, each secondary power return should be connected to chassis as close as possible to the transformer, in addition to grounding at the output connector. Filter capacitor ground leads should be connected to chassis and maintained as short as possible. Filter capacitors utilizing the case as ground are preferable where practical. In the case of converters or transformer-rectifiers

supplying secondary power to several units in addition to avoiding common dc power returns, care must be taken to provide adequate filtering or decoupling in each load unit to avoid interaction between units. Grounding dc power returns to chassis in each load unit precludes coupling via return lines .

Table 76. Analog Telemetry Measurements and Priorities

Sub Assembly	Parameter	Nominal Values of Parameter	Required Measurement Range (%)	Desired Measurement Accuracy (±%)	Priority	Notes
Solar array	Output voltage	20 to 50 V	50 to 250	3	3	Partial shunt regulator only. **Measurement range 98 to 102% for regulated bus systems. *Main bus voltage and current same as solar array voltage and current for shunt array control.
	Output current	5 to 50 A	10 to 150	3	3	
	Panel temperature	-200° to +150°C	----	5	3	
	Shunt element voltage	10 to 30 V	0 to 100	5	3	
	Shunt element current	5 to 150 A	0 to 100	5	3	
Array regulator	Shunt element temperature	-40° to 100°C	----	3	2	**Measurement range 98 to 102% for regulated bus systems. *Main bus voltage and current same as solar array voltage and current for shunt array control.
	Series regulator temperature	-40° to 100°C	----	3	5	
	Main bus voltage*	20 to 50 V	70 to 102%**	1/2	3	
	Main bus current*	5 to 50 A	10 to 150	3	2	
Battery	Charge current	0 1 to 50 A	0 to 200	0.5	2	Reconditioning discharge
	Discharge current	5 to 100 A	0 to 150	3	2	
	Terminal voltage	3 to 28 V	80 to 120	0.5	2	
	Terminal voltage	3 to 28 V	50 to 120	3	2	
	Baseplate temperature	0° to +50°C	----	3	2	
Line regulator	Baseplate temperature	-40° to +100°C	----	5	5	
	Output voltage	20 to 50 V	90 to 110	0.5	3	
	Output current	5 to 50 A	10 to 150	3	2	
Inverter	Output voltage	20 to 50 V ac	90 to 110	0.5	3	
	Output current	5 to 50 A ac	10 to 150	5	2	
	Baseplate temperature	-40° to +100°C	--	5	5	
Converter or transformer-rectifier	Input current	2 to 20 A	20 to 120	5	5	
	Output voltage	3 to 500 V	90 to 110	0.5	3	
	Baseplate temperature	-40° to +100°C	----	3	5	

6.5 CONCLUSIONS

In this study a large number of alternative power system configurations for several typical interplanetary missions were quantitatively compared. The primary study results are the computer program, which was developed to evaluate and optimize the reliability and weight of all candidate system configurations, and the preliminary determination of preferred system configurations for the interplanetary missions specified.

The study included the definition of model missions, model spacecraft configurations, the power requirements for each of these configurations, and the selection of specific designs for the large number of alternative power system functions required in the different system configurations.

6.5.1 Reliability -Weight Optimization Computer Program

The computer program resulting from this study provides a basic tool which can be used to quantitatively compare any set of power system configurations on the basis of reliability and weight. The absence of such a tool in the past has usually restricted the number of alternative system configurations to a relative few that are evaluated for any given mission. Considerable emphasis has then been placed on improving the reliability and minimizing the weight of the particular configuration that appeared best suited to the mission. This approach can obviously lead to the use of a system which is not optimum.

The fact that system considerations other than reliability and weight may strongly influence the selection of a particular power system design cannot be overlooked. Probably, the most significant considerations, other than reliability and weight, are cost and schedule. These considerations often lead to the adaptation of existing flight-proven equipment, which, although cost effective, frequently results in the use of a system that is neither the most reliable nor the least heavy for the new missions. Another consideration tending to deter power system optimization is a requirement that the power system be flexible in supporting a variety of payloads and/or missions; potential schedule improvements and cost savings again provide the reason for such a provision.

The reliability-weight optimization analyses performed in this study excluded spacecraft optimization requirements such as these, and, as a result, specific recommendations of preferred optimized power system designs for each of the interplanetary missions are not obtainable. However, the results of the computer program can provide the power system data needed to optimize the overall reliability and weight of the spacecraft for any specified mission.

Although considerations, such as cost, development time, and multiple missions, exist, the optimum design of any spacecraft requires proper apportioning of the total weight allowance defined by the booster capability among the various systems to achieve maximum complete spacecraft reliability.

The results of the computer runs for the power system define a largely narrowed-down range of system designs and the corresponding reliability and weight for each. These data, together with similar data for the communication system, payload, guidance and control, etc., can be combined in an overall system optimization program to select the optimum spacecraft configuration. Computer programs, capable of performing this type of spacecraft optimization already in use, facilitated the development of the power system optimization computer program for this study. The program approaches are similar in that various alternative configurations of elements within a system are defined, and, on the basis of reliability and weight, comparisons are made of possible combinations of these alternative elements. In this study, these comparisons were made for alternative power system configurations after each power system configuration was first optimized by comparing all combinations of redundant and nonredundant units within that power system configuration. The existence of this computer program permits the rapid development of reliability and weight data for optimized power system designs that can be used as an input to the overall spacecraft optimization process of future programs.

6.5.2 Preferred Power System Configurations

All power system configurations studied in this project were grouped into two categories:

- a) Those that combine the solar array and battery electrically at an unregulated bus.
- b) Those which use regulators on the solar array as well as for charging and discharging of the battery to permit their combination at a regulated bus.

The selection of the optimized configuration as well as the general type of power system was found to be a function of the load power profile of the mission, the solar array characteristics during the mission, and the allocated power system reliability or weight for the particular mission.

The principal advantage of directly generating a regulated bus results from the fact that a single, highly efficient solar array regulator may be used during sunlight operation when the solar array is supporting the load. When the battery is required to support the load for long periods, the losses incurred by battery charge and discharge regulation tend to offset the advantage of efficient solar array utilization obtained through the regulated bus approach. Conversely, unregulated bus systems provide a more efficient method of charging and discharging the battery but require supplementary regulation functions to accommodate the voltage variations of the main bus. These additional regulation functions reduce the efficiency of solar array power utilization in sunlight.

For all of the Jupiter missions, the weight of the very large solar array required to support the assumed loads at sun-spacecraft distances of 5.2 AU, combined with the attendant low utilization of battery energy, resulted in the selection of regulated bus systems for each mission. For the model spacecraft configured for these Jupiter missions, it was determined that solar array designs yielding at least 20 w/lb at 1 AU are virtually essential to achieve mission feasibility.

For the Venus Orbiter No. 1 mission, the regulated bus systems were again selected as the optimum configurations over the entire reliability range. For the Venus Orbiter No. 2 mission, the Mercury mission and the Mars Orbiter mission, the regulated and unregulated bus systems were intermixed over the reliability range.

There is a common characteristic among all of the reliability-weight plots for systems that consider the use of a single nonredundant battery, or a fully redundant *two*-battery approach for the orbiting missions. Starting from a nonredundant system of minimum weight and minimum reliability, a significant reliability gain with only a moderate weight increase can be achieved by first making all of the electronic equipment redundant. To further improve reliability, it was necessary to make the battery redundant; this increased system weight significantly for most of the missions. The reliability gained with the redundant battery permitted the elimination of some of the redundancy in the electronic equipment to minimize weight for intermediate reliability values. Further increases in system reliability are achieved by again making the electronic units redundant with only moderate weight increases.

The relative magnitude of the step increase in weight, incurred by making the battery redundant, is less for the flyby missions than for the orbiting missions. This is due to the fact that battery utilization is relatively small and the battery weight is less dominant in comparison to that of the solar array and conditioning equipment. Where low-voltage batteries are used, the nonredundant configuration was not considered. As a result, the characteristic step increase in weight occurring at intermediate reliability levels is not observed.

It was also noted in the analysis that the variation in particular implementation of a function within the several basic system configurations has a very small effect on the overall system reliability and weight; this was particularly true for the alternative battery charge control designs. The choice between dissipative bucking chargers and pulsewidth-modulated chargers, which of course have a higher efficiency, normally favored the dissipative approach. This results from the fact that the simplicity of the dissipative approach gives a reliability and weight advantage over the switching approach, and the efficiency advantage of the switching approach is not significant in terms of the low battery-charging power required for these model missions.

The selection of optimum systems as a function of reliability and weight was shown to include **both** ac and dc power distribution approaches. Analysis of the data has shown that the difference in reliability and weight

between an ac and dc distribution scheme is relatively small. As a result, the selection of either an ac or dc distribution system must be made on the basis of additional considerations such as flexibility, fault isolation and electromagnetic compatibility for a particular application.

The results of the power system reliability-weight optimization analyses have shown that for interplanetary probes or orbiting missions having relatively long orbit times and, as a result, relatively short eclipses, the use of power systems that electrically combine the solar array and battery at a regulated bus are usually advantageous.

An extension of this basic system approach which appears to offer significant improvements in system reliability and weight is the Modular Energy Storage and Control (MESAC) concept, which utilizes low-voltage batteries with a regulated bus approach. Although this system, as configured in the study, did not always appear to be optimum, an assumed use of three batteries, when only two are required to perform a mission, does not show the flexibility of this approach. The number of batteries used and the number of batteries required must be analyzed for any particular application to determine the optimum configuration of this low-voltage battery energy-storage concept.

The corollary to this conclusion is that those applications which require a significant amount of battery utilization because of a relatively low sunlight-to-total-orbit-period ratio are best served by power systems that incorporate the simplest battery control functions and an unregulated main bus. If these systems are configured with but one centralized line regulator, the overall weight and reliability of this approach is superior to that of any other approach.

6.5.3 Preferred Power Systems

Preferred power system configurations were determined, in the absence of reliability or weight allocations, by analyzing the results of the weight-reliability optimization for each of the seven model spacecraft. The locus of optimum systems (Section 5) for each model was scanned to determine those configurations which either were predominantly lightest over the entire reliability range or were significantly lighter than the

system having the next higher reliability. A single preferred system could not be selected for each mission because a weight limit or reliability allocation based on an overall spacecraft optimization was not available. The preferred system designations for each model and definitions of the major functional elements for each are as follows:

<u>MODEL</u>	<u>PREFERRED SYSTEMS</u>
Mercury Flyby	141, 495
Venus Orbiter No. 1	395, 3115
Venus Orbiter No. 2	141, 171, 4115
Mars Orbiter	161, 495, 423
Jupiter Flyby	395, 3115
Jupiter Orbiter No. 1	395, 3115
Jupiter Orbiter No. 2	395, 3115
System 141: No solar array voltage control, dissipative battery charger, momentary line booster or PWM bucking line regulator	
System 161: Same as 141 except PWM bucking battery charger	
System 171: Same as 141 except PWM buck-boost battery charger and no momentary line booster	
System 395: Dissipative shunt solar array regulator, dissipative battery-charge regulator, PWM boosting battery-discharge regulator and no line regulator (nominal 28-v battery)	
System 3115: Same as 395 except low voltage battery	
System 423: PWM series bucking solar array voltage limiter, resistive battery charge control, momentary line booster and PWM boosting line regulator	
System 425: Same as 395 except PWM series bucking solar array regulator	
System 4115: Same as 3115 except PWM series bucking solar array regulator	

situation is more perplexing. Several explanations are plausible. This small-size, high-velocity region involves the largest experimental uncertainties with respect to measurements of D and ϕ ; and certainly some measurement scatter appears in the data. But the velocity spread does decrease at some conditions (Fig. 28), and elimination of all questionable drops (0 quality factor) from the sample did not appreciably reduce the spread. Aside from the cases of newly formed drops at locations near the nozzle, the data indicate that the spray may produce unsteady entrainment and a grossly turbulent condition in the gas. Since the drop data are a composite of many instantaneous samples, the small drop data may indicate a statistical distribution of μ . The situation can only be clarified by more careful measurements.

Figure 31 compares the values of μ inferred by the two methods for the three axial positions at 25 psi. The trends are similar to profiles of mass flux or mass average velocity which are given in Section D below. Values of radial velocity estimated from the lower limit of $\langle v_r | D \rangle$ scatter about zero or remain slightly positive. Values obtained from the lower bound for the three pressures at the shortest downstream distances are shown in Fig. 32. All of these profiles are strongly dependent on the spatial distribution of mass in the spray which is

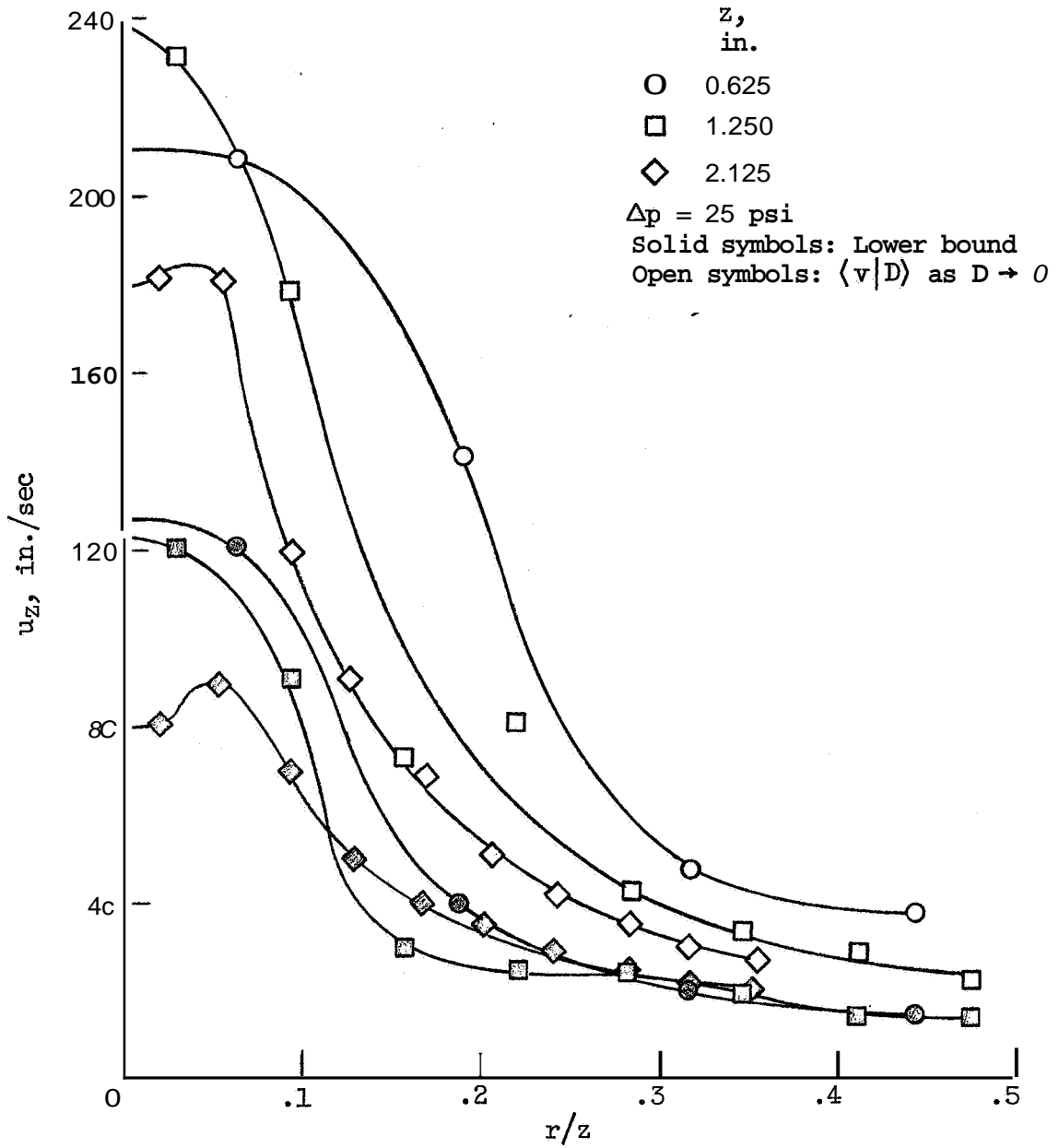


Fig. 31. - Comparison of Axial Air Velocities Obtained from the Regression Curve and the Lower Bound of the Data at Small Sizes.

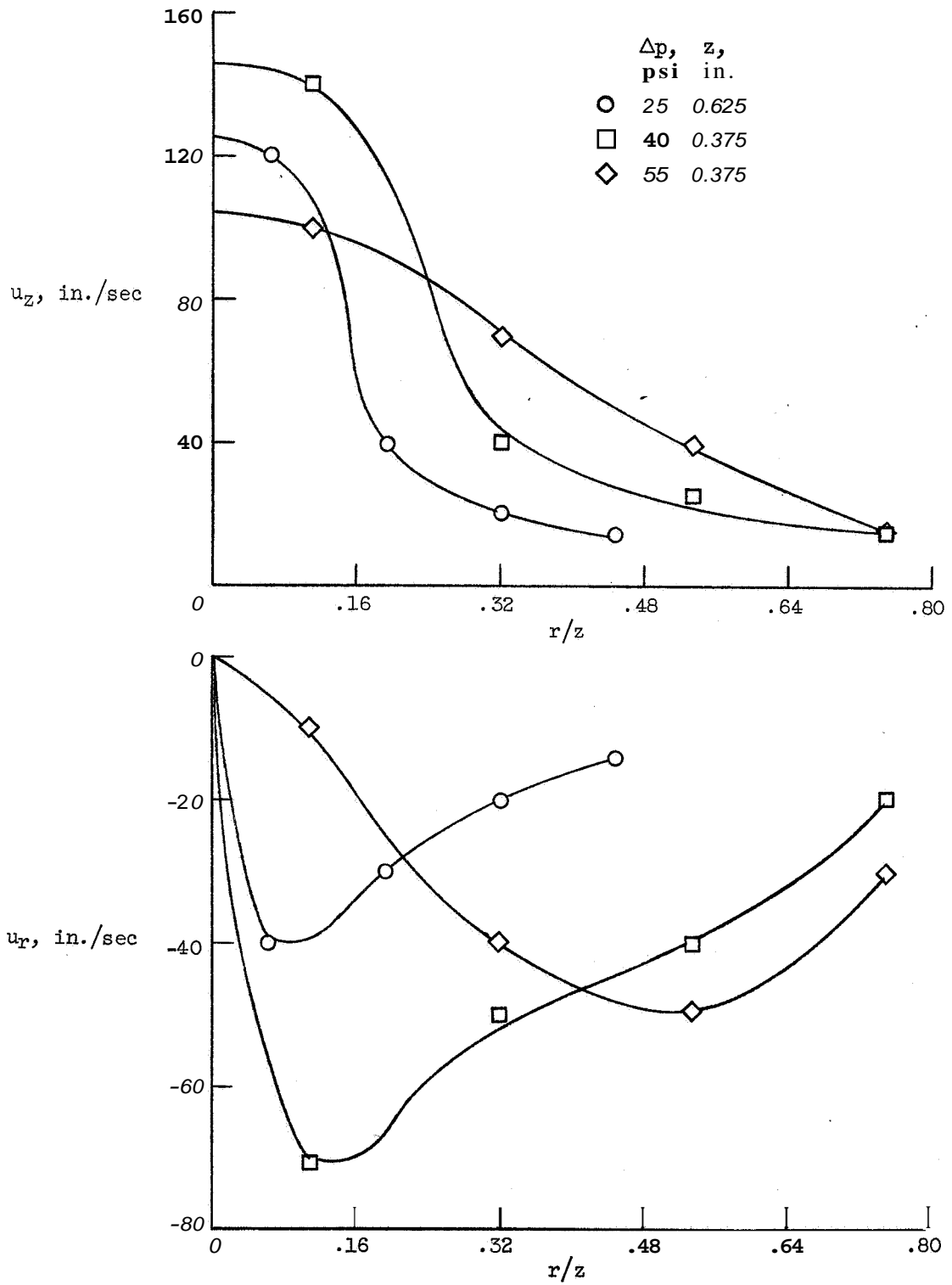


Fig. 32. Gas Velocities Inferred from the Lower Bound of the Velocity Data at Small Sizes.

initially determined by the injection conditions and is later modified by the gas flow.

It should be emphasized that the discussion above applies to the case of $v_E > \underline{u}$ as distinct from the conditions of $v_E < \underline{u}$ where the gas is decelerated by the spray and the inverse entrainment situation results.

C. Measured Size-Velocity Density Functions

Categorization of the type of data shown in Figs. 26-29 assigns measures to the observed frequencies so that density functions may be plotted. Rather than plotting histograms the alternate procedure followed here is to plot points at the mean values in each category and draw a smooth curve through them. Normalized density functions* are used with the normalization factors tabulated on the plots. The normalized form allows the size and velocity dependence at different conditions to be directly compared on the same linear plot, and the normalization factors provide the physical information about the magnitude of droplet number or mass densities and fluxes.

1. Variations in the Size-Velocity Density Functions with Position in the Spray.

Normalized spatial drop size distributions, f_g , at upstream positions are shown in Fig. 33. More exactly, these

*

Due to small variations in drawing the curves, the area under each curve may differ slightly from unity which is the area of all the bars in the corresponding histogram.

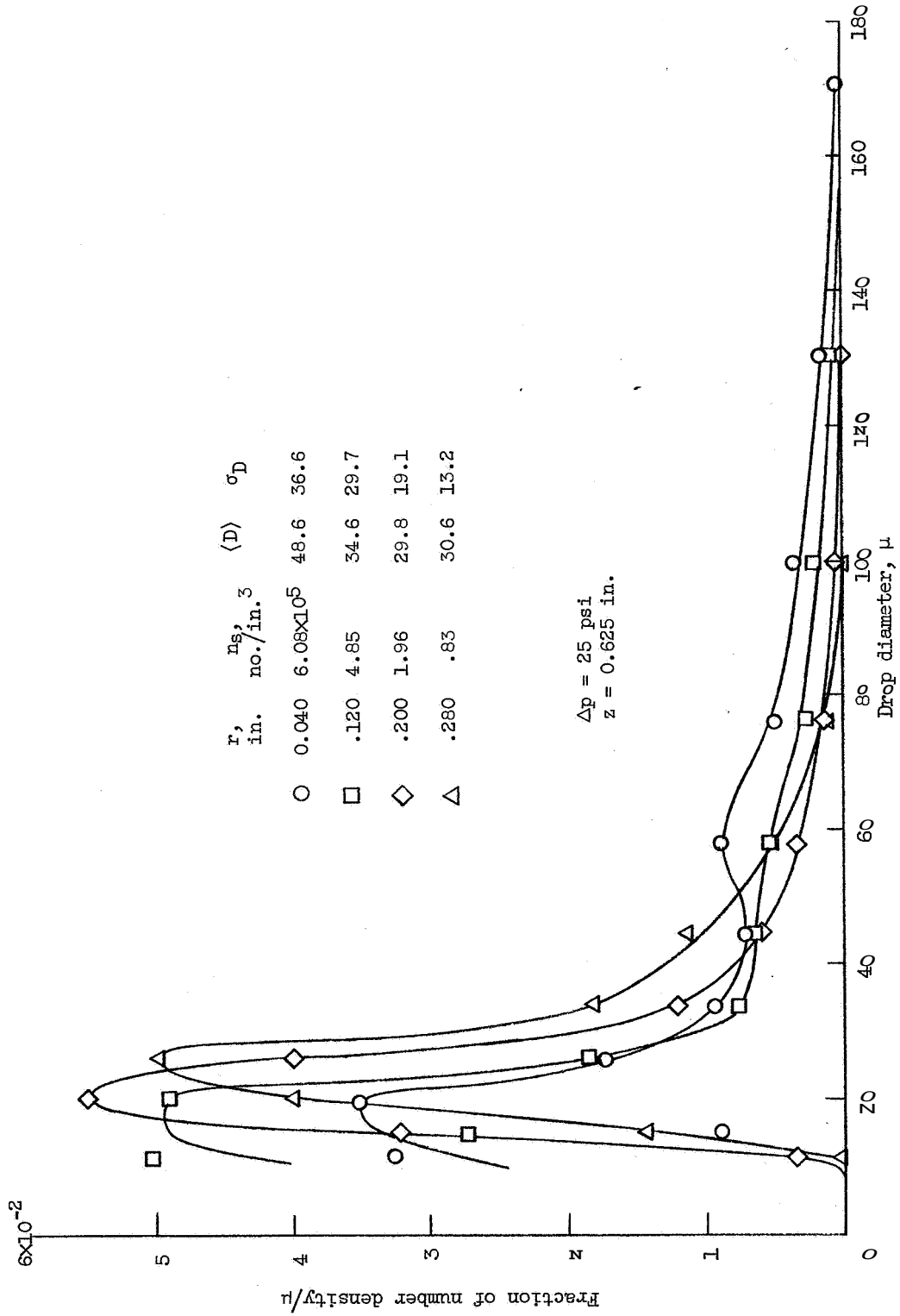


Figure 33 - Number densities as a function of drop size near the surface of formation.

are normalized number densities obtained by integrating over all droplet variables except D , r and z , i.e., only the distribution of drop sizes is considered at a given position. The normalization factor for each is the number of drops per unit volume as a function of position:

$$n_g(\underline{x}, t) = \iiint f(D, \underline{v}, \underline{x}, T_L, t) dD d\underline{v} dT_L \quad (4.9)$$

These familiar types of curves are greatly positively skewed -- they have a long "tail" extending to larger sizes. Uncertainties exist at the two extremes of size. As size decreases, measurement resolution eventually enters in; and the exact values of the peaks and shapes of the curves as size approaches zero are influenced by the resolution characteristic of the measuring system. At large sizes the sample size necessarily becomes small so that statistical uncertainties increase.

For the particular conditions noted on Fig. 33 the largest drops and greatest number concentrations are found near the center of the spray. As number density and mean size decrease with radius, so does the spread indicated by σ_D . These substantial variations of f_g with position are intimately connected with the atomizer geometry; and, especially at the outer edges of the spray, with the gas-liquid interaction.

The range of variation in number density with size is so large that effects at all but the smallest sizes

(which represent only a small fraction of the liquid mass) tend to be hidden. For this reason it is instructive to consider the mass weighted counterparts of the curves in Fig. 33. These normalized spatial mass densities, shown in Fig. 34, present a quite different picture of the data. Confidence in the ordinates is greatest in the medium-to-low size range since any statistical scatter at large sizes is amplified by the D^3 weighting. Compared to the number densities the extrapolation of the curve from the smallest measured sizes to zero can often be made with more confidence on a mass basis.

The densities of Fig. 34 are drawn to emphasize their strong bimodal character. Scatter at larger sizes has been neglected, and the progressively stronger occurrence of the mode at small sizes is evident at larger radii. Whether, in fact, other modes are present at larger sizes is an open question; but justification for the two modes shown will become clear as the discussion proceeds.

Figures 33 and 34 represent the type of spray data which are available from the many photographic studies conducted in the past. With the velocity information available in the present investigation, the corresponding number and mass densities may be plotted as a function of drop velocity as shown in Figs. 35 and 36. Now attention is focused only on the velocity, i.e., f is integrated over all droplet variables except velocity at a given

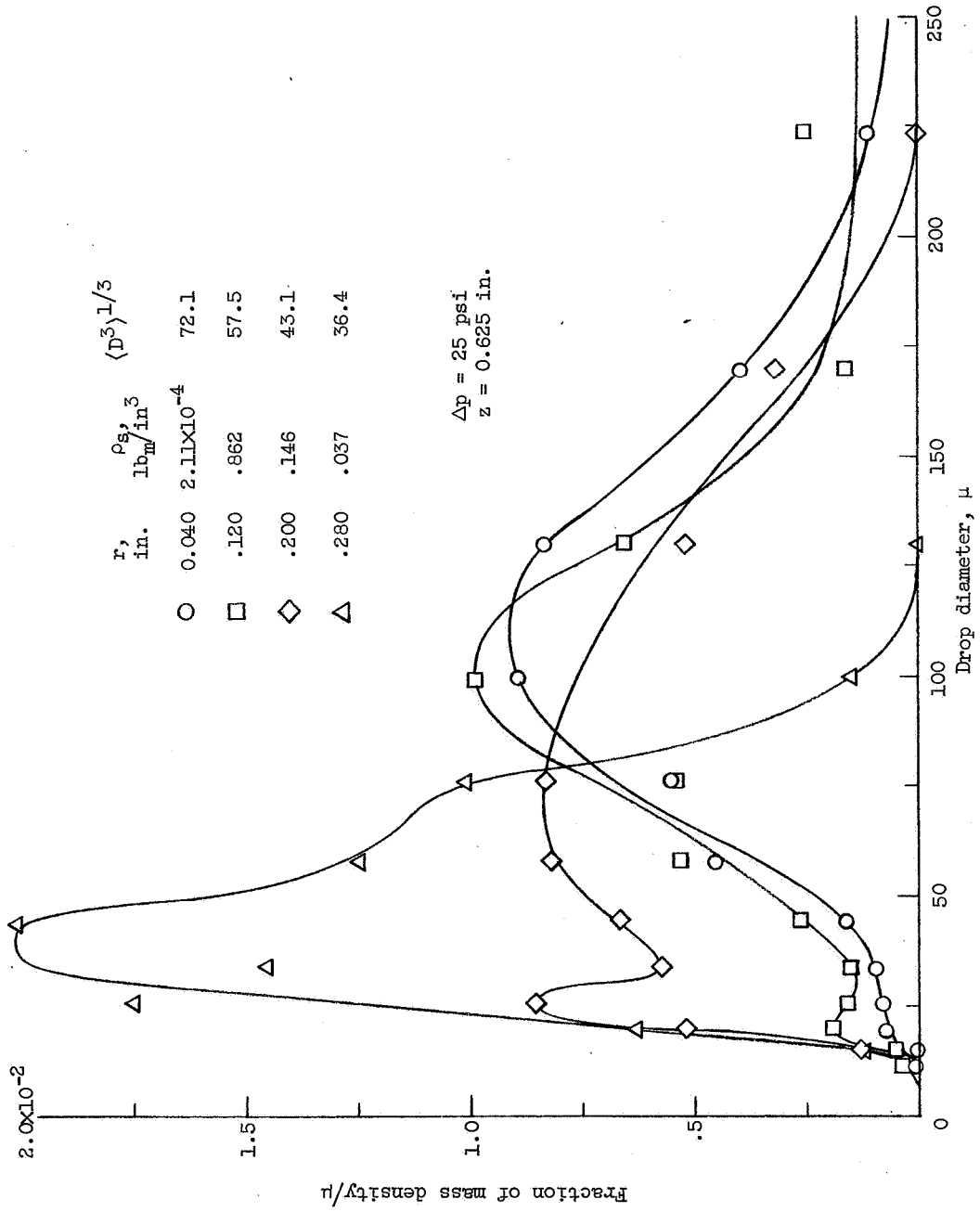


Figure 34. - Mass densities as a function of drop size near the surface of formation.

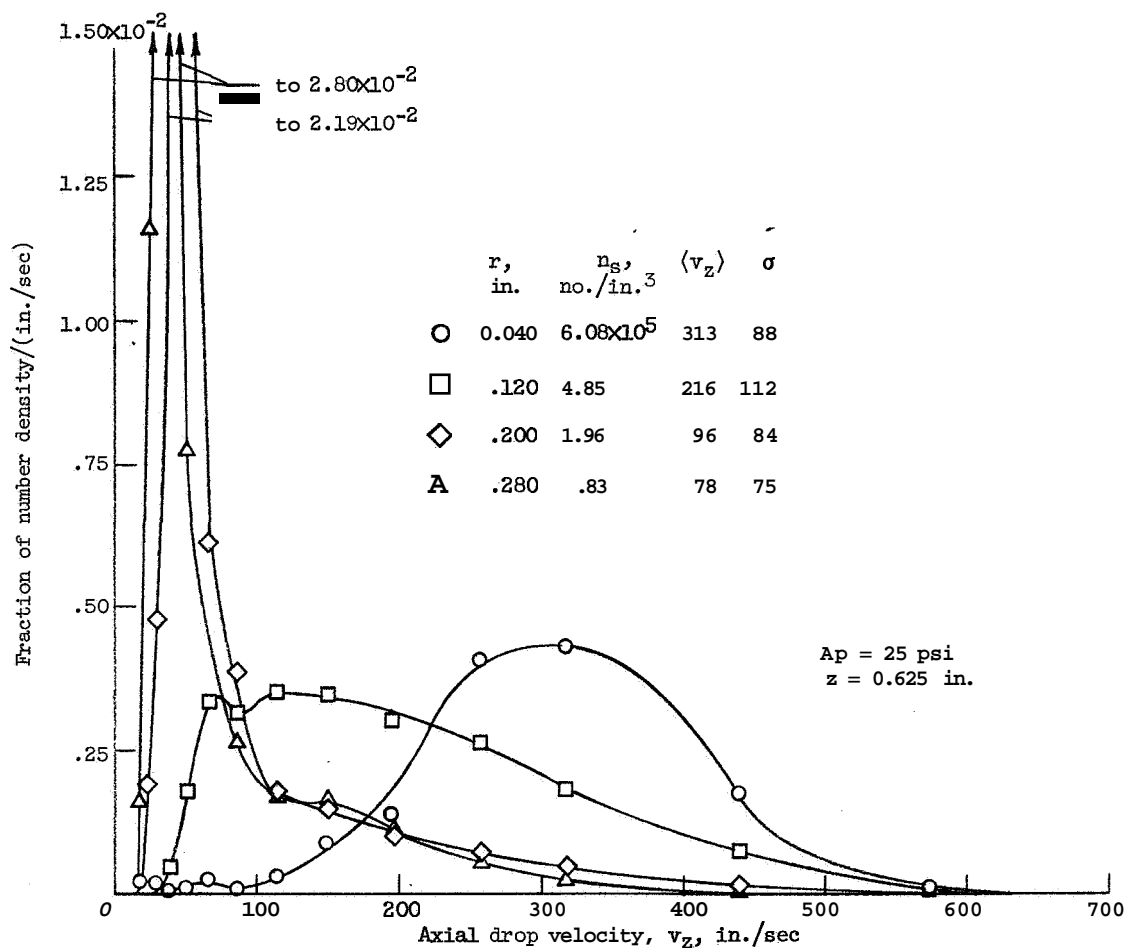


Figure 35. - Number densities as a function of axial drop velocity near the surface of formation.

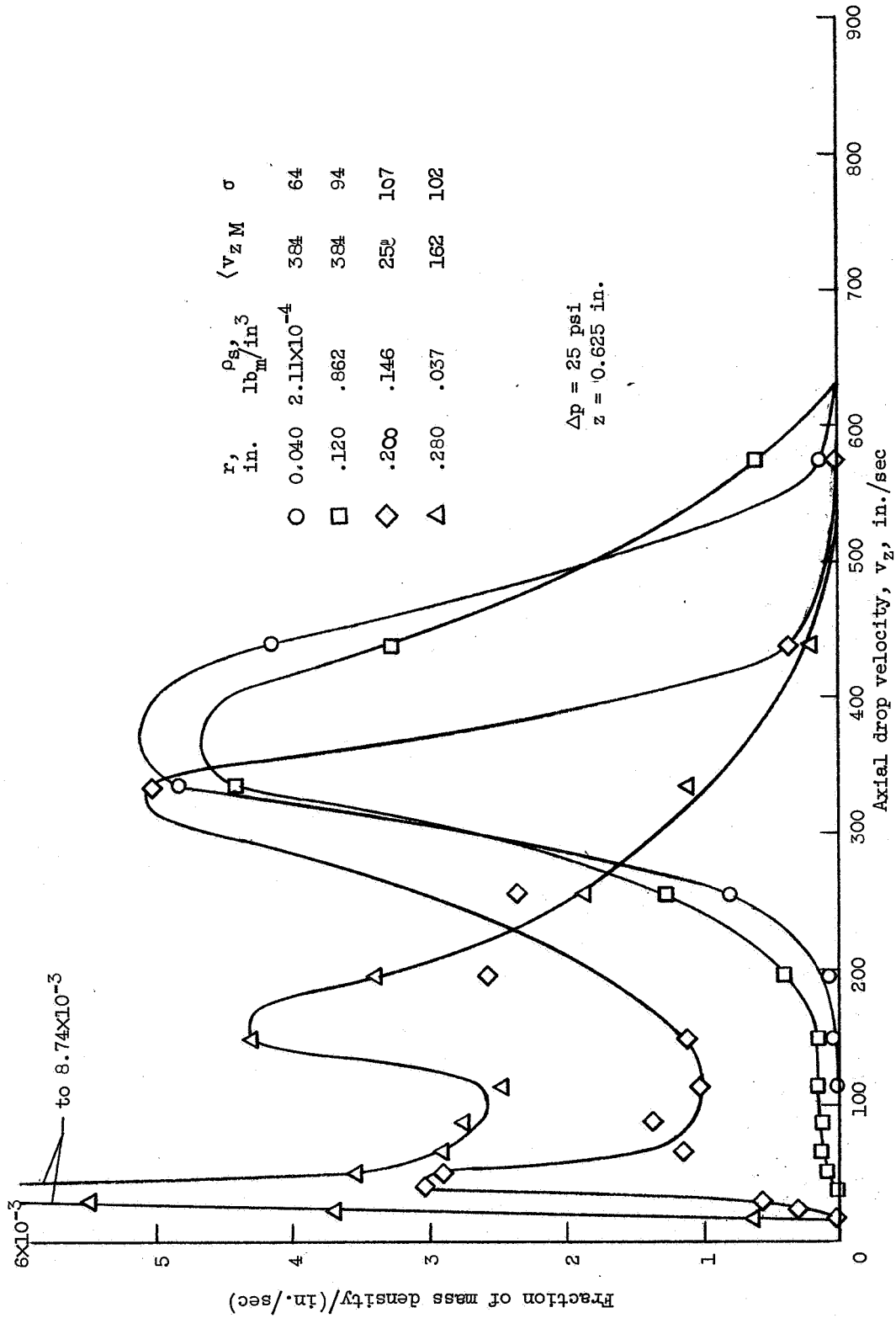


Figure 36. - Mass densities as a function of axial drop velocity near the surface of formation.

position. The normalization constants n_s and ρ_s remain the same.

As before, the mass density is the most revealing of the two showing the development of an unambiguous second mode at lower velocities. The significance of this mode is clear: drops are being decelerated to the local air velocity. At larger radii the deceleration process is more advanced since the spray is less dense and the drag forces have been acting for a longer time.

The family of mass densities for the same conditions are shown in Fig. 37 as a function of radial velocity. Two distinct modes are again present at each location. The mode at smaller velocities peaks at small negative values of v_r related to the inward flow of entrained air.

It should be noted that the means calculated for any of the bimodal density functions include the weighted effects of the two modes. If the modes enclose approximately equal areas, the mean will lie between the two peaks. Thus, measures of physical effects associated with either mode alone are not easily extracted from overall statistical moments such as the mean or standard deviation.

So far only marginal density functions in terms of one droplet variable have been considered. The physical situation leading to bimodal functions is clarified by examining the bivariate density in size and velocity.

Since v_r is usually much less than v_z and the amount of information in $f(D, v_z)$ is very large, the corresponding function $f(D, v_r)$ will be neglected.

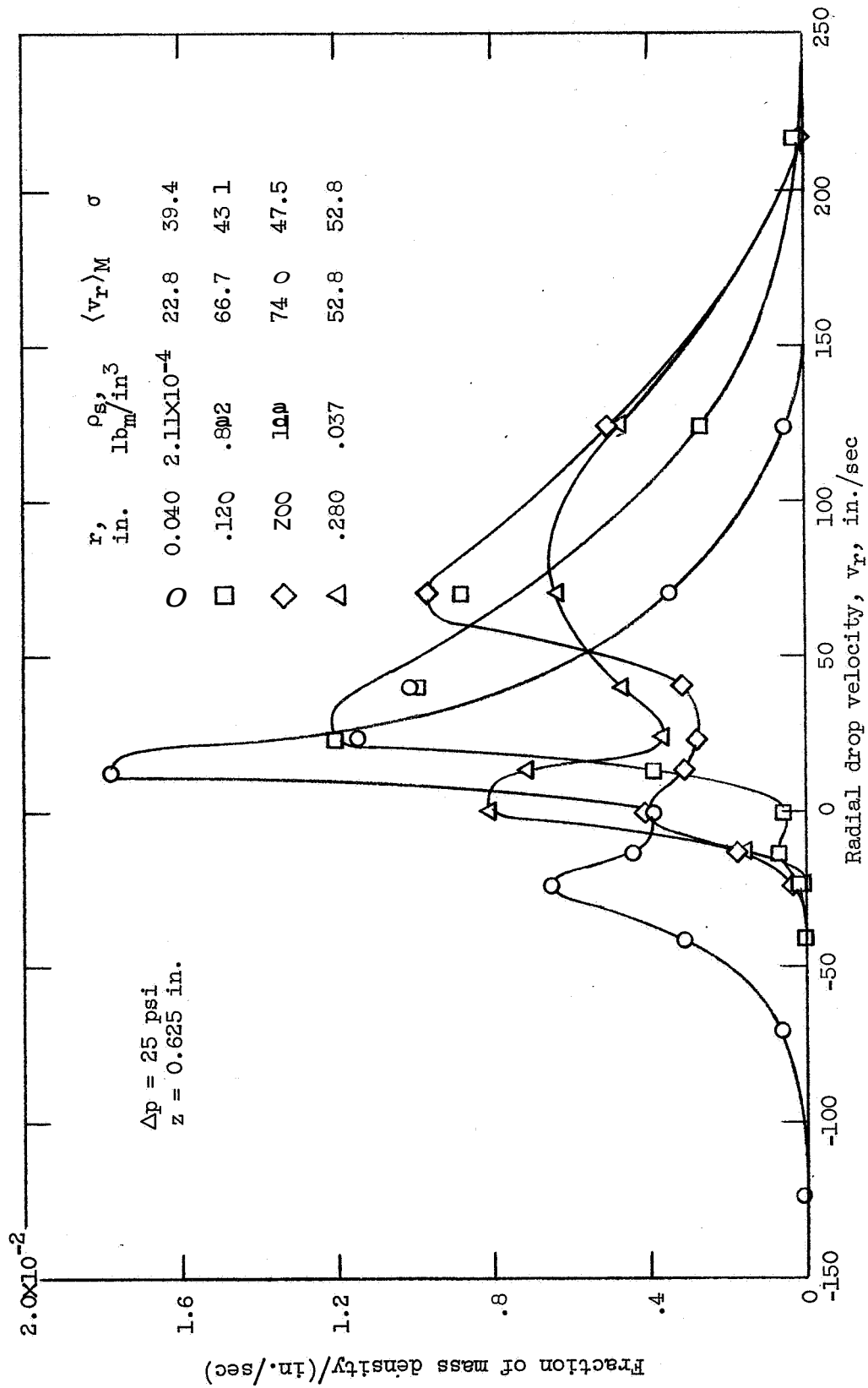


Figure 37. - Mass densities as a function of radial drop velocity near the surface of formation.

For the same reasons as before the mass-weighted, normalizer form* is used:

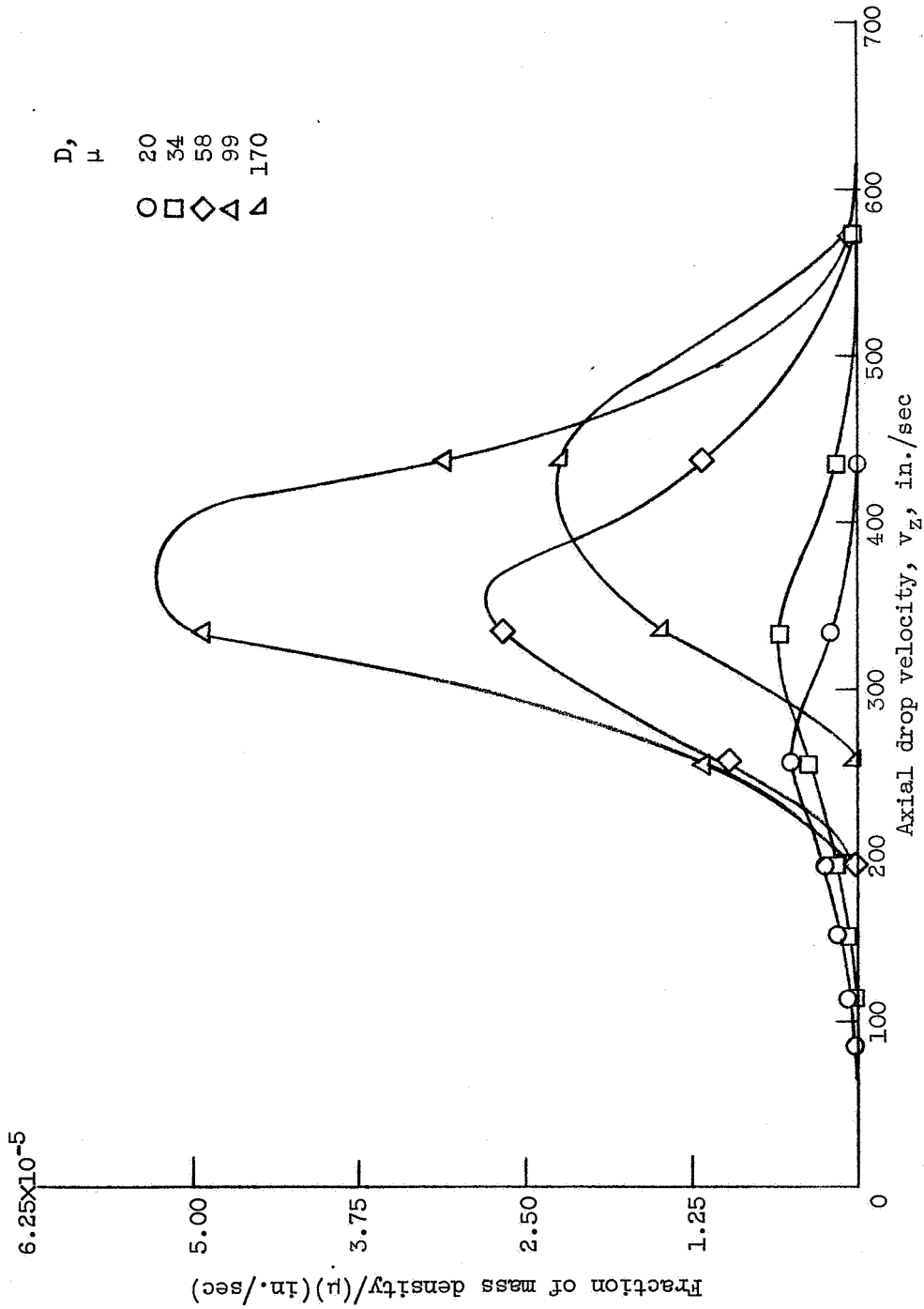
$$Mf_B = \rho_L \frac{\pi}{6} D^3 \frac{f_B(D, v_Z, r', z')}{\rho_s} \quad (4.10)$$

The family of mass densities at fixed sizes is shown in Fig. 38(a) as a function of v_Z at a location near the axis. A similar group near the edge of the spray is shown in Fig. 38(b). These curves represent cuts through the bivariate size-velocity surface at values of size corresponding to category means.** Figure 38(a) shows that only a small shift of the density toward the lower velocities occurs at smaller sizes. Here in the core of the spray near the surface of formation little air interaction has taken place. In contrast, the range of velocities is much greater at the outer radius as Fig. 38(b) shows. A steady progression occurs from small drops all moving near the air velocity, through a transition condition where two distinct modes exist, to large drops moving in a band below sheet velocity.

The complementary picture viewed with drop size as the abscissa and velocity as the parameter is presented in

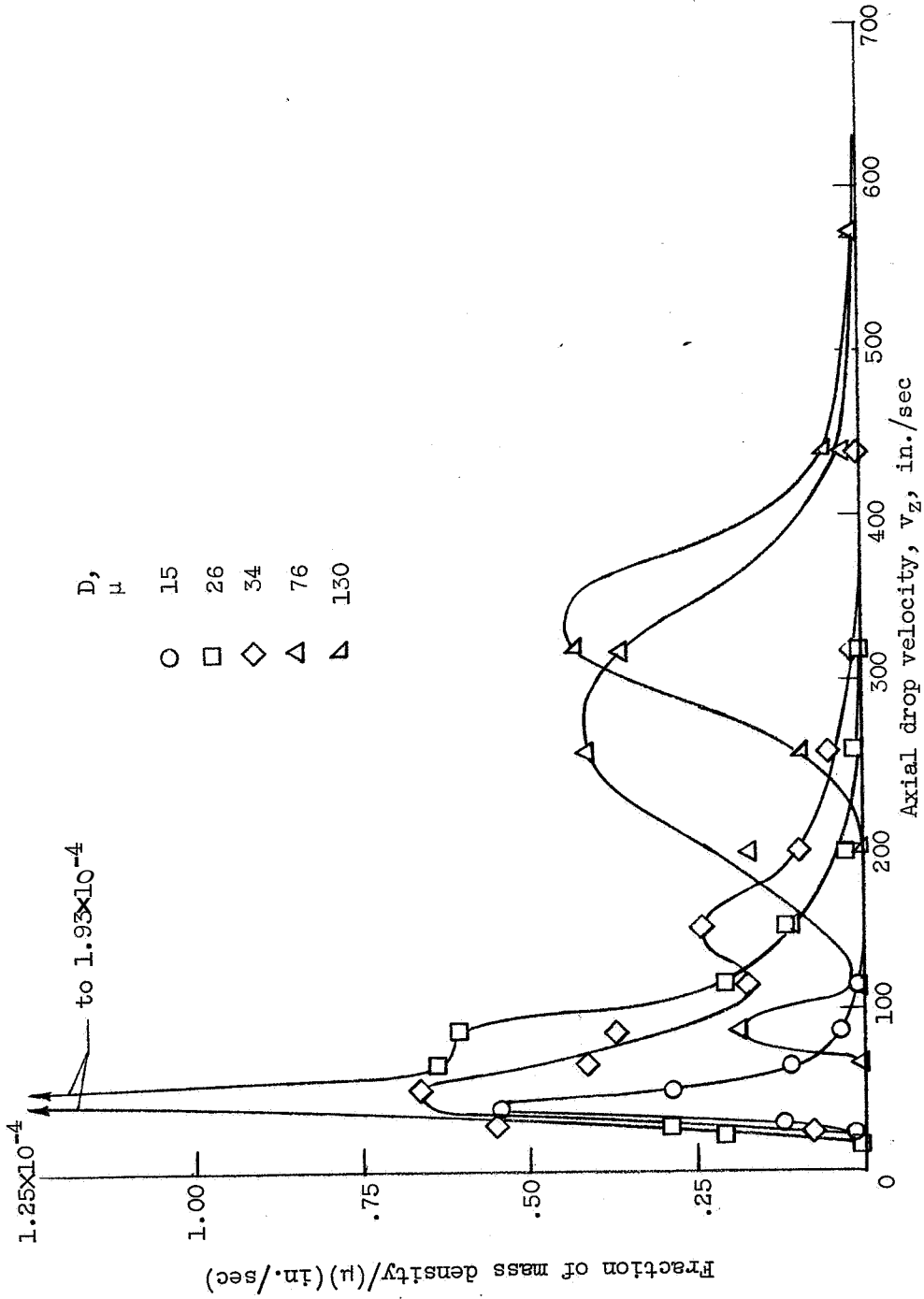
* The volume under the surface defined by f is always one due to normalization.

** They are not conditional density functions, $f(v_Z | D)$, since they have not been normalized separately to make the area under each equal to one.



(a) $z = 0.625$ in., $r = 0.040$ in.

Figure 38. - Comparison of bivariate mass densities at two locations as a function of drop velocity at selected values of drop size. $\Delta p = 25$ psi.



(b) $z = 0$ $Z \bar{z}$ in., $r = 0.200$ in.

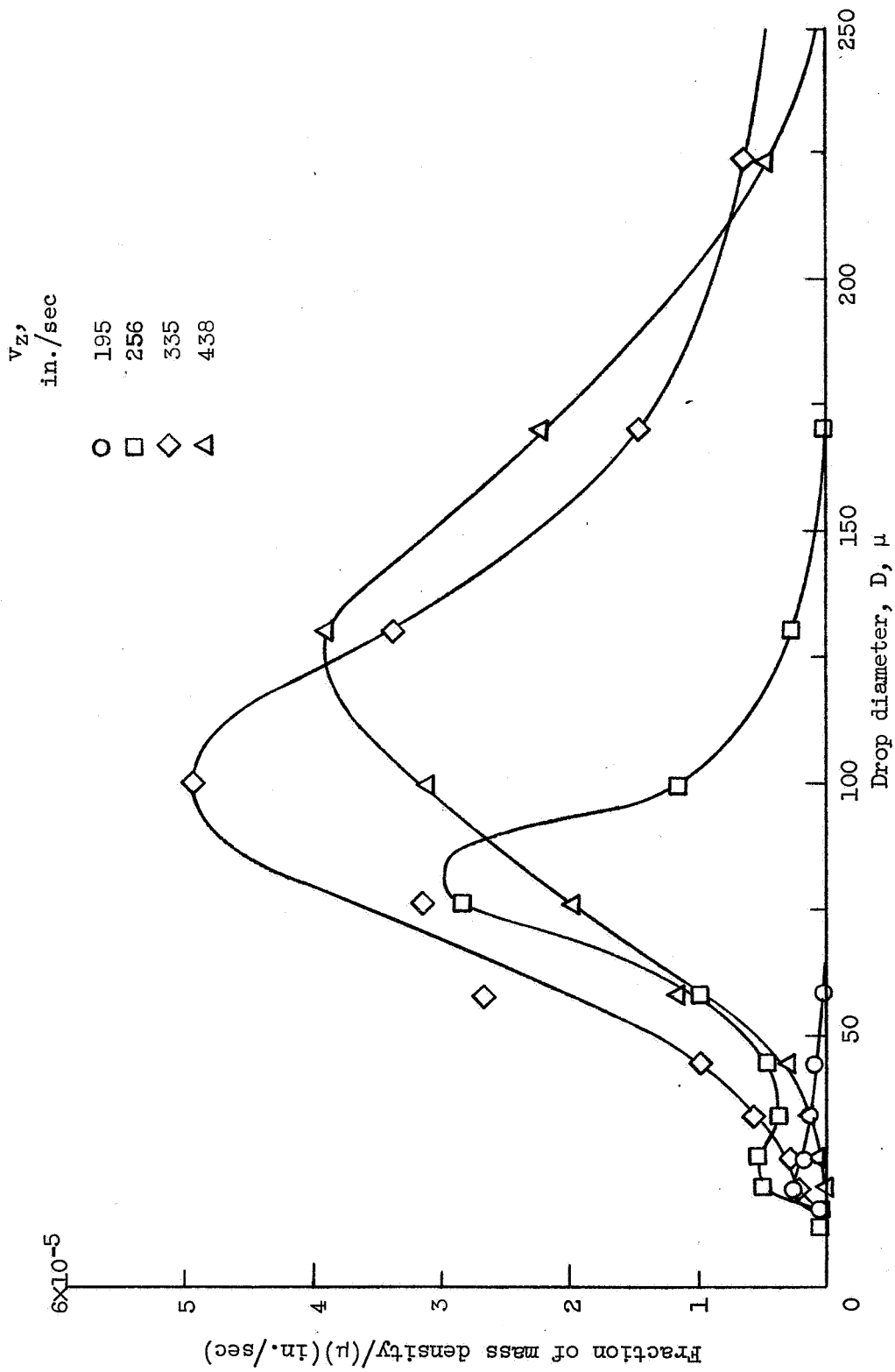
Figure 38. - Concluded.

Fig. 39. Near the axis the mode at lower sizes is just beginning to form (Fig. 39(a)) while at the outer radius the selective deceleration process is much more advanced.

Similar overall formation behavior of the local density functions is observed at injection pressures of 40 and 55 psig. Propagation characteristics are revealed by considering the local values of the density functions at downstream locations for $A_p = 25$ psi. The marginal mass density as a function of D is shown in Fig. 40 at $z = 2.125$ in. Its counterpart as a function of v_z is given in Fig. 41. As expected, bimodal behavior is more pronounced near the axis at this downstream location since more time has elapsed for segregation by drag. The same shift toward a dominant low velocity mode at small sizes is shown as r increases. Families of curves from the bivariate density function, $f(D, v_z)$, could be plotted at each position as was done in Figs. 38 and 39 and would show similar variations. As may be inferred from Figs. 40 and 41, two "humps" of varying prominence make up the surface defined by f , and a transition ridge connects the two.

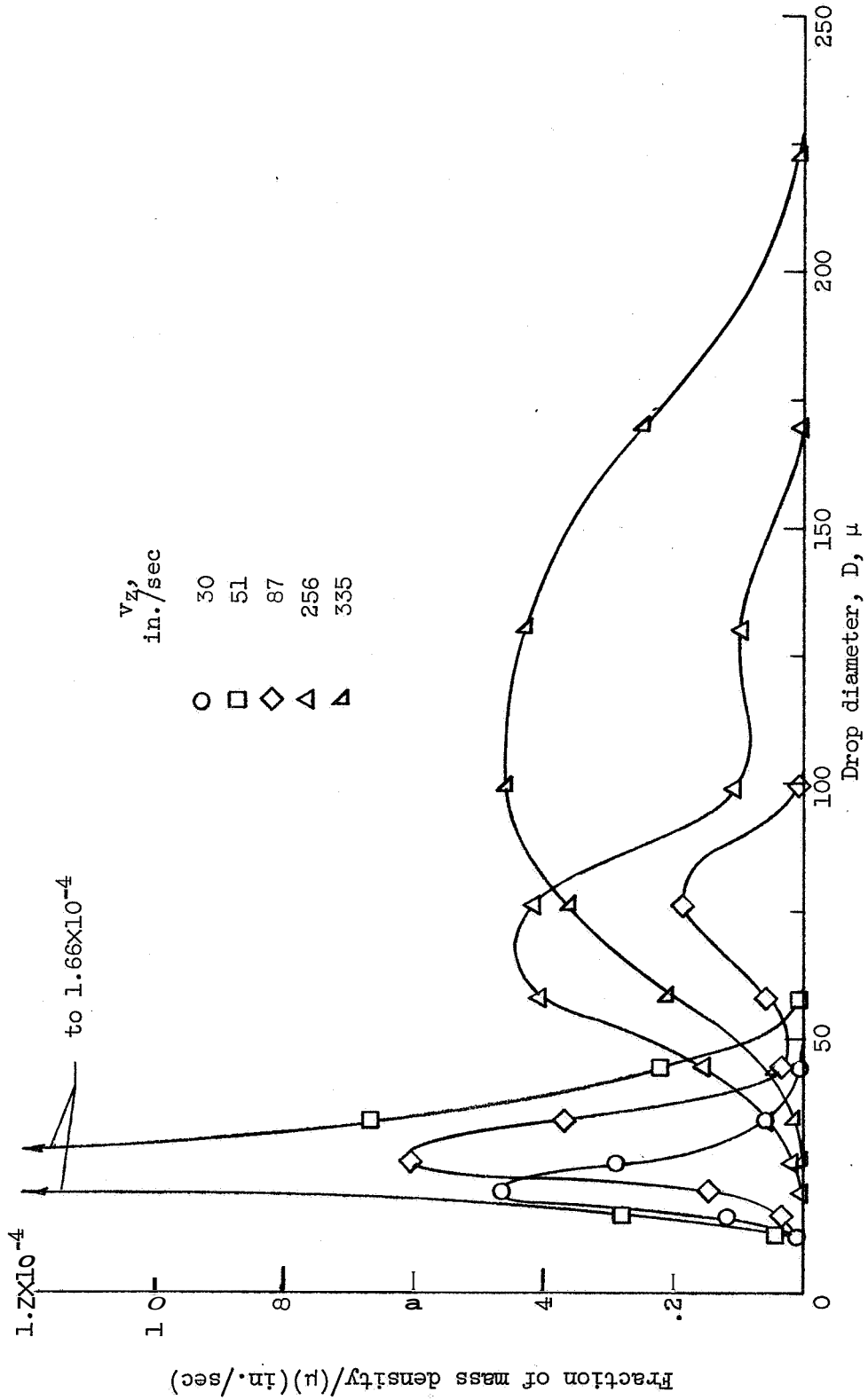
Thus, the entire local behavior of f is very diverse and strongly spatially dependent. This dependence is

* The reduction in the population of the smallest drops at larger radii suggests that entrained air sweeps small drops toward the axis.



(a) $z = 0.625$ in., $r = 0.040$ in.

Figure 39. - Comparison of bivariate mass densities at two locations as a function of drop size at selected values of drop velocity. $\Delta p = 25$ psi.



(b) $z = 0.625$ in., $r = 0.200$ in.

Figure 39. - Concluded.

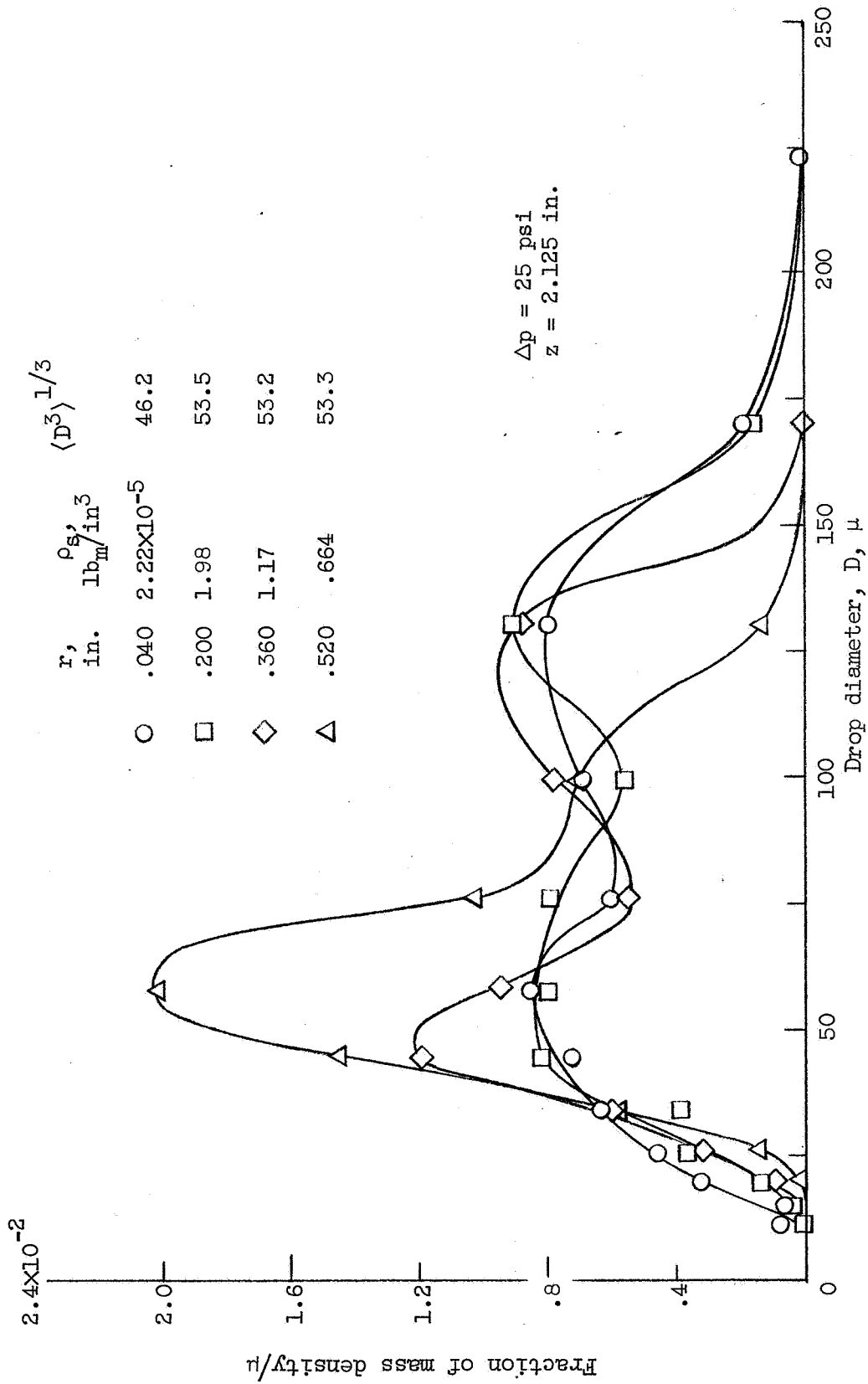


Figure 40. - Mass densities as a function of drop size at downstream locations.

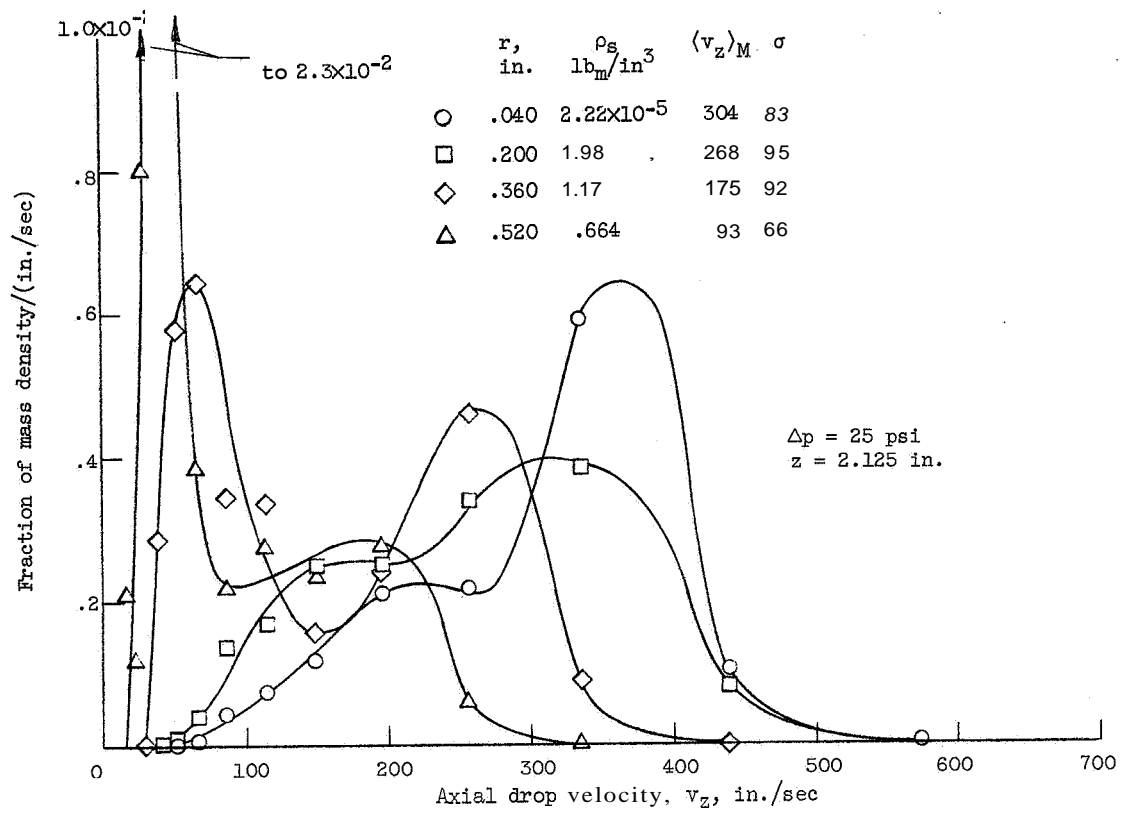


Figure 41. - Mass densities as a function of axial drop velocity at downstream locations.

initially determined primarily by the atomizer used and the spraying parameters. However, the spatial densities are radically modified by the gas-drop interactions (mainly drag in this case) as propagation proceeds. Local values of air velocity determine the location of the developing size-velocity mode which becomes more and more pronounced with increased travel time from the formation region. The coupling of the liquid flow with the gas is evidenced by air entrainment; and so the relative velocity, which is the main driving force for changes in f , is a function of position.

2. The Behavior of the Spatial and the Flux Distributions.

Bimodal spatial drop size distributions obtained by photographic methods have been reported by several investigators. The most similar study to the present one used a swirl atomizer injecting into stagnant air in a closed chamber (Ref. 72). Measured values of f_s were strongly dependent on location, and in many cases were decidedly bimodal. Atomization by impinging jets injecting into still air (Ref. 18) and higher velocity airstreams (Refs. 73, 74) have also produced spatial distributions with two modes. Due to the difficulties in separating true modes from statistical fluctuations in small samples and the complexity of treating bimodal data analytically, much data has been assumed to be unimodal. It is probable

that reanalysis of much existing photographic data would reveal the existence of two distinct modes.

There is also a body of data obtained by collection methods (Ref. 4) or velocity weighting of spatial distributions which corresponds to the flux distribution, \underline{f}_F . As stated in Eq. (2.28) the ratio of \underline{f}_F to f_S is the average drop velocity at a given size: $\langle v_z | D \rangle$. Figure 42 compares the two normalized distributions at a particular downstream location. The ratio of the mass-weighted, normalized forms is:

$$\frac{M \underline{f}_F}{\rho_S \langle v_z \rangle_M} \left(\frac{\rho_S}{M \underline{f}_S} \right) = \frac{\langle v_z | D \rangle}{\langle v_z \rangle_M} \quad (4.11)$$

as is clearly shown. In this case small drops have decelerated and their spatial density has increased while the largest drops continue to move much faster. Thus, for this gas flow condition photographs show the largest population of small drops while collectors intercept a greater number of large drops. Figure 42 emphasizes the fact that the two size distributions are not equivalent and may differ substantially. For example, note the differences in the tabulated means. Only in the special case where all drops are traveling at the same velocity are the normalized forms of \underline{f}_F and f_S equal.

*

This is true of Ref. 19, and the smooth curves of Fig. 5 are the result of a smoothing of the data by the form of correlation used.

**

Of course, perfect collection is assumed in the above discussion. If shattering occurs in the collector no basis of comparison exists.

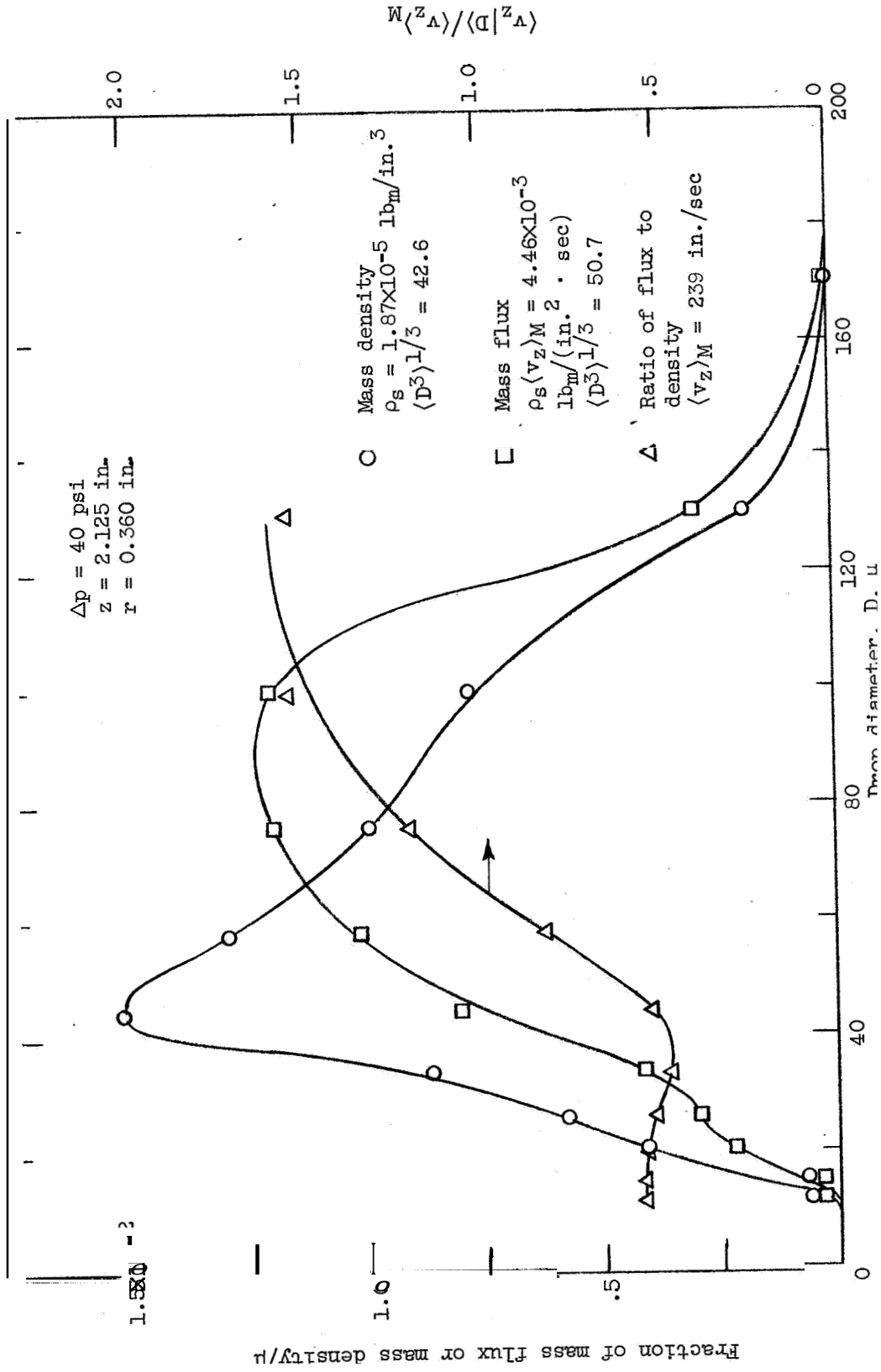


Figure 42. - Comparison of spatial and flux drop size distributions at a particular location.

The collection of regression curves (divided by $\langle v_z \rangle_M$) for different radii at a downstream location appear in Fig. 43. It can be seen that these weighting curves which relate the two types of distributions reflect the stage of deceleration so that their range increases with distance from the formation region.

The modal characteristics of \underline{f}_F can be drastically different from those of f_g as shown in Fig. 44. At this downstream position the spatial size distribution indicates that drops less than about 60μ have nearly reached the air velocity while larger drops continue to move faster and account for the mode at large sizes. But when the spatial density is weighted by the velocity regression curve to give mass flux, the dominant mode appears at large sizes with only a small inflection remaining in the small size range.

Equations of change for marginal density functions such as f_g and \underline{f}_F may be derived in order to investigate their propagation characteristics analytically.* In the special case where no processes occur to change the amount of liquid present inside the region of space under study; continuity requires that:

$$\nabla_x \cdot \underline{f}_F = 0 \quad \text{for} \quad \mathcal{D} = 0 \quad (4.12)$$

$\mathcal{J} = 0$, and steady-state

For the cylindrical coordinates r and z :

$$\frac{1}{r} \frac{\partial f_{Fr}}{\partial r} + \frac{\partial f_{Fz}}{\partial z} = 0 \quad (4.13a)$$

* See Appendix B.3 for details.

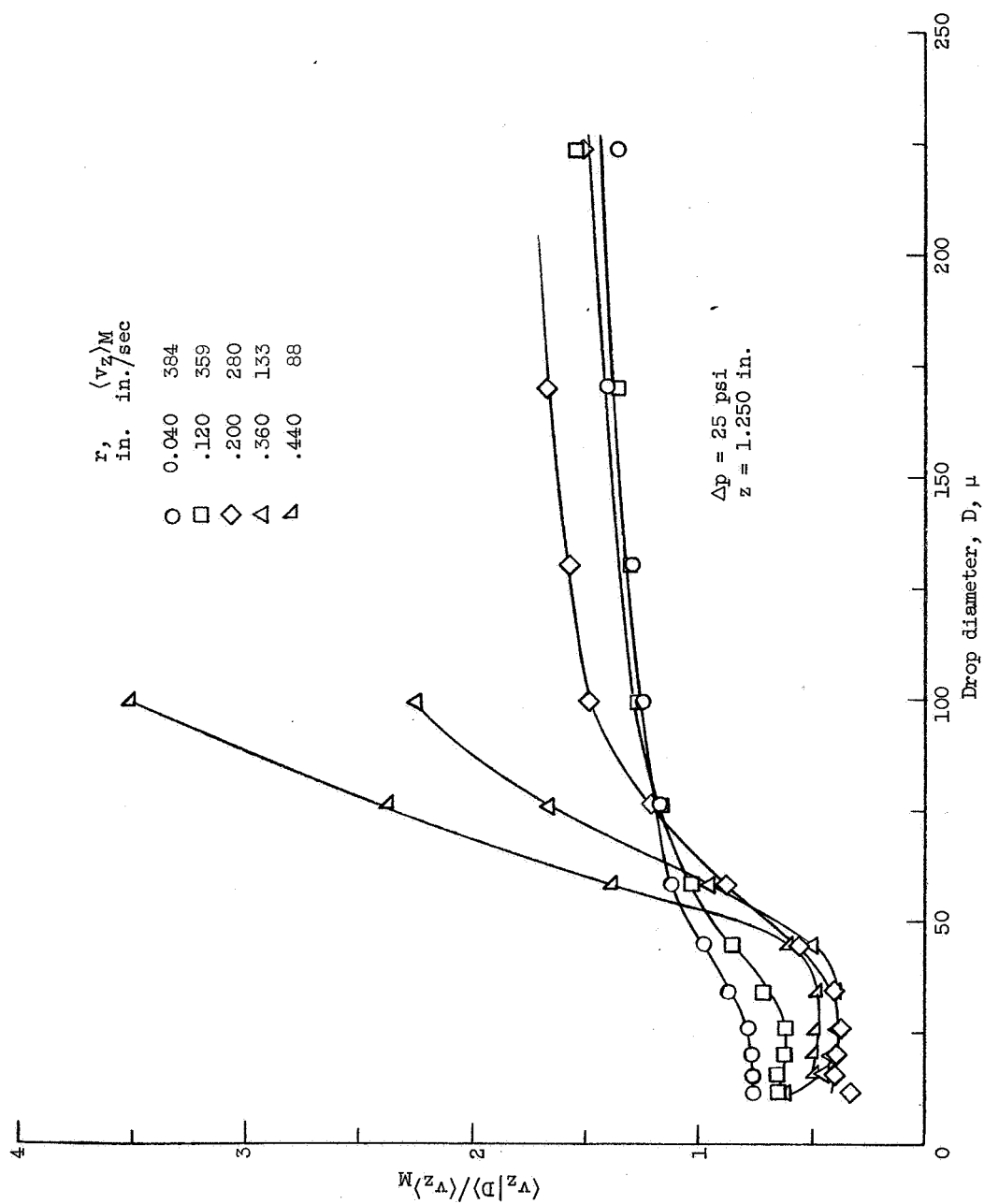


Figure 43. - Expected values of drop velocity as a function of size at several downstream locations.

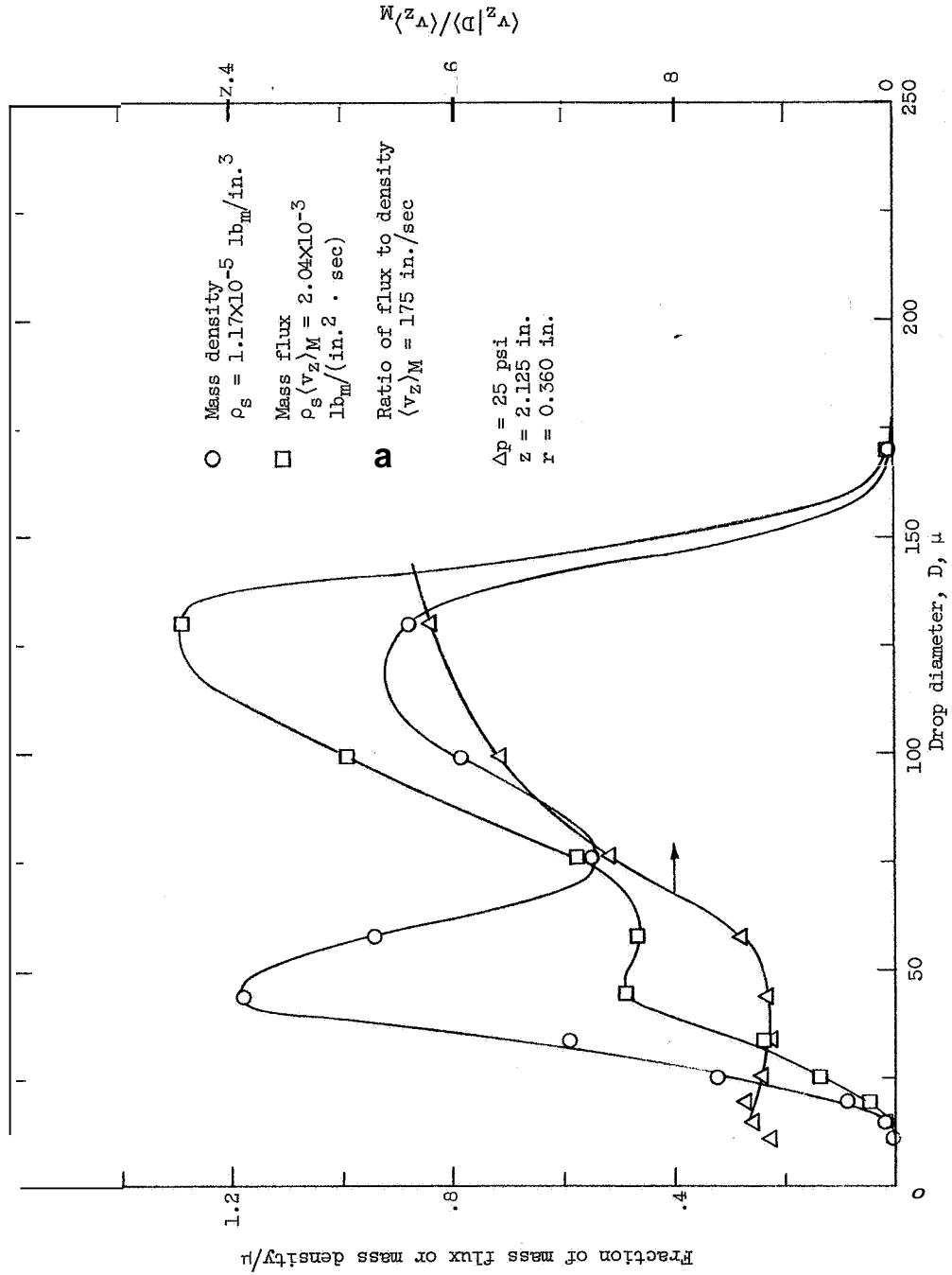


Figure 44. - Comparison of the modal characteristics of spatial and flux distributions at a particular location.

Substitution for \underline{f}_F in terms of f_S from Eq. 2.28 gives:

$$\frac{1}{r} \frac{\partial}{\partial r} (\langle v_r | D \rangle f_S) + \frac{\partial}{\partial z} (\langle v_z | D \rangle f_S) = 0 \quad (4.13b)$$

While propagation of \underline{f}_F is complicated in the two dimensional case, it can be seen that for no radial variations, \underline{f}_F is independent of z . In physical terms, the flux of numbers (or mass) as a function of D propagates unchanged. A one-dimensional description of the spray will now be considered so that such aspects of the data as the propagation of \underline{f}_F may be more easily treated.

3. One-Dimensional Spray Density Functions

A one-dimensional description of the spray at any axial location is obtained by integrating f over a cross-section. In cylindrical coordinates:

$$f_T = 2\pi \int_0^{\infty} f_B(D, v_z, r, z) r \, dr \quad (4.14)$$

The corresponding numerical approximation using experimental data is given by **Eq.** (4.4). Note that f_T is a one-dimensional "density" with units of drops per unit size, axial velocity and length in the z direction; and fluxes obtained from f_T are simply flow rates in the axial direction.

Normalized mass densities as a function of D are shown in Fig. 45 for the location near the surface of formation at the three injection pressures. The **small** first modes show the influence of the outer radii where drop deceleration is appreciable. A shift toward smaller

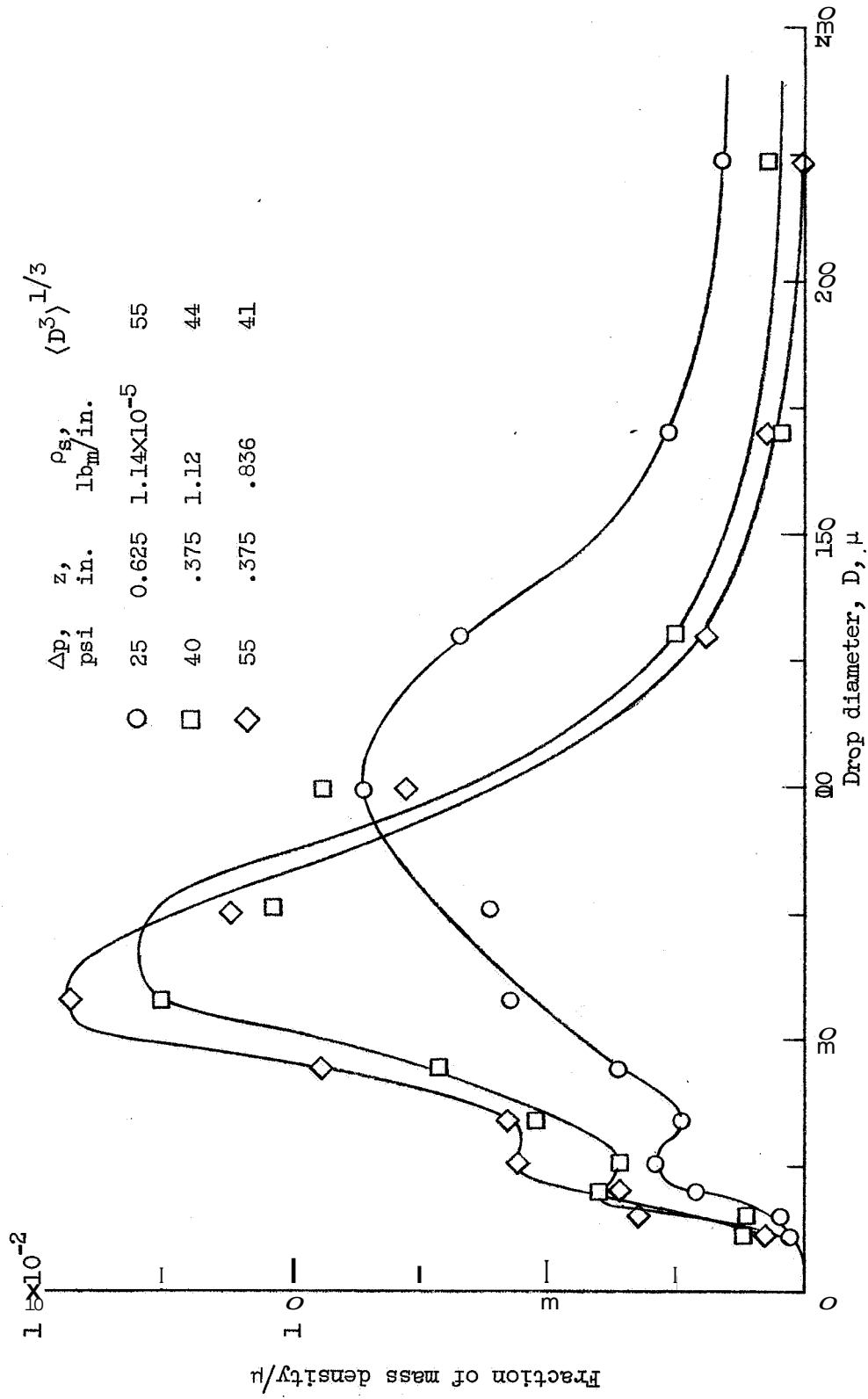


Figure 45. - One-dimensional mass densities as a function of drop size near the surface of formation.

sizes with increasing A_p indicates that the higher energy inputs produced smaller drops. Figure 46 shows the corresponding velocity dependence. Only small fractions of the mass have approached equilibrium with the air. The exact location and height of the first mode in each case depends on how well the sampling location approximated the surface of formation and the extent of the formation region which was greatest at 25, psig. Most of the mass is located in the second modes which broaden with increasing A_p and have means ranging from $2/3$ to $3/4$ of the axial sheet velocity.

The propagation of the mass densities with downstream distance is traced in Figs. 47 and 48. With respect to size there is the progression from a dominant second mode, through modes of comparable size, to a dominant first mode as more and more of the mass approaches gas velocity. A clearer picture of the changes occurring during propagation is given in Figs. 49(a-c) by the contour plots of the bivariate size-velocity function. Immediately after formation (Fig. 49(a)) the large "hill" representing the second, or what may be described as the formation mode, is dominant. Only a small peak representing the first, or more descriptively the propagation mode, appears. At the medium downstream distance (Fig. 49(b)) the propagation peak has sharpened; the formation mode has diminished; and a higher ridge connects the two. Finally the dominant feature of Fig. 49(c) is the high propagation

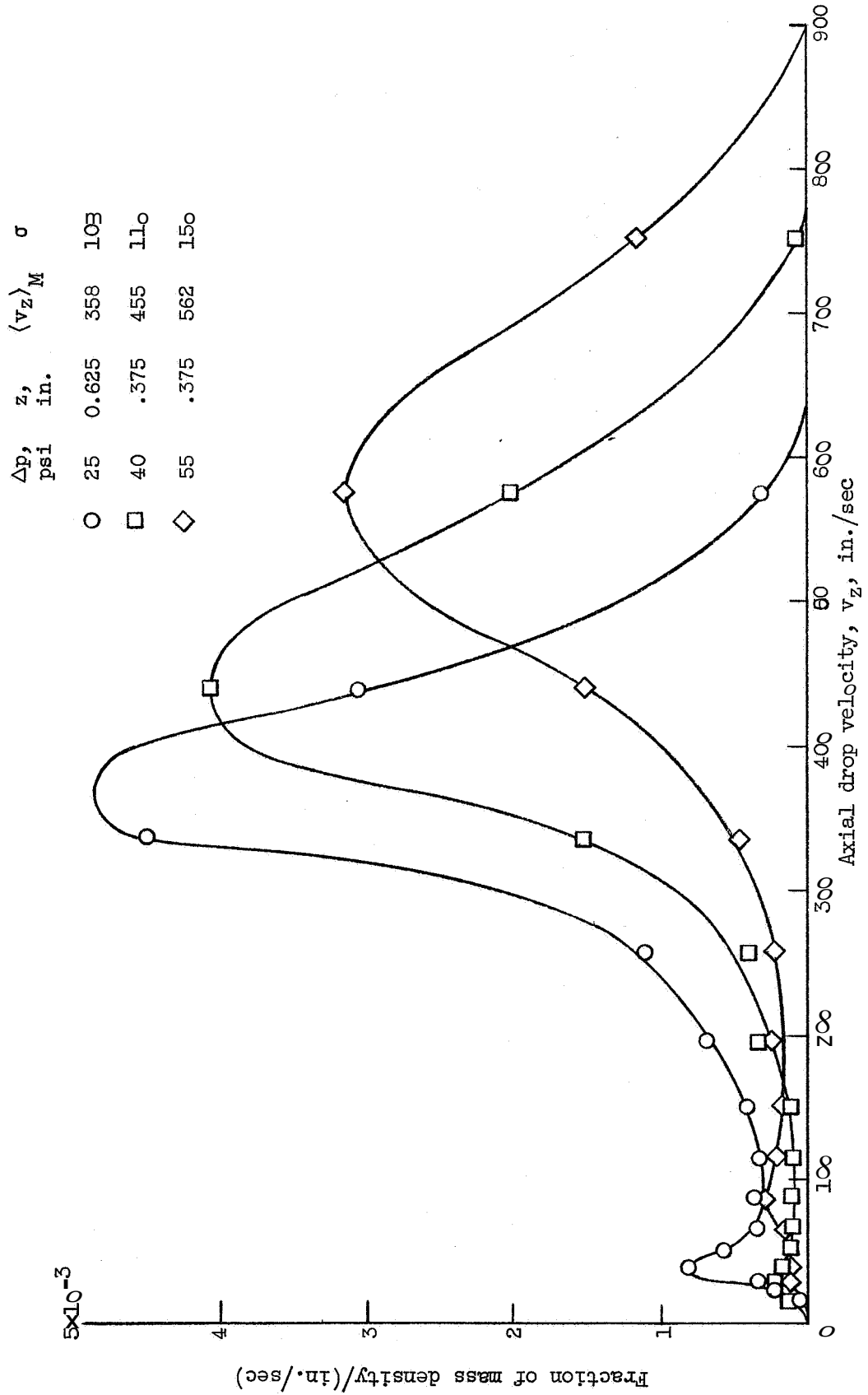


Figure 46. - One-dimensional mass densities as a function of axial drop velocity near the surface of formation.

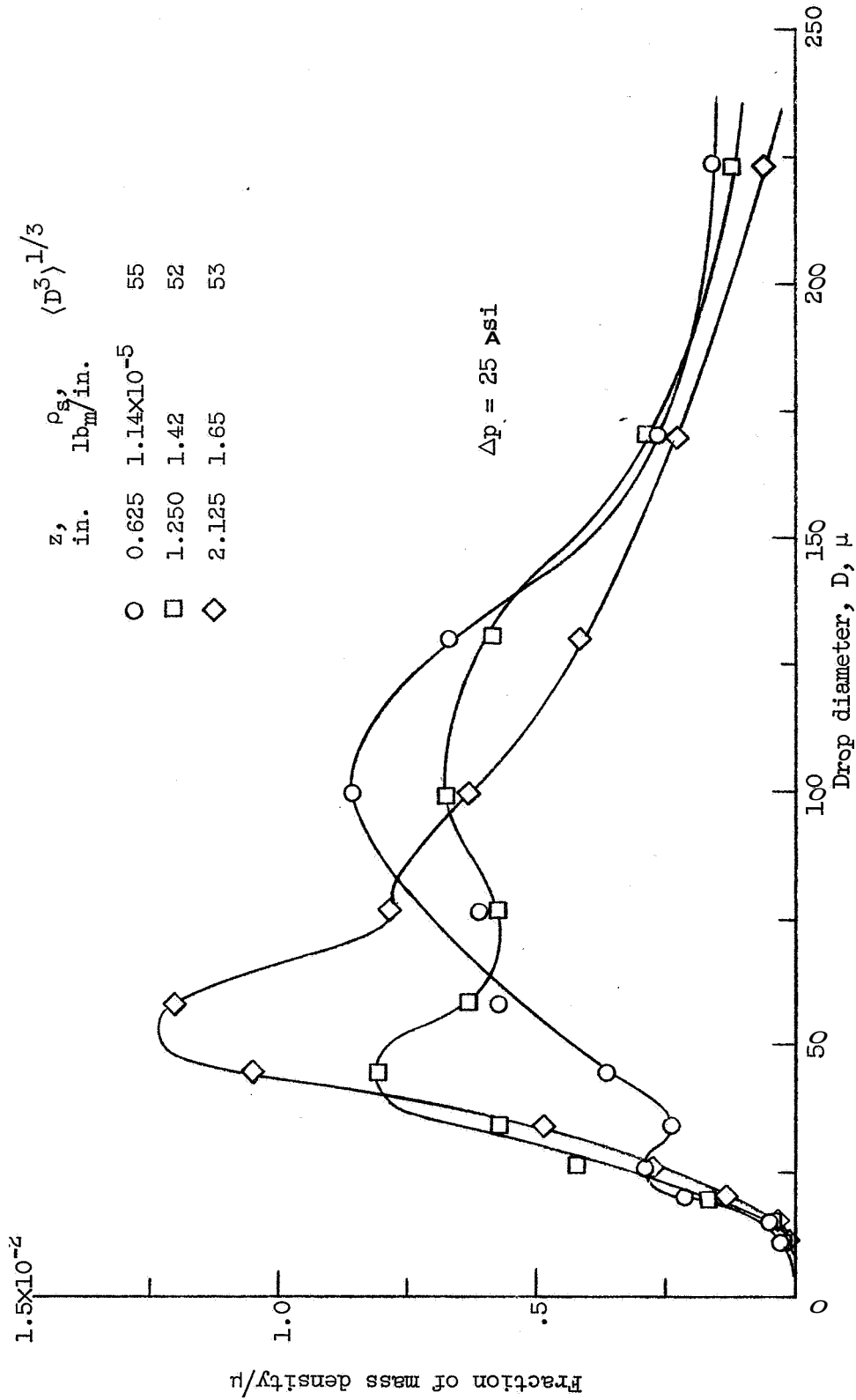


Figure 47. - Propagation characteristics of the one-dimensional mass densities as a function of drop size.

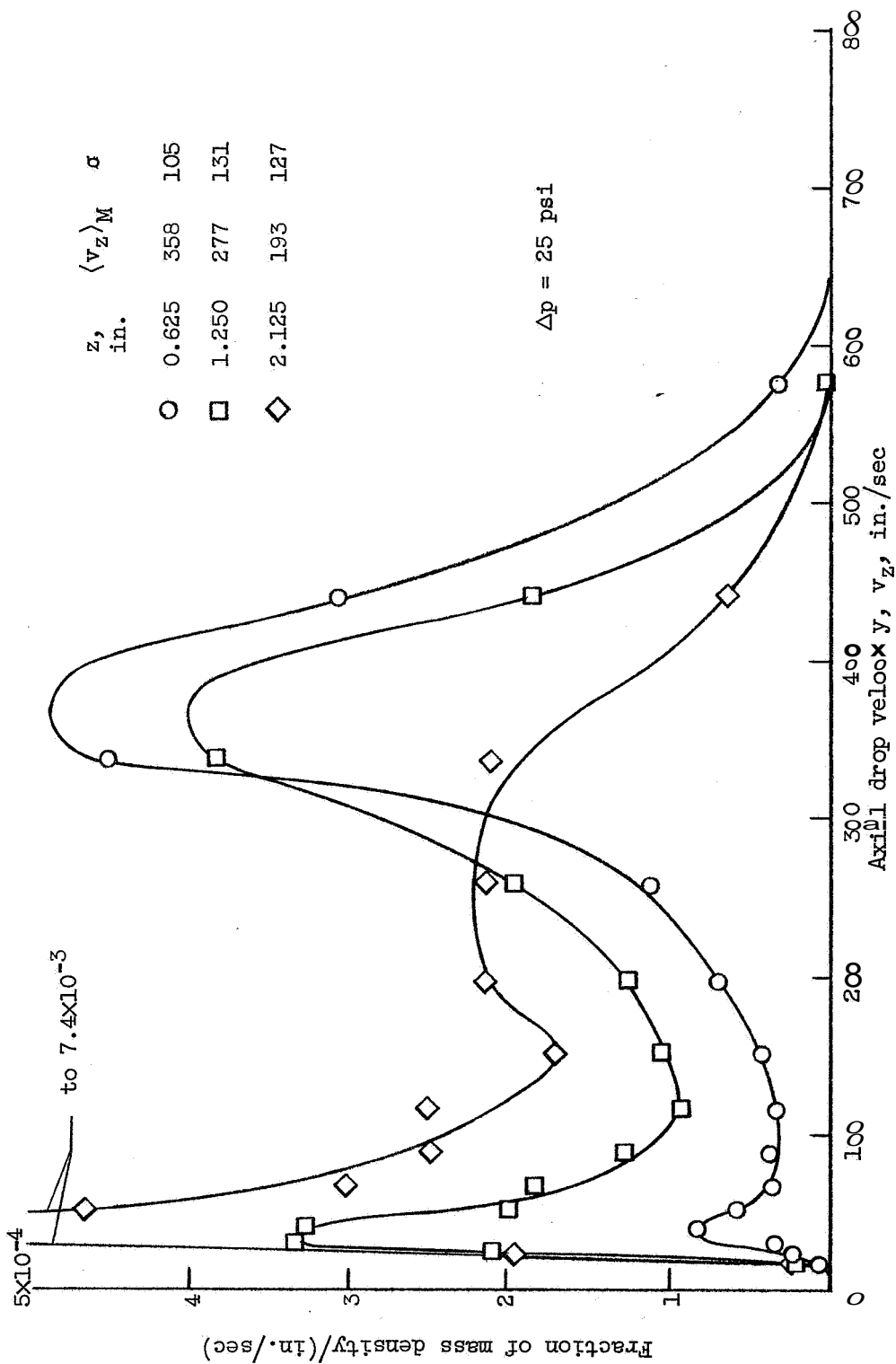
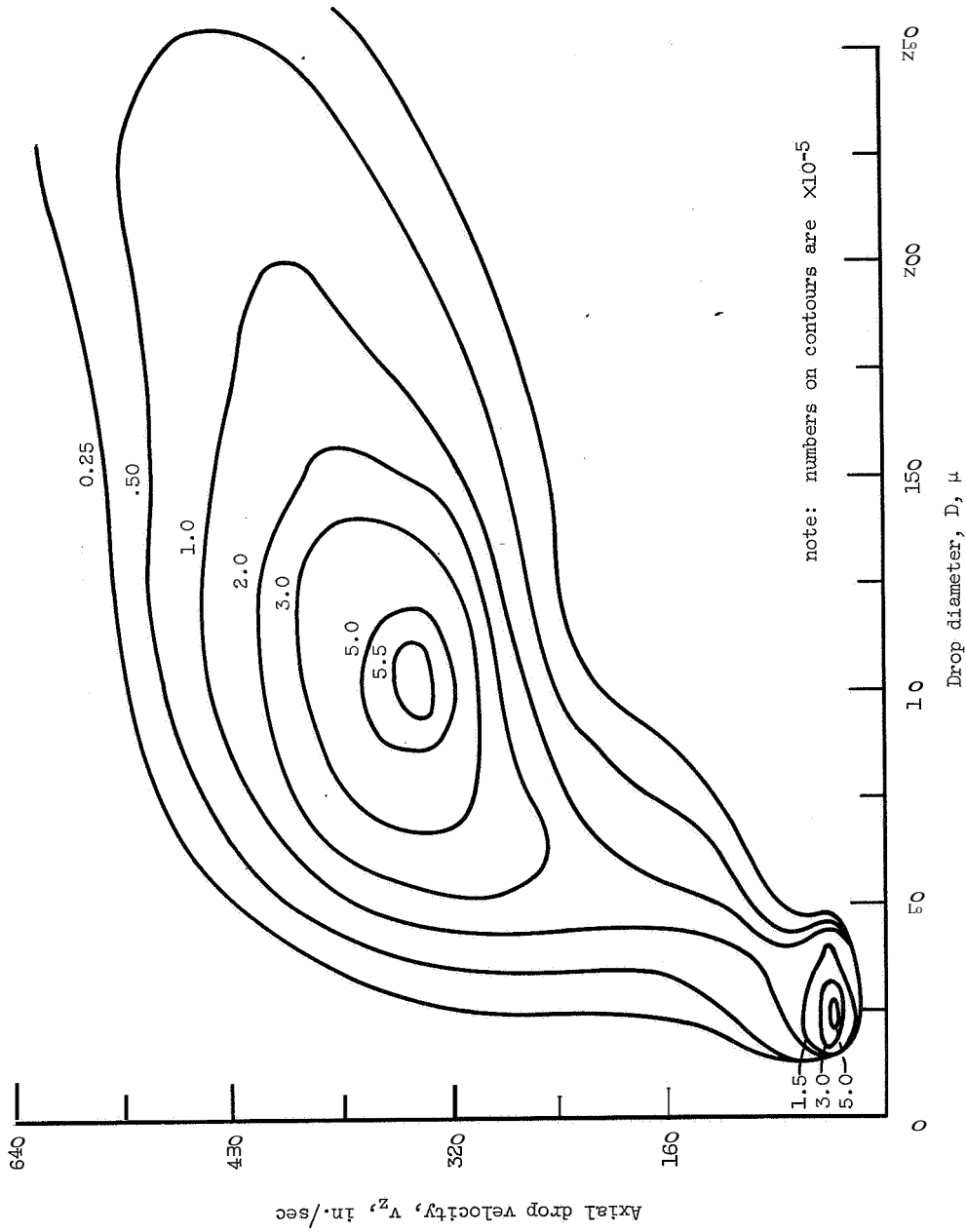
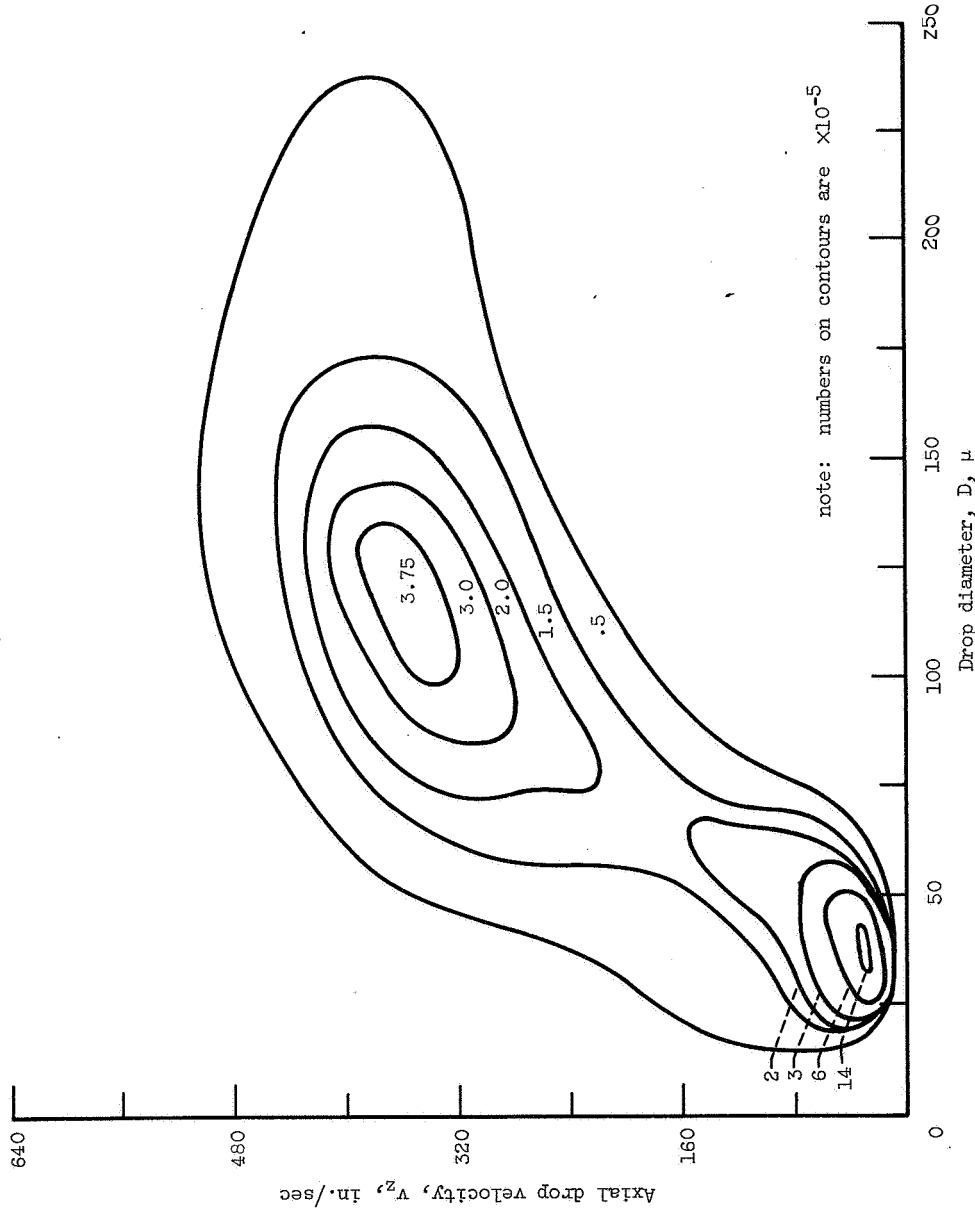


Figure 48. - Propagation characteristics of the one-dimensional mass densities as a function of axial drop velocity.



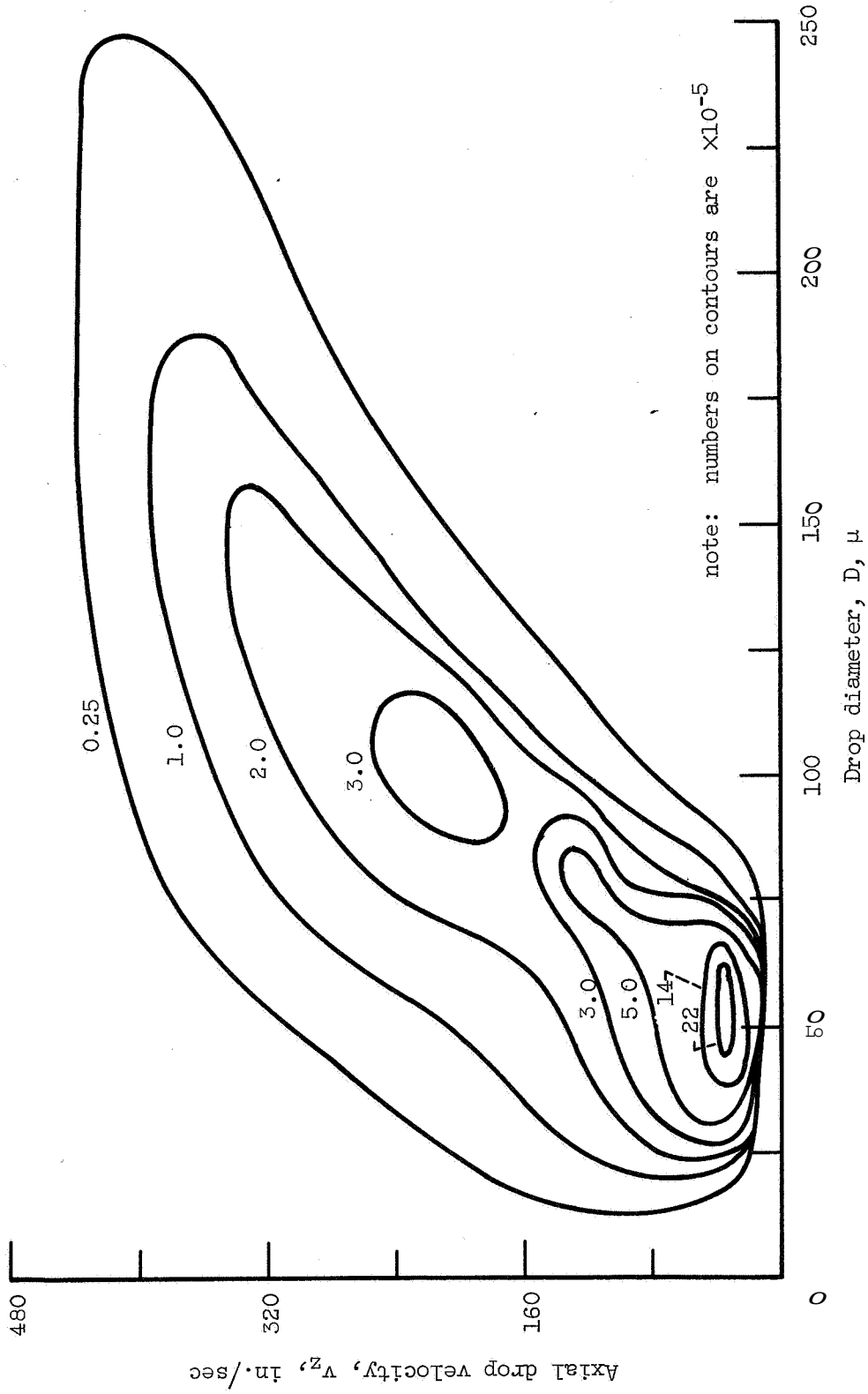
(a) $\infty = 25$ psi, $z = 0.625$ in.

Figure 49. - Contour maps of one-dimensional, bivariate mass densities.



(b) $\Delta p = 25$ psi, $z = 1.250$ in.

Figure 49. - Continued.



(c) $\Delta p = 25$ psi, $z = 2.128$ in.

Figure 49. - Concluded

mode whose base blends into the extensively altered formation mode.

It is of interest to note that in the studies where bimodal distributions were reported from samples taken at a constant downstream distance (Ref. 73, 74) it was the large size mode which showed the usual changes attributable to variations in injection parameters. This is compatible with the concept that it represented the formation mode while the first mode indicated the stage of propagation. The alternate hypothesis that the two modes resulted from two distinct formation processes is possible, and only velocity data could decide the question.

In the present study the possible existence of bimodal formation processes can be investigated by considering the one-dimensional mass flux distributions. Since vaporization was small (see section E below), Eq. 4.13(a) indicates that f_F should propagate unchanged with z^* . If definite modes are present at formation they should appear in the flux distribution. Figure 50, which includes both formation and propagation information, indicates that no definite modes are present for $A_p = 25$ psi. The strong bimodal spatial characteristic has almost completely disappeared at downstream locations. It is seen that the flux distribution does remain approximately constant for the three locations with the small shift toward smaller sizes probably being

* Flux distributions as a function of velocity propagate without change only for the case of no acceleration as shown in Appendix B.4.

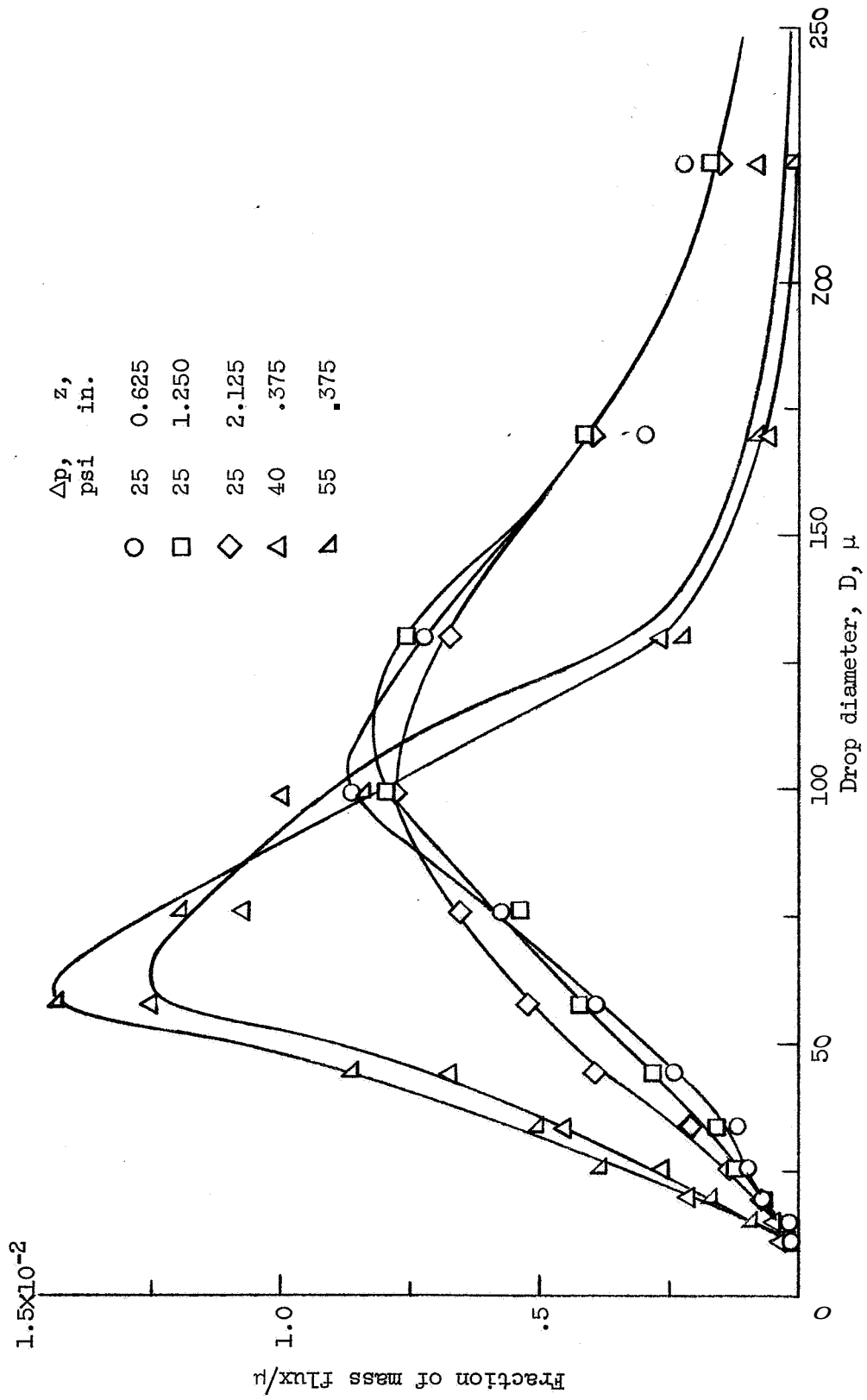


Figure 50. - One-dimensional mass flux distributions.

caused by the amount of vaporization present. Little difference exists between the two curves for higher pressures. The position of the two points at 75 and 100 μ for 40 psi could be interpreted as a bimodal formation tendency. However, the data are not extensive enough to warrant a definite conclusion. ~~What~~ is clear is that the two modes considered throughout the discussion of spatial density functions are the result of the drop-gas interactions and are not inherent in the spray formation process.

The problem of analytically representing $f(D, v_z)$ with a reasonably simple equation is formidable due to the bimodal property in addition to the bivariate form required. When the diversity in form of even the local single variable functions of size is considered, it is understandable that many equations have been proposed to fit measured size distributions (Ref. 3). Add to this situation the common failures to differentiate between spatial and flux data or between area-averaged and local data, and the reasons for confusion are clear. A logarithmic transformation of the normal or Gaussian distribution using a limited range of the independent variable results in a versatile form (Refs. 44, 70). This type of transformation has also been extended to the bivariate case (Ref. 71), but obtaining bimodal forms requires either a more complex equation or the use of a

sum of transformed bivariate normals. Near the surface of formation, the formation mode is dominant; and in some cases a useful approximation of f_0 may be obtained with an equation which neglects the propagation mode.

D. Mean Values of the Spray Variables

The mean quantities presented below emphasize the wide range of variation in the magnitudes and shapes of the density functions with position. Although they cannot reveal the bimodal propagation characteristics and necessarily represent the combined effects of the two modes, they do provide an overall view of spray variations with position and initial conditions.

1. Local Variations

The most basic means are the mass flux, $\dot{m}_z = \rho_s \langle v_z \rangle_M$; the mass average velocity, $\langle v_z \rangle_M$; and the density, ρ_s , which is the ratio of the first two. Figure 51 shows the profiles of $\langle v_z \rangle_M$ referred to the axial liquid sheet velocity. Suppression of the profile with downstream distance indicates the deceleration by the gas. At the lowest injection pressure (25 psig) the hollow liquid cone tends to collapse toward the axis due to the action of surface tension, and so the spray is confined to smaller radii.

This behavior is emphasized in the mass flux profiles given in Fig. 52 as fractions of the maximum value at each axial location. The development with injection pressure is peculiar to a swirl atomizer and near the surface of for-

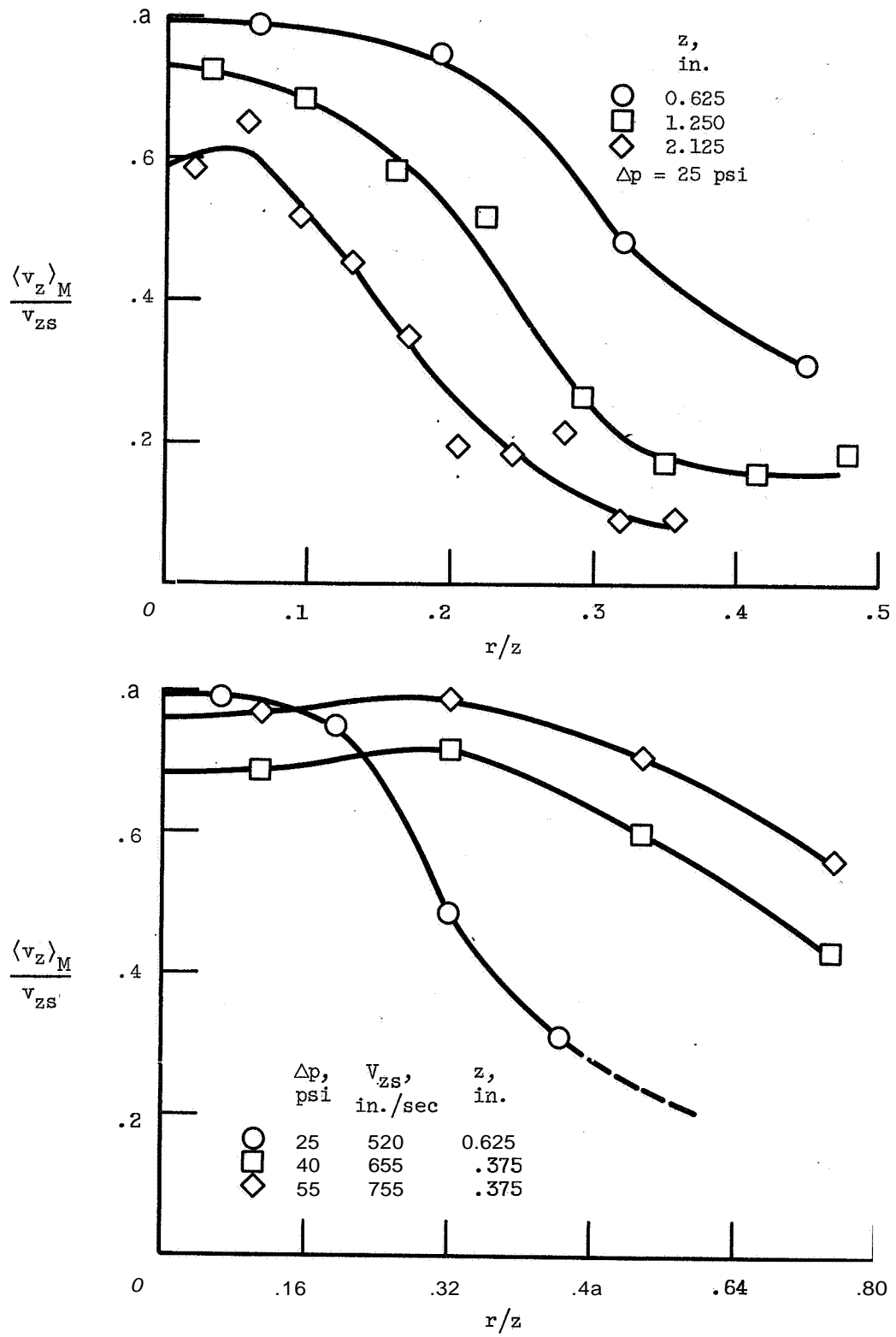


Figure 51. - Variation of mass average velocity with position and injection pressure.

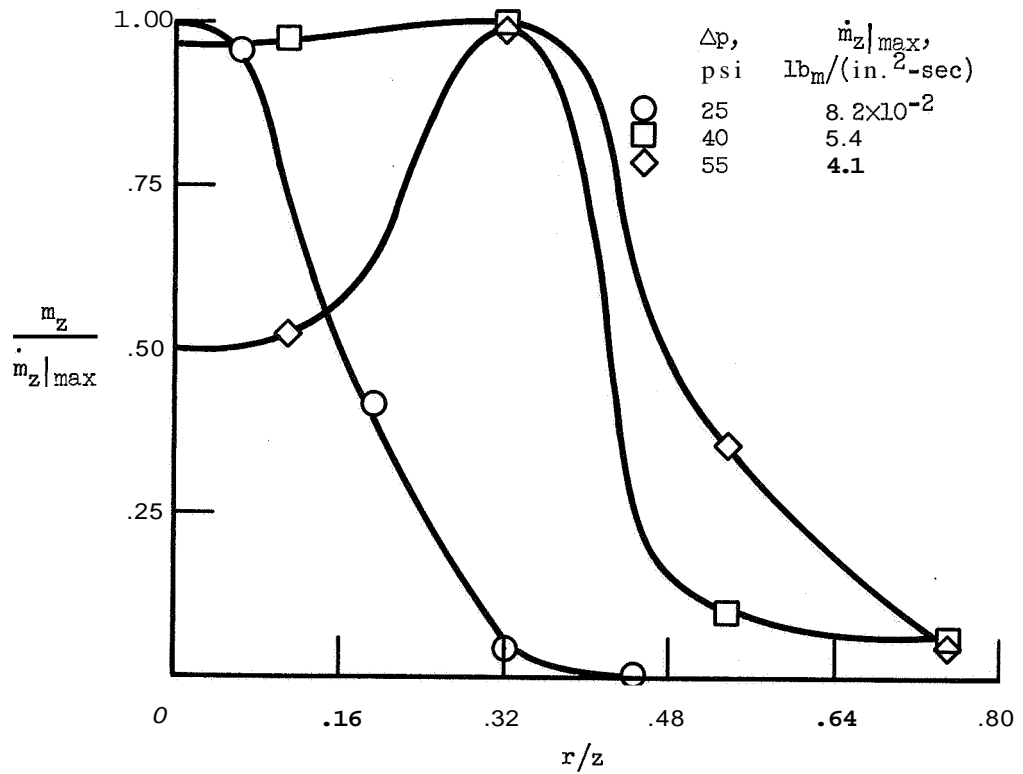
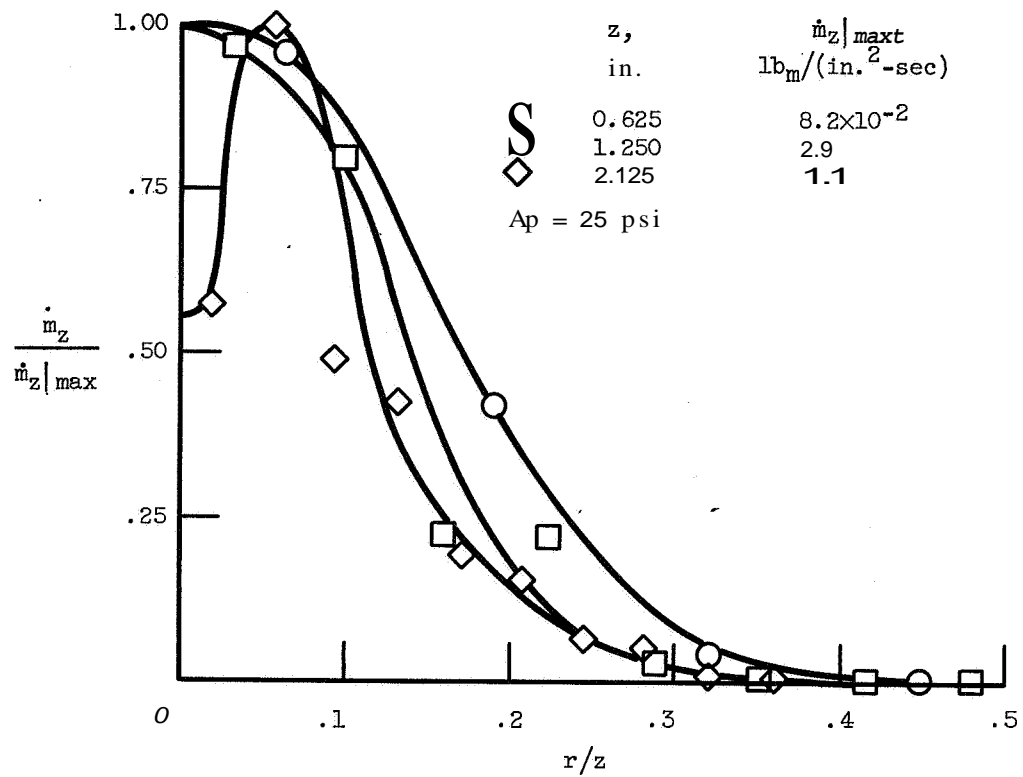


Figure 52. - Variation of mass flux profiles with position and injection pressure.

mation progresses from a "solid" cone, through a semi-hollow pattern, to an almost flat profile. Dispersion about the centerline decreases with downstream distance due to the inward flow of entrained air which warps the spray envelope from a conical toward a cylindrical form.*

Profiles of axial momentum flux, $\rho_s (\langle v_z^2 \rangle_M + \langle v_z v_r \rangle_M)$, and axial kinetic energy flux, $\rho_s (\langle v_z^3 \rangle_M + \langle v_z v_r^2 \rangle_M)$, vary in a manner similar to mass flux. However, note that the average of a product of velocities is not equal to the product of the averages. For example, $\langle v_z^2 \rangle_M \neq \langle v_z \rangle_M^2$ as indicated by the fact that $\langle v_z \rangle_M$ has a finite standard deviation. The coefficient of variation of $\langle v_z \rangle_M$ obtained by applying Eq. (4.6) to give:

$$\lambda_{\langle v_z \rangle_M} = \frac{\left(\langle v_z^2 \rangle_M - \langle v_z \rangle_M^2 \right)^{1/2}}{\langle v_z \rangle_M} \quad (4.14)$$

is plotted in Fig. 53. This "intensity of turbulence" which indicates the spread about the mean, increases toward the edges of the spray to values of .6 to .8.

The interdependence of $\langle v_z \rangle_M$ and $\langle v_r \rangle_M$ is indicated by their correlation (see Eq. (4.7), whose variation is shown in Fig. 54. At the centerline near the surface of formation the chaotic condition is indicated by the fact that the components are uncorrelated at all pres-

* The hollow profile at $z = 2.125$ and $Ap = 25$ may be due to drops crisscrossing the axis, an asymmetry of the spray pattern, or a small error in locating the downstream sampling position.

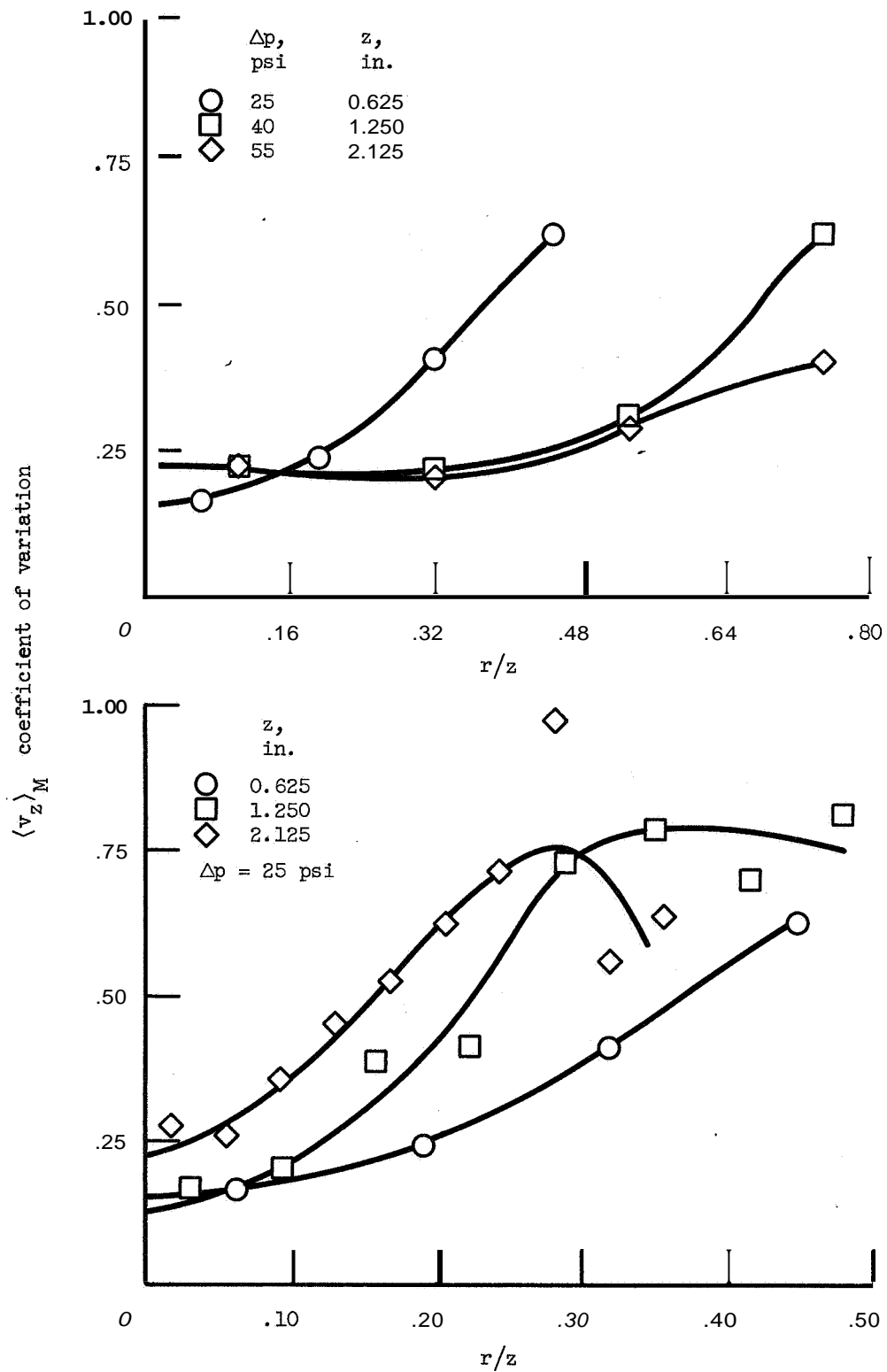


Figure 53. - Coefficient of variation for mass average axial velocity as a function of position and injection pressure.

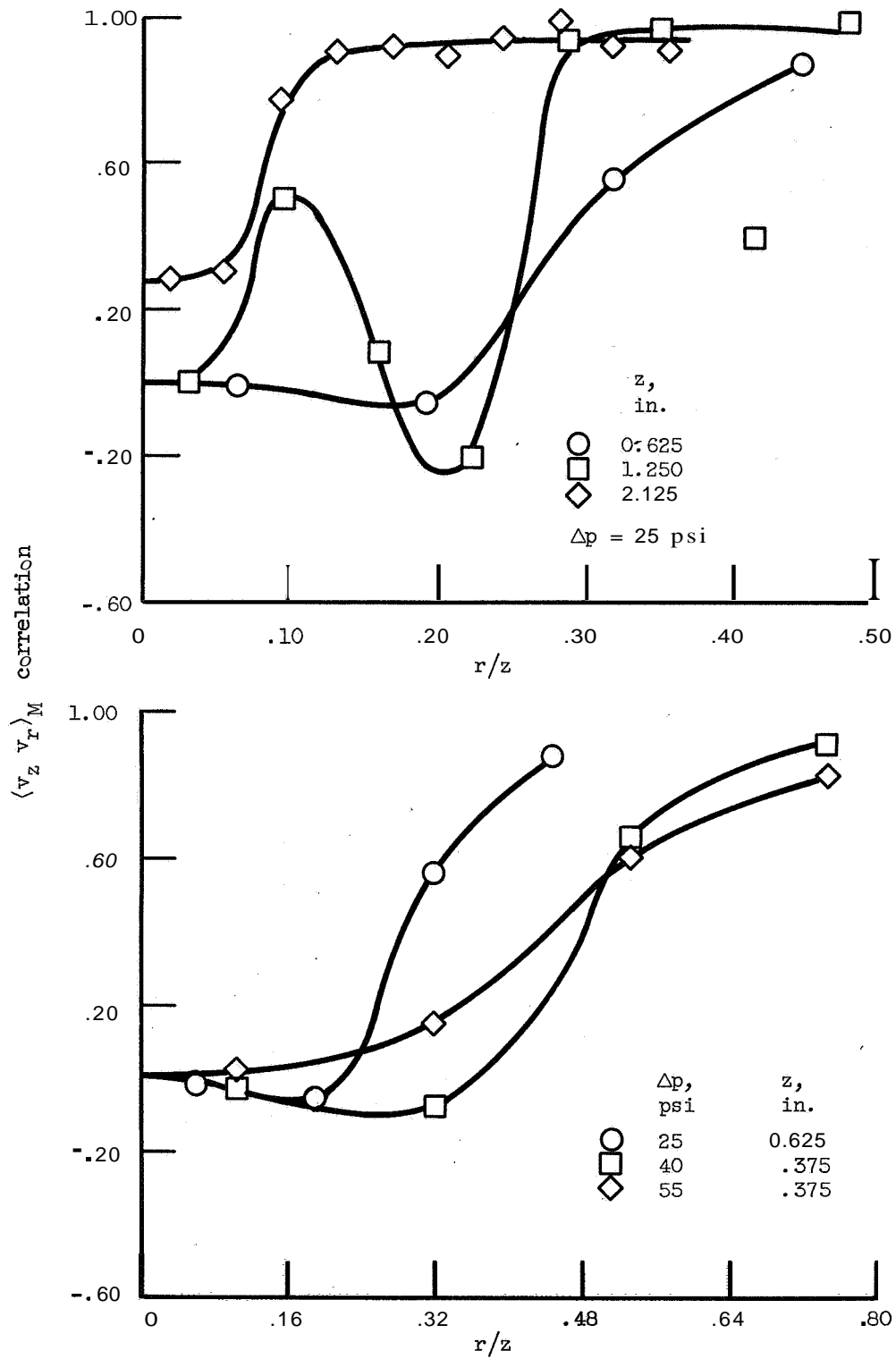


Figure 54. - Correlation of mass average radial and axial velocity components as a function of position and injection pressure.

sures. The negative values at intermediate radii show the tendency for some drops to be thrown inward from the conical sheet. Toward the edge of the spray, radial and axial components become highly correlated. The propagation behavior at 25 psig is complex at $z = 1.250$ apparently due to a pronounced crisscrossing of the larger drop trajectories. Farther downstream the inward sweep of the air leaves a much smaller, somewhat less chaotic core.

The third moment about the mean is incorporated in the shape parameter of Eq. (4.6): the skewness. This quantity is plotted in Fig. 55 for the mass average velocity. Although the interpretation is complicated by the bimodal form of the mass densities; the shifts from approximate symmetry to tailing-off toward small velocities; and then, to a high velocity tail can be compared with Figs. 36 and 41. The appearance of the propagation mode skews the density negatively, and deceleration continues until only a remnant of the formation mode remains to give a positive skewness.

The type of means just given for $\langle v_z \rangle_M$ can also be given for the number average velocity $\langle v_z \rangle_N$. In general, the range of variation tends to be somewhat larger without the moderating influence of mass weighting. The ratio of the mass average to number average velocities has significance as a comparison of spatial and flux distributions. Reference to Eqs. (2.7) to (2.10) shows

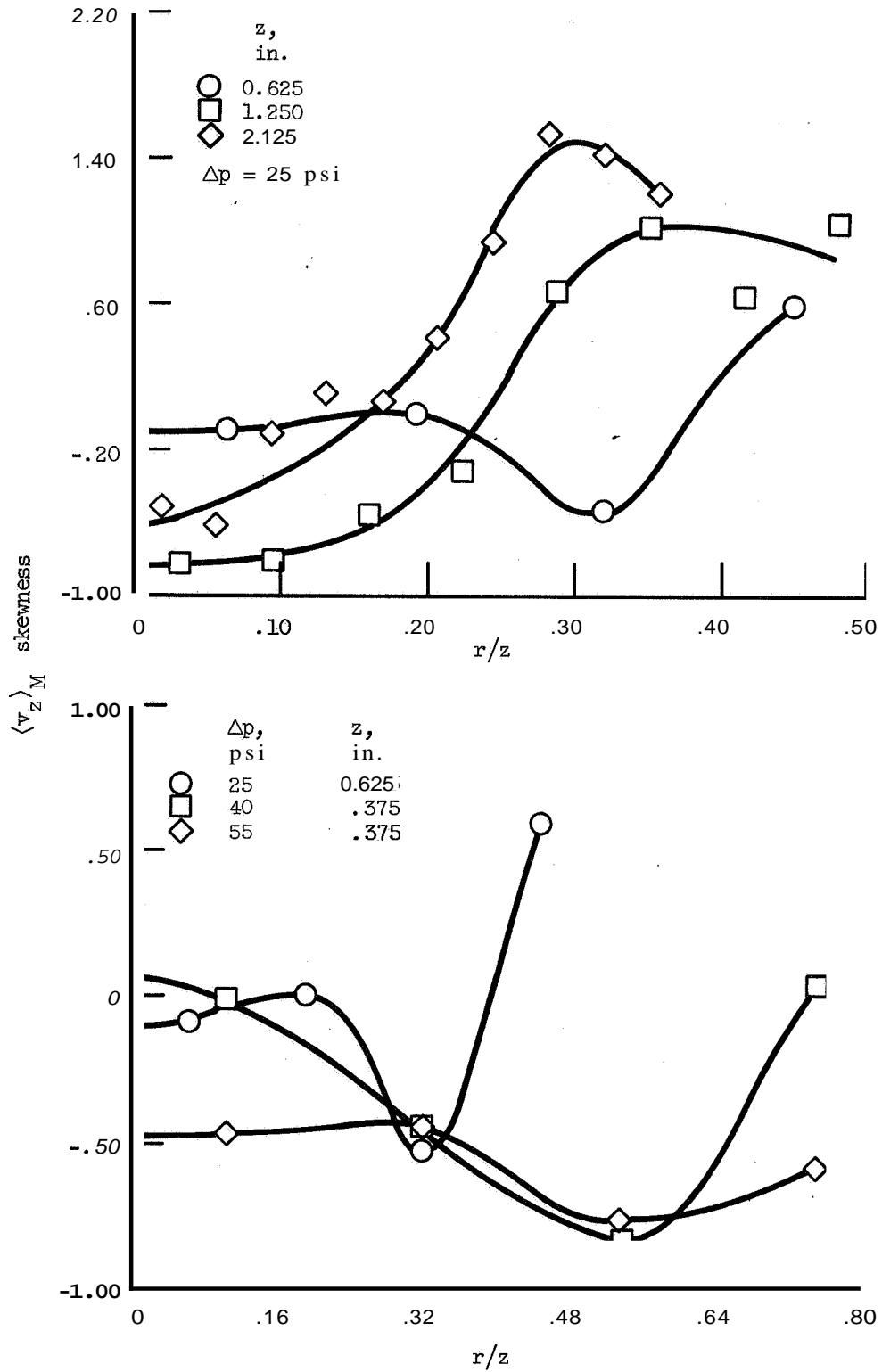


Figure 55. - Skewness for the mass average axial velocity as a function of position and injection pressure.

that the ratio of the velocity-weighted third moment of D to the same number - weighted moment is:

$$\frac{(D_{30})_v}{D_{30}} = \left(\frac{\rho_s \langle v_z \rangle_M n_s}{n_s \langle v_z \rangle \rho_s} \right)^{1/3} = \left(\frac{\langle v_z \rangle_M}{\langle v_z \rangle} \right)^{1/3} \quad (4.15)$$

Thus, this commonly used mean diameter, D_{30} , has a value for the mass-weighted spatial distribution which differs from the velocity-weighted counterpart obtained from the mass flux distribution. Figure 56 shows that substantial variations of this velocity ratio occur especially at the outer edges of the spray where deceleration results in a number average velocity which is much lower than the mass average. In the case of drops accelerating in a higher velocity gas stream, $\langle v_z \rangle$ is greater than $\langle v_z \rangle_M$ and the ratio is less than one. Another commonly used mean size is the Sauter mean, D_{32} . The ratio of this mean for the axial flux distribution to the spatial counterpart is given by:

$$\frac{(D_{32})_v}{D_{32}} = \frac{\rho_s \langle v_z \rangle_M \int D^2 f_S dD}{\int D^2 f_{FZ} dD} = \frac{\langle v_z \rangle_M}{\langle v_z \rangle_A} \quad (4.16)$$

Here $\langle v_z \rangle_A$ is the average velocity obtained by weighting the integrals by droplet surface area. Values of this velocity ratio show a range and type of variation which is very similar to Fig. 56. The above discussion again emphasizes the pitfalls of indiscriminately equating spatial with flux size **data**.

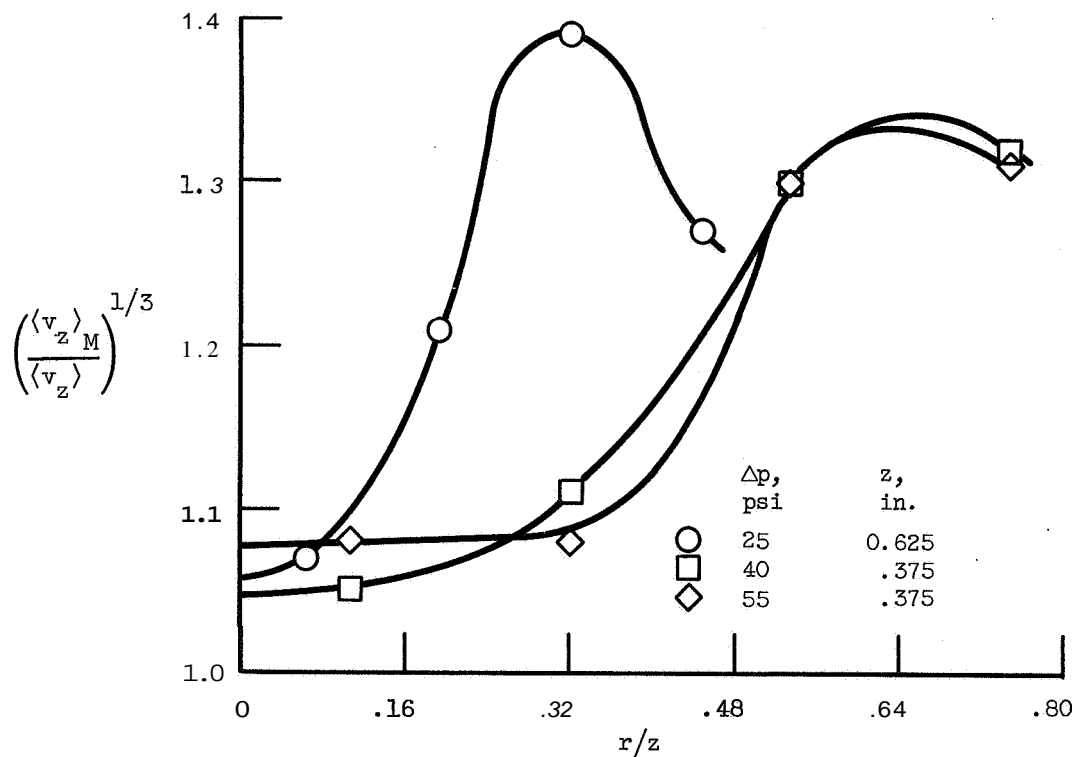
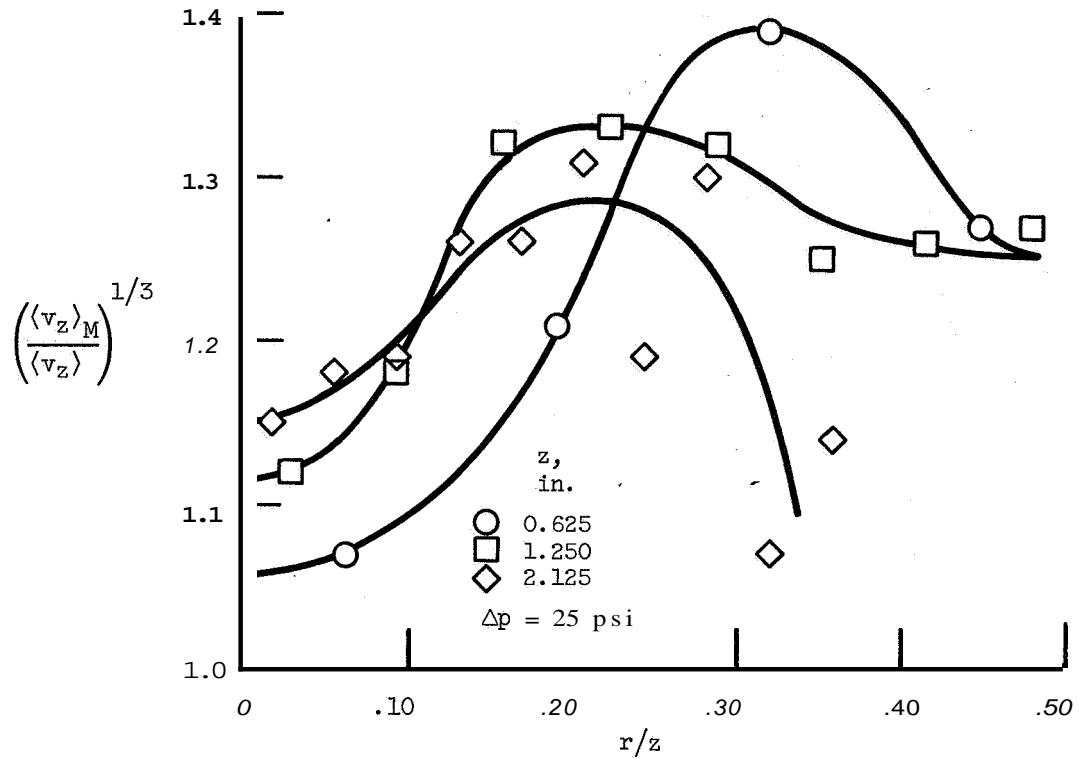


Figure 56. - Variation of mass to number average velocity ratio with position and injection pressure.

Moments with respect to drop size also yield widely varying profiles. Examples are provided by the mean drop size shown in Fig. 57 and the size coefficient of variation plotted in Fig. 58. Changes of the profiles are particularly extensive during propagation, with smaller drops apparently shifting toward the centerline. The formation profiles again reflect progressively greater dispersion of large drops about the spray axis with higher injection pressures. In contrast to mass average velocity, (Fig. 53), the size coefficient of variation (Fig. 58) remains high near the centerline and falls off toward the edge of the spray. Finally, the correlation of size with axial velocity is plotted in Fig. 59. Small drops in the core of the spray near the surface of formation have not decelerated, and so the correlation is lower. As propagation distance increases, higher correlations reflect the fact that most of the faster drops are the larger ones.

2. One-Dimensional Means

Performing the averaging operations on the density function integrated over the cross-section (f_T given by Eq. (4.4)) produces the quantities listed in Table XI. Comparison of these values with the figures given in Section C.3 confirms their gross indication of one-dimensional density function behavior.

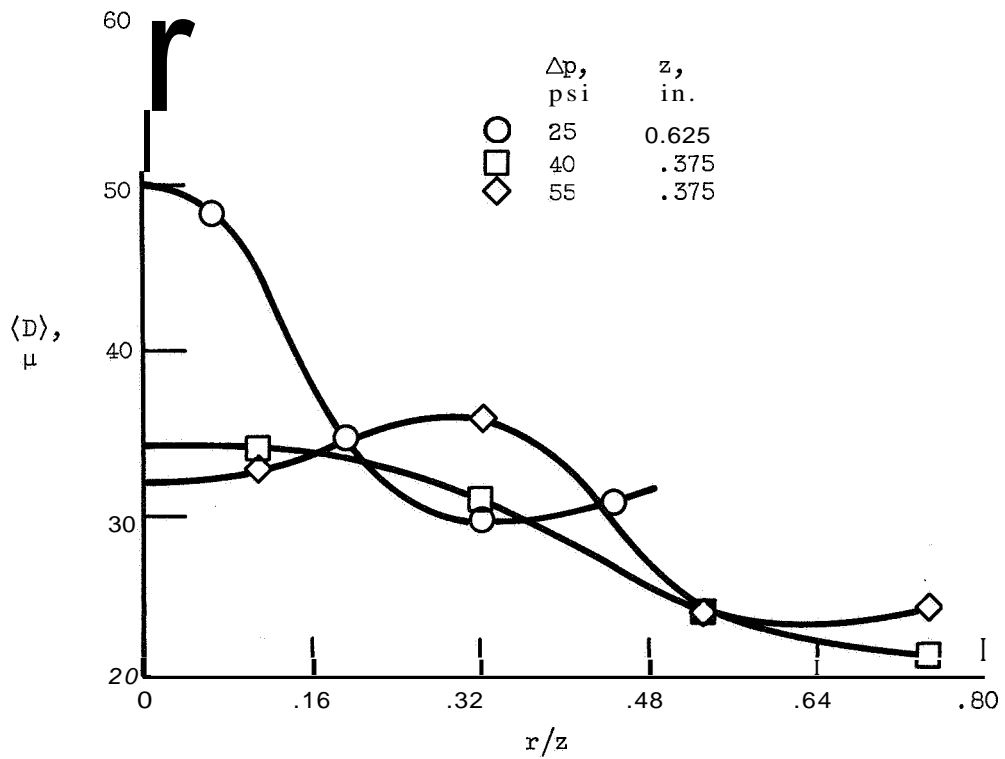
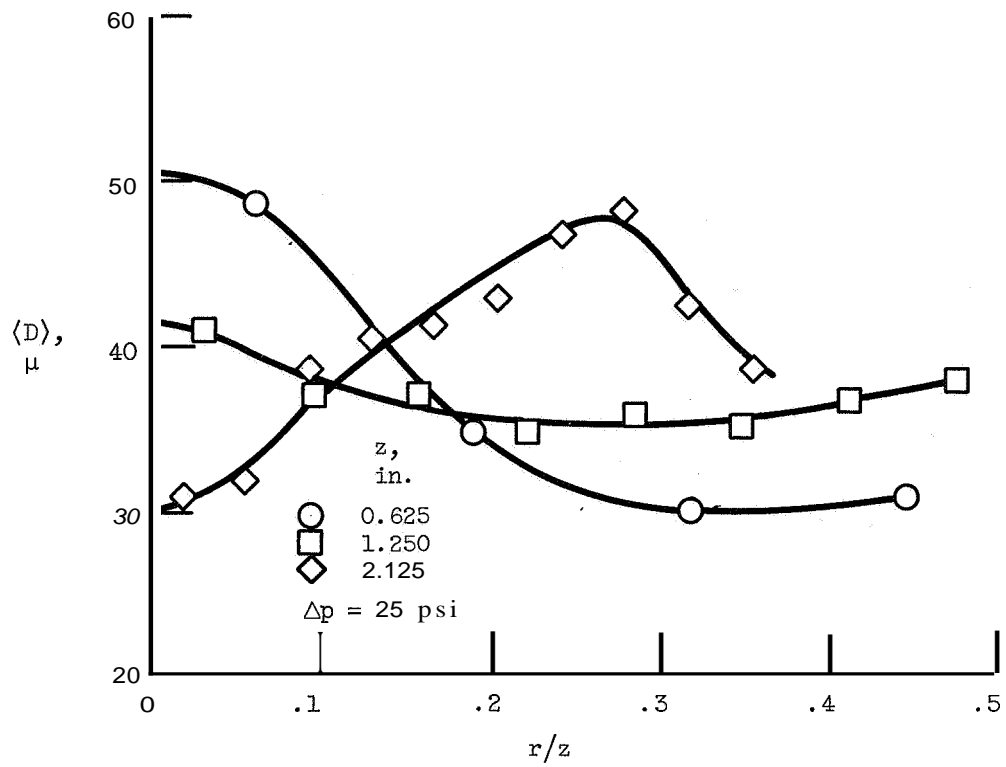


Figure 57. - Variation of mean drop diameter with position and injection pressure.

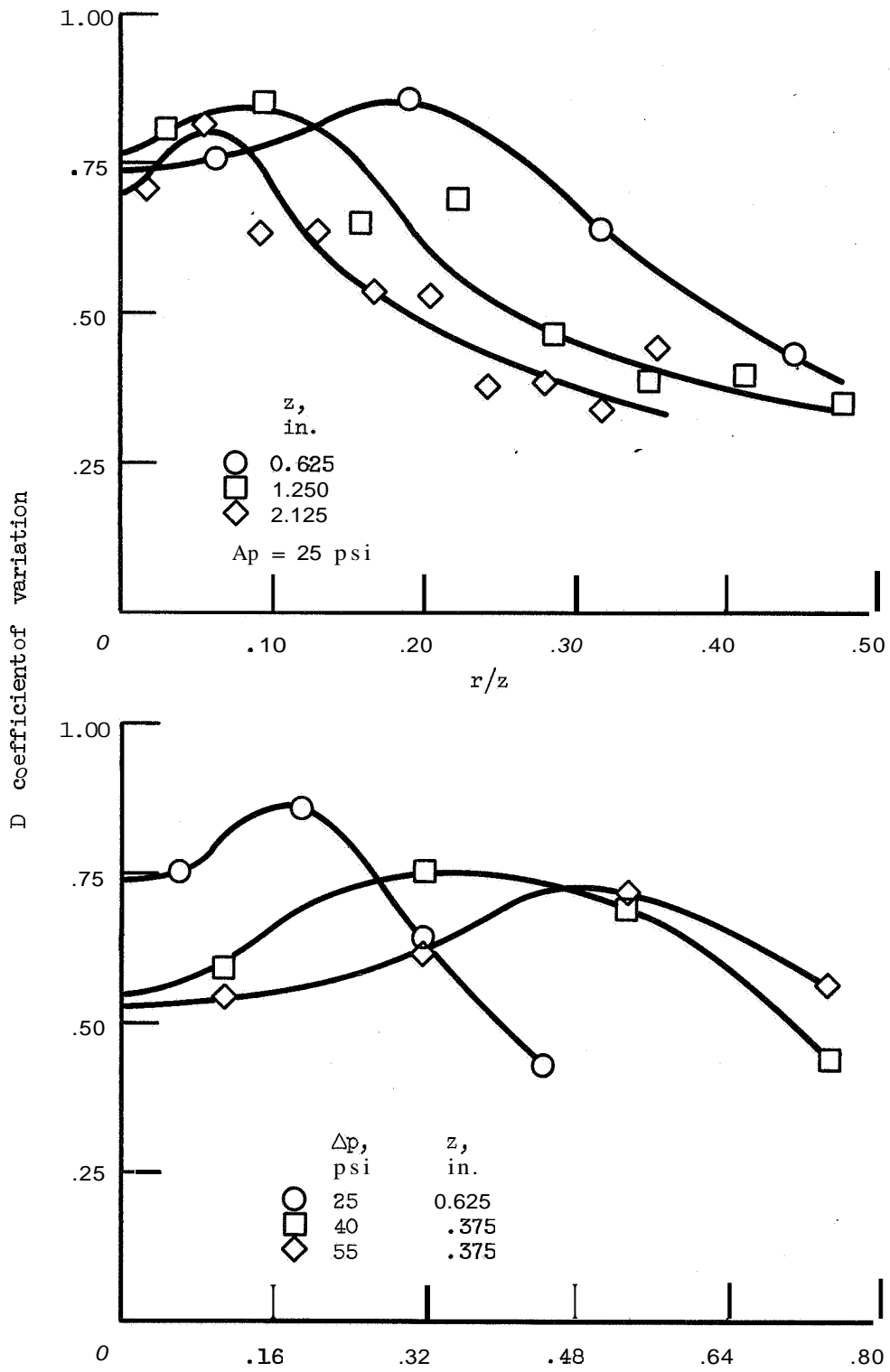


Figure 58. - Diameter coefficient of variation as a function of position and injection pressure.

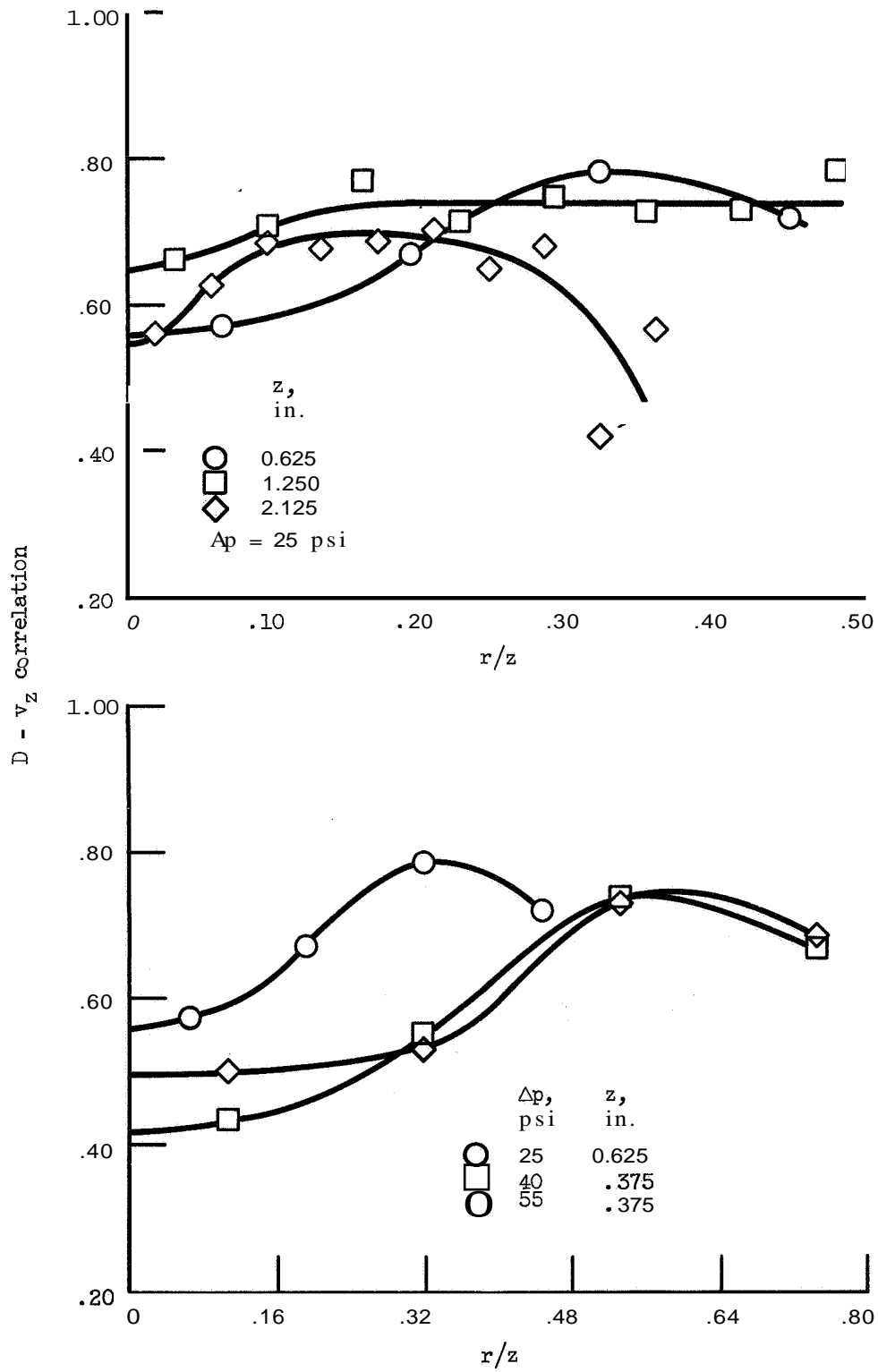


Figure 59. Diameter-axial velocity correlation as a function of position and injection pressure.

TABLE XI. - ONE-DIMENSIONAL MEAN QUANTITIES

Δp , psi	z, in.	$\langle D \rangle$, μ	$\langle v_z \rangle$, in./sec	$\langle v_z \rangle_M$ in./sec	Coefficient of variation of:	
					D	$\langle v_z \rangle$
25	0.625	35	178	358	0.780	0.718
	1.250	36	119	277	.643	.828
	2.125	40	104	193	.557	.713
40	0.375	30	303	455	0.714	0.545
	2.125	35	150	243	.541	.617
55	0.375	28	324	562	0.676	0.670

Δp , psi	z, in.	Skewness of:		ρ_{DV_z}	$\left(\frac{\langle v_z \rangle_M}{\langle v_z \rangle} \right)^{1/3}$	$\frac{\langle v_z \rangle_M}{\langle v_z \rangle_A}$
		D	$\langle v_z \rangle$			
25	0.625	2.35	0.62	0.617	1.26	1.16
	1.250	2.66	1.27	.522	1.33	1.31
	2.125	1.95	1.28	.279	1.23	1.32
40	0.375	1.99	-0.004	0.564	1.15	1.07
	2.125	1.39	1.13	.168	1.12	1.10
55	0.375	1.95	0.36	0.656	1.20	1.11

E. Source Terms Calculated from Measured Density Functions

The present experiment was not designed to specifically evaluate the predictive ability of existing single drop equations as applied to a spray. Precise values of local air velocity were unknown, and droplet temperature was not measured. However, some insight into the vaporization and drag processes is obtained by calculating the source terms and examining their trends and relative magnitudes.

1. Vaporization Terms

The primary equation of interest for vaporization is the continuity equation. For steady flow the difference in the total axial mass flux at two locations must equal the integral of the vaporization rate over the intervening volume:

$$\Delta \left(2\pi \int_0^M \rho_s \langle v_z \rangle r dr \right) = 2\pi \int_{z_1} \int_0 \omega r dr dz \quad (4.17)$$

Due to the ambiguity regarding the exact value of the sampling volume, the absolute magnitudes of mass flux obtained from the left side of Eq. (4.17) are uncertain. However, the relative decrease in mass flux with downstream distance indicates that at $A_p = 25$ psi a mean vaporization rate of 15 to 20% of the initial mass flow rate occurs per inch in the axial direction.

The evaluation of ω is carried out using the measured density functions, the continuity Eq. (1.1), and the empirical correlation Eq. (1.4). Two uncertainties accompany this calculation. The most serious one is due to an ignorance of the droplet temperatures and, consequently, the vaporization constant C_E . Although the mass average temperature for the spray must lie between T_g and T_{LS} , the vapor pressure of ethyl alcohol varies by a factor of 3.5 over this range. There is also an indication that the fluid properties from the literature and Eq. (1.1) may produce a vaporization constant which is too low in the low temperature range (see Fig. A2). The other unknowns are the exact values of local air velocity which effect the convective portion of ω . Values of \underline{u} from the lower bound of the size-velocity data are used in the calculation and are judged to be preferable after review of the detailed behavior of the density functions.*

The ratio of the convective to the stagnant portion of ω for an assumed value of the liquid temperature is given by:

$$\frac{\omega_{con}}{\omega_{stag}} = .3 Sc^{1/3} \left(\frac{\rho_m}{\mu_m} \right)^{1/2} \iint D^{1/2} (\underline{v} - \underline{u})^{1/2} f_B dD d\underline{v} \quad (4.18)$$

* For example, see the low velocity modes of Figs. 36 and 37.

The profiles of this ratio, which are plotted in Fig. 60, are very similar in shape to those for mass average velocity given in Fig. 51. However, it is of interest to note that the velocity averaged with respect to the weighting factor of rate of change of mass, $\langle v_z \rangle_{\dot{M}}$, is lower than $\langle v_z \rangle_M$ by as much as 25% at some locations.

Since the amount of vaporization is relatively small; the momentum and energy source terms due to change of phase, $\omega \langle v_z \rangle_{\dot{M}}$ and $\omega \left\langle \frac{v^2}{2} \right\rangle_{\dot{M}}$, are less than about 20 and 10% of the respective drag terms, $\rho_S \langle v_z \rangle_M$ and $\rho_S \langle v_z v_z \rangle_M$.

The relative contributions of the various drop sizes to vaporization are shown by the one-dimensional density functions for ω as a function of drop size given in Fig. 61. The two modes are the result of the combination of the stagnant and convective portions of ω which have different dependence on D and v . Tabulated values of ω integrated over the cross sections are for $T_L = 500^\circ R$ and so should be considered as only a relative indication. Rough numerical integration of ω over the volume gives a vaporization rate which is too low compared to differences in mass flux. This indicates that the mass average temperature for the spray is considerably higher than the steady-state value.

2. Drag Terms

The integrated form of the one-dimensional, steady-state momentum equation which governs droplet deceleration is:

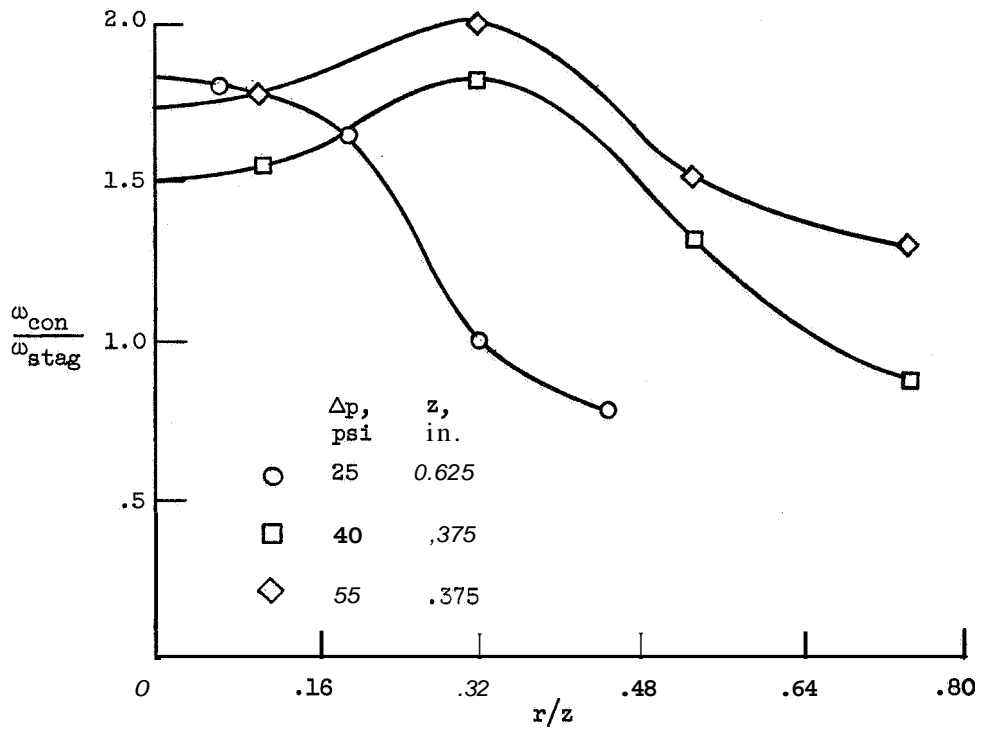
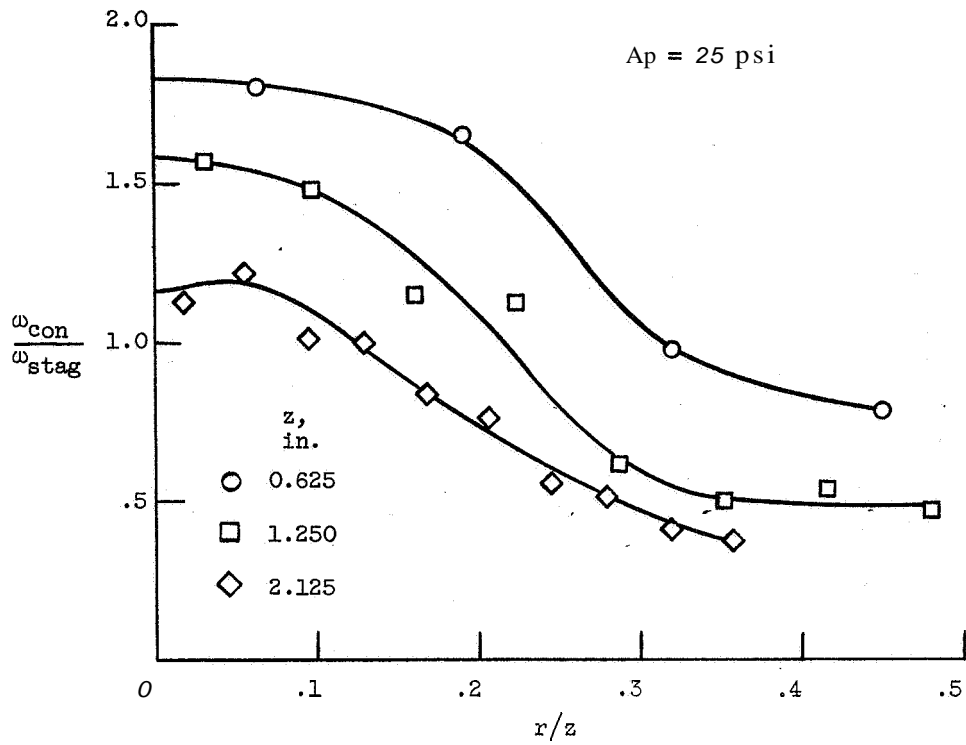


Figure 60. Ratio of convective to stagnant vaporization source terms as a function of position and injection pressure.

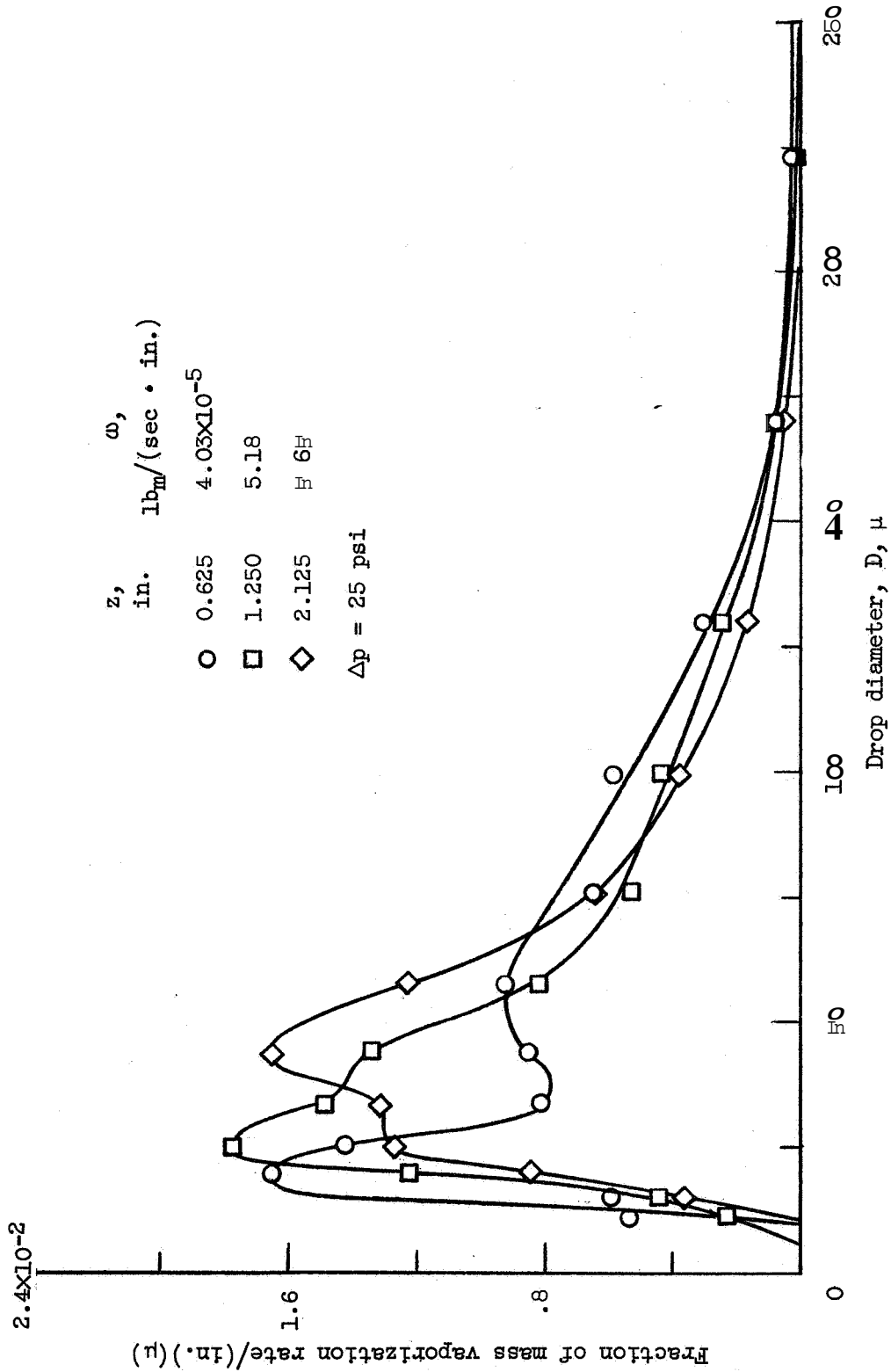


Figure 61. - One-dimensional density functions for the vaporization source as a function of drop size.

$$\Delta \left[2\pi \int_0^\infty \rho_s \langle v_z^2 + v_z v_r \rangle_M r dr \right]$$

$$\int_{z_1}^{z_2} \int_0^\infty \left(\omega \langle v_z \rangle_M + \rho_s \langle \mathcal{A}_z \rangle_M \right) r dr dz \quad (4.19)$$

Neglecting the radial momentum which is transported axially and the liquid momentum lost due to conversion to gas gives:

$$\Delta \left(2\pi \int_0^\infty \rho_s \langle v_z^2 \rangle_M r dr \right)$$

$$= 2\pi \int_{z_1}^{z_2} \int_0^\infty \rho_s \langle \mathcal{A}_z \rangle_M r dr dz \quad (4.19a)$$

The uncertainties in ρ_s again mean that absolute magnitudes of the momentum flux are in doubt. Evaluation of $\rho_s \langle \mathcal{A}_z \rangle_M$ is carried out using the measured $f(D, v_z)$, the motion Eq. (1.2) and Eq. (1.6) for C_D . The two uncertainties in this calculation are the choice of the drag correlation and the values of air velocity used. Use of the alternate drag expressions, Eqs. (1.5), reduces the magnitudes of $\rho_s \langle \mathcal{A}_z \rangle_M$ by about 30% for this data. The values of μ from the lower bound are used as in the case of vaporization.

Profiles of the mass average accelerations are shown in Fig. 62. The minus signs on $\langle \mathcal{A}_z \rangle_M$ indicating that the drops are slowing down have been omitted, and the

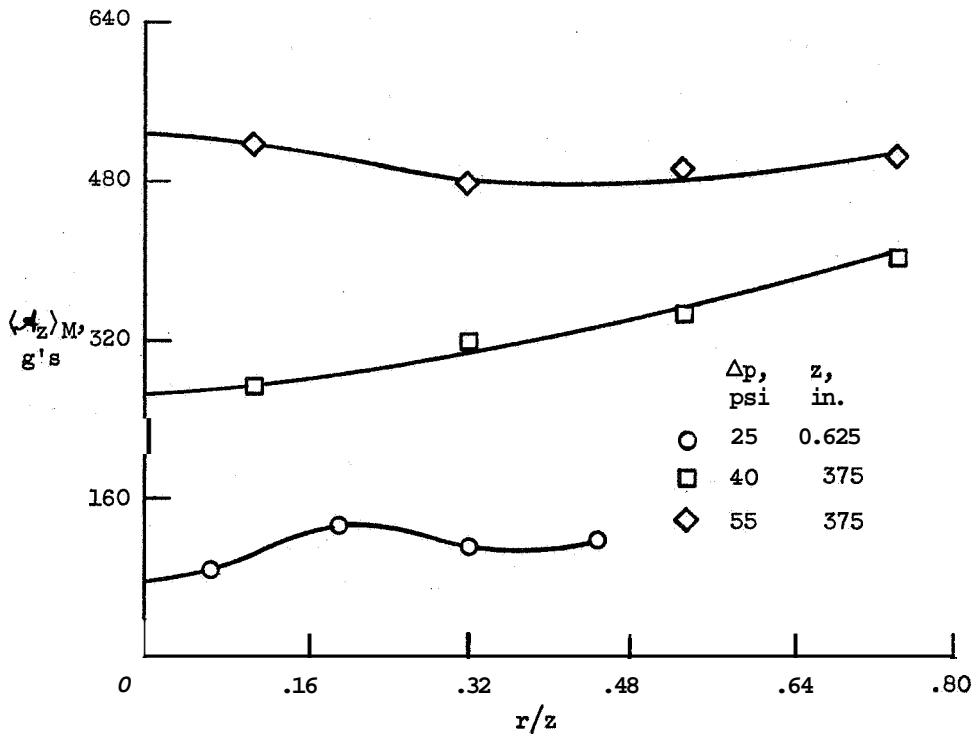
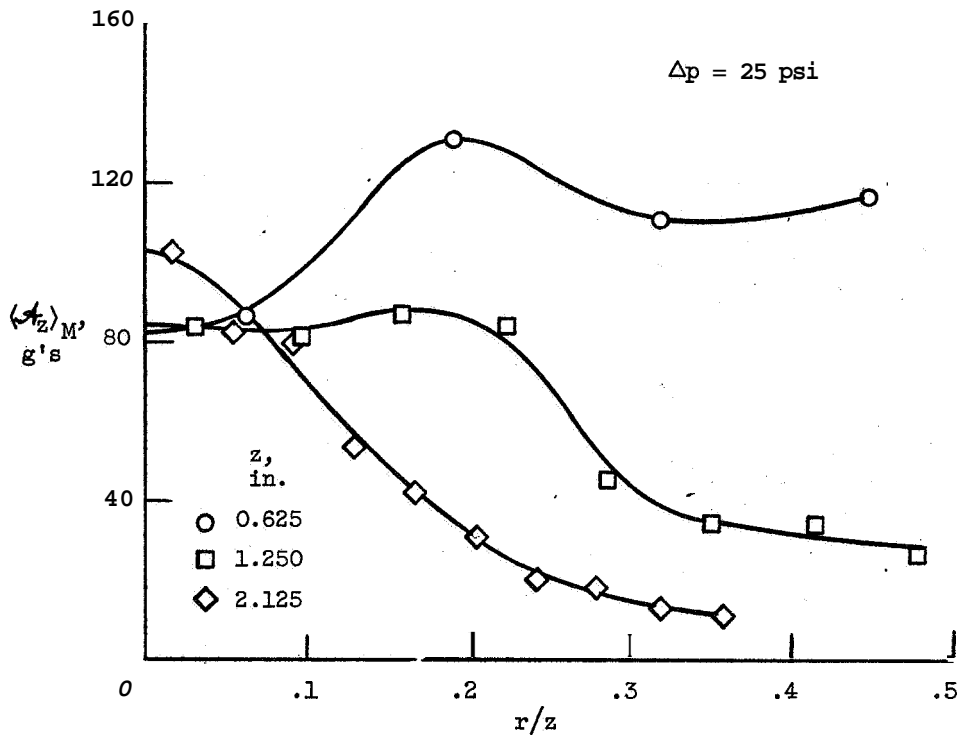


Figure 62. - Mass-average acceleration as a function of position and injection pressure.

units of g's are used to emphasize the unimportance of gravitational forces. The edges of the spray approach velocity equilibrium with the gas at the downstream location, but the dense core requires more time.

One-dimensional density functions for $\rho_s \langle A_z \rangle_M$ as a function of drop velocity are shown in Fig. 63. At higher velocities the curves are somewhat similar to those of Fig. 48 for mass density, but the sharp peaks at low velocity do not appear since they represent drops whose deceleration is complete. Although numerical integrations of $\rho_s \langle A_z \rangle_M$ and $\rho_s \langle v_z^2 \rangle_M$ do satisfy Eq. (4.19a), this does not mean that the drag Eq. (1.6) is preferable to Eqs. (1.5) since values of air velocity were not precisely known.

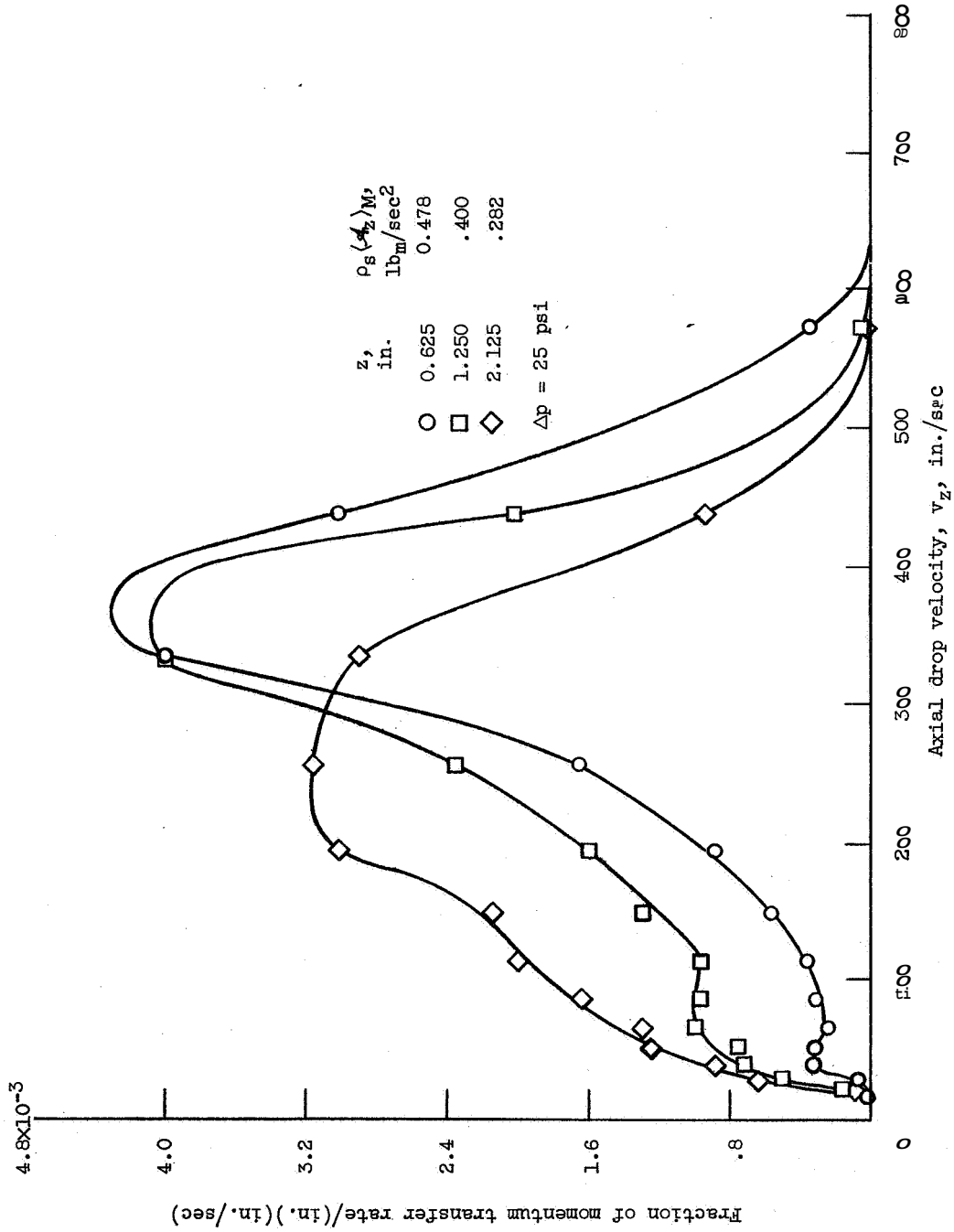


Figure 63. - One-dimensional density functions for the drag source as a function of drop velocity.

Chapter V
SUMMARY AND CONCLUSIONS REGARDING
STATISTICAL SPRAY DESCRIPTION

A. Summary of the Investigation

1. Conceptual and Physical Background

In order to provide a definite framework for a discussion of spray description some basic definitions are given. A spray is defined as a collection of liquid droplets each of whose mass and dynamic behavior can be adequately described with reference to one characteristic size dimension. The spray is said to be formed at downstream locations constituting a "surface of formation" where highly aspherical shapes are rare. Quantitative characterization of a spray at the surface of formation, prediction of these characteristics from a knowledge of injection parameters, and determination of the downstream behavior are called, respectively: the description, formation and propagation problems.

A solution to the description problem begins with the choice of the droplet variables as size, velocity, position, and temperature; and the recognition that a coordinated description of the gas phase must be included. Physical evidence of the random nature of spray processes is reviewed for the purpose of showing that the droplet variables must be considered as distributed in a statistical sense. Particular emphasis is placed on the role of

drop velocity and its treatment on an equal statistical basis with drop size. A review of established single droplet behavior shows the kind of information which must be built into a spray model. It also points out the uniqueness of each droplet history as related to its initial size, velocity, and temperature at formation and to the properties of the surrounding gas through which it travels. Spray observations confirm that the random formation processes are distributed in space. This indicates that at the surface of formation, individual drops have a range of ages and have experienced different environments. For these reasons it is concluded that drop velocities, sizes, and in all probability, droplet temperatures should be considered as being distributed over a range of values at any position in the spray.

2. The Theoretical Model

A theoretical treatment which embodies these ideas is available from an adaptation of molecular statistical mechanics. The key quantity in the theory is the spray density function which specifies the statistical distribution of the variables describing the dynamic state of a droplet. In the present investigation the droplet internal energy in terms of liquid temperature is included in addition to size, velocity, and position in order to complete the incorporation of existing single drop theory and data into the statistical model.

A theoretical basis for the study of spray propagation is presented in the equations of change for the spray density function. The most fundamental relationship is the spray transport equation which is the analog of the Boltzmann equation of molecular statistical mechanics. From this continuity equation for the spray density function, equations of change for liquid mass, momentum, and energy are developed in terms of average spray variables which are functions of only position and time. These equations are the liquid phase counterparts of the more familiar equations for the gas phase. The two sets are coupled by interphase transport terms which disappear when corresponding equations for liquid and gas are added to obtain the equations for the overall mixture. At several places in the development the similarities and differences between the molecular and spray situations are pointed out.

Approaches to applying the propagation theory are reviewed in terms of existing and required experimental information. The two types of size data available, spatial and flux drop size distributions, are related to the general spray density function, and their physical interpretations are discussed. Required experimental information is concluded to be the spray density function at the surface of formation or initial values of mean spray quantities defined by the equations of change.

3. Measurement Methods and Results

The experimental technique of double-exposure, fluorescent photography, which **was** developed to measure individual drop sizes and velocities at known locations in a spray, is discussed. Application of this method to an unconfined spray formed by steady injection of ethyl alcohol through a swirl atomizer is explained. The **two** kinds of samples taken are: (a) traverses near the surface of formation over a small range of injection pressure to show formation characteristics, and (b) surveys at two distances farther downstream to indicate propagation characteristics. Measurements of the size and velocity of more than 32,000 drops form the raw data from which bivariate, size-velocity density functions are constructed as a function of position.

Quantities calculated from these experimental density functions include: (a) bivariate mass densities, (b) marginal mass densities as a function of size (the spatial drop size distribution), (c) marginal mass densities as a function of velocity, (d) mass flux as a function of size (the flux drop size distribution), (e) one-dimensional forms of all these density functions obtained by integration over the spray cross section, (f) profiles of mean spray quantities obtained by integrating over size and velocity, and (g) spray vaporization and drag terms using the single drop expressions.

The most important results are summarized schematically in Fig. 64. For the situation existing in the present study where the mean velocity at the exit of the atomizer, v_E , is greater than the ambient air velocity, u ; Fig. 64(a) illustrates the situation. Each contour plot of the mass density surface in the size-velocity plane is accompanied by the marginal density functions of D or v alone obtained by integration over one of the two variables. The mass density as a function of D is the traditional spatial drop size distribution measured by photographic methods, while the counterpart as a function of velocity has not been measured previously. The relationship between these two distributions is also noted for each case. Since no vaporization is considered, the mass flux as a function of drop size must propagate unchanged.

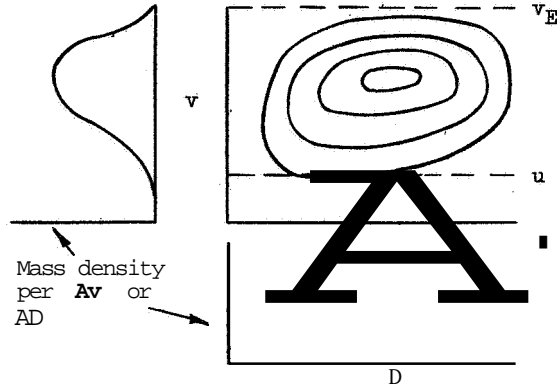
Immediately after formation one large "hill" forms the mass density surface. It is slightly distorted at smaller sizes and velocities by the deceleration process which has already begun for the oldest of the smaller droplets. Droplet mass per unit spatial volume is definitely distributed with respect to velocity to as great a degree as with respect to size. Note that the mass average velocity is less than injection velocity due to dissipation in the break-up process. The expected value of velocity at any size is approximately constant. This means that the mass flux distribution is simply this constant times the mass density.

Stage of spray development

contours of
droplet mass density
(Δv) (ΔD)

Relationship of spatial
to flux drop size
distributions

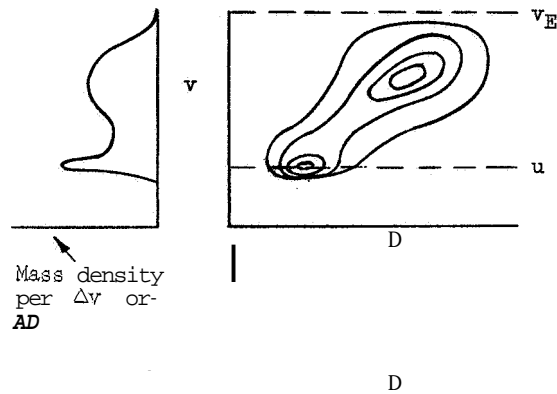
Formation



$$\langle v|D \rangle \approx \text{constant} = v_0$$

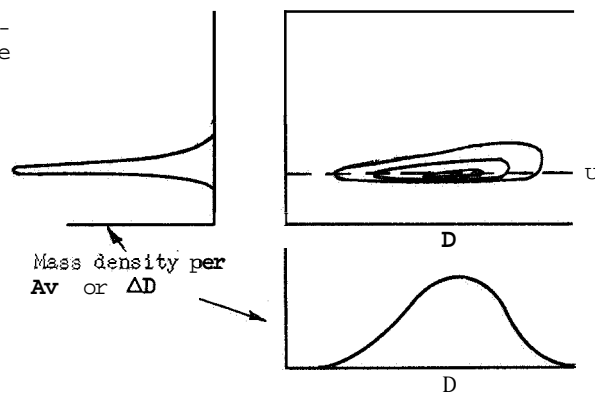
$$f_F \approx v_0 f_S$$

Intermediate
propagation



$$f_F = \langle v|D \rangle f_S$$

Near equilib-
rium with the
gas



$$\langle v|D \rangle \approx u$$

$$f_F \approx u f_S$$

(a) Injection into a lower velocity gas, $v_E > u$.

Figure 64. Schematic formation-propagation characteristics of mass density functions with no vaporization.

At an intermediate condition where considerable gas-drop interaction has occurred, selective deceleration according to size has divided the original "hill" into two peaks connected by a ridge. Consequently, the marginal densities are bimodal. The original single formation mode had diminished; the spatial density of small drops has increased with respect to larger drops; and a sharp peak has formed at the gas velocity. Average values of drop velocity at any size now vary greatly with size. In fact, the shape of the $\langle v|D \rangle$ curve is exactly the form that will transform the bimodal spatial mass distribution back into the original unimodal mass flux distribution.

Finally, if the gas velocity is nearly constant, a location far downstream may be found where the spray and gas are near velocity equilibrium. Nearly all of the drops have approached gas velocity forming a long, narrow, and very high peak. Since $\langle v|D \rangle \approx u$, the flux distribution differs from the spatial distribution by simply this constant multiplier.

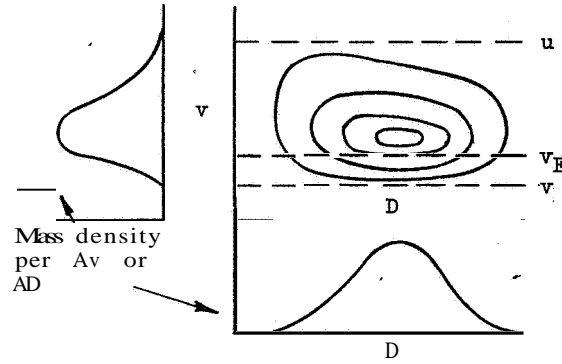
Reasoning from Fig. 64(a), the corresponding curves for the case of injection into a higher velocity gas stream can be constructed as shown in Fig. 64(b). Since measurements were not made on a spray under these conditions, some details may be missing; but the overall behavior is illustrated. The situation is one of acceleration during propagation; and as always, small drops

Stage of spray development

Contours of droplet mass density $(\Delta v)(AD)$

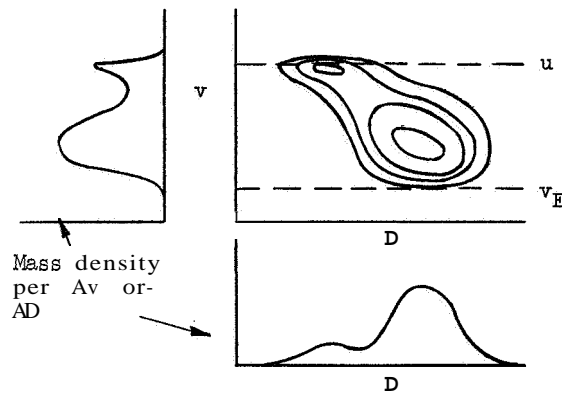
Relationship of spatial to flux drop size distributions

Formation



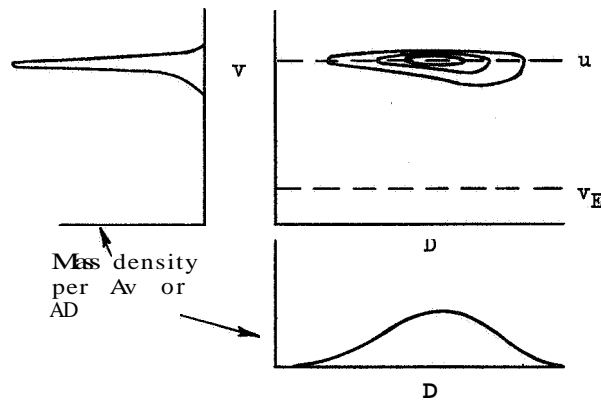
$\langle v|D \rangle \approx \text{constant} = v_0$
 $f_F \approx v_0 f_S$

Intermediate propagation



$f_F = \langle v|D \rangle f_S$

Near equilibrium with the gas



$\langle v|D \rangle \approx u$
 $f_F \approx u f_S$

(b) Injection into a higher velocity gas, $v_E < u$.

Figure 64. - Concluded.

are the most responsive. Contours of the mass density are inverted with respect to the velocity axis compared to Fig. 64(a). At the intermediate condition the spatial density of small drops decreases compared to large drops which continue to move more slowly.

When substantial vaporization is present, removal of liquid mass, which is greatest in the low-to-medium size range, will distort the entire picture; and the flux distribution no longer propagates unchanged.

Profiles of mean quantities, of course, reflect in a gross manner the detailed behavior just reviewed. However, in the case of bimodal density functions, it becomes very difficult to extract the physical picture from the single set of means representing combined characteristics.

B. Conclusions and Their Implications

1. Spray Data and Its Interpretation

DROP VELOCITY IN A SPRAY IS A STATISTICALLY DISTRIBUTED VARIABLE THE KNOWLEDGE OF WHICH IS EQUALLY IMPORTANT TO DROP SIZE. Without such information to fix the dynamic state of the spray, little insight into formation or propagation mechanisms can be gained. For example, the processes which produce bimodal density functions can only be conjectured; and calculations of liquid mass or momentum transport rest on questionable, assumed values of mean velocity.

THE CHARACTERISTICS OF THE BIVARIATE, 'SIZE-VELOCITY DENSITY FUNCTION ARE STRONGLY DEPENDENT ON POSITION WITH

THE KEY FEATURE DETERMINING THE VARIATIONS BEING THE AMOUNT OF DROPLET-GAS INTERACTION THAT HAS OCCURRED. An extremely wide range of shapes and modal conditions of the spatial distribution can be found in the same spray simply by sampling at different locations. Unless the sampling conditions are clearly specified, no basis for the comparison of spatial drop size data exists.

IN MANY CASES THE DIFFERENCES IN THE SHAPE AND MODAL CHARACTERISTICS OF SPATIAL AND FLUX DISTRIBUTIONS ARE LARGE. Only in very special situations where the spray approaches velocity equilibrium with the gas are photographic and collection data equivalent. The flux distribution implicitly contains drop velocity information although it is not readily extractable without some additional data on spatial densities. In cases where vaporization is negligible, the shape of the one-dimensional flux distribution indicates whether or not drops were actually formed with more than one mode with respect to size.

Failure to recognize the significance of velocity, the degree of spatial dependence, and the distinction between densities and fluxes has led to much confusion in interpreting spray data. It is understandable that no general agreement exists as to the most useful empirical equation to fit measured distributions. If data representing a myriad of spray situations are lumped together

to obtain a "general" correlation, the most versatile equation (usually the one with the largest number of parameters) is bound to give the best fit. The actual generality and usefulness of such a correlation are questionable. Statistical sampling uncertainties are always present, but all inconsistencies in data should not be assigned to this catch-all excuse. Basic differences in the physical situations which the data represent are factors which deserve equal scrutiny.

2. Analytic Description of Spray Situations

In its present stage of analytical development, the primary usefulness of the statistical mechanical formalism is as a conceptual aid to organizing the attack on spray problems. The reduction of the general spray transport equation to equations of change provides a unified treatment of the gas and liquid phase dynamics. Resultant mean spray quantities defined on a physical basis can then be associated with the traditional statistical moments defined strictly in terms of mathematical operations.

Two barriers to realistic solutions of spray propagation problems exist. Mathematically, the available solutions to transport problems similar to the one posed by the spray equation are few and of very restricted form. Numerical methods appear to be a necessary-resort since analytically simplifying assumptions such as Stokes Law

drag or stagnant vaporization cannot represent many spray situations of practical interest. The other impediment is the ignorance of initial conditions in the form of the spray density function in the case of the general spray equation or the mean quantities in cases where integrated equations of change are used.

3. Suggestions for Future Experiments

The significance of the spray density function measured at the surface of formation justifies further experimental efforts to measure it for a wider range of injection parameters. In addition to providing initial conditions for propagation calculations, such information is necessary for new efforts to develop a theory of spray formation. More quantitative criteria for locating the surface of formation are desirable extensions of past break-up length studies.

Methods of measuring spray droplet temperatures need to be developed so that its inclusion as a random variable in the spray density function can be verified.

The characterization of gas properties in a spray deserves more attention. Reliable values of local gas velocities and temperatures are required before definite conclusions can be drawn about the ability to calculate local vaporization rates and droplet concentrations.

Time variations in the spray properties remain largely unexplored. Unsteady spray density functions,

even for size alone, have rarely been measured; and a knowledge of continuous time histories under steady-state conditions would shed light on the ergodic problem and the possible excitation of resonant phenomena by spray fluctuations.

At present, the general spray density function is too difficult to measure and contains more information than can be readily handled in practical applications. Use of the mean spray properties in the form of overall macroscopic balances obtained from the equations of change seems to be a more expedient design or development approach. However, such methods can only be implemented if experimental techniques are developed to measure mean spray properties, such as the spray density, directly without resorting to individual drop measurements.

The problem of obtaining reliable experimental estimates of statistical quantities suggests the development of more automated data collection and reduction techniques so that larger samples can be obtained. It should be realized, however, that complex hardware may tend to obscure the familiar experimental calibration difficulties. Television cameras have recording thresholds and exposure characteristics affecting the apparent particle size just as film does. Flying-spot film scanners require careful monitoring of signal clipping levels to

realize the possible, but not automatic, advantage of consistency over manual measurements. At **times** it may be preferable to sacrifice quantity and rapidity **for** the sake **of** directly examining an additional droplet variable.

APPENDIX A: Supplementary Information Pertaining to the Calculation of Ethyl Alcohol Drop Histories in Air at Atmospheric Pressure.

1. Fluid Properties

Film Averages: Equations must be defined for averages of thermodynamic and transport properties over the vapor-gas mixture in the film surrounding a drop.

The following notation is used:

B = an arbitrary property

c = concentration of a constituent

Subscripts:

f = vaporizing fluid

g = gas property at a great distance from a drop

I = value at the liquid-gas interface

m = mean value defined over the film

Define an arithmetic mean:

$$B_m = \frac{1}{2} (B_I + B_g)$$

If a binary mixture rule $B = c_g B_g + c_f B_f$ is used where

$c_f = p_{fL}/p$ and $c_g = 1 - p_{fL}/p$:

$$B_I = \left(1 - \frac{p_{fL}}{p}\right) B_g + \frac{p_{fL}}{p} B_f$$

From the definition of B_m :

$$B_m = \left(1 - \frac{p_{fL}}{2p}\right) B_g + \frac{p_{fL}}{2p} B_f \quad (\text{A.1})$$

Thus, the expressions used were

$$\mu_m = \left(1 - \frac{p_{fL}}{2p}\right) \mu_g + \frac{p_{fL}}{2p} \mu_f \quad (\text{A.2a})$$

$$k_m = \left(1 - \frac{p_{fL}}{2p}\right) k_g + \frac{p_{fL}}{2p} k_f \quad (\text{A.2b})$$

$$M_m = \left(1 - \frac{p_{fL}}{2p}\right) M_g + \frac{p_{fL}}{2p} M_f \quad (\text{A.2c})$$

M = molecular weight

$$C_{pm} = \left(1 - \frac{p_{fL}}{2p}\right) \frac{M_g}{M_m} C_{pg} + \frac{p_{fL}}{2p} \frac{M_f}{M_m} C_{pf} \quad (\text{A.2d})$$

$$T_m = \frac{T_g + T_L}{2} \quad (\text{A.2e})$$

$$\rho_m = \frac{p M_m}{R T_m} \quad (\text{A.2f})$$

D_v , μ_g , μ_f , k_g , k_f , C_{pg} , C_{pf} are evaluated at T_m and p_{fL} , ρ_L , C_{pL} , h_{fL} , σ are evaluated at T_L .

Ethyl Alcohol Properties: units are lb_m, in., sec, BTU, °R

Diffusivity for C₂H₅OH - Air (Ref. 51)

$$D_v = 0.01581 \left(\frac{T}{491.69}\right)^2 \quad (\text{A.3a})$$

Viscosity of vapor (Ref. 52)

$$\mu_f = \frac{49.08388 \times 10^{-9} \sqrt{T}}{1 + \frac{733.14}{T}} \quad 490 \leq T \leq 800 \text{ } ^\circ\text{R} \quad (\text{A.3b})$$

Thermal conductivity of vapor (Ref. 51)

$$k_f = -1.1435 \times 10^{-6} + 4.1063 \times 10^{-9} T - 2.9979 \times 10^{-12} T^2 \quad (\text{A.3c})$$

490 ≤ T ≤ 690 °R Parabola through 3 points

Liquid density (Refs. 51, 53)

$$\rho_L = 3.4382 \times 10^{-2} - 5.0887 \times 10^{-6} T - 1.1399 \times 10^{-8} T^2 \quad (\text{A.3d})$$

$$490 \leq T \leq 660 \text{ } ^\circ\text{R} \quad \text{least squares fit to data,} \\ \text{standard error} = 7.676 \times 10^{-6}$$

Vapor pressure (Refs. 51, 53)

$$\ln p_{fL} = 14.358 - \frac{6004.9}{T} - \frac{8.7297 \times 10^{-5}}{T^2} \quad (\text{A.3e})$$

$$490 \leq T \leq 650 \text{ } ^\circ\text{R} \quad \text{least squares fit to data}$$

Specific heat of liquid (Ref. 54)

$$C_{pL} = 0.90377 - 2.2858 \times 10^{-3} T + 3.1481 \times 10^{-6} T^2 \quad (\text{A.3f})$$

$$490 \leq T \leq 670 \text{ } ^\circ\text{R}$$

Specific heat of vapor (Ref. 55)

$$C_{pv} = 0.10729 + 5.9155 \times 10^{-4} T - 1.59711 \times 10^{-7} T^2 \\ + 1.67376 \times 10^{-11} T^3 \quad (\text{A.3g})$$

$$490 \leq T \leq 890 \text{ } ^\circ\text{R}$$

Latent heat of vaporization (Ref. 54)

$$h_{fL} = -5.3966 \times 10^{-4} T'^2 + 0.52499 T' + 61.5519 T'^{1/4} \quad (\text{A.3h})$$

$$T' = 923.69 - T$$

$$490 \leq T \leq 655 \text{ } ^\circ\text{R}$$

Surface tension: $\text{C}_2\text{H}_5\text{OH} - \text{Air}$ (Ref. 51)

$$\sigma = 1.31652 \times 10^{-3} T'' - 1.73778 \times 10^{-3} T''^2 \\ + 7.93007 \times 10^{-4} T''^2 \quad (\text{A.3i})$$

where $T'' = 1 - \frac{T}{929.16}$

Air properties (Ref. 56) units lb_M, in., sec, Btu, °R

Specific heat

$$C_{pg} = 0.24061485 \cong T \cong 550 \text{ °R} \pm 0.2\%$$

viscosity

$$\mu_g = \frac{60.8540 \times 10^{-9} T^{3/2}}{T + 198.72} \quad (\text{A.3j})$$

Thermal conductivity

$$k_g = \frac{2.6382 \times 10^{-8} T^{1/2}}{1 + \frac{441.72 \times 10^{-21.6/T}}{T}} \quad (\text{A.3k})$$

2. Steady State Temperature, T_{LS}

Steady-state temperatures were calculated for a range of air temperatures by iteration on Eq. (1.8) using the temperature dependent property expressions listed above. The results are shown in Fig. A1 along with measured values from the literature.

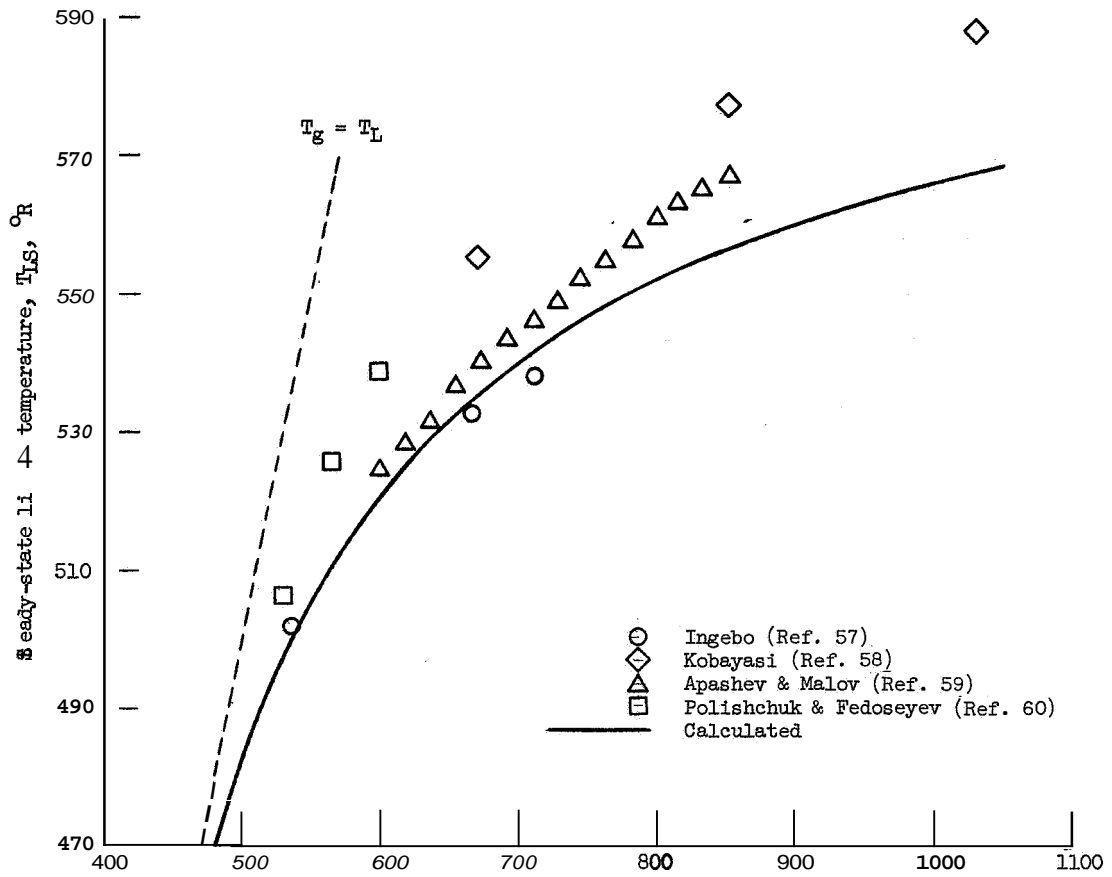
3. Equilibrium Vaporization Constant, C_E

If the relative velocity between the drop and gas is zero and the liquid is at the steady-state temperature, the continuity Eq. (1.1) may be integrated to give:

$$D^2 = D_0^2 - C_E t \quad \text{for } \underline{v} - \underline{u} = 0 \quad \text{and} \quad T_L = T_{LS} \quad (\text{A.4})$$

where:

$$C_E = \frac{8D_v p_f L}{R_f T_M \rho_L} \quad (\text{A.5a})$$



An alternate expression for C_E is obtained under the same assumptions by integrating the energy Eq. (1.3):

$$C_E = \frac{8k_m(T_g - T_{LS})\xi}{\rho_L \lambda} \quad (A5b)$$

Calculated values are compared with some data from the literature in Fig. A2. The calculation is particularly sensitive to T_{LS} through p_{fL} .

4. Calculation of Ethyl Alcohol Drop Histories

The three first order nonlinear differential equations, (1.1) to (1.3) were integrated numerically on a digital computer using a Runga-Kutta technique. Equations for the empirical correlations (1.4 to 1.7), film means (A.2), and temperature dependent fluid properties (A.3) were included. Over the small range from room temperature down to the steady-state liquid temperature ($500 \leq T \leq 535^\circ \text{R}$), by far the most important property variation is the vapor pressure ($0.315 \leq p_{fL} \leq 1.08 \text{ psi}$). The factors a and ξ differ from 1.0 by less than 4% and 8%, respectively.

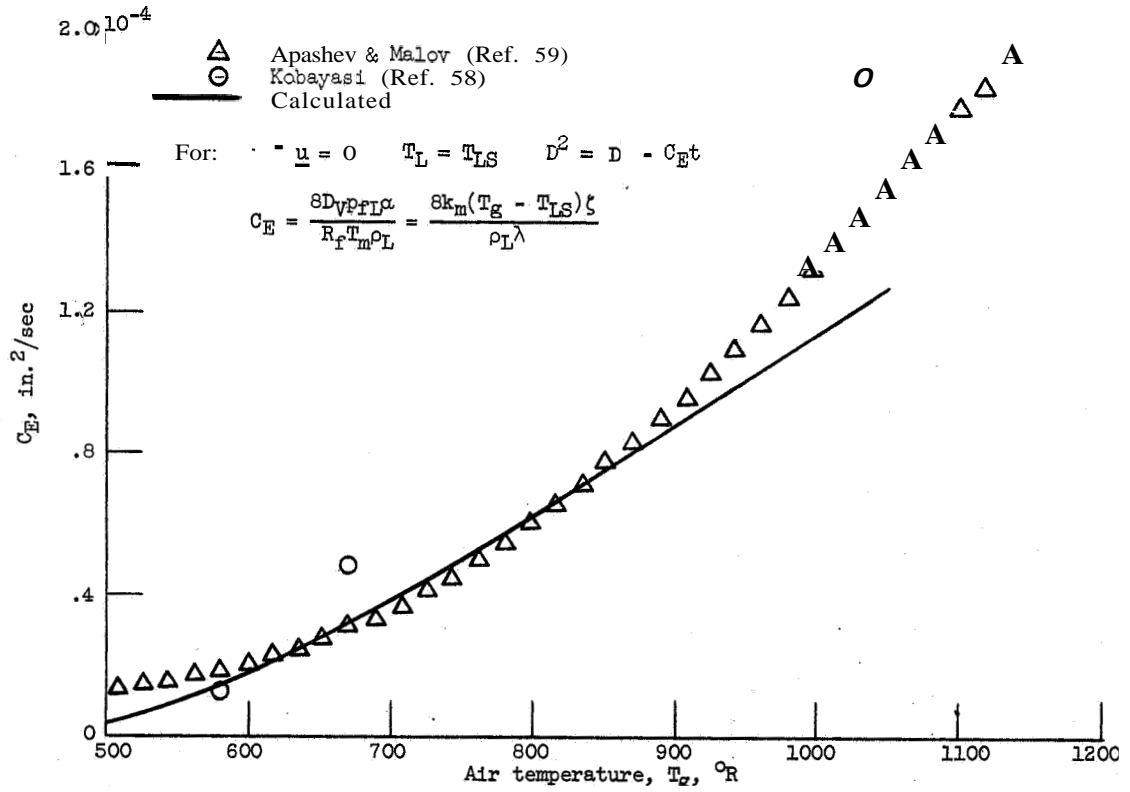


Fig. A2. - Vaporization Constant for Ethyl Alcohol Droplets as a Function of Air Temperature.

APPENDIX B: Manipulations of Equations Involving the Density Function $f(\Gamma_i, t)$ For Droplets..

1. Outline of a Derivation of the Continuity Equation for f

Consider a property $f(\Gamma_i, t)$ of a system which has the characteristics of a generalized density in the i dimensional space of Γ_i (e.g., number of drops per unit Γ_i).

Let:

$d\Gamma_i$ = the volume element of a volume V fixed in Γ_i space

dS = the surface area element of the surface S which encloses V

n_i = the i th component of the outwardly directed unit vector normal to any point on S

$\lambda(\Gamma_i, t)$ = sources of the quantity described by f inside V (e.g., number of drops created per unit Γ_i per unit time)

The conservation of f in V requires that:

$$\frac{d}{dt} \int_V f d\Gamma_i = - \int_S f \Gamma_i n_i dS + \int_V \lambda d\Gamma_i$$

$$\left\{ \begin{array}{l} \text{rate of change of} \\ f \text{ inside } V \end{array} \right\} = \left\{ \begin{array}{l} \text{net flux of } f \text{ for } \\ \text{into } V \text{ through } S \end{array} \right\} + \left\{ \begin{array}{l} \text{internal} \\ \text{sources} \end{array} \right\}$$

Applying generalized forms of Leibnitz formula for differentiating an integral and the divergence theorem for converting surface integrals to volume integrals:

$$\int_V \frac{\partial f}{\partial t} d\Gamma_i = - \int_V \frac{\partial}{\partial \Gamma_i} (f \dot{\Gamma}_i) d\Gamma_i + \int_V \dot{\Gamma}_i d\Gamma_i$$

Since the volume V is arbitrary, the integrals may be removed and Eq. (2.4) results:

$$\frac{\partial f}{\partial t} + \frac{\partial(\dot{\Gamma}_i f)}{\partial \Gamma_i} = \dot{\Gamma}_i \quad (2.4)$$

2. Derivation of the Equation of Change for $\psi_j(D, \underline{v}, T_L)$, Eq. (2.6), From the Equation of Change for $f(D, \underline{x}, \underline{v}, T_L, t)$, Eq. (2.5).

The terms resulting from the multiplication of Eq. (2.5) by ψ_j and integration are:

$$\text{i. } \iiint \psi_j \frac{\partial f}{\partial t} dD d\underline{v} dT_L = \frac{\partial}{\partial t} \iiint \psi_j f dD d\underline{v} dT_L - \iiint f \frac{\partial \psi_j}{\partial t} dD d\underline{v} dT_L$$

The underlined term vanishes since ψ_j is not a function of time t : $\frac{\partial \psi_j}{\partial t} = 0$

$$\text{ii. } \iiint \psi_j (\nabla_{\underline{x}} \cdot \underline{v} f) dD d\underline{v} dT_L = \nabla_{\underline{x}} \cdot \iiint \psi_j \underline{v} f dD d\underline{v} dT_L - \iiint (\underline{v} f \cdot \nabla_{\underline{x}} \psi_j) dD d\underline{v} dT_L$$

The underlined term vanishes since ψ_j is not a function of \underline{x} : $\nabla_{\underline{x}}\psi_j = 0$

$$\begin{aligned}
 \text{iii. } & \iiint \psi_j \frac{\partial}{\partial D} (\mathcal{D}f) dD d\underline{v} dT_L \\
 &= \iiint \frac{\partial}{\partial D} (\psi_j \mathcal{D}f) dD d\underline{v} dT_L - \iiint \mathcal{D}f \frac{\partial \psi_j}{\partial D} dD d\underline{v} dT_L \\
 &= \underline{\iint (\psi_j \mathcal{D}f) \Big|_{D_{\min}}^{D_{\max}} d\underline{v} dT_L} - \iiint \mathcal{D}f \frac{\partial \psi_j}{\partial D} dD d\underline{v} dT_L
 \end{aligned}$$

The underlined term vanishes since the product $\psi_j \mathcal{D}f$ vanishes at the limits of D if ψ_j is dependent on D to at least the first power. For ψ_j independent of D , $\mathcal{D}f$ may be finite at the lower limit of D .

$$\begin{aligned}
 \text{iv. } & \iiint \psi_j (\nabla_{\underline{v}} \cdot \underline{\mathcal{A}}f) dD d\underline{v} dT_L \\
 &= \iiint \nabla_{\underline{v}} \cdot (\psi_j \underline{\mathcal{A}}f) dD d\underline{v} dT_L - \iiint (\underline{\mathcal{A}}f \cdot \nabla_{\underline{v}} \psi_j) dD d\underline{v} dT_L \\
 &= \underline{\iint (\psi_j \underline{\mathcal{A}}f) \Big|_{\underline{v}=-\infty}^{\underline{v}=\infty} dD dT_L} - \iiint (\underline{\mathcal{A}}f \cdot \nabla_{\underline{v}} \psi_j) dD d\underline{v} dT_L
 \end{aligned}$$

The underlined term vanishes since the product $\psi_j \underline{\mathcal{A}}f$ vanishes at the limits of \underline{v} .

$$\begin{aligned}
v. \quad & \iiint \psi_j \frac{\partial}{\partial T_L} (\mathcal{E}f) dD \, d\underline{v} \, dT_L \\
& = \iiint \frac{\partial}{\partial T} (\psi_j \mathcal{E}f) dD \, d\underline{v} \, dT_L - \iiint \mathcal{E}f \frac{\partial \psi_j}{\partial T} dD \, d\underline{v} \, dT_L \\
& = \underbrace{\iint (\psi_j \mathcal{E}f) \Big|_{T_{\min}}^{T_{\max}} dD \, d\underline{v}} - \iiint \mathcal{E}f \frac{\partial \psi_j}{\partial T_L} dD \, d\underline{v} \, dT_L
\end{aligned}$$

The underlined term vanishes since the product $\psi_j \mathcal{E}f$ vanishes at the limits of T_L .

3. Derivation of the Equation of Change for the Spatial Drop Size Distribution.

Following the procedure of the previous section with the exception that the integral over D is not carried out gives:

$$\begin{aligned}
\frac{\partial}{\partial t} \iint \psi_j f \, d\underline{v} \, dT_L + \nabla_{\underline{x}} \cdot \iint \psi_j \underline{v} f \, d\underline{v} \, dT_L \\
= \iint \psi_j \frac{\partial}{\partial D} (\mathcal{D}f) d\underline{v} \, dT_L + \iint (\mathcal{A}f \cdot \nabla_{\underline{v}} \psi_j) d\underline{v} \, dT_L \\
+ \iint \mathcal{E}f \frac{\partial \psi_j}{\partial T_L} d\underline{v} \, dT_L \quad (B.1)
\end{aligned}$$

For $\psi_j = 1$ and using the definition of f_S and \underline{f}_F from Eqs. (2.24) and (2.25):

$$\frac{\partial f_S}{\partial t} + \nabla_{\underline{x}} \cdot \underline{f}_F = \iint \frac{\partial}{\partial D} (\mathcal{D}f) d\underline{v} \, dT_L \quad (B.2)$$

For steady-state conditions and $\mathcal{D} = 0$:

$$\nabla_{\underline{x}} \cdot \underline{f}_F = 0 \quad (4.12)$$

4. Derivation of the Equation of Change for the Marginal Number Density as a Function of Velocity.

Again, by taking moments of Eq. (2.5) for f but, in this case, not integrating over \underline{v} gives:

$$\begin{aligned}
 \frac{\partial}{\partial t} \iint \psi_j f \, dD \, dT_L + \underline{\nabla}_{\underline{x}} \cdot \iint \psi_j \underline{v} f \, dD \, dT_L \\
 = \iint \mathfrak{D} f \frac{\partial \psi_j}{\partial D} \, dD \, dT + \underline{\nabla}_{\underline{v}} \cdot \iint (\psi_j \underline{\mathcal{A}} f) \, dD \, dT_L \\
 + \iint (\underline{\mathcal{A}} f \cdot \underline{\nabla}_{\underline{v}} \psi_j) \, dD \, dT_L + \iint \mathcal{F} f \frac{\partial \psi_j}{\partial T} \, dD \, dT_L
 \end{aligned} \tag{B.3}$$

For $\psi_j = 1$ and defining a spacial distribution as a function of \underline{v} :

$$\frac{\partial f_{SV}}{\partial t} + \underline{v} \cdot \underline{\nabla}_{\underline{x}} f_{SV} = \iint \mathfrak{D} f \, dD \, dT_L + \underline{\nabla}_{\underline{v}} \cdot \iint \underline{\mathcal{A}} f \, dD \, dT_L \tag{B.4}$$

where:

$$f_{SV} = \iint f \, dD \, dT_L$$

For steady-state conditions and $\mathfrak{D} = 0$:

$$\underline{v} \cdot \underline{\nabla}_{\underline{x}} f_{SV} = \underline{\nabla}_{\underline{v}} \cdot \iint \underline{\mathcal{A}} f \, dD \, dT_L \tag{B.5}$$

APPENDIX C: Manipulations of Average Quantities

1. Alternate Form of the Terms $\omega \left\langle \frac{v^2}{2} + c_{pL} T_L \right\rangle_M$ and $\rho_s \langle c_{pL} \mathcal{E} \rangle_M$ in the Droplet Energy Eq. (2.13).

From Eq. (1.3):

$$M C_{pL} = Q_s + h_{fL} \frac{dM}{dt}$$

where:

Q_s = heat transferred from the gas to the liquid

h_{fL} = heat of vaporization, $h_f - h_L$

h_f = enthalpy of the vapor leaving the droplet surface

$$\begin{aligned} & \omega \left\langle \frac{v^2}{2} + c_{pL} T_L \right\rangle_M + \rho_s \langle c_{pL} \mathcal{E} \rangle_M \\ &= \iiint \left[\frac{dM}{dt} \left(\frac{v^2}{2} + c_{pL} T_L \right) + M C_{pL} \frac{dT_L}{dt} \right] f \, dD \, d\underline{v} \, dT_L \\ &= \iiint \left[\frac{dM}{dt} \frac{v^2}{2} + c_{pL} T_L \frac{dM}{dt} + Q_s \right. \\ & \quad \left. + h_f \frac{dM}{dt} - h_L \frac{dM}{dt} \right] f \, dD \, d\underline{v} \, dT_L \\ &= \iiint \left[\frac{dM}{dt} \left(\frac{v^2}{2} + h_f \right) + Q_s \right] f \, dD \, d\underline{v} \, dT_L \\ &= \omega \left\langle \frac{v^2}{2} + h_f \right\rangle_M + q_s \end{aligned} \tag{C.1}$$

where:

$$q_s = \iiint Q_s f \, dD \, d\underline{v} \, dT_L$$

2. Analagous Notation for Gas and Liquid Phase Average Quantities

The mass average gas velocity \underline{u} is given by the

molecular statistical mechanics expression analogous to Eq. (2.8):

$$\underline{u} \equiv \langle \underline{c} \rangle_M = \frac{\sum_k \frac{m_k}{\eta} \int \underline{c} f_k(\underline{x}, \underline{c}, t) d\underline{c}}{\sum_k \frac{m_k}{\eta} \int f_k(\underline{x}, \underline{c}, t) d\underline{c}} = \frac{1}{\rho_f} \sum_k \frac{m_k}{\eta} \int \underline{c} f_k d\underline{c} \quad (\text{C.2})$$

where

\underline{c} = molecular velocity

$f_k(\underline{x}, \underline{c}, t)$ = density function representing the statistical behavior of the k^{th} species in the gas

m_k = molecular weight of the k^{th} species

η = Avogadro's number

Here no internal energy of the molecules is considered so an analog of T_L does not appear. The summation over the k species replaces the operation of integrating over size in a spray.

It is customary in molecular statistical mechanics to consider deviations about the mass average behavior. For this purpose a peculiar velocity is defined:

$$\underline{c} = \underline{c} - \langle \underline{c} \rangle_M \quad (\text{C.3})$$

The variables \underline{u}_T , \underline{u} and \underline{q} are defined in terms of \underline{c} and \underline{c} in Table XII. Note that spray analogs may be defined by replacing ρ_f by ρ_s , \underline{c} by \underline{v} , and \underline{c} by \underline{v} where the peculiar drop velocity is:

$$\underline{v} = \underline{v} - \langle \underline{v} \rangle_M \quad (\text{C.4})$$

TABLE XII.- GAS DYNAMIC QUANTITIES IN TERMS OF THE PECULIAR VELOCITY \underline{C} AND THE MOLECULAR VELOCITY \underline{c} *

Quantity	Definition in terms of \underline{C}	Equivalent expression in terms of \underline{c}
u_T , Translational kinetic energy	$\left\langle \frac{c^2}{2} \right\rangle_M$	$\left\langle \frac{c^2}{2} \right\rangle_M - \frac{\langle c \rangle_M^2}{2}$
$\pi_{\underline{f}}$, Pressure tensor	$\rho_f \langle \underline{c} \underline{c} \rangle_M$	$\rho_f \left(\langle \underline{c} \underline{c} \rangle_M - \langle \underline{c} \rangle_M \langle \underline{c} \rangle_M \right)$
\underline{q} , Heat flux	$\rho_f \left\langle \frac{c^2}{2} \underline{c} \right\rangle_M$	$\rho_f \left(\left\langle \frac{c^2}{2} \underline{c} \right\rangle_M - \left\langle \frac{c^2}{2} \right\rangle_M \langle \underline{c} \rangle_M \right) - \langle \underline{c} \rangle_M \cdot \pi_{\underline{f}}$

* Note: for any function $G(\underline{c})$

$$\langle G \rangle_M \equiv \frac{\sum_K \frac{m_K}{n} \int G f_k d\underline{c}}{\rho_f}$$

$$\underline{c}^2 = \underline{c} \cdot \underline{c} \quad c^2 = \underline{c} \cdot \underline{c}$$

APPENDIX D: A Laser as a Light Source for Fluorescent Droplet Photography

The excitation of the fluorescence with a thin sheet of light was a major stumbling block in the application of the fluorescent technique. In the present system only a very small fraction of the total emitted energy (10^{-5} to 10^{-6}) could be collected and used by the beam shaping and focusing system. Thus, total pulse energy had to be high; and, consequently, the duration was relatively long. The result was a sampling system which was marginal from the standpoint of film exposure by the fluorescence and limited to studies of sprays with relatively low injection velocities.

Several properties of a laser seem aptly suited to the source requirements of the fluorescent technique, and offer the possibility of extending its range of applicability. Presently available Q-switched lasers are capable of producing 10 to 100 megawatt output pulses. Such pulse powers are of the same order as the input of 20-40 megawatts to the spark gap sources which were used, but two unique characteristics of the laser are highly significant for the present application. First, the pulse durations are in the range of 20-50 ns which is approximately two orders of magnitude shorter than the conventional sources. And secondly, the energy output of 0.1 to 1 joules per pulse is emitted in a small diameter,

highly collimated beam. Thus, the entire energy output is available for focusing and shaping, and the coherence of the beam offers the possibility of more closely approaching the ideal square-wave intensity profile of the sheet over the required axial distance.

In order to assess the problems involved in using a laser source, a feasibility test was conducted with the present apparatus by substituting a laser for one of the spark gap sources. The specific goals of the test were to answer the following questions:

1. Could a combination of fluorescent dye absorption-emission characteristics and laser wavelength be found that would produce sharp, well-exposed droplet images on film?
2. Could true droplet size be easily determined from the photographs or would the unique properties of laser light (monochromatic, plane polarized, coherent) cause an image structure which would make measurement uncertain or difficult?

APPARATUS AND PROCEDURE

Laser Source: The two high energy, Q-switched lasers commercially available were ruby and neodymium-doped glass emitting at wavelengths of 6943 Å and 1.06 μ, respectively. Since neither laser wavelength fell within the absorption band of available fluorescent dyes, a frequency doubling technique (optical harmonic generation) was used (Ref. 61). A ruby laser was chosen for the tests since its second harmonic at 3475 Å fell within the absorption spectrum of uranin (fluorescein sodium) dye.

A schematic diagram of the experimental apparatus is shown in Fig. D1. The Q-switched ruby laser used was capable of emitting single pulses at 6943 Å having energies of 0.3 to 1.0 joule and pulse durations of 20 to 50 nsec. A KDP (potassium dihydrogen phosphate) crystal converted 0.01 to 0.02 joule of the fundamental to the second harmonic at 3471 Å. A CuSO₄ filter solution was used to absorb unconverted ruby light while transmitting the ultraviolet. The energy output at 3471 Å was limited by the allowable energy density in the KDP and not by the laser's output capability.

Due to the preliminary nature of these tests, a cylindrical lens system was not used to form a precise sheet of light. Rather, during some of the tests a simple convex lens was used to concentrate the laser output in a small region of the spray.

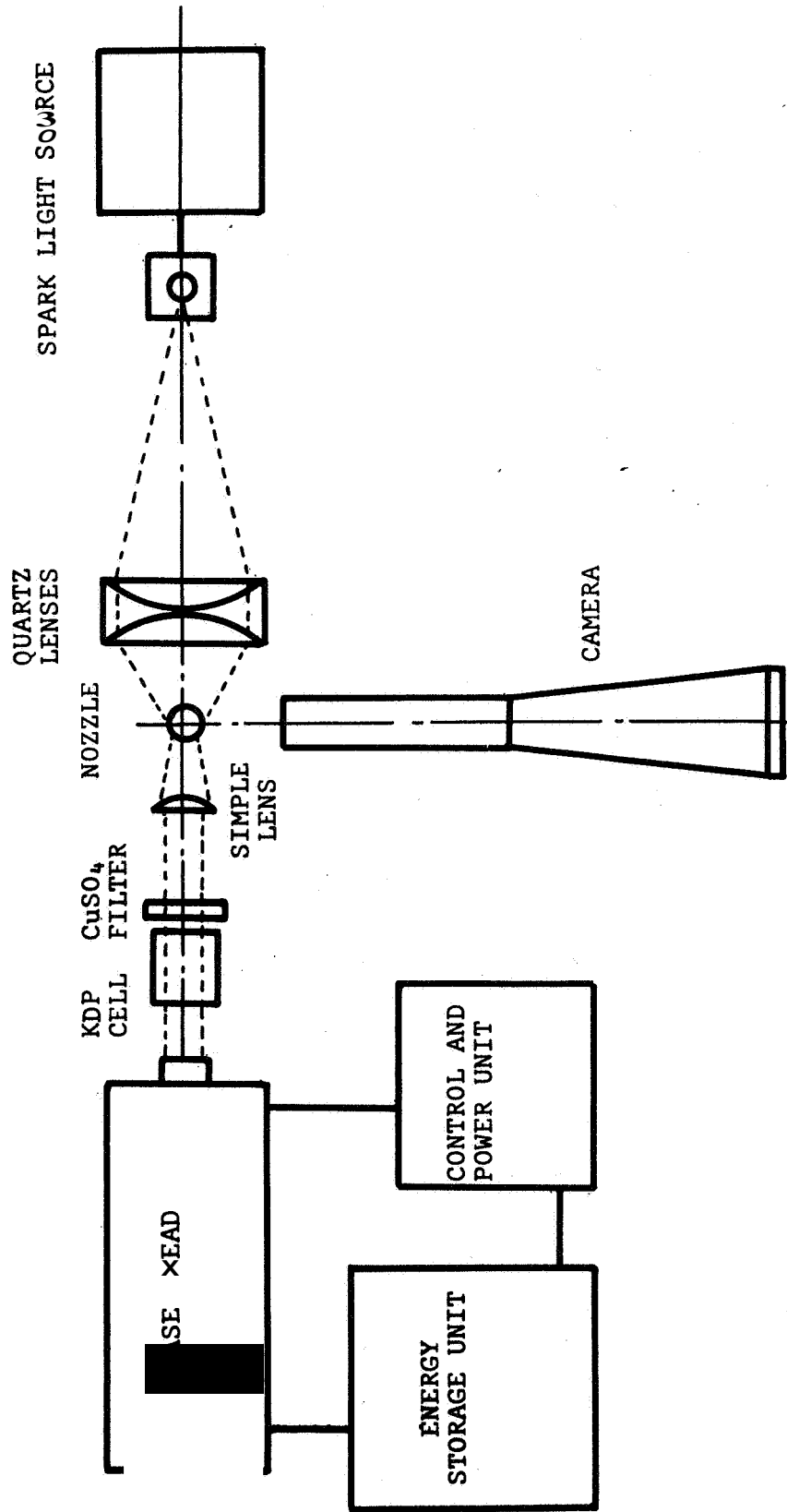


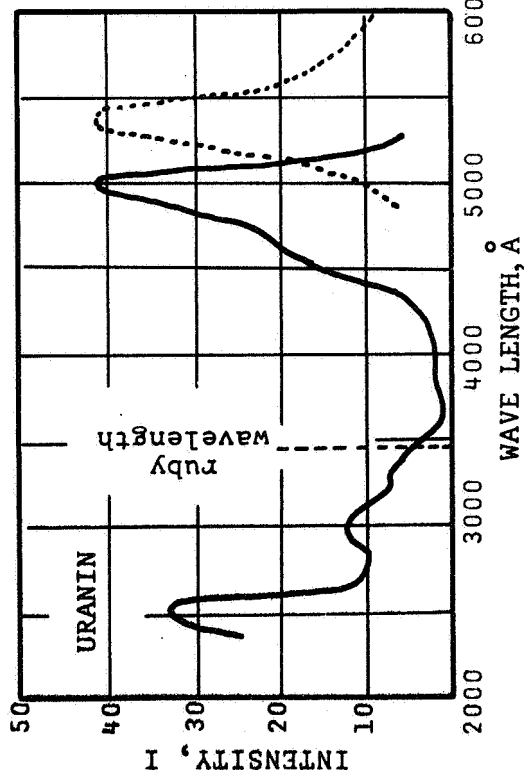
Figure D1. - Block diagram of apparatus for laser test.

Fluorescent Dyes: The spray liquid used in the test was ethanol containing either 5g/liter of uranin or 4.5 g/liter of rhodamine B extra. Absorption-emission curves for these two dyes are given in Fig. D2.. These curves are not for the exact dye concentrations used, but should indicate the trends expected. It can be seen that the 3471 Å wavelength available from the ruby-harmonic generator combination falls at a relatively low point in the absorption band of both dyes.

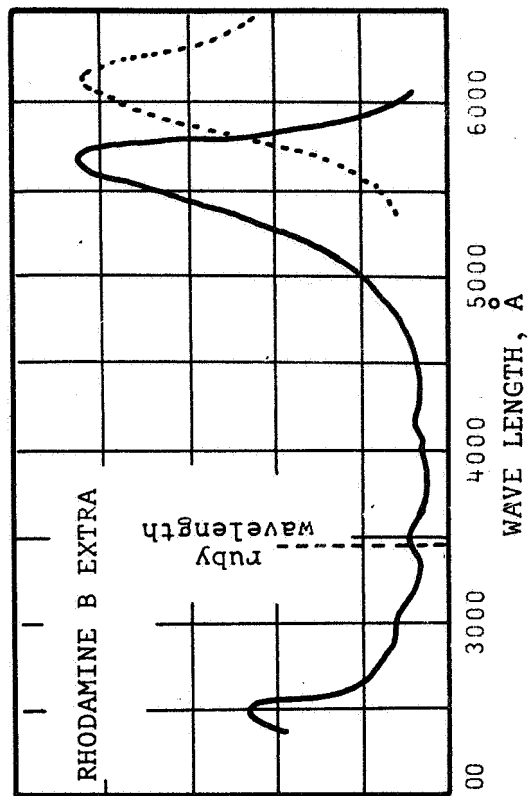
The second harmonic of neodymium at 5300 Å is incompatible with uranin while the absorption of rhodamine B extra is substantial at this wavelength. Rubrene dye in benzene also absorbs strongly at 5300 Å; however, the availability, low cost, and solubility of fluorescein in alcohols, glycerine, and water made its use attractive. It is possible that some dye may be found in the cyanine family which could absorb 6943 Å directly. However, the fluorescent emission at longer wavelengths would require the use of an infrared sensitive film.

The peak emission of uranin is in the green at about 5200 Å while the peak for rhodamine occurs in the red at about 6100 Å. This separation in emission peaks for dyes excited by the same wavelength provides a feature which may be useful in mixing studies. Fluorescent lifetimes of uranin and rhodamine B have been measured as 4 and 6 nsec, respectively (Ref. 62).

— ABSORPTION
- - - EMISSION



(a) Uranin



(b) Rhodamine B Extra

Figure D2. - Spectral characteristics of dye absorption and emission (ref. 67).

Photographic Materials: Films having a range of speeds were used in order to assess the strength of the fluorescence and display varying amounts of image detail. Since past experiments employing the fluorescent technique used Royal-X Pan developed in DK60a for 12 minutes plus intensification to increase contrast, this combination served as the basis for judging the behavior of the fluorescence under conditions of laser excitation.

Conditions for Drop Photography: Fluorescing droplets were photographed under both statically suspended and dynamically sprayed conditions.

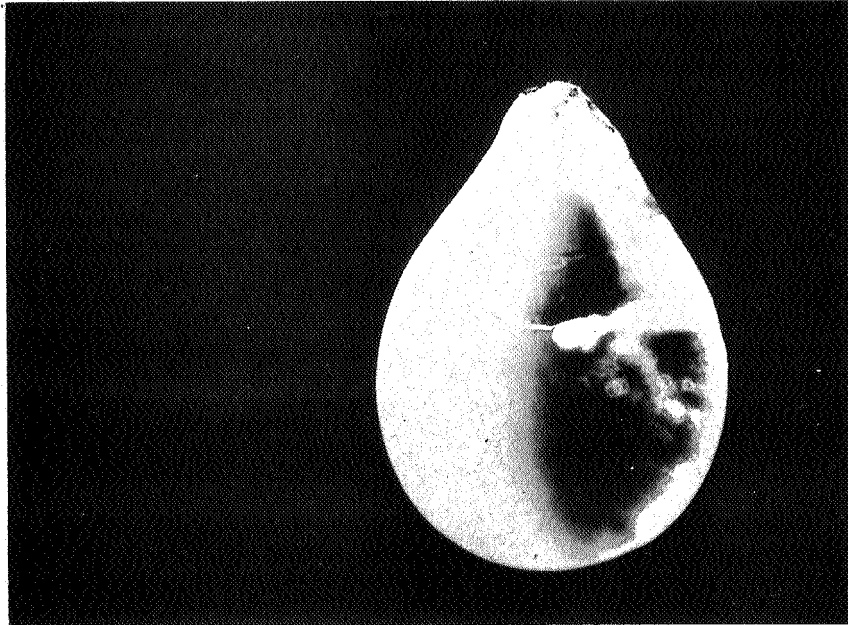
The static tests were conducted by suspending relatively large drops (1 to 2 mm in diameter) from a 0.7 mm diameter hypodermic needle. This situation aided in the alignment of the laser beam with respect to the camera, ruled out small drop size effects, and provided an initial indication of the fluorescent behavior.

The sprays were formed by a low flow (0.75 gal/hr at 100 psi) swirl-type nozzle. Injection pressures were varied from 20 to 300 psi, giving a maximum injection velocity of approximately 100 m/sec as a check on the motion-stopping ability of the laser excited fluorescent method. Direct comparison photographs of the same group of droplets were taken by lighting them first with the laser and then the spark gap separated in time by about 10 μ s.

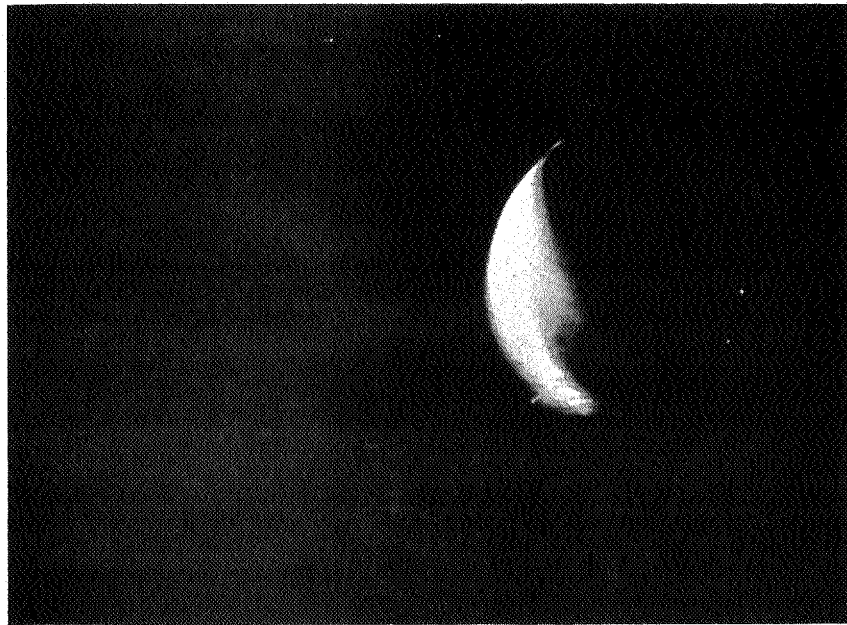
DISCUSSION OF TEST RESULTS

Photographs of Single Suspended Drops: Fluorescent photographs of ethanol drops containing either uranin or rhodamine B extra were taken using $3471 \overset{0}{\text{Å}}$ as the exciting wavelength. The resulting images formed on Royal-X Pan film are shown in Fig. D3. Part of the differences in image density produced by the two dyes is due to the decreasing spectral sensitivity of the film in the longer wavelength portion of the rhodamine emission band.

Examples of various image patterns that were observed in single drop photos of ethanol-uranin solutions are shown in Fig. D4. All of the droplets were lighted from the left side as they appear in the figure. In examining these photos it must be kept in mind that these drops are 10 to 20 times larger than the camera's depth of field for 10μ objects. The twin highlights in Fig. D4(a) appear to be a geometric effect which also occurs for small spray droplets whose fluorescence is excited by a spark source. Distributed "hot spots" of intense emission within a drop have also been observed previously with the fluorescent technique. These hot spots may be the primary cause of the ring patterns shown in Figs. D4(b) and (c). Intense "point" sources of light within the drop could be distorted by the convex liquid surface and depth of field effects to produce modified Airy patterns similar to the rings observed. Filtering of the fluorescent solution to remove any larger suspended dye particles did not

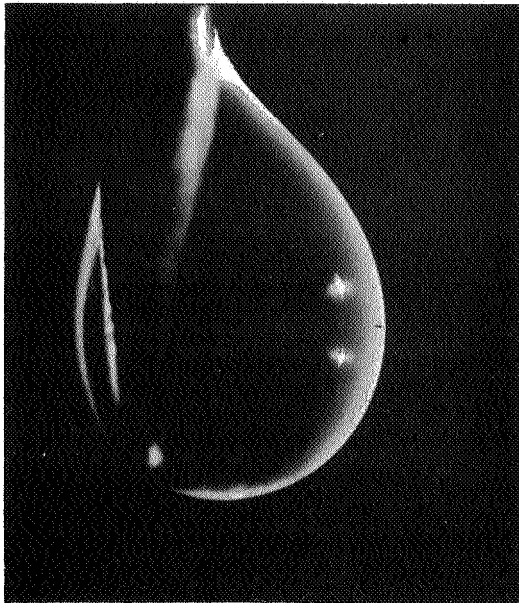


fa) Uranin.

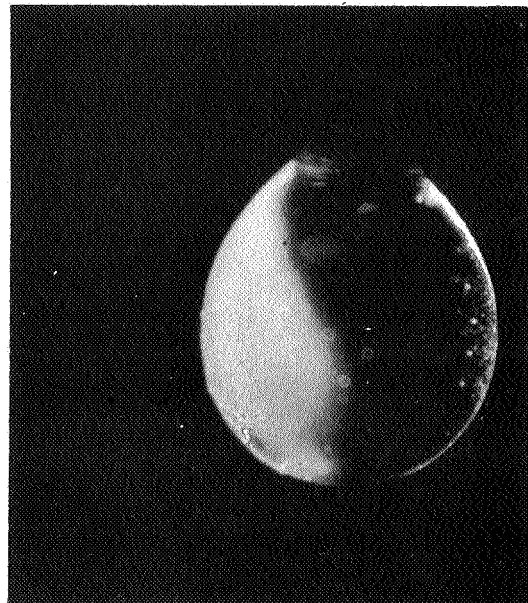


(b) Rhodamine B extra.

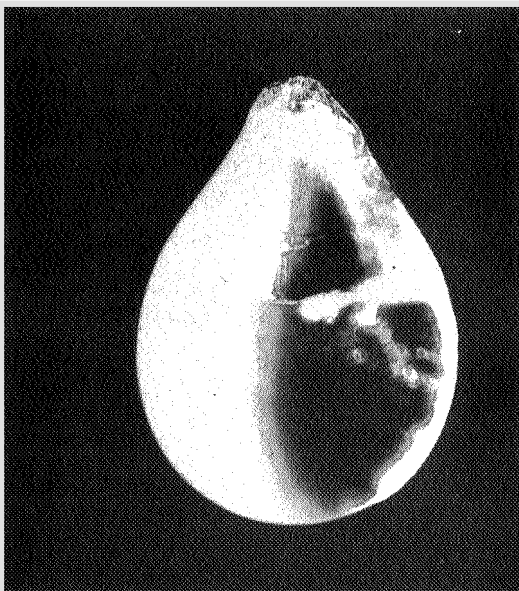
Fig. D3. - Single suspended drops photographed by
Laser light.



(a)



(b)



(c)



(d)

Fig. D4. - Photographs of suspended drops showing patterns.

eliminate these patterns. As to the horizontal striations of Fig. D4(d) one may only speculate that these result from some sort of stress pattern inside the drop.

Figure D5 shows an example of the disruptive effects of the incident light on the liquid which were observed as the intensity was increased. The question immediately arises as to how the image of material outside the confines of the drop was produced. Three possible answers are: First, material capable of fluorescing was already located in the position shown in the photos at the beginning of the light pulse. Under this supposition the misty portions in Fig. D5 suggest that alcohol vapor or the products of its photodecomposition may fluoresce. Second, under high intensity excitation the fluorescent decay time was lengthened thereby increasing the exposure time. Third, the material moved the distance shown during the duration of the laser pulse. This last possibility is supported by the reported observation of plumes of material leaving the surface of metals with velocities as high as 2×10^6 cm/sec after being struck by a beam from a Q-switched laser (Ref. 63). A velocity of the same order of magnitude is obtained from Fig. D5 by measuring the apparent distance moved during an assumed exposure time of 20 nsec. The use of a positive shutter operating in the nanosecond range would be required in order to definitely specify the mechanisms causing the observed results.

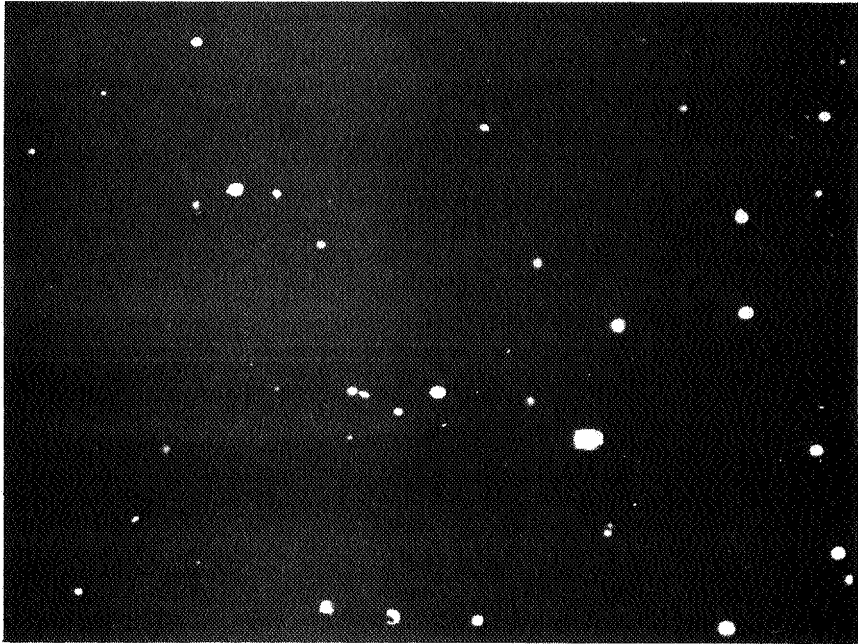


Fig. D5. - Material disturbance of a suspended drop caused by incident Laser light..

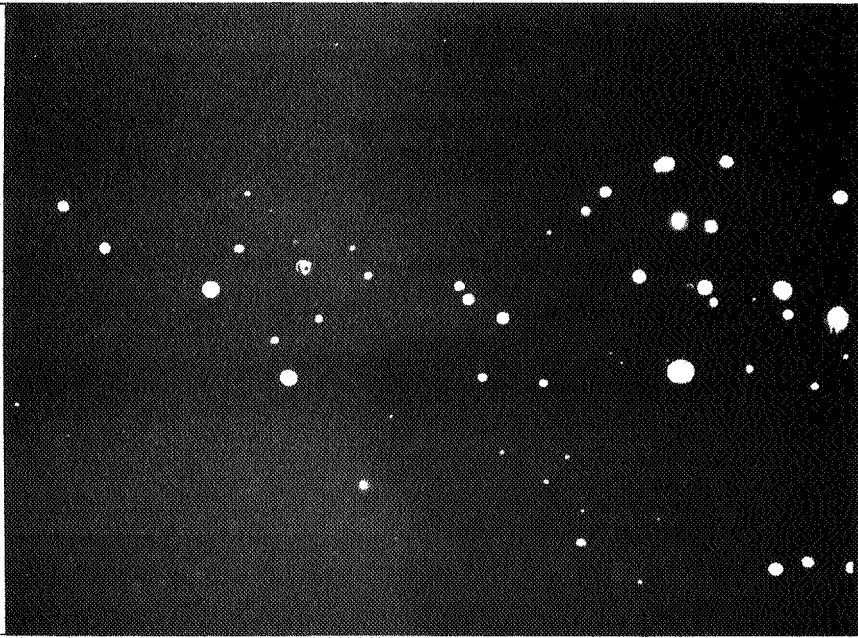
Removal of the CuSO_4 filter which allowed a large amount of light at 6943 \AA to be focused on the drop in addition to that at 3471 \AA resulted in complete removal of the liquid from the end of the hypodermic needle.

As control tests, attempts were made to photograph single undyed drops of ethanol and milk. Under the same lighting conditions, the pure ethanol showed no exposure on Polaroid 3000 ASA film and milk showed only extremely faint exposure probably due to scattering.

Spray Photography: Figure D6 shows the effect on film exposure produced by varying the intensity of the 3471 \AA laser light. In the first case (Fig. D6(a)) the unfocused beam was used just as it emerged from the CuSO_4 filter while in the second case (Fig. D6(b)) a small lens was used to increase the intensity in the spray by at least 10 times. In both cases out of focus drops are illuminated since special optics were not used to form a thin light sheet. The degree of exposure and sharpness of the images in Fig. D6(b) are far superior to those obtained using the guided spark source and the same film (Royal-X Pan) with intensification. Photographs taken with slower films under the same lighting conditions indicated that finer grained emulsions such as Ansco Super Hypan might be used to improve image quality. However, given the experimental conditions existing in this test, it would not be possible to form a 0.008 in. thick light sheet of sufficient intensity simply by passing the laser beam through a



(a) Incident beam unfocused.

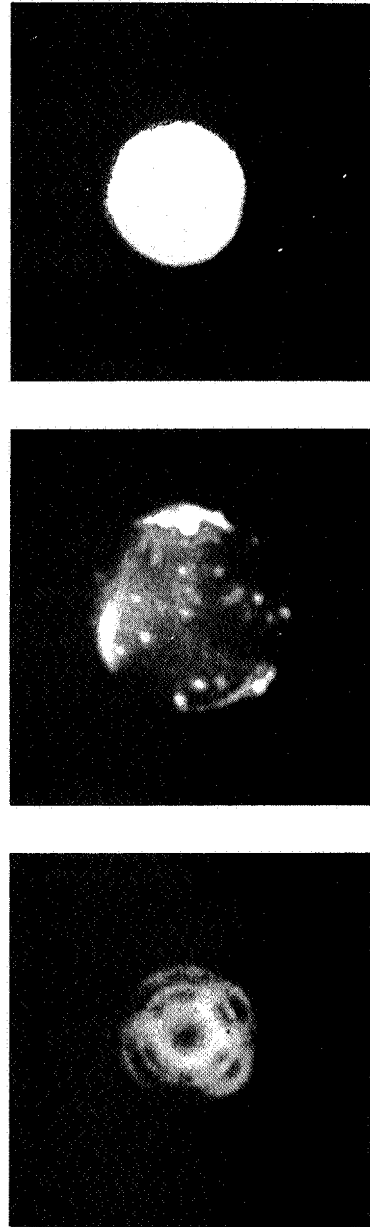


(b) Incident beam focused.

Fig. D6. - Spray photographs showing the effect of incident light intensity.

set of slit's. Rather, a cylindrical lens system which gathered the entire beam would have to be used.

Three types of image structure that were observed have been enlarged 15X from the negatives (initial magnification 25X) and are shown in Fig. D7. Figures D7(a) and (b) were taken on Super Hypan, and Fig. D7(c) was taken on Royal X Pan. Images that were not strongly overexposed often showed either cellular patterns such as the "star" superimposed upon rings in Fig. D7(a) or "hot spots" such as those in Fig. D7(b). To rule out the possibility that these patterns might be caused by scattered laser fundamental ($6943 \overset{O}{\text{\AA}}$) or second harmonic ($3471 \overset{O}{\text{\AA}}$); a green pass filter, Wratten no. 74, was placed on the camera to exclude these wavelengths. No change other than a reduction in film exposure occurred. The cellular pattern may be a diffraction effect originating from small, intensely lighted droplets which lie outside the camera's depth of field. The star effect may result from some internal construction feature of the camera lenses. An alternate explanation would be to attribute the cell patterns to some type of interference or resonance effect within the droplet. "Hot spots" inside and at the boundaries of apparently in-focus droplets are the same phenomena observed on a larger scale in the images of single suspended drops. Droplets that were in focus and intensely lighted frequently exhibited the "lumpy"



(a) Cellular.

(b) H spots

(c) Lumpy.

Fig. D7 - Types of image fine structure.

edge effect shown in Fig. D7(c). In these cases all internal image structure was obliterated by overexposure.

In order to assess the consequences that these image structures might, have in terms of the ability to measure drop sizes, the double-flash photographs were taken. The same droplet was exposed to laser radiation followed by illumination from the guided spark about 10μ sec later. Approximately 80 pairs of images were measured from several different films. These data are plotted in Fig. D8 as image size produced by the spark source versus image size produced by the laser. In general, the laser-produced image of a drop ~~is slightly larger.~~ This result appears to be largely due to the fact that the laser images were usually more dense due to greater exposure. In those cases where the drop image produced by the spark source is the larger of the two, it is also more dense. Thus, drop size can be obtained from the laser photographs with confidence provided reasonable care is taken to obtain proper exposure.

A spray photograph was obtained using rhodamine B extra in ethanol and 3000 ASA film. As suggested by the single drop tests, rhodamine can be used to produce sharp spray droplet images. Best results would be obtained with a film having extended red sensitivity.

As a matter of interest, the KDP cell was removed and a spray picture was taken using only ruby light picked

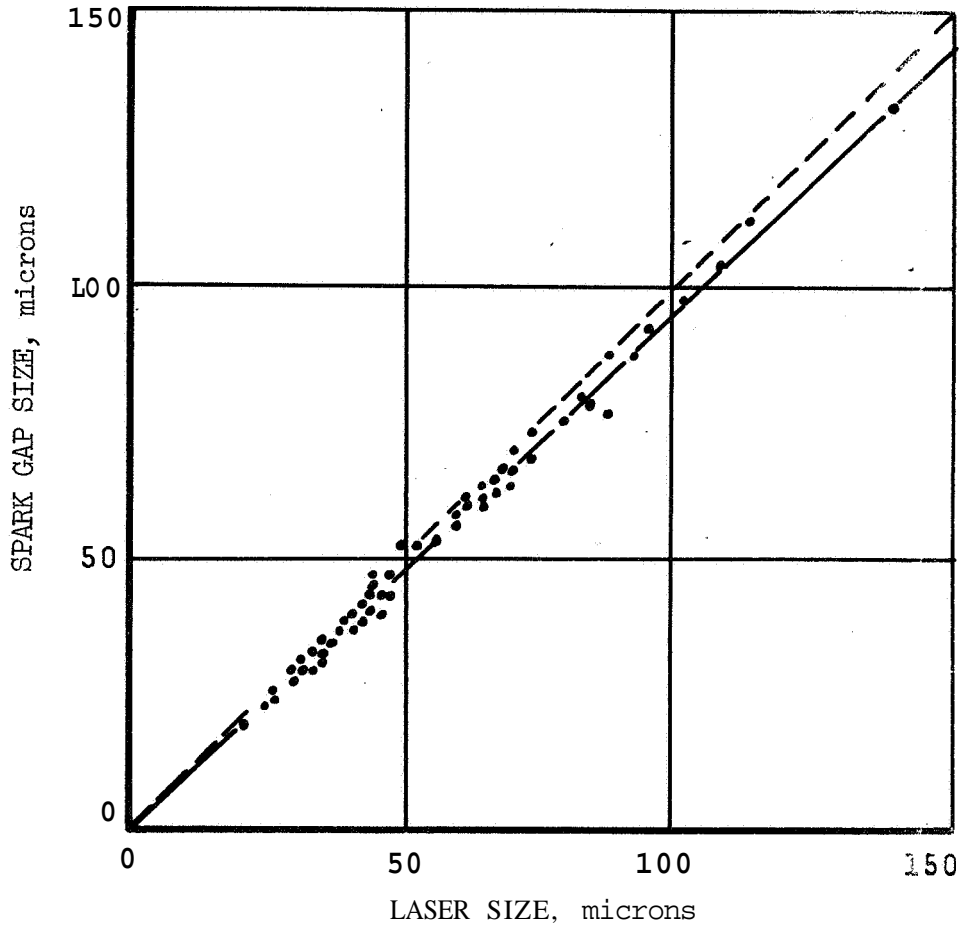


Figure D8. - Comparison of measured drop sizes for the two lighting methods.

up at a 90° scattering angle by the camera. The film used was Kodak 2475 which is Royal-X Pan with extended red sensitivity. The extremely complex diffraction patterns which resulted are roughly reproduced in Fig. D9 at an overall magnification of approximately 100.

SUMMARY OF RESULTS

As a result of the tests performed the following conclusions are drawn regarding the use of a Q-switched laser source with the fluorescent method of spray photography.

1. Both uranin (disodium fluorescein) and rhodamine B extra dyes in ethanol were strongly excited by the second harmonic of ruby at $3471 \overset{0}{\text{Å}}$. In spite of the fact that this wavelength falls at a low point in dye absorption; sharp, well-exposed droplet images were produced. However, the harmonic generator was operating near peak output so that care must be taken to gather the entire converted beam when forming the 0.008 m. thick light sheet required by the present apparatus.

2. The time resolution or motion-stopping ability', of the laser-fluorescent combination was excellent as demonstrated by the sharpness of images of 10μ drops formed over a range of injection velocities to a maximum of approximately 100 m/sec.

3. In spite of some image fine structure, a direct, dynamic calibration demonstrated that droplet sizes could be accurately determined.

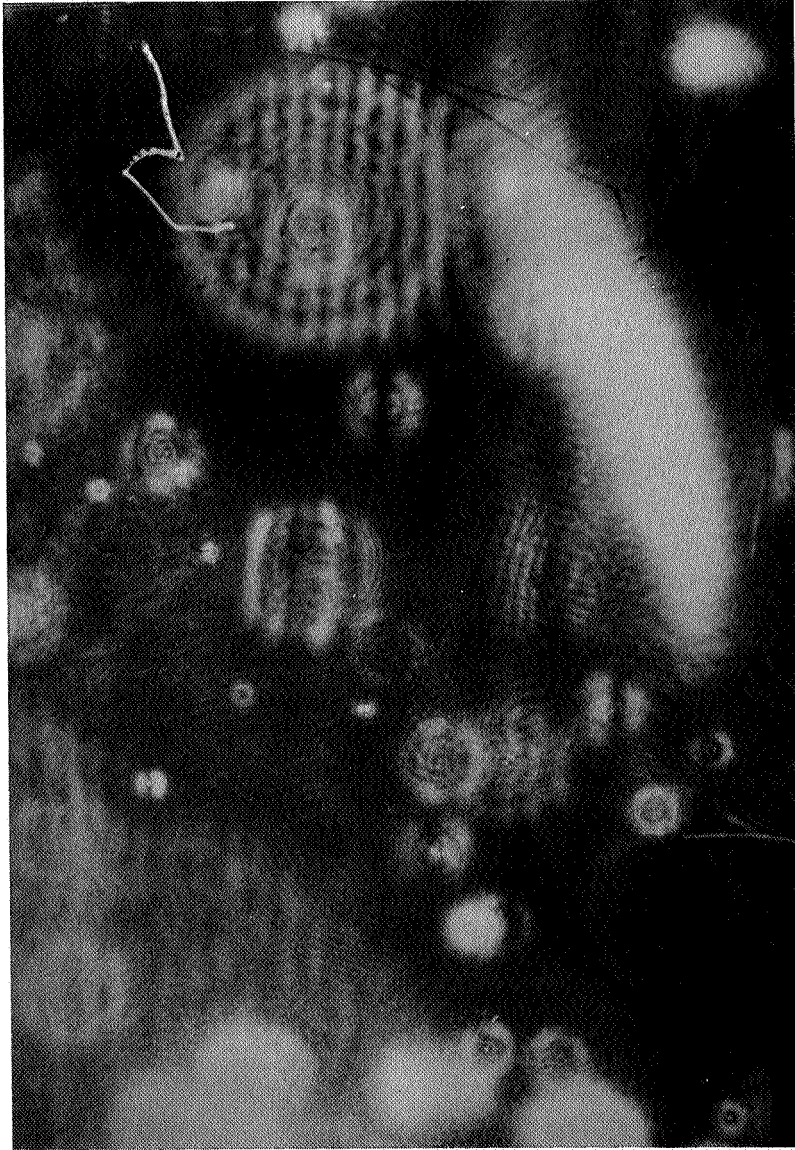


Fig. D9. - Diffraction patterns formed by ruby Laser light scattered at 90° by drops in a spray.

Several aspects of the application of lasers to fluorescent photography remain to be explored. A more efficient spectral match of laser wavelength with dye absorption deserves attention. Avoiding the process of converting the primary laser wavelength has obvious advantages in terms of available intensity and experimental convenience.

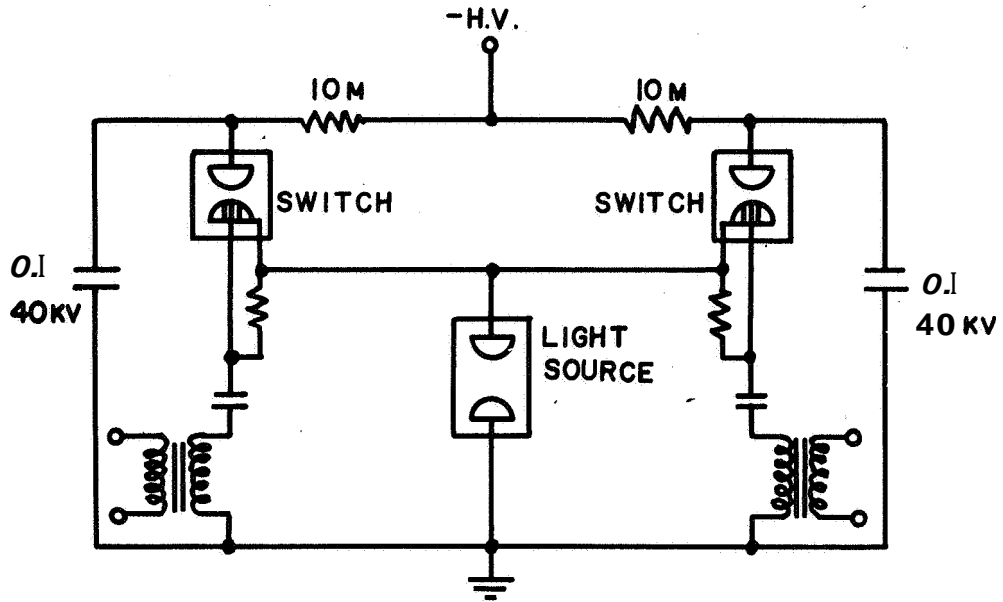
The laser used in the tests did not have the capability of producing two or more flashes of sufficient intensity to record multiple images for the purpose of velocity measurement. The Q-switch was of the passive, saturable-filter type and was designed to produce maximum single pulses. However, precisely controlled pulse trains have been produced by using Kerr cell Q-switching, (Ref. 64). Development work is required on an effective method of producing multiple pulses of high intensity at a precisely repeatable interval. If at least three pulses were produced, local values of drop acceleration could be measured. Such information would be extremely valuable in clarifying droplet drag relationships.

In summary, the use of a laser source seems to offer the most fruitful approach to further application of fluorescent spray photography.

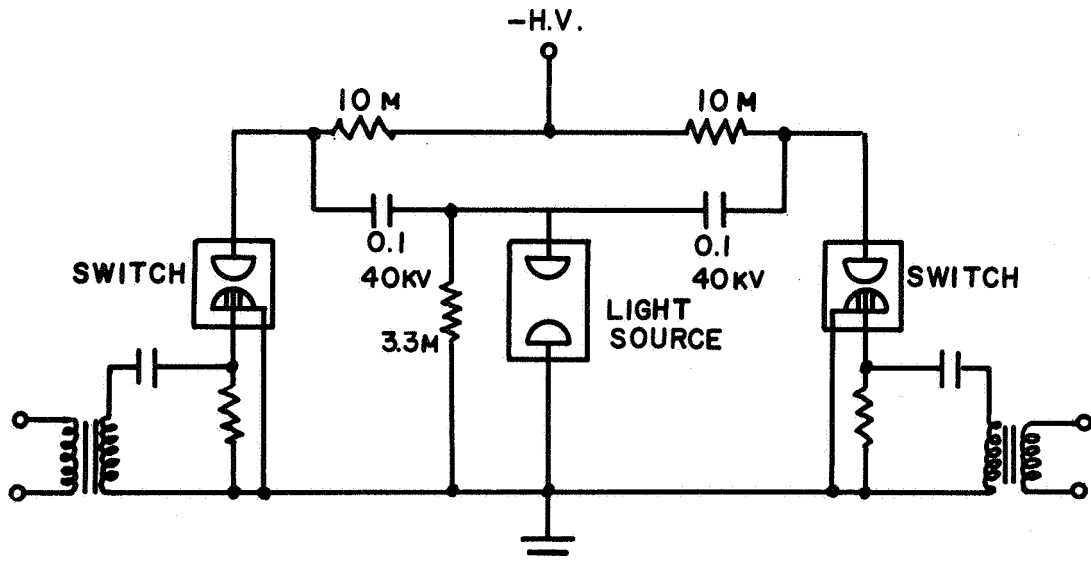
APPENDIX E: Problems Associated with a Single-Gap,
Double-Flash Source

Two circuit diagrams for controlled double pulsing of the same gap are given in Fig. E1. Successful application of the upper circuit (Fig. E1(a)) at energy inputs of less than 0.5 joule has been reported (Ref. 65). The output from the second flash was found to be considerably weaker than the first and so twice the capacitance was used in the circuit to be fired second. These results were duplicated at input energies up to 10 joules with minimum delays between flashes of $10\mu\text{s}$. However, at the 80 joule level, delays shorter than $100\mu\text{s}$ could not be accomplished. It appeared that a combination of poor gap recovery under the high current fluxes and strong transients induced in the circuit by the first discharge were responsible for the erratic behavior at short delays. In an attempt to stabilize the voltages occurring at the hollow electrodes of the spark gap switches, the second circuit (Fig. E1(b) Ref. 66)) was used in which the switches are grounded. The performance at delays less than $100\mu\text{s}$ remained unsatisfactory, and the direct flashing of a single source was abandoned.

A modified geometry in which two gaps were very close to each other but were physically separated by a quartz window is shown in Fig. E2. This design was unsuccessful for two reasons. The quartz was shattered by the shock waves from the discharges and the solid angle in which the



(a) Ungrounded triggers



(b) Grounded triggers

Figure E1. - Two double flash light source circuits.

- 1 Brass Double Electrode
- 2 Slotted Teflon Arc Guide
- 3 Lucite Body
- 4 Fused Quartz Window
- 5 Brass Single Electrode

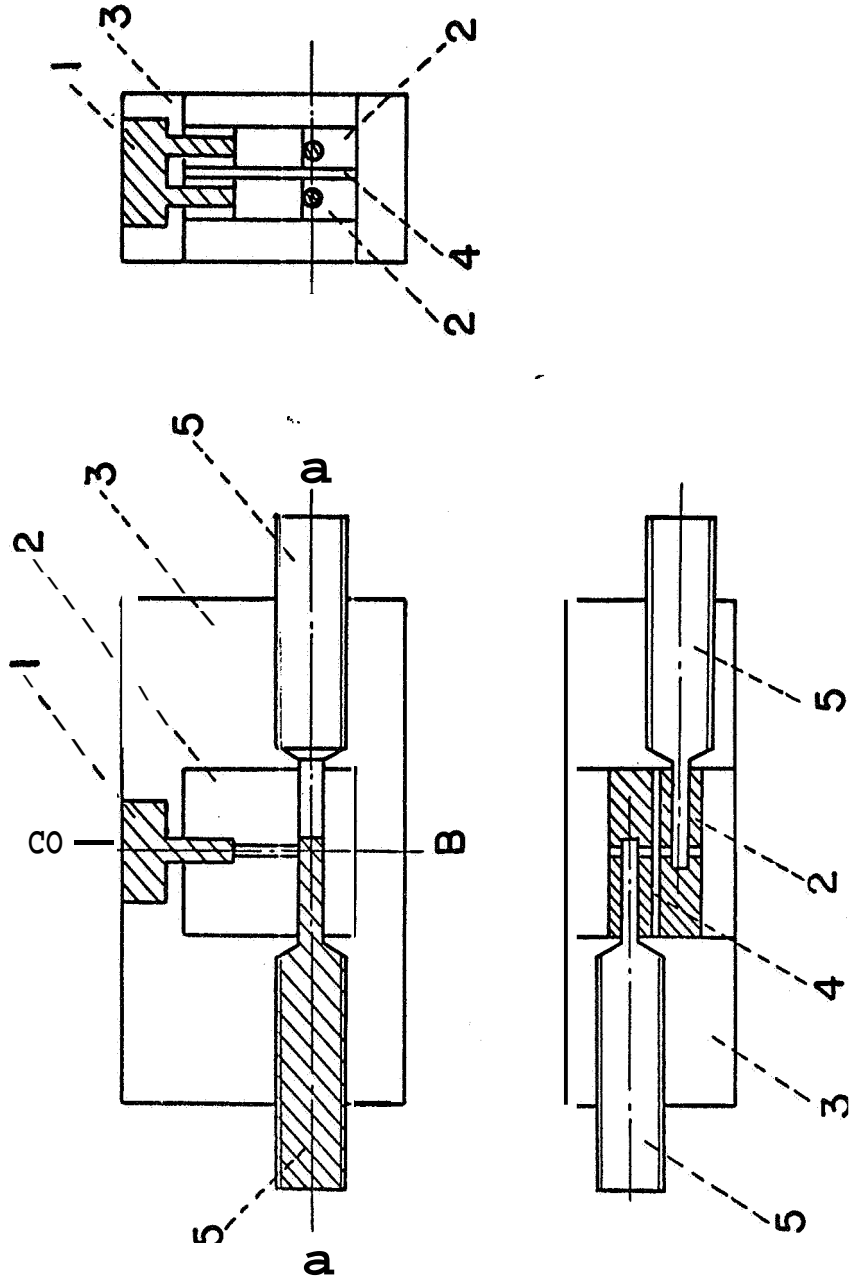


Figure E2. - Single location double flash source.

rear gap could radiate was limited when viewed from the front. A plexiglass barrier which was substituted for the quartz did not shatter, but surface erosion decreased the optical transmission to an unacceptable level.

In view of these results it was necessary to use two sources which were independent electrically and separated physically.

APPENDIX F: Tabulation of Raw Size-Velocity Matrices as
a Function of Position in the Spray

NOTE: Categories used are given in Table X
Sample Volume corresponding to each
location: 10^{-4} in.³

Units used are: position in inches,
velocity in inches/
second, and drop size
in microns

RAW VZ-DIAMETER MATRICES

DELTA P=25.		R=0.520										TOTAL EXPOSURES=40.													
AVE.VZ	CAT.NO.	1	2	3	4	5	6	7	8	9	10	11	12	1	2	3	4	5	6	7	8	9	10	11	12
985.8	16	0.	0.	0.	0.	0.	0.	0.	0.	0.	0.	0.	0.	0.	0.	0.	0.	0.	0.	0.	0.	0.	0.	0.	
752.5	15	0.	0.	0.	0.	0.	0.	0.	0.	0.	0.	0.	0.	0.	0.	0.	0.	0.	0.	0.	0.	0.	0.	0.	
574.5	14	0.	0.	0.	0.	0.	0.	0.	0.	0.	0.	0.	0.	0.	0.	0.	0.	0.	0.	0.	0.	0.	0.	0.	
438.5	13	0.	0.	0.	0.	0.	0.	0.	0.	0.	0.	0.	0.	0.	0.	0.	0.	0.	0.	0.	0.	0.	0.	0.	
334.7	12	0.	0.	0.	0.	0.	0.	0.	0.	0.	0.	0.	0.	0.	0.	0.	0.	0.	0.	0.	0.	0.	0.	0.	
255.5	11	0.	0.	0.	0.	0.	0.	0.	0.	0.	0.	0.	0.	0.	0.	0.	0.	0.	0.	0.	0.	0.	0.	0.	
195.1	10	0.	0.	0.	0.	0.	0.	0.	0.	0.	0.	0.	0.	0.	0.	0.	0.	0.	0.	0.	0.	0.	0.	0.	
148.9	9	0.	0.	0.	0.	0.	0.	0.	0.	0.	0.	0.	0.	0.	0.	0.	0.	0.	0.	0.	0.	0.	0.	0.	
113.7	8	0.	0.	0.	0.	0.	0.	0.	0.	0.	0.	0.	0.	0.	0.	0.	0.	0.	0.	0.	0.	0.	0.	0.	
86.8	7	0.	0.	0.	0.	0.	0.	0.	0.	0.	0.	0.	0.	0.	0.	0.	0.	0.	0.	0.	0.	0.	0.	0.	
66.2	6	0.	0.	0.	0.	0.	0.	0.	0.	0.	0.	0.	0.	0.	0.	0.	0.	0.	0.	0.	0.	0.	0.	0.	
50.6	5	0.	0.	0.	0.	0.	0.	0.	0.	0.	0.	0.	0.	0.	0.	0.	0.	0.	0.	0.	0.	0.	0.	0.	
38.6	4	0.	0.	0.	0.	0.	0.	0.	0.	0.	0.	0.	0.	0.	0.	0.	0.	0.	0.	0.	0.	0.	0.	0.	
29.5	3	0.	0.	0.	0.	0.	0.	0.	0.	0.	0.	0.	0.	0.	0.	0.	0.	0.	0.	0.	0.	0.	0.	0.	
17.2	1	0.	0.	0.	0.	0.	0.	0.	0.	0.	0.	0.	0.	0.	0.	0.	0.	0.	0.	0.	0.	0.	0.	0.	

DELTA P=25.		R=0.600										TOTAL EXPOSURES=40.													
AVE.VZ	CAT.NO.	1	2	3	4	5	6	7	8	9	10	11	12	1	2	3	4	5	6	7	8	9	10	11	12
985.8	16	0.	0.	0.	0.	0.	0.	0.	0.	0.	0.	0.	0.	0.	0.	0.	0.	0.	0.	0.	0.	0.	0.	0.	
752.5	15	0.	0.	0.	0.	0.	0.	0.	0.	0.	0.	0.	0.	0.	0.	0.	0.	0.	0.	0.	0.	0.	0.	0.	
574.5	14	0.	0.	0.	0.	0.	0.	0.	0.	0.	0.	0.	0.	0.	0.	0.	0.	0.	0.	0.	0.	0.	0.	0.	
438.5	13	0.	0.	0.	0.	0.	0.	0.	0.	0.	0.	0.	0.	0.	0.	0.	0.	0.	0.	0.	0.	0.	0.	0.	
334.7	12	0.	0.	0.	0.	0.	0.	0.	0.	0.	0.	0.	0.	0.	0.	0.	0.	0.	0.	0.	0.	0.	0.	0.	
255.5	11	0.	0.	0.	0.	0.	0.	0.	0.	0.	0.	0.	0.	0.	0.	0.	0.	0.	0.	0.	0.	0.	0.	0.	
195.1	10	0.	0.	0.	0.	0.	0.	0.	0.	0.	0.	0.	0.	0.	0.	0.	0.	0.	0.	0.	0.	0.	0.	0.	
148.9	9	0.	0.	0.	0.	0.	0.	0.	0.	0.	0.	0.	0.	0.	0.	0.	0.	0.	0.	0.	0.	0.	0.	0.	
113.7	8	0.	0.	0.	0.	0.	0.	0.	0.	0.	0.	0.	0.	0.	0.	0.	0.	0.	0.	0.	0.	0.	0.	0.	
86.8	7	0.	0.	0.	0.	0.	0.	0.	0.	0.	0.	0.	0.	0.	0.	0.	0.	0.	0.	0.	0.	0.	0.	0.	
66.2	6	0.	0.	0.	0.	0.	0.	0.	0.	0.	0.	0.	0.	0.	0.	0.	0.	0.	0.	0.	0.	0.	0.	0.	
50.6	5	0.	0.	0.	0.	0.	0.	0.	0.	0.	0.	0.	0.	0.	0.	0.	0.	0.	0.	0.	0.	0.	0.	0.	
38.6	4	0.	0.	0.	0.	0.	0.	0.	0.	0.	0.	0.	0.	0.	0.	0.	0.	0.	0.	0.	0.	0.	0.	0.	
29.5	3	0.	0.	0.	0.	0.	0.	0.	0.	0.	0.	0.	0.	0.	0.	0.	0.	0.	0.	0.	0.	0.	0.	0.	
17.2	1	0.	0.	0.	0.	0.	0.	0.	0.	0.	0.	0.	0.	0.	0.	0.	0.	0.	0.	0.	0.	0.	0.	0.	

CAT. NO. 1 2 3 4 5 6 7 8 9 10 11 12
 AVE. DIA. 11.4 15.0 19.6 25.7 33.7 44.2 57.8 75.8 99.3 130.0 170.4 223.2

RAW VZ-DIAMETER MATRICES

DELTA P=25 Z=2.125 R=0.680 TOTAL EXPOSURES=40

AVE.VZ	CAT.NO.	1	2	3	4	5	6	7	8	9	10	11	12
985.8	16	0.	0.	0.	0.	0.	0.	0.	0.	0.	0.	0.	0.
752.5	15	0.	0.	0.	0.	0.	0.	0.	0.	0.	0.	0.	0.
574.5	14	0.	0.	0.	0.	0.	0.	0.	0.	0.	0.	0.	0.
438.5	13	0.	0.	0.	0.	0.	0.	0.	0.	0.	0.	0.	0.
334.7	12	0.	0.	0.	0.	0.	0.	0.	0.	0.	0.	0.	0.
255.5	11	0.	0.	0.	0.	0.	0.	0.	0.	0.	0.	0.	0.
195.1	10	0.	0.	0.	0.	0.	0.	0.	0.	0.	0.	0.	0.
148.9	9	0.	0.	0.	0.	0.	0.	0.	0.	0.	0.	0.	0.
113.7	8	0.	0.	0.	0.	0.	0.	0.	0.	0.	0.	0.	0.
86.8	7	0.	0.	0.	0.	0.	0.	0.	0.	0.	0.	0.	0.
66.2	6	0.	0.	0.	0.	0.	0.	0.	0.	0.	0.	0.	0.
50.6	5	0.	0.	0.	0.	0.	0.	0.	0.	0.	0.	0.	0.
38.6	4	0.	0.	0.	0.	0.	0.	0.	0.	0.	0.	0.	0.
29.5	3	0.	0.	0.	0.	0.	0.	0.	0.	0.	0.	0.	0.
22.5	2	0.	0.	0.	0.	0.	0.	0.	0.	0.	0.	0.	0.
17.2	1	0.	0.	0.	0.	0.	0.	0.	0.	0.	0.	0.	0.

CAT. NO. 1 2 3 4 5 6 7 8 9 10 11 12
 AVE. DIA. 11.4 15.0 19.6 25.7 33.7 44.2 57.8 75.8 99.3 130.0 170.4 223.2

DELTA P=25 Z=2.125 R=0.680 TOTAL EXPOSURES=40

AVE.VZ	CAT.NO.	1	2	3	4	5	6	7	8	9	10	11	12
985.8	16	0.	0.	0.	0.	0.	0.	0.	0.	0.	0.	0.	0.
752.5	15	0.	0.	0.	0.	0.	0.	0.	0.	0.	0.	0.	0.
574.5	14	0.	0.	0.	0.	0.	0.	0.	0.	0.	0.	0.	0.
438.5	13	0.	0.	0.	0.	0.	0.	0.	0.	0.	0.	0.	0.
334.7	12	0.	0.	0.	0.	0.	0.	0.	0.	0.	0.	0.	0.
255.5	11	0.	0.	0.	0.	0.	0.	0.	0.	0.	0.	0.	0.
195.1	10	0.	0.	0.	0.	0.	0.	0.	0.	0.	0.	0.	0.
148.9	9	0.	0.	0.	0.	0.	0.	0.	0.	0.	0.	0.	0.
113.7	8	0.	0.	0.	0.	0.	0.	0.	0.	0.	0.	0.	0.
86.8	7	0.	0.	0.	0.	0.	0.	0.	0.	0.	0.	0.	0.
66.2	6	0.	0.	0.	0.	0.	0.	0.	0.	0.	0.	0.	0.
50.6	5	0.	0.	0.	0.	0.	0.	0.	0.	0.	0.	0.	0.
38.6	4	0.	0.	0.	0.	0.	0.	0.	0.	0.	0.	0.	0.
29.5	3	0.	0.	0.	0.	0.	0.	0.	0.	0.	0.	0.	0.
22.5	2	0.	0.	0.	0.	0.	0.	0.	0.	0.	0.	0.	0.
17.2	1	0.	0.	0.	0.	0.	0.	0.	0.	0.	0.	0.	0.

CAT. NO. 1 2 3 4 5 6 7 8 9 10 11 12
 AVE. DIA. 11.4 15.0 19.6 25.7 33.7 44.2 57.8 75.8 99.3 130.0 170.4 223.2

C 17 0 MPTE M T PSES

DELTA P=40. Z=2.125 R=0.360 TOTAL EXPOSURES=48.

AVE. VZ	CAT. NO.	1	2	3	4	5	6	7	8	9	10	11	12
985.8	16	0.	0.	0.	0.	0.	0.	0.	0.	0.	0.	0.	0.
752.5	15	0.	0.	0.	0.	0.	0.	0.	0.	0.	0.	0.	0.
574.5	14	0.	0.	0.	0.	0.	0.	0.	0.	1.	0.	0.	0.
438.5	13	0.	0.	0.	0.	0.	0.	0.	0.	2.	7.	1.	0.
334.7	12	1.	0.	0.	0.	0.	1.	9.	19.	11.	2.	0.	0.
255.5	11	2.	0.	3.	2.	2.	8.	29.	19.	1.	0.	0.	0.
195.1	10	8.	8.	26.	18.	17.	39.	29.	6.	1.	0.	0.	0.
148.9	9	47.	33.	96.	58.	39.	41.	17.	0.	0.	0.	0.	0.
113.7	8	38.	28.	105.	90.	65.	37.	10.	0.	0.	0.	0.	0.
86.8	7	10.	8.	44.	47.	53.	45.	1.	0.	0.	0.	0.	0.
66.2	6	5.	0.	5.	10.	18.	16.	0.	0.	0.	0.	0.	0.
50.6	5	1.	2.	0.	5.	17.	7.	0.	0.	0.	0.	0.	0.
38.6	4	1.	0.	0.	0.	0.	2.	0.	0.	0.	0.	0.	0.
29.5	3	0.	0.	1.	0.	1.	1.	1.	0.	0.	0.	0.	0.
22.5	2	0.	0.	0.	1.	2.	1.	0.	0.	0.	0.	0.	0.
17.2	1	0.	0.	0.	0.	1.	0.	0.	0.	0.	0.	0.	0.

DELTA P=40. Z=2.125 R=0.440 TOTAL EXPOSURES=48.

AVE. VZ	CAT. NO.	1	2	3	4	5	6	7	8	9	10	11	12
985.8	16	0.	0.	0.	0.	0.	0.	0.	0.	0.	0.	0.	0.
752.5	15	0.	0.	0.	0.	0.	0.	0.	0.	0.	0.	0.	0.
574.5	14	0.	0.	0.	0.	0.	0.	0.	0.	1.	0.	0.	0.
438.5	13	0.	0.	0.	0.	0.	0.	0.	0.	4.	0.	0.	0.
334.7	12	0.	0.	0.	0.	0.	1.	1.	5.	8.	1.	0.	0.
255.5	11	0.	0.	0.	0.	2.	2.	11.	14.	5.	0.	0.	0.
195.1	10	1.	0.	2.	4.	5.	16.	18.	13.	1.	0.	0.	0.
148.9	9	11.	4.	21.	13.	13.	18.	30.	2.	0.	0.	0.	0.
113.7	8	19.	16.	41.	36.	21.	27.	23.	1.	0.	0.	0.	0.
86.8	7	10.	15.	65.	85.	87.	38.	12.	1.	0.	0.	0.	0.
66.2	6	7.	0.	8.	35.	61.	32.	7.	1.	0.	0.	0.	0.
50.6	5	1.	2.	5.	17.	33.	22.	4.	0.	0.	0.	0.	0.
38.6	4	0.	0.	1.	2.	6.	14.	6.	1.	0.	0.	0.	0.
29.5	3	0.	0.	0.	0.	6.	8.	0.	0.	0.	0.	0.	0.
22.5	2	1.	0.	0.	0.	1.	2.	0.	0.	0.	0.	0.	0.
17.2	1	0.	0.	0.	1.	1.	4.	0.	0.	0.	0.	0.	0.

DELTA P=40. Z=2.125 R=0.440 TOTAL EXPOSURES=48.

AVE. VZ	CAT. NO.	1	2	3	4	5	6	7	8	9	10	11	12
985.8	16	0.	0.	0.	0.	0.	0.	0.	0.	0.	0.	0.	0.
752.5	15	0.	0.	0.	0.	0.	0.	0.	0.	0.	0.	0.	0.
574.5	14	0.	0.	0.	0.	0.	0.	0.	0.	1.	0.	0.	0.
438.5	13	0.	0.	0.	0.	0.	0.	0.	0.	4.	0.	0.	0.
334.7	12	0.	0.	0.	0.	0.	1.	1.	5.	8.	1.	0.	0.
255.5	11	0.	0.	0.	0.	2.	2.	11.	14.	5.	0.	0.	0.
195.1	10	1.	0.	2.	4.	5.	16.	18.	13.	1.	0.	0.	0.
148.9	9	11.	4.	21.	13.	13.	18.	30.	2.	0.	0.	0.	0.
113.7	8	19.	16.	41.	36.	21.	27.	23.	1.	0.	0.	0.	0.
86.8	7	10.	15.	65.	85.	87.	38.	12.	1.	0.	0.	0.	0.
66.2	6	7.	0.	8.	35.	61.	32.	7.	1.	0.	0.	0.	0.
50.6	5	1.	2.	5.	17.	33.	22.	4.	0.	0.	0.	0.	0.
38.6	4	0.	0.	1.	2.	6.	14.	6.	1.	0.	0.	0.	0.
29.5	3	0.	0.	0.	0.	6.	8.	0.	0.	0.	0.	0.	0.
22.5	2	1.	0.	0.	0.	1.	2.	0.	0.	0.	0.	0.	0.
17.2	1	0.	0.	0.	1.	1.	4.	0.	0.	0.	0.	0.	0.

REFERENCES

1. DeJuhasz, Kalman, J., ed: Spray Literature Abstracts, ASME, 1959.
2. DeJuhasz, Kalman, J: ed; : Spray Literature Abstracts, Vol. 11, ASME, 1964.
3. Putnam, A. A. and Thomas R. E., eds.: "Injection and Combustion of Liquid Fuels," Battelle Memorial Institute, 1957 (WADC TR 56-344, ASTIA No. AD 118142).
4. Marshall, W. R.,: Atomization and Spray Drying, Chem. Eng. Prog., Monograph Series, No. 2, Vol. 50, 1954.
5. Priem, Richard J., and Heidmann, Marcus F.,: "Propellant Vaporization as a Design Criterion for Rocket-Engine Combustion Chambers," NASA TR R-67 1960 (Supersedes NACA TN's 3883, 3985, 4098, and 4219).
6. El-Wakil, M. M., Myers, P. S., Uyehara, O. A.: "Fuel Vaporization and Ignition Lag in Diesel Combustion," SAE Trans., Vol. 64, 1956, pp. 712-729.
7. Priem, Richard J.: "Combustion Process Influence on Stability;" Chem, Eng. Prog. Sym. Series, Vol. 62, No. 61, 1966, pp. 103-112 See also NASA TN D-2957, 1965.
8. Hoglund, Richard F.: "Recent Advances in Gas-Particle Nozzle Flows," ARS J., Vol. 32, No. 5, May 1962, pp. 662-671.
9. York, J. L. and Stubbs, H. E.: "Photographic Analysis of Sprays," Trans. ASME, Vol. 74, No. 7, October 1952, pp. 1157-1162.

10. Ingebo, R. D.: "Vaporization Rates and Drag Coefficients for Isoctane Sprays in Turbulent Air Streams," NACA TN 3265, 1954.
11. Manning, W. P., and Gauwin, W. H.: "Heat and Mass Transfer to Decelerating Finely Atomized Sprays." A.I.Ch.E. J., Vol. 6, No. 2, June 1960, pp. 184-190.
12. Short, W. L.: Some Properties of Sprays Formed by the Disintegration of a Superheated Liquid Jet, Ph. D. Thesis, University of Michigan, 1963.
13. Williams, F. A.: Theoretical Studies in Heterogenous Combustion, Ph. D. Thesis, Calif. Inst. Tech., 1958.
14. Williams F. A.: "Progress in Spray Combustion Analysis," Eighth (International) Symposium on Combustion, Williams and Wilkins, 1962, pp. 50-69.
15. Giffen, E., and Muraszew, A.: The Atomization of Liquid Fuels, Wiley, 1953.
16. Crandall, Stephen H., and Mark, William D.: Random Vibration in Mechanical Systems, Academic Press, 1963.
17. Heidmann, Marcus F., Priem, Richard J., and Humphrey, Jack C.: "A Study of Sprays Formed by Two Impinging Jets," NACA TN 3835, 1957.
18. Heidmann, Marcus. F.: "Photography and Analysis of Time Variation in Drop Size Distribution of a Liquid Spray," Proc. of 5th International Congress on High Speed Photography, Soc. Motion Picture and Television Engineers, 1962, pp. 519-524.

19. Rice, Edward J.: The Effect of Selected Fluid Parameters on Spatial Drop Size Distribution, Ph.D. Thesis, University of Wisconsin, 1966.
20. Lane, W. R.: "Shatter of Drops in Streams of Air," *Ind. Eng. Chem.*, Vol. 43, No. 6, June 1951, pp. 1312-1317.
21. Hanson, A. R., Domich, E. G., and Adams, H. S.: "An Experimental Investigation of Impact and Shock-Wave Break-Up of Liquid Drops," Res. Rep. 125, University of Minnesota, Jan. 1956,
22. Hinze, J. O.: "Fundamentals of the Hydrodynamic Mechanisms of Splitting in Dispersion Processes," *A.I.Ch.E. J.*, Vol. 1, Sept. 1955, pp. 289-295.
23. Magarvey, R. A, and Taylor, B. W.: "Free Fall Breakup of Large Drops," *J. Appl. Phys.*, Vol. 27, No. 10, 1956, pp. 1129-1135.
24. Telford, J. W., and Thorndike, N. S.: "Observations of Small Drop Collisions," *J. of Meteor.*, Vol. 18, 1961, p. 382.
25. Hocking, L. M.: "The Collision Efficiency of Small Drops," *Quart. J. Roy. Meteor. Soc.*, Vol. 85, 1959, p. 44.
26. Dunsikii, V. F.: "On Coagulation During the Atomization of a Liquid," *Sov. Phys. Tech. Phys.* (trans.) Vol. 1, 1956, p. 1232.

27. El-Wakil, M. M., Uyehara, O. A., and Myers, P. S.:
"A Theoretical Investigation of the Heating-Up
Period of Injected Fuel Droplets Vaporizing in Air,"
NACA TN 3179, 1954.
28. Borman, G. L., and Johnson, J. H.: "Unsteady Vaporization Histories and Trajectories of Fuel Drops Injected into Swirling Air," SAE Paper No. 598C, presented at National Powerplant Meeting (Phila.), 1962.
29. Crowe, C. T., Nicholls, J. A., and Morrison, R. B.:
"Drag Coefficients of Inert and Burning Particles Accelerating in Gas Streams," Ninth' (International) Symposium on Combustion, Academic Press, 1963, pp. 395-406.
30. Ranz, W. E., and Marshall, W. R.: "Evaporation From Drops," Chem. Eng. Prog., Vol. 48, No. 3, March 1952, pp. 141-146 and No. 4, April 1952, pp. 173-180.
31. Hsu, N. T., Sato, K., and Sage, B. H.: "Influence of Shape on Evaporation of Drops of N-Heptane," Ind. Eng. Chem., Vol. 46, No. 5, May 1954, pp. 870-876.
32. Torobin, L. B., and Gauvin, W. H.: "The Drag Coefficients of Single Spheres Moving in Steady and Accelerated Motion in Turbulent Fluid," A.I.Ch.E. J., Vol. 7, No. 4, Dec. 1961, pp. 615-619.
33. El-Wakil, M. M., Priem, R. J., Brikowski, H. J., Myers, P. S., and Uyehara, O. A.: "Experimental and Calculated Temperature and Mass Histories of Vaporizing Fuel Drops," NACA TN 3490, 1956.

34. Priem, R. J., Borman, G. L., El-Wakil, M. M., Ueyehara, O. A., and Myers, P. S.: "Experimental and Calculated Histories of Vaporizing Fuel Drops," NACA TN 3988, 1957.
35. Ingebo, R. D.: "Drag Coefficients for Droplets and Solid Spheres in Clouds Accelerating in Airstreams," NACA TN 3762, 1956.
36. Rabin, E., Schallenmuller, A. R., and Lawhead, R. B.: "Displacement and Shattering of Propellant Droplets," Final Summary Report AFOSR TR 60-75, March 1960.
37. Lambiris, S., and Combs, L. P.: "Steady State Combustion Measurements in a LOX/RP-1 Rocket Chamber and Related Spray Burning Analysis," in Detonation and Two-Phase Flow, S. S. Penner ed., Academic Press, 1962, pp. 269-304.
38. Hughes, R. R., and Gilliland, E. R.: "The Mechanics of Drops," Chem. Eng. Prog., Vol. 48, 1952, p. 497.
39. Gauvin, W. H., Pasternak, I. S.; Torobin, L. B., and Yaffe, L.: "A Radioactive Tracer Technique for Particle Velocity Measurement in Solids-Gas Systems," Can. J. Chem. Eng., Vol. 37, June 1959, pp. 95-98.
40. Torobin, L. B., and Gauvin, W. H.: "Fundamental Aspects of Solids-Gas Flow," Can. J. Chem. Eng.
(a) I. Introductory Concepts and Idealized Motion in a Viscous Regime, Vol. 37, Aug. 1959, pp. 129-141.

- (b) II. The Sphere Wake in Steady Laminar Fluids,
Vol. 37, Aug. 1959, pp. 167-176.
- (c) III. Accelerated Motion of a Particle in a Fluid,
Vol. 37, Dec. 1959, pp. 224-236.
- (d) IV. The Effects of Particle Rotation, Roughness and
Shape, Vol. 38, Oct. 1960, pp. 142-153.
- (e) V. The Effects of Fluid Turbulence on Particle Drag
Coefficients, Vol. 38, Dec. 1960, pp. 189-200.
- (f) VI. Multiparticle Behavior in Turbulent Fluids,
Vol. 39, June 1961, pp. 113-120.
41. Williams, F. A. : Combustion Theory, Addison-Wesley,
1965.
42. Hirschfelder, J. O., Curtiss, C. F., and Bird, R. B.:
Molecular Theory of Gases and Liquids, John Wiley &
Sons, 1962.
43. Panter, P. F.: Modulation, Noise, and Spectral
Analysis, McGraw-Hill, 1965.
44. Mugele, R. A., and Evans, H. D.: "Droplet Size Dis-
tributions in Sprays," Ind. Eng. Chem., Vol. 43,
No. 6, June 1951, pp. 1317-1324.
45. Bird, R. B., Stewart, W. E., and Lightfoot, E. N. :
Transport Phenomena, John Wiley and Sons, 1960.
46. Khinchin, A. I.: Mathematical Foundations of Sta-
tistical Mechanics, Dover, 1949.
47. DeCorso, S. M., and Kemeny, G. A.: "Effect of Ambient
and Fuel Pressure on Nozzle Spray Angle;" Trans.
ASME, Vol. 79, No. 3, April 1957, pp. 607-615.

48. Ranz, W. E.: "On Sprays and Spraying," Eng. Research Bull. B-65, Penn. St. Univ., 1956.
49. Benson, G. M.: The Determination Of Cross-Sectional Drop-Size Distributions of Liquid Sprays by a Fluorescent Technique, Ph.D. Thesis, Univ. of Wisc., 1963.
50. Benson, G. M.; El-Wakil, M. M.; Myers, P. S., and Uyehara, O. A.: "Fluorescent Technique for Determining the Cross-Sectional Drop-Size Distributions of Liquid Sprays," ARS J., Vol. 30, No. 5, May 1960, pp. 447-454.
51. International Critical Tables, McGraw-Hill, 1928.
52. Titani: Bull. Chem. Soc. Japan, Vol. 8, 1937, p. 255.
53. Timmermans, J.: Physico-Chemical Constants of Pure Organic Compounds, Elsevier, 1950.
54. Fiock, E. F., et. al.: "Calorimetric Determination of Thermal Properties of Methyl Alcohol, and Benzene," J. of Research NBS, Vol. 6, 1931, p. 881.
55. Spencer, H. M.: "Empirical Heat Capacity Equations of Gases and Graphite; Ind. Engr. Chem., Vol. 40, 1948, pp. 2152-2154. data of Brickwedde et. al., J. of Research NBS, Vol. 37, p. 263.
56. Hilsenrath, J.: Tables of Thermodynamic and Transport Properties, Pergamon Press, 1960.
57. Ingebo, R. D.: "Vaporization Rates and Heat Transfer Coefficients for Pure Liquid Drops," NACA TN 2368, 1951.

58. Kobayasi, K. : "A Study of the Evaporation Velocity of a Single Liquid Droplet," Technology Repts. of Tohoku Univ., Vol. 18, No. 2, 1954, pp. 209-222.
59. Apashev, M. D., and Malov, P. V. : "Evaporation of Single Free Droplets of Various Liquids with Small Reynolds Number Values for the Stream Flowing Past the Droplets," ARS J., Vol. 32, No. 3, March 1962 (translation) pp. 467-472.
60. Fedoseyev, V. A., and Polishchuk, D. I.: (cited in Apashov & Malov) "Evaporation of Droplets of Some Organic Liquids," Collected Papers, Faculty of Physics and Mathematics, Odessa Stat Univ., 1954, No. 5.
61. Miller, R. C., and Savage A.: "Harmonic Generation and Mixing of $\text{CaWO}_4: \text{Nd}^{3+}$ and Ruby Pulsed Laser Beams in Piezoelectric Crystals," Phys Rev, Vol. 128, No. 5, Dec. 1, 1962.
62. Strickler, S. J., and Berg, R. A.: "Relationship Between Adsorption Intensity and Fluorescence Lifetime of Molecules," J. Chem. Phys., Vol. 37, No. 4, Aug. 15, 1962, pp. 814-822.
63. Ready, John E.: "Effects of Laser Radiations," Ind. Res., Vol. 7, No. 8, Aug 1965, pp. 44-50.
64. Ellis, A. T., and Fourney, M. E.: "Application of a Ruby Laser to High Speed Photography," Proc. IEEE, Vol. 51, June 1963, pp. 942-943.

65. Edgerton, H. E. : "Double-Flash Microsecond Silhouette Photography," Rev. Sci, Inst., Vol. 23, No. 10, Oct. 1952, pp. ~~532-533~~.
66. Adams, G. K.: "A Repetitive Spark Source for Shadow and Schlieren Photography," J. Sci Instru., Vol. 28, Dec. 1951, pp. 379-384.
67. Pringsheim, Peter: Fluorescence and Phosphorescence, Interscience, 1949.
68. Briffa, Francis E. J., and Dombrowski, Norman: "Entrainment of Air into a Liquid Spray," A.I.Ch.E. J., Vol. 21, No. 4, July 1966, pp. 708-717.
69. Binark, Hikmet, and Ranz, W. E. : "Induced Air Flows in Fuel Sprays; ASME Paper No. 58-A-284, 1958.
70. Johnson, N. L. : "Systems of Frequency Curves Generated by Methods of Translation: Biometrika, Vol. 36, 1949, pp. 149-176.
71. Johnson, N. L.: "Bivariate Distributions Based on Simple Translation Systems:' Biometrika, Vol. 36, 1949, pp. 279-304.
72. DeCorso, S. M.: "Effect of Ambient and Fuel Pressure on Spray Drop Size," ASME Paper No. 59-GTP-3, (presented at ASME Gas Turbine Power Conference, March 1959).
73. Heidmann, Marcus F., and Foster, Hampton H. : "Effect of Impingement Angle on Drop Size Distribution and Spray Pattern of Two Impinging Water Jets," NASA TN D-872, 1961.

74. Bittker, David A.: "Effect of Ambient Air Velocity on Atomization of Two Impinging Water Jets," NASA TN D-2087, 1964.